A GENETIC TEST

FOR

MALIGNANT HYPERTHERMIA

A dissertation presented to Massey University in partial fulfilment of the requirements for the degree of Doctor of Philosophy in biochemistry.

Rosemary L. Brown

2000

ACKNOWLEDGEMENTS

I would like to extend my sincere gratitude to my principal supervisor, Dr. Kathryn Stowell for her enduring encouragement, dedication and reassurance, throughout the (prolonged) term of my PhD studies. Thanks also to Prof, John Tweedie for guidance, and enthusiastic assistance with computer-related tasks.

This work would not have been possible without the dedication of Neil Pollock, (specialist anaesthetist, Palmerston North hospital), who organised the collection of blood and tissue samples and provided vital clinical expertise in the field of MH. I would also like to thank other members of the Palmerston North hospital department of Anaesthesia and intensive care, for the provision of IVCT data and helpful discussion, particularly Ken Couchman and Mike Hodges.

Many members of the former Department of Biochemistry and the current IMBS have provided assistance, encouragement and enjoyable diversion along the way. In particular, I am indebted to Danielle James for her persistently cheerful dedication of to the task of endless DNA extractions, and for keeping tabs on the pedigree data. Much of this work also relied on the efficiency of Lorraine Berry, who was in charge the automatic sequencing. I would also like to thank friends and colleagues in the Twilight Zone, for friendship and technical advice, especially, Catherine, Robyn, Jakki, Bec and Carole. Special thanks to Stan Moore for his dedicated provision of comic relief, and likewise, the members of the IMBS touch team, numerous flatmates, and friends from the Massey alpine club. I am particularly indebted to Lee Davies for helping to salvage my data, and for reformatting and replacing my hard drive (sadly, on more than one occasion).

I am sincerely grateful to my parents for their support and acceptance throughout the duration of my studies, and to Andrew, for his love and continued encouragement during my PhD and for abiding the protracted separation associated with the preparation of this thesis.

TABLE OF CONTENTS

ABSTRACT

Malignant Hyperthermia (MH) is an inherited disorder of skeletal muscle in which an abnormality in the regulation of calcium release from internal stores can result in a fatal hypermetabolic reaction on exposure to general anesthetics. Mutations in the gene encoding the skeletal muscle ryanodine receptor/ calcium release channel (RYR1) have been linked to MHS in 50% of overseas families examined, and at least five additional MH susceptibility loci have since been proposed. Current diagnosis of MH in New Zealand relies on the *in vitro* contracture testing (IVCT) of excised muscle bundles with caffeine and halothane. The genetic basis of MH in NZ families was investigated, with the goal of developing genetic tests to replace the muscle biopsy test.

A search for previously published RYR1 mutations in susceptible members of 33 NZ MH families revealed three RYR1 mutations; Arg163Cys, Gly341Arg, and Gly2434Arg, which co-segregated completely with susceptibility to MH (MHS). None of the 17 published RYR1 mutations were detected in a local MHS Maori family in which several anaesthetic deaths have occurred. This is the largest characterised MH family in the world. An examination of the segregation of a panel of chromosome 19q markers with MHS in over 200 members of this family revealed that MHS was linked to the RYR1-flanking markers. This implicated the involvement of a novel RYR1 defect.

The entire 15.3 kb RYR1 coding region was combed for mutations by RT-PCR and automatic sequence analysis. A novel point mutation was detected that changed threonine 4826 to isoleucine in the C-terminal region of the RyR1 protein. This mutation was not found in 220 chromosomes from the normal population, or in 94 members of the family who had been diagnosed MHN (normal). A screen for the mutation in 210 key family members revealed a direct correlation between inheritance of the mutation and highly abnormal muscle contracture results in 36 individuals. 22 MHS individuals lacked the mutation; consequently the false positive rate of the IVCT and the possible segregation of at least one additional MHS gene complicated genetic linkage analysis. These problems were addressed by investigating increasingly stringent models for MH diagnosis.

Four additional novel RYR1 mutations were detected in other MHS families investigated by sequence analysis of cDNA and genomic DNA, Arg401Cys, Arg2452Trp, Arg2454His and His4833Tyr. The detection of the Thr4826Ile and His 4833Tyr mutations established the channel domain of the ryanodine receptor as a new MHS domain. Genetic testing for MHS can now be applied with caution to predict MH susceptibility in approximately 40 % of at-risk individual in NZ, thus reducing the number of patients requiring an expensive and invasive surgical procedure.

ABBREVIATIONS

A	absorbance
ACRS	amplification-created restriction site
ARMS	amplification refractory mutation system
ASO	allele-specific oligonucleotide
bp	base pair
BRL	Bethseda research laboratories
cDNA	complementary DNA
Caf.	Caffeine
CaM	calmodulin
CFLP	cleavase fragment length polymorphism
CHCT	caffeine/halothane contracture test (North American protocol)
CK	Creatine phosphokinase
cs	chromosome
ddNTP	2',3'-dideoxyribonucleotide 5'-triphosphate
dH_2O	distilled water
DEPC	diethylpyrocarbonate
DHPR	dihydropyridine receptor
DMD	Duchenne muscular dystrophy
DMSO	dimethyl sulphoxide
dNTP	deoxyribonucleoside 5'-triphosphate
ds DNA	double-stranded DNA
DTT	dithiothreitol
ECC	Excitation-contraction coupling
EDTA	ethylene diamine tetra-acetate
EEO	electroendosmosis
EMHG	European Malignant Hyperthermia Group
EtBr	ethidium Bromide
Hal.	halothane
HEPES	N-[2-hydroxyethyl]piperazine-N'-[4-butanesulphonic acid]
IP_3R	inositol 1,4,5-trisphosphate receptor
IVCT	*in vitro* contracture test (European protocol)
kb	kilobase
KR	Krebs-Ringer
MH	malignant hyperthermia
MHE	malignant hyperthermia equivocal diagnosis
MHN	malignant hyperthermia negative diagnosis
MHS	malignant hyperthermia susceptible diagnosis
MPC	magnetic particle concentrator
mRNA	Messenger RNA
MOPS	3-[N-morpholino]propanesulphonic acid
NCE	Na^{+}/Ca^{+2} exchanger
PAGE	polyacylamide gel electrophoresis
PCR	polymerase chain reaction
PMCA	plasma membrane calcium ATPase
PSS	porcine stress syndrome
RE	restriction endonuclease

RFLP	restriction fragment length polymorphism
RNase	ribonuclease
rRNA	ribosomal RNA
RT	reverse transcriptase
RT-PCR	reverse transcription-polymerase chain reaction
RYR	ryanodine receptor (gene)
RyR	ryanodine receptor (protein)
SDS	sodium dodecyl sulphate
SERCA	Sarco(endo)plasmic reticulum ATPase
ss DNA	single-stranded DNA
SSCP	single-stranded conformation polymorphism
SR	sarcoplasmic reticulum
TAE	Tris-acetate-EDTA buffer
Taq	*Thermus aquaticus*
TBE	Tris-borate-EDTA buffer
TC	Terminal cisternae
TE	Tris-EDTA buffer
TEMED	N,N,N',N'-tetramethylenediamine
Tm	melting temperature

LIST OF FIGURES

1. INTRODUCTION

1.1 OVERVIEW OF THE GENETICS AND BIOCHEMISTRY OF MALIGNANT HYPERTHERMIA

Malignant hyperthermia (MH) is an autosomal dominant skeletal muscle disorder that predisposes susceptible individuals to a potentially fatal reaction during general anaesthesia [1]. The reaction apparently results from a defect in the mechanism regulating the release of Ca^{+2} from internal stores, leading to a rapid sustained increase in myoplasmic Ca^{+2} [2-4]. The reaction is triggered in susceptible individuals upon exposure to commonly used inhalational anaesthetics, alone, or in combination with depolarising muscle relaxants. MH manifests as a hyper-metabolic crisis, characterised by high fever, sustained muscle contracture and metabolic acidosis. Unless the reaction is halted with early treatment (rapid cooling, and administration of the Ca^{+2} channel blocking agent, dantrolene sodium) the patient will invariably die from cardiac arrest [5,6]. Permanent neurological or kidney damage sustained during the MH crisis contributes to the morbidity. An analogous condition in swine (porcine stress syndrome) is triggered by anaesthetics and stress factors, including overheating, fighting and weaning [7,8]. The possible involvement of stress and other environmental factors as triggers of sudden death in human MH is a current area of debate [9-11]. MH has been associated with a number of neuromuscular diseases, in particular, central core disease (CCD) a severe myopathy characterised by muscle weakness [12-16].

Muscle from MHS individuals is hypersensitive to the contracture inducing effects of agents that stimulate Ca^{+2} release from the sarcoplasmic reticulum (SR). Current diagnosis relies on the measured in vitro contracture response of excised muscle bundles to caffeine and halothane. Biochemical and electrophysiological studies of MH in swine and humans pointed to the skeletal muscle SR Ca^{+2} release channel, known as the ryanodine receptor (RyR1) as a likely candidate for the molecular defect [17-19]. The name RyR is derived from the neutral plant alkaloid, which binds to the receptor with high affinity and has been used as a label to purify and study the functional properties of the RyR1 calcium channel. RyR1 forms a large tetrameric protein consisting of a C-terminal channel embedded in the SR membrane, and a large cytoplasmic foot domain, which is believed to communicate with a voltage-dependent Ca^{+2} channel in the opposing T-tubule membrane [20].

Molecular genetic studies mapped the primary MH susceptibility locus to chromosome 19q13.1, in the vicinity of the gene encoding the ryanodine receptor, RYR1 [21,22]. The involvement of RYR1 in MHS has been corroborated by the identification of RYR1 point mutations that co-segregate with MH susceptibility in swine [23,24] and in a subset of human MH susceptible pedigrees [25]. In other pedigrees, susceptibility to MH is not linked to the RYR1 gene [26-29]. Five additional MH susceptibility loci have been revealed on chromosomes 17q [30], 7q [29] 3q [31], 1q [32,33] and 5p [32] where genes involved in muscle ion homeostasis and excitation-contraction coupling have been proposed as candidates. A mutation in the CACNLIA3 gene encoding the main subunit of the L-type voltage dependent calcium channel has been confirmed for the 1q locus [33]. Consequently, MH has been redefined as a complex syndrome representing the final common pathway of any number of defects in muscle ion homeostasis [34]. A major objective for MH research is the introduction of a general genetic test to replace the invasive skeletal muscle biopsy test currently in use. However, the development of a genetic screening test for MH has been

constrained by the emerging genetic and clinical heterogeneity of the MH syndrome and the lack of a "gold standard" by which to define an individual's true MH status.

1.2 CLINICAL FEATURES OF MALIGNANT HYPERTHERMIA

1.2.1 History and incidence

Episodes of anaesthetic deaths with unexpected fever and muscle contracture were reported as early as 1900, as "ether convulsions" [35]. Denborough *et. al.* first described a familial predisposition to the so-called malignant hyperexia syndrome in a family in which ten related individuals had died suddenly with fever and convulsions during general anaesthesia [1]. An autosomal dominant mode of inheritance was subsequently defined [36,37]. The incidence of MH during general anaesthesia varies age dependently from 1:15,000 children to 1:50,000 adults anaesthetised [37-40]. However, these figures underestimate the true prevalence of the genetic disposition since susceptible individuals do not always display symptoms when exposed to triggering anaesthetic [41]. Estimates of the clinical penetrance of the MHS phenotype vary between 3.3 % and 37 % [42,43].

1.2.2 Clinical symptoms

MH reactions are highly variable and difficult to diagnose. A standardised clinical grading scale was recently devised to provide a clinical definition of the MH syndrome and to assist diagnosis [44]. A classic MH reaction is characterised by skeletal muscle rigidity and muscle hypermetabolism (presenting as tachypnea, tachycardia, metabolic and respiratory acidosis and hyperthermia) and rhabdomyolysis [45,46]. About 75% of patients during a crisis develop skeletal muscle rigidity [47], and jaw muscle spasms are an early sign of an impending MH crisis in 50% of cases [10,48]. Unless controlled, a futile hypermetabolic cycle ensues, which can lead to death by cardiac arrest or brain oedema. Patients who survive the initial MH crisis may later suffer complications ranging from muscle pain and weakness to kidney failure and permanent brain damage [5].

1.2.3 Triggering agents

MH may be triggered by: 1) volatile non-halogenated anaesthetics (such as ether, and cyclopropane); 2) all commonly used halogenated anaesthetics (halothane, isoflurane, ethyl chloride, trichloroethylene) and; 3) by depolarising muscle relaxants such as succinylcholine [49-51]. The manifestation of MH is more severe and the onset more abrupt when both halothane and succinylcholine are received concomitantly [52]. Conversely, non-depolarising neuromuscular blockers and barbiturates can delay the onset [53]. Succinylcholine may trigger MH via effects on the motor end plate (where it binds acetylcholine receptors, causing muscle paralysis). In addition, the preservative in succinylcholine solutions (4-chloro-m-cresol) is in itself a specific and potent activator of Ca^{+2} release channel [54]. The binding affinity for 4-chloro-m-cresol [55] and the contracture inducing effects of this drug are exaggerated in MHS muscle [56] thus it may be a trigger of clinical MH [57]. Drugs other than the volatile agents and succinylcholine have produced MH-like responses, including ketamine, phencyclidine, some tranquilizers and tricyclic antidepressants [58,59]. Elevated body temperatures resulting from infection or external environment or physical exertion prior to anaesthesia [60] can aggravate the progression of the MH crisis. MH-like episodes triggered in the absence of anaesthesia have been described in susceptible persons in association with overheating [61,62], exertional heatstroke [63-66] alcohol ingestion, viral infection [11] and stress [42,67-70]. A higher

incidence of the sudden infant death syndrome (SIDS) has been noted in MHS families, compared to controls [70-72], however the link between SIDS and MH is controversial.

1.2.4 Management of the MHS patient

The mortality associated with MH episodes has been reduced from 80% [73,74] to 3-4% with improved awareness and the therapeutic use of a clinical antidote, sodium dantrolene [75,76] however MH is still recognised as the leading cause of preventable anaesthetic deaths. Dantrolene is a lipid soluble hydantoin derivative that terminates MH episodes by inhibiting the release of Ca^{+2} from the SR [77] and thus lowering the sarcoplasmic Ca^{+2} concentration in MHS muscle. Early intervention is the key to MH treatment since the progressive decline in cardiac activity restricts the drug's distribution [46] and to be effective, dantrolene must be administered before the SR Ca^{+2} stores are depleted. Further treatment involves discontinuing anaesthesia, reducing body temperature through artificial cooling, correcting hypoxia and supporting cardiovascular function [78]. Anaesthetic agents considered safe for susceptible individuals include local anaesthetics, nitrous oxide, thiopental and other barbiturates, althesin, opiates, droperidol and pancuronium [5].

1.3 THE PORCINE MODEL OF MALIGNANT HYPERTHERMIA

A disorder that is homologous to human MH occurring in swine, known porcine stress syndrome (PSS) has been used as a model to study the pathophysiology of human MH and to identify triggering agents and therapeutic drugs. Animals homozygous for the abnormality have a MH-like response to stress, manifesting as muscle rigidity, hypermetabolism, fever, flushing of the skin and rapid death followed by instant *rigor-mortis* [7,8]. The syndrome is precipitated by separation, fighting, mating and slaughter, after which the carcass is rendered worthless due to a post-mortem deterioration of the meat quality known as soft, exudative pork [7].

Predisposition to PSS is controlled by a recessive gene [79] also associated with beneficial effects on muscle mass, lean meat quality and sensitivity to inhalational anaesthetics, which manifests as a malignant hyperthermic reaction on exposure to halothane [80]. Affected swine can be detected by the "barnyard test" in which susceptible animals develop limb rigidity when challenged with halothane [80]. Heterozygotes are identified by a simultaneous administration of 1% halothane and succinylcholine [81] and by skeletal muscle *in vitro* contracture tests [38]. In one breed of swine, homozygotes for the MH gene defect are resistant to halothane, suggesting some strain-dependent modulation of the response [82,83]. Modifying factors that are thought to influence the onset and severity of the syndrome include free fatty acids [83], inositol-1,4,5-triphosphate [84] and the antioxidant defence system [85].

A mutation in the gene encoding the skeletal muscle sarcoplasmic reticulum Ca^{+2} release channel (RYR1) is responsible for all known cases of porcine MH [23,24]. Animals heterozygous for the Arg615Cys mutation are characterised by large muscle mass similar to homozygous pigs, and stress resistance. Consequently, DNA tests have since replaced the barnyard challenge [86,87] and are applied to selectively breed heterozygous litters. MH-like syndromes have been reported in a number of other species, most notably dogs [88,89]. However, the molecular basis of canine MH has not yet been identified.

1.4 DIAGNOSIS OF MALIGNANT HYPERTHERMIA

Although a significant elevation of serum creatine kinase (CK) is characteristic of MH [90,91], measurement of serum CK is unsatisfactory as a test in that 30% of carriers are not detected [92,93]. Currently the only accurate and reliable diagnostic test for MH is the *in vitro* caffeine/halothane contracture test (IVCT), which requires the patient to undergo an expensive and highly invasive open *quadriceps* muscle biopsy. The contracture test was based on observations that muscle fascicles from MH susceptible (MHS) patients develop contractures on exposure to lower concentrations of halothane or caffeine than do specimens from normal, MH negative (MHN) subjects [35,94,95].

Two alternate protocols for the diagnosis of MH are currently used by the European (IVCT) [96,97] and North American (CHCT) [98] MH groups. The European Malignant Hyperthermia group (EMHG) IVCT standardised protocol classifies patients into three diagnostic categories: MHS (susceptible), MHN (normal), and MHE (equivocal). The MHE group was created to reduce the incidence of false positive or false negative diagnoses, and is clinically regarded as susceptible to MH [96]. The North American procedure does not include an equivocal category, and designates an abnormal contracture response to a single test agent as an MHS result. The CHCT thus generates more false positive diagnoses than the IVCT, which has hampered genetic investigations of American families [99]. The NZ IVCT testing centre (Palmerston North hospital) is affiliated with the European MH group and adopted the standardised EMHG test procedure in 1985.

1.4.1 European MH group IVCT procedure

The procedure requires the excision of a segment of *quadriceps* muscle (5 cm by 2 cm) to provide several muscle specimens, 15 mm-25 mm in length by 2-3 mm in width. The fresh muscle sample is suspended immediately in a bath of carboxygenated Krebs-Ringer (KR) solution and transported to the laboratory for testing within 5 hours of the biopsy. The IVCT measures the contracture of dissected muscle fascicles (suspended in a 40 ml bath of KR buffer at 37°C) over a background of twitches that ascertain the viability of the fiber. Tension is measured by a transducer before and after the addition of the test drug. The recorded test parameter in each case is the threshold drug concentration; the lowest drug concentration to elicit a sustained increase of 0.2 g in baseline tension. The measurement of the caffeine threshold involves a stepwise increase of 0.25, 0.5, 1.0, 1.5, 2.0, 3.0 and 4.0 mM caffeine in the tissue bath each at 3 minute periods, until a contraction occurs. The static halothane test measures the contracture response to 0.5, 1.0, 2.0, and 3.0 % halothane [93,96]. Subjects are diagnosed MHS if an "abnormal" threshold tension of 0.2 g or greater is obtained, at a threshold caffeine concentration of 2 mM or less, and independently, at a threshold halothane concentration of 2% or less. Subjects registering muscle contracture responses of $\geq$ 0.2 g tension in response to only one of the test agents are designated MH equivocal (MHE). Subjects with muscle tensions within the normal range (< 0.2 g) at both 2 mM caffeine and 2 % halothane are diagnosed MHN.

1.4.2 Limitations of the IVCT

Although the IVCT is regarded as the "gold standard" for MH diagnosis it has many limitations. The test is expensive, highly invasive and technically demanding. Patients may take weeks to fully recover and suffer permanent scarring. Children under the age of ten, and the elderly can not be diagnosed due to uncertainty of test viability and insufficient tissue [96]. Halothane is a volatile anaesthetic with low solubility in water; consequently, actual

concentrations of halothane in solution can vary. Temperature, Ca^{+2} and Mg^{+2} ion levels in the bath influence the magnitude of the induced contractures, causing variability in results between laboratories [100]. Some pharmaceuticals including dantrolene, verapamil (Ca^{+2} channel blocker), propranolol (β blocker), and procaine can interfere with contracture tests and must be discontinued before patients are admitted for muscle biopsy [93]. Inconclusive tests, in most circumstances cannot be repeated.

In light of these problems, and the availability of non-triggering anaesthetics for susceptible individuals, clinicians may elect to assume MHS status for the relatives of a proband rather than subjecting them to the muscle biopsy test. However, the number of assumed MHS individuals within susceptible families may increase exponentially over two or more generations unless negative branches are established. The risks of anaesthesia for patients who will have to be managed as MHS are greater, as the range of applicable drugs are limited, and the alternatives less safe [101]. This can pose problems for patients with difficult airways, asthma, or with full stomachs (as in emergency or obstetrics cases), where intubation is difficult and the danger of aspiration (inhalation of vomit) is increased [101].

1.4.3 The sensitivity and specificity of the IVCT

The IVCT measures the interaction among many components of a system involving several channels, pumps and contractile proteins. Consequently, within the varied population, results encompass a wide spectrum of values, and, as with most pharmaco-physiologic tests, do not fall naturally into clear positive and negative categories. The IVCT diagnostic cut-points were set to maximise the sensitivity of the test (to avoid potentially fatal false-negative results), and were arrived at by comparing the IVCT data from a groups of MHS probands and normal control patients [96,98]. The compromise of a test with high sensitivity is a reduced specificity, in other words, some false IVCT positives will be assigned [98].

The European MH group IVCT was found to have 99% sensitivity and 93.6 % specificity [97,102], while the equivalent values for the North American CHCT procedure were 97% and 78% respectively [102]. The retrospective analysis of exposure to triggering anaesthetics in subjects diagnosed MHN confirms the rarity of false negative diagnosis and supports the confidence placed in an MHN diagnosis [41,103]. Four patients diagnosed MHN by the IVCT at one centre later suffered hypermetabolic reactions during anaesthesia [104]. However, no other reports of false negative IVCT results have been published by European testing centres [105]. The accuracy of the European protocol has been further validated by the discovery of causative mutations in the RYR1 gene that correlate well with positive contracture tests [13,106-111].

The high sensitivity and moderate specificity of the IVCT is appropriate for the clinical diagnosis of a life-threatening condition in which false positive diagnoses do not pose a risk for the patient [101]. However, the significant false positive rate of the IVCT can pose a challenge to the genetic studies of MH. The use of altered (more stringent) IVCT cut-off points has, in some cases, revealed linkage between a candidate MHS mutation and MHS that was previously obscured when standard cut-off points were applied [99,105,112].

Specific activators of the Ca^{+2} release pathway, including ryanodine [113] and 4-m-chlorocresol [56] have been recently proposed as potentially specific tests for malignant hyperthermia (MH). These agents are now used routinely by some groups to supplement the caffeine and halothane tests, and can assist the phenotypic categorisation of MHE individuals [56,114,115]. The

sensitivity and specificity of the ryanodine and 4-chloro-m-cresol tests has not yet been formally determined.

1.5 MOLECULAR COMPONENTS OF SKELETAL MUSCLE CONTRACTION

Skeletal muscle was recognised as the site of the primary abnormality in MH, after isolated swine hind-limb preparations were shown to respond to triggering agents in a similar manner to intact animals [116] and excised skeletal muscle bundles responded abnormally to triggering agents *in vitro* [35]. The role of Ca^{+2} in the progression of the crisis was established by *in vivo* experiments on swine. A sudden rise in intracellular Ca^{+2} accompanying the onset of an induced crisis was measured directly by the use of ion specific electrodes inserted into the myocytes of a MHS pig. A fall in Ca^{+2} was observed as dantrolene controlled the syndrome and the muscles relaxed [2]. A defect in the regulation of intracellular Ca^{+2} could theoretically account for the full cascade of biochemical events observed during the MH crisis since muscle contraction, relaxation and energy metabolism are all regulated by Ca^{+2} [47].

1.5.1 The role of calcium as a second messenger

A wide range of events essential for life are modulated by Ca^{+2}, including fertilisation, cell division differentiation and growth, control of metabolic pathways, endocrine secretion, neuronal signal transduction, muscle contraction, and cognitive function [117,118]. The spatial organisation, timing, amplitude and frequency of Ca^{+2} signals are tailored to control the intensity and nature of the physiological response [118]. However, prolonged high concentrations of intracellular Ca^{+2} are toxic, leading to cell death [118]. Muscle cells thus have complex systems of Ca^{+2} pumps and channels to extrude Ca^{+2} from the cell and tightly regulate Ca^{+2} influx.

1.5.1.1 Control of calcium efflux

The resting cell maintains low cytoplasmic free calcium levels (10^{-7} M) compared to the extracellular fluid (10^{-3} M). This steep gradient is partly achieved by the action of Ca^{+2} ATPases (PMCA) present on the plasma membrane that drive Ca^{+2} into the extracellular space in return for H^+. A low affinity Na^+/Ca^{+2} exchanger on the plasma membrane also expels Ca^{+2} by using the Na^+ gradient established by the Na^+-K^+ pump and operates when Ca^{+2} concentrations rise up to ten times their normal level (to 10^{-6} M) [119]. The Ca^{+2} ATPase (SERCA) residing in the membranes of internal organelles provides the predominant mechanism by which Ca^{+2} is removed from the cytosol. The Ca^{+2} ATPase pump has a higher affinity for Ca^{+2} than the Na^+/Ca^{+2} exchanger and constitutes approximately 90% of the SR membrane protein [117]. During Ca^{+2} stress mitochondria can transport Ca^{+2} into the matrix spaces, thereby protecting the cell from Ca^{+2}-induced necrosis. In addition to a Na^+/Ca^{+2} exchanger that admits Ca^{+2} down the electrical gradient of the inner mitochondrial membrane, mitochondria have a high capacity Ca^{+2} pump that operates under Ca^{+2} stress (10^{-3} M) to take up Ca^{+2} from the cytosol [120]. Under these conditions, the production of ATP through mitochondrial oxidative phosphorylation is arrested [120].

1.5.1.2 Control of calcium influx

Cellular processes are controlled by Ca^{+2} ion release from intracellular stores within the endoplasmic reticulum, or the sarcoplasmic reticulum (SR) in muscle. Two related families of intracellular Ca^{+2} release channels have been characterised that release Ca^{+2} from these sources: the inositol-1,4,5-trisphosphate (IP_3) receptors and the ryanodine receptors (RyR) [121]. The

RyRs and IP_3 receptors are distant relatives, sharing amino acid sequence homology (particularly in the channel region) and a similar quaternary structure [117,122]. Both RyR and IP_3R are present in the sarcoplasmic reticulum of skeletal muscle fibers. In skeletal muscle, the RyR1 Ca^{+2} release channel isoform plays the major role in muscle contraction, and opens in response to neuronal induced depolarisation of the surface membrane. The IP_3 receptor of skeletal muscle releases Ca^{+2} upon the binding of IP_3 to the cytoplasmic portion of the 1200 kDa tetramer. The role of the IP_3 receptor in skeletal muscle Ca^{+2} mobilisation remains an area of controversy [119]. Calcium flux is also mediated by the entry of extracellular Ca^{+2} ions. A voltage-dependent, dihydropyridine sensitive Ca^{+2} channel (DHPR) concentrated in the extensions of the surface membrane, is activated in response to electrical stimulation. The influx of Ca^{+2} into the cell through this channel triggers the opening of RyR receptors, at least in cardiac muscle, but is not in itself sufficient to directly initiate muscle contraction.

1.5.2 Skeletal muscle morphology at the triad junction

Skeletal myofibers are elongated multinucleated cells, about 100 μm wide and up to 30 cm in length. Cylindrical myofibrils composed of thin (actin, troponin) and thick (myosin) myofilaments run longitudinally through the fiber. Myofibrils are arranged compartments (sarcomeres) that are separated from each other by a layer of dense material known as the Z line. The thin myofilaments are anchored to the Z lines and extend inwards from each end of the sarcomere to inter-digitate centrally with the thick filaments.

An elaborate network of membranous Ca^{+2}-filled sacs known as the sarcoplasmic reticulum (SR) surrounds the myofibrils. Finger-like extensions of the plasma membrane known as transverse tubules (T-tubules) run transversely through the fiber. The T-tubules form small openings on the surface of the muscle fiber, and as extensions of the plasma membrane, they are filled with extracellular fluid. The T-tubules encircle the myofibrils, and interrupt the longitudinal SR channels where they are embraced on either side by dilated sacs of the SR known as terminal cisterns (see Figure 1-1). Ca^{+2} ions are concentrated mostly in the terminal cisternae of the SR where they are bound to calsequestrin. The T-tubule, together with the segments of SR on either side is collectively known as the triad.

Excitation begins with the arrival of a neurotransmitter (acetylcholine) at the plasma membrane, which opens a Na^{+} channel to establish an action potential. The principal function of the T-tubules is to conduct electrical impulses from the fiber surface, deep into the interior, and to bring about muscle contraction by initiating the release of Ca^{+2} from the SR, in a process known as excitation contraction coupling (ECC). Ca^{+2} activates the contractile apparatus by binding troponin C, thus shifting the troponin-tropomyosin complex and exposing the activated myosin-binding sites on actin. The myosin cross-bridges move like the oars of a boat on the surface of the actin filaments, causing the filaments to slide past each other. At the end of this power stroke, the detachment of the cross-bridge from actin requires the binding of a new ATP molecule to myosin. The abundant Ca^{+2} ATPase pumps on the SR actively sequester Ca^{+2} ions back into the SR and restore Ca^{+2} to resting levels.

The missing link in the current understanding of the ECC in skeletal muscle is the mechanism by which the signal to release Ca^{+2} from the SR is transmitted from the T-Tubule at the triad junction. It is this process that is believed to malfunction in MH, resulting in unregulated SR Ca^{+2} release. The current "mechanical coupling hypothesis" for ECC proposes a direct protein-protein interaction between two large Ca^{+2} channel complexes in the T-tubule and SR membranes of the triad junction [123,124]. In favour of this model, the DHPR or voltage sensor Ca^{+2} channel of the T-tubule directly opposes the large tetrameric Ca^{+2} release channel (RyR)

embedded in the SR membrane [123]. The cytoplasmic domain of the SR channel is broad enough to bridge the 15 nm gap between the two membranes and constitutes the "foot domain" in triad junctions observed spanning junctional gap under light microscopy [125]. The carboxy terminal third of the RyR forms the membrane-spanning base-plate and the Ca^{+2} pore in the SR membrane [126,127]. Not all RyR1s are located in the triad junctions. Some are positioned in the SR membranes between triad junctions, and are probably activated by Ca^{+2} ions released in their neighbourhood, to amplify the signal [128].

The DHPR on the T-tubule membrane is an L-type (long lasting, high voltage, slow current) voltage-operated Ca^{+2} channel, composed of 5 subunits, designated α_1 (185 kDa), α_2, (143 kDa), β (54kDa), γ (30 kDa) and δ (26 kDa). The α_2 and β subunits are generated by post-translational proteolytic processing of a single peptide. The α_1 subunit performs both the voltage sensing and Ca^{+2} conduction functions and contains the binding site of the namesake dihydropyridine drugs. The remaining subunits are believed to be regulatory. Four DHPR complexes form a diamond shaped tetrad array within the T-tubule membrane [129]. In skeletal muscle, each tetrad is aligned with the large RyR tetramer in the SR membrane. Interestingly, only alternate RyR tetramers are aligned with DHPR tetrads, in keeping with an average RyR: DHPR ratio of 2:1 observed in biochemical studies [130]. This forms the basis of a model for the dual mechanism for Ca^{+2} release, involving direct contact and a secondary calcium-induced amplification signal [128] (discussed further in section 1.10)

Figure 1-1 Ion channels involved in skeletal muscle EC coupling

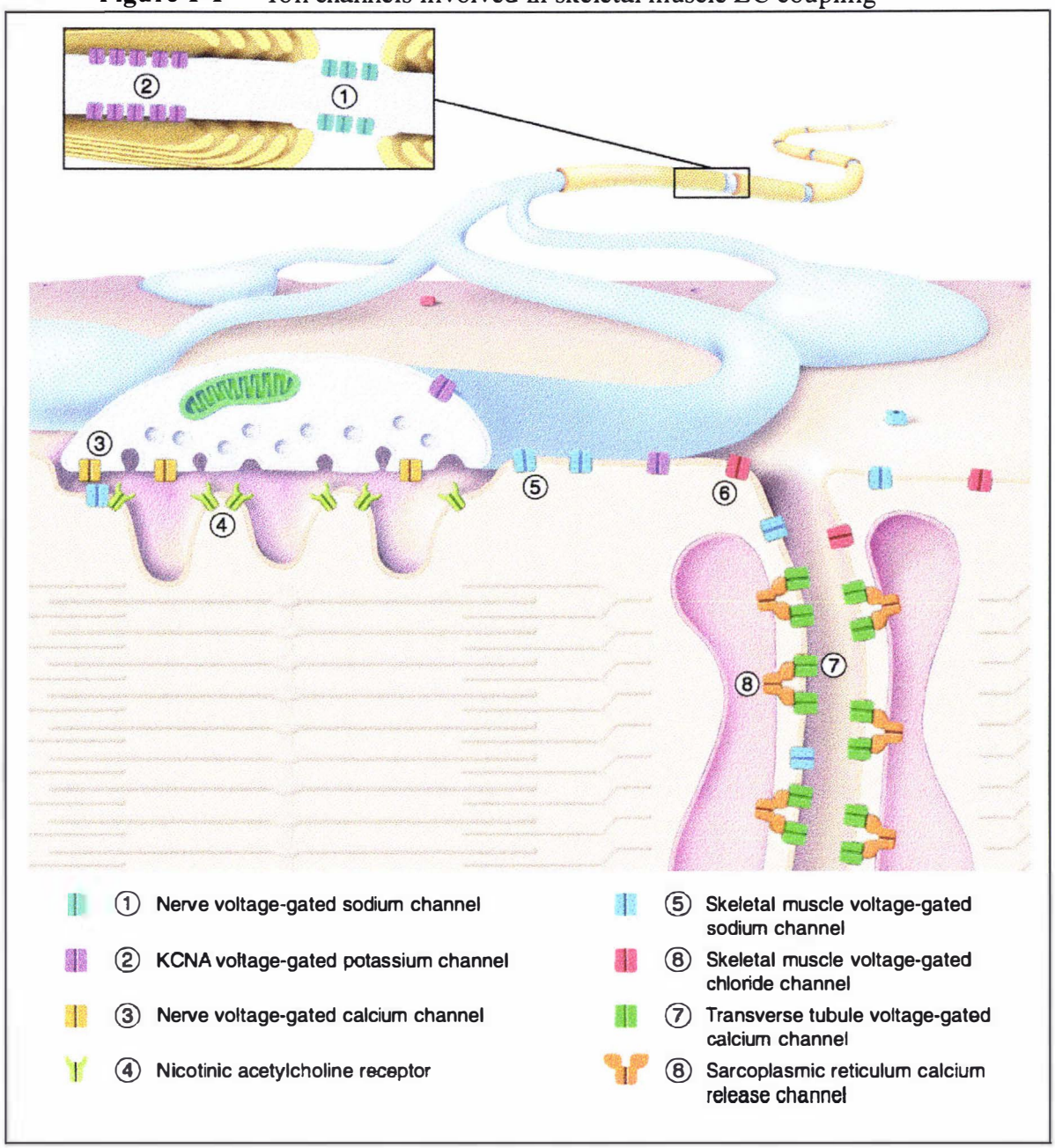

In the upper portion of the diagram, a nerve axon forms synaptic contact with the muscle fiber (enlarged). The contractile apparatus and membrane components of the muscle cell are shown in the lower portion. The T- tubule extension of the plasma membrane is surrounded by the terminal cisternae of the SR. The junction between the two membranes features two large calcium channel complexes; the voltage gated (DHPR) (7) on the T-tubule membrane and the calcium release channel (RyR1) (8) on the SR membrane. MH results from defects in RyR1 (8). Muscle diseases associated with MHS result from mutations in ion channels upstream of RyR1 in ECC including 4,5, 6, 7, and 8. (From reference [131]).

1.6 THE PATHOPHYSIOLOGY OF MH

MH results from a defect in SR calcium release, leading to sustained rise in myoplasmic free Ca^{+2} [2]. This initiates muscle contracture, accelerates both aerobic and anaerobic metabolism and can account for the irreversible cascade of biochemical events observed during an MH crisis, as summarised in Figure 1-2.

Ca^{+2} promotes glycogenolysis and glycolysis by binding to and activating phosphorylase kinase, leading to a build up of lactic acid and CO_2, an early feature of the MH crisis. Ca^{+2} also activates the mitochondrial oxidative cycle, leading to high CO_2 production (hypercapnia) and oxygen consumption (contributing to hypoxemia). Respiratory acidosis ensues, as the increase in ventilation (tachypnea) is unable to control the rising CO_2. Tachycardia (rapid heart rate), vasoconstriction and high blood pressure accompany an increase in circulating catecholamines, which is triggered by acidosis [5,46,132,133].

Unlike normal muscle contraction which is brief, reversible, and initiated by a membrane action potential [50], generalised skeletal muscle contractures associated with MH are prolonged and occur when Ca^{+2} levels exceed the threshold for the initiation of contractile activity (6×10^{-7} M). Muscle rigidity can lead to rigor; an irreversible condition that develops when the fiber is deleted of ATP and the muscle is unable to relax (as observed in *rigor mortis*). Muscle contractile activity and a compensatory increase in Ca^{+2} ion pumping deplete ATP stores. Furthermore, when exposed to a high Ca^{+2} load, mitochondria actively sequester Ca^{+2} [134]. The resultant depression of the energy transduction pathways in mitochondria by compensatory Ca^{+2} uptake further aggravates the existing energy imbalance [5,47,134]. Factors that contribute to the heat produced during the MH episode include: the hydrolysis of ATP during contraction, ion pumping to restore ion imbalances, aerobic and anaerobic glycolysis, and buffering of the resultant H^+ [46,133,135]. Core body temperature may increase by up to 1°C per 5 min, and can exceed 43°C if uncontrolled [38].

The integrity of the muscle cell is destroyed as calcium-activated proteolytic enzymes degrade the fiber scaffolding and energy sources required by enzymes that maintain membrane stability are depleted. In addition, Ca^{+2}-activated phospholipases release fatty acids from the membrane [133] while raised temperature and acidity denature functional proteins and increase membrane fluidity [46,134]. A combination of acid inactivation of Ca^{+2} transport, exhaustion of ATP substrate, and increased membrane permeability impair Ca^{+2} re-uptake, which exacerbates the existing calcium stress. The resultant skeletal muscle breakdown (rhabdomyolysis) is indicated by elevated serum creatine kinase (>10,000 IU/L), excessive myoglobin in the urine, and raised serum potassium [44]. Potassium efflux from damaged muscle results in plasma hyperkalemia, causing hypotension, ventricular fibrillations, arrythmia, and ultimately, cardiac arrest in fulminant MH cases [46,136]. Kidney tubules can be blocked with myoglobin, leading to kidney damage. In fulminant cases of MH, disseminated intravascular coagulopathy (DIC) may occur when humoral factors that activate the coagulation cascade are released during hemolysis and tissue breakdown. Fibrin deposits in the kidney tubules cause further damage to the kidneys [6].

Early intravenous administration of sodium dantrolene, or a prophylactic oral dose before surgery can halt the progression of the MH reaction [137,138]. The point at which the reaction becomes irreversible may occur when ATP is depleted to half its resting concentration, at which point contraction becomes independent of Ca^{+2}, (presenting as rigor)

and a breakdown of mitochondrial and plasma membranes ensues. Further complications range from muscle pain to irreversible neurological damage by anoxia, acidosis, hyperkalemia, hyperthermia, and ATP depletion [46]. Cerebral oedema and coma may proceed to brain death.

Figure 1-2 A proposed mechanism for the induction of human and porcine MH

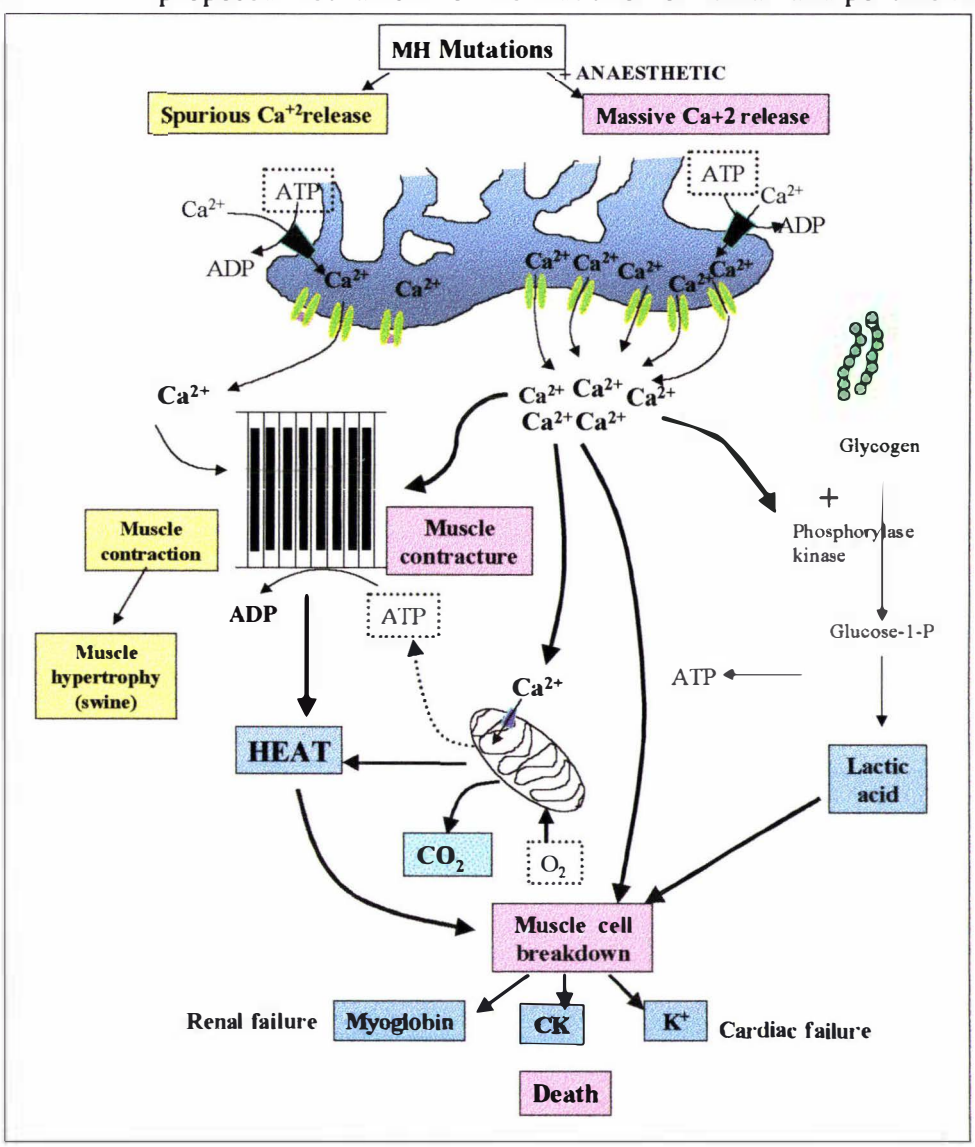

In normal muscle, brief depolarisation induced RyR Ca^{+2} release triggers muscle contraction, and Ca^{+2} is pumped back into the SR by the Ca^{+2}ATPase pump to allow relaxation. MHS RyR channels are more sensitive to agonists (e.g. caffeine, halothane, Ca^{+2}) and insensitive to antagonists. In pigs heterozygous for a RYR1 mutation, spontaneous Ca^{+2} release events might lead to muscle hypertrophy and lean muscle mass (yellow boxes). In human MHS muscle, RyR1 opening is activated in the presence of halothane. Ca^{+2} floods the cell, overpowering the Ca^{+2} ATPase pump. Ca^{+2} induces sustained contraction, accelerated glycolytic and aerobic metabolism, generating lactic acid, CO_2, heat (blue boxes) and ATP and oxygen depletion (dashed boxes). Muscle tissue breakdown results in leakage of cellular constituents and plasma ion imbalances culminating in multiple organ failure and death. (Adapted from refs. [47] and [15]).

1.7 MUSCLE DISORDERS ASSOCIATED WITH MH

A predisposition to a classical presentation of MH has been firmly established for three rare myopathies: Central core disease, Evans myopathy and King-Denborough syndrome [40,139]. Like true MH, these conditions predispose to a drug-induced increase in myoplasmic Ca^{+2} that leads to life-threatening hyperthermia, hypoxia and acidosis [13,140]. Special anaesthetic precautions must be taken with all patients with these conditions unless they have been diagnosed MHN by IVCT. In fact, MH was recorded as the major cause of death in a review of patients afflicted with King-Denborough syndrome [10,141]

1.7.1 CCD

Central core disease (CCD) is a rare, dominantly inherited, clinically variable myopathy that is closely associated with MH. CCD is characterised by muscle weakness, muscle cramps after exercise, and neonatal hypotonia (floppy infant syndrome), leading to delayed motor development [142]. Diagnosis relies on the histological investigation of muscle tissue, for signs of muscle atrophy and amorphous central areas (cores) in the muscle fiber that are devoid of mitochondria and oxidative enzyme activity [143]. Other features include a predominance of type 1 (slow twitch) fibers and fatty tissue and occasional skeletal deformity [144]. Electron microscopy has revealed central disintegration of the contractile apparatus, and a proliferation of SR and transverse tubules [143]. A number of RYR1 mutations have been identified in CCD pedigrees, which may or may not be associated with MHS diagnosis.

A mechanism has been proposed by which defects in the RyR Ca^{+2} release channel could give rise to two contrasting phenotypes; muscle hypertrophy in swine, and muscle atrophy in human CCD [13,15,47] (Figure 1-2). In swine heterozygous for the Arg615Cys RYR1 mutation, transient calcium "leak" is thought to promote spontaneous contraction without causing cell damage, leading to muscle hypertrophy and lean muscle traits [23,24]. In contrast, the human MHS and CCD mutations sensitise the RyR1 channel to anaesthetic-induced Ca^{+2} release, resulting in excessive Ca^{+2} efflux from the SR on exposure to triggering substances. Mitochondria in the peripheral regions of the muscle fiber could be protected by the action of PMCA and Ca^{+2} exchangers (NCE) that extrude Ca^{+2} into the extracellular space. However, mitochondrial function in the centre of the cell may be impaired, due to the participation of this organelle as an emergency Ca^{+2} sink, leading to diminished ATP synthesis. Uneven Ca^{+2} gradients in the cell would lead to differential contraction of the core of the muscle fiber in relation to the periphery [15], giving rise to the disorganisation of the central myofibrils, the appearance of central cores, muscle weakness and atrophy. Further histological aspects of CCD, including an increased proportion of type I muscle fibers and sarcotubular membrane might result from the Ca^{+2}-induced transcription of genes encoding compensatory proteins [15,40].

1.7.2 Other muscle disorders

Variable associations with MHS are recognised for a number of other musculo-skeletal disorders, including X-linked Duchennes muscular dystrophy (DMD) and Becker muscular dystrophy (BMD) caused by deficiency or defects in dystrophin (respectively) [145]. Typical MH episodes have been reported in Duchenne muscular dystrophic patients [145,146] and DMD patients often [147](but not always [145]) register MHS responses in the caffeine-halothane contracture test. Mortality (resulting from cardiac arrest) in DMD patients exposed to succinylcholine, may be more than 60 % [10,148,149]. The occurrence of MHS in DMD patients

is thought to be consequence of elevated myoplasmic Ca^{+2} associated with the general disintegration of the muscle cell structure in subjects lacking functional dystrophin [10].

The association between MH and other myopathies including myotonia congenita, syndrome, myotonia fluctuans and hyperkalemic periodic paralysis is less clear [12,150]. Non-dystrophic myotonias and primary periodic paralyses are non-specific disorders, characterised by uncontrollable muscle stiffness or myotonia (delayed relaxation) [131,151-153]. These symptoms are attributed to defects in either sodium or chloride channels that lead to membrane hyperexcitability (See Figure 1-1). Anaesthetic-induced myotonic events have been attributed to the increased vulnerability of the hyperexcitable fiber membrane to certain drugs. A Gly1306 to Ala mutation in the adult sodium gene (SCNA4) has been linked to masseter muscle rigidity (MMR) and abnormal IVCT results in a family with a very mild form of myotonia, known as myotonia fluctuans [154]. Although MMR is considered to herald a MH crisis, it is a non-specific genetically heterogeneous event and not all forms progress to the hypermetabolic state.

1.8 THE GENETIC BASIS OF MALIGNANT HYPERTHERMIA

1.8.1 Linkage of the MHS1 locus to RYR1

The first clue aiding the identification of the MH gene came from the linkage of the porcine syndrome (the so-called HAL locus) with the glucose phosphate isomerase (GPI) locus on chromosome 6 [79]. Meanwhile, biochemical studies had pointed to the SR Ca^{+2} release channel as the site of the primary MH defect, making it a strong candidate gene. The region of porcine chromosome 6 including the GPI and Hal locus was syntenic to the human chromosome 19q12-13.2 where the human GPI locus had been previously mapped. The co-segregation of human MHS with GPI markers was subsequently demonstrated in Irish MHS pedigrees [22]. At the same time, the human and porcine RYR1 genes were cloned [155] and mapped to chromosome 19q13.1 [156] and 6 [157] respectively. Human MHS was subsequently linked to polymorphic RYR1 markers with a lod score of 4.20 in nine Canadian families [21]. The quest for a genetic test for MH gathered momentum with the description of the first RYR1 gene mutations in affected swine [23] and human [106] subjects.

1.8.2 The involvement of RYR1 mutations in MHS

A single point mutation (C1843T) in porcine RYR1 that substituted Arg615 for Cys correlated with MHS in five major breeds of lean, heavily muscled swine [23] and was linked to MH with a lod score of 102 in 338 informative meiosis [24]. This finding firmly established the role of RYR1 in MHS. The Arg615Cys mutation alone accounts for all known cases of MH in swine suggesting it originated in a single animal and was transmitted by the founder effect [24]. The corresponding substitution (Arg614Cys) was subsequently identified in two human MHS pedigrees [106,158]. Contrary to the porcine MHS, human MH is a genetically heterogeneous disorder. In fact, the Arg614Cys mutation accounts for less than 5 % of human MHS cases worldwide [25]. Furthermore, while stress-susceptible MH pigs are homozygous for the Arg615Cys gene defect, human MH is associated with heterozygosity for RYR1 mutations. In addition, the presence of a variety of RYR1 haplotypes of unrelated MHS families identified with the same RYR1 mutations suggests that recurrent identical mutations have arisen independently in man [159].

The RYR1 gene is one of the largest genes in the human genome, coding for 5038 amino acid residues [160]. Screening the 15,393 bp coding sequence for candidate mutations in MHS probands therefore poses a formidable challenge for the molecular genetic study of MH. Nevertheless, 22 candidate mutations have been identified to date in the RYR1 gene [25,161-163], and shown to co-segregate, to varying degrees with the IVCT MHS phenotype in MHS families (listed in Table 1-1). Mutations that cause MHS are also associated with more severe CCD phenotype in some families. The search for RYR1 mutations has been assisted by the fact that the majority of MHS/CCD mutations are tightly clustered within two regions of the RyR1 polypeptide sequence: the cytoplasmic N-terminal region bracketed by residues Arg35 and Arg614 and a cytoplasmic central region between residues Arg2163 and Arg2458. This has considerably narrowed the target region. An Ile4898Thr mutation was recently identified in the C- terminal transmembrane region of the RyR1 protein, well outside the two previously defined mutation regions [164]. This mutation was associated with a severe form of CCD but did not coincide with clinical susceptibility to MH.

Table 1-1 RYR1 mutations associated with MHS and/or CCD

Substitution	Nucleotide change	Reference	Year	Proportion of MHS families
Cys35Arg	T103C	[165]	1997	1 family
Arg163Cys *	C487G	[13]	1993	2 %
Gly248Arg	G742A	[107]	1992	2 %
Gly341Arg	G1021A	[109]	1994	6 %
Ile403Arg *	C1209G	[13]	1993	1 family
Tyr522Arg *	A1565C	[108]	1994	1 family
Arg552Trp	C1654T	[111]	1997	1 family
Arg614Cys	C1840T	[106]	1991	4 %
Arg614Leu	G1841T	[166]	1997	2 %
Arg2163Cys	C6487T	[25]	1998	4 %
Arg2163His	G6488A	[25]	1998	1 family
Arg2163Pro	G6488C	[162]	1999	1 family
Val2168Met	G6502A	[25]	1998	7 %
Thr2206Met	C6617T	[25]	1998	3%
Thr2206Arg	C6617G	[162]	1999	1 family
Gly2434Arg	G7303A	[110,167]	1994	4 %
Arg2435His *	G7307A	[168]	1993	1 family
Arg2435Leu	G7307T	[161]	1999	1 family
Arg2454His	G7361A	[161]	1999	2 families
Arg2454Cys	C7360T	[163]	2000	2 families
Arg2458Cys	C7372T	[169]	1998	4 %
Arg2458His	G7373A	[169]	1998	4 %
Ile4898Thr *	T14693C	[164]	1999	4 %

Associated with MHS and/or CCD

1.8.3 Discrepancies between RYR1 mutations and IVCT phenotype

The IVCT results do not correlate with the results from the genetic analysis of RYR1 mutations in 100 % of cases [99,105,170,171]. Discrepancies between genetic results and IVCT diagnoses in families segregating for RYR1 mutations has raised concerns about the causative nature of the RYR1 mutations, the accuracy of the IVCT, or the possibility that more than one MHS mutation may be segregating in some families [172]. In most cases, phenotype/genotype discrepancies arise from a MHS diagnosis in subjects who lack the segregating mutation. This pattern is

consistent with false positive diagnosis, bearing in mind that the IVCT is highly sensitive and results in more false positive than false negative results [97]. For example, the high-incidence Gly341Arg mutation co-segregated precisely with the MHS phenotype in all 48 MHS patients from 11 families [109] [173]. False positive diagnosis [105] and segregation of a second MHS gene [170,174] has been invoked to reconcile discrepancies between Gly341Arg and the MHS phenotype in other studies [105][170]. Discordance between the segregation of the Arg614Cys mutation and IVCT results has also been reported [99,175,176]. MHN diagnoses have been recorded in subjects identified with the Arg614Cys [175] and Gly2434Arg mutations [167] suggesting compensatory factors may be operating to negate the effects of the mutations *in vitro* [175]. RYR1 mutations (Gly341Arg, Arg2458His) have been detected in MHE subjects, supporting the cautious clinical management of ambiguous MHE patients as MHS [109]. The IVCT phenotypes of individuals homozygous for the Arg614Cys [175] and Cys35Arg [165] mutations did not differ remarkably from those of the heterozygous MHS relatives [165].

1.8.4 Alternate MHS loci

In contrast to the porcine disorder, human MH displays both allelic and locus heterogeneity [26,27,29,31-33,177,178] and linkage to RYR1 is found in only 50% of families [38]. The human MH syndrome may in fact represent the final common pathway of defects in any number of proteins involved in ECC and Ca^{+2} homeostasis [172,179]. In view of the association between the DHPR and RYR1 in excitation-contraction coupling, the genes encoding the α_1, β, γ and α_2/δ subunits of the DHPR have cone under scrutiny as potential MHS gene candidates in families that do not demonstrate linkage to the MHS1 RYR1 locus [28,29,180-182]. Other ion channel genes that function upstream of RyR1 in signal transduction and ECC are also potential MHS gene candidates (Figure 1-1).

Genetic linkage analyses have proposed five additional MH loci (listed in Table 1-2). Using the candidate gene approach, MHS was linked to chromosome 17q11-24 [30,177,178] (where the adult muscle sodium channel gene, SCNA4 is a candidate). The genes encoding the DHPR β and γ subunits (CACNLB1 and CACNLG) also map to the chromosome 17q11.2-q24 region [180] reported to contain the MHS2 locus, however, these genes were excluded as candidate MHS genes in two European studies [28,180]. The third MHS locus was mapped to chromosome 7q21-22 (where the CACNL2A gene encoding the α_2/δ subunit of the DHPR was a strong candidate)[29]. In genome-wide linkage screens, MHS3, MHS4 and MHS5 loci were proposed at chromosomes 3q13.1 [31], and 1q31 and 5p respectively [32]. Gene candidates at 3q13.1 and 5p have not yet been established. The CACNL1A3 gene was a strong candidate at the 1q31 locus, since it encodes the voltage dependent calcium channel (DHPR α_1 subunit) that participates with RyR1 in excitation-contraction coupling. An Arg 1086 to His mutation in the CACNL1A3 gene was subsequently identified in an MHS pedigree [33], confirming the 1q31 locus. A second mutation at the same codon, resulting in an Arg1086Cys mutation was reported recently [40]. Mutations have not yet been described for the candidate genes, SCNA4 (MHS2) and CACNL2A (MHS3). Since several of the pedigrees examined did not display linkage to the MHS1-MHS6 loci, the presence of additional MH loci can be inferred [32].

Mutations in the voltage sensing regions of the DHPR α_1 subunit have been associated with hypokalemic periodic paralysis, characterised by episodic muscle weakness with low serum potassium levels [183]. Similarly, mutations in the SCNA4 gene are linked to other myotonias such as periodic paralysis and paramyotonia congenita and masseter muscle rigidity [154]. As anaesthetic related events similar but clinically distinct from MH are common in myotonic patients [184] the involvement of the SCNA4 locus in MHS [177] may be secondary to an underlying myopathy.

Genetic heterogeneity is clearly evident in MH, and has important ramifications for the future development of a diagnostic test. Nevertheless, the MHS1 RYR1 locus remains the predominant source of MHS mutations. No MHS-linked mutations have yet been reported for the families that demonstrated linkage to alternate loci MHS2 and MHS3 and the evidence in favour of linkage to the chromosome 17q MHS locus was weak [177].

Table 1-2 Proposed MHS loci

Loci	Gene	Protein	Chromosomal position	Reference
MHS1	RYR1	ryanodine receptor (SR)	19q13.1	[21]
MHS2	SCN4A	adult sodium channel α subunit IV	17q11.2-q24	[30,177]
MHS3	CACNL2A	DHPR Ca^{+2} channel $\alpha_2\delta$ subunit	7q21-q22	[29]
MHS4	Unknown	Unknown	3q13.1	[31]
MHS5	CACNL1A3	DHPR Ca^{+2} channel α_1s subunit	1q32	[33]
MHS6	Unknown	unknown	5p	[32],

1.8.5 The genetic basis of CCD

CCD is often [142] (but not always [185]) associated with MHS. CCD and MH are allelic disorders, in that a subset of RYR1 that give rise to MHS can present as CCD in some individuals [13,25,108]. However, unknown genetic and/or environmental factors influence the expression of the CCD phenotype, as revealed by combinations of CCD/MHS, MHS (only), and CCD/MHN phenotypes, even within the same family [13,108,185]. Consistent with the association with MHS and RYR1 mutations the CCD locus was mapped to chromosome 19q13.1 [14]. However like MH, CCD exhibits both allelic and locus heterogeneity. Recombination between RYR1 and CCD has been described in two recent studies [185,186]. While the recombinant haplotypes presented in the first report [186] may have been erroneous, recombination between CCD and MHS was clearly demonstrated in families in a large family presented in the second study [185]. Alternate CCD loci have not yet been described.

1.9 THE RYANODINE RECEPTOR: STRUCTURE AND FUNCTION

1.9.1 RyR isoforms

Three different isoforms of mammalian RyRs have been identified: RyR1 (skeletal), RyR2 (cardiac) and RyR3 (brain). They are encoded by different genes, localised to human chromosomes 19q12-13.2 (RYR1) [22], 1q42.1 (RYR2) [187] and 15q14-q15 (RYR3) [188]. Northern blot and [3H]-ryanodine binding experiments have revealed complex and overlapping expression patterns for the three isoforms. RYR1 expression is highest in skeletal muscle [155], though it is expressed at low levels in other tissues such as the stomach, spleen, and the Purkinje cells of the cerebellum [189,190]. RyR1 is also found in human B-lymphocytes where it plays a role in the B-cell antigen receptor-stimulated Ca^{+2}-signalling process [191]. RyR2 is expressed principally in the heart, and to a lesser degree in the brain, lung, stomach and kidney but not skeletal muscle. RyR3 is ubiquitously distributed throughout various tissues [192-194], including the skeletal muscle where it constitutes less than 1% of total RyR protein [195]. Although RyR3 is known as the brain ryanodine receptor, this is misleading since RyR3 comprises, on average, only 2% of brain RyR, the major brain isoform being RyR2 [196,197]. RyR3 is expressed in T-lymphocytes where it may contribute to cell proliferation and activation [198,199]. Two RyR isoforms, co-expressed in the skeletal muscle of fish, birds and amphibians are known as known

as α-RyR and β-RyR and are homologues of RyR1 and RyR3 respectively. In addition, a distinct cardiac form is expressed in the chicken heart [200].

Although the RyR1 and RyR3 may be co-expressed in triads of the same muscle fiber [201], they do not appear to form heterotetramers [195]. RYR3 is not a plausible candidate MHS gene, since the Ca^{+2} sensitivity for activation is about 7 times lower than that of RyR1 [195]. RyR3 content is minimal in skeletal muscle, and RYR3 deficient mice show no gross abnormality [195,202], suggesting the functional contribution of RyR3 to skeletal muscle ECC may be negligible.

Mammalian RYR1 cDNAs have been cloned from man [126], rabbit [126,155] and pig [23,203]. Human RYR1 cDNA is 15,393 bp, made up of a 130 bp 5' untranslated region (UTR), an open reading frame of 15,117 bp encodes 5038 amino acids, followed by a 146 bp 3' UTR [160]. The genomic structure of human RYR1 has been recently characterised [160] and consists of 106 exons spanning 160 kb of genomic DNA [160]. Human RYR2 and RYR3 cDNAs encoding the cardiac and brain RyR isoforms have slightly shorter open reading frames, coding for 4967 [204] and 4870 [205,206] amino acids respectively. The overall sequence identity among RyR isoforms is about 66% [204,207,208]. Alternatively spliced transcripts occur for all three RyR cDNAs [168,206,209-211] and show tissue-specific and developmentally regulated patterns of expression [209].

1.9.2 RyR-deficient animal models

The generation of RyR1-deficient knockout ("dyspedic") mice confirmed the fundamental role of RyR1 in mammalian excitation contraction coupling. Homozygous RYR1-/- mice had gross abnormalities of the skeletal muscle and died perinatally of respiratory failure [212]. In contrast, homozygous RYR3-/- deficient mice were viable and the only obvious abnormality was an increase in locomotor activity [213] and impaired learning capacity associated with altered synaptic plasticity [213], suggesting a mild effect on certain neurons in the central nervous system. The expression of RyR3 in skeletal muscle may be particularly important during the post-natal phase of muscle development, since it increased until 3-4 weeks after birth and then declined [202,214] consistent with improvement of skeletal muscle function in transition from the neonate to the adult RyR-/- mouse [202]. Double mutant mice carrying a targeted disruption of both the RyR1 and the RyR3 genes (RyR1-/-; RyR3-/-) had degenerated myofibrils and showed no caffeine or ryanodine response [215]. The junctions between the T-tubule and SR membranes were still observed in muscle from these mice, implying that other proteins are involved in the association of the two membranes [215]. RyR2 plays an essential role in cardiac ECC. Mutant mice lacking RyR2 died at embryonic day 10 with morphological abnormalities in the heart tube. Homozygous mutant cardiomyocytes displayed structurally abnormal mitochondria and large vacuolate SR [216].

1.9.3 RyR 3D structure

The three RyR isoforms are predicted to share the same basic structure [207]. About 80% of the protein is hydrophilic and forms the cytoplasmic foot domain, while the carboxy terminal 20% constitutes the transmembrane channel assembly, consisting of between four [155,217] and ≥ 10 [126,207] transmembrane helices, according to two alternate models for the membrane topology [218]. With a molecular mass of 560 kDa, giving rise to a tetramer of 2.3 million Daltons, the RyR is the largest known ion channel [208].

Cryoelectron microscopic investigations of frozen, single Ca^{+2} channels have provided 3D images of the RyR1 tetramer, at 3 nm resolution [219-221] (Figure 1-3). They reveal a large four-leaf clover-like structure, with a transmembrane domain forming the Ca^{+2} pore. The

cytoplasmic assembly is composed of distinct domains and has a very open "scaffolding" type structure [122]. Four bridges connect the cytoplasmic assembly to the transmembrane channel [219]. In the open state structure, a 1.8 nm hole is visible running through the transmembrane assembly [219]. The transition from the closed to open state is also accompanied by the opening of two "clamp" domains in the cytoplasmic assembly (domains 9 and 10) [221,222] and a 4° rotation of the cytoplasmic assembly relative to the transmembrane assembly [122]. Cryoelectron microscopy has also provided images of RyR1 bound to channel-modulating junctional proteins, FKBP12 and calmodulin [221,223-226]. These images showed FKBP12 bound to RyR1 along each of the four edges of the cytoplasmic assembly, and calmodulin bound in a crevice (below domain 4) of each subunit near the peripheral region of the cytoplasmic assembly.

Figure 1-3 Three-dimensional structural reconstruction of RyR from cryoelectron-micrographs of isolated single channels

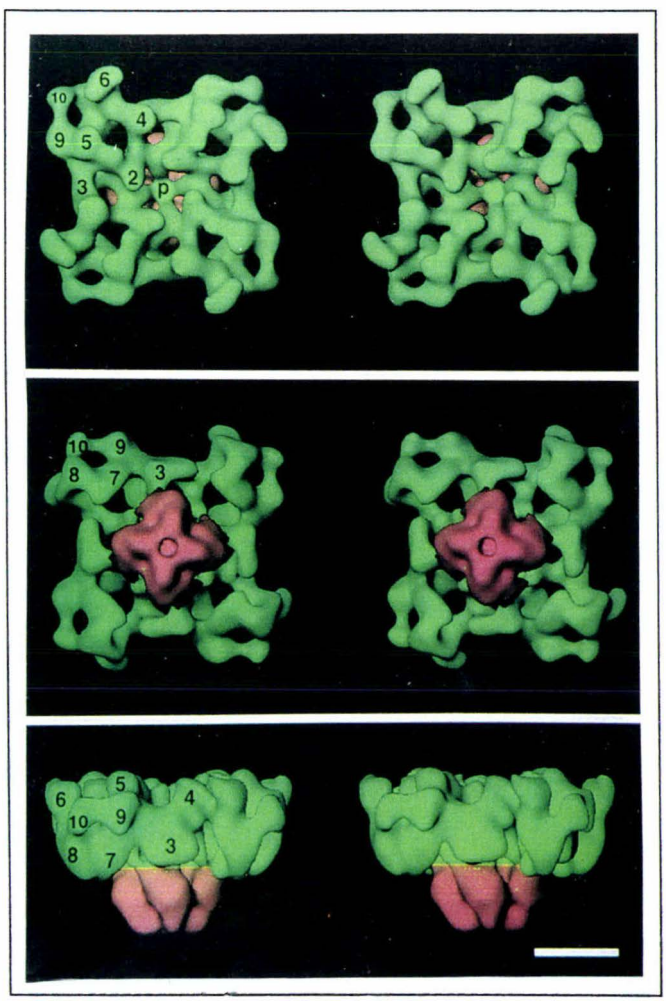

3D reconstruction of RyR1
a. From T-tubule
b. From inside SR
c. Side-view.

The cytoplasmic and transmembrane assembles are coloured green and pink, respectively. Scale bar = 10 nm. Reproduced from Samso, 1998 [122]. Numbers refer to arbitrarily labelled domains. For an idea of scale: the smallest domain (domain 10) is the size of the globular protein ribonuclease [122].

1.9.3.1 Regulation of RyR1 calcium release

The regulation of the RyR channel has been investigated *in vitro* using four complementary techniques. Firstly, muscle fibers were chemically or mechanically skinned to remove the plasma membrane and provide direct access to the intracellular space, allowing the observation of force activation in defined myoplasmic solutions [227,228]. Secondly, isolated SR vesicles with the T-

tubule attached (triads) or detached (the heavy fraction) derived from the junctional membranes can be passively or actively loaded with labelled Ca^{+2} to study the in vitro effects of various agonists using rapid mixing or filtration devices [208]. The neutral plant alkaloid, ryanodine, binds preferentially to the open state of the Ca^{+2} release channel, therefore the analysis of [^{3}H]-ryanodine binding has been used extensively in these experiments to probe the functional state of the channel [229]. Thirdly, direct information has been gained from single channel recordings of heavy SR vesicles or detergent-solubilised RyR channels following their incorporation into planar lipid bilayers. Fourthly, various mutated rabbit RYR cDNAs have been functionally expressed in non-muscle cells to explore the effects of human RYR1 mutations on Ca^{+2} release.

A number of detailed reviews have explored the interaction of a wide range of endogenous and pharmacological agonists and antagonists of RyR Ca^{+2} release [230-236]. Activators of the Ca^{+2} channel include Ca^{+2} (in micromolar concentrations), caffeine, halothane, adenine nucleotides, inositol-triphosphate, sulf-hydryl reagents and ryanodine (in micromolar concentrations). RyR1 activity is inhibited by Mg^{+2}, calmodulin, ryanodine (in millimolar concentrations), Ca^{+2} (in millimolar concentrations), ruthenium red and local anaesthetics. The following discussion focuses on the major endogenous modulators and the pharmacological agonists relevant to the pathophysiology of MH.

1.9.3.2 Endogenous soluble modulators

Cytoplasmic concentrations of Ca^{+2} regulate the channel in a biphasic manner, producing a characteristic bell-shaped Ca^{+2} response curve [235]. The channel activity is enhanced at lower Ca^{+2} concentrations within the nM to μM range, reaching a maximum at 100-200 μM [232], and is inhibited at higher concentrations (above 200 μM Ca^{+2} [237]). In this way both the activation and attenuation of Ca^{+2} release are synchronised, as both are controlled by feedback Ca^{+2} [238]. The biphasic Ca^{+2} dependence suggests two classes of Ca^{+2} regulatory sites are involved; a high-affinity activation site and a low-affinity inhibitory site. The high affinity binding site has been mapped to a proline-glutamate repeat sequence in the putative transmembrane sequence (M2) [239] and a mutation of a glutamate residue in this region reduced Ca^{+2} sensitivity by 10,000 fold [240]. A recent study mapped the low-affinity calcium inactivating sites to the C-terminus of RyR1 [241]. Ca^{+2} alone is not sufficient to fully activate the channel. The addition of millimolar ATP in the together with micromolar Ca^{+2} produces a synergetic activation of the channel [242].

Mg^{+2} inhibits the RyR1 channel and may exert its inhibitory effects by (a) competing with Ca^{+2} for the high affinity Ca^{+2} activation sites and/or (b) binding to the low affinity inhibitory sites [231,243]. In the resting cell, the inhibitory site is believed to be occupied completely by Mg^{+2}, which is present in mM concentrations. Upon depolarisation a conformational change displaces Mg^{+2} from the inhibitory site, allowing partial channel opening [234]. According to this model, the released intracellular Ca^{+2} (>10 μM) then out-competes Mg^{+2} at the high affinity binding site, and initiates maximal opening of the channel [238,244,245].

1.9.3.3 Proteins that modulate RyR1 activity

Calmodulin interacts with RyR in a Ca^{+2}-dependent fashion and counteracts the effects that Ca^{+2} alone would have on the channel. At Ca^{+2} concentrations in the optimal range (10 - 100 μM), 4 molecules of calmodulin bind per tetramer, and inhibit the channel [246,247]. At low resting Ca^{+2} concentrations up to 16 calmodulin molecules bind to the tetramer, and activate the channel [246]. Three-dimensional images of the RyR with calmodulin bound suggest the binding sites

are close together in the folded protein [226]. Calmodulin binding sites have been mapped to two regions in the cytoplasmic domain: 2937-3225 (PM1) and 3546-3655 (PM2) (that bound calmodulin under activating (0.1 μM) Ca^{+2} concentrations [248,249]. The inhibitory RyR calmodulin site, which specifically bound calmodulin at high Ca^{+2} concentrations (100 – 500 μM) was mapped to residues 4534-4552 (PM3) in the transmembrane domain [249].

RyR1 co-purifies with a 12 kDa immunophillin known as FKBP12. This small protein is a cytoplasmic receptor for immunosuppressant drugs: FK506 and rapamycin [250]. FKBP12 is a prolyl-isomerase, and is thought to have a physiological role in protein folding [251]. FKBP12 promotes co-operativity between the RyR subunits to stabilise the channel in the fully closed or fully open conductance state. [252,253].

Calsequestrin is a highly acidic, high capacity Ca^{+2} storage membrane in the SR membrane, that co-sediments with RyR1, and increases the open probability of purified RyR1 [251]. Activation of RyR is accompanied by the release of bound Ca^{+2} from calsequestrin within the SR lumen, suggesting a reciprocal coupling mechanism operates between calsequestrin and RyR [254]. Other proteins at the triad junction that interact with RyR either directly or indirectly include triadin (which may act as a linker between RyR and calsequestrin) [255-258] and junctin (which may anchor calsequestrin to the SR membrane) [259], sarcalumenin, calreticulin and a histidine-rich glycoprotein with unknown function [251]. Defects in any of the proteins involved in the elaborate process of muscle Ca^{+2} homeostasis may be linked to MHS and/or other disease states.

1.9.3.4 *Exogenous modulators*

Caffeine is well known for its ability to initiate muscle contraction and SR Ca^{+2} release and like many other ligands, exerts its effects by influencing the Ca^{+2} sensitivity of RyR [232]. Caffeine operates in two ways. At low concentrations, caffeine acts at the activation sites of the RyR/Ca^{+2} release channel, and transfers the receptor to a pre-activated state [245]. This renders RyR more sensitive to the activating effects of depolarisation, Ca^{+2} and ATP, and less sensitive to the inhibitory Mg^{+2}. At higher concentrations (>5 mM) caffeine activates the channel by a direct mechanism that is independent of Ca^{+2} [245]. The truncated carboxy-terminal RyR1 channel is not activated by caffeine, indicating the caffeine binding site is located in the N-terminal foot region [127]. All RYR1 MHS mutations increase the sensitivity of SR Ca^{+2} release for caffeine [16].

Halothane (2-bromo-2-chloro-1,1,1-triflouro-ethane) is a widely employed inhalational anaesthetic. Until recently the mode of operation of this volatile agent was unknown. Volatile anaesthetics promote hydrophobic interactions between Ca^{+2} regulatory proteins within skeletal muscle triads, inducing oligomerization of the RyR, the DHPR, α_1 subunit and calsequestrin [260] [261-265]. A direct interaction between volatile anaesthetics and RyR promotes SR Ca^{+2} release [4]. The resultant increase in myoplasmic Ca^{+2} concentration might be sufficient to trigger a MH crisis in susceptible muscle tissue [235,260,266].

The ability of dantrolene to halt an MH crisis stems from its action on the SR, where it inhibits Ca^{+2} release. Dantrolene has been shown to act directly and specifically on single purified RyR channels where it limits the activation by calmodulin and Ca^{+2} [267]. At low concentrations however, dantrolene activated the RyR [268].

Ryanodine is a secondary metabolite purified from the stem and root of the South American plant *Ryania Speciosa*. Pharmacologically, the alkaloid first gained attention because of its insecticidal properties, causing flaccid paralysis of invertebrate muscle [234]. Ryanodine

also induces irreversible contracture of vertebrate skeletal muscle, and cardiac decline in mammals [234]. In nanomolar to micromolar concentrations, ryanodine binds specifically to the open channel, and locks the RyR channel in a 50% sub-conductance state. Higher concentrations of ryanodine permanently close the channel.

1.10 EXCITATION-CONTRACTION COUPLING

Excitation contraction coupling (ECC) describes the process by which the depolarisation of the plasma membrane is coupled to the opening of the SR Ca^{+2} channel (RyR) to initiate Ca^{+2} release and muscle contraction. ECC occurs at the internal triad junctions between the T-tubule and SR membranes and involves an interaction between two proteins; the voltage gated calcium channel of the T-tubule (the DHPR) and the calcium release channel of the SR membrane (RyR). Regarded as the missing link in the current understanding of cardiac and skeletal muscle contraction, ECC has been the subject of numerous extensive reviews [128,208,233,235,269-275]. Abnormalities in EC coupling in skeletal muscle somehow uncouple the opening of the SR channel to depolarisation of the T-tubule membrane. Deciphering the ECC mechanism of skeletal muscle will therefore play a pivotal role in future investigations into the biochemical aetiology of MH.

Normal signal transduction at the triad junction involves: 1) the depolarisation of the T-tubule membrane; 2) a depolarisation–induced charge movement in the DHPR voltage sensing L-type calcium channel, followed by; 3) an inward calcium current via the DHPR and; 4) the release of Ca^{+2} from internal stores through the RyR/Ca^{+2} release channel [271].

Two mechanisms for ECC are observed in cardiac and skeletal muscle, respectively. In cardiac muscle, EC coupling is dependent on a fast inward calcium current through the DHPR calcium channel to induce Ca^{+2} release from RyR2 (calcium induced calcium release, or CICR). In skeletal muscle, an influx of Ca^{+2} ions through the DHPR calcium channel is not essential for ECC, since Ca^{+2} release and muscle force can be induced in the absence of external Ca^{+2} [233]. The primary mechanism for basis of EC coupling in skeletal muscle is thought to involve a direct molecular interaction between the RyR1 and the DHPR, whereby a voltage-induced conformational change in the DHPR is transmitted directly to the RyR by protein-protein interactions [124]. Although not essential to skeletal muscle EC coupling, CICR functions in skeletal muscle *in vitro*, and may operate as a secondary mechanism *in vivo* to amplify the DHPR-mediated signal [119].

1.10.1 DHPR/RyR interactions in skeletal muscle EC coupling

The molecular basis of the distinct cardiac and skeletal muscle EC-coupling mechanisms has been investigated using myotubes from two mutant mouse lines; dysgenic (a naturally occurring mutant lacking the skeletal muscle DHPR α_1 subunit [276], and dyspedic (engineered with a mutation to abolish RyR1 expression) [212]. The DHPR α_1-subunit is responsible for both the calcium current and voltage sensing functions of the DHPR [276,277]. The protein consists of four domains of internal homology, each with six transmembrane helical segments, numbered S1 – S6 (see Figure 1-4). The four domains are connected by three cytoplasmic linkers (I-II, II-III and III-IV) that interact with RyR1 in skeletal-type EC coupling [275].

A cytoplasmic loop between DHPR α_1 subunit domains II and III has been shown to be a critical determinant of skeletal muscle type EC coupling [277,279,280][278]. The II-III loop is comprised of both a "trigger" peptide (Thr671-Lue690) involved in the depolarisation-induced

RyR1 activation and a "blocker" peptide (residues 724-760), believed to replace the trigger peptide, thus returning RyR to the original conformation) [244]. A region of the DHPR α_1 subunit C-terminal tail was also shown to inhibit the RyR1 receptor reconstituted into planar lipid bilayers [281]. The peptides implicated so far in DHPR/RyR1 mechanical coupling are depicted in Figure 1-4.

The cytoplasmic loop between domains III and IV contains the first DHPR α_1 (Arg1086His) mutation associated with MH [33]. This loop has been shown to interact directly with RyR1 [282], providing a molecular mechanism for the indistinguishable phenotypes conferred by RyR1 and DHPR α_1 defects [33]. The corresponding regions of RyR1 that bind the DHPR II-III and III-IV loops have been mapped to overlapping sites on RyR1 between Lys954 and Asp1112 [280,282]. A second region of RyR1 that binds DHPR and is essential role in EC coupling includes the divergent D2 region (residues 1303-1406) [283]. In addition to the activating signal received from DHPR, RyR1 sends a retrograde signal to the DHPR [284,285].

Figure 1-4 Proposed interactions between the skeletal muscle DHPR α_1 subunit and RyR1

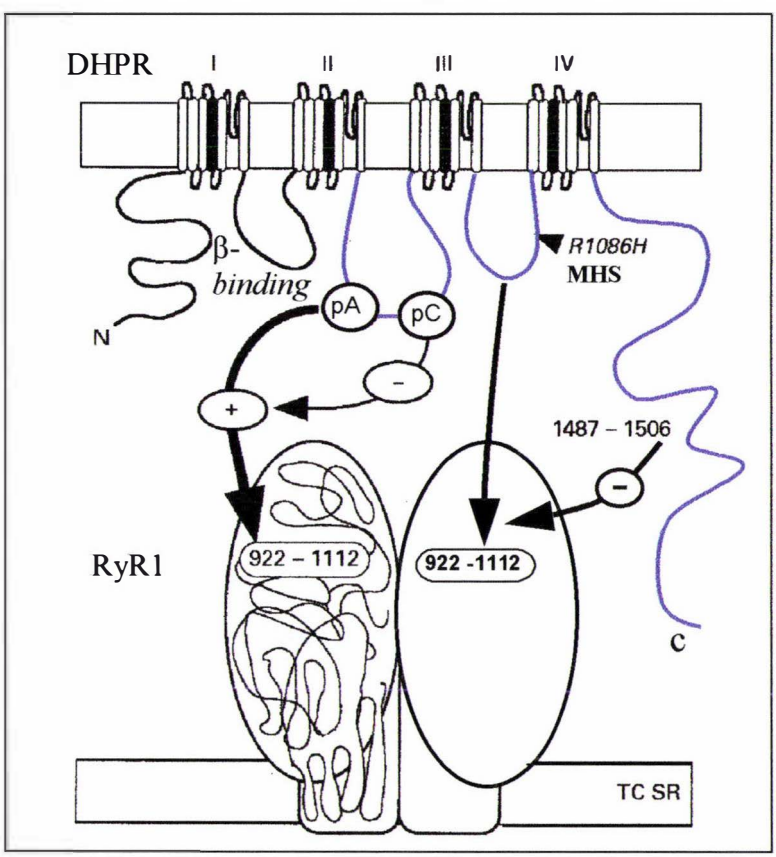

Diagram adapted from [251], to show recently described interactions between DHPR cytoplasmic loops and RyR1 [275]. The DHPR has four repeat domains (I-IV) each with transmembrane segments S1-S6. S4 (black) forms the voltage sensor. The I-II intracellular loop interacts with the DHPR β–subunit [33]. Hydrophilic loops on the extracellular surface between S5 and S6 within domains III and IV are involved in pore formation. The DHPR II–III loop is essential to ECC and contains a peptide (Pa, residues 681-690) that activates RyR1. This effect is abolished by peptide Pb (residues 724-760). The DHPR II-IV loop is the site of a MHS mutation and interacts with RyR peptide 952-1112 [282]. Residues 1487-1506 of the DHPR α_1 inhibit the RyR1 channel.

1.11 MOLECULAR PREDICTIONS FOR MHS MUTATIONS

The majority of MHS mutations are clustered in two regions, either at the amino terminus or in the central regions of RyR1 (Figure 1-5). The recent identification of the Ile4898Thr mutation suggests a third MHS domain, in the C-terminal region of the receptor [164]. The N-terminal MHS mutation domain is homologous to the IP_3-binding domain of the IP_3 receptor [286], and may contain binding sites for regulatory ligands [23]. However, there is no evidence to date that MHS and CCD mutations [25] have a direct consequence on known binding sites for RyR agonists or antagonists [15,20,251,274]. This is perhaps not surprising in view of the sub-clinical nature of MH. Except on exposure to halogenated anaesthetics most MHS individuals are asymptomatic, suggesting that a mutation associated with the MHS trait would not dramatically alter the essential functions of the receptor.

Recent evidence suggests that RYR1 mutations may perturb protein-protein interactions between RyR monomers, and/or intramolecular interaction between the MHS domain and a regulatory domain of the RyR1 protein [251]. These effects could be further exacerbated by halothane, since volatile anaesthetics are known to modify hydrophobic interactions that promote SR Ca^{+2} release [235,260]. Some support of a role for a role of the MHS domains in protein-protein interactions has been provided by antibody binding studies [287]. An N-terminal region (residues 163 to 522) that encompassed four MHS mutation sites was shown to interact with a central calmodulin-binding site (PM1) and with a domain at residues 799-1172 in ligand overlay experiments [287].

Although the three MHS domains are widely spaced in terms of the primary sequence, they may be closely situated in the folded protein through proposed long-range interactions between the N-terminal, central and C-terminal domains [287-289], which would account for the similar MHS observed for mutations in different regions of the RYR1 gene. In support of this hypothesis, two domains predicted to be involved in RyR subunit interactions correspond to the N-terminal and central MHS domains [287,289]. Four repeat domains identified in the N-terminal region (termed MIR) present in the RyR and IP3 receptor [286] encompass residues 97 – 360 of RyR1, including three MHS-associated mutations. In addition, two internally repeated domains RyR and IP3 homology domains (RIH) have been identified, (encompassing residues 466- 643 and 2186 –2364 of RyR1) [286]. A number of MHS and CCD-associated mutations occurred within these RIH domains. Protein binding functions between these regions and C-terminal transmembrane regions have been proposed [286].

Figure 1-5 Location of RyR1 MHS/CCD mutations and regulatory sites

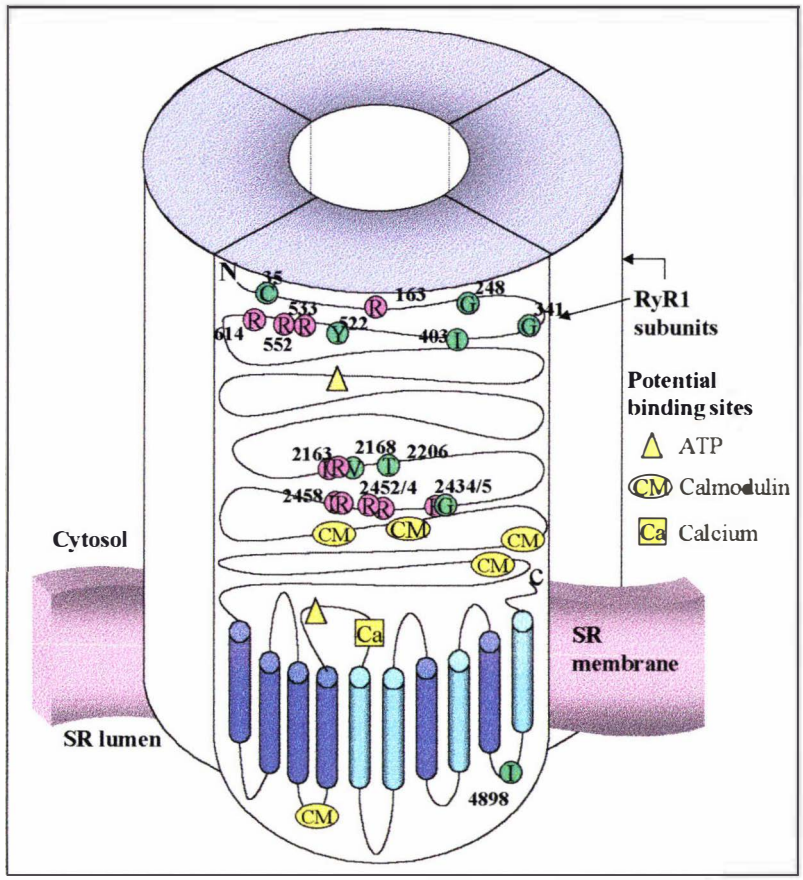

Diagram adapted from references [233] and [245].

1.12 BIOCHEMICAL CHARACTERISATION OF MHS MUTATIONS

A large number of biochemical studies of muscle fibers, SR vesicles and purified RyR1 channels have convincingly shown that the porcine Arg614Cys mutation is directly responsible for an alteration in the SR release mechanism. Rates of calcium induced calcium release (CICR) were increased by two to three fold in MHS SR vesicles from both porcine [17,290-293] and human muscle fibers [294], SR vesicles [17] and single RyR1 channels [18,19]. Ryanodine binding was enhanced in both human [295] and porcine [17] MHS SR. MHS SR vesicles also showed an exaggerated sensitivity to the activating effects of calmodulin at low Ca^{+2} concentrations [296]. There is some disagreement in the literature regarding the calcium dependence of calcium release for MHS versus normal RyR1 [235]. Single RyR channels purified from MHS muscle of pig [18] were resistant to the inhibitory effects of high calcium concentrations, but showed unaltered sensitivity to activating calcium, suggesting that a defect in a low-affinity calcium binding site was responsible for the altered gating of MHS SR channels [18,297,298]. Resistance to channel inactivation was not observed in human MHS RyR1 [19,295], though an abnormally increased sensitivity to calcium [295] and caffeine [19] was observed in human MHS RyR1 single

channels. Halothane acted directly on purified human RyR channels and increased the sensitivity of calcium release to activating calcium to a higher degree for MHS RyR1 [3,4]. Results from human MHS RyR1 and SR were variable, probably reflecting the heterogeneous genetic background RyR [19,295].

Two studies have investigated the functional effects of specific human RyR1 substitutions on muscle cell homeostasis. In the first study, cultured human skeletal myotubes derived from MHS individuals with the Arg163Cys mutation were significantly more sensitive to halothane-induced SR Ca^{+2} release compared to cells from MHN individuals [299]. In the second study, skeletal muscle SR vesicles prepared from individuals heterozygous for the Gly2434Arg mutation demonstrated an increase in affinity for ryanodine at activating Ca^{+2} concentration, increased sensitivity to the activating effects of Ca^{+2} and caffeine and resistance to inactivating Ca^{+2} concentrations [300]. Contrary to the porcine Arg615Cys mutation, the human Gly2434Arg mutation also conferred a distinct resistance to the inhibitory effects of calmodulin at activating Ca^{+2} concentrations, which could be explained by the close vicinity of the Gly2434Arg mutation to calmodulin binding sites [249,301] (see Figure1-5).

1.12.1 Functional expression of mutated RYR1

The functional expression of cloned rabbit RYR1 cDNA has provided a means to assess the effects of RYR1 mutations, and has provided valuable insights into the aetiology of MH and CCD. The porcine Arg615Cys mutation conferred an increased sensitivity to Ca^{+2} release induced by caffeine, halothane [207] and 4-chloro-m-cresol [302] in transfected myoblast (C2C12) [207] and COS-7 [302] cells but had no effect on the resting Ca^{+2} concentration [207,302]. By examining the functional expression of mutant RYR1 in HEK-293 cells (kidney origin), loaded with fluorescent Ca^{+2} indicator, Tong *et al.* showed that both the caffeine and halothane sensitivity of intracellular Ca^{+2} release was altered by 15 RYR1 human MH and/or CCD mutations [16]. This provided essential evidence that RYR1 mutations are causative of human MH. A spectrum of sensitivity to the test agents was conferred by the different mutations, and results correlated well with the IVCT caffeine tensions [16]. In a further study, higher resting Ca^{+2} concentrations were observed in HEK-293 cells expressing CCD-mutant RYR1 compared to those expressing the MHS-mutant RYR1, or wild type RYR1 supporting the theory that SR of CCD muscle is "leaky" [303]. Functional expression of the Ile4898Thr mutation in HEK-293 cells revealed that this mutation produced the most leaky channels of those investigated, in keeping with the severe CCD phenotype associated with this mutation [164].

In summary, MHS RyR1 has increased rates of calcium induced calcium release (CICR) and is hypersensitive to ligands that stimulate this process, and resistant to the ligands that inhibit calcium release. The increase in myocellular Ca^{+2} in the presence of halothane may be tolerated in normal muscle, but in MHS muscle could be sufficient to trigger CICR, leading to uncontrolled SR Ca^{+2} release, muscle contraction and hypermetabolism. The functional expression studies provide strong support for the causative role of RYR1 mutations in MH [16]. In light of this new evidence, the discrepancies often observed between the segregation of MHS mutations and MHS IVCT phenotype could be attributed to complex genetic and environmental effects that modulate both the *in vitro* and *in vivo* manifestation of RYR1 mutations.

1.13 RESEARCH GOALS

Susceptibility to MH may be secondarily associated with various congenital myopathies [10], but in the majority of cases, there are no signs of the disease outside of anaesthesia. Affected individuals thus lead normal healthy lives, providing the susceptibility to MH is recognised and exposure to triggering anaesthetics is meticulously avoided. Hence, the primary motive fuelling MHS research is the development of accurate diagnostic tests to detect in advance of anaesthesia the abnormalities that predispose an individual to MH.

MH in NZ has an estimated national incidence of 1 per 70,000 anaesthetics. However, the incidence MH is much higher in Palmerston North, due to a large susceptible Maori family residing in the Manawatu region. This family (CH) is of particular interest, being the largest and most extensively clinically characterised MHS family worldwide, and contributing to approximately 40% of MHS diagnoses at the Palmerston North hospital. On average, one in every 130 patients presenting for anaesthesia in Palmerston North has suspected susceptibility to MH.

The goal of this project was to determine the genetic basis of MH in susceptible NZ families with a view to the future introduction of DNA based diagnostic tests to replace the highly invasive and expensive *quadriceps* muscle biopsy *in vitro* contracture test (IVCT) currently in use. To this end, four phases of the research project were proposed and carried out as follows:

1. MHS subjects from 33 NZ MHS pedigrees were initially screened for the presence of published RYR1 mutations (Chapter 3).

2. Members of the large Maori (CH) family were genotyped for chromosome 19q markers flanking the RYR1 gene (RFLP and microsatellite polymorphisms). Genotype and IVCT phenotype data were then used in genetic linkage analysis to investigate the possible involvement of a RYR1 defect in the MHS phenotype in this family (Chapter 4).

3. After ruling out the presence of previously published mutations, and ascertaining the involvement of a novel RYR1 defect, MHS probands of the large Maori family, and other NZ MHS families were screened for novel RYR1 mutations. RYR1 cDNA from MHS probands was amplified by PCR and combed systematically for heterozygous mutations by automatic DNA sequencing (Chapter 5).

4. The segregation of candidate mutations with the MHS phenotype was then studied to explore the evidence for a causative role of novel RYR1 mutations and to investigate the sensitivity and specificity of the current diagnostic procedure (Chapter 6).

In addition to their diagnostic potential, it was envisaged that novel mutations predisposing to MH in NZ families would provide valuable insights into the intricate mechanisms that regulate skeletal muscle Ca^{+2} release, just as investigations into the excitation contraction coupling process are continuing to unravel the complex aetiology of the MH syndrome.

1.13.1 Role of Collaborators

This study has involved collaboration with members of the Department of Anaesthesia and Intensive care; Palmerston North Hospital where the sole IVCT testing centre for MH in NZ is situated. Muscle biopsy contracture testing has been conducted in accordance with the European protocol since 1986, primarily by Dr. Ken Couchman (Medical research laboratory, Palmerston North hospital). Over 380 muscle biopsies have been performed in this time. A database of all suspected MH reactions in NZ has been created and susceptible pedigrees traced by Dr. Neil Pollock (specialist anaesthetist, Palmerston North Hospital) and Dr. Ken Couchman, with the assistance of Mr. Rupene Waaka, a representative of the Ngati Raukawa ki te Tonga. The collection of blood samples from MHS probands and their family members was organised by Dr. Neil Pollock.

1.13.2 Collection and analysis of blood and tissue specimens

Blood samples from patients admitted for contracture testing, and their relatives have been collected and sent to Massey from 1989. Between 1989 and August of 1994, 130 blood samples were processed to extract DNA from white blood cells under the direction of Dr. Brian Mansfield, Molecular Genetics Unit, Massey University. DNA extraction from fresh, venous blood samples has continued at Massey University in the Department of Biochemistry and the Institute of Molecular BioSciences, under the direction of Dr. Kathryn Stowell. A registry of 720 DNA samples from NZ MHS families has now been established. The extraction of DNA form venous blood samples has largely been the responsibility of Ms. Danielle James, who was employed as a research technician from 1997. In addition, fresh muscle tissue samples have been obtained from patients undergoing skeletal muscle biopsy, and stored, frozen in liquid nitrogen to enable the extraction of muscle RNA.

Genomic DNA samples were used in a screen for published MHS mutations in individual RYR1 exons and for genotyping of RYR1-linked chromosome 19q markers. Skeletal muscle RNA was extracted from frozen MHS muscle specimens and used in reverse transcriptase (RT)-PCR to synthesise cDNA. Skeletal muscle cDNA was then used as a template in PCR to amplify RYR1 coding sequence in overlapping segments. These segments were screened for the presence of candidate heterozygous MHS mutations by automatic DNA sequence analysis. Genomic DNA samples collected from the relatives of subjects identified with RYR1 mutations were examined to assess the segregation of candidate mutations with the MHS phenotype. Procedures employed in the investigation of genomic DNA and cDNA for candidate MHS mutations are outlined in the following chapter.

2. MATERIALS AND METHODS

2.1 PURIFICATION OF GENOMIC DNA

2.1.1 Precautions for the handling of human blood.

The following precautions were observed to minimise the risk of infection by blood-borne pathogens during handling of human blood.

- All personnel involved in primary processing of human blood were vaccinated against Hepatitis B.
- Gloves, facemasks, safety eye-goggles and protective clothing were worn at all stages.
- Blood processing was performed in a dedicated, labelled bench in the laboratory.
- Tubes were capped for all centrifugation steps to minimise the production of aerosols.
- Blood waste products and collection tubes were decontaminated in large plastic discard jars with a 1% Virkon™ solution. Decontaminated tubes were incinerated.
- Spills were decontaminated by applying powdered Virkon™ directly to the affected area for 5 minutes. The powder was then scraped in a discard container, and the area cleaned with 1% Virkon™ solution.

2.1.2 Extraction of genomic DNA from peripheral blood

Blood samples were obtained with informed consent from members of 33 MH families participating in this study. Approximately 15 - 30 ml blood were provided per subject, in 6 ml Vacutainer™ tubes coated with EDTA to prevent coagulation of the blood and DNA degradation. DNA was extracted successfully from blood samples that had been stored for up to 12 days, however yields were significantly diminished for samples stored more than two days at 4°C.

Various DNA extraction procedures were employed. All procedures involved red blood cell lysis in a hypotonic salt solution followed by preferential harvesting of white blood cells by slow centrifugation. After white blood cell nuclei lysis and removal of proteins by precipitation and centrifugation, the DNA was precipitated from the supernatant with alcohol. A sample of white blood cells (approximately one third of the total) was removed for long term storage at -20°C.

The viscosity of high molecular weight genomic DNA solutions prohibits accurate DNA quantitation by spectrophotometric methods [304]. The quantity and integrity of the extracted, solubilised DNA was assessed by loading 1µl of each sample on a 1% agarose gel containing 10 mg/ml ethidium bromide alongside DNA concentration standards. Typically, 30-60 µg of DNA was obtained per ml of blood. DNA samples were diluted to 100-200 ng/µl for use in PCR.

2.1.2.1 Extraction of human DNA from white blood cells using laboratory reagents

The initial 200 DNA samples were purified from venous blood using laboratory-prepared reagents according to the method of Kunkel *et al.* [305]. 10-25 ml of blood was mixed with three volumes of ice-cold red blood cell lysing solution (155 mM NH_4Cl, 10 mM $KHCO_3$, 0.1 mM EDTA), incubated on ice for 10 minutes and centrifuged at 160X g for 10 minutes. The white blood cell pellet was washed in 10 ml 0.83% NH_4CL in 10 mM HEPES (pH 7.0) for 10 minutes at 37°C and recovered by centrifugation at 650X g for 7 minutes. Pellets were washed with 10 ml

0.9 % NaCl and collected by centrifugation at 5000 rpm in an SS-34 rotor for 5 minutes. A 1.5 ml sample of the resuspended pellet was transferred to a micro-centrifuge tube, and the cells collected by a 1 minute spin at 5000 rpm, and stored at -20°C.

2.1.2.2 Preparation of DNA from white blood cells

White blood cells from 10- 25 ml of blood were resuspended in 3.95 ml of TE (pH 8.0), and vortexed thoroughly to break up any cell clumps. Cells were mixed with 500 µl 0.5 M EDTA (pH 8.0), 50 µl of 40 mg/ml proteinase K and 500 µl of 10% SDS, and incubated with gentle mixing at 50°C for 3 hours. The viscous solution was mixed vigorously for 30 seconds with 2.2 ml of a saturated solution of NaCl and centrifuged for 10 minutes at 5000 rpm in an SS-34 rotor to collect the precipitated protein. DNA was precipitated from the supernatant with the addition of two volumes of 95% ethanol and gentle inversion of the tube. DNA appeared as a white strand, which was spooled out of solution with a sealed Pasteur pipette, washed in 75% ethanol and blotted dry on filter paper. The DNA was transferred to a 1.5 ml micro-centrifuge tube and dissolved overnight in 1 ml of TE buffer (pH 8.0). Samples were stored at - 20°C.

2.1.2.3 DNA purification with Wizard™ DNA extraction kit.

DNA was extracted from 3 ml blood with the Wizard™ DNA extraction (Promega) kit according to manufacturers' instructions. A scaled-down version of the protocol was used to prepare DNA from 300 µl blood samples from new-born infants.

2.1.3 Extraction of genomic DNA from paraffin-embedded tissue.

Paraffin-embedded autopsy spleen tissue specimens from members of an MHS family were obtained from the Palmerston North Hospital pathology department. DNA was extracted according to the method of Goelz *et al* [306].

Approximately 500 mg of the spleen tissue was frozen in liquid nitrogen and pulverised in a steel mortar. Crushed tissue was vortexed with 10 ml of a solution containing 1% SDS and 125 µl of 40 mg/ml proteinase K in TE (pH 9.0) and digested for two days at 50° C. The solution was forced through an 18 gauge needle three times and extracted three times with phenol. The final aqueous phase was vortexed with an equal volume of chloroform and centrifuged. DNA was precipitated from the final aqueous phase with the addition of 0.33X volume of 10 M ammonium acetate and 2.5 volumes of 95% ethanol followed by incubation at -70° C for two hours. The DNA precipitate was harvested by centrifugation at 9000X g for one hour, washed in 70 % ethanol, and collected with a 5 minute spin at 9000X g. The pellet was air-dried and resuspended in 250 µl of TE (pH 8.0).

2.2 PURIFICATION OF HUMAN SKELETAL MUSCLE RNA

2.2.1 Collection and storage of human skeletal muscle tissue

Vastus skeletal muscle tissue samples were obtained with informed consent from patients undergoing muscle biopsy at the Palmerston North Hospital for the *in vitro* contracture test. Tissue intended for future RNA extraction was frozen immediately to limit degradation by RNases. Approximately 150 mg of tissue was immersed in liquid nitrogen immediately after excision. Frozen samples were transferred to Massey University where they were stored in liquid nitrogen in sterile cryogenic 15 ml vials. Samples of skeletal muscle tissue from previous muscle

biopsies had been stored at -20° C in glass vials at Palmerston North Hospital. These were transferred to Massey University for continued storage at -70° C.

2.2.2 Maximizing yields of RNA from skeletal muscle

Skeletal muscle tissue typically contains lower concentrations of RNA compared to other tissues due to low cell density and the polynucleate nature of muscle tissue [307]. Furthermore, skeletal muscle tissue is difficult to homogenise compared to tissues such as the liver and kidney due to the abundance of connective tissue and contractile proteins. Yields of RNA from human skeletal muscle tissue (0.35 µg/ mg tissue) are also reportedly lower than that from other species investigated [307,308]. Maximising yields of RNA from small samples of human skeletal muscle tissue was therefore critical.

Isolation of high yields of pure, biologically intact RNA relies on denaturation of endogenous RNase activity and complete tissue homogenisation [309]. RNA is protected from the degradative action of RNases in the presence of Trizol™ solution and other organic solvents such as chloroform and ethanol [310]. Tubes, pipette tips and solutions intended for the transfer and storage of aqueous RNA solutions were pre-treated with a 0.05 % solution of diethylpyrocarbonate (DEPC), a non-competitive irreversible inhibitor of RNase activity [307]. Tris buffers that cannot be treated with DEPC were prepared using DEPC-treated water and glassware. Solutions and plastic-ware were then autoclaved repeatedly to remove traces of the DEPC, which can inhibit subsequent enzymatic steps [309]. RNasin™ (Promega) recombinant ribonuclease inhibitor was used to swab pipettes and apparatus for RNA gel electrophoresis. RNase-free barrier pipette tips were used to resuspend RNA or aliquot RNA solutions.

Total RNA was isolated rapidly with the Trizol™ RNA extraction reagent (Life Technologies) after extensive tissue homogenisation of crushed frozen tissue. The RNA extraction procedure is based on the single-step acid-guanidinium thiocyanate phenol-chloroform RNA extraction method of Chomczynski and Saachi [308]. During sample homogenisation, the Trizol™ reagent maintains the RNA integrity by inactivating RNases, while disrupting cells, disintegrating cellular structures and disassociating nucleoprotein complexes. Addition of chloroform and centrifugation separates the solution into an aqueous phase and an organic phase, with RNA remaining exclusively in the aqueous phase.

2.2.3 Tissue homogenization

50-150 mg samples of frozen muscle tissue were immersed in liquid nitrogen, and crushed to a fine powder in a cooled steel mortar designed for rock-crushing. The powdered, frozen tissue was transferred quickly to a weighed 1.5 ml microcentrifuge tube containing 1 ml of Trizol™. The tube was re-weighed, and the mass of the muscle tissue calculated by difference. The volume of Trizol™ was adjusted to achieve a ratio of 1 ml per 50 mg of tissue. The tissue/Trizol™ solution was transferred quantitatively to a 15 ml round-bottom centrifuge tube and homogenised to a smooth consistency with an ultra-Turrax T25.

2.2.4 RNA extraction with Trizol™

The homogenised tissue/Trizol™ mixture was transferred evenly to two 1.5 ml microcentrifuge tubes and RNA extracted according to Trizol™ manufacturers' instructions. The RNA pellet was collected by centrifugation at 7500X g for 5 minutes at 4°C and left to air-dry after removal of all the supernatant. One RNA pellet was re-dissolved in 25-30 ml of DEPC -treated sterile,

distilled water (Superscript™ kit) by heating to 55° C for five minutes. The remaining pellet was stored under 95% ethanol at -20 C.

The pure RNA precipitate dried to a translucent gel-like pellet. The Trizol™ reagent information advised against drying the RNA pellet to completion to aid solubilisation. However, the partially dried RNA pellet appeared opaque-white, and was insoluble. When re-precipitated in ethanol, harvested by centrifugation and dried completely to a translucent form, the pellet dissolved readily. Gel electrophoresis (see below) revealed the RNA was relatively undegraded and free of genomic DNA contamination.

2.2.4.1 Inspection of RNA purity

The concentration and purity of the RNA was assessed spectroscopically in a 100 µl quartz cuvette using 1 µl of the RNA solution diluted 100-fold in DEPC-treated HEPES pH 7.6 (10 mM HEPES, 0.001 mM EDTA). An A_{260}/A_{280}nm absorbance ratio approaching 2.0 is expected of pure RNA, while ratios of less than 1.8 are indicative contamination with protein or residual phenol [309]. The concentration of the RNA was calculated from the absorbance at 260nm assuming a concentration of 40 ug/ml for a solution with an absorbance of 1.0 [309].

2.2.4.2 Agarose gel electrophoresis for RNA

The integrity of the RNA preparation was ascertained by denaturing gel electrophoresis. RNA sample buffer was prepared fresh by mixing 0.14 ml sterile distilled water, 0.5 ml deionised formamide, 0.16 ml formaldehyde, and 0.2 ml 5X MOPS running gel buffer (1 M MOPS, 250 mM sodium acetate, 5 mM EDTA, pH 7.0). 10 - 20 µg of RNA was mixed with 20 µl of sample buffer, denatured at 60°C for 10 minutes, cooled on ice, and mixed with 2 µl of 10 mg/ml ethidium bromide and 1 µl of loading buffer (50% glycerol, 0.4% bromophenol blue, 1 mM EDTA). Two blanks were prepared containing 20 µl of sample buffer and 1 µl of loading buffer (containing 0.4% bromophenol blue and 0.4 % xylene cyanol).

0.75 g of low EEO agarose was melted in 31.25 ml of RNase-free water. 10 ml of hot (55°C) 5X MOPS running buffer was added to the agarose solution followed by 8.8 ml of formaldehyde. The gel was poured into a gel tray pre-treated with RNasin™ RNase inhibitor, allowed to set, then submerged in 1X MOPS loading buffer (made up with sterile DEPC-treated water). Samples were separated by electrophoresis at 100 mA for 3-4 hours in the fume hood. The gel was visualised and photographed under UV.

Successful purification of high quality, intact RNA was indicated by:

- A lack of visible high molecular weight DNA near the well.
- The presence of an approximate ratio of 2:1 between discrete ribosomal RNA 28S (~ 5 kb) and the 18S (~ 2 kb) ribosomal bands.
- The presence of high molecular weight mRNA, running as a smear between the 2 ribosomal RNA (rRNA) bands.
- The absence of an abundance of low molecular weight RNA species running below the 18 S rRNA .

Yields of 0.35 µg of RNA per mg of human skeletal muscle can be expected for extraction procedures based on the Chomczynski method [307,308].

2.3 STANDARD PCR PROCEDURES

2.3.1 PCR reagents

PCR primers were obtained from Life Technologies (Gibco BRL) "Custom Primers" service. Lyophilised oligonucleotides (~ 50 nmol) were dissolved in sterile distilled water to 10 µg/µl (or ~1.6 nmol/µl) stock solutions. These were diluted 10-fold to 1 µg/µl (or ~160 µM) stocks. The 1 µg/µl stock solutions were diluted as required, to 100 µl volumes of 50 ng/µl (~8 µM) or 20 ng/µl (~3.2 µM) working primer solutions. Working 3 mM dNTP solutions were prepared in 100 µl volumes from stock dNTP solutions containing 25 mM of each of dTTP, dATP, dCTP and dGTP, and stored at -20°C.

2.3.2 Basic PCR protocol

PCR reaction conditions were tailored for each primer set and are described within the relevant sections. Generally, 5 µl of genomic DNA (100-400 ng) was used as a template in 50 µl PCR reaction volumes containing 1.5 mM $MgCl_2$, 1X PCR buffer, 0.3 mM dNTP's, 250 ng (~ 40 pmol) each primer and 1.5 U of *Taq* polymerase.

A template designed to assist the preparation of standard PCR reactions and the recording of relevant details is presented in Table 2-1. Reagents (excluding the genomic DNA template) were combined in a PCR reagent master-mix, to ensure uniformity of reactions, and to minimise opportunities for contamination. The reagent mixture was dispensed in 45 µl aliquots into appropriately labelled, sterile 0.5 ml PCR tubes. Diluted genomic DNA solutions (20 - 100 ng/µl) were mixed, centrifuged and dispensed in 5 µl aliquots into each of the reaction tubes. 5 µl of sterile dH_2O was added to the negative control tube in place of DNA. Reactions were mixed, centrifuged briefly and overlaid with 1-2 drops (25 µl - 50 µl) of sterile nuclease-free mineral oil.

2.3.2.1 Thermal cycle

PCR was performed with Hybaid OmnE™ or Corbett™ thermal cyclers. Typical PCR thermal programs consisted of a 4 minute denaturation at 94°C, followed by 30 cycles of a 3-step program consisting of a 30 second denaturation at 94°C, a 30 second annealing step at the specified temperature and a 1 minute extension at 72°C. A final extension was performed at 72°C for 2 minutes. Completed reactions were stored at 4°C.

The initial annealing temperature selected was approximately 5°C below the lower calculated Tm for the oligonucleotide pair, as computed with the following formula [304];

$$T_m = 81.5 + 16.6\,(\log_{10}[Na^+]) + 0.41\,(\%\ G + C) - 675/n$$

(Where $[Na^+]$ = the molar salt concentration of monovalent cations and n = the number of bases in the primer.)

Table 2-1 Template for Basic PCR protocol

PCR Code:	***Date :*** / /
Primers:	
***Notes*:**	

Component	Conc.	Volume		Master Mix		React No.	DNA ID	React No.	DNA ID
PCR Buffer	X 10	*5 µl*		*50 µl*		1	M	11	M
$MgCl_2$	25 mM	*3 µl*	X *10*	*30 µl*		2	M	12	M
dH_2O	-	*21.7 µl*	n+10 %	*217 µl*		3	M	13	M
Primer (F)	50 ng/µl	*5 µl*		*50 µl*		4	M	14	M
Primer (R)	50 ng/µl	*5 µl*		*50 µl*		5	M	15	M
dNTP's	3 mM	*5 µl*		*50 µl*		6	M	16	M
Taq Poly.	5 U/µl	*0.3 µl*		*3 µl*		7	M	17	M
DNA	~50 ng/µl	*5 µl*		-		8	M	18	M
Total volume		*50 µl*		*450 µl*		9	M	19	M
Aliquot per reaction				*45 µl*		10	M	20	M

Thermal Cycle:

Example volumes are shown in grey Italics. PCR tubes were labelled with the PCR code number followed by the reaction number for unique identification and accurate cross-referencing.

2.3.3 Detection and prevention of PCR contamination.

A control reaction containing dH_2O in place of DNA was used in all reactions to check for contamination of PCR reagents. The most likely source of contamination of PCR is PCR product generated from a previous reaction [311]. The following procedures were adopted to limit the chance of cross-contamination.

- Separate work areas were assigned for pre and post-amplification steps. Dedicated centrifuge and pipettes, tubes and racks and bench areas were assigned for PCR.
- Barrier-tips were used for setting up PCR with cDNA, or dispensing PCR primers.
- Gloves were worn and changed between handling DNA solutions and PCR reagents.
- Buffers and sterile water were discarded frequently.

PCR contamination was revealed as the presence of a band in the negative control. In the event of contamination, PCR reagents including buffers dNTP's and diluted primers were disposed of, and reactions repeated under especially sterile conditions. Alternatively, different primer sets (with at least one oligonucleotide outside the region encompassed by the contaminating species) were chosen such that the original PCR product could not act as a template.

2.4 PROCEDURES FOR OPTIMISIMG PCR

2.4.1 Critical variables

The free magnesium ion concentration, annealing temperature and DNA are critical variables which can be readily modified to influence the PCR specificity. Non-specific PCR priming was primarily addressed by increasing the annealing temperature, to favour the annealing of the primer to the correct target sequence over the thermodynamically less stable non-specific primer/template interactions.

Excess $MgCl_2$ concentrations stabilise mismatched primer/template interactions and can reduce *Taq* polymerase fidelity [312] and concentrations above 10 mM are inhibitory [313,314]. The optimal $MgCl_2$ concentration was empirically defined for each primer set by performing magnesium titrations in the 1.0 - 2.5 mM range (2 - 5 µl of 25 mM $MgCl_2$ per 50 µl reaction). The dNTP concentration in all PCR procedures was 0.3 mM.

Amplification of very high molecular weight DNA was improved by pippetting and vortexing the DNA solutions to shear the DNA into smaller fragments (< 50 kb) to aid template denaturation and dispersion [311]. Excessive amounts of genomic DNA template were found to be inhibitory and lead to a high molecular weight smear of DNA extending above the amplified target and non-specific amplification.

Other critical factors that shift the PCR reaction towards the accumulation of non-specific product include excess enzyme, excess primers, prolonged extension times and continued thermal cycling beyond the PCR plateau stage [311,315]. The plateau phase is reached after approximately 30 cycles, as the enzyme becomes self-limiting and self-annealing of synthesised DNA surpasses primer annealing [315]. Continued cycling beyond the plateau phase was avoided where possible to minimise the preferential exponential accumulation of unwanted products that have not yet reached saturation.

2.4.2 Touchdown PCR

Touchdown PCR is a one-step procedure that can be used to avoid time-consuming optimisation procedures by ensuring a competitive advantage for the target product at annealing temperatures below the Tm that would otherwise promote spurious amplification [316]. The strategy involves incremental decreases in annealing temperature designed to bracket the melting temperature of the oligonucleotides [317]. At stringent initial annealing temperature, priming of non-specific sequences is de-stabilised, and the solution is enriched for the desired PCR product. Subsequent cycles are performed at progressively lower annealing temperatures to increase the efficiency of the reaction, during which time the specific product is preferentially amplified.

2.4.3 Hot-start PCR

Primer-dimers are PCR products resulting from the self-annealing of the 3' ends of primers and compete effectively with the desired product. The amplification of primer-dimers and other products formed through mismatched annealing and extension of mixed reactions at ambient temperatures is minimised in hot-start PCR by withholding a vital PCR component (either $MgCl_2$ or enzyme) until the reactions have reached the 94°C denaturation temperature. An antibody/polymerase preparation (Platinum *Taq* polymerase™) was utilised to achieve specific hot-start amplification of select RYR1 cDNA regions. The antibody binds the *Taq* polymerase and prevents extension at ambient temperature but is released at higher temperatures to yield a

functional polymerase [318]. Most hot-start procedures were performed manually, with standard *Taq* polymerase by mixing the enzyme to the PCR reactions at 94°C.

2.4.4 Nested PCR

Products from an initial PCR reaction were diluted and used to seed a second PCR reaction in which at least one PCR primer is internal to the original primer set to prevent the amplification of non-specific products. Best results generally obtained when the primary product was diluted 1/1000 - 10,000 fold. The use of excess seeding template in the second reaction resulted in smeared bands due to a sub-optimal primer template ratio and concatemerisation of PCR products [311]. Amplification of very dilute template solutions can result in allele amplification bias or amplification of PCR errors, which can give rise to false positive results in mutation scanning [311]. Furthermore, the second round of PCR is extremely sensitive to contamination with the products of the first round. For these reasons, the nested PCR strategy was generally avoided in applications that were designed to detect novel mutations.

2.4.5 Primer design

PCR specificity was improved by observing particular guidelines for primer design to eliminate 3' mismatch tolerance and primer-dimer artifacts.

- T nucleotides at the 3' terminus were avoided since *Taq* polymerase can extend from T mismatches [319].
- Oligonucleotides with GC-rich sequence at the 3' termini were avoided to destabilise the extension from non-target sequences [311].
- Regions containing polynucleotide stretches or common microsatellite repeat elements were also avoided.
- Primer pairs with internal complementarily, or between-primer 3' complementarity were rejected to limit the formation of primer-dimers.
- Oligonucleotides with similar melting temperatures were selected for PCR pairs where possible.

Primer selection was assisted with the use of the "Primer3" program made available by the Whitehead institute for Biomedical Research at the URL: http://www-genome.wi.mit.edu/cgi-bin/primer/primer3.cgi) [320]. Optimal primer pairs within a designated sequence were selected to conform to guidelines for ideal primer design and to the user-specified criteria including product size range, target regions, excluded regions and maximum and minimum primer lengths. Potential primers were screened against human repetitive sequence elements within a Primer3 mispriming library.

2.5 METHODS OF MUTATION DETECTION

2.5.1 Restriction fragment length polymorphism analysis (PCR-RFLP).

Mutations that destroy or introduce restriction endonuclease (RE) recognition sites for affordable enzymes were detected by the presence of undigested or digested DNA fragments respectively after RE digestion of PCR-amplified regions of genomic DNA.

PCR

PCR was performed according to standard procedure in 50 µl total reaction volumes. All components aside from the DNA template were pre-mixed in a reagent cocktail (sufficient for *n+1* reactions). PCR conditions were optimised with respect to $MgCl_2$ and annealing temperature to generate adequate yields of discrete PCR products (Table 2-2). 5 µl of each PCR product was analysed on a 3% Nusieve™ agarose gel to confirm that a single product of the expected size was obtained and that the negative PCR control was free of contamination.

Table 2-2 MH mutation screening by PCR-RFLP

Mutation	Base change	Ref.	PCR primers (F / R)	Size (bp)	$MgCl_2$ (mM)	T anneal	RE Changed
RYR1							
R163C	C487T	[13]	163F-bio / 163R,	76	2.0	58°C	-*Bst* UI
			163F-bio / 163I-R	200	2.0	56°C	-B*st* UI
I403	C1209G	[13]	403Fseq /403R-bio	75	1.5	58°C	-*Mbo* I
R552W	C1654T	[111]	552F-bio/ 522R	202	1.5	57°C	-*Sau*3A
R614C	C1840T	[106]	614F-bio / 614R	132	1.5	60°C	-*Rsa* I
R2163C	C6487T	[25]	38int / 39intR	331	2.0	61°C	-*Bsr* BI
R2163H	G6488A	[25]	38int / 39intR	331	2.0	61°C	-*Bsr* BI
G2434R	G7297A	[110,167]	2434F /2434R-bio	210	1.8	60°C	+*Dde* 1
R2435H	G7301A	[168]	2434F / 2434R-bio	210	1.8	60°C	-*Hga* I
R2458H	G7373A	[169]	45intF / 47exR	348	1.5	60°C	-*Bsr* BI
CACNLA3							
R1086H	G3333A	[33]	CACNLA3.25iF - CACNLA3.25iR,	226	1.5	58°C	+*Hha* I +*Cfo* I

-bio : 5' biotinylated primer. Primer sequences are given in appendix 1.

Restriction endonuclease digestion and concentration of PCR products.

20 µl of each PCR product was digested with 2-3 µl (4 - 9U) of the appropriate enzyme in a 50 µl total reaction volume. 30 µl aliquots of a cocktail reagent comprising the RE enzyme, RE 10X buffer and water were dispensed into 1.5 ml microcentrifuge tubes containing 20 µl of PCR product. Reactions were incubated at the appropriate temperature for 1-2 hours. DNA was precipitated with the addition of 0.1X volume of 3 M sodium acetate (pH 5.2) and 2.5 volumes of cold 95% ethanol. Tubes were mixed thoroughly and stored at -70°C for 20 minutes. The DNA precipitate was recovered by centrifugation for 15 minutes at 4°C, washed in 70 % ethanol, centrifuged briefly, drained and dried under vacuum for 5 minutes.

Gel electrophoresis

Dried DNA pellets were dissolved in 10 µl of distilled H_20 and 2 µl of DNA loading dye (40 % sucrose, 0.05 % bromophenol blue, 0.05 % xylene cyanol). The entire sample was loaded onto

an 3-4% Nusieve™ agarose gel containing 1X TAE, adjacent to 8 µl of undigested PCR product and 5 µl of a DNA size marker (Gibco-BRL 1 Kb ladder). The agarose concentration and electrophoresis time was tailored for each RFLP with reference to Nusieve™ product specifications. Electrophoresis was carried out at 80-90 V for 1-1.5 hours, stained in 0.5 µg/ml ethidium bromide (EtBr) for 15 minutes. Gels were destained in 1X TAE and photographed under UV light.

2.5.2 Mutation screening by direct sequencing

2.5.2.1 Purification of template DNA with strepatavidin-coated Dynabeads™

Manual dideoxy sequence analysis was used to screen for MH-linked RYR1 mutations that did not alter RE sites. PCR was performed with one 5' biotinylated primer (Table 2-3) to enable purification of single-stranded DNA template for sequencing. PCR specificity was verified by analysing 5 µl of PCR product on 3 % Nusieve™ agarose gels.

Dynal Dynabeads-streptavidin (20 µl per template) were washed in 1X washing buffer (5 mM Tris.HCl pH 7.5, 0.5 mM EDTA, 1.0 M NaCl) and resuspended in 2X washing buffer (40 µl per template). Dynabeads were recovered out of solution at each stage by use of a magnetic particle concentrator (MPC) to collect the beads to one side of the tube, allowing removal of the supernatant from the opposing side. 40 µl aliquots of the prepared dynabeads were mixed with 40 µl of each PCR reaction for 15 minutes to allow the dynabeads-streptavidin complex to selectively bind the biotinylated DNA. The beads were washed in 40 µl of 1X washing buffer. DNA was denatured by incubation with 0.1 M NaOH for 10 minutes at room temperature. The biotinylated DNA strand was selectively purified by collecting the beads, removing the supernatant, and washing sequentially with 50 µl of NaOH, 40 µl of 1X washing buffer and 50 µl of TE (pH 8.0). Finally, the beads were recovered and resuspended in 6 µl of dH_2O.

Table 2-3 RYR1 mutation screening by PCR/direct sequencing

Mutation		Ref.	PCR primers (F/R)	Sequencing primer	Product Size (bp)	[$MgCl_2$ mM	T Anneal
C35R	T103C	[165]	RYR-C35Fbio / C35-R	RYRC35Rseq	170	1.5	58°C
G248R	G742A	[107]	248F-bio / 248R	248Rseq	228	2.2	60°C
G341R	G1021A	[109]	341F-bio / 341R	341R-seq	127	1.5	58°C
R552W	C1654T	[111]	RYR552F-bio / RYR522R	RYR552Rseq	183	1.8	56°C
R614L	C1841T	[166]	614F-bio / 614R	614Rseq	134	1.5	60°C
V2168M	G6502A	[25]	RYR38intF /RYR39intR	RYR38intF	331	2.0	61°C

Primer sequences are given in appendix 1.

2.5.2.2 Labelling templates for manual dideoxy sequencing

Sequence analysis was performed using the Sequenase™ version 2.0 DNA sequencing kit. 7 µl of the purified template (dynabead/single-stranded DNA complex) was mixed with 2 µl of sequenase buffer and 1 µl of oligonucleotide primer (0.5 pmol/µl) in 0.5 ml tubes and heated to 65°C for 2 minutes in 15 ml test-tubes. Test-tubes were removed from the heating block and allowed to cool gradually to < 35°C. Labelling reaction mixture sufficient for eight templates was prepared by mixing 8 µl of DTT, 3.2 µl of labelling mix, 14 µl of enzyme dilution buffer, 4 µl of ^{35}S[dATP] 14 µl of dH_2O and 2 µl of undiluted Sequenase version 2.0™ T7 DNA polymerase. 5.5 µl of the labelling reaction mixture was added to each annealed template/primer mixture. Tubes were incubated at room temperature for 3 minutes. 3.5 µl of this reaction mixture was added to 2.5 µl of each of four dideoxy NTP's (ddNTP) termination mix solutions, dispensed in 32-well microtitre plates. Reactions were incubated at 37°C for 5 minutes and terminated by mixing 98 % formamide/dye stop solution to each well. Reactions were stored at -20°C for up to one week.

2.5.2.3 Preparation and electrophoresis of DNA sequencing gels

Matched glass plates were cleaned thoroughly and wiped with ethanol. The shorter plate was siliconised on one side with 2% dichloromethylsilane in dichloromethane. Glass plates were assembled with matching spacers, and secured with a rubber seal. 80 ml of acrylamide solution (6 % 19:1 acrylamide:N,N'-methylenebisacrylamide, 6 M urea, 1X TBE) was mixed with 250 µl of a freshly prepared 10 % ammonium persulphate solution and 80 µl of TEMED to initiate polymerisation. The gel was poured immediately taking care to avoid the generation of bubbles.

Sharks-tooth combs were inserted with the flat edge against the gel and secured with bulldog clips. Once set, the gel was assembled into the S2 sequencing gel electrophoresis unit (BRL). After pre-running the gel for 30 minutes at 65 W constant power (1500V, 45 mA) in 1X TBE, excess urea was flushed from the gel surface and sharks-tooth combs were inserted, so that the teeth made small indentations in the gel surface. Labelled templates were heated for 2 minutes and 3.5 µl of each reaction loaded in the order AGCT. Gels were electrophoresed as before for 1.5 - 2.5 hours, fixed in 7% acetic acid/15 % methanol for 15 minutes to remove urea, drained and transferred to a sheet of Whatman 3 MM chromatography paper. The gel was dried for 40 minutes at 80°C and autoradiographed overnight (up to 3 days for weak signals). X-ray films were developed for 3 - 5 minutes in developing solution (KODAK), rinsed, fixed for 5 minutes and washed well with water.

2.5.3 Amplification created restriction site analysis (ARMS)

Mismatch oligonucleotides were designed to selectively introduce a new RE site in the PCR product derived from the mutant allele to detect the A1565C (Tyr522Ser) mutation in preference to direct sequence analysis. A forward primer (RYR522F) containing a 1 bp miss-match was designed to direct the incorporation of a *Bsm*A1 restriction site (and removal of a *Mbo* II site) in the presence of the A1565C mutation. After *Bsm* AI digestion of the PCR products (prepared with RYR522F/RYR522Rbio primer pair), and high-resolution agarose gel electrophoresis, the normal allele is represented by a 180 bp band, while the mutant allele is cleaved to 166 and 24 bp fragments. An alternate set of primers (522F-wt/RYR-R522R-Pst) was also employed, with a miss-match reverse primer to selectively introduce a *Pst* I site in the 100 bp PCR product derived from the mutant allele.

2.5.3.1 Single-stranded conformation polymorphism analysis (SSCP) of amplified genomic DNA

SSCP mutation detection exploits the sequence and conformation-dependent mobility of single-stranded DNA on non-denaturing polyacrylamide gels [321,322]. Non-radioactive SSCP was employed for large scale screening of genomic DNA samples for the presence of 5 novel mutations identified in NZ families. The method was based on that described by Orita *et al.* [321] and Hongyo *et al.* [323], modified by trial and error for each PCR product to facilitate discrimination of normal and mutant alleles by ethidium bromide detection. Products amplified from PCR reagent mixes with different buffer, $MgCl_2$, DNA or oligonucleotide compositions could not be reliably compared since these variables effect the stability of intramolecular duplexes, and the resultant SSCP profiles [324].

2.5.3.2 PCR for SSCP

- ❑ PCR was performed under standard conditions, in 25 µl reactions, with 50 ng each primer, 0.15 µl of *Taq* polymerase (5U/µl) per reaction, and 1.5 µl (50 -100 ng) genomic DNA. Cocktail reagent mixtures containing all components (aside from the genomic DNA template) were prepared for up to 35 reactions at a time (sufficient for two gels). 23.5 µl of the PCR master mix was aliquoted into each tube containing 1.5 µl of genomic DNA (or water in the case of the negative control). Three positive mutation controls were included. PCR conditions optimised for the SSCP screening for each mutation (see Table 2-4).
- ❑ A 3.5 µl sample of each product was analysed on a 3% Nusieve gel to assess the specificity and of the reaction, leaving sufficient DNA for two 10 µl SSCP analyses.

2.5.3.3 Preparation of SSCP gels

- ❑ 40 ml of 8% non-denaturing polyacrylamide gel solution was prepared by mixing 8 ml 40 % 39:1 acrylamide:N,N'-methylenebisacrylamide, 8 ml 5X TBE and dH_2O to volume. Polymerisation was initiated with the addition of 40 µl of TEMED and 160 µl of 10% ammonium persulphate.
- ❑ The gel was poured immediately into a 16 cm X 16 cm gel apparatus (Horizon V15:17, Life Technologies). After removal of any bubbles, a 20 well comb was inserted, and the gel left to set for 30 minutes.
- ❑ Gel plates were cleaned to remove any spilled acrylamide, and assembled onto the electrophoresis unit in the cold room (4°C). Top and bottom reservoirs were filled with 0.5X TBE.

2.5.3.4 Sample preparation and electrophoresis

- ❑ 5 µl of each PCR product was mixed with 20 µl of 0.5 X TBE and 5 µl of 98% formamide dye (98% deionised formamide, 0.25% bromophenol blue, 0.25% xylene cyanol). At least 3 samples of a positive control (carrying the mutation) were prepared to be loaded at regular intervals across the gel.
- ❑ Samples were heated at 99°C for 5 minutes and cooled suddenly by plunging immediately into an ice/acetone bath. 5 µl of one of the PCR products was mixed with 20 µl of the 0.5X TBE and 5 µl of the dye, mixed and left on ice. This sample was not denatured and served as a reference marker for double-stranded DNA.
- ❑ 25 µl of each sample, including the double stranded control was loaded immediately onto the 8% polyacrylamide gel and electrophoresed at 4°C with power limiting at 3W and voltage set to 280 V for approximately 3 hours and twenty minutes. The current usually decreased from 13 mA to 9 mA during electrophoresis.

- After the bromophenol blue had reached the bottom of the gel, electrophoresis was discontinued, and the plates dismantled so that the gel adhered to the smaller glass plate.
- The gel (adhered to the glass plate) was stained in 1 µg/ml ethidium bromide solution for 10-15 minutes, destained for 15 minutes in 0.5X TBE, and viewed under UV light.

Double-stranded DNA migrated ahead of the single-stranded DNA on the SSCP gels. Generally two or more bands corresponding to single-stranded DNA were observed. Sequence polymorphisms were revealed by the appearance of additional bands or by the increase or reduction of intensity of particular single-stranded DNA bands.

Table 2-4 PCR and gel conditions: RYR1 mutation screening by SSCP

Mutation	PCR Primers	size, bp	[$MgCl_2$]	T anneal	PA Gel %,Run time
R2452W, R2454H	45iF - 7393	200	1.5 mM	60°C	8%, 3 hrs 20 min
T4826IH4833Y	144662 - 100iR	208	1.6 mM	60°C	8%, 3 hrs
G341R	341F-341R-bio	134	1.5 mM	59°C	12%, 4.5 hrs
R401C	401iF- 403Rseq	185	1.5 mM	57°C	8.5 %, 3.5 hrs

Standard PCR programs involved of an initial 4 min denaturation at 94°C, followed by 30 cycles of 20 sec denaturation at 94°C, 30 sec annealing at the specified temperature, and 1 min extension at 72°C, with a final extension at 72°C for 3 min. Primer sequences are given in appendix 1.

2.5.4 Automated DNA sequencing

Members of NZ MH families identified with published (R163C, G341R, G2434R) and novel (R401C, R2452W, R2454H, T4826I, H4833Y) RYR1 mutations were screened for diagnostic purposes by direct automatic sequence analysis of PCR-amplified genomic DNA with dye terminator chemistry. After verification of the PCR specificity by agarose gel electrophoresis, PCR products were purified away from contaminants, including primer-dimers and amplification primers with Wizard™ PCR DNA purification resin and Wizard™ minicolumns (according to manufacturers' instructions). DNA was eluted in dH_2O and a 1-2 µl sample run adjacent to a range of quantitation standards (10 - 100 ng) on a Nusieve™ agarose gel to ascertain the DNA purity and concentration. Primers for sequencing were diluted to 3.2 pmol/µl. Automatic sequencing was performed by the Massey University DNA sequencing service on an Applied Biosystems 377-36 automatic sequencer.

2.6 ANALYSIS OF CHROMOSOME 19q MARKERS

2.6.1 Restriction fragment length polymorphism analysis (RFLP)

Genotyping with respect to restriction fragment length polymorphisms was performed as described in section 2.3.1 for mutation detection by PCR-RFLP. Members of the Maori family were typed with respect to three published intragenic RYR1 RFLP polymorphisms [107] (Ile^{1151}, Asp^{2729}, and Ser^{2862}) analysed by digestion of PCR-amplified regions of genomic DNA with *Taq* I, *Fok* I and *Cfo* I respectively. Digested PCR products were separated by gel electrophoresis using 3% Nusieve™ agarose. Primer sequences, optimal PCR conditions, and digest products are

presented in Table 2-5. In the case of the Asp^{2729} polymorphism, a second non-polymorphic *Fok*I site served as a useful internal control for enzyme activity.

Undigested PCR products were recorded as the "1" allele while cleaved fragments are registered as the "2" allele. Heterozygous status is indicated by the presence of both the uncut and digested fragments, where the intensity of the undigested PCR product representing the "1" allele should be approximately equal to the combined intensity of each of the cut fragments derived from the "2" allele. Deviation from the expected relative band intensities indicated incomplete digestion or PCR cross-contamination.

Table 2-5 Primers and reaction conditions for RYR1 PCR-RFLP analysis.

RFLP site	RE	PCR primers (5'-3')	[$MgCl_2$] mM	Anneal Temp.	PCR Product	Fragment sizes Allele 1	Allele 2
Ile^{1151}	*Taq* I	RYR1151F, RYR1151R	1.75	58°C	120 bp	120 bp	72, 48 bp
Asp^{2729}	*Fok* I	RYR 2729F, RYR 2729RiBio	1.5	58°C	205 bp	205 bp	153, 50 bp
Ser^{2862}	*Cfo* I	RYR2862F, RYR2862R	1.5	60°C	250 bp	149, 91 bp	105, 91, 38 bp

Primer sequences are given in appendix 1.

2.6.2 Microsatellite analysis

Members of a large MH Maori family were typed with respect to four chromosome 19 microsatellite repeat markers flanking the RYR1 locus. Informative markers chosen included dinucleotide CA-repeat polymorphisms: D19S220 [325,326], RYR1CA [327] and D19S47 [178,328] and the trinucleotide CAG-repeat polymorphism D19S190 [329]. Microsatellite markers were amplified by PCR on genomic DNA using ^{33}P-labelled primers and resolved on denaturing 5-8% polyacrylamide gels.

2.6.2.1 5'labeling of oligonucleotides with $\gamma^{33}P[ATP]$

5 µl of a 20 µM solution of the forward PCR primer was incubated with 5 µl of 5X forward reaction buffer, 2.5 µl of 10 U/µl T4 Polynucleotide kinase and 5 µl of $\gamma^{33}P[ATP]$ (10 µCi/µl) in a total volume of 25 µl in at 37°C for 45 minutes. The labelled primer solution was heated for 10 minutes at 68°C to heat-inactivate the kinase, cooled on ice and stored at -20°C. The final concentration of the labelled primer was 4 µM (4 pmol/µl). The above reaction provided sufficient labelled primer to perform 50 (10µl) PCR reactions.

2.6.2.2 Preparation of reference M13 sequence ladder

An M13 sequencing ladder served as a size-marker to ascertain microsatellite band size for accurate allele assignment. M13 single-stranded DNA template and -40 primer was supplied in the Sequenase Version 2.0™ DNA sequencing kit. The protocol was modified as follows to provide sufficient sequencing ladder for 10 gels.

Primer annealing

5 µg of the single-stranded M13 template (0.25 µg/ml) was mixed with 4 µl of the -40 primer (0.5 pmol/µl) and 8 µl of the Sequenase™ buffer in a total volume of 40 µl in a 0.5 ml tube. The annealing mixture was heated for 2 minutes in 15 ml test-tubes filled with water at 68°C. The primer was annealed to the template by removing the test tubes from the heat block and slowly cooling the mixture to < 35°C.

Labelling reaction
22 µl of a labelling reaction mix (comprised of 1.6 µl of Sequenase™ 5X labelling mix, 4 µl of 0.1 M DTT, 7 µl of enzyme dilution buffer, 2 µl of $\alpha^{35}S$ [dATP] and 1µl of Sequenase 2.0™) was mixed with the annealed primer/template and incubated at room temperature for 2-5 minutes.

Termination.
10 µl of each of four ddNTP's were dispensed into four tubes marked A, T, G and C and preheated at 37°C for 5 minutes. 14 µl of the labelling reaction was transferred to each of the four tubes, which were mixed and incubated at 37°C for 5 minutes. Reactions were terminated with the addition of 16 µl of stop solution (98% formamide, 0.25% bromophenol blue, 0.25% xylene cyanol) to each tube. The reactions were stable for approximately 1 month stored at -20°C.

2.6.2.3 Microsatellite PCR

The protocol was adapted from a published procedure [330], to accommodate detection with $\gamma^{33}P$[ATP] (in preference to $\gamma^{32}P$[ATP] detection). The standard protocol [330] was adjusted to permit more economical (10 µl) PCR volumes. A mixed primer solution containing a 2:3 molar ratio of the forward to reverse primer (6 µM F and 8 µM R) was prepared by diluting 3.75 µl of the forward primer (160 µM) and 5 µl of the reverse primer (160 µM) with 91.25 µl of sterile dH_2O. The asymmetric primer ratio compensated for the extra labelled forward primer included in the PCR.

Individual PCR components and concentrations are presented in Table 2-6. A cocktail PCR mixture including all the PCR reagents, excluding the template genomic DNA was prepared for *n + 10%* reactions (including the negative control), to allow for pippetting error. Up to 40 PCR reactions were prepared at a time. 8 µl aliquots of the combined reaction mixture were dispensed into appropriately labelled 0.5 ml reaction tubes. 2 µl of each diluted genomic DNA sample was added to each tube, or 2 µl of sterile dH_2O in the negative control. Tubes were vortexed, centrifuged, and overlaid with sterile mineral oil.

Thermal cycles typically included a initial 3 minute denaturation at 94°C, followed by 35 rounds of a 3-step cycle including denaturation at 94°C for 25 seconds, annealing for 30 seconds (at the primer-specific temperature) and extension at 72°C for 45 seconds, followed by a final extension at 72°C. PCR primers, $MgCl_2$ and annealing temperatures specific to each microsatellite marker are detailed in Table 2-7. Completed reactions were diluted 3-fold with 20 µl of 98 % formamide stop solution (98% deionised formamide, 20 mM EDTA, 0.05 % bromophenol blue, 0.05 % xylene cyanol) and stored at -20°C.

Table 2-6 Microsatellite PCR.

Component	Concentration	Volume	Final Concentration
PCR buffer	10X	1 µl	1X
$MgCl_2$	25 mM	0.7 µl	1.75 mM
Sterile dH_2O	--	3.7 µl	--
dNTP's	3 mM	1 µl	0.3 µM
Combined Primers	6 µM F 8 µM R	1 µl	pmol/µl F, 0.8 pmol/µl R
Labelled F primer	4 µM (^{33}P labelled)	0.5 µl	0.2 pmol/µl
Taq DNA polymerase	5 U/µl	0.1 µl	0.05 U/µl
Genomic DNA	50 - 150 ng/µl	2 µl	100- 300 ng/ 10 µl

2.6.2.4 Polyacrylamide gel electrophoresis of microsatellite PCR products

Denatured PCR products were separated on large denaturing polyacrylamide sequencing-type gels. 5 -8% acrylamide gel solutions (containing 6M Urea) were prepared fresh, in 80 ml volumes in a 200 ml beaker, by mixing the appropriate volume of 40% 19:1 acrylamide:N,N'-methylenebisacrylamide, 8 ml of 10X TBE, 38.4 g of urea and dH_2O to volume.

Polymerisation of the dissolved acrylamide solution was initiated with the addition of 250 µl of a fresh 10 % ammonium persulphate solution and 80 µl of TEMED. The acrylamide solution was poured into a glass plate sandwich (as described in section 2.3.2.3). Gels were left to set for 30 minutes, and pre-run in 1X TBE at 65 W constant power for 45 minutes (voltage was set to 2000 V, and current to 50 mA). Voltage and current stabilised at 1700 V and 38 mA respectively.

After flushing leached urea from the gel surface, sharks-tooth combs were inserted and clamped in place with bulldog clips to prevent leakage while loading the gel. PCR tubes (and the M13 sequence reference ladder were heated to 95°C for 5 minutes in a thermal cycler. 5 µl of each sample was loaded directly off the heating block. Electrophoresis was performed with 65 W constant power (referring to tables outlining the migration of single-stranded DNA) at varying concentrations of polyacrylamide relative to the dye markers to achieve optimal separation of the polymorphic DNA bands [304]. Gels were run for approximately 3 hours or until the bromophenol blue dye front had migrated approximately 3/4 the length of the gel (as described in Table 2-7).

Gels were dismantled, fixed in 5% acetic acid and 15% methanol, dried on sheets of Whatmann 3MM blotting paper, exposed to X-ray film for 1-3 days and developed as described for manual sequencing gels in section 2.3.2.3.

Table 2-7 PCR and electrophoretic conditions for microsatellite analysis

Marker	PCR primers	Product size range (bp)	PCR T anneal	PCR [$MgCl_2$]	PA gel %	Approx. run time
D19S220	D19S220-F/ D19S220-R	265 - 283	57°C	1.75 mM	5 %	3 ½ hr.
RYRCA	RYRCA-F/ RYRCA-R	266 - 278	58°C	1.75 mM	6 %	3 hr.
D19S190	D19S190-F/ D19S190-R	111 - 117	60°C	1.4 mM	7.5 %	2 ¼ hr.
D19S47	D19S47-F/ D19S47-R	88- 106	55°C	1.75 mM	7.5 %	2 ¼ hr.

Primer sequences are given in appendix 1.2

2.7 GENETIC LINKAGE ANALYSIS

2.7.1 Installing LINKAGE programs

Versions of LINKAGE analysis program package [331,332] are available for DOS, UNIX, OS2 and Win32 operating systems (MacIntosh versions are currently unavailable.). The DOS and Window's versions of the Linkage program package (LINKAGE 5.1) were obtained by anonymous FTP from Rockerfeller University site (URL: ftp://linkage.rockefeller.edu/software/linkage).

Executable programs including (ILINK, LINKMAP, LODSCORE, LOOPS, MLINK, PREPLINK, UNKNOWN) are contained within the compressed gedos.zip (DOS) and gewin.zip (Windows platform) files. Additional linkage auxiliary programs (including MAKEPED, LINKLODS and the LCP batch program shell) are contained in the supdos.zip file.

The lines FILES = 20 and DEVICE = ANSI.SYS were inserted into the config.sys file in the root directory to enable use of the LCP batch program. The line SET PATH = C:\DOS;C:\LINKAGE;%PATH% was inserted into the AUTOEXEC.BAT file in the root directory to ensure that the linkage directory is accessible by DOS.

Linkage analysis requires two input files; the pedigree file, containing pedigree structure, genotype and phenotype data and a parameter file, describing the locus types, disease and allele frequencies, mutation rates and the genetic model.

2.7.2 Pedigree files

The preliminary pedigree file was prepared with a simple text editor capable of producing ASCII files. One line is entered per individual consisting of eight or more fields delimited by spaces. Data fields were entered according to standard format: Family number, individual ID, Father ID, Mother ID, gender (1 = male, 2 = female), affection status, liability class, allele 1 (marker 1), allele 2 (marker 1), allele 1 (marker 2), allele 2 (marker 2) and so forth for all the marker loci. Phenotype and marker data were entered in the order stipulated in the associated parameter file. Zeros were entered as placeholders for missing phenotype and marker data and in the parental fields for founders and unrelated spouses.

The preliminary pedigree file is processed by the MAKEPED batch program to convert the data into a format appropriate for the MLINK or ILINK analysis programs. MAKEPED checks for

pedigree structural inconsistencies and adds a proband field and three pointer fields per individual indicating the first offspring, first paternal sibling and first maternal sibling. The LOOPS program is invoked by MAKEPED to identify any marriage or consanguinity loops within the pedigree. Any known loops were specified at the MAKEPED prompt when the program is first initiated.

2.7.3 Parameter files

The PREPLINK program was used to generate a parameter file for the linkage analysis. Variables specific to the genetic model such as the number of loci and locus types, mutation rates, allele frequencies, disease gene frequency and penetrance were entered according to published recommendations [333] and are discussed in Chapter 4.

2.7.4 Performing linkage analysis with LCP

The Linkage Control Program (LCP) was used to perform all linkage calculations. This program provides a user interface between the user and the linkage programs, and prepares a file to conduct multiple analyses non-interactively in batch mode. Required input files are the MAKEPED output pedigree file and the parameter file generated by PREPLINK. LCP automatically initiates the UNKNOWN program which checks for data inconsistencies such as non-Mendelian segregation of alleles, excludes impossible genotypes from inclusion in the likelihood calculations for individuals with missing data, and incorporates genotypes of untyped individuals that can be inferred with certainty [333].

2.7.4.1 LINKAGE programs for general Pedigrees

MLINK was used to calculate 2-point likelihood estimates for two loci under predefined values of θ. ILINK was used to compute lod scores at the maximum likelihood estimate of the iterated parameter. The LINKMAP program is used in multipoint analysis to place a locus on a fixed map with user-defined loci order and θ intervals. Liklihoods were calculated as the locus of interest was shifted through each map interval.

2.7.4.2 Interpreting LINKAGE output files

Linkage results were viewed directly in the final.out file, or alternatively, the stream.out files were converted into tabular format using the Linkage Report Program (LRP). The LINKLODS support program was used to manipulate the LINKMAP output file (stream.out) to compute lod scores and convert recombination fractions into genetic distance (cM) estimates under the Kosambi level of interference. Multipoint location scores were calculated from the stream.out file with the LRP support program. Graphical representations of the multipoint linkage results were prepared with the SigmaPlot™ statistical analysis software.

2.7.5 Multipoint linkage analysis

2.7.5.1 LINKMAP

Multipoint analysis was performed initially with the LINKMAP program (LINKAGE 5.1) using the LCP interface. Memory constraints severely limited the computation of multipoint lod scores with LINKMAP for highly polymorphic markers [333] and imposed restrictions on the allowable number of loci and alleles at each loci. Alleles for the highly polymorphic markers were each down-coded to 4 alleles prior to running LINKMAP to conform to the MAXHAP (maximum

haplotypes) = 256 program constraint. To achieve this, alleles introduced by unrelated spouses were recoded to preserve linkage information and where possible, alleles with similar population frequencies were grouped. Allele frequencies for pooled alleles were adjusted accordingly in the parameter file. Alleles observed at the highly polymorphic D19S220 and D19S47 loci were each collapsed into four allele groups. The integrity of each recoding scheme was checked by calculating 2-point lod scores. By convention, the lod scores from the recoded markers should be within a range spanning the original score ± 0.30 [330].

2.7.5.2 FASTLINK

The FASTLINK programs are modified versions of the LINKAGE executable programs that have improved computational efficiency. The FASTLINK (DOS) version of LINKMAP allows for increased alleles at each locus and is free of a number of bugs associated with the LINKAGE programs. Versions of FASTLINK for both UNIX and DOS operating systems are distributed by Rice University. FASTLINK was obtained via anonymous FTP from the site ftp://softlib.cs.rice.edu/pub/fastlink. It transpired that the distributed programs had been recompiled with a version 486 PC (DJGPP compiler) and would not run independently on a Pentium processor (Prof. Alejandro Schaffer, personal communication). A memory manager program (CWSDPMI.EXE) was obtained with the DJGPP software for compiling UNIX software to run on the DOS operating system (URL: http://www.delorie.com, Dr. David Duffy, personal communication).

The fixed map order, recombination frequencies and intervals to be tested were defined for the LINKMAP and FASTLINK programs using the LCP interface. Recombination frequencies were obtained from the sex-averaged CHLC chromosome 19 linkage map (version 2.0) [330,334]. The use of the standard LINKMAP and FASTLINK programs in multipoint analysis is described further in Chapter 4.

2.8 SCREENING FOR NOVEL RYR1 MUTATIONS BY RT-PCR

2.8.1 Synthesis of cDNA from purified skeletal muscle total RNA

Synthesis of cDNA from purified skeletal muscle RNA template was performed with the SuperScript™ pre-amplification system. First strand cDNA synthesis reaction was catalysed by SuperScript II RNase H$^-$ Reverse Transcriptase. SuperScript has been engineered from the MMLV RT to remove the RNase activity that degrades mRNA during the reaction (SuperScript product information). The enzyme has increased thermal stability and can be used at temperatures up to 50°C to aid extension of templates with 2° structure.

Annealing and first-strand synthesis procedures were prepared with RNase-free barrier tips in DEPC-treated 0.5 ml tubes to avoid introduction of RNase activity. Temperature shifts were accomplished with the use of a pre-programmed Corbett™ thermal cycler.

2.8.1.1 First-strand synthesis with random hexamers.

Random hexamers were used to prime the first-strand synthesis for amplification of the 5' half of the RYR1 cDNA. A low ratio of random hexamers (RH) to template was used to favour the synthesis of longer cDNA molecules. Four primer/RNA annealing mixtures were prepared: two (reactions 1 and 2) with template RNA derived from the MHS muscle specimen, and two (reactions 3 and 4) with RNA extracted from the MHN control muscle specimen. Reactions 2

and 4 served as "no enzyme" controls to screen for genomic DNA (or other template) contamination in subsequent PCR procedures.

- 4-5 µg of total RNA (~1µg/µl) was mixed with 1 µl of the random hexamers (50 ng/µl) and DEPC-treated dH_2O to achieve a 12 µl total volume. Annealing mixtures were heated to 70°C for 10 minutes and chilled on ice for at least 1 minute.
- A cocktail reaction mixture was prepared, sufficient for *n + 1* (5) reactions; containing 10 µl of 10X PCR buffer, 10 µl $MgCl_2$ (25 mM), 5 µl of a 10 mM dNTP solution and 10 µl of 0.1 M DDT. 7 µl of this reaction mixture was added to each of the chilled, primer/RNA annealing mixtures from (2). Tubes were centrifuged and pre-incubated for 5 min. at 25°C.
- SuperScript™ II RT (1 µl) was added to one MHS and one MHN reaction (tubes 1 and 3). Enzyme was substituted with 1 µl of sterile DEPC-treated water in the two "no enzyme" control tubes (2 and 4). Reactions were pre-incubated for 10 minutes at 25°C to allow primary extension of the annealed hexamers before incubating for one hour at 42°C.
- First-strand synthesis was terminated by heating reactions to 70°C for 15 minutes. Reaction mixtures were chilled on ice and collected by brief centrifugation.
- 1 µl of RNase H (SuperScript kit) was added to each tube to remove the RNA template from the cDNA:RNA hybrid molecule. Reactions were incubated at 37°C for 20 minutes to allow RNA digestion, cooled to 4°C and stored at -20°C.

2.8.1.2 First-strand synthesis using Oligo(dT)

Oligo(dT) was also employed to prime synthesis of cDNA by hybridisation and extension from 3' poly (A) mRNA tails. The procedure was identical to that described for the random hexamer primed cDNA, apart from the following adjustments. 1 µl of 0.5 µg/µl oligo$(dT)_{12-18}$ was used in place of 1 µl of random hexamers in the annealing step. The 25°C pre-incubation steps were omitted. A 48°C extended incubation was selected to promote synthesis through template regions rich in secondary structure.

2.8.2 Amplification of cDNA for mutation screening by PCR (general method)

2.8.2.1 Primers for amplification of RYR1 cDNA

Amplification of the RYR1 cDNA was accomplished using primers provided from Professor T. McCarthy from the University of Cork, together with exon-based primers designed for RYR1 mutation analysis and PCR-RFLP. The chosen automatic sequence analysis strategy (in preference to SSCP or manual sequence analysis) permitted the use of larger fragments (up to 1800 bp).

2.8.2.2 Amplification of target cDNA

The SuperScript™ kit protocol recommends the use of 10% of the first strand reaction (i.e. 2 µl) in subsequent amplification of the target cDNA. However, optimal results were obtained using less than 0.5 % - 1% of the first strand synthesis reaction in each PCR (1 - 2 µl of a 15 - 20-fold dilution of random hexamer (RH)-primed cDNA, or 2µl of a 10-fold dilution of oligo-T primed cDNA). Barrier tips were used to aliquot all PCR reagents and templates to limit opportunities for PCR cross-contamination.

Hot-start PCR was performed in 50 µl reactions prepared with a cocktail reagent mixture (Table 2-8). 1-2 µl of the diluted cDNA template was added to 48 µl of the cocktail mixture. Sterile dH_2O was added to the negative control tube in place of cDNA. An identical set of reactions

were prepared for the "minus RT" controls. Tubes were mixed, overlaid with mineral oil and heated to 94°C. 0.5 µl (2.5 U) of *Taq* polymerase was mixed with each of heated reactions, finishing with the negative controls, and thermal cycles commenced as described below.

Table 2-8 Reaction components for amplification of cDNA.

Component	Concentration	Volume	Final Conc.	Cocktail (3 reactions +)
PCR buffer	10X	5 µl	1X	20 µl
$MgCl_2$	25 mM	3 µl	1.5 mM*	12 µl
Sterile dH_2O	--	25.5 µl	--	102 µl
dNTP's	3 mM	5 µl	0.3 µM	20 µl
Forward Primers	20 ng/µl	5 µl	2 ng/µl	20 µl
Reverse Primer	20 ng/µl	5 µl	2 ng/µl	20 µl
Aliquot per reaction				48 µl
cDNA template	1/15 dil. RH *or* 1/10 dil.Oligo(dT)	1.5 µl	0.5 % RT reaction	added to 48 µl of cocktail mix
Taq polymerase	5 U/µl	0.5 µl	0.05 U/µl	addition @ 94°C

* $MgCl_2$ concentration optimised for each primer set

2.8.2.3 Thermal cycle

Touchdown PCR was employed to minimise the trial and error process of PCR optimisation. A typical preliminary program would consist of an initial 3 minute denaturation at 94°C, followed by 5 amplification cycles at a stringent annealing temperature (94°C X 15 seconds, 61°C X 30 seconds, 72°C X 2 min) then 5 amplification cycles at a lowered annealing temperature (94°C X 15 seconds, 60°C X 30 seconds, 72°C X 2 min). This was followed by two or three 5-cycle amplifications with progressively lower annealing temperatures, before continuing with 30 repeats of a low-stringency amplification cycle (94°C X 15 seconds, 57°C X 30 seconds, 72°C X 2 min), concluding with a final 5 minute 72°C extension and a 4°C hold.

The negative control was scrutinised for DNA amplification indicative of contamination of one or more PCR reagents with template DNA. The "no RT" control was checked for amplification products which would indicate genomic DNA contamination of the RNA samples. In most cases, the amplification of genomic DNA was prohibited by the use of primers that spanned multiple exons.

2.8.3 Purification of amplified cDNA for automatic DNA sequencing

Contaminants such as primer-dimers and amplification primers and unincorporated nucleotides were removed from PCR products before sequencing with Wizard™ PCR DNA purification resin and Wizard™ minicolumns (according to manufacturers instructions). DNA was eluted in 50 - 100 µl of dH_2O, and larger products (> 800 bp) concentrated with a SpeedVac to approximately 20 µl volumes. Purified product yields were assessed by running a 1 µl sample of the solution on a standard agarose gels adjacent to a set of quantitation standards (20 - 100 ng). Products were either diluted with dH_2O or concentrated by SpeedVac to a concentration suitable for automatic sequencing. 400 bp - 800 bp fragments were concentrated to 20 - 50 ng/ µl, while 800 - 1600 bp products were adjusted to 40 - 80 ng/ µl).

2.8.3.1 Gel-purification

Where PCR reactions failed to yield discrete bands after repeated attempts, the fragment of interest was isolated away from contaminating PCR products, and primers by gel-purification from Nusieve™ agarose gel slices. The PCR product was concentrated by ethanol precipitation (with the addition of 0.1 vol 3 M sodium acetate, pH 5.2 and 2.5 vol 95% ethanol), dried, rehydrated and separated from contaminating products on a low melting point Nusieve™ gel, containing 0.5 μg/ml EtBr. The desired band was excised quickly from the gel with a sterile scalpel under UV light. The agarose slice (approximately 300 mg) was melted at 70°C; mixed with 1 ml of Wizard™ PCR preps purification resin, and purified using a 3 ml disposable syringe and a Wizard™ minicolumn as directed by the manufacturers' instructions.

2.8.4 Automated DNA sequence-analysis of amplified cDNA

Purified RYR1 PCR fragments amplified from cDNA of MHS and MHN were submitted together for automatic cycle sequence analysis with an Applied Biosystems 377-36 automatic sequencer with dye terminator chemistry. A 3.2 pmol/μl (~ 20 ng/μl) solution of the appropriate sequencing primer (PCR primer or internal oligonucleotide) was provided. Sequence strategies were designed to favour the use of internal primers where possible. Sequence obtained from the MHS sample was compared to that of the control (MHN) and published RYR1 sequence (accession number J05200) [126] using the GCG 'gap' and 'pileup' programs.

2.9 REAGENTS AND CHEMICALS

Specialised reagents used in this study are listed below, together with the name of the supplier. Unless otherwise stated, chemicals used in the preparation of buffers and other solutions were from Sigma™ chemicals, St. Louis, MO. USA.

Wizard™ DNA extraction kits were purchased from Promega Corporation, W.I , USA. The Genomix™ DNA extraction kit was purchased from Talent, Italy.
The 1 Kb DNA ladder, oligonucleotide primers for PCR, Trizol™ RNA extraction reagent and T4 Polynucleotide kinase were obtained from GibcoBRL/Life Technologies Inc. M.D, USA.
40 % 29: 1 and 19:1 bis-acrylamide was supplied by BDH chemicals Ltd., England. Nusieve™ agarose was from FMC Bioproducts, Rockland, Maine, USA.
Dynabeads-streptavidin complex was supplied by Dynal International, Norway.
Restriction endonucleases were obtained from Life Technologies, New England Biolabs Inc., M.A, USA and Promega Corporation, WI, USA.
Taq polymerase and reagents for PCR were purchased from Roche Diagnostics, NZ. and Promega Corporation, WI., USA.
RNasin RNAse inhibitor was obtained from Promega Corporation, WI., USA..
Sequenase™ Version 2.0 sequencing kit was from Amersham, UK.
X-Ray film and developing reagents were from KODAK, N.Y. USA.
Radioisotopes; γ^{33}P[ATP], and α^{35}S [dATP], were purchased from Amersham, UK. and New England Nuclear, Dupont, USA.

3. SCREENING FOR PUBLISHED RYR1 MUTATIONS

3.1 APPROACH TO THE SEARCH FOR REPORTED MH MUTATIONS

At the initiation of the project in 1994, 8 RYR1 mutations had been reported that were linked to MH in North American [106,107,167,168] and European families [13,109,110]. Linkage studies had revealed evidence of heterogeneity [26,27] with tentative linkage to a chromosome 17q MHS2 locus in a South African study [177]. Candidates at this locus included the adult sodium channel SCNA4 gene and genes encoding the β_1 and γ-subunits of the human skeletal muscle L-type voltage-dependent calcium channel [177]. However another study did not support linkage to the chromosome 17q locus [180]. Mutations had not been identified in any other genes at this time.

3.1.1 Preliminary mutation-screening

Five of the early reported RYR1 mutations listed in Table 3-1 alter commercially available RE recognition sites and could be detected by simple PCR-RFLP analysis. Three mutations did not alter recognition sites for commercially available RE and were investigated by manual direct sequence analysis of PCR-amplified regions of genomic DNA (Table 3-1). The amplification created restriction site (ACRS) method [311,335] was also used to screen for the Tyr522Ser mutation.

Table 3-1 Early RYR1 mutations and methods of detection

Substitution	Nucleotide transition	Reference	Method of detection
Arg163Cys	C487T	[13]	RFLP (*Bst* UI)
Ile403Met	C1209G	[13]	RFLP (*Mbo* I)
Arg614Cys	C1840T	[106]	RFLP (*Rsa* I)
Gly2434Arg	G7297A	[110,167]	RFLP (*Dde* I or *Alw* NI)
Arg2435Cys	G7301A	[168]	RFLP (*Hga* I)
Gly248Arg	G742A	[107]	Direct sequence analysis
Gly341Arg	G1021A	[109]	Direct sequence analysis
Tyr522Ser	A1565C	[108]	Direct sequence analysis or ACRS

PCR primer sequences are given in appendix A 1. MHS subjects from 33 NZ MH families were screened for 8 mutations in the RYR1 gene that were known when the project was initiated.

3.1.2 Screening for mutations in selected families

Nine additional RYR1 mutations were revealed at the eighth International MH workshop in September 1996 taking the total number to 17 at that time. Three were located in the N-terminal mutation region while six were clustered in exons 39, 40 and 46 of the central RYR1 region, as described in Table 3-2. Conveniently, four of the mutations in the central mutation region removed recognition sites for *Bsr* BI, facilitating simultaneous PCR-RFLP screening. Restriction endonuclease maps of genomic DNA sequence [167] surrounding each of the new reported mutations were generated with the GCG package to investigate opportunities for simple RFLP screening methods (as indicated in Table 3-2). The nucleotide and amino acid positions and

substitutions pertaining to each of the reported RYR1 mutations, and associated exon-based primer sequences are marked on the corrected RYR1 sequence presented in Appendix 2.

In view of the increasing number of RYR1 mutations and reports of genetic heterogeneity in MH [27,29,32,177] together with the relatively low frequency of other reported mutations in NZ MH families, the approach to the RYR1 mutation screening was subsequently revised. Individuals were studied from only five relatively well characterized NZ families in which MH events have been confirmed by IVCT examination were screened for the new mutations.

Table 3-2 RYR1 mutations and methods of detection in selected families

Substitution	Nucleotide transition	Reference	Method of detection
Cys35Arg	T103C	[165]	Direct sequence analysis
Arg614Leu	G1841T	[109]	Direct sequence analysis
Arg552Trp	C1654T	[111]	PCR-RFLP (- *Mbo* I)
Arg2163Cys	C6847T	[25]	PCR-RFLP (- *Bsr* BI, + *Bgl* II)
Arg2163His	G6848A	[25]	PCR-RFLP (- *Bsr* BI)
Arg2458His	C7372T	[169]	PCR-RFLP (- *Bsr* BI)
Arg2458Cys	G7373A	[169]	PCR-RFLP (- *Bsr* BI)
Val2168Met	G6502A	[25]	Direct sequence analysis
Thr2206Met	C6617T	[25]	Direct sequence analysis

PCR primer sequences are given in appendix A 1. Cys35Arg introduced a recognition site for the *Aci* I enzyme, however several nearby non-polymorphic *Aci* I sites prevented simple RFLP analysis. The Arg552Trp mutation removed recognition sites for the enzymes S*au* 3 AI, *Mbo* I, *Nde* II, *Dpn* II and *Dpn* I. MHS individuals from 33 MHS families were screened for the Arg552Trp mutation with *Mbo* I. Only five important families were investigated for the remaining mutations. The Val2168Met substitution introduces *Nla* III and *Msl* II sites and removes a *Bsg* I site; however the enzyme cost prohibited RFLP screening. The presence of the Arg2458Cys/His mutations in 31 NZ MH families was later excluded by SSCP analysis of exon 46, as described in Chapter 5, section 5.6.2.

3.1.3 Screening for a mutation in the CACNL1A3 gene

The first mutation in a gene other than RYR1 was reported in the CACNL1A3 gene encoding the α_1 subunit of the voltage dependent calcium channel [33]. The G3333A transition in exon 25 of this gene substitutes Arg1086 for His and removes a *Cfo* I (*Hha* I) cleavage site. Representative members of each of the NZ MH families were screened for the presence of the Arg1086His mutation by PCR-RFLP with *Cfo* I.

3.2 MUTATION SCREENING BY PCR-RFLP ANALYSIS

Susceptibility to MH has been identified in individuals from 33 NZ families. DNA was extracted from fresh blood samples collected from representative individuals in each family, and used in a screen for published mutations within the RYR1 gene [13,25,106-111,165,167-169]. Several reports of discordance between MH and RYR1 mutations have attributed MHE and weak MHS phenotypes in individuals with normal genotype to the lack of specificity of the IVCT [105,112,167]. Consequently, MHS individuals with the strongest muscle contracture responses in the IVCT from each family were preferentially selected for mutation screening.

The genetic and IVCT details for the NZ families investigated for susceptibility to MH and RYR1 mutations are summarised in appendix 5.

3.2.1 PCR

PCR primers were designed to amplify regions of genomic DNA encompassing each mutation. Each initial primer set included one biotinylated oligonucleotide and one internal sequencing primer to facilitate confirmation of any mutations by direct sequence analysis. PCR conditions were optimised for each primer set by varying annealing temperatures and $MgCl_2$ concentration. Examples of the effects of a $MgCl_2$ titration and annealing temperature on the yield and specificity of PCR reactions is shown in Figure 3-1. PCR primer sequences are detailed in appendix 1.

3.2.2 RFLP digests

The Arg163Cys [13], Ile403Met [13], Arg614Cys [106], Gly2434Arg [110] and Arg2435Cys [168] mutations remove recognition sequences for *Bst* UI, *Mbo* I, *Rsa* I and *Hga* I respectively. In each case, DNA corresponding to the normal allele was cleaved into two fragments of appropriate size that permitted differentiation from any uncut material (indicative of a mutant allele) by gel electrophoresis. Expected fragment sizes derived from the digestion of the normal and mutant alleles for each RYR1 mutation are presented in Table 3-3. The screen for the Arg163Cys mutation was refined with the design of a new primer set, made possible with the publication of RYR1 intron sequences [160]. PCR with the 163Fi-bio and 163iR primers yielded a 207 bp PCR product and larger B*st* UI digest fragments that were more readily resolved by agarose gel electrophoresis.

The chosen strategy for screening for the detection of the Gly2434Arg mutation differed to that reported [110,167]. The region was amplified with primers designed for the screening of the adjacent Arg2435Cys mutation [168] and digested with either *Dde* I or *Alw* NI. The PCR product encompassed an additional, non-polymorphic *Dde* I site that served as an internal positive control for enzyme activity

Figure 3-1 Effects of $[Mg^{+2}]$ on PCR amplification yield and specificity

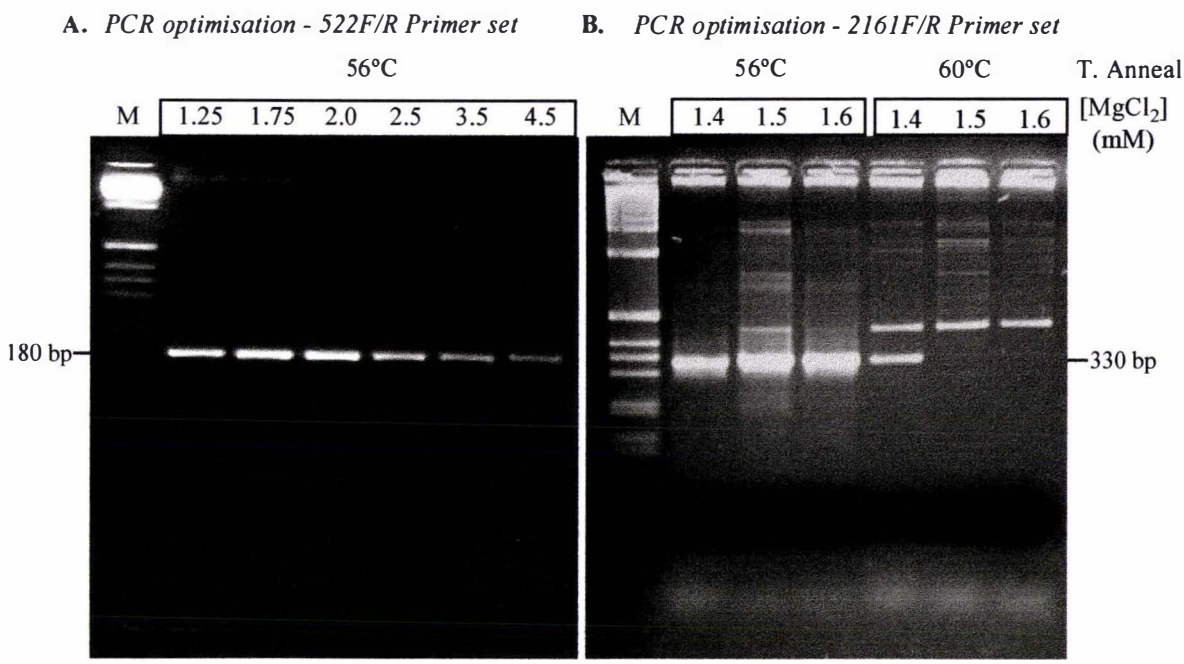

A. Amplification of a 180 bp product including the Y522S mutation site at varying $[Mg^{+2}]$. M = 1kb DNA ladder. 50 µl reactions include 250 ng 522F and R primers, 0.3 mM dNTP, ~250 ng genomic DNA. 5 µl of each reaction was loaded. Electrophoresis: 3 % Nusieve™ gel in 1X TAE. Gel stained in 0.5 µg/ml EtBr, and photographed under UV light.

B. Amplification of the 330 bp R2163H/C mutation region with 2161F and 2161R primer set. Reaction conditions as for Figure A. A non-specific higher molecular weight product is preferentially amplified at higher $[Mg^{+2}]$ and annealing temperatures. 5 µl of each reaction was loaded. Electrophoresis: 3 % Nusieve™ gel in 1X TAE. Gel stained in 0.5 µg/ml EtBr, and photographed under UV light.

Table 3-3 PCR-RFLP analysis of published RYR1 mutations.

Mutation [ref]	**PCR Primers**	**RE site altered**	**Fragment size**	
			Normal allele	**Mutant**
R163C [13]	163F- bio - 163R	- *Bst* UI	76 bp	44, 32 bp
R163C [13]	163F-bio - 163I-R	- *Bst* UI	207 bp	121, 86 bp
I403M [13]	403Fseq - 403R-bio	- *Mbo* I	80 bp	53, 27 bp
R614C [106]	614F-bio - 614R	- *Rsa* I	132 bp	86, 44 bp
G2434R [110,167]	2434F - 2434R-bio	+ *Dde* I, *Alw* NI	130, 62 bp	95, 24 bp
R2435C [3]	2434F - 2434R-bio	- *Hga* I	210 bp	110 , 90 bp

Primer sequences are given in appendix 1. PCR conditions are outlined in Materials and Methods, section 2.5.

An inherent problem in this type of analysis is incomplete RE digestion of the PCR products. This can be misinterpreted as heterozygous status for mutations that are revealed by the presence of undigested DNA. Digest failure was signalled by a lower than expected ratio of uncut to cut fragments and residual undigested DNA in the control digests. Various DNA purification procedures were investigated unsuccessfully to improve digest efficiency. These included micro-dialysis, ethanol precipitation, purification with Strataclean™ resin and centricon™ spin columns.

Substantial quantities of both enzyme (2-3 µl) and DNA (15-25 µl PCR product) in 30-40 µl reaction volumes were required to achieve complete RE digestion and visualisation of small PCR products. The inhibitory action of glycerol and PCR reaction components prevented the use of small reaction volumes (15 µl). Samples were therefore concentrated by ethanol precipitation to remove salt and reduce volumes to 10- 15 µl, convenient for gel electrophoresis. Digest products were resolved by PAGE on 10-15 % gels in 1X TBE or by agarose gel electrophoresis with 3.5 % Nusieve™ agarose.

PCR-RFLP results for two MHS individuals investigated for the Arg163Cys, Arg614Cys, Ile403Met and Arg2434His mutations are presented in Figure 3-2. Both individuals display the digest pattern characteristic of the normal genotype (-/-) for the Arg614Cys, Ile403Met and Arg2434His mutations as indicated by complete digestion of the PCR products with *Rsa* I, *Mbo* I and *Hga* I respectively. Individual M218 (family 35) is heterozygous for the Arg163Cys (C487T) mutation (+/-). This was revealed by the presence of the uncut 76 bp band in the *Bst* UI digest of DNA derived from the mutant allele in combination with the 44 and 32 bp bands derived from cleavage of the normal allele. Individual M230 displays the *Bst* UI digest pattern representative of the homozygous normal genotype for Arg163Cys.

Figure 3.2 Screening for published RYR1 mutations by PCR-RFLP

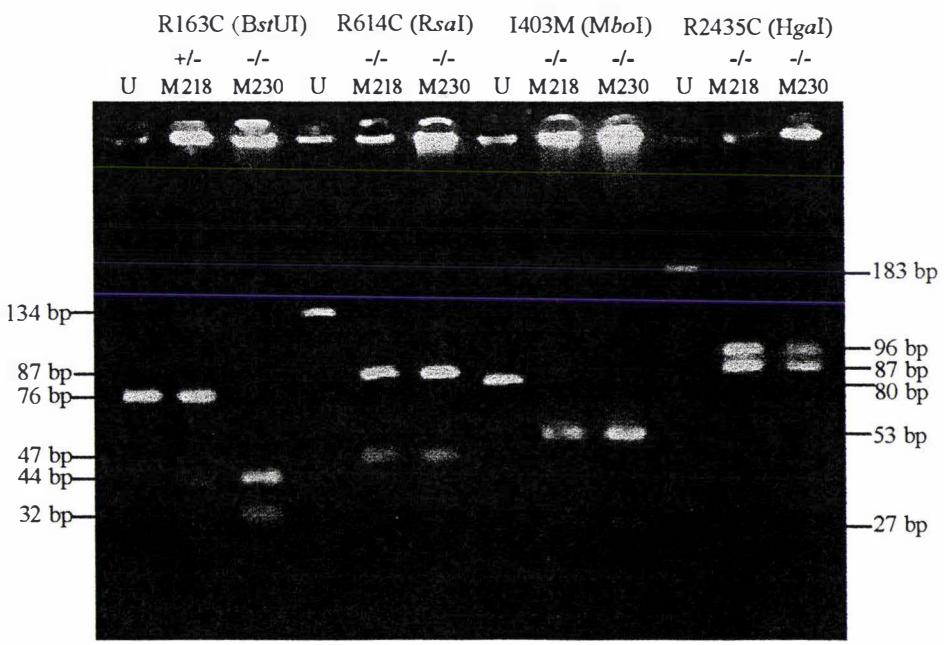

Regions encompassing RYR1 mutations were PCR-amplified from genomic DNA from two MHS probands and screened for published mutations by RE diegestion. Digest products were concentrated by ethanol precipitation, resolved on a 3.5% Nusieve™ gel in 1X TAE and stained in 0.5 µg/ml EtBr. U= undigested DNA.

Members of 33 NZ MH families, including four representative MHS members of the large Maori CH family were screened for the presence of 5 of the early reported RYR1 mutations (described in Table 3.1) by PCR-RFLP. The Ile403Met, Arg614Cys and Arg2435Cys mutations were not detected in any of the samples examined. Two mutations, Arg163Cys and Gly2434Arg were detected in two unrelated NZ families by PCR-RFLP.

3.2.3 Detection of the Arg163Cys mutation in family 35

The C487T transition that substitutes Arg163 for Cys was detected in the DNA of a single proband who had survived an MH reaction upon exposure to isoflurane for repair of the ulnar collateral ligament of the left thumb. The reaction ranked five on the MH clinical grading scale [44] indicating MH was very likely (A clinical case report is given in appendix 6.5). The proband and her father were subsequently subjected to a muscle biopsy, and both were diagnosed MHS by IVCT with strong abnormal contracture responses to both halothane and caffeine. The Arg163Cys mutation was also detected in the DNA from the proband's sister (M219) and her father (M218) by the loss of the *Bst* UI restriction site (Figure 3-3). The mother (M220) was normal with respect to the Arg163Cys mutation. Both the mother and the sister of the proband have declined muscle biopsy examination.

The presence of the C487T transition in the PCR-amplified DNA of the MHS father (M218) was confirmed by direct manual sequence analysis (Figure 3-4), and subsequently by automatic sequence analysis (Figure 3-5). The mutation was revealed by the presence of bands in adjacent lanes (Figure 3-4) and by two overlapping peaks in the automated sequence electropherogram (Figure 3-5), demonstrating the efficacy of both methods in the detection of RYR1 point mutations.

Figure 3.3 Detection of the C487T (Arg163Cys) mutation by PCR-RFLP

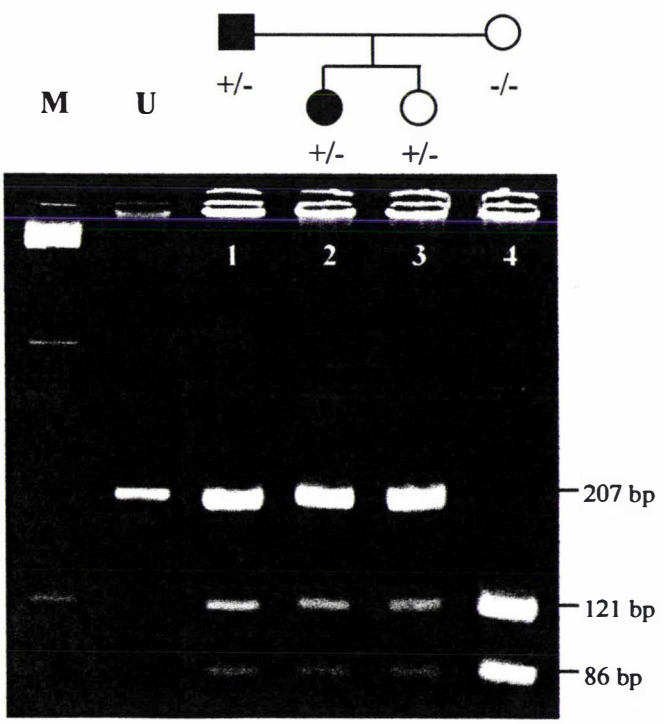

Agarose gel electrophoresis of PCR products before (lane U) and after (lanes 1 - 4) digestion with *Bst* U1 restriction enzyme. (3.5 % Nuiseve™ gel in IXTAE, stained in 0.5 µg/ml EtBr). The C487T mutation is revealed by the presence of undigested 207 bp PCR product. Genomic DNA was amplified with the amplified with the 163iF and 163iR primer pair.

Lane 1; M218, MHS, positive
Lane 2; M142, MHS proband, positive
Lane 3; M219, Not tested, positive
Lane 4, M220, Not tested, negative.

Figure 3-4 Manual sequence analysis of the C487T (Arg163Cys) mutation

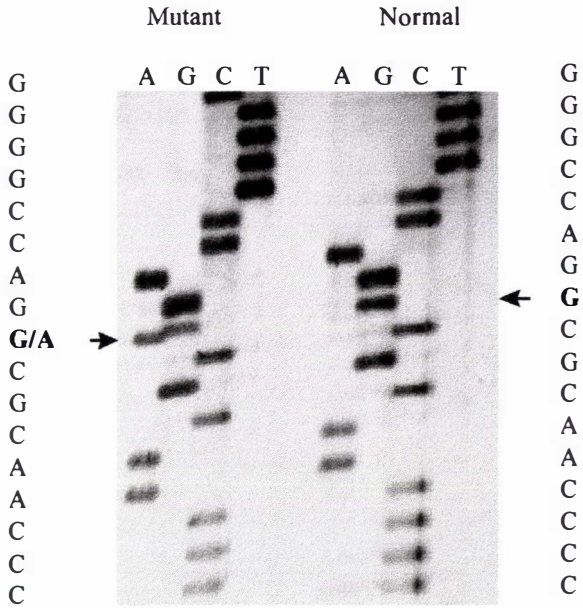

The C487T mutation was confirmed in the amplified genomic DNA of MHS individual M218 (left) by direct solid-phase sequence analysis. The normal sequence is displayed by his spouse, M220 (right). Arrows indicate the position of normal and mutated nucleotides.

The biotinylated 207 bp PCR product generated by PCR with the 163Fi-bio and 163Ri primer pair. Sequencing was performed with the reverse PCR primer (antisense strand is shown). Sequencing reactions were resolved by 7% denaturing PAGE in 1XTBE, at 60W (constant power).

Figure 3-5 Automated sequence analysis of the C487T (Arg163Cys) mutation

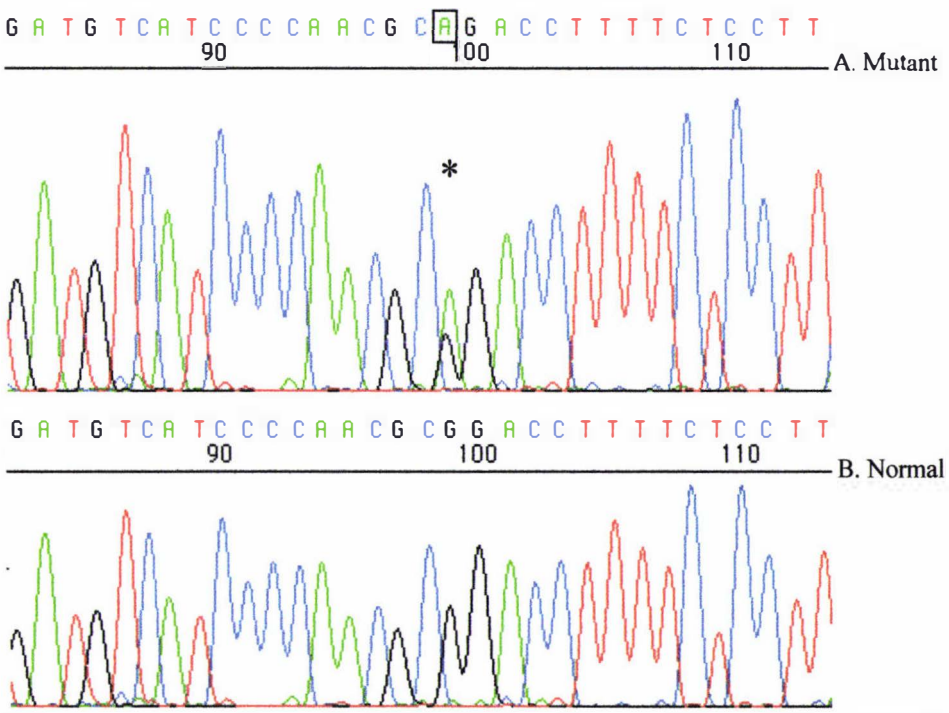

Direct sequence analysis of the 207 bp PCR product amplified with the 163Fi-bio/163iR primers. Sequencing reactions were primed with the reverse 163iR PCR primer. PCR products were purified using the Wizard™ PCR preps purification system and sequenced with an ABI-377-18 automatic sequencer using dye terminator chemistry. The mutation is indicated with an asterisk. A: MHS individual M218 (+/-). B: Individual M220 (-/-).

3.2.4 Segregation analysis of the Arg163Cys mutation in family 35

The RFLP and sequence analysis indicated that the proband and her sibling had inherited the Arg163Cys mutation paternally, in keeping with the IVCT diagnosis of MHS in the father. The father has one brother (M280) who was normal with respect to the Arg163Cys mutation. Both paternal grandparents of the proband are deceased and post-mortem DNA samples from these individuals were not available.

In an attempt to identify the origin of the mutation, DNA was isolated from the blood of 32 extended relatives of both paternal grandparents and screened for the mutation by PCR-RFLP as described. Individuals from the extended pedigree screened for the Arg163Cys mutation are indicated in Figure 3-6. One of the paternal grandparents is of Danish descent, and there may be some familial link to a Danish kindred in which the Arg163Cys mutation has been reported [13,336]. However, a link between this NZ family and MH families on the Danish MH register could not be established (H. Ording, personal communication). The sole surviving sibling of the paternal grandfather tested negative for the mutation. Eight fourth-generation offspring of four other siblings also tested negative. DNA from descendants of the remaining eight siblings was not available. Distant cousins of the paternal grandfather; M358 and M295 were both normal.

All relatives of the paternal grandmother were also negative with respect to the Arg163Cys mutation. Tested individuals included two surviving siblings of the paternal grandmother and eight representative offspring of three other third generation siblings. Further analysis was limited by the availability of DNA samples, thus the presence of the mutation can not be ruled out in other extended family members from either side of the family.

There is no history of MH in family 35 aside from the single MH reaction in the proband (M142). The mutation may have occurred *de novo* in the father of the proband (M218) or in the previous generation. A segregation analysis was performed using a panel of chromosome 19q markers flanking the RYR1 locus in an attempt to trace the affected RYR1 haplotype within the immediate family of the proband. DNA samples were genotyped for the RYR1 gene microsatellite (RYR1CA) [327], three RYR1 intragenic RFLPs (RYR-RFLP3) and RYR1 linked microsatellites D19S220 [325,326], D19S190 [329] and D19S47 [328], as described in Chapter 4 (section 4.6).

The identification of a common chromosome 19q pattern shared by individuals with and without the C487T mutation would support the occurrence of a *de novo* mutation in the father of the proband. An analysis of the chromosome 19q markers indicated that the mutation coincided with the inheritance of the 7-1-1-1-8 haplotype, which was shared by both the MHS father (M218) and his daughter (M219), as presented in Figure 3.6. Insufficient DNA from the proband (M142) was available to include this individual in the analysis. A paternal uncle of the proband (M280) who was diagnosed negative for the mutation has also inherited the 7-1-1-1-8 haplotype. The occurrence of the putative disease-linked 7-1-1-1-8 haplotype in both the affected (M218) and unaffected (M280) brothers would suggest that the C487T transition has occurred *de novo* in the father of the proband. However, because the haplotypes could not be ascertained for the deceased grandparents, the possibility that the two brothers (M218 and M280) have inherited the same 7-1-1-1-8 pattern from different parents cannot be excluded. Thus, the source of the Arg163Cys mutation in this pedigree can not be defined.

Figure 3.6 Segregation of the R163C mutation in family 35.

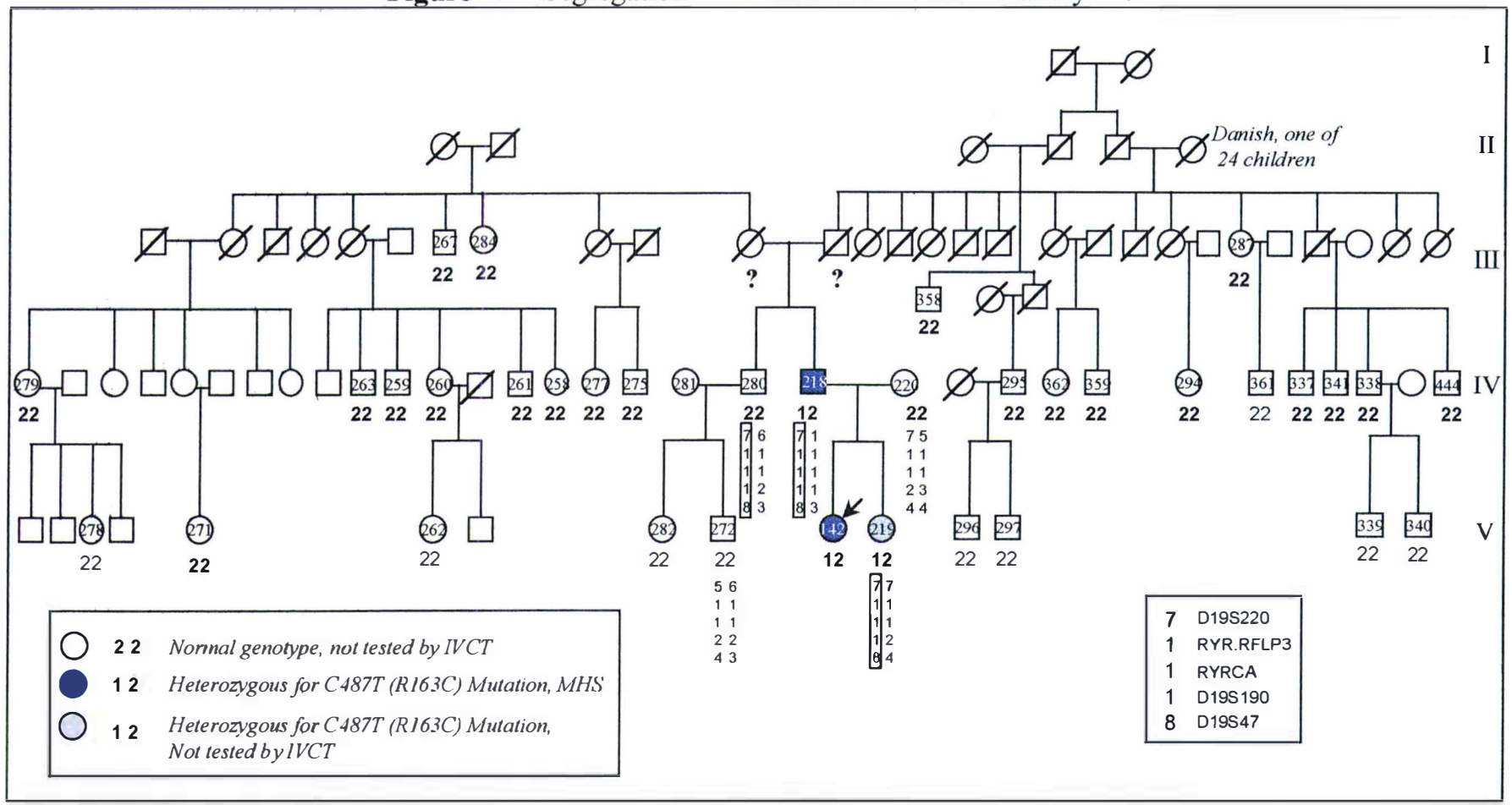

Partial pedigree of family 35, indicating representative families with members tested for the R163C mutation by PCR-RFLP. and haplotype analysis with chromsome 19q markers. DNA identification numbers are shown within symbols. The proband (indicated with an arrow) suffered a fulminant MH crisis and together with her sibling, inherited the mutation (**12**) paternally. All tested relatives (**22** genotype) and their offspring (22) are normal with respect to the R163C mutation.

3.2.5 Detection of the Gly2434Arg mutation in family 5

A RYR1 mutation that substituted Gly2434 for Arg [110,167] was revealed in a single NZ pedigree by the introduction of a restriction site for the enzyme *Dde* I (Figure 3-7). Automatic sequence analysis of the region amplified from genomic DNA of an MHS individual confirmed the G7297A mutation was identical to that reported previously (Figure 3-8). Sequence was compared to that from an MHS individual from the CH family who had previously tested negative for the Gly2434Arg mutation by PCR-RFLP. Sequence analysis indicated both individuals were normal with respect to the adjacent Arg2435His mutation, confirming the results of earlier *Hga* I RFLP analysis. A silent C to A mutation was detected in intron 45 sequence from the MHS CH family member (M221). This polymorphism did not alter any recognition sites for any commercially available restriction enzymes.

Figure 3-7 PCR-RFLP detection of the Gly2434Arg mutation in Family 5

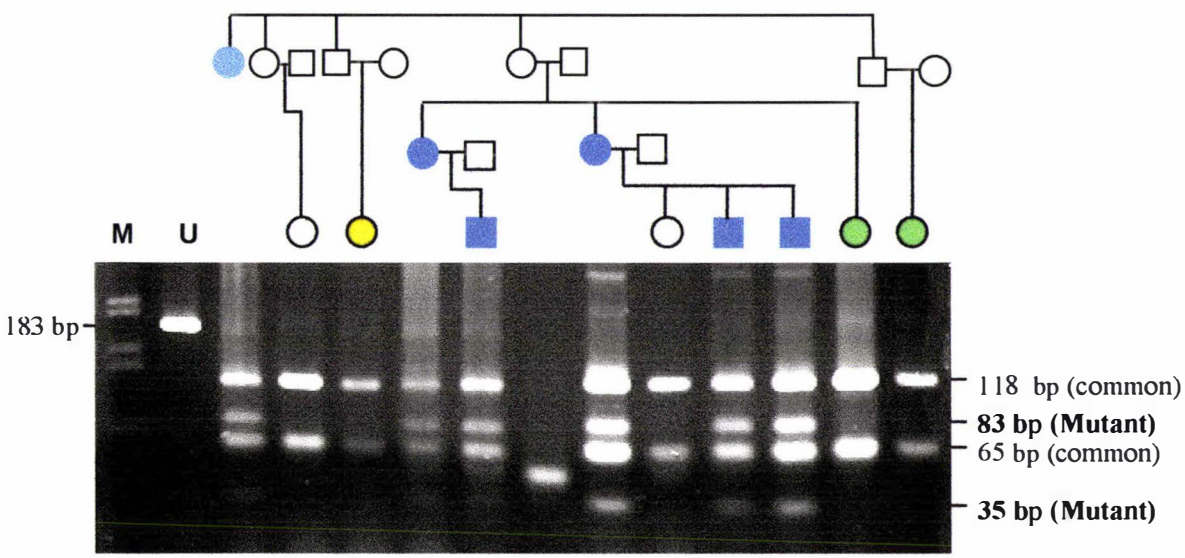

Detection of the G7297A (Gly2434Arg) mutation with IVCT phenotype in members of family 5 by the introduction of a cleavage site for *Dde* I. Normal alleles are cleaved into two 118 and 65 bp fragments. The G7301A mutation is revealed by further digestion of the 118 bp fragment into 83 bp and 35 bp. Electrophoresis: 3.5% Nusieve™ gel in 1X TAE. 20 µl of each PCR product was digested with *Dde* I. The entire volume was concentrated by ethanol precipitation, redissolved in 10 µl of buffer and loaded onto the gel.

Figure 3-8 Confirmation of the Gly2434Arg mutation by automated DNA sequence analysis

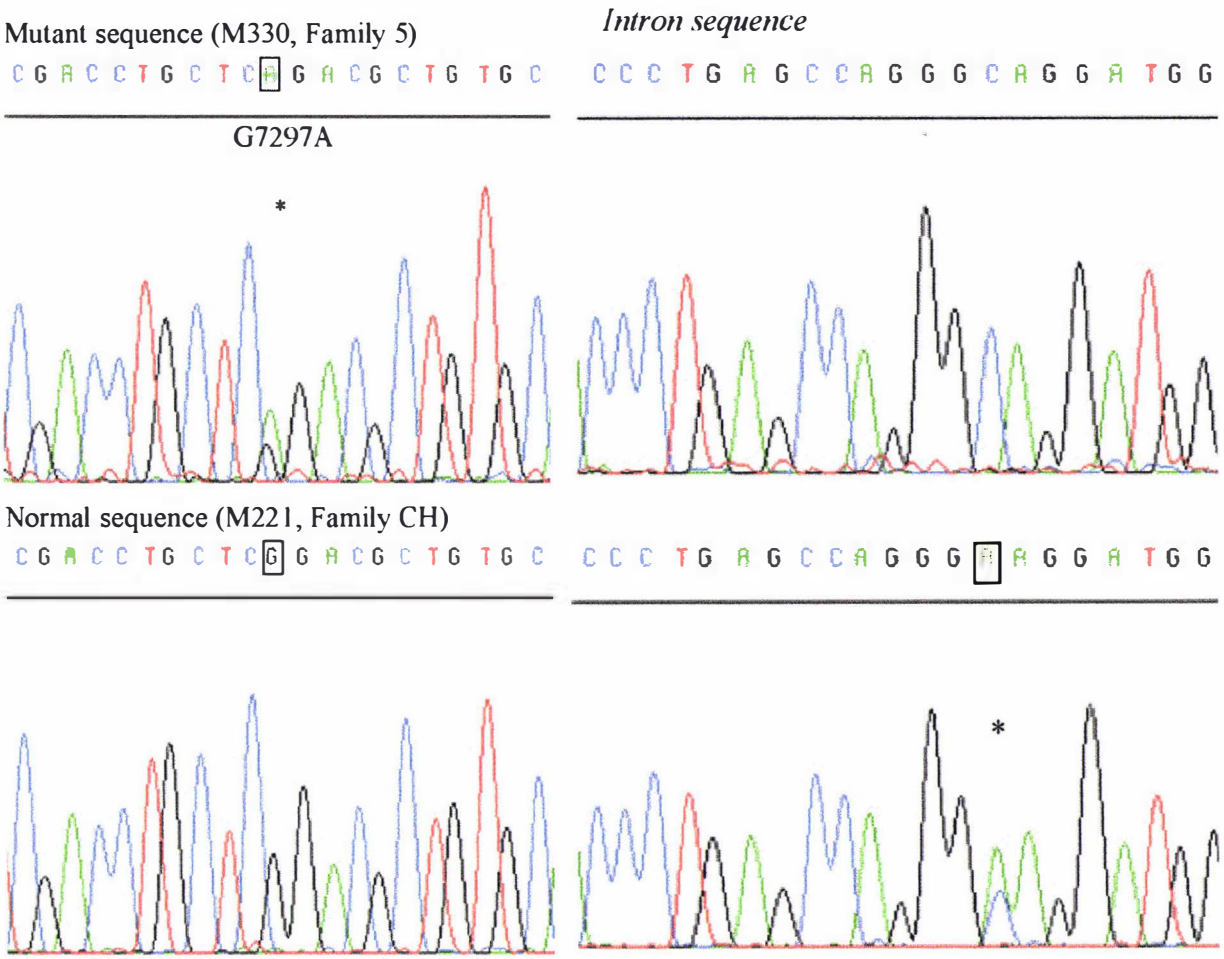

Electropherogram, confirming the presence of the G7297A mutation (Gly2434Arg) in amplified genomic DNA from MHS member of family 5 (M330, top left). The normal sequence, shown for comparison was derived from an MHS member of the CH family (M221, bottom left). A silent C to A polymorphism located individual 20 bp into intron 45 sequence was detected nearby in the sequence from this individual (M221, bottom right). PCR primers; 2434F/2434R. Sequencing primer: 2434F-seq. Sequencing performed using an ABI-377-18 automatic sequencer with dye terminator chemistry.

3.2.6 Segregation of the Gly2434Arg mutation in family 5.

The proband (M317) was a 15 year-old male who suffered an MH episode whilst undergoing emergency surgery for a broken leg. A clinical case report is given in appendix 6.3. Extended family members were screened for the Gly2434Arg mutation by PCR-RFLP with either D*de* I or A*lw* NI. The mutation was not detected in the DNA of 8 individuals diagnosed MHN or MHE(h). 7 MHS family members and one obligate carrier displayed the RFLP pattern indicating heterozygous status for the Gly2434Arg mutation. Thus, the mutation segregated with MHS in this pedigree, consistent with a causative role in the MH syndrome.

The association between the mutation and the MHS phenotype was assessed statistically by conducting genetic linkage analysis. LINKAGE 5.1 program parameters included a disease and mutation allele frequency of 0.0001 and 0.0001 respectively, a mutation rate of 0.00001, a phenocopy rate of 0.01 and 0.99 penetrance of the disease allele.

Theoretical and practical aspects of genetic linkage analysis are discussed in Chapter 4. A pairwise linkage analysis of the pedigree summarised in Figure 3-9 generated a lod score of 2.86 ($\theta = 0$) for linkage of MHS to the RYR1 mutation locus, consistent with a causative role for the Gly2434Arg mutation in MH in this kindred. MHE(h) individuals who recorded normal (<0.2 g) IVCT contracture responses to 2 mM caffeine and contracture responses to 2% halothane in excess of the 0.2 g threshold were entered as "status unknown" in the linkage calculations. When the affection status of the four individuals with MHE IVCT responses was changed to the "normal" (1 1) phenotype, the support for linkage increased to a maximum lod score of 3.32 at $\theta = 0$.

The caffeine test data correlates more closely with the Gly2434Arg genotype than does the halothane test data. Of the seven subjects examined by muscle biopsy who were negative for the mutation, only one registered a response to the 2 mM caffeine test (0.15 g). This individual (M110) was initially diagnosed MHS, and was screened for the presence of the eight early RYR1 mutations, including the Gly2434Arg mutation before DNA samples from definite MHS family members were available. This finding reinforced the importance of selecting individuals with the strongest contracture responses from families undergoing mutation analysis.

Several factors support a causative relationship between the Gly2434Arg mutation and MHS in this family. These include: 1) reports of the mutation in at least nine other MH families [110,161,167], 2) the strict conservation of the residue across all known sequences of the ryanodine receptor gene family (Chapter 6, Figure 6.7B), 3) evidence from biochemical studies supporting a causative relationship with MH [300] and 4) Complete co-segregation of the Gly2434Arg mutation with MHS in the family 5.

Figure 3.8 Segregation of the G2434R mutation with MH in family 5

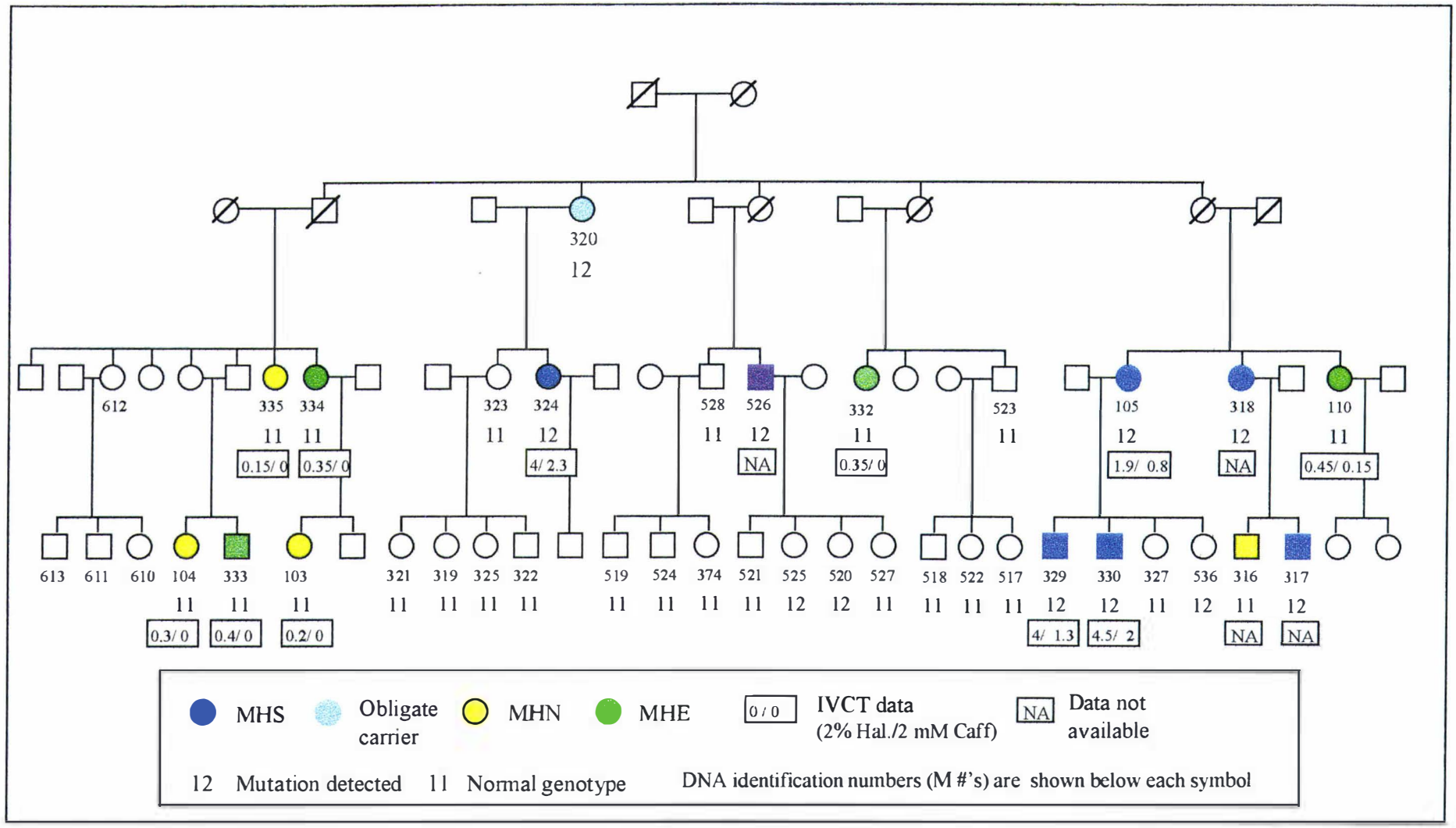

3.2.7 Screening for further RYR1 mutations by PCR-RFLP in key families

Members of four key NZ families were screened for the Arg552Trp mutation by direct sequence analysis and probands from 25 families were examined by PCR-RFLP analysis with *Mbo* I. None of the DNA samples from MHS individuals displayed the expected sequence profile or RFLP pattern characteristic of the Arg552Trp mutation.

Repeated attempts to amplify exon 39 to search for the Arg2163Cys, Arg2163His mutations and Val2168Met mutations with the 2161F and 2161R intron-based primers failed to generate discrete products. A product of the expected size was eventually amplified with the use of a touchdown PCR cycle (annealing temperature varied from 56°C to 54°C) under stringent conditions (1.25 mM $MgCl_2$) as demonstrated in Figure 3-1. The use of more stringent annealing temperatures unexpectedly enriched the reactions for a non-specific, higher molecular weight product. The Arg2163Cys mutation introduces a site for *Bgl* II and removes a *Bsr*BI site. One MHS member of the CH family screened for the Arg2163Cys mutation by PCR-RFLP with *Bgl* II displayed the pattern expected of the normal genotype (no B*gl* II digestion). A *Bgl* II digest of a 134 bp DNA fragment known to contain a *Bgl* II site was included as a positive control for enzyme activity (Figure 3-10 B).

An alternative set of primers was designed from published intron sequences (38int286F and 39int616R) [160] to amplify exon 39. A search for the Arg2163Cys or Arg2163His mutations in regions of amplified genomic DNA from four key families was accomplished by *Bsr*BI digestion of the resultant 331 bp product. The involvement of the Val2168Met in the large Maori CH family was excluded by direct sequence analysis of exon 39, amplified from the DNA of a representative MHS individuals with the new primer set. This site was not investigated in other MH families due to the difficulties in obtaining pure PCR products, and the expense associated with DNA sequencing.

The Arg2458Cys and Arg2458His mutations in exon 46 were investigated by PCR-RFLP with *Bsr* BI . The initial primer set was designed from intron 45 and 46 sequence (2456F, 2456R) submitted to Genbank [160], (accession number, U48477). Repeated amplification attempts failed to yield a discrete product of the expected size. A second primer set designed from intron 45 (RYR45intF) and exon 47 sequences (47exR) successfully amplified a product of the appropriate size. According to the published sequence, the resultant PCR product should have been cleaved by *Bsr* BI into two 155 bp and 193 bp fragments in the absence of the Arg2458His/Cys mutations. However, the *Bsr* BI digest unexpectedly resulted in three fragments of 155 bp, 115 bp and 78 bp, consistent with the presence of an extra *Bsr*BI cleavage site (Figure 3-10 A).

Exon 46 of theRYR1 gene was subsequently amplified from an MHS DNA with the 45int(616)F and 47exR primer set and examined by automated sequence analysis. This revealed a number of discrepancies between the submitted sequence [160] and the actual sequence (Figure 3-11). The errors in the original sequence encompass the original reverse primer binding site, explaining the failure of all PCR attempts employing the 2456R oligonucleotide. In addition, the corrected sequence contained an extra, non-polymorphic *Bsr* BI cleavage site, in agreement with the observed RFLP digest results. The *Bsr*BI digest pattern was consistent for samples investigated from five unrelated families. This confirmed that the sequence discrepancy was the result of errors in the published intron sequence. The sequence discrepancies may have resulted from a series of compressions in the original manual sequencing that are usually resolved by automatic DNA sequence analysis [330].

Compression artifacts may have resulted in errors in other published RYR1 intron sequences. If so, PCR with primers designed to anneal to intron sequences may be particularly problematic. The difficulties encountered during the amplification of exons 39 and 40 with intron-based primers may have been related to further sequence errors, although this has not yet been confirmed by automatic sequence analysis.

Figure 3-10 PCR-RFLP screen for Arg2458His/Cys and Arg2163Cys mutations

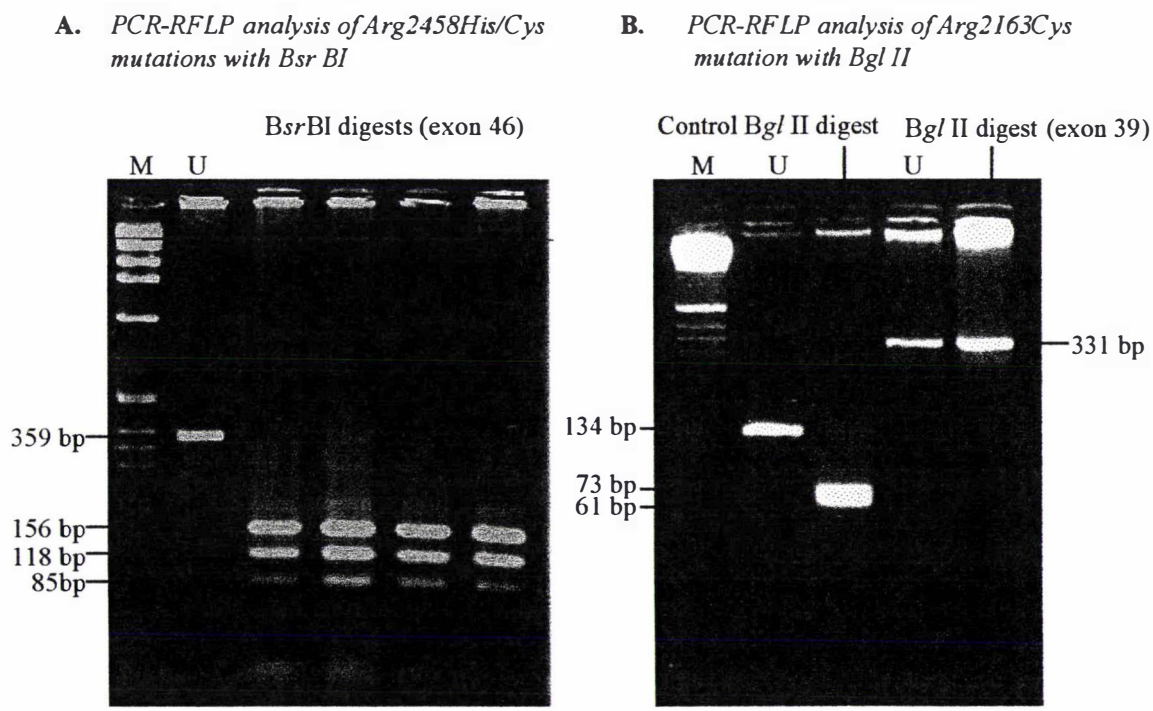

A. The 359 bp products were amplified from genomic DNA with RYR45intF and RYR47exR primers, digested with B*sr*BI, concentrated and separated on a 3% Nusieve gel in 1X TAE (stained with 0.5 μg/ml EtBr). The Arg2458Cys/His mutation would be detected by the removal of a *Bsr* BI site and the appearance of a 274 bp fragment (cleaved in the normal sequence to 156 and 118 bp fragments). All four individuals are normal with respect to these mutations. U = uncut DNA. M = 1 kb DNA marker.

B. RFLP analysis of the Arg2163Cys mutation site. Digested PCR products were concentrated and separated on a 3.5% Nusieve™ gel in 1X TAE (stained in 0.5 μg/ ml EtBr). The C6487T (Arg2163Cys) mutation would be revealed by *Bgl* II digestion of the 331 bp PCR product into 234 bp and 97 bp fragments. DNA amplified from a MHS individual from the CH family with the RYR38intF and RYR39intR primer set (lane 4) is not cleaved by *Bgl* II (lane 5), indicating normal Arg2163 genotype. The *Bgl* II digestion of a 134 bp PCR product (amplified with the 614F and 614R primer pair), into 73 and 61 bp fragments served as a positive control for enzyme activity.

Figure 3-11 Detection of errors in intron 46 published sequence

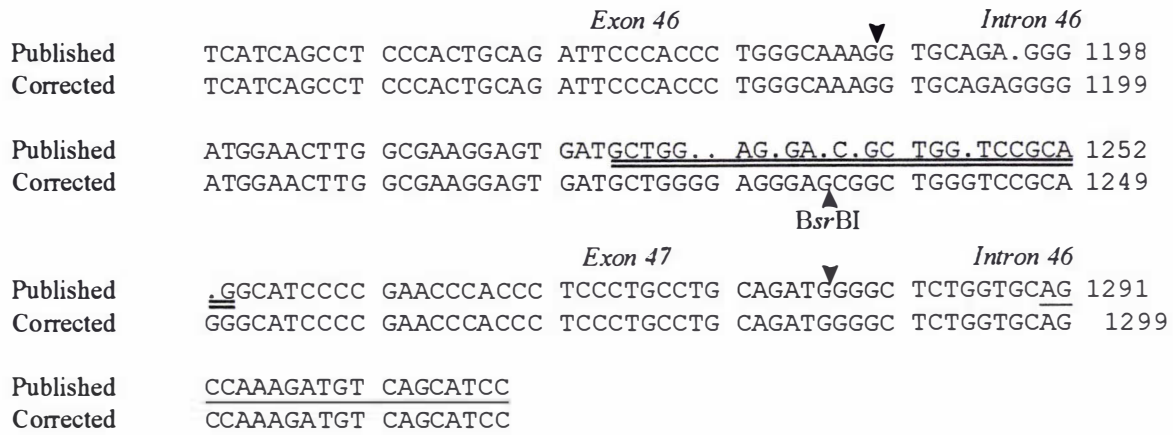

Published sequence for intron 46 as submitted by Phillips *et al.*, 1996 (Genbank accession number; U48477). Corrected sequence was determined by automatic sequence analysis of a PCR product generated with primers complementary to intron 45 and exon 47 (RYR45intF, RYR47exR). Nucleotides are numbered according to the original submitted sequence encompassing exons 44-47. The position of the RYR47exR reverse PCR primer is underlined with a single line. The location of the original reverse primer (2456R), complementary to the published sequence is indicated with double lines. Seven errors in the published sequence in this region can account for failure of PCR reactions with the 2456R primer. The corrected sequence results in an extra recognition site for *Bsr* BI (GAGCGG), explaining the unexpected fragmentation pattern generated in the *Bsr* BI RFLP analysis of the Arg2458Cys/His mutations.

3.2.8 Screening for the Tyr522Ser mutation using amplification created restriction sites

The Tyr522Ser mutation, resulting from an A1565C transversion in exon 14 of RYR1 was detected in a single French MH pedigree in association with central core disease [108]. The mutation was initially reported at a MH workshop in 1994, and a screen for this mutation in NZ families was developed before publication of the mutation [108]. The A1565C mutation did not alter any naturally occurring restriction sites, excluding simple RFLP analysis as a method of detection. The amplification created restriction sites method (ACRS), as depicted in Figure 3-12 was investigated as an alternative to manual sequencing.

A forward primer was designed to anneal immediately upstream of the mutation site with a mismatched nucleotide at the 3' end such that amplification of the target sequence would direct the incorporation of a *Bsm* AI recognition site exclusively in the presence of the A1565C mutation. The reverse primer was positioned to yield a 100 bp PCR product to enable electrophoretic separation from the 76 bp RE digest product that would be generated in the presence of the mutation by cleavage at the 3' end of the mismatched oligonucleotide. Primers were designed from the RYR1 cDNA sequence (Genbank accession number; J05200)[126]. Exon/intron boundaries were tentatively assigned to the human sequence based on the partial structural organization of the porcine RYR1 gene [Brenig, 1992 #1274]. The resultant 180 bp PCR product encompassing the A1565C mutation was 80 bp larger than anticipated due to the presence of an intron within the target region. This was confirmed by direct, manual sequence

analysis of the region amplified with the 522F and R primers and (and subsequently by a published report of the Tyr522Ser mutation [108]).

To test the efficacy of the ACRS method, a primer set was designed that introduced a *Fok*I recognition site in the amplification of both the normal and mutant alleles. The successful primer-directed incorporation of a *Fok*I site resulted in cleavage of the 180 bp PCR product into fragments of 147 bp and 33 bp. The 180 bp fragment was readily resolved from the 147 bp digest product by Nusieve™ agarose gel electrophoresis (Figure 3-13 A). Since this method of detection was clearly successful, representative DNA samples from 32 NZ families were screened by *Bsm* AI digestion of a 180 bp product amplified with the primers designed to incorporate a *Bsm* AI site in the presence of the Tyr522Ser mutation. None of the 30 samples investigated displayed the pattern expected for the digestion of the amplified mutant sequence. Enzyme activity was assessed by the digestion of a 300 bp PCR product known to contain a *Bsm* AI cleavage site (data not shown).

DNA from an individual harboring the Tyr522Ser mutation was not available to act as a positive control, to ensure the detection method worked and that the *Bsm* AI enzyme cleaved the PCR product at the introduced recognition site. To guard against the possibility that the *Bsm* AI ACRS procedure was not effective, an alternative mismatch ACRS scheme was devised to provide an internal positive control for enzyme activity. A reverse mismatch primer was designed to introduce a mutation-specific *Pst* I site in a 145 bp product, in addition to a forward mismatch primer that incorporates a non-polymorphic *Pst* I site to act as an internal control for *Pst* I activity (Figure 3-12 C). However, the presence of multiple mismatches in both primers was found to compromise PCR specificity. Successful amplification required a primary amplification with a complementary forward primer (522F-wt) in conjunction with the mutation-specific mismatched reverse primer (522R-Pst1), followed by secondary amplification of the resultant product with both mismatched primers (522Pst and 522R-Pst). Interpretation of the *Pst* I digest product was complicated by the presence of non-specific PCR products and incomplete digestion. Nevertheless, resolution of the digest products by non-denaturing PAGE indicated a *Pst* I site had been successfully introduced by the forward primer Figure 3-13 B). The absence of a second *Pst* I site in the reverse primer region was consistent with the expected profile for homozygous normal genotype. Due to difficulties in obtaining pure PCR products, this approach was restricted screening the DNA samples from the Maori CH family (M91), the CCD pedigree (M181, family 94) and one MHN control (M69). Both MHS and CCD DNA samples exhibited the RFLP pattern characteristic of the homozygous normal A1565 genotype.

Figure 3-12 Screening for the A1564C (Tyr522Ser) mutation by ACRS

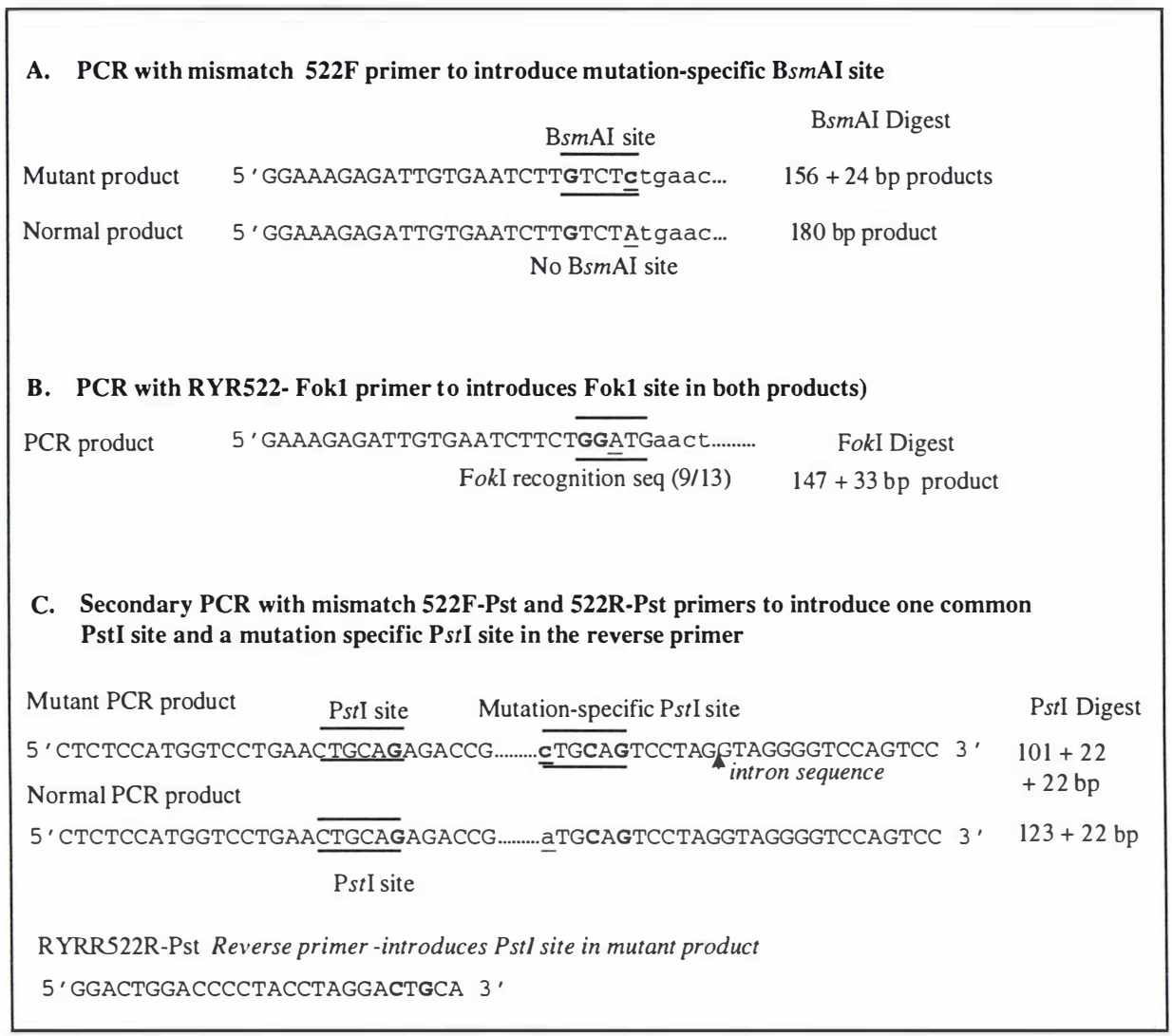

Scheme for detection of Y522S mutation by the mutation-specific incorporation of a site for *Bsm* AI (A) or *Pst* I (C). The efficacy of this method was demonstrated by the primer mediated introduction of a common *Fok* I site (B). Primer sequences are displayed in large caps with mismatched nucleotides in bold. The mutation site is underlined. Expected RFLP digest products for the amplified normal and mutant sequences are indicated.

Figure 3-13 A screen for theTyr522Ser mutation using amplification-created restriction sites.

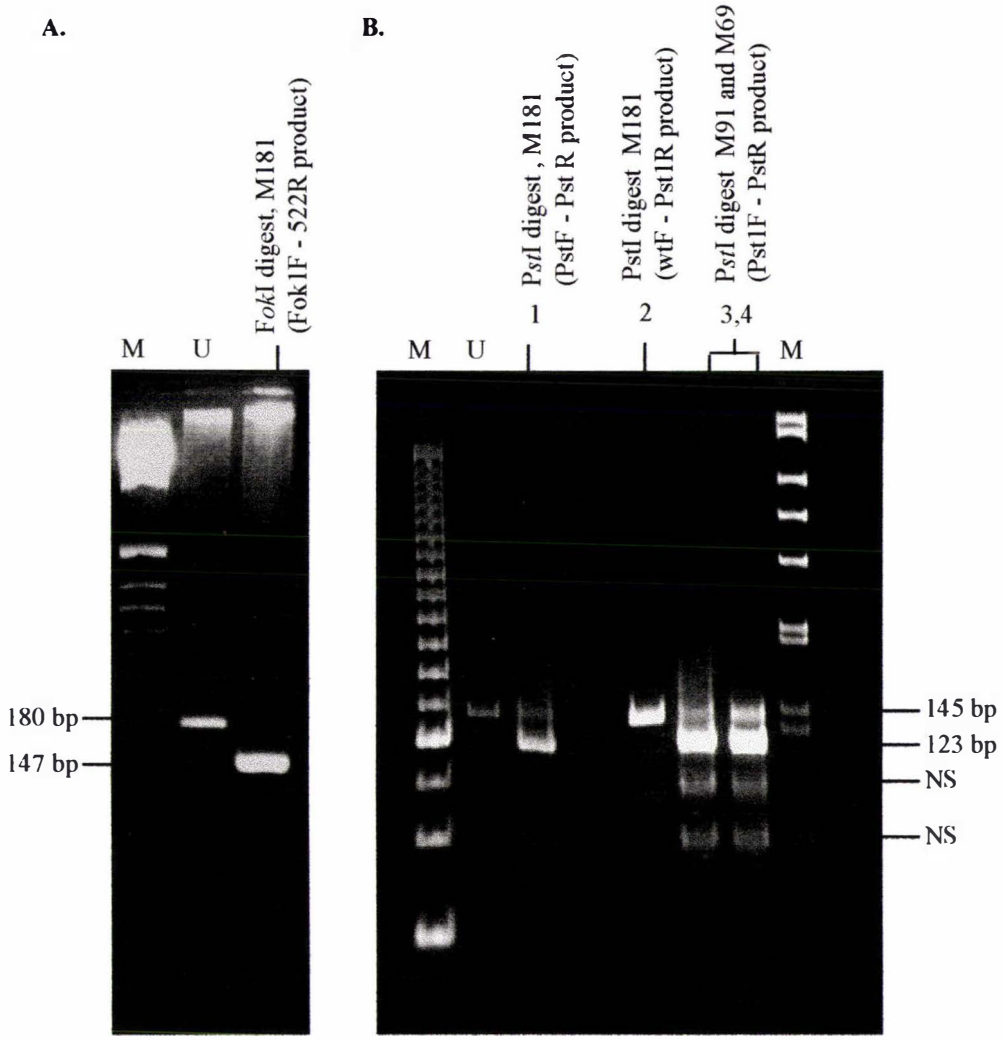

A. Separation of *Fok*I digest products on a 3.5 % Nusieve™ gel, in 1X TAE (stained in 0.5 μg/ml EtBr). M = 1 kb DNA ladder. U = Uncut DNA. The primer-directed introduction of a *Fok* I site by amplification with the 522F-Fok - 522Rbio primer set, followed by *Fok* I digestion results in the cleavage of the 180 bp PCR product into fragments of 147 bp and 33 bp (not visible) in the presence of the normal allele.

B. Separation of *Pst* I digest products on a non-denaturing, 16 X 16 cm 14% polyacrylamide gel. The gel was electrophoresed in 1X TBE for 8 hr, at 150 V and stained in 0.5 μg/ml EtBr. M (left) = 25 bp DNA ladder. M (right) = 1 kb DNA ladder . U = uncut DNA.
Lanes 1,3 and 4: *Pst* I digest of PCR products amplified with the 522F-Pst and 522R-Pst primers designed to introduce both a common *Pst* I site with the forward primer and a mutation-specific *Pst* I site with the reverse primer. The generation of a single cleavage product is consistent with normal genotype at the Tyr522Ser mutation site in three individuals M181 (CCD), M91 (MHS) and M69 (MHN). NS = non-specific PCR products.
Lane 2: *Pst* I digest of product generated with normal 522F-wt forward primer and the 522R-Pst mutation-specific reverse primer. The absence of digestion of the 145 bp PCR product by *Pst* I was consistent with the homozygous normal A1565 (Tyr522) genotype in this individual.

3.3 SCREENING FOR PUBLISHED RYR1 MUTATIONS BY DIRECT SEQUENCE ANALYSIS.

3.3.1 Screening for the Gly248Arg , Gly341Arg and Arg35Cys mutations

Due to the difficulties encountered with the ACRS detection method, screening for the Gly248Arg and Gly341Arg mutations was accomplished by direct sequence analysis of the mutation regions amplified from genomic DNA samples from MHS individuals. PCR was performed with one 5'-biotinylated primer to facilitate purification of single-stranded templates with Dynal™ streptavidin-coated paramagnetic beads. Sequencing reactions were primed with internal oligonucleotides and performed with the Sequenase™ Version 2.0 system, incorporating [α–^{35}S]dATP as a label. Reactions were optimised to intensify bands corresponding to sequence close to the primer to facilitate analysis of the mutation region. This was achieved by diluting the labelling mix 1:15 (instead of 1:5), limiting reaction times to 3 minutes and by the addition of 1 µl of Mn buffer (0.15 M Isocitrate, 0.1 M $MnCl_2$) to the labelling reaction mixture (sufficient four 4 templates). The addition of Mn^{+2} reduces the discrimination against incorporation of dideoxynucleotides [337], thus reducing the average length of DNA fragments synthesized in the termination step.

Sequence analysis of the Gly341Arg mutation region was impaired by the high GC-content of the region, which can promote the formation of secondary structure during electrophoresis and compression artifacts. The substitution of dGTP with dITP in the labelling reaction was investigated as a means of eliminating the secondary structure. However, sequence generated with dITP was of poor quality, characterized by frequent pause sites and low intensity bands. The occurrence of compressions in the sequence was reduced by heating to 80°C immediately before loading and performing electrophoresis at 70 - 75 W to encourage complete denaturation of the DNA during electrophoresis.

Examples of sequence profiles for the Gly248Arg (G742A) and Gly341Arg (G1021A) mutation regions are shown in Figure 3-14 (B) and (C). All MHS and MHE representative members of 30 NZ families investigated by direct manual sequence analysis of amplified genomic DNA were normal with respect to these mutations.

Selected members of four important families, including the large Maori CH family were screened for the presence of the Arg35Cys mutation by direct manual sequence analysis as described above. All displayed the homozygous normal (T103) genotype at the mutation site (Figure 3-14 A).

3.3.2 Screening for the Thr2206Met mutation

Primers were designed from intron sequences flanking exon 40 (Genbank accession number = U48474) [160] to screen samples from key families for the Thr2206Met mutation by direct sequence analysis. PCR reactions with the RYR1 intron39F and RYR1 intron40R primers failed to yield pure products of the correct size despite repeated efforts over a range of magnesium concentrations and annealing temperatures with hot start and touchdown PCR programs. A secondary PCR approach was required to generate discrete products amenable to sequence analysis. PCR was performed with the intron 39F and intron40R primer pair using a genomic

Figure 3-14 Direct manual sequence analysis of published RYR1 mutation sites

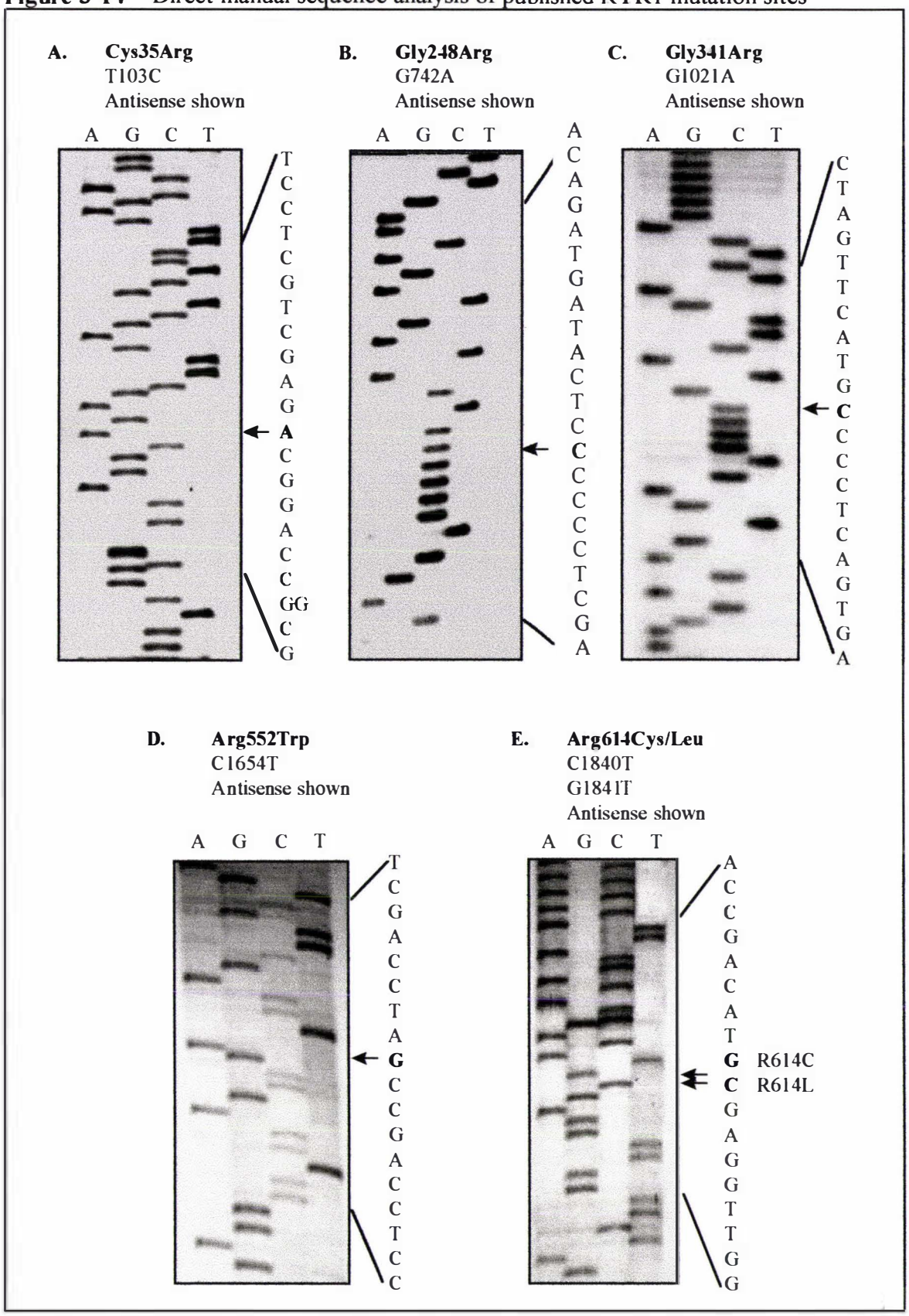

Biotinylated SS DNA templates for sequencing were prepared from PCR reactions using streptavidin-coated paramagnetic beads. Sequence reactions were performed with Sequenase™ and labelled with ^{35}S-α[ATP] using internal reverse primers. 3.5 µl of each sequence reaction was resolved on a 7% denaturing polyacrylamide gel, containing 5 M urea in 1X TBE at 60 W, constant power (until the xylene cyanol dye front had migrated ~3/5 the total distance). Sequences (A -E) were derived from a genomic DNA sample from an MHS member of the CH family (M60). All sequence profiles were normal with respect to the 6 published RYR1 mutations.

DNA sample (M91) from an MHS member of the CH family. A product of the appropriate size was isolated from contaminating species by gel purification. The purified DNA was diluted and used as a template in a secondary round of PCR using the same primer pair. The amplification of the desired target region was favoured over the non-specific amplification products in the secondary PCR reaction, however contaminating species were still observed. The desired secondary PCR product was excised from a 3% Nusieve™ gel, purified with the Wizard™ PCR preps system and subjected to automatic DNA sequence analysis using the forward PCR primer (39iF). The sequence derived from the MHS individual contained considerable background noise but could be clearly interpreted at the mutation site as negative for the Thr2206Met mutation.

3.3.3 Screening for a reported mutation in CACNL1A3

A search for the reported G3333A (Arg1086 for His) mutation in the CACNL1A3 gene in DNA samples from 32 NZ families was achieved by PCR-RFLP with the *Cfo* I enzyme. Primers were as published in the original report [33]. 6 MHS members of the large CH Maori family who were identified as discordant with respect to a RYR1 haplotype that co-segregated with the MHS phenotype in this family were also screened for the CACNL1A3 mutation to investigate the possibility of genetic heterogeneity in this pedigree. All samples investigated demonstrated the normal, homozygous G3333 genotype, characterised by complete digestion 226 bp product with *Cfo*I into 190 bp and 36 bp fragments (data not shown).

3.3.4 Continued analysis of published MH mutations in new MHS probands

In view of both the increasing number of rare RYR1 mutations and the ongoing referral of new MH families for testing, the search for all the individual MH mutations in amplified genomic DNA, while aided by the publication of intron sequences, was no longer economically feasible. Although sequence analysis of the 15.3 kb RYR1 cDNA for each new MH family was also outside the scope of the project, the tight clustering of the reported mutations in one of two regions of the RYR1 coding region effectively reduced the target region to approximately 2 kb. With the introduction of automated DNA sequencing facility at Massey University, amplification and automated sequence analysis of amplified cDNA encoding the N-terminal and central "hot-spot" regions is now the chosen, most efficient method of mutation analysis. Accordingly, the project emphasis shifted from a search for published mutations to the identification and characterisation of novel mutations. This approach narrowed the focus to key families from whom muscle biopsy tissue from the IVCT had been collected and stored appropriately to allow extraction of pure, intact RNA.

4. GENETIC LINKAGE ANALYSIS OF A LARGE MHS PEDIGREE

The establishment of linkage between the MHS phenotype and a candidate locus has been limited in overseas studies by small pedigree size and the lack of definitive phenotypic data. A principal objective of the genetic study of MH in NZ was to investigate the genetic etiology of the MH disorder in a very large Maori MHS kindred from the lower North Island (the CH pedigree). The following factors were considered in the selection of this pedigree for linkage analysis.

1. The CH family includes over 1400 individuals documented over seven generations, and is potentially one of the most extensively characterised MH pedigrees in the world. Over 140 individuals have been investigated by IVCT. This provided a unique opportunity to investigate genotype/phenotype relationships for any candidate mutation, and assess the performance of the IVCT.

2. Fifteen fulminant MH events have been documented in the CH family that were highly indicative of susceptibility to MH (N. Pollock, personal communication). Several of these events scored the maximum value of six on the clinical grading scale, which is interpreted as "almost certainly" MH [44]. Examples of documented MH case reports for members of the CH pedigree are presented in appendix 6.1).

3. The inheritance of MH in this pedigree was traced to a marriage between a Maori individual and an individual of Scottish descent. It is not known whether the disorder originated in the Maori lineage, but if this were so, a novel mutation would be likely to be involved, since no previous genetic studies of the MH disorder have included families of Maori descent.

4. The discovery of a mutation in this family could have significant diagnostic potential, allowing many family members to forego a highly invasive surgical procedure. In view of the size of the pedigree, an alternate diagnostic test would have a considerable impact on the management and diagnosis of MH in NZ, and would yield considerable financial savings for the Palmerston North Hospital.

5. DNA samples from members of this family were readily available. Most family members reside in the Manawatu /Horowhenua region and were generally highly cooperative in the provision of blood specimens. Over 350 DNA samples from representative members of this kindred were collected, with informed consent during the course of this study. Patient consent forms for the supply of blood and tissue specimens are included in appendix 7.

6. Ethical approval for the project was successfully obtained from the Manawatu-Whanganui and Massey University ethics committees, under consultation with a Ngati Raukawa Ki te Tonga tribal authority.

4.1 CH PEDIGREE STRUCTURE

The seven-generation pedigree structure is portrayed in appendix 9. Branches of the family are labelled according to the original scheme devised by Dr. Ken Couchman (Palmerston North

Hospital), and ID numbers refer to the pedigree identification number assigned by the pedigree/draw database. DNA identification numbers are also indicated (M prefix). Only essential individuals from whom genotype and phenotype data are available are shown, although over 1500 members of the family have been traced.

The first generation founders are of Maori (individual I-2) and Scottish (I-1) descent. It is not known whether MH was introduced by the Maori or Scottish sides of the pedigree, or whether a *de novo* mutation has occurred in one of the first generation individuals. Descendants of two male and one female offspring of I-1 and I-2 have been traced. No MH reactions or positive MHS diagnoses have been reported in direct descendants of the first son (II-3) (labelled the RO and TH branches) including children from a first cousin marriage (EM branch). MH reactions have occurred in descendants of the daughter (II-31) and one son (II-11), indicating they are obligate carriers of the gene defect. The daughter (II-31), was born in 1852 and had six children. Descendants of four children of II-31 gave rise to the EM (III-33), EH (III-35), EA (III-40) and ES (III-37) branches of the pedigree. No descendants of the fifth child (EW branch) have been investigated by IVCT, and no descendants of the sixth child have been recorded. MHS diagnoses have been obtained in members of the EA, ES and EH branches, indicating that at least three of the six children from individual II-31 had inherited the gene defect. Individual III-33 (CHEM) married a first cousin and produced one child (IV- 205). All six fifth generation CHEM individuals have been diagnosed either MHE or MHN, which suggests that this is a negative branch of the family.

Individual II-11 had one son (III-13) and one daughter, though descendants of the latter have not been investigated. The son (III-13) had eight children from his first marriage. Descendants of four out of the eight offspring have been traced (giving rise to the NG, RA, AR and TA branches). MH reactions have been documented and MHS diagnoses have been made for members of the NG and RA branches (though in the latter case, the MH defect may have been re-introduced by a consanguineous marriage with an obligate MHS carrier from the ES branch). Two children, a son and daughter, were born to individual III-13 in a second marriage. No descendants of the daughter (IV-29, RU branch) have been diagnosed MHS. The son (IV-24) produced 15 children from four marriages, giving rise to the KW, KM and KC and KH branches of the family tree. MHS individuals were identified in the KW, KM and KC branches. At least three consanguineous marriages have occurred within the seventh generation in these families. IVCT results were equivocal for the representative members of the fourth marriage (KH branch).

None of the 18 published mutations that had been linked to MHS in overseas studies [25] were detected in MHS probands from the large Maori CH family, indicating a novel mutation could underlie the MH disorder in this pedigree. While the MHS1 RYR1 locus remains the principal candidate for a gene defect, locus heterogeneity in MH has now been firmly established [32,33]. Genetic linkage analysis was therefore conducted to investigate the role of the RYR1 gene in MHS in this pedigree (CH) before embarking on a costly and labour intensive screen of the 15.3 kb RYR1 coding region.

4.2 PRINCIPLES OF GENETIC LINKAGE ANALYSIS

The mapping of genes on chromosomes is made possible by the phenomenon of genetic recombination, during which segments of chromosomes undergo homologous exchanges at frequencies relative to the chromosome length. The frequency of recombination events between

the marker and disease locus is related to the physical distance between the two. Since each crossover affects only two of the four chromatids, the recombination fraction between such genes approaches 50% for genes far apart on the same chromosome [338]. In addition, genes on different chromosomes segregate independently so that they also recombine with a frequency of 50%. Thus, the recombination fraction (θ) can range between zero (for tightly linked genes) and 0.5 (for unlinked genes).

The unit of measurement of distance is the map unit, where 1 map unit = 1 centimorgan or cM, which corresponds approximately to a recombination fraction of 0.01. However, the relationship between θ and the genetic distance is indirect, since the probability of multiple, undetected recombination events increases with increasing distance between two loci. The genetic distance is estimated from θ using Haldane or Kosambi mathematical mapping functions that correct for interference factors [338,339]. Assuming a total genetic map length of 3,000 cM and 3×10^9 bp of DNA in the haploid genome, a genetic distance of 1 cM corresponds to an approximate physical distance of 1 million base pairs [338]. However, the genetic map distance (in cM) does not always correlate well with physical distance (in bp) since the recombination intensity and interference are not constant throughout the genome. Nevertheless, linkage analysis provides estimates of recombination fraction and corresponding genetic distances, which are more relevant to issues in genetic counselling than physical map distance.

The positioning of genetic markers across the genome and the development of statistical methods for analysing the segregation of markers and genes has paved the way for the positional cloning of disease genes without prior biochemical characterisation of the gene defect [340,341]. In this approach, the probable location of a disease locus is established by testing linkage to a panel of markers representing the entire genome at 10 cM intervals [340]. Potential linkage regions are then further defined through the identification of important recombinant events between the disease locus and flanking marker loci that define the proximal and distal boundaries of linkage. The candidate gene region may then be physically characterized with YAC clones and candidate genes with functional significance screened for mutations that co-segregate with the disease. This approach has led to the mapping and subsequent cloning of over 100 disease genes including cystic fibrosis [342], neurofibromatosis [343], early [344] and late-onset [345] Alzheimer disease, Huntington disease [346], polycystic kidney disease [347], and familial breast cancer [330,348]. Approximately 7100 human genes had been mapped to chromosomal locations, and an additional 643 "unassigned" genes have been documented whose locations have not yet been determined unequivocally (GDB Reports and Statistics, July 1999 [349]).

Methods of genetic linkage analysis can be divided into two major groups: parametric and non-parametric. Non-parametric methods such as the sib-pair analysis [350] and the affected pedigree member analysis [351] rely on the identification of common allele in affected relatives. These approaches do not require a thorough understanding of the modes of transmission of the disease, and are suitable for diseases with complex genetic etiologies [351] but require accurate phenotypic assessment as they are extremely sensitive to phenotypic or marker misclassification [352]. Non-parametric methods do not attempt to assess linkage by direct detection for recombinant events and thus provide no estimate distance between the disease gene and a marker.

In contrast, parametric analyses require the definition of the genetic model parameters such as the mode of inheritance, penetrance, disease and allele frequencies and mutation rates [331]. Parametric analyses are more powerful, although positive evidence for linkage can be obscured by the adoption of an incorrect genetic model [352,353] and false positive evidence for linkage can be obtained if incorrect allele or disease frequencies are applied [354]. An autosomal dominant

mode of transmission for MH susceptibility has been established [39,355] and other relevant parameters for MH linkage analysis have been previously defined [27]. A parametric approach to MH linkage analysis was therefore the preferred strategy, particularly in view of the potential for IVCT diagnostic errors.

The likelihood ratio method or "Lod score analysis" is the primary parametric analysis method in use [356]. Lod score analysis measures the likelihood of obtaining a set of data under the hypothesis that a disease and marker loci are linked at a particular value of θ versus the likelihood of obtaining the data assuming the two loci are unlinked ($\theta = 0.5$). The reported parameter (z) is the $\log_{10}$ of the ratio of these two probabilities, known as a lod score (logarithm of odds ratio). In practice, a range of values of θ are tested, and the θ_{max} for which the likelihood estimate (z) is maximal is reported as the most probable indicator of the recombination fraction or genetic distance between two loci. A maximal lod score at $\theta = 0$ is generated when no recombination events are observed between the disease phenotype and a genetic marker. A more thorough explanation of lod score analysis and working examples are given in section 4.2.3.

4.2.1 Analysis of polymorphisms

4.2.1.1 Strategies for genotype generation

A genetic marker is defined as any detectable inheritable variation within the study population [357]. A number of genetic markers and their methods of detection are described below. Restriction fragments length polymorphisms (RFLP) occur as a result of single base changes that create or eliminate restriction sites, or alternatively by insertions or deletions which alter the distance between two restriction sites. RFLP are detected using labelled genomic DNA fragments as probes in southern blots of restriction digests [359] or by digestion of the amplified polymorphic region.

Microsatellites are short (2 - 5 bp) tandem nucleotide repeats that are scattered throughout the genomes of eukaryotes. The large variation in the number of copies of the repeated unit among individuals of a species, make these simple sequence length polymorphisms (SSLP's) valuable sources of detectable molecular variation for genetic linkage studies [328]. Proposed functions for the sequence repeats include participation in gene regulation and 'hot-spots' for recombination [360]. The evolutionary origins of microsatellites are unclear. The initial development of repeat units appears to occur slowly, in stepwise fashion whereby short arrays decrease or increase in the repeat number by replication slippage [360]. Loci with fewer than 5 - 8 CA repeat units are almost never polymorphic in humans [360] whereas most arrays with more than 20 CA repeats have heterozygosities of greater than 80% [361]. CA repeats are the most abundant class of simple sequence repeats. Trinucleotide and tetranucleotide repeats [362] produce band patterns that are more easily distinguished. Arrays of repeated units of 9 to 62 nucleotides are referred to as variable number tandem repeats (VNTR) or minisatellites and are highly polymorphic [363].

SSLP's offer several advantages over RFLP markers. They can be typed simply by amplifying the polymorphic region and determining the fragment lengths by PAGE, and are amenable to multiplex analysis. SSLP's are more likely to be informative for a particular mating due to their highly polymorphic potential [361]. They are frequent in human genome, occurring at approximately every 30-60 kb, and thus have permitted the construction of high-resolution human genome maps [325,326,364]. Comprehensive chromosome maps, including locations and details

of genes, contigs, polymorphic markers and associated primers are available as online resources. These are detailed in appendix 3.

4.2.1.2 Marker selection

The usefulness of a particular marker for evaluating linkage is a function of the informativeness of the marker, its proximity to a candidate gene region, and pedigree structure. For a mating to be potentially informative for linkage between two loci, at least one of the parents must be doubly heterozygous [338]. Therefore, a marker's usefulness for linkage analysis depends on the number of alleles and their frequencies, since increased polymorphism leads to an increased probability of heterozygosity [338]. The standard measure of polymorphism for a marker is the heterozygosity or HET value [330]. HET values for specific markers available from the GDB are calculated from allele frequencies obtained from genotyping 80 - 100 individuals [349]. Microsatellite markers often have HET values > 70% and are the preferred choice for linkage studies [328]. RFLP markers generally have HET values in the 0.25 - 0.5 range [357].

4.2.1.3 Specification of allele frequencies

Unless all individuals can be genotyped or the genotypes inferred directly, allele frequencies must be accurately specified in the linkage analysis. Incorrect specification of allele frequencies at marker loci can result in extreme biases and false positive evidence for linkage [354,365]. The impact of errors in the assigned allele frequencies is more severe when large amounts of data are missing [330]. The genome database [349,357] provides estimates of allele frequencies for marker loci however, these frequencies may not apply to particular isolated populations [330,366]. Gene frequencies can be estimated if necessary, by genotyping representative control individuals or unrelated individuals who have married into the family being studied [366].

4.2.2 Defining the genetic model

Before conducting genetic linkage analysis, clinical and epidemiological data are studied to define the mode of transmission (dominant or recessive) and to determine whether the disorder is polygenic or has a single gene component. It is also necessary to investigate genotype/phenotype relationships to derive estimates of the disease penetrance, expressivity, diagnostic error rates, and the incidence of phenocopies. These factors are defined below and discussed with a view to the impact they may have on the outcome of linkage analysis of MH families.

4.2.2.1 The mode of inheritance

The mode of inheritance (recessive, dominant, monogenic, polygenic) of the disease must be ascertained before conducting linkage analysis using segregation analysis techniques [367]. Formal segregation analyses require strict adherence to guidelines for sequential sampling of members of extended pedigrees to be included to avoid ascertainment bias [330,368,369]. Ascertainment bias occurs where samples are not representative of the general disease population. This can result in inflated estimates of the penetrance of the disorder, or mistaken modes of inheritance [330]. Calculating linkage under a correct genetic model usually generates higher lod scores compared to analyses performed with an inappropriate model [370]. However, maximising the lod score over the genetic model parameters can result in inflated lod scores and an increased probability of false positive evidence for linkage [338,371,372].

4.2.2.2 Penetrance

Reduced penetrance, in which the disease trait is not observed in genetically susceptible individuals, is a feature of a variety of genetic disorders including Huntingtons disease [346], familial Alzheimer disease [345] and retinoblastoma [373]. Penetrance is quantitatively defined as the conditional probability that an individual with a specific genotype will express the predicted phenotype. A numerical estimate of the penetrance is incorporated into the genetic model in the linkage parameter file.

Most diseases such as familial hypercholesterolemia [374], or emphysema associated with α_1 antitrypsin deficiency [375] depend on a complex interaction of both genetic and environmental factors [376]. Ecogenetic or pharmacogenetic traits are those that do not manifest unless accompanied by specific environmental stimuli. MH is an example of a classic pharmacogenetic disorder revealed only upon exposure to anaesthesia.

The clinical penetrance of MH is predicted to be between 0.1 - 0.33, which represents the likelihood that a genetically susceptible individual will suffer an MH reaction on exposure to triggering agents [42,43]. While it would be ethically unacceptable to test susceptibility to MH by exposing relatives of probands to triggering anaesthetics, even if this were possible, many genetically predisposed individuals would appear normal. The IVCT is the only currently available method by which to identify MHS relatives of a proband. Consequently, for the purpose of linkage analysis, the penetrance of the MHS phenotype is equivalent to the probability that a genetically susceptible individual will be designated MHS by the IVCT. This is equal to the sensitivity of the IVCT test, which is about 99% [97]. Even when incomplete penetrances are factored into the calculation, the ambiguity in the genotype/phenotype relationship results in a loss of information and lower lod scores.

4.2.2.3 Phenotypic uncertainty

Phenotypic misclassification in MH arises predominantly from the adoption of diagnostic criteria that maintain a high sensitivity at the expense of a significant false positive rate [96]. Misdiagnosis of the disease phenotype can lead to an overestimation of the genetic distance between the marker and disease locus [377,378] and remains a significant problem in MH genetics [34,172].

The false positive rate of the IVCT is defined as the probability of a MHS diagnosis in a genetically normal individual [101]. In many diseases, phenocopies (sporadic cases) occur through alternate etiologies, for example by unspecified environmental causes. The probability of misclassification is a general form of incomplete penetrance [338]. The presence of phenocopies and the false positive rate of the IVCT are therefore modelled in MH linkage studies by assigning a non-zero penetrance to the normal genotype. For example, a penetrance of 0.1 for the normal genotype incorporates a 10% likelihood that an unaffected individual is labelled as susceptible. This corrects for both the IVCT error rate and the occurrence of phenocopies. Correcting for phenotypic uncertainty in this way protects against an inflated estimate of θ. However, it results in a loss of power of the data. For example, at $\theta = 0.01$, and a misclassification rate of 0.1, twice as much data are required to obtain the same power of analysis [338].

It is possible to assign different probabilities for misdiagnosis to different individuals with the use of liability classes. Each individual is allocated a number immediately after the affected status field in the pedigree file, which assigns them to a particular liability class. The penetrances of the normal and disease genes are specified for each liability class in the associated parameter file. For example, the probability that an MHS result represents a false positive diagnosis is lower for

individuals who have suffered a fulminant MH crisis before being examined by IVCT than it is for other MHS individuals. Accordingly, these individuals can be assigned to a separate liability class for which the penetrance of the normal genotype (false positive or phenocopy rate) is set to zero.

4.2.2.4 Variable expressivity

Expressivity of a genetic disease describes the severity of a phenotype and can be variable, particularly for pleiotropic genes that may affect multiple tissues or organs such as neurofibromatosis [379]. In the case of MH, variable expressivity is apparent in the range of responses to the IVCT test agents registered by a group of susceptible individuals harbouring the same mutation [100]. Individual variation in the IVCT responses may contribute to the false positive rate of the IVCT, particularly as diagnoses are made from the maximum contracture responses of duplicate tests, and not the average of two or more tests [97].

4.2.2.5 Genetic heterogeneity

Allelic heterogeneity refers to the expression of the same phenotype from alternate genotypes at the same locus. Locus heterogeneity refers to disorders that are caused by genetic defects at different loci [345]. MH demonstrates both allelic and locus heterogeneity, with multiple mutations in the RYR1 gene [25] and an unknown number of mutations in up to 5 other genes potentially resulting in a similar phenotype [29,31,32,177].

Genetic heterogeneity complicates linkage studies and can obscure evidence of linkage where lod scores are summed across a mixture of linked and unlinked pedigrees. Formal tests of heterogeneity have been devised including the M test [380] the B test [381] and the admixture analysis which is applied in the HOMOG program package [365] for assessing genetic heterogeneity within a set of pedigrees. If the HOMOG analysis indicates significant evidence for genetic heterogeneity, lod scores can be summed for families demonstrating linkage to the locus of interest after excluding data from unlinked families.

4.2.3 Analysis of genetic linkage

4.2.3.1 Determination of chromosomal phase

If an individual is heterozygous at both the disease (Mm) and marker (12) loci, the disease allele (M) could have been inherited from the affected parent in coupling with either the 1 or the 2 allele. These two possibilities are known as the two phases of the double heterozygote. For a mating involving a phase-known doubly heterozygous parent (M1/m2), it is possible to determine unequivocally if offspring have inherited non-recombinant (M1 or m2) or recombinant (M2 or m1) gametes from the parent, in which case they are referred to as 'informative for linkage'.

Alleles at two or more loci received by an individual from one parent are referred to as a haplotype. Often it is unclear which of the two alleles were received as a haplotype from one parent; hence, the phase is unknown. There are two ways in which chromosomal phase can be determined. For genotypes with a maximum of one heterozygous gene, the phase can be determined directly, since it is clear which alleles were received as haplotype from each parent. Alternatively, the phase can be inferred directly from the data from the grandparents. A three-generation family in which all members are typed consequently provides more information about linkage than a two-generation pedigree.

The contribution of the third generation to the information content and phase determination for a small pedigree is demonstrated in Figure 4-1. This represents a family from the Maori pedigree typed for the intragenic RYR1 *Taq* I RFLP. In example A, the phase of the doubly heterozygous father can be discerned from the affected grandmother, and the offspring can be uniquely categorised as recombinant or non-recombinant. In the absence of data from the grandparent, two alternate phases with equal probability are possible for the MHS father shown in B and C. Where the phase cannot be determined unequivocally, the probabilities for the alternate phases can be determined from the configurations of disease and marker loci in the children, assuming various values for θ [338].

Figure 4-1 Representative three-generation family segregating for MHS showing the effect of third generation data on phase determination.

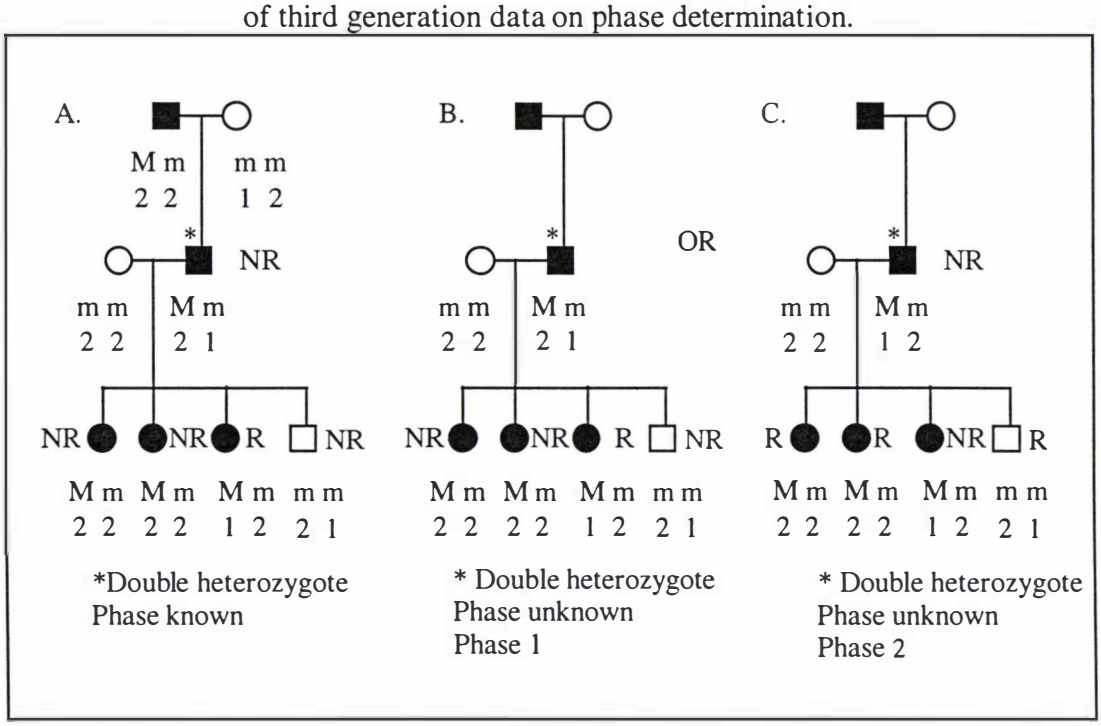

Genotypes for the *Taq*1 RYR1 marker are shown. M and m refer MHS and MHN status for the MH disorder respectively. NR = non-recombinant. R = Recombinant. In A, the phase of the father (*) can be determined. Without the grandparents data, two alternate phases are possible (B and C). Data are derived from the CH pedigree. Alleles for grandparents and the unrelated spouse were deduced from extended family data. In this case, the apparent recombinant M1 haplotype may in fact reflect a false MHS diagnosis.

4.2.3.2 Calculation of 2-point lod scores - theoretical considerations.

The likelihood ratio approach to the calculation of lod scores was developed by Morton (1955) [356]. This strategy combines the standard probability ratio tests [382] with a method of sequential sampling analysis to allow the further addition of data before the decision to accept or reject the null hypothesis is made [383].

According to likelihood theory, the likelihood of a hypothetical value for a given parameter is a function of the probability of that parameter being true for the observed data. In other words, a greater degree of belief is placed upon hypotheses that would make the observed outcome more likely [384]. By maximising the likelihood of a set of data with respect to a parameter, a consistent maximum likelihood estimate (MLE) for that parameter can be obtained. This approach

is used in linkage analysis to find the value of θ at which the probability of a data set is maximised. This value of θ represents the best estimate of the recombination fraction (θ_{max}) between two loci.

The measure of support for the hypothesis (that θ is equal to a particular value) is expressed as the ratio of the likelihood of the hypothesis (linkage), versus that of a null hypothesis (no linkage, θ = 0.5). The likelihood of the pedigree data (L) is computed at a chosen value of θ, and at θ = 0.5. The support for linkage is measured by the ratio of these two probabilities. Conventionally linkage, or Z (x), is presented as the $\log_{10}$ of the probability ratio where x is some value θ.

$$Z(\theta) = \log_{10}\left[\frac{L\ (\text{pedigree given } \theta = x)}{L\ (\text{pedigree given } \theta = 0.5\ )}\right]$$

The probability of a recombination is equal to θ and the probability of a no recombination is equal to 1-θ. The likelihood of achieving the observed frequencies of parental and non-parental haplotypes in the offspring from an informative mating at a specified recombination fraction (θ) is therefore given by

$$\theta^{R}\ (1 - \theta)^{NR}$$

Where "R" and "NR" refer to individuals who are recombinant (disease and marker loci in opposite configuration to that of the affected parent) or non-recombinant (disease and marker loci in same chromosomal configuration as the affected parent) respectively. The lod score for the data is computed with the equation

$$z(x) = \log_{10}\left[\frac{\theta^{R}\ (1-\theta)^{NR}}{(0.5)^{R}\ (0.5)^{NR}}\right]$$

Calculations are performed over a range of θ (conventionally, 0.01. 0.05, 0.1, 0.2, 0.3, 0.4). The properties of the likelihood ratio permit additive combination of $\log_{10}$ likelihood ratios from different families until a threshold is reached at which linkage is either accepted or rejected [384]. Lod scores can be summed across families provided they are calculated under the same model and at the same value of θ [331].

In the case of the MH pedigree example presented in Figure 4-1 A, the phase of the father (marked with an asterisk) can be determined unambiguously as M2/m1 from the genotypes of the grandparents, since the affected grandfather is homozygous (22) at the marker locus. Because the phase-known father is heterozygous at both the disease and marker loci, the gametes inherited by his four offspring can be unambiguously defined as recombinant or non-recombinant. In this case, three of the offspring are non-recombinant while the fourth is recombinant. The lod score for the pedigree at θ = 0.05 is computed as follows:

$$z(0.05) = \log_{10}\left[\frac{0.05^{R}\,(1-0.05)^{NR}}{(0.5)^{R}\,(0.5)^{NR}}\right]$$

$$z(0.05) = \log_{10}\left[\frac{0.05^{1}\,(1-0.05)^{3}}{(0.5)^{1}\,(0.5)^{3}}\right]$$

$$z(0.05) = \log_{10} 0.686$$

$$z(0.05) = -0.164$$

Linkage is not supported at this level of θ. In simple pedigrees, the value of θ for which the lod score is maximal (θ_{max}) is equivalent to the proportion of children carrying a recombinant genotype [333]. Hence, the maximum likelihood estimate for this pedigree ($z_{max} = 0.23$) is obtained at $\theta = 0.25$. These results were verified by computing the data with the LINKAGE 5.1 program [331].

If the grandparents had not been genotyped, two linkage phases (shown in B and C) would be possible, each with a 50% chance of being correct. Two terms are now included into the calculation of the likelihood of the pedigree, representing likelihood of observing the data under each of the phases [$\theta^{R}\,(1-\theta)^{NR}$] each of which has a probability of 0.5.

$$z(0.05) = \log_{10}\left[\frac{1/2\,[0.05^{1}\,(1-0.05)^{3}] \;+\; 1/2\,[0.05^{3}\,(1-0.05)^{1}]}{(0.5)^{R}\,(0.5)^{NR}}\right]$$

$$z(0.05) = \log_{10} 0.344$$

$$z(0.05) = -0.46$$

In this case, the loss of phase information has reduced the power of the data, and the negative lod score indicates linkage is not supported at this value of θ.

Manual calculation of lod scores is straightforward for small nuclear families. However, in most cases, data sets are incomplete and additional factors such as allele frequencies, disease penetrance and misclassification must be incorporated. Calculation of lod scores in complex pedigrees demands the application of linkage analysis software such as LIPED, MENDEL [385], LODLINK, and LINKAGE [331,332]. The LINKAGE package is a commonly used and freely available program that facilitates calculation of both pairwise and multipoint lod scores [331]. The LINKAGE program is based on the modified Elston and Stewart logarithm (1971) [367,386] which calculates the probability of the whole pedigree recursively, beginning with the most recent generation (later modified to include complex pedigrees [387]). The use of this software is described in section 4.4.

4.2.3.3 Interpretation of lod scores

Positive lod scores indicate evidence for linkage, and negative lod scores indicate absence of linkage. However, conclusive demonstration of linkage requires sufficient evidence to reject the null hypothesis of no linkage ($\theta = 0.5$) between the marker and disease loci. The data are said to convey significant evidence for linkage if a lod score exceeds a critical value. According to the

critical values originally proposed by Morton (1955) [356], lod scores of greater than 3.0 provide significant evidence in favour of linkage, while scores less than -2.0 exclude linkage. Lod scores in the range of - 2.0 to 3.0 are inconclusive and require collection of additional data.

The threshold of $Z_{max} > 3.0$ for accepting linkage is based on the relative probabilities of type 1 errors (mistakenly accepting linkage) and type 2 errors (failure to accept linkage when it exists). A lod score of 3.0 is associated with a likelihood ratio of 1000 and a significance level (p) of 0.001. In other words, the probability of obtaining a lod score or larger than 3.0 for a truly unlinked ($\theta = 0.5$) locus is 0.001 [356,382,383]. The significance level (α) of 0.001 for the linkage test may appear much more stringent than the values of $\alpha = 0.01$ and 0.05 that are usually applied in statistical tests. This level of significance was chosen in view of the prior probability that two random loci will fall within measurable distance of each other, which has been approximated at 2% [388]. Consequently, the conventional lod score of 3.0 corresponds to a (posterior) probability of linkage of 95% (100 % - 1000 x 0.02), and a false positive rate of 5%. A thorough account of the statistical interpretation of the likelihood ratio test and significance levels is reviewed by Ott, 1991 [338].

4.2.3.4 Planning the linkage analysis

Prior to conducting a linkage analysis, the mode of inheritance and estimates of the population frequency and penetrance were required. A formal segregation analysis (to avoid ascertainment bias) [37,39,389,390] could not be performed on the NZ MH pedigrees since sampling for MH testing has occurred in a non-systematic fashion and under the presumption of dominant transmission. Visual inspection of the pedigree indicated that the transmission of the disease was largely consistent with an autosomal dominant inheritance pattern. Recommendations for the definition of other relevant parameters useful in MH linkage analysis including disease frequency and penetrance have been reported by the European MH group [175].

The second consideration in planning the linkage analyses was to consider the method for assigning the phenotype. In the case of phenotypes measured with a continuous variable, values for affected and normal individuals typically belong to two normal distributions that may overlap somewhat. In such cases, the disease locus can be coded as a 'quantitative trait type locus' (instead of an 'affection status' type locus) [333]. This approach requires prior estimation of the means and variances of the data distributions from normal and affected groups [333]. Alternatively, the more common approach is to define a threshold by which to classify normal and disease phenotypes, so that the disease can be coded as an 'affection status' type locus. According to the established EMHG protocol, the clinical diagnosis of MHS is defined by a threshold tensions of 0.2 g in response to 2 mM caffeine and 2% halothane [96]. The standardised EMHG diagnostic protocol was therefore deemed the most convenient and clinically relevant method to define MH status.

The third consideration when collating data for linkage analysis was the number of individuals from the family required to provide sufficient data to either exclude or prove linkage to the candidate gene. Disproving a candidate gene amounts simply to finding an obligate recombinant. For example, if two loci are truly unlinked (assuming $\theta = 0.5$), only seven fully informative meiosis are necessary to be 99% certain of encountering at least one recombinant [338]. To disprove linkage between RYR1 and MHS with a lod score of ≤ -2, at a given value of θ (e.g. $\theta < 0.01$), on average only 3 fully informative meiotic events should need to be investigated. Thus, it

was anticipated that RYR1 would be excluded as a candidate relatively quickly if MHS in this family was not linked to a RYR1 defect.

It is more difficult to prove linkage to a candidate gene. Under ideal circumstances (fully informative meioses, no recombinants) each offspring thus contributes log2 = 0.301 towards the total lod score. Accordingly, a minimum of 10 non-recombinant informative meiotic events must be observed to prove linkage ($Z \geq 3.0$) when the true recombination fraction is 0, and 16 when the true recombination fraction is 0.01 [338]. In other words, when investigating a candidate gene, 16 meiotic events provide good power (90%) to prove linkage (that $\theta < 0.5$) [338]. However, to prove that a locus is a candidate gene requires a much smaller confidence interval for the true recombination fraction [338]. For example, to be 95% sure that θ lies between 0.0 and 0.05, at least 59 fully informative meiosis must be investigated (according to the equation, $n = \log(\alpha)/\log(1-\theta)$, assuming no recombinants are observed [338]). Even higher numbers are required in the presence of complicating factors (heterogeneity , misclassification) that reduce the information content of the data, and in practice, only a fraction of meioses are fully informative. It is evident that linkage analysis in MH requires very large, well-characterised pedigrees in order to prove linkage to a new candidate gene. The CH family is the only NZ (and one of few in the world) that can meet these criteria. If the results clearly excluded the involvement of RYR1, (lod score < -2) other proposed candidate gene loci on chromosomes 1 (CACLN1A3 [33]), 7 (CACNL2A, [29], 3 [31] or 17 (SCN4A [391]), could then be investigated.

4.3 DATA COLLECTION

4.3.1 RFLP analysis with intragenic RYR1 markers

A number of intragenic RFLP markers have been described for the RYR1 locus. Primers for three intragenic RYR1 RFLP Ile1151 (*Taq* I) Asp2729 (*Fok* I) and Ser2862 (*Cfo* I) [107] were provided by Dr. Andrew Wallace (St. Mary's Hospital, Manchester). These were typed by RE digestion of the amplified polymorphic regions. By convention, alleles which lack the polymorphic RE sites are denoted "1" and those with the polymorphic RE site allocated the "2" allele. The region encompassing the Asp2729 (F*ok* I) polymorphism includes a second, non-polymorphic site that served as an internal positive control for digestion.

RFLP analysis of family 94

RFLP markers were typed initially for NZ descendants of a British family for whom linkage to the RYR1 locus had been established [392]. An example of RFLP analysis of the Asp2729 marker with *Fok* I is presented in Figure 4-2. The position of the common and polymorphic *Fok* I sites and the corresponding fragmentation patterns are indicated in Figure 4-3. Results were entirely consistent with the previously published data for this family [392]. The MHS phenotype was associated with the "1-1-2" haplotype for the *Taq* I, *Fok* I and *Cfo* I markers respectively, as shown in Figure 4-2A.

Figure 4-2 Segregation of RYR1 RFLP markers in NZ members of a RYR1-linked family (family 94).

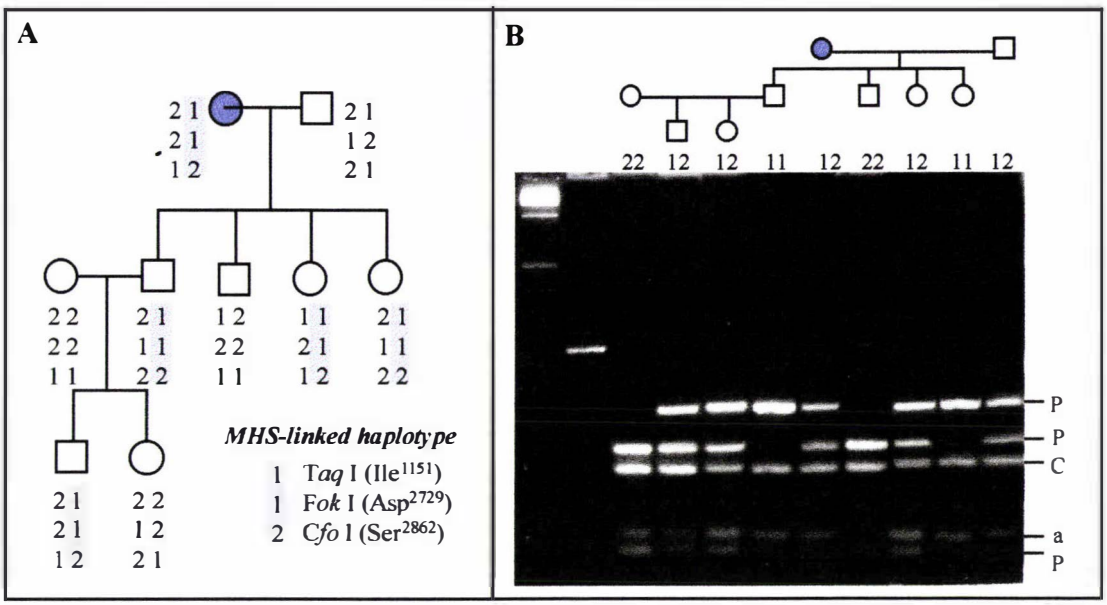

A. MHS coincides with "1-1-2" RYR1-RFLP3 haplotype detected in one MHS individual (filled symbol). Results are consistent with a published segregation of RYR1 RFLP markers with MHS in British relatives of this family (family 94) [392].

B. RFLP analysis of the Asp2729 polymorphism by PCR-RFLP with *Fok* I. 25 µl of each PCR product was digested with *Fok* I, concentrated by precipitation with ethanol and resolved on a 3% Nusieve gel, in 1 X TAE, stained in 0.5 µg/ml EtBr. Allele 1: Cleaved at a non-polymorphic *Fok* I site to 149 bp and 91 bp fragments (C= common bands). Allele 2: The 149 bp *Fok* I fragment is cleaved at the polymorphic *Fok* I site to yield 106 bp and 38 bp fragments (P = polymorphic bands, a = PCR artifact).

RFLP analysis of the CH family

Individuals from the large Maori CH family were typed for the three RYR1 intragenic RFLP markers. Two well-characterised branches (CHEH and CHEA, appendix 9) were selected principally because of the availability of DNA samples from individuals who had been examined by IVCT. RFLP alleles were aligned into probable haplotypes based on the data from key homozygous offspring. Examples of RFLP analysis in the CHEH branch of the family are given in Figure 4-3A and Figure 4-3B.

Alleles at the Asp2729 (*Fok* I) and Ser2862 (*Cfo* I) RFLP loci were found to be in linkage disequilibrium. Where it was possible to assign phase unambiguously, the "1" allele for the *Fok* I marker was consistently observed in conjunction with the "2" allele for the *Cfo* I marker and vice versa. This limited phase pattern applied to all individuals investigated from the CH family, in addition to individuals from unrelated pedigrees. These polymorphisms are very tightly linked (separated by approximately 1.5 kb [107], thus recombination between the two loci would occur at an extremely low frequency (~ 1.5 x10^{-5}). The *Taq* I marker "2" allele was observed in conjunction with either the "1" and "2" *Fok* I marker alleles, though the "2-2" and "1-1" configurations were disproportionately represented.

Assigning single allele numbers to the four observed haplotypes (Table 4-1) reduced the data complexity whilst retaining the relevant information. Combining alleles in this way effectively compensated for the low polymorphic nature of the RFLP markers [392] and was performed under the assumption of zero intragenic recombination between the markers.

Table 4-1 Alleles assigned to combined RYR-RFLP haplotypes

Taq I, *Fok* I, *Cfo* I RYR-RFLP haplotype	Allele
221	1
121	2
212	3
112	4

The '2-2-1' RYR1-RFLP3 haplotype (indicating alleles corresponding to the presence of the polymorphic restriction sites at for *Taq* I, *Fok* I and *Cfo* I respectively) was common to 14 key MHS individuals. This pattern was notably absent from three individuals diagnosed MHN in the CHEH family. The putative MHS-linked '2-2-1' RFLP haplotype differed from the '1-1-2' pattern that was observed to segregate with MHS in the previously examined NZ/British pedigree [392](family 94) indicating these two MH pedigrees do not share a common founder.

Figure 4-3A RFLP analysis of the Ser2862 polymorphism with *Cfo* I.

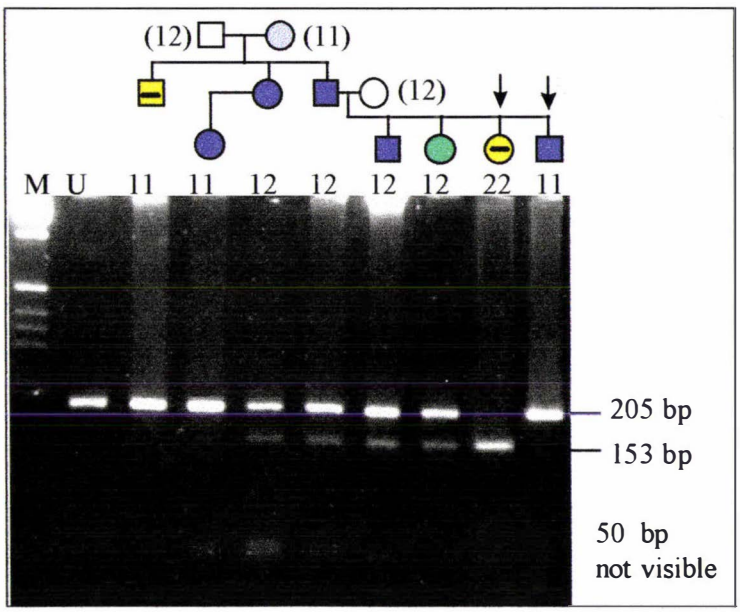

PCR products encompassing the Ser2862 polymorphism were digested with *Cfo* I and resolved on a 3% Nusieve gel in 1X TAE. The gel was stained in 0.5 µg/ml EtBr and photographed under UV light.

Genotypes for members of the CHEH family are shown. Symbols: Blue = MHS, Green = MHE. Yellow = MHN.

All MHS individuals from this family share the "1" allele. Individuals who are informative for this marker are marked with arrows. The '1" allele was not inherited by an MHN individual.

Figure 4-3B PCR-RFLP analysis of RYR1 polymorphisms with *Taq* I and *Fok* I .

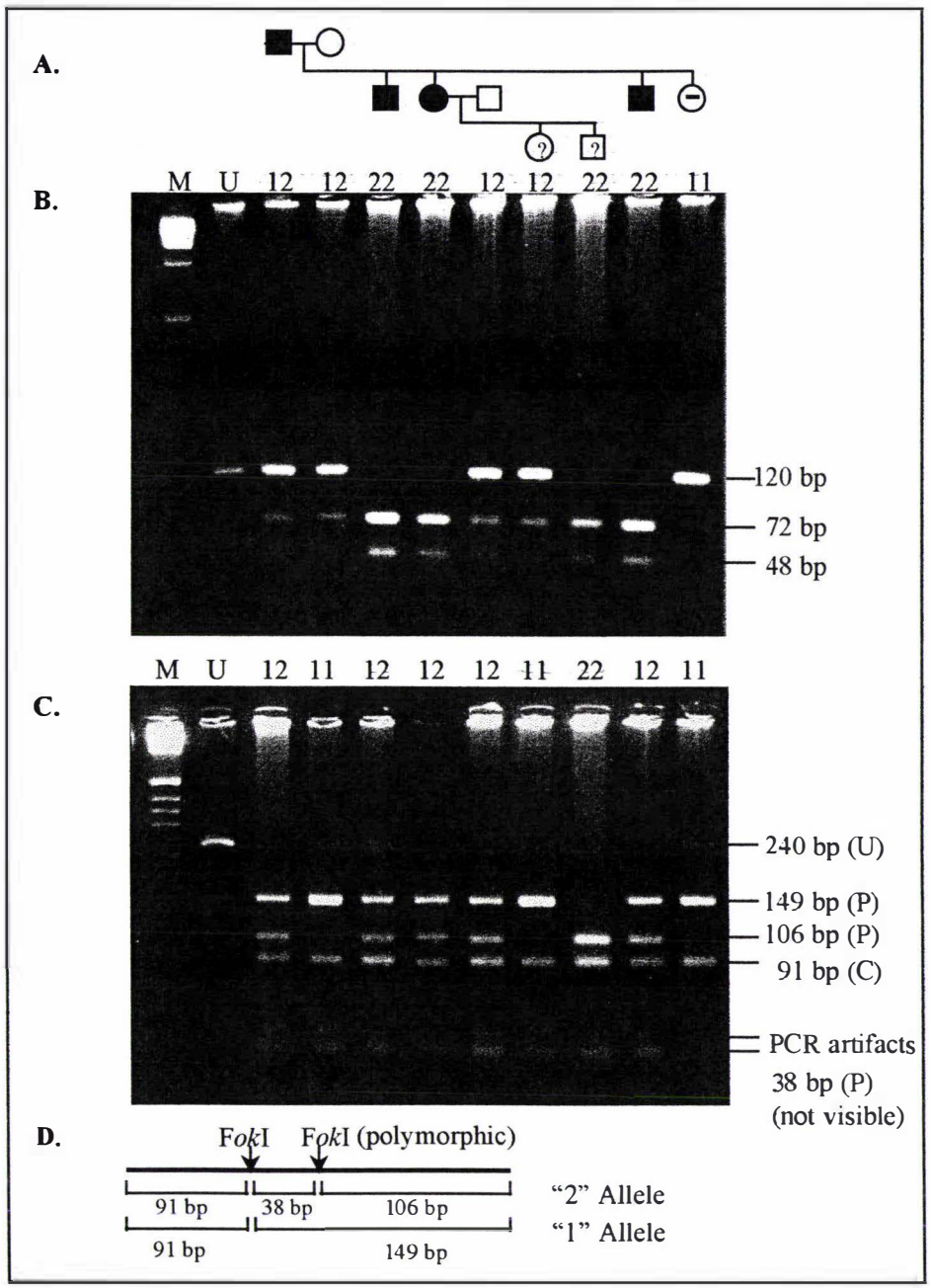

A. Segregation of MHS with the "2-2" (Ile1151, Asp2729) RYR1-RFLP haplotype in members of the CHEH pedigree. Symbols: Black = MHS, ? = Not tested, - = MHN.

B. PCR-RFLP analysis of the Ile1151 polymorphism revealed by *Taq* I digestion of PCR products (3.5% Nusieve gel in 1X TAE, stained in 0.5 µg/ml EtBr, and visualised under UV light).

C. RFLP analysis of the Asp2729 polymorphism by *Fok* I digestion of PCR products (3.5% Nusieve gel in 1X TAE, stained in 0.5 µg/ml EtBr, photographed under UV light). C= common bands. P = polymorphic bands associated with the "2" allele.

D. Illustration of RFLP fragments generated by *Fok* I digestion of the 240 bp PCR product at common and polymorphic (Asp2729) F*ok* I sites.

4.3.2 Analysis of sequence length polymorphisms flanking the RYR1 locus

In order to investigate linkage of MHS to the RYR1 locus, members of the Maori pedigree were typed for four chromosome 19q microsatellite markers that are tightly linked to the RYR1 locus: D19S220 [325,326], RYR1-CA [327], D19S190 [329] and D19S47 [328]. These markers were selected because of their proximity RYR1 (Figure 4-4) and their usage in published linkage studies [180,329,392,393]. Marker loci are indicated in the chromosome 19 physical and genetic maps shown in Figure 4-4 and Table 4.2 respectively.

Figure 4-4 Location of RYR1 markers

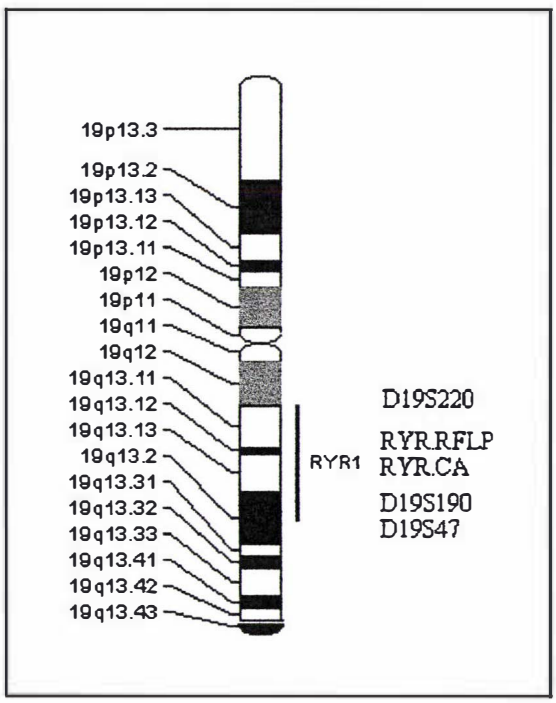

(Above) Adapted from current online GDB integrated chromosome 19 map (MAPVIEW) [349].

(Right) CHLC sex-averaged chromosome 19 framework map (version 3) [334]. Genetic distances are in Kosambi cM.

Table 4-2 Chromosome19q genetic map

Locus	θ	Interval cM	Total cM
D19S247	0.0091	0.9	0
D19S424	0.1346	13.8	0.9
INSR	0.0720	7.3	14.7
D19S413	0.0361	3.6	22.0
D19S394	0.0202	2.0	25.6
D19S221	0.0850	8.6	27.6
D19S432	0.0342	3.4	36.2
D19S410	0.0438	4.4	39.6
D19S434	0.0295	3.0	44.0
D19S433	0.0402	4.0	47.0
D19S431	0.0410	4.1	51.0
D19S248	0.0177	1.8	55.1
D19S191	0.0199	2.0	56.9
D19S220	0.0080	0.8	58.9
RYR1	0.0073	0.7	59.7
D19S190	0.0000	0.0	60.4
D19S47	0.0047	0.5	60.4
D19S200	0.0057	0.6	60.9
D19S197	0.0409	4.1	61.4
D19S537	0.0000	0.0	65.5
D19S178	0.0184	1.8	65.5
APOC2	0.0084	0.8	67.4
DM	0.0621	6.2	68.2
HRC	0.0378	3.8	74.4
D19S246	0.0354	3.5	78.2
KLK	0.0356	3.6	81.8
D19S601	0.0943	9.5	85.3
D19S418	0.0833	8.4	94.9
D19S254			103.3

Genotyping chromosome 19q markers

PCR primers were ordered according to published sequences to amplify the four chromosome 19q SSLP markers; D19S220 [325,326], RYRCA CA [327], D19S190 [329] and D19S47 [328]. The SSLP's were amplified by PCR using a single γ-^{33}P end-labelled primer, then resolved on 5- 8% denaturing polyacrylamide gels. An appropriate method for SSLP analysis of the RYR-CA marker was developed by trial and error and was used in the analysis of all four SSLP markers. The successful protocol was based on published methods [330] with an increased ratio of labelled to unlabelled primer to accommodate the use of the γ-^{33}P -labelled primer, which is a weaker β-

emitter than γ-^{32}P. PCR annealing temperatures and gel percentages and run times were tailored for each marker, as outlined in Chapter 2, section 2.6.2 and Table 2.7.

The interpretation of the SSLP gels was complicated by the presence of multiple bands representing each allele, termed "stutter" bands. These appeared as a 2 bp ladder of decreasing intensity below the major 'true' band. The stutter effect is thought to be due to slippage of *Taq* polymerase during DNA amplification [328]. Members of a British family residing in NZ (family 94) who had previously been investigated for these markers [392] were genotyped first to standardize the allocation of the correct allele numbers to the SSLP bands.

4.3.3 Procedures for maintaining data integrity

Ideally, genotyping should be performed by individuals who do not have knowledge of the disease phenotypes to prevent interpretation bias in the case of ambiguous results in favour of co-segregation of the disease and marker loci [330]. In this case, the assessment of phenotypic data, pedigree analyses, and cataloguing of DNA samples was performed in conjunction with regular consultation with clinicians and it was not possible to avoid prior knowledge of patient MH status.

The following precautions were observed to limit inadvertent interpretation bias and genotyping error:

- PCR reaction details were recorded on templates (Materials and Methods, Table 2.1) on which a unique PCR code number was assigned to each reaction as the primary field. DNA identification numbers were recorded under each PCR code number. In this way, repeated analyses of a particular DNA sample with the same primer set could be uniquely identified.
- Samples were identified only by their DNA numbers and unique PCR code numbers without reference to names or MH status when performing PCR and loading gels.
- Bands were compared against previously typed standards that were loaded at regular intervals across the gel to ensure consistency in allele assignment.
- Data sheets for recording genotypes were prepared in advance of the SSLP interpretation. Details included PCR code numbers, gel lane numbers, allele sizes for previously typed standards, and the position of M13 sequencing size standards.
- A blind interpretation of each autoradiogram was performed in which alleles were assigned and recorded with respect to the gel lane and PCR code number before cross-referencing results with DNA numbers from the PCR template forms.
- DNA samples were organised with parents and children adjacent to each other to aid comparison of inherited alleles. Any ambiguities were resolved by re-loading key samples adjacent to an array of previously typed samples.
- Reference samples from known homozygotes and heterozygotes with alleles that differed by one repeat unit were included to assist discrimination between the similar banding patterns produced by these alternate genotypes.

Details assisting interpretation of the four microsatellite markers, including the number of alleles observed and size range for each are given in Table 4-3. The sizes, assigned numbers and population frequencies of the alleles described for each of the markers are outlined in Table 4-4. These data were obtained from the genome database [349] and published information [327,329]. Examples of SSLP band patterns and allele assignment for members of the CH family typed for the D19S220, RYRCA, D19S190 and D19S47 markers are presented in Figure 4-5 to Figure 4-8.

Table 4-3 Chromosome 19q SSLP marker details

Marker	Allele set (GDB ID)	Primers	Product size (bp)	Repeat unit	No. of alleles, [HET]	Ref.
D19S220	GDB:62907	D19S220 F/R	265 - 283	CA	10 [0.846]	[325,326]
RYR-CA	GDB:61184	RYR-CA F/R	266 - 278	CA	7 [0.392]	[327]
D19S190	GDB:61127	D19S190 F/R	111 - 117	ACC	3 [0.625]	[329]
D19S47	GDB:58371	D19S47 F/R	88- 106	CA	9 [0.739]	[328]

Marker primer sequences are given in appendix 1.2

Table 4-4 Chromosome 19q marker allele frequencies (Taken from the GDB)

Locus	Allele number (fragment size {bp}, frequency)
D19S220	1(265, 0.03) 2(267, 0.09) 3(269, 0.01) 4(271, 0.09) 5(273, 0.27) 6(275, 0.16) 7(277, 0.16) 8(279, 0.11) 9(281, 0.01) 10(283, 0.01)
RYR-CA	1(278 0.01) 2(276, 0.01) 3(274, 0.1) 4(272, 0.77) 5(270, 0.03) 6(268, 0.03) 7(266, 0.05)
D19S190	1 (117, 0.170) 2(114, 0.44) 3(111, 0.39)
D19S47	1 (106, 0.03) 2(104, 0.01) 3(102, 0.110) 4(100, 0.38) 5(98, 0.06) 6(96, 0.04) 7(94, 0.04) 8(92, 0.310) 9(88, 0.01)
Combined RYR-RFLP	Allele number *(Taq* I, *Fok* I, *Cfo* I haplotype, observed frequency) 1(221, 0.53) 2(121, 0.15) 3(212,0.09) 4(112, 0.23)

Figure 4-5 Analysis of the RYR-CA dinucleotide repeat marker in the CHEA pedigree

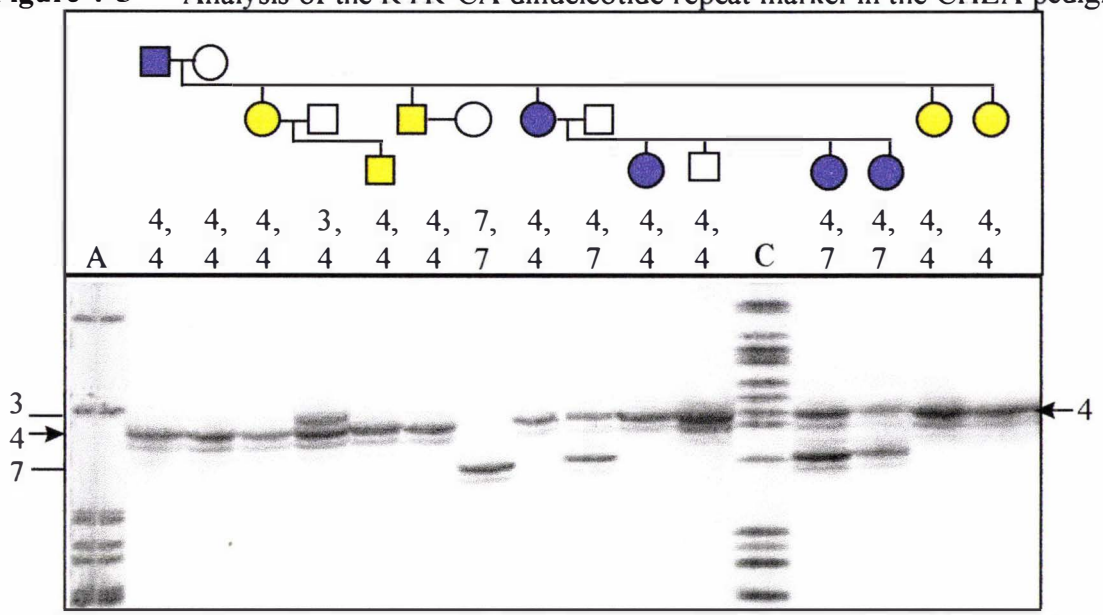

Representative gel showing members of the CHEA branch of the large Maori family typed for the RYR-CA marker. The γ^{33}P-labelled RYRCA-F/RYRCA-R products were denatured and resolved by 6% denaturing PAGE (3 hr. at 60 W in 1X TBE). Blue symbols are MHS; yellow symbols are MHN or MHE. Allele sizes were determined by comparison with the M13 sequence ladder (lanes "A "and "C"). The MHS phenotype coincides with the occurrence of the common 272 bp "4" allele (marked with an arrow). The RYR-CA marker was not informative for this branch.

Figure 4-6 Analysis of the D19S220 dinucleotide repeat marker in the CHES pedigree

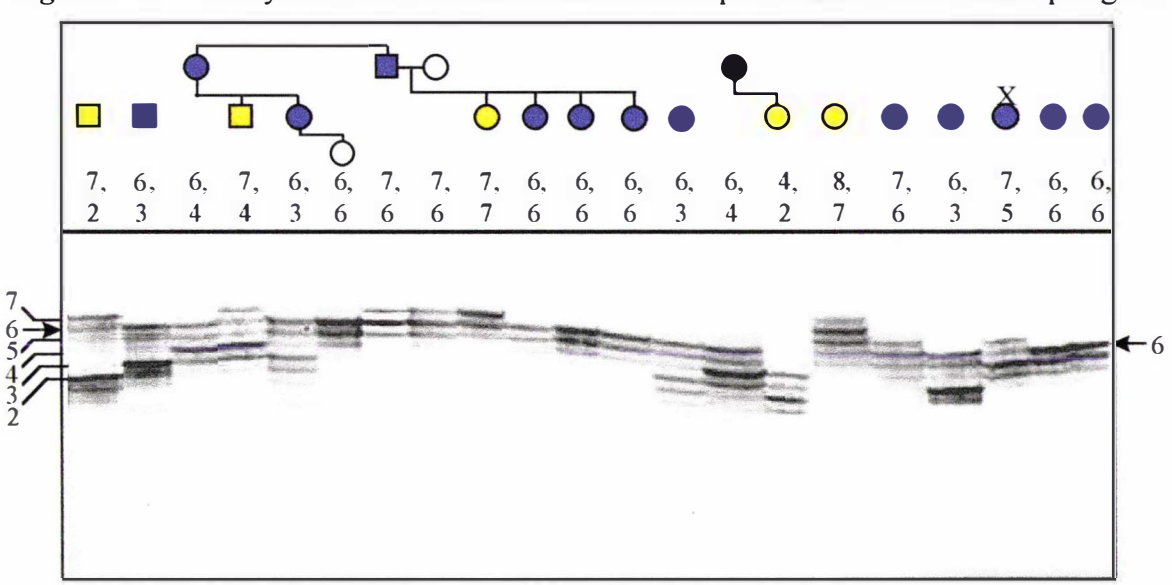

Representative SSLP gel showing members of the CHES branch of the large Maori family typed for the D19S220 marker. Samples were amplified with the γ^{33}P-D19S220-F/D19S220-R primer pair and resolved by 5% denaturing PAGE (3 hr. 40 min at 65 W in 1X TBE). MHS individuals are represented by blue symbols. MHN and MHE individuals are represented by yellow symbols. The MHS phenotype coincides with the occurrence of the 275 bp "6" allele (marked with an arrow) which was not inherited by any of the four MHN/MHE individuals. One recombinant MHS individual (M395, indicated with a cross) has not inherited the "6" allele. Reference samples were loaded in adjacent lanes to confirm the 7,5 genotype that was assigned to this recombinant individual in a previous analysis.

Figure 4-7 Analysis of the D19S47 dinucleotide repeat marker in the CHEH pedigree

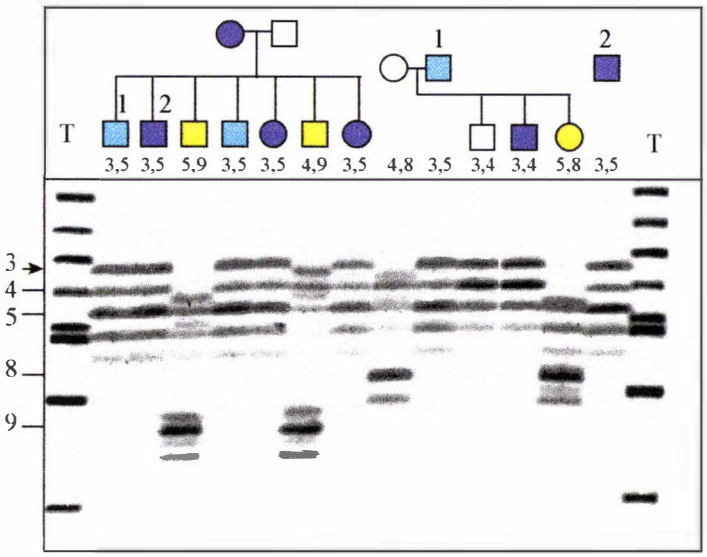

The γ^{33}P-labelled D19S47-F/D19S47-R PCR products were denatured and resolved by 8% denaturing PAGE (2 hr. 40 min at 65 W in 1X TBE). Blue symbols are MHS, yellow symbols are MHE or MHN, and pale blue symbols represent obligate MHS subjects. The MHS phenotype coincides with the inheritance of the 102 bp "3" allele, which is absent from the three MHN individuals. Allele sizes were determined by comparison with the M13 sequencing ladder ("T"). Additional bands migrating ~1 bp above the principle bands in lanes 4, 7 and 9 are gel artifacts (conformation polymorphisms) and were not observed upon repeated electrophoresis of the same PCR products.

Figure 4.8 Analysis of the D19S47 CA-repeat marker in the CHES pedigree

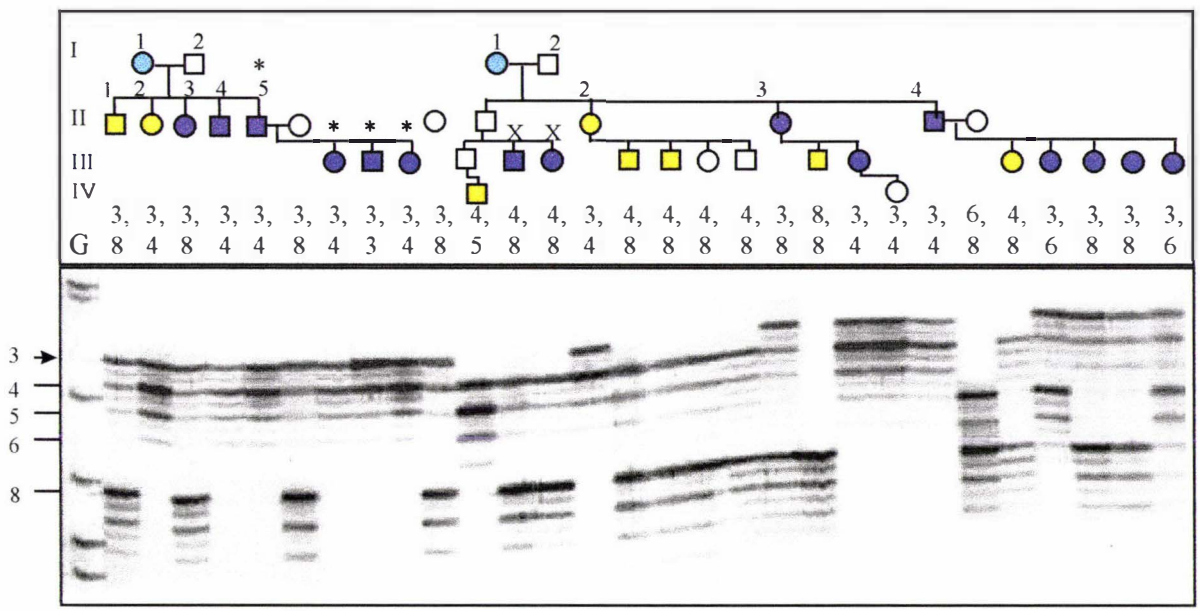

Members of the CHES branch of the pedigree were typed for the D19S47 marker 7.5% denaturing PAGE (2 hr. 15 min at 65 W in 1X TBE). Blue symbols are MHS; yellow symbols are MHE or MHN. The MHS phenotype coincides with the inheritance of the "3" allele, which was not detected in five of the eight MHE/MHN subjects. However, two MHS siblings are recombinant. Individuals M42 and M206 (marked with crosses) were diagnosed MHS before the adoption of the standard IVCT protocol and both have the "4,8" genotype. These individuals, together with other members the CHES branch (*) appeared to be recombinant with respect to the RYR-RFLP and D19S220 markers.

Figure 4-9 Analysis of the D19S190 trinucleotide repeat marker in the CHEA pedigree

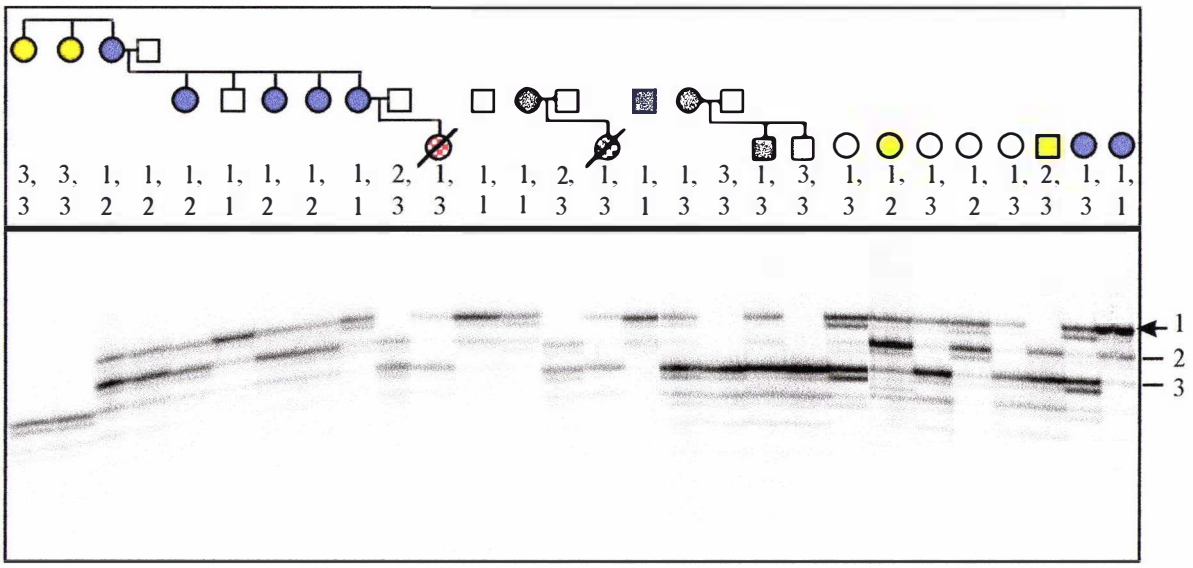

Representative gel showing members of the CHEA branch of the large Maori family typed for the D19S190 marker. The γ^{33}P-labelled D19S190-F/D19S190-R PCR products were denatured and resolved by 7.5% denaturing PAGE (2 hr. 15 min. at 65 W in 1X TBE). Blue symbols are MHS; yellow symbols are MHE or MHN. Red chequered symbols represent individual M412, who suffered sudden unexplained death. The MHS phenotype coincides with the occurrence of the 117 bp "1" allele (marked with an arrow) which was not observed in three MHN individuals.

4.3.4 Resolving data inconsistencies

Genotype data error is often revealed by apparent non-Mendelian transmission of alleles from parents to offspring. The apparent occurrence of multiple crossovers between markers is also highly indicative of undetected genotyping error [349]. Non-Mendelian data inconsistencies resulting from genotyping error are detected and reported by the LINKAGE program. However in some cases errors may pass undetected as recombination events [330,394] that can lead to inflated recombination fractions in linkage analysis [353,377,378].

All genetic data inconsistencies were scrutinized by repeated PCR and SSLP analysis of the original DNA sample followed by analysis of a second DNA sample extracted from stored leukocytes. If inconsistencies persisted, the analysis was repeated on DNA extracted from a new blood sample, where possible. Genotyping errors were found to be very infrequent, however three cases of mistaken DNA sample identity were identified. DNA was re-extracted from fresh blood samples from these subjects.

Inconsistencies suggestive of errors in the IVCT diagnosis (for example, the apparent inheritance of MHS from an MHN parent) were difficult to resolve. Before conducting linkage analysis, the raw IVCT data sheets for each patient were obtained from the Palmerston North Hospital, and details were entered into a database. The data was reviewed for methodological inconsistencies and breaches of standard IVCT protocol, under consultation with Dr. Neil Pollock, and data were omitted or substituted where appropriate (as described further in a discussion at the end of this chapter).

4.4 SEGREGATION OF MHS WITH CHROMOSOME 19q MARKERS IN THE CH FAMILY

4.4.1 The CHEH branch

The segregation of chromosome 19q markers with the MHS phenotype was investigated in four major branches of the CH family (CHEH, CHEA, CHK and CHES, appendix 9). Members of one large branch (CHEH) of the Maori pedigree were sampled initially. Haplotypes were constructed for the RYR1 intragenic markers (RYR-RFLP3) and the four RYR1 linked microsatellites. The segregation of chromosome 19q13.1-13.2 markers with the MHS phenotype in members of the CHEH branch (descended from individual III-35) is illustrated in Figure 4-10.

The inheritance of a "high risk" haplotype of alleles 6-1-4-1-3 for the markers D19S220, RFLP3, RYRCA, D19S190 and D19S47, respectively was found to coincide with the inheritance of MHS phenotype in eight MHS individuals in the CHEH branch, one of whom (M10) had suffered a fulminant MH reaction. The same haplotype was also observed in two obligate carriers. The putative MHS-linked haplotype was not detected in any of the three MHN patients, or in four individuals diagnosed MHE, consistent with the involvement of a RYR1 gene defect in this pedigree.

However, MHS did not segregate completely with the chromosome 19q markers. Individuals M231 and M130 who were both diagnosed MHS according to EMHG diagnostic criteria have not inherited the 6-1-4-1-3 haplotype. This result suggests that MHS in the CH pedigree arose from a mutation in gene outside the region bound by the D19S47 and D19S220 markers rather than RYR1 itself. However, this would require the improbable event of at least two independent recombinant events between the disease locus and the panel of markers.

The MHS diagnosis in individual M130 is particularly problematic, since the father of this individual (an expected obligate carrier) was diagnosed MHN. The haplotype data corroborates the alleged paternity for both M130 and M231. The mothers of the recombinant individuals have declined a muscle biopsy, so the possibility of genetic heterogeneity and introduction of MH susceptibility from an unrelated spouse cannot be ruled out in either case. Another possibility is that the father of M130 may have been falsely diagnosed MHN, however this is highly improbable in view of the rarity of false negative IVCT diagnoses [97,102]. An alternative explanation is that, as the IVCT does not achieve absolute specificity [97], individuals M130 and M231 may be false positives. In fact, an inspection of the IVCT data revealed that these two discordant MHS individuals registered the weakest IVCT tensions of the MHS group. These individuals are therefore likely candidates for false positive diagnoses.

Figure 4.10 Segregation of with MHSchromosome 19q markers : Pedigree branch CHEH

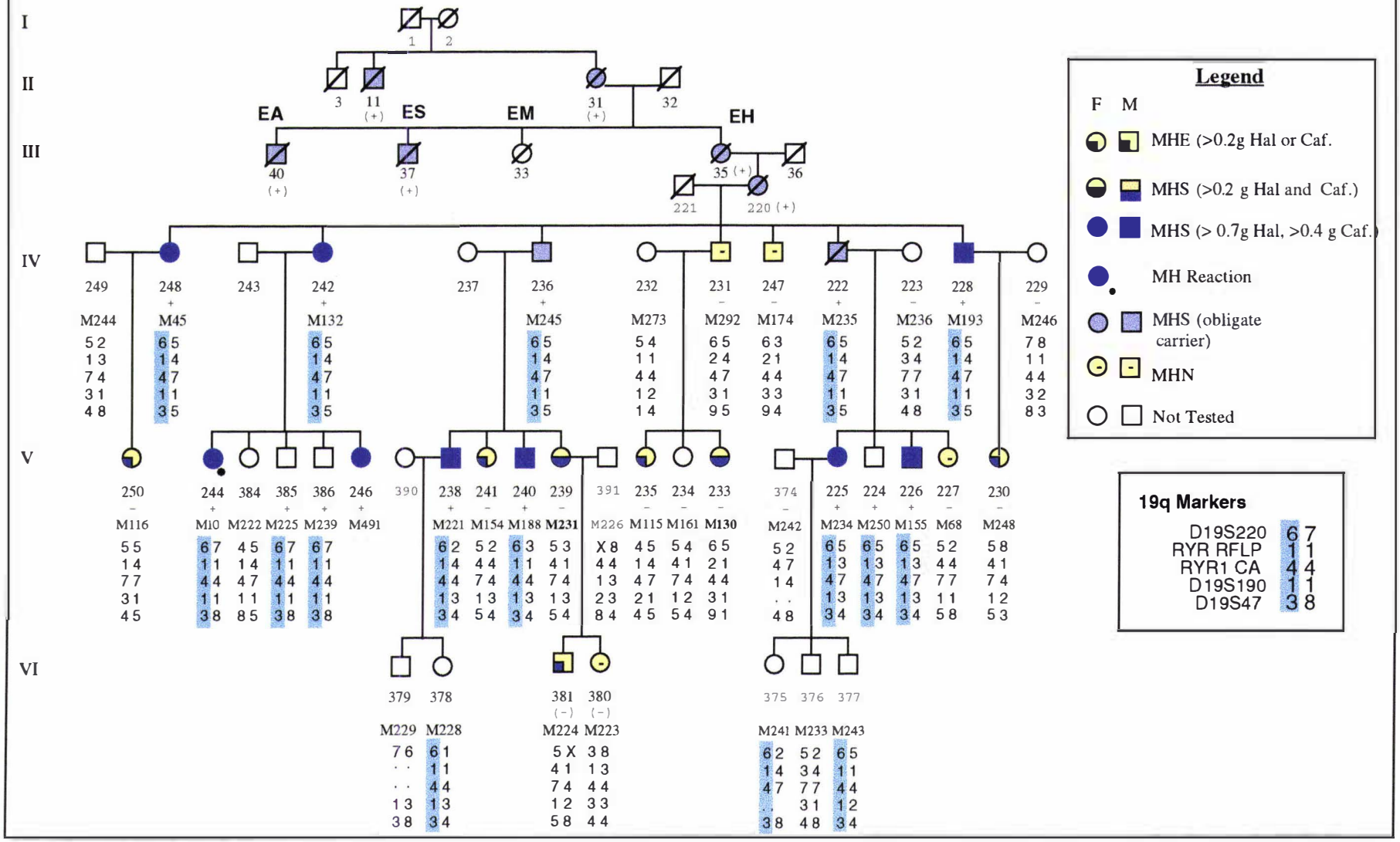

4.4.2 The CHEA branch

The haplotype analysis was extended to the CHEA branch (Figure 4-11) as DNA samples became available. The inheritance of the MHS phenotype coincided with the 6-1-4-1-3 haplotype in eight MHS individuals (including the sister of individual 337 who had died from a MH reaction), and one obligate carrier (M21) as shown in Figure 4-11. The 6-1-4-1-3 haplotype was not observed in eight MHN patients or nine MHE patients consistent with linkage to the RYR1 locus in this branch of the family.

Two families demonstrated incomplete segregation of the RYR1 markers with MHS. In the first case, the high-risk haplotype was not observed in individual M408 (Figure 4-11), who was presumed to be an obligate MHS carrier based on MHS diagnoses in two offspring. Alleles at the RYR-RFLP and D19S47 loci were consistent with the MHS-associated haplotype, however individual M408 has the "7,2" genotype at the D19S220 locus, and therefore is recombinant at this locus. Genotypes were confirmed by repeated analysis and comparison with control samples presenting the "6" and "7" D19S220 alleles. The data could be explained by a genetic recombination between the D19S220 locus and the RYR1 gene in the previous generation (i.e. in a parent of M408). This is difficult to ascertain in the absence of IVCT data from M408 and his brother, M352. The situation is further complicated by the apparent non-Mendelian segregation of the D19S190 alleles, since the "3,2" and "2,2" genotypes for M175 and M33 at this locus are both incompatible with parental alleles. Consistent results were obtained on repeated analysis therefore this discrepancy has not been resolved. Non-paternity or sampling errors were not excluded, but would seem unlikely given the compatibility of alleles with parental types at other loci.

The second case of discordance involves individual M54 (Figure 4-11) who inherited a 2-4-4-(1)-4 maternal haplotype and a 3-1-4-(-)-4 paternal haplotype, yet was diagnosed MHS. This discrepancy could not be explained by a single recombination event between RYR1 and the flanking markers because alleles at both the D19S220 and D19S47 loci do not concur with the 6-1-4-1-3 pattern. An alternate possibility is that MHS in this family arises from a mutation in a linked gene other than RYR1. However, this would require at least two recombinant events distal to the D19S220 locus. Other plausible explanations for this discrepancy include false positive diagnosis or paternal inheritance of an alternate MH gene defect. The MHE diagnosis for the mother (M47) of M54 supports the latter hypothesis. In further support, the mother (M47) does not carry the MHS-linked haplotype, and instead has inherited a normal chromosome 19q haplotype that was also transmitted to her MHN and MHE half-siblings. This suggests that that M47 did not inherit the MHS trait and consequently, could not have transmitted MHS to her son. The father of M54 was not available for muscle biopsy examination; therefore, paternal inheritance of the MHS defect was not excluded.

The CHEH and CHEA branches of the Maori family were condensed into a single pedigree file for the purpose of genetic linkage analysis and are collectively referred to as the "CH1 pedigree".

Figure 4.11 **Segregation of MHS with chromsome 19q markers : Pedigree branch CHEA**

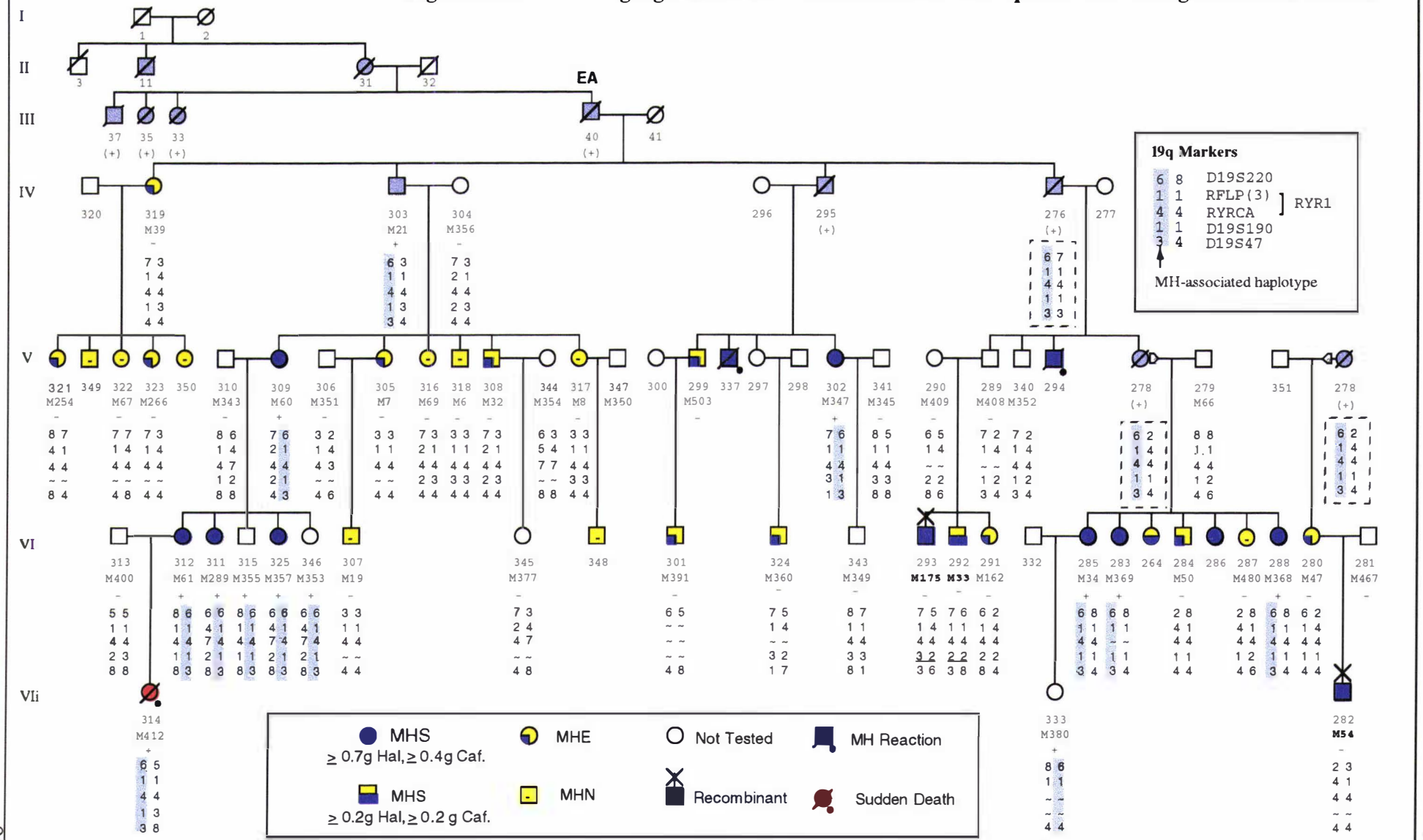

4.4.3 The CH2 pedigree

Following the analysis of the CHEH and CHEA branches, descendants of individual II-11 comprising the "CHK" families were typed for the chromosome 19q markers. These branches of the large Maori CH family are collectively referred to as the CH2 pedigree in Figure 4-12. Consistent with the observations from the CHEH and CHEA branches, the 6-1-4-1-3 haplotype was found to coincide with the MH trait in seven MHS individuals, one patient who had survived an MH episode, (M29) and two obligate MHS carriers. The 6-1-4-1-3 pattern was not observed in six patients that were diagnosed MHN or MHE.

However, segregation is incomplete in two nuclear families. In the first case, a presumed obligate MHS individual (M93) from the CHKM branch lacked the high-risk 6-1-4-1-3 haplotype. Consequently, her two MHS daughters and MHS granddaughter also lacked the haplotype characteristic of MHS in the CH family. The grandmother, M93, registered an abnormal IVCT halothane test but recorded a normal response to 2 mM caffeine. She was therefore classified MHE. Two MHS daughters (M98, M199) and MHS granddaughter (M99) do not share common maternal chromosome 19q haplotypes. Four possible explanations were considered in an attempt to reconcile these discrepancies. Firstly, the discordance in this branch of the family could be attributed to diagnostic error, which would require the acceptance of three false positive diagnoses. This is unlikely given the specificity of the IVCT. Secondly, instead of a RYR1 mutation, a mutation in a linked gene outside the region defined by the RYR1 flanking markers might actually be causative of MH susceptibility. However, if this were true, multiple recombination events and a false negative caffeine test (for M93) must be invoked to explain the data in this pedigree. Thirdly, it is possible the MHS defect in M98 was inherited paternally. However, if this were true, a false positive diagnosis in M199 is still required to reconcile the data since M98 and M199 have different fathers. A fourth, and more probable possibility is that M93 may have inherited or incurred a mutation in a second gene not linked to the RYR1 region. This would account for the abnormal IVCT halothane test result in M93, the MHS diagnoses in four of her descendants and the lack of a common chromosome 19q haplotype in these individuals.

The second discrepancy involves an individual from the CHKW branch (M102). This individual carries the D19S220 "6" and D19S47 "3" alleles consistent with inheritance of the high-risk haplotype, but has the "1,1" genotype for the single RYR1 *Taq*I RFLP marker. M102 therefore could not have inherited the MHS-associated RYR1 allele carried by his MHS sibling (M5). A single false positive in M102 could account for this discrepancy. In support of this conclusion, the contracture data from seven muscle strips from this individual subjected to the halothane test were very inconsistent, with only two of the seven strips registering responses above the 0.2 g threshold for MHS diagnosis. Furthermore, out of three muscle strips subjected to the caffeine contracture test, the maximum tension recorded was only 0.2 g for this individual. The MHS diagnosis for M102 was only the third MHS diagnosis made at the Palmerston North testing centre. It has been suggested that these tests performed in early the stages of development of the Palmerston North Hospital IVCT laboratory were less reliable than current tests (N. Pollock, personal communication).

Figure 4-12 Segregation of MHS with chromsomome 19q markers: Pedigree CH2

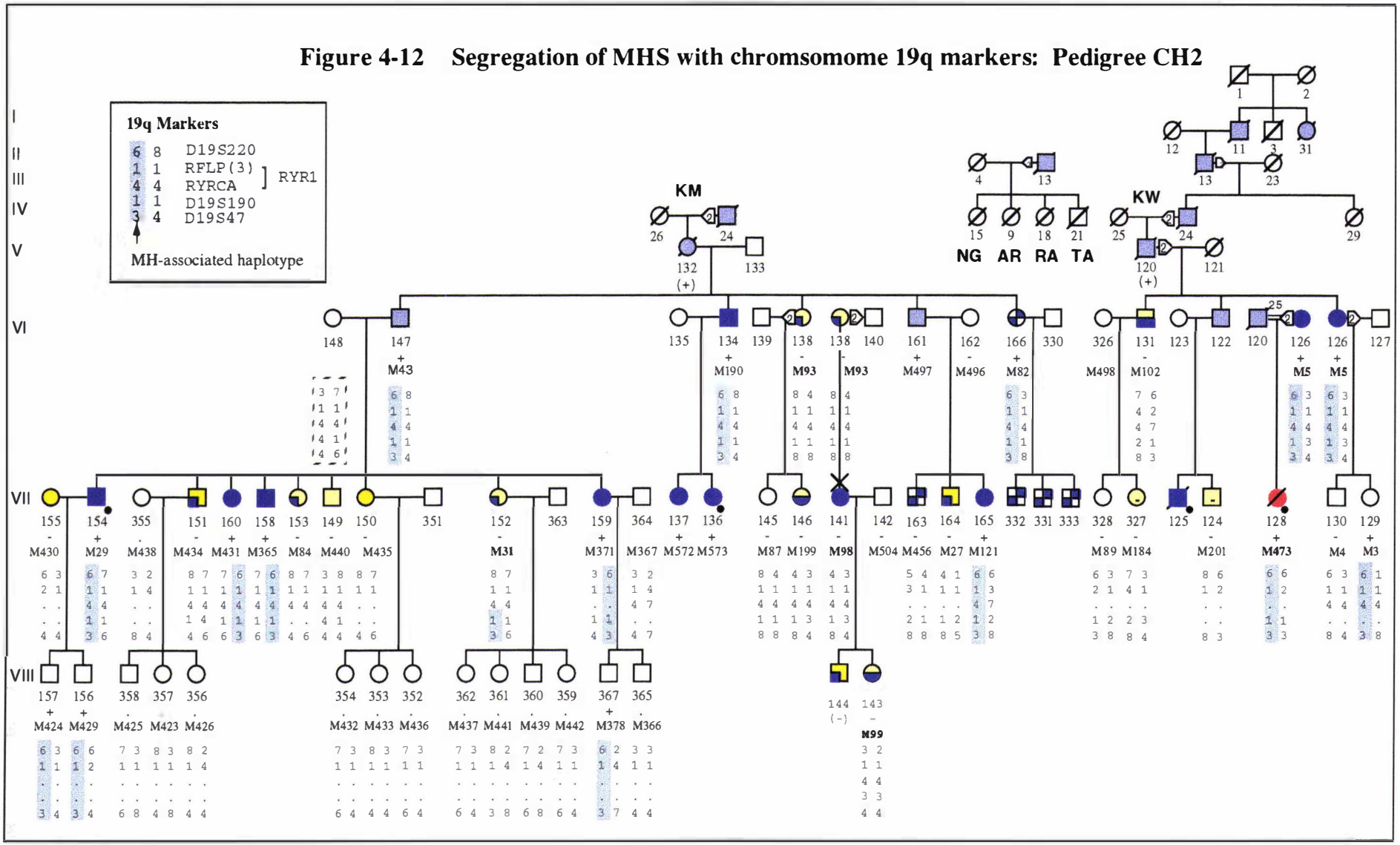

4.4.4 The CH3 pedigree

The haplotype analysis was extended to the remaining branches of the CH pedigree, restricting the panel of markers to the more informative D19S220 and D19S47 dinucleotide repeat and combined RFLP polymorphisms. The ES, EM, NG and RA branches were condensed into the CH3 pedigree (Figure 4-13). One marriage loop and three consanguineous marriages link the families in this diagram. Consistent with the results from the other branches, individuals positive with respect to the MHS-associated haplotype (6-1-3) registered strong positive IVCT results.

CHEM family

The high-risk (6-1-3) haplotype was absent from all members of the CHEM branch of the family. A single (weak) MHS diagnosis was recorded in this branch. Interestingly both parents of the MHS individual (M86) have been diagnosed MHN, suggesting M86 was falsely diagnosed MHS. These data suggest that MH is not present in this branch of the family.

CHNG family

The NG branch of the family involves a consanguineous marriage between two distant MHN cousins. Both lacked the 6-1-3 haplotype as did their two MHN offspring (and four other offspring not included in the pedigree diagram). The data indicate that the NG branch is a negative line of inheritance for both the MHS defect and the associated RYR1-haplotype.

CHRA family

The segregation of the chromosome 19q haplotypes with the MHS phenotype in the RA branch of the family is entirely consistent with linkage to the RYR1 locus. The 6-1-3 pattern was detected in the DNA of six MHS individuals, including individual M74, who had suffered two MHS reactions. The mother of this individual had died of a fulminant MH crisis. The 6-1-3 haplotype was not detected in the DNA of two MHN and two MHE individuals from the RA branch. One consanguineous marriage involved a male (ID 20) from the CHRA branch who has a 50% likelihood of MHS status and a female second cousin from the CHES branch (ID 18) who has obligate MHS status (with MHS offspring from a previous marriage). The maternal haplotypes (ID 18) could be deduced as 6-1-3/2-1-4 from the genotypes of four other offspring, but the paternal haplotypes (ID 20) could not be ascertained. Their sole MHS child (M197) therefore has a 0.125 probability of homozygosity for the gene defect. Inspection of the haplotype data indicated M197 was heterozygous for 6-1-3 haplotype and the putative RYR1 gene defect.

CHES family

The founders of the ES branch are individuals III-37 and III-38, whose haplotypes were deduced from the genotypes of five offspring. Two of these offspring (M58 and M22) were diagnosed MHN and have not inherited the maternal 6-1-3 "high-risk" haplotype. Two other offspring (M40 and M48) were diagnosed MHS and have transmitted the 6-1-3 haplotype to four MHS children and the non disease-linked haplotypes to two MHN individuals. The segregation of chromosome 19q markers is therefore consistent with linkage to MHS in ten individuals on the left-hand side of the CHES pedigree.

However, MHS does not segregate with the chromosome 19q markers in the right hand branch of the CHES family. The fifth child of III-37 and 1II-38 (ID251) was diagnosed MHS but neither he nor his four MHS children or three MHS grandchildren could possibly have inherited the 6-1-3 haplotype. These eight discordant MHS individuals do not share a single common chromosome 19q haplotype. One individual (M395) does not carry the "1" RYR1-RFLP allele that associates

with the MHS in the rest of the family, thus the discrepancies cannot be accounted for by recombination between the RYR1 locus and the flanking markers.

Genotyping errors were excluded by repeated analysis with fresh DNA samples. The haplotypes are also consistent with the alleged paternity. Errors in phenotype classification are harder to discern, but eight false positive MHS diagnoses in one small family are highly improbable, based on the reported specificity of the IVCT [97]. The incidence of the MHS phenotype in several members of the CH family who have clearly not inherited the 6-1-4-1-3 haplotype challenges the causative role of the RYR1 gene or other nearby RYR1-linked gene under a single gene model. Multiple recombination events within the short genetic distance of 1.5 cM between D19S220 and D19S47 would have to be invoked to reconcile the involvement of a gene within or nearby the region represented by these markers. The discordance in the CHES branch is more readily explained by the introduction of an additional inherited factor that predisposes to abnormal IVCT responses and/or MH susceptibility. This may have been introduced by one of the unrelated spouses or by *de novo* mutation.

4.4.5 Identification of crossovers

Detecting important recombination events is an essential step in defining the proximal and distal boundaries of linkage to a panel of markers. A crossover detected in one individual (M31, CHK family, Figure 4-13) between the disease locus and the D19S47 locus placed the disease locus centromeric to the D19S47 marker, which is 0.71 cM from the RYR1 gene. This individual (M31) was diagnosed MHN but has inherited the "3" D19S47 allele derived from the MHS-associated haplotype together with the unlinked D19S220 '8' allele. Genotypes at RYR-RFLP3 and D19S190 loci were not informative in this meiosis; therefore, the position of the crossover between could not be further defined. Genotyping error was excluded by repeating the data collection. Furthermore, M31 transmitted the recombinant haplotype to two offspring in fully informative meioses. This observation indicates that the recombinant haplotype inherited by M31 is the result of genetic crossover rather than genotyping error.

A crossover between the RYR1 locus and the D19S47 marker was detected in a second individual (M147, CHES branch, Figure 4-13). This individual has inherited the 6-1-8 haplotype which is not compatible with either the maternal (7-2-8 / 6-1-6) or paternal (6-1-3 / 7-4-4). This inconsistency is readily explained by the occurrence of a recombination between the maternal chromatids, telomeric to the RYR1 locus. The maternal 7-2-8 haplotype and the associated region of the recombinant 6-1-8 haplotype are shaded pink in Figure 4-13. The possibility of non-paternity is excluded by the paternal transmission of both the 6-1-3 haplotype and MHS to M147. This recombination was not informative for linkage because it involved a chromatid from an unrelated individual. The centromeric boundary for linkage was not defined in this study.

Figure 4-13 Segregation of MHS with chromosome 19q markers: Pedigree branch CH3

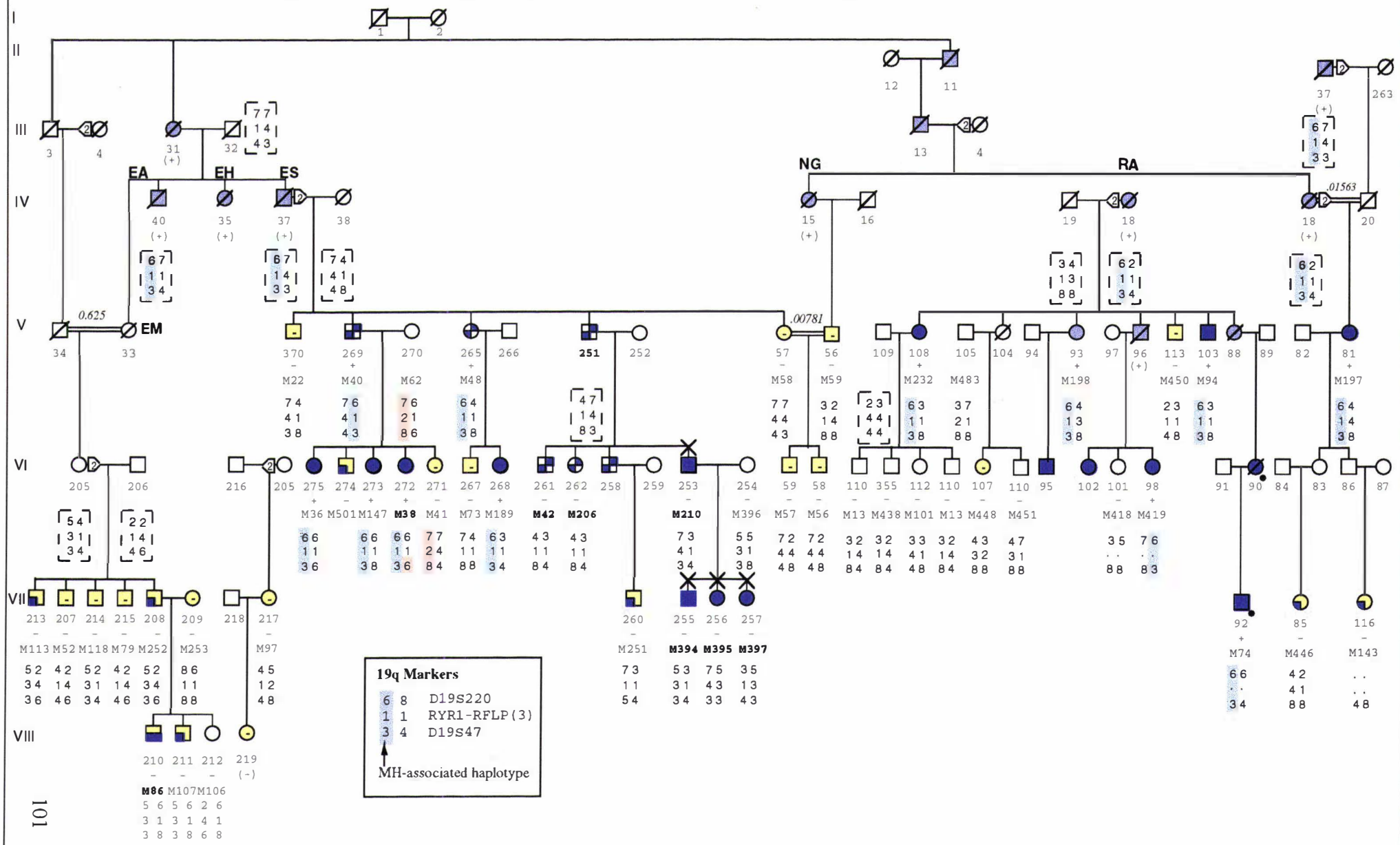

4.4.6 Haplotype analysis of SIDS victims

Two distantly related children aged 9 and 24 months born to MHS parents in the CH family died sudden unexplained deaths in the absence of any known triggering agents. These cases of sudden death are unique in that febrile seizures were noted before death, and symptoms resembled an awake episode of MH with both hyperthermia and muscle rigidity (N. Pollock, personal communication). It is noteworthy that the parents of the nine-month-old infant were closely related (inbreeding coefficient 0.25), therefore the infant had a 25% probability of homozygosity for the putative RYR1 gene defect. A possible role of the RYR1 gene defect in predisposing these children to sudden death was investigated by retrospective analysis of DNA extracted from paraffin embedded autopsy tissue.

Autopsy specimens were obtained from the 9-month-old infant and the 24-month-old child to determine whether they had inherited the MHS-linked haplotype, and if so, whether they were heterozygous or homozygous for the putative RYR1 gene defect. DNA extracted from paraffin embedded tissue (PET) is typically of a poor quality, due to damage by fixation in formalin, long term storage in paraffin and the shearing that can occur during vigorous extraction processes [311]. Difficulties in the PCR amplification of DNA from PET were therefore anticipated due to the fragmentation of the DNA and inhibition by fixatives.

Extraction and analysis of DNA from paraffin embedded tissue

Autopsy spleen tissue was obtained from the Palmerston North Hospital. DNA extracts were visualized by gel electrophoresis as a smear in the 300 bp - 2 kb size range, indicating significant degradation had occurred.

An inverse relationship between the DNA concentration and amplification yield was observed, presumably due to the inhibitory effects of residual tissue fixatives carried over in the DNA extraction. PCR amplification of the RYR1 RFLP sites from a 1/40 dilution of the templates generated bands of the expected size. The primary PCR products were diluted and reamplified in order to obtain sufficient DNA for RFLP analysis. Particular care was taken to avoid cross-contamination of the PCR by the use of barrier tips and the inclusion of several negative PCR controls.

After repeated attempts, the D19S47, D19S190 markers were amplified and genotypes established for both PET DNA samples. Genotypes for the D19S220 and RYR1-CA markers were also determined for the autopsy DNA sample extracted from tissue taken from the 24-month-old child in 1996 (M412, Figure 4-15). The D19S220 and RYRCA PCR products are approximately twice the size of the D19S47 products. These proved difficult to amplify from the older, highly degraded DNA from the 9-month-old infant who had died in 1962 (M473, Figure 4-15). Consequently, PCR failure precluded genotyping the older DNA sample for these markers despite repeated attempts. Haplotypes for the deceased children and their families were constructed and presented in Figure 4-15.

Examination of the segregation of the panel of chromosome 19q markers revealed the inbred child was homozygous for the D19S47 "3" allele but was heterozygous for the T*aq*I RFLP marker as shown in Figure 4-14. Therefore, we can not attribute this case of sudden death to homozygosity for the RYR1 gene defect.

The haplotype data revealed that both young children who suffered sudden unexplained deaths in the absence of any known triggering agents were heterozygous for the MHS-linked haplotype. Although this association may be coincidental, the possibility that inheritance of the putative RYR1 gene defect may have played a role in the deaths of these two infants could not be excluded.

Figure 4-14 Analysis of the *Taq*I marker in a family of a SIDS child

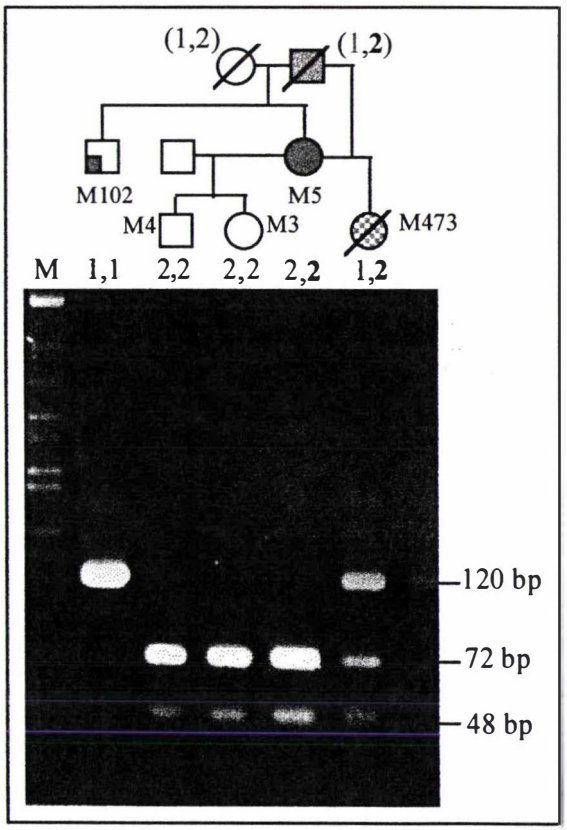

DNA samples from the CHKW family were amplified with the RYR11151-F/R primer set, digested with T*aq* I and resolved on a 3% Nusieve gel in 1X TAE, The gel was stained in 0.5 μg/ml EtBr and photographed under UV light.

Individual M473 died in infancy (sudden infant death). DNA was extracted from autopsy spleen tissue. Both closely related MHS parents of this child carry the MHS-associated "2" T*aq* I allele. M473 is heterozygous for the T*aq* I RFLP marker and has inherited the "2" allele maternally (bold type).

Discordant Individual M102 was diagnosed MHS according to EMHG protocol but has inherited the non-disease linked "1" allele (red type) paternally.

Figure 4-15 Association of the MHS-linked haplotype with sudden unexplained death.

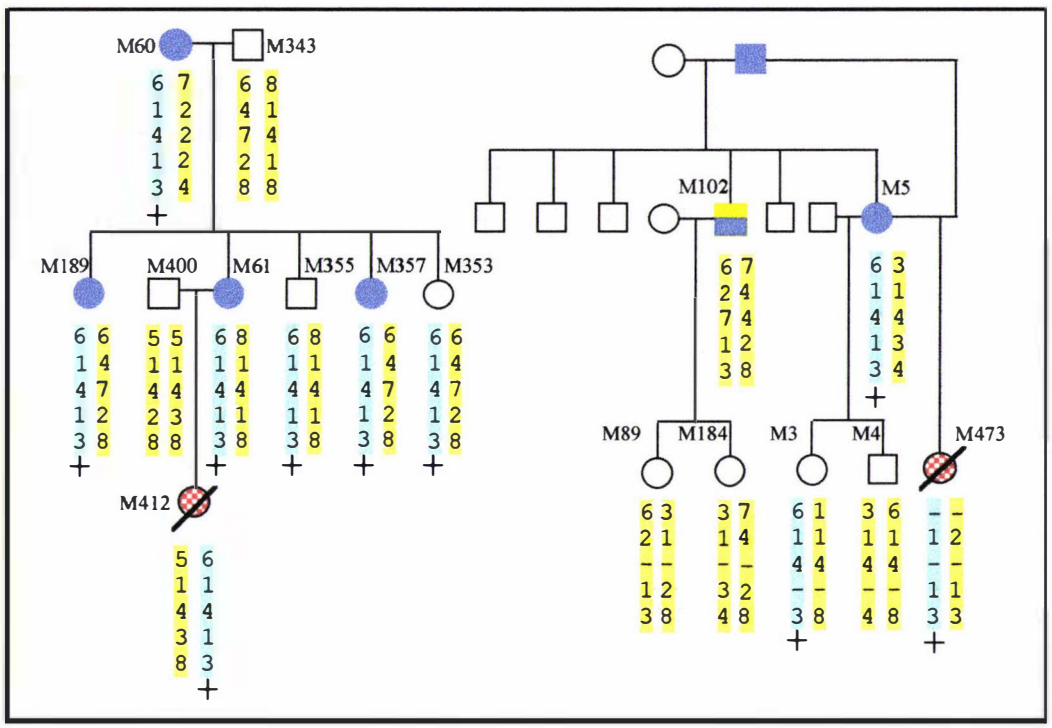

Symbols are as described for Figure 4-11. Red chequered symbols indicate young children who died sudden unexplained deaths. DNA identity numbers are shown. DNA sample M412 was from a 2 year old girl who died in 1997. DNA sample M473 is from a 9 month-old infant who died in 1962. DNA was extracted from paraffin embedded autopsy spleen tissue specimens. + Signs denote the positive status for an MHS-linked RYR1 mutation subsequently identified in the CH family.

4.4.7 Haplotype analysis of other Maori MHS families

Two other MH families of Maori descent were referred to the Palmerston North Hospital for IVCT examination (families 48 and 70). A link between these families and the CH family was not established within the branches of the CH family that had been traced (K. Couchman, personal communication). Selected individuals from these families and a MHS child of Polynesian descent (family 99) were typed for the D19S220 and D19S47 markers to examine the possibility that two or more of these families may have common ancestry and share the same RYR1 gene defect. None of the MHS or MHE individuals examined from the three families shared any alleles in common with the 6-1-4-1-3 high-risk haplotype identified for the CH family at either the D19S220 or D19S47 locus (data not shown). It is therefore unlikely that any of the four Maori or Polynesian families could have inherited the same RYR1 defect via a common founder.

4.5 TWO-POINT LINKAGE ANALYSIS

The investigation of the segregation of chromosome 19q markers flanking the RYR1 locus in the CH family implicated the involvement of a RYR1 defect in MHS. The inheritance of a unique 6-1-4-1-3 haplotype coincided with the MHS phenotype (or obligate MHS status) in 40 individuals from four distantly related branches of the family. However, several cases of discordance were encountered in which individuals who were diagnosed MHS lacked the RYR1 6-1-4-1-3 haplotype. This contradicted the assumption of linkage to the RYR1 locus in the CH pedigree. In order to determine the probability of linkage of MHS to the RYR1 locus, the data were quantified statistically by performing genetic linkage analysis. Linkage to the chromosome 19q region was assessed separately for each of the markers in pairwise (or two-point) analyses.

4.5.1 Estimation of allele frequencies

Allele frequencies for the disease and marker loci were stipulated in the parameter file for linkage analysis. Allele frequencies for the D19S220 [325,326], RYR-CA [327], D19S190 [329] and D19S47 [328] markers were taken from published data and online information from the genome database [349]. Data from the three RFLP markers were combined and presented as the RYR1-RFLP3 locus. Haplotype frequencies for this combined locus were not available. Consequently, the frequencies of each of the combine RYR1-RFLP3 haplotypes were estimated from the proportion of each haplotype amongst 38 unrelated spouses in the CH pedigree according to recommended procedures [330,395][396]. The RYR1-RFLP3 allele frequencies calculated for the CH pedigree are given in Table 4-5.

Table 4-5 Allele frequencies observed for combined RYR1-RFLP3 locus

Allele No.	RFLP haplotype (Ile1151, Ser2862, Asp2729)	Observed frequency (CH pedigree)
1.	221	0.53
2.	121	0.15
3.	212	0.09
4.	112	0.23

Only four configurations of alleles for the three RFLP marker loci were observed, since the Asp2729 and Ser2862 markers appeared to be in linkage disequilibrium. It transpired that the MHS-linked 2-2-1 haplotype (allele 1) was the most frequently observed haplotype in the population. This reduced the likelihood that the combined RYR-RFLP3 marker would be informative for linkage in this family, since individuals are less likely to be heterozygous for a common allele.

4.5.2 Organization of pedigrees for linkage analysis

The CHEH and CHEA branches of the large Maori family shown in Figure 4-10 and Figure 4-11. were combined in one pedigree termed CH1, for linkage analysis. The CH2 branch, displayed in Figure 4-12, comprises descendants of individual ID24. The remaining branches of the complex pedigree were combined in the CH3 pedigree shown in Figure 4-13. This included descendants of ID13 (RA and NG branches), ID3 and ID33 (EM branch) and ID 37 (ES branch), who are all

linked by consanguineous marriages and other marriage loops. The decision to break the large complex family into three groups for linkage analysis was based primarily on the memory demands associated with linkage programs. Memory restrictions did not accommodate calculation of two-point lod scores for the complex pedigree under a range of genetic models. In addition, the impact of subtle changes in the genetic model or diagnostic parameters may have been obscured in the analysis of the complex pedigree. Memory restrictions entirely excluded multipoint analysis of the complex pedigree using the LINKAGE 5.1 program package, under a DOS platform.

4.5.3 Pedigree and parameter files for linkage analysis

Two input files are required for linkage analysis with the LINKAGE 5.1 program: a pedigree file and a parameter file. Data were entered in the pedigree file in columns with one line per individual. Each line contained the following information in the order shown: Pedigree identifier, . IN the phenotype field, MHS individuals were designated "2", MHN individuals were designated "1" and untested and MHE individuals were entered as unknown status (0) in the affection status field. MHE individuals therefore did not contribute to the lod scores of the pedigrees. While these individuals are managed clinically as susceptible, from the geneticist's perspective, their exclusion from the analysis, although reducing the statistical power of the data, significantly improves the validity of the assigned phenotypes by improving the specificity of the IVCT [32].

The mode of transmission of the disorder was specified in the parameter file by the penetrances assigned to each genotype. By convention, a fully penetrant autosomal dominant disorder is specified by assigning the "11" genotype (normal) a penetrance of 0.0, and both the "12" and "22" genotypes penetrances of 1.0 [333]. The penetrance of the normal "11" genotype was set to a value above zero to accommodate phenocopies and a level of uncertainty in the MHS diagnosis. In general, linkage was calculated with a penetrance of 0.01 for the "11" genotype as described elsewhere [27]. The penetrance of the affected genotypes (12 and 22) was set to 0.99, to accommodate a 1% false negative rate for the IVCT [97]. The penetrance of the affected genotype in individuals who have suffered MH crises was set to 1.0, as described in previous studies [31,32].

The normal (1) and disease (2) alleles were defined by the frequencies assigned to each allele. The incidence of the MHS trait was approximated at 1/5000 [31,180]. This is probably an overestimate of the true incidence [70,397], but conservative in terms of generating false positive lod scores [180]. Moreover, evidence is accumulating that the frequency of MHS IVCT result exceeds the incidence of clinical susceptibility [32]. The 1/5000 estimate is therefore appropriate for linkage analysis in which the affected phenotype status is based on IVCT diagnoses, and not the clinical incidence of MHS. The frequency of the disease allele (2) was consequently calculated as 0.0001 under the assumption of Hardy-Weinberg equilibrium [330]. The frequency of the normal allele (1) was therefore taken to be 0.9999 and the mutation rate was set to 0.00001. The parameters applied in this study are in accordance with the standard genetic model defined by the EMHG genetics section [27,28,32]. Pairwise lod scores for linkage of the disease trait to each of the markers were computed with the MLINK program, and maximum likelihood estimates for θ were calculated for linkage to each marker with the ILINK program [331,333].

4.5.4 Accommodating IVCT false positive diagnoses in the genetic model

Phenotyping errors can adversely effect linkage analysis. Potential phenotypic inaccuracies were accommodated in the genetic model by setting the phenocopy rate above zero. Secondly, the use of different diagnostic thresholds for the MHS diagnosis was investigated to examine the effect of diagnostic stringency on the evidence for linkage. The false positive rate of the IVCT

in accordance with EMHG protocol was estimated at 3.5 - 10.8% [97]. The parameters for genetic linkage analysis as recommended by the EMHG genetics section [27,28,32,175] include a phenocopy rate of 0.01- 0.02 to allow for potential false positive IVCT diagnoses.

The effect of the defined phenocopy rate on the calculated support for linkage was investigated by calculating 2-point lod scores (at $\theta = 0$) for the CH1 pedigree at increasing phenocopy rates. Results are presented graphically in Figure 4-16.

Linkage to the RYR1 flanking markers was excluded under the assumption of a zero phenocopy rate and standard EMHG diagnostic parameters ($Z = -4.69$ at $\theta = 0$ for the D19S220 locus, $Z = -1.37$ at $\theta = 0$ at the D19S47 locus). In this case, the five discordant MHS individuals imply genetic recombination between the disease locus and the chromosome 19q markers. Support for linkage increased when the phenocopy rate was raised gradually from 0 to 0.1, as the impact of the recombinant MHS individuals was reduced by the inclusion of a low level of diagnostic uncertainty into the genetic model. When the phenocopy rate was raised above 0.1, a reduction in the power of the non-recombinant data resulted in a decrease in lod scores calculated for most loci.

Figure 4-16 Influence of the phenocopy parameter on support for linkage to RYR1

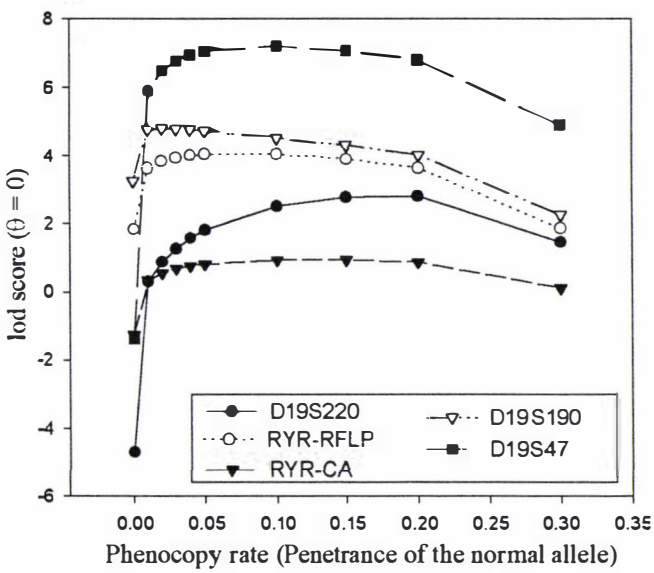

Two point lod scores were calculated (at $\theta = 0$) under various phenocopy rates to accommodate the false positive rate of the IVCT for the CH1 pedigree. Phenotype was assigned according to conventional EMHG thresholds (0.2 g at 2 mM caf. and 2 % hal.).

Parameters for linkage analysis included a penetrance of 0.99 for the disease allele, a disease allele frequency of 0.0001, and a mutation rate of 0.00001.

A phenocopy rate of 0.01 was assumed in all subsequent analyses. This is more conservative in terms of imparting false positive bias in the analysis than the 0.02 phenocopy rate applied in other MH linkage reports [31,32,180].

4.5.5 Increasing the stringency of the diagnostic criteria

The specificity of the IVCT is less than absolute [97], therefore, the five recombinant individuals in the CH1 pedigree classified MHS by conventional diagnostic thresholds may actually represent false positive diagnoses. To test this possibility, linkage was performed under increasingly stringent diagnostic criteria. This approach has been applied to other discordant families where alteration of the IVCT diagnostic cut-off points has permitted investigators to expose linkage of MHS families to the RYR1 gene that was obscured when the conventional EMHG thresholds were applied [99,105,112]. Pairwise lod scores were recalculated at the standard EMHG

thresholds (≥ 0.2 g tension at 2mM caf and 2 % hal) and with increasingly stringent criteria, where subjects generating a tension ≥ 0.4, 0.6, 0.8, 1.0 and 1.5 g in response to 2 mM caffeine or a tension ≥ 0.4, 0.6, 0.8, 1.0 or 1.5 g in response to 2 % halothane were classified as MHS. Subjects producing responses below the selected thresholds for both tests were classified as MHN, while those attaining the threshold response to only one test agent were classed as MHE.

Lod scores calculated at various values of θ under the EMHG (0.2 g/ 0.2 g) thresholds are displayed in Table 4-6. Equivalent analyses were performed under more stringent thresholds of 0.4 g/ 0.8 g and 1.0 g/ 1.5 g for caffeine/halothane respectively. The lod scores were maximised over θ for each marker using the ILINK program to estimate the recombination fraction between the marker and the disease locus (θ_{max}). The relationship between the diagnostic stringency and the evidence for linkage to the RYR1 locus for the CH1 pedigree is summarised in Table 4-7. The number of concordant and discordant individuals are shown for each diagnostic scheme together with lod scores calculated at θ = 0, and maximal lod scores for the most informative marker (D19S47).

Table 4-6 Pairwise lod scores for linkage of MHS to chromosome 19q markers in CH1 .

A. ≥ 0.2 g at 2mM caf and ≥ 0.2 g at 2 % hal (EMHG thresholds)

			Z at Recombination fraction (θ) =						
MH v.	θ_{max}	$Z(\theta)_{max}$	0	0.01	0.05	0.10	0.2	0.3	0.4
D19S220	0.092	3.24	0.31	1.93	3.06	3.23	2.72	1.76	0.61
RYRRFLP	0.038	3.97	3.62	3.84	3.96	3.75	2.96	1.94	0.82
RYRCA	0.102	1.01	0.34	0.61	0.94	1.01	0.89	0.62	0.27
D19S190	0.000	4.76	4.76	4.68	4.33	3.88	2.92	1.90	0.85
D19S47	0.041	6.45	5.91	6.22	6.44	6.12	4.90	3.28	1.43

Under the conventional EMHG thresholds of ≥ 0.2 g tension at 2 mM caffeine and 2 % halothane, five MHS individuals were recombinant at the D19S220 locus. Consequently, linkage to the D19S220 locus is not supported at θ = 0 under the EMHG thresholds for the CH1 pedigree (Z = 0.31 at θ = 0).

Lod scores in favour of linkage of MHS to the markers increased with incremental increases in the stringency of the diagnostic criteria, concomitant with a reduction in the number of MHS recombinant individuals, as shown in Table 4-7. The lod score for linkage to the D19S220 locus increased from 0.31 to 5.76 θ = 0 under the new thresholds. A maximum lod score of 9.81 in favour of linkage to the D19S47 locus at θ = 0.012 was obtained. Examination of the IVCT data from the CHEH and CHEA branches revealed that three discordant individuals: M33 (Figure 4-11); M130 and M231 (Figure 4-10) recorded the weakest contracture responses of the MHS group. When the cut-off point for MHS diagnosis was raised to 0.4 g tension at 2 mM caffeine and 0.8 g tension at 2 % halothane (as applied by Healy *et al.* 1996), individuals M33, M130 and M231 were classified MHN, MHE and MHE respectively. In addition, 12 MHE individuals were reclassified as MHN, improving overall support for linkage.

Two discordant individuals (M175 and M54) from the CHEA branch (Figure 4-11) remained MHS under the intermediate thresholds of 0.4 g (at 2 mM caf) and 0.8 g (at 2% hal). When the diagnostic thresholds were raised to ≥ 1.0 g in at 2 mM caffeine and ≥ 1.5 g at 2 % halothane, the two remaining discordant individuals were classified MHE while all individuals who were positive for the 6-1-4-1-3 haplotype remained MHS. Complete concordance between MHS and the

genetic data was reflected by the calculation of maximal lod scores at $\theta = 0$ for all marker loci. As the cut-points were raised further to 1.5 g for both the caffeine and halothane tests, two MHS individuals who were positive for the MHS-linked haplotype (M60, M289, Figure 4-11) were classified MHE, and the lod scores decreased accordingly.

These results clearly show that MHS is linked to the RYR1 locus in the CH1 pedigree, and support the assumption of false positive diagnosis in at least three discordant MHS individuals who have relatively weak contracture responses. This suggests that diagnostic errors imposed by the adoption of the low EMHG thresholds rather than true genetic recombination resulted in the inflated estimates of the genetic distance between the disease locus and the RYR1 markers in this pedigree.

Table 4-7 The relationship between diagnostic stringency and evidence for linkage to RYR1 in the CH1 pedigree.

Cut-point	No. of individuals Haplotype (+)			Haplotype (-)			Lod score at $\theta = 0$ MHS *vs.*					D19S47	
Caf/Hal	S	E	N Rec	S Rec	E	N	D19-S220	RYR-RFLP	RYR-CA	D19-S190	D19-S47	θ Max	Z(θ) Max
0.2/ 0.2	16	0	0	5[c-g]	15	9	0.31	3.62	0.34	4.76	5.91	0.041	6.45
0.4/ 0.4	16	0	0	3[e-g]	5	21	3.67	5.17	1.04	4.19	9.55	0.013	9.67
0.4/ 0.8	16	0	0	2[f,g]	3	24	5.76	5.32	2.57	4.31	9.72	0.012	9.81
0.8/ 0.8	16	0	0	2[f,g]	1[d]	26	5.93	5.5	2.74	4.19	9.9	0.011	9.99
1.0/ 1.0	15	1[a]	0	1[e]	2[d,f]	26	6.96	6.42	2.73	4.05	10.02	0.00	10.0
1.0/ 1.5	15	1[a]	0	0	2[d]	27	7.13	6.54	2.73	4.04	10.20	0.00	10.2
1.5/ 1.5	14	2[a,b]	0	0	1[f]	28	6.83	6.24	2.73	4.03	9.88	0.00	9.88

Patients were classified MH S, E, or N depending on whether threshold tensions were obtained in response to both, one or neither of the IVCT tests respectively. The haplotype (+) or (-) refers to the presence or absence of the MHS-associated 6-1-4-1-3 chromosome 19q haplotype. Rec. = recombinant.
a: M60 (0.9 g at 1.5 mM caf., 1.6 g at 1 % hal.), b: M289 (1.3 g at 2 mM caf, 2.2 g at 2 % hal),
c: M33 (0.25 g at 2 mM caf, 0.6 g at 2 % hal), d: M130* (0.3 g at 2 mM caf, 1.2 g at 2 % hal),
e: M231* (0.6 g at 2 mM caf, 0.4 g at 2% hal), f: M175 (0.9 g at 2 mM caf, 3.7 g at 2% hal),
g: M54 (1.0 g at 2 mM caf, 1.4 g at 2 % hal)
* Denotes individuals from the CHEH branch (Figure 4-10). All other individuals are from the CHEA branch of the pedigree (Figure 4-11).

4.5.6 Two-point linkage analysis of the CH2 branch

Two-point linkage analysis was conducted for the CH2 pedigree branches (Figure 4-12), under both the standard EMHG parameters and increasingly stringent diagnostic thresholds. A phenocopy rate of 0.01 was assumed. The influence of the diagnostic thresholds on the support for linkage in the CH2 pedigree is shown in Table 4-8. Linkage to the RYR1 locus in the CH2 pedigree (Figure 4-12) was excluded under the standardized diagnostic criteria of the EMHG group ($Z = -5.04$ at $\theta = 0$ at the D19S220 locus). Support for linkage increased as the diagnostic cut-points were raised, concomitant with a reduction in the number of MHS recombinants from 6 to 1. Lod scores decreased as the thresholds were raised above 0.8 g for both caffeine and halothane. At these thresholds, individual M5 (who is positive for the MHS-linked haplotype) is classified MHN and recombinant with respect to the RYR1 flanking marker. However, in this

case, poor quality muscle may have resulted in the relatively low IVCT responses. An unambiguous genetic recombination observed between the disease locus and D19S47 marker in MHN individual M31 (CHKM branch) also reduced the apparent support for linkage to the D19S47 locus under the raised thresholds.

Table 4-8 The relationship between the diagnostic stringency and evidence for linkage to RYR1 in the CH2 pedigree (shown in Figure 4-12).

Cut-point	Haplotype (+)			Haplotype (-)			Lod score at θ = 0 MHS *vs.*			D19S47	
Caf/Hal	S	E	N Rec	S Rec	E	N	D19-S220	RYR-RFLP	D19-S47	θ Max	Z(θ) Max
0.2/ 0.2	8	0	0	6	5	4	-5.04	-0.52	-1.85	0.22	0.49
0.4/ 0.4	8	0	0	1[c]	9	5	0.94	0.61	-1.17	0.06	1.48
0.4/ 0.8	8	0	0	1[c]	0	14	2.50	0.73	0.59	0.11	1.44
0.8/ 0.8	8	0	0	1[c]	0	14	2.50	0.73	0.59	0.11	1.44
1.0/ 1.0	7	0	1[a]	1[c]	0	14	2.26	0.20	0.40	0.11	1.24
1.0/ 1.5	7	0	1[a]	1[c]	0	14	2.26	0.20	0.40	0.11	1.24
1.5/ 1.5	6	1[b]	1[a]	0	1[c]	15	2.73	0.03	0.86	0.07	1.4

a M5 (0.8 g at 2 mM caf and 1.0 g at 2 % hal. Note: early test, poor muscle twitch noted)
b M365 (1.2 g at 2 mM caf and 3.9 g at 2 % hal)
c M98 (1 g at 2 mM caf and 1.8 g at 2 % hal)

4.5.7 Two-point linkage analysis of the CH3 pedigree

Linkage to RYR1 was also investigated for the CH3 pedigree (Figure 4-13) under various diagnostic schemes. Results are presented in Table 4-9. Eight MHS individuals from the CH3 pedigree are discordant with respect to the RYR1 haplotype. Accordingly, linkage to the RYR1 region is not supported ($Z = -1.34$ at $\theta = 0$ for the D19S220 locus) under conventional IVCT thresholds.

IVCT tensions recorded for four discordant MHS individuals from the CHES branch (M210, M394, M395 and M397) were sufficient to secure an MHS diagnosis under the raised thresholds of ≥ 0.4 g at 2 mM caf and ≥ 0.8 g at 2 % hal. Consequently, linkage to the D19S220 locus was not supported at $\theta = 0$ ($z = -0.07$) even under these stringent thresholds. The analysis was limited by the lack of contracture data for four additional discordant individuals (M42, M206, ID251, ID258) who were diagnosed MHS before the Palmerston North Hospital IVCT testing centre was established. These individuals were classified MHS under conventional thresholds and "status unknown" under the raised diagnostic schemes. When an MHS status was assumed for these four individuals at the 0.4g /0.8 g threshold tensions the lod score at the D19S220 locus decreased to -2.01 at $\theta = 0$, and was maximal at a $\theta = 0.143$. D19S220 is tightly linked to the RYR1 gene ($\theta = 0.008$, CHLC sex-average genetic map). Consequently, this result excludes linkage to the RYR1 locus under the raised diagnostic parameters recommended in an earlier study [105].

Maximal lod scores were achieved under the highest thresholds of 1.5 g tension at both 2 mM caffeine and 2 % halothane ($Z_{max} = 4.84$, for the D19S220 locus at $\theta = 0$). At these thresholds, the four discordant CHES individuals (for whom data was available) were classified as MHE.

However, two individuals with the high risk 6-1-3 haplotype were also re-classified MHE at these thresholds, so there is some loss of power in the analysis, due to overlap between the contracture responses from the discordant and concordant MHS individuals.

Table 4-9 The relationship between the diagnostic stringency and evidence for linkage to RYR1 in the CH3 pedigree (shown in Figure 4-13).

Cut-point	Haplotype (+)			Haplotype (-)			Lod score at θ = 0 MHS *vs.*			D19S220	
Caf/Hal	S	E	N Rec	S Rec	E	N	D19-S220	RYR-RFLP	D19-S47	θ Max	Z(θ) Max
0.2/ 0.2*	12	0	0	9[c-k]	6	15	-1.34	0.78	1.72	0.038	0.79
0.4/ 0.4	10	2	0	4[h-k]	7	19	-0.19	0.49	1.85	0.094	2.04
0.4/ 0.8*	12	0	0	8[d-k]	0	22	- 2.01	0.67	1.69	0.143	1.11
0.4/ 0.8	10	2	0	4[h-k]	4	22	-0.07	0.53	2.09	0.075	2.57
0.8/ 0.8	10	2	0	2[j,k]	6	22	2.27	2.22	2.10	0.000	2.27
1.0/ 1.0	10	2	0	1[k]	7	22	3.74	1.92	3.39	0.000	3.74
1.0/ 1.5	10	2[a,b]	0	1[k]	6	23	4.01	2.19	3.36	0.000	4.01
1.5/ 1.5	10	2[a,b]	0	0	7	23	4.84	1.90	4.20	0.000	4.84

a, b: M40, M48. IVCT data not available.
c: M86 (0.4 g, 0.65 g)
d - g: M42, M206, ID251, ID258. IVCT data not available.
h - k: M395 (0.5 g, 1.4 g) M210 (0.5 g, 1.5 g), M397 (1.0. g, 2.6 g), M394 (1.2 g, 1.7 g). Tensions at 2 mM caf, and 2% hal respectively).
* Four MHS individuals for whom data was not available diagnosed MHS (M42, M206, ID251, ID258)

4.5.8 Summed 2-point lod scores for the CH family

Lod scores summed across the three pedigree branches are presented in Table 4-10. Under the standard EMGH 0.2 g thresholds, linkage to MHS is not supported for either the D19S47 or RYR1-EFLP3 loci, and was excluded for the D19S220 marker (Z = -6.29). Under the raised diagnostic thresholds of 0.4 g at 2 mM and 0.8 g at 2 % halothane (described in a previous study [105]), conclusive evidence for linkage was obtained, with combined lod scores > 6.0 generated for each of the D19S220, RYR-RFLP3 and D19S47 markers. The combined 2-point lod scores therefore provide convincing support for linkage of MHS to the RYR1 region in the CH pedigree. However, combining the data in this way obscured the observed recombination between the MHS and the chromosome 19q markers. The evidence of genetic heterogeneity within this pedigree advocates the scrutiny of separate branches of large MH pedigrees before combining data.

A limitation of 2-point linkage analysis is that loci examined individually can appear to be linked with a disease, even though an inspection for the haplotypes for the family might strongly suggest that the entire region under investigation fails to segregate with the disorder. The distortional effects of including incomplete data in linkage calculations have been described [180,365]. This can be overcome by performing multipoint linkage analysis [332], whereby the inclusion of data reflecting the observed haplotypes would exclude MHS from the whole interval between D19S220 and D19S47 in the CHES family.

Table 4-10 Summed 2-point lod scores for linkage of MHS to chromosome 19q markers in CH1 CH2 and CH3 pedigree branches

A. *≥0.2 g at 2mM caf and ≥0.2 g at 2 % hal (EMHG thresholds)*

	Z at Recombination fraction (θ) =						
MH v.	0	0.01	0.05	0.10	0.2	0.3	0.4
D19S220	-6.288	-0.25	-1.2	1.34	3.24	3.25	2.46
RYRRFLP	0.298	4.45	4.35	4.65	4.68	4.18	3.08
D19S47	-0.139	6.59	7.15	7.86	7.87	6.83	5.07

B *≥0.4 g at 2 mM caf and ≥0.8 g at 2 % hal (as applied by Healy et al., 1996)*

	Z at Recombination fraction (θ) =						
MHS v.	0	0.01	0.05	0.10	0.2	0.3	0.4
D19S220	8.19	9.04	9.58	9.17	7.23	4.44	1.42
RYRRFLP	6.58	6.79	6.77	6.27	4.81	3.07	1.24
D19S47	12.4	13.02	13.55	12.91	10.34	6.9	2.95

4.6 MULTIPOINT LINKAGE ANALYSIS

After the approximate location of a disease gene has been mapped with 2-point linkage analysis, multipoint linkage analysis is used to map the location of a disease gene accurately to a fixed point on an established map of loci. Multipoint analysis effectively evaluates an extended haplotype, and maximises the information content of the data set. The multipoint lod score is described by the equation

$$Z(x) = \log_{10}\left[\frac{L(x)}{L(\infty)}\right]$$

Where x is the location of the disease gene on the fixed map [398]. The denominator assumes the disease locus is unlinked to the established map of markers where ∞ denotes the infinite map distance corresponding to $\theta = 0.5$.

4.6.1 Multipoint analysis with the LINKMAP program

The LINKMAP program is used for disease mapping of general pedigrees in which there may be complex penetrance models [332]. Due to the heavy memory requirements of the LINKMAP program, only four loci can be assessed at a time. This limitation is overcome by sliding the group of four loci down the map, in one locus increments, placing the disease locus in the middle interval of each set of four markers [333]. The disease locus is then moved through each interval on the fixed map, beginning at the left of the first marker locus (interval 0), up to interval 2 (between markers 2 and 3). At least one evaluation is required with the disease fixed at $\theta = 0.5$ to the left of the leftmost marker with each set of four alleles.

The three major branches of the CH pedigree (CH1, CH2, and CH3) were investigated in separate multipoint linkage analyses. This reduced the computational demands and permitted a comparison of the influence of genetic heterogeneity in each branch of the pedigree.

4.6.1.1 Condensing alleles

Linkage program limitations prevented evaluation of more than three highly polymorphic SSLP with more than 3 or 4 alleles at each locus in addition to the disease locus (LINKAGE 5.1 users guide). To accommodate these limitations, the genotypes were recoded to a maximum of four at each locus. This was achieved by reducing the genotypes to alleles observed in the root family and adjusting the alleles of individuals married into the family to preserve all the linkage information, according to standard procedure [31,330,365]. Allele frequencies of the informative alleles were preserved; while the remaining alleles were pooled into groups of approximately equal frequency, where possible. The D19S190 and RYRCA markers were omitted from the multipoint analysis to improve computation efficiency.

The 2-point lod scores for the recoded pedigrees were compared with the lod scores for the original pedigrees to check that no linkage information had been erroneously introduced or lost by recoding the alleles. For each pedigree branch (CH1, CH2, CH3) the 2-point lod scores for the recoded pedigrees fell within the +/- 0.3 guidelines for maintaining consistency with recoded allele data [330].

4.6.2 Multipoint analysis with LINKMAP and FASTLINK

The disease phenotype in the pedigree file was defined using the raised IVCT diagnostic contracture thresholds of 0.4 g at 2 mM caffeine and 0.8 g at 2% halothane that were employed by Healy *et al.* [105]. The chromosome 19q marker map order was fixed as D19S220-RYR RFLP-D19S47, with recombination frequencies of 0.008 and 0.0071 defining the first and second map intervals (obtained from the online CHLC sex-averaged chromosome 19 linkage map [334]). The MHS locus was moved through each interval, from 0 to 3 with 5 increments in each interval. Map distances were calculated from the recombination fractions with the Kosambi mapping function using the LINKLODS auxiliary program. The LINKMAP program was used to calculate multipoint scores for the CH1 pedigree. Multipoint analysis of the CH2 and CH3 pedigrees was performed with FASTLINK (a faster version of the LINKMAP recompiled from the UNIX source code to operate under DOS). Multipoint linkage scores obtained for the CH1, CH2 and CH3 pedigrees are represented graphically in Figure 4-17, Figure 4-18 and Figure 4-19 respectively.

Linkage to the RYR1 region was conclusive for the CH1 pedigree, with a maximum multipoint lod score of 9.88 obtained at a genetic distance of ($\theta = 0.008$) from the D19S220 marker (Figure 4-17). This corresponds to the position of the RYR1 gene locus (CHLC sex-averaged map).

A maximum multipoint lod score of 2.9 in favour of linkage was obtained for the CH2 pedigree at the position of the D19S220 locus (0 cM). This is close to the level at which linkage is accepted as conclusive ($Z = 3.0$). The lod score dropped to 0.99 at 1.5 cM telomeric to the D19S47 locus, corresponding to the D19S47 locus position. This reflects the crossover observed between the disease trait and the D19S47 marker in a single individual (M31, CHKM branch, Figure 4-12).

In contrast to the results from the CH1 pedigree branch, multipoint analysis of the CH3 pedigree branch did not support linkage of MHS to RYR1 (Figure 4-19). Allowances for the IVCT false positive rate were included in the analysis of all three pedigree branches by the application of raised diagnostic thresholds and a 0.01 phenocopy rate in the genetic model. Even with these adjustments, a negative multipoint score of –0.330 was generated at the RYR1 locus position for the CH3 pedigree branch. This reflects the significant discordance between the MHS and the RYR1 haplotype observed in the CH3 branch (specifically in the CHES family).

In multipoint analysis, if the defined genetic model differs significantly from the true model, inflated estimates of θ can drive the trait outside of a candidate map region even if it includes the trait locus [333]. The haplotype data for the CHES family pointed to the segregation of a second genetic defect not linked to RYR1 that predisposes the affected individuals to MHS. The possible segregation of two MHS genes in the family was not accommodated in the single gene model applied. Inconsistencies, possibly attributable to the segregation of a second MHS gene were therefore be interpreted by the program as genetic recombination between the MHS trait and the RYR1 locus, hence the negative multipoint lod score at RYR1.

Figure 4-17 Multipoint linkage analysis of the CH1 pedigree branch.

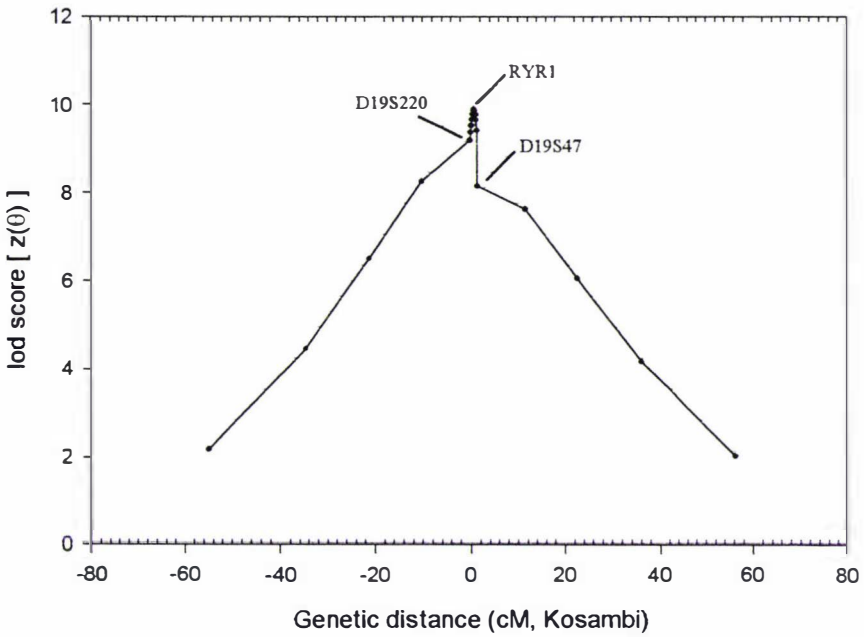

The location map indicates lod scores for MHS at various map positions in a fixed marker map comprising markers D19S220, RYR-RFLP3 and D19S47. Liklihoods were calculated with LINKMAP and converted to lod scores with LINKLODS. The D19S220 locus is arbitrarily placed at 0 cM. Markers were positioned according to sex-averaged CHLC maps for this region. Genetic distance refers to distance (cM) from the D19S220 locus (Kosambi mapping function). The MHS phenotype was established according to raised diagnostic criteria (0.8g at 2 % Hal., 0.4 g at 2 mM Caf.), with MHE individuals entered as unknown status. $Z(\theta)_{max}$ = 9.88 at 0.8 cM telomeric to the D19S220 locus (corresponding to the RYR1-RFLP3 locus). Parameters for linkage analysis included a penetrance of 0.99 for the disease allele, a phenocopy rate of 0.01 and a disease allele frequency of 0.0001.

Figure 4-18 Multipoint analysis of the CH2 pedigree branch

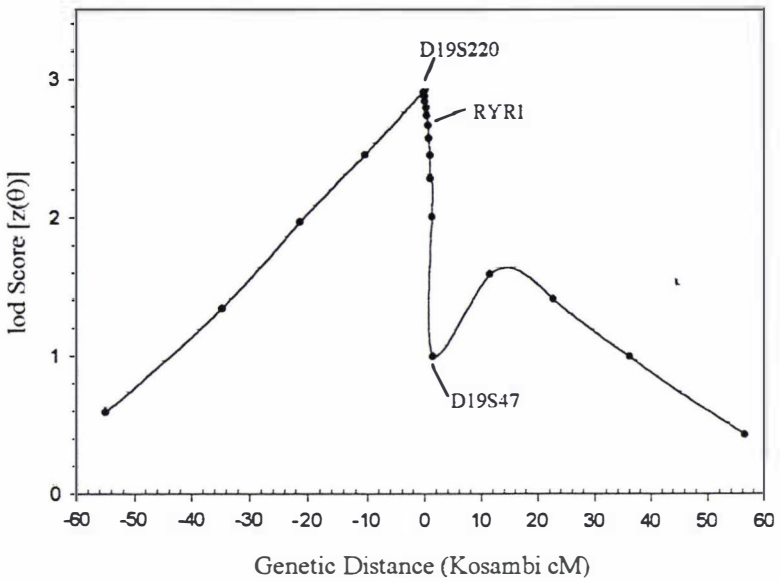

Multipoint lod scores for the CH2 pedigree (Figure 4-12) were computed with LINKMAP (FASTLINK). Linkage and diagnostic parameters are as described in Figure 4-17. The maximum multipoint lod score, $Z_{max} = 2.9$ was generated at 0 cM (the D19S220 locus). A genetic recombination event between MHS and the D19S47 marker placed the disease locus centromeric to D19S47, consistent with linkage to RYR! in this family.

Figure 4-19 Multipoint analysis of the CH3 pedigree branch

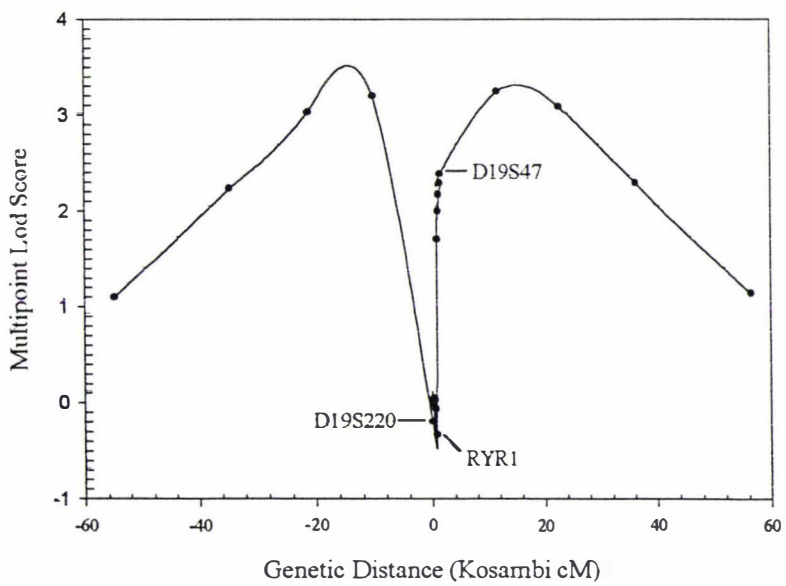

Multipoint lod scores were calculated using LINKMAP (FASTLINK) as described for figure 4-17. Linkage to RYR1 was not supported; Multipoint lod score = -0.331 at the RYR1 locus. This is a reflection of the discordance between MHS and the RYR1 haplotype in the CH3 pedigree, (specifically in the CHES family, Figure 4-13).

4.7 DISCUSSION OF RESULTS

4.7.1 Troubleshooting SSLP analysis

Several difficulties were encountered in the typing of microsatellites. The chosen method was developed from standard protocols for typing γ-^{32}P-labelled products that recommend a 30-fold dilution of PCR products in 98% formamide loading dye [330,361]. The lower emission levels of the γ-^{33}P label necessitated an increased DNA/formamide ratio to visualize bands within a practical exposure time-frame. The reduced concentration of formamide in the samples may have resulted in incomplete denaturation of the DNA, leading to blurred bands and other artifacts that complicated genotype interpretation. The problem was resolved by heating samples to 95°C in batches and loading the denatured DNA immediately. The band artifacts and poor resolution were attributed to the formation of secondary structure in the single-stranded DNA.

In addition to the stutter bands that occurred in 2 bp increments, faint bands were also observed in 1 bp increments above the associated major bands. These extra bands could have resulted from the partial non-template directed nucleotide addition of a nucleotide to the 3' end of amplification products during PCR ("A tailing") [399]. Approximately 86% of PCR products generated by *Taq* polymerase have the extra 3' A addition [400]. Despite the potential problems with PCR of repeat sequences, the band patterns were found to be consistent for DNA samples amplified under identical PCR conditions.

The D19S47 marker proved the most informative for the CH family, as the MHS phenotype appeared to segregate with a relatively rare allele. A complex highly polymorphic VNTR (WUT1.9) flanking RYR1 was reported during the data collection phase [401] was also investigated as a potentially useful RYR1 marker. The marker is composed of a 25 bp minisatellite sequence, a compound microsatellite (AC)(AT), and an oligo-T stretch [401]. The WUT1.9 polymorphism was not informative for the CH family as the MHS phenotype appeared to co-segregate with a common allele that was difficult to discern from a complex array of similarly sized bands. Analysis of the WUT1.9 marker was therefore not extended to other branches of the family.

4.7.2 Eliminating genetic and IVCT data errors

In view of the significant discordance between phenotypic and genetic data in branches of the CH family, the genotypes were verified by repeating microsatellite and RFLP analysis on all recombinant samples prior to conducting linkage analysis (with fresh DNA samples where possible). It is unlikely that genotyping errors have been made repeatedly for the same samples in the collection of marker data at all 5 loci, thus the genetic data for the recombinant individuals was taken to be sound.

Before conducting genetic linkage analysis, the IVCT data from members of the CH family tested at the Palmerston North was reviewed and entered into a database. Details recorded included the contracture responses at each drug concentration, muscle twitch and results from duplicate muscle strips. Any departure from the standard protocol, such as the bolus addition of the test agents, or the addition of other drugs to the bath was noted.

Some inconsistencies in test procedure were observed that might have contributed to aberrant contracture responses in some tests.

Data from individual muscle strips was void in the following circumstances: Where additional agents were added to the bath; where zero or poor twitch response (< 0.5 g) was noted, and; where the test agent was added to the bath as a bolus dose instead of the standard incremental addition. The bolus addition of the test reagents is know to induce stronger muscle tensions than incremental addition, therefore this procedure might have contributed to abnormal contracture responses in some individuals [100,102]. A further source of variability was the use of acid-dissolved caffeine, and the addition of drugs such as suxamethonium, profofol, or diprivan to the bath. It is unclear how these agents might have affected the resultant tensions, though exaggerated tensions were noted with the addition of suxamethonium (which would be expected since this agent is a potent trigger of MH). Where the maximal tension was achieved in a test that departed from the accepted protocol, data was substituted with the next highest tension from muscle bundles tested with the correct procedure. All biopsy test results were similarly evaluated to avoid positive bias.

Aberrations in the IVCT procedure were noted for three recombinant MHS individuals. In the first case, (son of discordant individual M98, CHKM branch, Figure 4-12), an abnormal tension of 0.7 g was induced by acid-dissolved caffeine whereas normal results (< 0.2 g) were obtained with standard caffeine solution. It is unclear whether the potency of the acid caffeine solution differs from standard caffeine solution used in most tests. The MHS diagnosis in the grandmother of this individual (M93, CHKM branch, Figure 4-12) was also suspect. M93 registered normal caffeine responses (< 0.2 g) in all three strips tested according to standard procedure, however, a contracture of 0.6 g was recorded with a bolus dose of halothane in the fourth. Prior expectation of an MHS result due to the previous MHS diagnosis in a child of this individual may have influenced the test procedure and interpretation. An unknown MH status was entered for these individuals in the linkage analysis.

Prominent inconsistencies in the results from duplicate muscle strips also suggested the influence of IVCT error. In the case of discordant MHS individual M102 (CHKW branch, Figure 4-12), three caffeine tests were performed, registering normal tensions of 0.0, 0.15 and 0.2 g. Seven halothane tests were performed, with tensions ranging from 0.15 to 1.5 g. In a deviation from standard procedure, caffeine was added to the halothane bath in three tests, and residual caffeine may have influenced a fourth. The remaining three strips registered 0.15, 0.2 and 1.0 g tension. The striking abnormal halothane response in one of the strips warrants clinical suspicion of MHS status. However, for genetic analysis, this ambiguous result was excluded by entering the phenotype status as unknown.

There were no noticeable deviations from the standard IVCT procedure for the 4 discordant MHS individuals from the CH3 pedigree (Figure 4.13; M210, M394, M395, M397), the CH2 pedigree (Figure 4-12, M98) or from the CHEA branch of the family (Figure 4-11; M54, M175, M33). Data from one MHS patient who carried the high-risk haplotype (M5, biopsy 18, 0.8 g at 2 mM caf. and 1.0 g at 2 % hal) was excluded because of zero twitch response and breach of standard protocol (only one muscle strip was tested in each case). Data from a second MHS patient who also carried the high-risk haplotype (M60, biopsy 13, 0.9 g at 2 mM caf. and 1.6 g at 2 % hal.) was excluded from statistical analysis of the data because tensions were not recorded at the standard IVCT threshold concentrations.

4.7.3 Overview of evidence for linkage of MHS to RYR1

The analysis of the segregation of RYR1 markers in the CH family supports the existence of a RYR1 mutation segregating across 4 major branches of the family which could account for the 15 clinically observed cases of MH susceptibility. All members of the family identified with the unique 6-1-4-1-3 haplotype across distantly related branches of the family examined by IVCT were diagnosed MHS. This strongly implicated the involvement of the RYR1 locus in this family. This assumption was confirmed by conclusive evidence for linkage obtained at the RYR1-RFLP3, D19S190 and D19S47 loci from the two-point analysis of the CH1 pedigree under the standard EMHG thresholds. The analysis was extended to additional branches of the family with a view to the future application of the defined MHS-linked haplotype in indirect diagnosis, as has been described in previous studies where the causative mutation was unknown [392,402]. However, multiple cases of genotype/phenotype discordance were encountered in which individuals who were diagnosed MHS clearly had not inherited the MHS-linked 6-1-4-1-3 haplotype. Consequently, the negative two-point lod scores excluded linkage to the D19S220 locus in both the CH2 and CH3 pedigrees when individuals were diagnosed according to the standard diagnostic thresholds (0.2 g at 2 mM caffeine and 2 % halothane) and estimates of θ_{max} placed the disease locus outside the RYR1 region. This challenged linkage to the RYR1 locus in the CH pedigree, and cautioned against the use of the chromosome 19q markers in any diagnostic capacity.

The following possibilities could be considered to account for the MHS phenotype in discordant individuals lacking the 6-1-4-1-3 haplotype: 1) genetic recombination between the RYR1 locus and flanking markers; 2) the involvement of a chromosome 19q gene positioned outside the region defined by the RYR1 flanking markers (thus excluding the involvement of a RYR1 gene defect in MHS in the CH pedigree); 3) false positive IVCT diagnosis; 4) the introduction of additional gene defect(s) at a different locus or loci.

Genetic recombination between the RYR1 locus and the flanking markers used in this study would be expected to be rare, since the markers were chosen on the basis of their tight linkage to RYR1 (being separated at most, by a genetic distance of 0.8 cM). The rationale behind the selection of tightly linked markers related to the potential application of any defined MHS-associated haplotypes in indirect diagnosis [392,402]. None of the discordant MHS individuals in any of the branches could be explained by a single genetic recombination between RYR1 and a flanking marker. In each case, haplotypes were consistent with those of their parents (with the exception of M175, CHEA branch, Figure 4-11) and alleles at two or more loci conflicted with the 6-1-4-1-3 haplotype.

A crossover between MHS and the D19S47 marker in an MHE mapped the disease locus centromeric to the D19S47 consistent with the involvement of RYR1. The centromeric boundary for linkage was not defined in this study due to the selection of markers that were tightly linked to RYR1. If the true MHS locus was positioned centromeric to D19S220 (i.e not involving RYR1), MHS could have been separated from the 6-1-4-1-3 haplotype by genetic recombination and transmitted together with the recombinant haplotype to MHS offspring. However, haplotype data did not support this conclusion. In the CHES branch of the family (Figure 4-13) at least five recombination events between MHS and the chromosome 19q markers would be required to account for the observed data if a gene defect centromeric to D19S220 was causative of MHS in this pedigree. Similarly, multiple genetic recombination events would be required to explain the transmission of the MHS phenotype from individual M93 to discordant MHS individuals, M98, M199 and M99 in the KM branch (Figure 4-12). This frequency of recombination would position

the hypothetical disease locus at some distance from the chromosome 19q markers. If this were true, an equivalent number of recombinant MHN individuals harbouring the 6-1-4-1-3 haplotype would be expected to result from crossovers between the hypothetical disease locus and the chromosome 19q markers. A significant observation is that no such MHN recombinants were observed. Furthermore, scrutiny of the CHLC and GDB chromosome 19 maps [334,349] did not reveal a strong candidate MHS gene other than RYR1 near the D19S220 or D19S47 chromosome 19q markers (see appendix 4). Therefore, the genotype/phenotype discordance in this family could not be explained by the occurrence of an alternate disease locus on chromosome 19q.

The potential for false positive diagnosis was accommodated with a 0.01 phenocopy rate in the genetic model and by performing the linkage analysis under increasingly stringent diagnostic thresholds. In all three branches of the family, the evidence in favour of linkage to the RYR1 markers increased with incremental increases in the diagnostic stringency. This supported the assumption of false positive diagnosis in 11 borderline MHS individuals who were discordant under the standard diagnostic thresholds. False positive diagnosis can be reasonable invoked to account for the discordant MHS individuals with weak MHS results. However, a total of seven individuals who lacked the MHS-linked haplotype were still classified MHS under the maximum diagnostic cut-off points of 0.4g/0.8 g that were applied in an earlier study to reveal linkage to the Gly341Arg mutation [105] (M130, Figure 4-10; M54, Figure 4-11; M98, Figure 4-12; M210, M395, M394, M397, Figure 4-13). The possibility that alternate MHS genes may be segregating in these seven individuals was raised. True linkage to a disease gene may be obscured by genetic heterogeneity [180,330,338]. This may have contributed to the negative multipoint lod score obtained in multipoint analysis of the CH3 pedigree. Evidence supporting the segregation of multiple MHS genes in the CH family is discussed further in chapter 6.

In spite of the incomplete segregation of the chromosome 19q markers with MHS , sufficient evidence in favour of at least one RYR1 defect in this large family prompted a systematic search of the RYR1 cDNA for a novel mutation, as outlined in chapter 5.

5. IDENTIFICATION OF MUTATIONS BY SEQUENCE ANALYSIS OF RYR1 cDNA

5.1 SEARCH FOR A NOVEL RYR1 MUTATION IN THE CH FAMILY

The screen for published RYR1 mutations, together with the demonstration of linkage of MHS to the RYR1 region pointed to the involvement of a novel RYR1 defect in the large Maori CH pedigree. Various methods of mutation detection were contemplated before embarking on a search for a novel RYR1 mutation in this family. These are summarised below.

5.1.1 Comparison of strategies for screening for novel mutations

5.1.1.1 SSCP

The majority of RYR1 mutations reported in overseas MH families were detected by the method of single-strand conformation polymorphism (SSCP) analysis of amplified RYR1 cDNA. [107,108,110,165,167]. SSCP analysis is limited to relatively short, overlapping 250-300 bp DNA fragments [321] and would therefore necessitate approximately 70 - 80 PCR reactions to cover the RYR1 coding region. SSCP analysis is less sensitive than DNA sequencing and more technically demanding [322]. Many factors can influence the sensitivity of SSCP, and its optimisation is highly empirical [322]. Moreover, fragments encompassing silent DNA polymorphisms that are detected by SSCP must be further investigated by DNA sequence analysis to identify the nucleotide change. SSCP is therefore a high-throughput, low sensitivity method of detection, suited to the simultaneous analysis of multiple samples. This was outside the scope of the current project, which aimed to identify the causative defect in a small number of well-characterised families. However, SSCP analysis could be a useful method for screening a large number of individuals once a mutation was identified.

5.1.1.2 CFLP

A new method to detect mutations, termed cleavase fragment length polymorphism, or CFLP, [405,406] was investigated as an alternative to SSCP. This technique is similar to SSCP in that it relies on the detection of sequence-dependent conformational polymorphisms associated with single nucleotide changes. CFLP is based on the action of a structure-specific endonuclease Cleavase I [405] that recognizes and cleaves single-stranded DNA at the position of hairpins. Mutations are revealed by the differences in fragmentation patterns after electrophoretic separation of the cleavase digests by denaturing PAGE. Consequently, CFLP offers an advantage over SSCP in that the detection of conformational polymorphisms is not dependent on a defined set of electrophoretic conditions. In addition, larger PCR products (up to 1 kb) may be investigated [406]. CFLP with silver staining detection (CFLP-SS) has been described as a rapid and cost efficient method of mutation detection [406]. However, attempts to use CFLP-SS to detect a known R163C mutation amplified genomic DNA were unsuccessful. A complex array of fragments was generated and there were no differences observed between the fragmentation pattern generated for the mutant and control samples (data not shown). There are relatively few reports in the literature of the CFLP technique being used successfully and the sensitivity of CFLP is reportedly lower than that of other methods [407].

5.1.1.3 Sequencing strategies

Previous investigations had employed manual sequencing methods to characterise RYR1 mutations detected in MH pedigrees [110,111,164,167,168,408]. The recent development of an automated DNA sequence analysis facility at Massey University offered new opportunities for rapid and sensitive mutation detection. While automated DNA sequence analysis is relatively expensive at $25 per lane, the cost is partially offset by the larger stretches of sequence that can be investigated, compared to SSCP, CFLP or manual sequence analysis. Approximately 500 bp of high-resolution sequence is generally obtained from the ABI-377 automatic sequencer. Consequently, PCR products of up to 1 kb can be covered, using each of the PCR primers to initiate two sequencing reactions. Even longer fragments may be investigated with the use of additional internal sequencing primers.

The recent structural characterisation of the RYR1 gene and the publication of intron sequences [160] has improved prospects for mutation detection by sequence analysis of RYR1 exons amplified from genomic DNA. However, this approach would have required at least 106 PCR primer sets to amplify each exon and an equivalent number of sequencing reactions. Moreover, intron-based PCR primers were not readily available, and published intron sequences [160] were found to be unreliable during attempts to amplify exons encompassing published RYR1 mutation sites. Several fresh muscle specimens had been salvaged from IVCT muscle biopsies of both MHS and MHN members of the CH family. This permitted the extraction of high quality, intact RNA and, consequently the sequence analysis of RYR1 cDNA as an alternative to genomic DNA.

Due to financial limitations, the cost associated with the design of PCR and sequencing primers was an important consideration in the project design. This prompted collaboration with Professor Tommie McCarthy from the University of Cork, Ireland, who generously provided a set of primers designed to amplify the entire RYR1 coding region from cDNA [13].

While automatic sequence analysis with dye-primer chemistry is promoted as the most sensitive method of heterozygote detection [409], the expense associated with fluorescent-labelled primers excluded this approach. This method can be cost effective if the primers are used to sequence a large number of samples for a known mutation, but is unfeasible in this project where a range of different products were to be sequenced from a small number of individuals. Automatic sequence analysis with dye-terminator chemistry was investigated as an alternative and more affordable method since it permitted the use of the available standard primers. However, sequence generated with dye-terminator chemistry is less clear due to different ease of incorporation of the fluorescently labelled ddNTPs. The signal intensity of a particular nucleotide is affected by the preceding sequence, for example, "A" is easily incorporated and a characteristic low peak occurs if incorporated directly after an "A" [409]. Sequence navigator software can be used to compensate for peak height variability. However, this was not available due to financial constraints.

The efficacy of the dye-terminator strategy in the detection of heterozygotes was assured by the successful detection of RYR1 mutations in amplified genomic DNA, as described in Chapter 3. Subsequently, automatic sequence analysis of RYR1 cDNA with dye terminator chemistry was selected as the most sensitive and cost effective strategy to search for a novel RYR1 mutation in the CH family.

5.1.2 Selection of muscle tissue specimens

Subjects chosen for RYR1 sequence were selected on the basis of genotype and tissue availability and are indicated with arrows in Figure 5-1. *Vastus* skeletal muscle tissue was obtained from the MHS individual (M221) bearing the paternal MH-linked haplotype and from an MHE sibling (M154) who carried the normal paternal haplotype. Both siblings share a common maternal haplotype, but different paternal haplotypes. The phase of new polymorphisms with respect to the established RYR1 haplotypes could therefore be immediately defined. This strategy aided the distinction of candidate mutations from non disease-linked polymorphisms, since any sequence variants unique to the MHS individual could be attributed to the inheritance of the MH-linked haplotype.

Figure 5-1 Subjects chosen for mutation screen

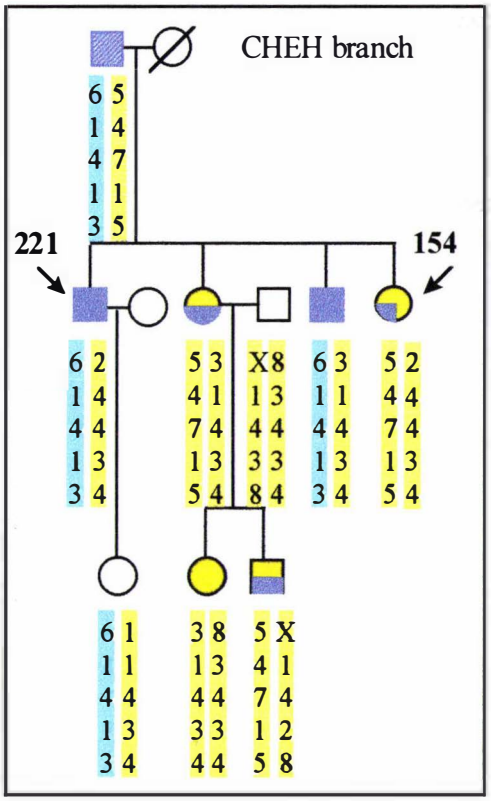

Right: *Genomic DNA samples were typed for D19S220, RYR-RFLP3, RYR-CA, D19S47 and D19S190 markers. MHS co-segregates with the 6-1-4-1-3 haplotype. Blue symbols represent individuals diagnosed MHS by stringent diagnostic criteria (≥ 0.4 g caf, and ≥ 0.8 g hal.). Half and quarter filled symbols are MHS and MHE by EMHG diagnostic criteria. Yellow symbols are MHN. Arrows indicate individuals selected for cDNA sequence analysis.*

5.1.3 RNA yields and purity

Both the MHS and MHE tissue specimens were stored at -20°C for up to 2 years before being transferred to Massey University for continued storage for at -70°C. Both muscle specimens may have been left at room temperature for several hours before being frozen. The possibility that the RNA may have been degraded during this time by endogenous tissue RNases was considered [309]. Trial RNA extractions were performed on other human IVCT muscle specimens that had been collected and stored in a similar fashion. Pure, intact RNA was successfully extracted from these specimens, although yields were lower than those obtained from tissue that had been frozen in liquid N_2 immediately after excision.

RNA was then extracted from the MHS and MHE tissue specimens selected from the CH family. Approximately 200 mg of muscle tissue was frozen in liquid N_2, crushed to a fine powder and homogenized extensively in Trizol™ RNA extraction reagent to a fine slurry (1 ml per 70 mg) using an ultra-Turrax T-25. RNA was purified according to Trizol™ manufacturers' instructions. Estimates of the RNA yields and purity based on the spectroscopic analysis are presented in Table 5-1. Additional organic solvent extraction and ethanol precipitation steps required to remove an insoluble white precipitate (presumed to be glycogen) may have reduced the yield from the MHE sample. Nevertheless, yields of 500-650 μg/g were still higher than published yields of 350 μg/g of human muscle tissue [307]. Spectroscopic analysis [309] indicated the nucleic acid was free of protein contamination (A_{280}/A_{260} values approaching 2.0).

Table 5-1 Spectroscopic analysis of RNA (diluted 1/200)

Specimen	Mass Tissue (g)	A280	A260	Ratio	Conc. µg/µl	Total µg	Yield (µg/g tissue)
MHS (M221)	0.233	0.111	0.221	1.98	1.80	144	618
MHE (M154)	0.205	0.053	0.105	2.00	0.84	121	590

The integrity and the purity the RNA was verified by examining approximately 10 µg of each sample by denaturing agarose gel electrophoresis (Figure 5-2). Pure, intact RNA was isolated, as revealed the appearance of prominent 28S and 18S ribosomal RNA bands, and the absence of low molecular weight RNA species [309]. The mRNA appeared as a smear running from the 18S band to the well.

Figure 5-2 RNA gel electrophoresis

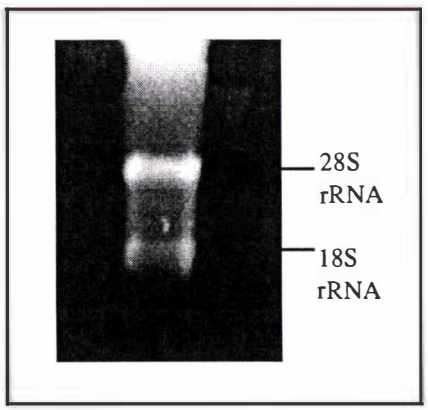

10 µg of total RNA from MHE individual (154) was resolved on 1.5 % denaturing agarose gel in 1X MOPS buffer, pH 7.0. Excess ethidium bromide appears as a brightly fluorescing region at the top of the gel (this was also observed in a lane in which sample buffer alone was loaded, and is therefore not likely to be the result of genomic DNA contamination).

5.2 RT-PCR STRATEGY

5.2.1 cDNA synthesis

The Superscript II ™ RT-PCR preamplification system (Life technologies) was chosen to prepare cDNA from total skeletal muscle RNA. This system employs the Moloney murine leukemia virus (MMLV) RNase H-Minus reverse transcriptase modified to favour the synthesis of longer transcripts (> 12 kb) [410]. Reverse transcription (RT) reactions can be initiated using oligo-dT, random hexamers or gene-specific primers. RT reactions primed with either oligo-dT or gene specific oligonucleotides provide a more specific substrate for PCR than those primed with random hexamers [309,311]. However, reactions must be optimised for each gene-specific primer, and cDNA synthesised in this way can only be used as a substrate for the amplification of regions 5' of the primer site. In view of the length of the RYR1 transcript and the presence of a 75% GC-rich stretch in the 12600- 13400 bp region of the RYR1 sequence [126], it was anticipated that the reverse transcription of full length RYR1 cDNA from oligo-dT primers would not be feasible. Furthermore, an adenine-rich region between residues 8501 and 8512 is thought to serve as a secondary priming site for cDNA synthesis, which may stop transcription from the 3' end and create a gap in the cDNA [126]. Therefore, a strategy employing both random hexamers and oligo-dT to prime the RT reactions was employed.

5.2.2 PCR

Collaboration was initiated with Professor Tommie McCarthy (University of Cork, Ireland) who generously provided a set of 50 RYR1 PCR primers. These were designed from the published human RYR1 sequence [126] to amplify the RYR1 coding region from -10 to 15175 bp. A strategy was devised to employ the provided primer set in conjunction with existing exon-based primers to amplify the entire RYR1 cDNA in overlapping fragments of 400-1600 bp that would be amenable to automatic sequence analysis. Additional primers were designed to be used as internal sequencing primers. Primers were also designed from the updated RYR1 sequence [160] to amplify and sequence exon 1 from genomic DNA (from -156 to +20 bp of intron 1).

The quality of sequence obtained using dye-terminator chemistry can be improved with the use of internal sequencing primers in place of the PCR primers, particularly if the PCR products contain non-specific contaminating species. Therefore, PCR primer pairs were selected to generate large overlapping fragments that would facilitate the use of adjacent PCR primers as internal sequencing primers. Where possible, forward and reverse PCR primers with similar melting temperatures were selected. The Irish MH group employed SSCP to screen for RYR1 mutations in amplified cDNA. The primer set provided had been used to generate long primary PCR products which were used as substrates for secondary PCR reactions to generate shorter fragments for SSCP analysis [13,108-111,166]. While the practice of using PCR products as templates in secondary PCR reactions with nested primers can greatly assist the production of discrete reaction products, it can increase the chances of PCR contamination and allele amplification bias [311]. A different amplification strategy was devised in order to use the additional primers available from our own laboratory and to avoid the reamplification of PCR products.

In view of the size of the RYR1 cDNA, it was decided to initially amplify and sequence specific areas of interest rather than a systematic analysis of the entire cDNA in the 5' to 3' direction. At the time the sequencing project was initiated, all reported RYR1 MH mutations were clustered within two mutation-rich regions in the N-terminal (residues Cys35 to Arg614 [13,106-109,111,165,166]) and central (residues Arg2123 to Arg2458 [25,110,167-169]) regions of RYR1. These regions were examined initially as likely sites for a novel RYR1 mutation in the CH family. The chosen amplification strategy is summarised diagrammatically in (Figure 5-3). Primer sequences and annealing sites are detailed in appendices 1 and 2.

Figure 5-3 Strategy for the amplification of RYR1 cDNA

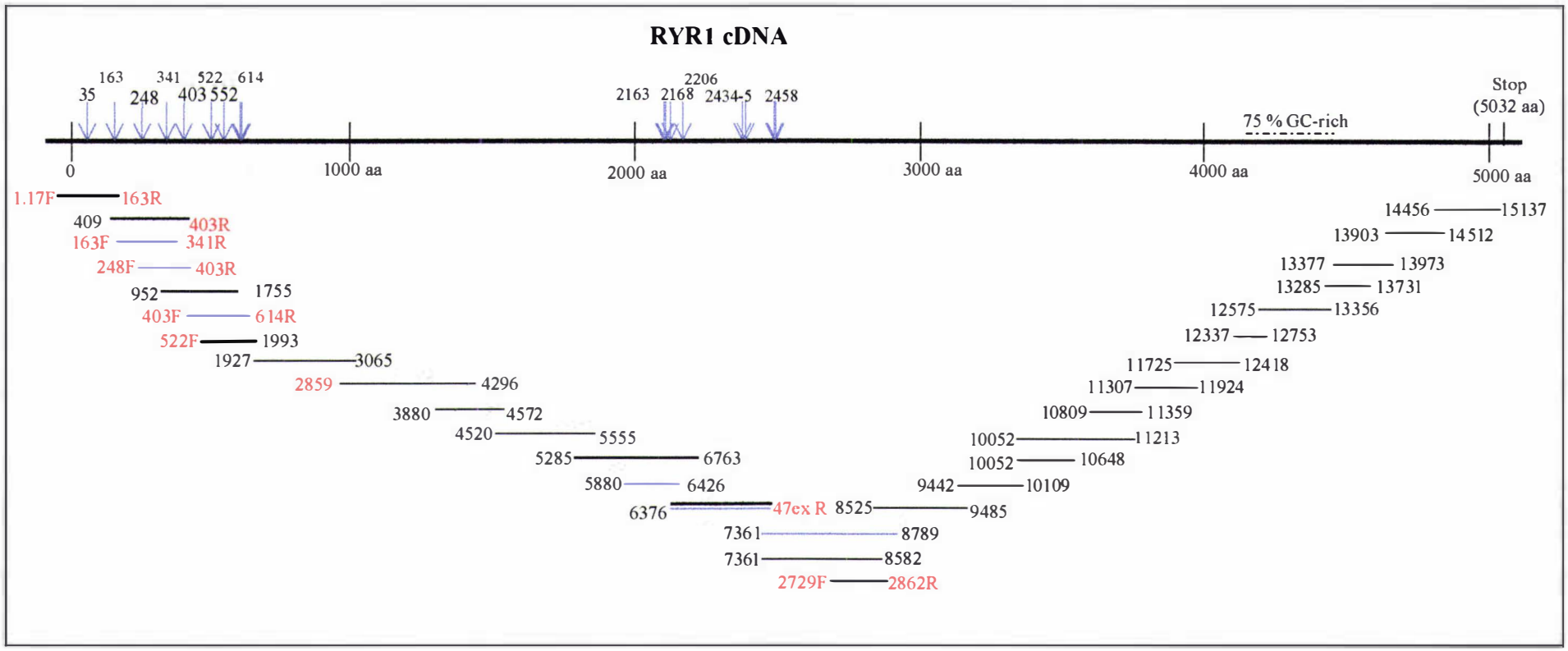

The RYR1 cDNA sequence is represented as a bold line at the top of the diagram. 17 RYR1 mutations reported at the time the sequencing project was commenced are indicated with blue arrows. Amino acids (aa) are numbered according to the updated RYR1 sequence (Phillips *et al.*, 1996). Overlapping PCR products amplified from the MHS (c221) and MHE (c154) cDNA samples are indicated below. Primers obtained from Professor Tommie McCarthy (University of Cork, Ireland) are labelled according to nucleotide sequence and are shown in black text. Other available primers are presented in red text. Bold lines indicate fragments encompassing mutation-rich regions. These fragments were investigated initially as likely sites for a novel mutation and were sequenced in both directions. Different PCR primer sets were used to repeat the amplification of the mutation-rich regions from c221 and from cDNA synthesized from a second MHS individual (c369). These fragments are represented with blue lines. Precise primer positions and sequencing primers are shown in appendix (). Primer sequences are given in appendix ().

Table 5-2 PCR primers and reaction conditions for the amplification of RYR1 cDNA

F Primer	R Primer	Boundaries (bp) 5'	3'	Prod. size (bp)	PCR: Annealing Temp. (X number of cycles) $MgCl_2$	Template	Sequencing primers employed
RYR176F	intron 1 R	-176	intron 1	240	55°C (X3), 54°C (X3), 53°C (X10), 52°C (X20), 1.5 mM	Genomic DNA	RYR-176F
RYR1.17F	163R	-114	531	645	60°C (X4) , 59°C (X4), 58°C (X38), 1.6 mM	RH cDNA	Not sequenced
RYR1.17F	275R	-114	276	390	58°C (X3) , 57°C (X5), 56°C (X30), 1.5 mM	1.17F/163R	275R
-7	163R	-16	531	546	60°C (X43), 1.5 mM	RH cDNA	163R-seq
409	403R	409	1224	816	59°C (X10) , 58°C (X35), 1.5 mM	RH cDNA	163F, 1204
163F	341R	457	1085	629	59°C (X42), 1.5 mM	RH cDNA	163F
248F	403R	702	1224	523	61°C (X35), 1.5 mM	RH cDNA	1204R
952	1755	952	1775	824	60°C (X35), 1.8 mM	RH cDNA	341F, 522R
403F	614R	1150	1925	776	60°C (X4), 59°C (X3), 57°C (X33), 1.5 mM	RH cDNA	403F-seq
522F	1993	1447	2013	567	60°C (X45), 1.5 mM	RH cDNA	522F, 1993
1927	3065	1927	3085	1159	60°C (X45), 1.5 mM	RH cDNA	1927, 2447, 2536, 2770
2859	4296	2877	4319	1443	54°C (X45), 1.5 mM	RH cDNA	3016, 3988, 3277
3016	4296	3016	4319	1304	60°C (X45), 1.5 mM (Elongase enzyme)	OT cDNA	3277
3880	4572	3880	4595	716	62°C (X5), 61°C (X5), 60°C(X10), 59°C (X30) 1.6 mM	RH cDNA	4296, 4572
4262	4800	4265	4823	559	61°C(X4), 60°C (X4), 59°C (X10), 58°C (X30) 1.4 mM	RH cDNA*	4800
4520	5555	4523	5578	1056	59°C (X45), 1.4 mm	RH cDNA*	4766, 5430
5285	6763	5288	6786	1499	62°C(X5), 61°C(X5), 60.5°C (X5), 60°C (X30) 1.5 mM	OT cDNA	5285, 6426
5880	6426	5883	6449	567	61°C (X5), 60°C (X40) , 1.5 mM	RH cDNA	5880, 6163
6376	47exR	6379	7479	1101	61°C (X20), 60°C (X24), 1.5 mM	RH cDNA	6763, 7039, 47exR, 2434F
7361	8789	7364	8812	1449	58°C (X5), 57°C (X40), 1.5 mM	OT cDNA	7361, 8132, 8332, 2729F
7361	8582	7364	8605	1242	59°C (X45), 1.5 mM	RH cDNA	7361, 8132, 8332, 2729F
2729F	2862R	8068	8640	573	57°C (X38), 1.6 mM	OT cDNA	2729F
8525	9485	8528	9507	980	58.5°C (X30), 1.5 mM	RH cDNA	2862F, 9022, 9485
9442	10109	9445	10131	687	60.5 (X15), 59.5°C (X35), 1.5 mM	OT cDNA	9696, 9769
10052	10648	10055	10686	632	54°C (X5), 53°C (X5), 52°C (X37), 1.8 mM	OT cDNA	10052, 10518
10052	11213	10055	11250	1196	53°C (X45), 1.5 mM	OT cDNA	10884
10809	11359	10827	11377	551	60°C (X4), 59°C (X5), 58°C (X20), 57°C (X20), 1.5 mM	OT cDNA	10809, 11359
11307	11924	11325	11961	637	59°C (X4), 58°C (X4), 57°C (X10), 56°C (X30), 1.5 mM	OT cDNA	11307, 11924
11725	12418	11744	12456	713	59°C (X4), 57°C (X4), 56°C (X33), 1.5 mM	OT cDNA*	12418, 11725

F Primer	R Primer	Boundaries (bp) 5'	3'	Prod. size (bp)	PCR: Annealing Temp. (X number of cycles) $MgCl_2$	Template	Sequencing primers employed
12337	12753	12357	12790	434	60°C (X45)	OT cDNA	12753
12575	13356	12592	13394	803	61°C (X3), 60°C (X3), 59°C (X5), 58°C (X32), (3 min @ 72°C), 1.5 mM $MgCl_2$, 8% DMSO, 7% glycerol	OT cDNA⌘	12892, 12974
13285	13731	13303	13769	467	62°C (X9), 60°C (X10), 59°C (X21), 1.5 mM	OT cDNA	13285
13377	13973	13405	14011	606	59°C (X45), 1.75 mM	OT cDNA	13377, 13973
13903	14512	13921	14550	630	58°C (X45), 1.75 mM	OT cDNA	13903, 14512
14456	15137	14474	15175	702	58°C (X45), 1.75 mM	OT cDNA	14456, 15137

Forward (F) and reverse (R) PCR primers, product sizes and reaction conditions are represented for the amplification of RYR1 cDNA. Products were purified and sequenced using an ABI-377 automatic sequencer. OT cDNA = oligo T-primed cDNA. RH cDNA = random hexamer-primed cDNA. Products were purified before sequencing using Wizard™ PCR purification system. ⌘ = PCR product s purified from agarose gel using the Wizard™ system.

Underlined primers were designed from RYR1 cDNA sequence for the amplification of specific mutation sites. Other primers were obtained from Professor Tommie McCarthy, University of Cork, Ireland. The amplification strategy is shown diagrammatically in Figure 5-3. Precise primer positions are indicated on the updated RYR1 coding sequence in appendix 3. Primer sequences are given in appendix 2.

PCR

Reactions were performed in 50 µl volumes. Reaction components were pre-mixed mixed in a cocktail to provide the following final concentrations: 1X PCR Buffer, 1.5 - 1.8 mM $MgCl_2$, 0.3 mM dNTP's, 2 ng/µl of each forward and reverse primer. The reaction mix was aliquoted into 0.5 ml tubes and template DNA added (1-1.5 µl of a 1/20 dilution of random hexamer-primed cDNA or 2-3 µl of a 1/10 dilution of the oligo T -primed cDNA). Tubes were overlaid with 50 - 100 µl of mineral oil. Hot-start PCR was performed in each case with the addition of 0.5 µl of *Taq* polymerase (or 2 µl of 2 U/µl Elongase™) to the reaction mixtures pre-heated to 94°C.

Standard PCR cycles consisted of an initial 3 minute denaturation at 94°C followed by repeated cycles of 15 seconds at 94°C, 30 seconds at the appropriate annealing temperature, and a 1-3 minute extension at 72°C. Programs were completed with a final 5 minute incubation at 72°C. Touchdown cycles involving progressively less stringent annealing temperatures were frequently performed to assist optimisation of reactions. The number of cycles at each annealing temperature is indicated in brackets.

5.3 RT-PCR METHODOLOGY

5.3.1 Sample identification

First strand cDNA was synthesised from 4 μg of each RNA sample with the Superscript™ preamplification system using random hexamers or oligo-dT to prime the reactions. The cDNA samples from the MHS and MHE individuals were identified with their respective genomic DNA identity numbers (M221 and M154) with a "c" prefix used in place of "M". Sequence data was labelled with the cDNA codes, together with the PCR reaction number and the sequencing primer. This allowed all samples to be traced in case of PCR contamination or detection of any candidate mutations.

5.3.2 Standard PCR methodology

PCR primers, product sizes and amplification procedures for the amplification of sequenced RYR1 gene segments are detailed in Table 5.2. A hot-start procedure was used in all PCR reactions to reduce the amplification of primer-dimers and contaminating products generated from non-specific priming during the reaction preparation at ambient temperatures. Optimal results were achieved using hot-start PCR with 0.2 μl of the oligo-dT primed cDNA template (2 μl of a ten-fold dilution) or 0.05 μl of the random hexamer-primed cDNA template (1 μl of a 20-fold dilution) per 50 μl PCR reaction. A $MgCl_2$ concentration of 1.5 mM was used in most reactions. To limit opportunities for PCR cross-contamination, dedicated pipettes were used to prepare all PCR reactions. These were not used in the downstream purification and handling of PCR products. Barrier tips were also used, when available.

5.3.3 Amplification of a polymorphic region

Polymorphic RYR1 regions were amplified and scrutinized to test the sensitivity of the mutation detection and also to verify the identity of the cDNA samples in the event of PCR cross contamination. A region containing a number of published silent polymorphisms, including Ile2704, Asp2729 and Ser2862 [107] was amplified from both random hexamer and oligo-dT primed cDNA as a 573 bp fragment using the 2739F/2862R primer set. This region was also encompassed within a 1428 bp fragment amplified with the 7361/8789 primer set or alternatively, a 1242 bp fragment prepared with the 7361/8582 primer set. Reaction conditions are given in Table 5-2.

5.3.4 Amplification of the N-terminal and central mutation-rich regions

The N-terminal mutation-rich region (excluding the Cys35Arg mutation) was amplified in three fragments as detailed in Figure 5.3 and Table 5-2. The 409/403R primer set was used to amplify an 816 bp fragment, which encompassed amino acid residues 144 to 401including the sites of three RYR1 mutations (Arg163Cys, Gly248Arg and Gly341Arg). Products were purified and sequenced in both directions using the 163F-bio and 1204 internal primers. An overlapping 824 bp fragment that included the sites of the Ile403Met, Tyr522Ser and Arg552Trp mutations was amplified with the 952-1755 primer set and sequenced with the 341F and 522R internal primers. A third overlapping segment was amplified with the 522Fwt/1993 primer set included amino acid residues 493- 664 (spanning the Tyr522Ser, Arg552Trp,Arg614Cys and Arg614Leu mutations) and was sequenced in the reverse direction region using the 1993 PCR primer.

The central mutation-rich region, which covered amino acid residues 2134 to 2486 (including the Arg2163Cys, Arg2163His, Val2168Met, Thr2206Met, Gly2434Arg, Arg24535His, Arg2458Cys and Arg2458His mutations), was amplified with the 6376/47exR primer set. This segment was sequenced with the forward 6376 and 2434F forward primers and the 6763, 7039 and 7393 internal reverse primers.

5.3.5 Amplification of the 5' RYR1 terminus

The primer set obtained from the Irish MH group did not encompass the 5' terminus or 5' UTR region of the RYR1 sequence. In order to amplify and sequence the entire RYR1 transcript, a forward 1.17F primer was designed using Primer 3 software program [320] to anneal 114 bp upstream of the initiator methionine codon. Repetitive sequence elements and the high GC content within the 5' UTR region hampered the design of primers to amplify this region. The 5' terminus of the RYR1 cDNA was amplified in a 555 bp fragment with the -1.17F/163R primer pair using random hexamer-primed cDNA. The –1.17F primer was designed from the revised RYR1 sequence [160] as there were several discrepancies within the 5' UTR between this sequence and the original published cDNA sequence [126]. Primers were also designed from the updated RYR1 sequence [160] to amplify and sequence exon 1 from genomic DNA (from -156 to +20 bp of intron 1).

5.3.6 Amplification of a GC-rich region

A region of the RYR1 sequence spanning residues 12890 - 13360 with 75-81 percentage GC content is reportedly refractory to amplification from cDNA (Dr. Patrick Lynch, Prof. Tommie McCarthy, personal communication). Amplification of this region was not possible using the standard PCR procedure described above, and appropriate conditions were arrived at by trial and error. The amplification of an 802 bp GC-rich fragment from oligo-dT primed cDNA was performed using 12575/13356 primer set with the addition of 7% glycerol and 8% DMSO using a 'touchdown' PCR program. Three cycles were performed at each annealing temperature, which was reduced in 1°C increments from 61°C to 58°C. An extended incubation period (6 minutes at 95°C) was included at the beginning of the program and denaturation steps within the PCR program were increased from the standard time of 15 seconds to 45 seconds to assist denaturation of the high GC template [411].

5.4 RESULTS: RT-PCR AND RYR1 SEQUENCE ANALYSIS

Both oligo-dT and random hexamer-primed cDNA were used successfully as substrates in PCR reactions, indicating that the extraction of intact RYR1 mRNA and cDNA synthesis was successful. RYR1 cDNA transcripts of at least 7.5 kb in length were synthesised as inferred from the successful amplification of nucleotides 8068 to 8640 from oligo-dT primed cDNA.

5.4.1 Detection of heterozygotes

A cDNA segment encompassing RYR1 nucleotides 8068 to 8640 including three published polymorphisms [107] was amplified and sequenced initially to test the efficacy of the dye-terminator chemistry in the detection of heterozygotes. A product of the appropriate size was obtained from oligo-dT primed cDNA and the identity of the 575 bp PCR product was confirmed by *Rsa* I digestion into fragments of 360, 192 and 20 bp, as expected (data not shown). The sequence from the MHS individual clearly indicated heterozygosity at positions corresponding to the Ile2706, Asp2730 and Ser2863 polymorphisms. This was revealed by the occurrence of overlapping signals in conjunction with a commensurate reduction in the relative peak intensity of the mutated nucleotide (data not shown). The MHE control individual was homozygous for the rare allele for each of these polymorphisms. The sequence profiles for the Asp2729 and Ser2862 polymorphism were thus consistent with the genotypes determined earlier by RFLP analysis of genomic DNA samples (M221 and M154) from the same individuals, confirming the identity of the muscle tissue specimens used to extract RNA.

5.4.2 Sequence analysis of the N-terminal and central mutation-rich regions

After the dye-terminator chemistry was shown to detect points of heterozygous sequence, the N-terminal and central mutation-rich regions were investigated as the most likely sites for a MH mutation in the CH family. These regions were amplified and sequenced in both directions as described above. High-resolution sequence (extending up to 400 –450 bp from the primer site) was examined for potential mutations and sequence discrepancies by computer-assisted alignment of the sequence from the MHS individual with that from the MHE individual and also the published RYR1 sequence [126]. Sequences were also scrutinized manually for any overlapping signals characteristic of heterozygosity. True polymorphisms were distinguished from sequence artifacts by careful scrutiny of the corresponding sequence from the control sample, and by sequencing the opposite strand of the region of interest.

None of the published RYR1 mutations were detected in the sequence analysis of the N-terminal (amino acid residues 144 - 664) or central (amino acid residues 2134 to 2930) RYR1 mutation-rich regions amplified from the MHS (c221) cDNA sample. This was expected from an earlier screen for these mutations by RFLP and sequence analysis of genomic DNA from MHS members of the CH family (Chapter 3). The N-terminal and central mutation-rich regions were also devoid of any candidate disease-linked mutations. This result was unexpected, since the linkage analysis strongly implicated the involvement of a RYR1 defect in this family and all previously reported RYR1 mutations were confined to these regions. Therefore, the mutation-rich regions were amplified from the cDNA of a second MHS individual (c369) and re-sequenced in case a mutation had gone undetected in the initial screen. Different primer sets and amplification strategies were employed such that, in the event of PCR contamination, the products of previous reactions could not act as templates in the amplification of the cDNA from the second MHS individual. For example, the 409/403R, 952/1755 and 522/1993 primer sets were substituted with 163F/341R,

248F/403R and 341F/614R primer combinations respectively. The 7361/8789 primer pair was used in place of the 7361/8582 primer set. Sequence analysis of cDNA from the second MHS individual revealed a number of silent polymorphisms, however no candidate mutations were identified in this individual. In view of the proven sensitivity of the chosen sequencing chemistry in the detection of silent polymorphisms, it was highly unlikely that a mutation would have been overlooked in the repeated analysis. Therefore it was concluded that if a RYR1 mutation was involved in the CH family, it must lie outside the mutation "hot-spot" regions where all previously reported mutations had been located.

5.4.3 Analysis of polymorphic region

After excluding the N-terminal and central regions from containing a causative mutation in the CH family, a highly polymorphic region [107], immediately 3' to the central mutation-rich region, was investigated next as a potential site for a novel mutation in this family. This region was amplified initially with the 7361/8789 primer set but the reactions failed to yield discrete products. The desired 1449 bp fragment was consequently excised under UV-light, purified from the agarose gel and re-amplified to obtain a pure product. Automatic sequence analysis of this fragment revealed an apparent novel Val2715 to Ala substitution resulting from a C8144 to T transition, as shown in Figure 5-4. Two overlapping peaks of equivalent intensity were observed in the sequence, which was otherwise devoid of any background noise.

Figure 5-4 Detection of a probable UV-induced mutation amplified in secondary PCR

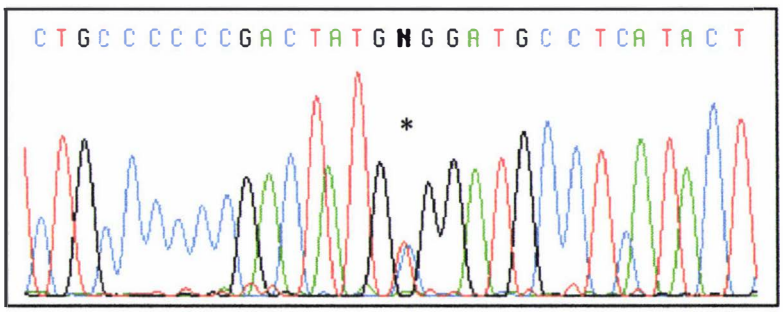

Electropherogram obtained from an ABI-377-18 automatic sequencer using dye-terminator chemistry. Sequence is shown from the MHS (c221) individual bearing an apparent C2744 to T transition (Val 2715 to Ala). The 1428 bp DNA fragment was re-amplified with the 7361/8789 primer pair from gel-purified PCR product. Sequence was initiated with the 7631 primer. The bases change was not observed when the region was amplified from cDNA and sequenced in both directions.

To verify the existence of this candidate novel substitution, the region was amplified with an alternate 7361/8572 primer set directly from the cDNA template and sequenced in both directions. The putative mutation was not observed in this repeat sequence. This suggested the mutation detected in the gel-purified PCR product might have been induced by UV-light during gel-purification and then amplified in the second round of PCR. Interestingly, the sequence derived from the gel-purified DNA indicated homozygous status for the common alleles at the Ile2704, Asp2729 and Ser2862 polymorphisms. This indicated allele amplification bias might also

have occurred, as the genotypes were not consistent with the expected profiles for either the MHS or MHE sequences. In light of the problems encountered in this analysis, the secondary amplification of gel-purified products commonly used to improve PCR specificity [411] was not employed to amplify other products for RYR1 cDNA sequence analysis.

After excluding the N-terminal and central regions and adjacent polymorphic region as sites for the causative mutation in the CH family, the remaining RYR1 coding sequence was examined. The 5'UTR and 5' coding region was investigated initially, followed by the intervening segment between the N-terminal and central mutation regions. The remaining 6.4 kb of 3' sequence was then examined sequentially in the 5' to 3' direction. Segments outside the mutation-rich regions were generally sequenced in one direction only, except to resolve ambiguities, and to confirm new polymorphisms and candidate mutations. Problems encountered during this investigation, included evidence of PCR cross-contamination an apparent PCR-induced deletion and complex sequence derived from fragments encompassing alternatively spliced regions.

5.4.3.1 Detection of a PCR-induced deletion in the 5' untranslated region

Primers were designed from updated sequence information [160] to amplify the 5' UTR in a 390 bp product, which included the site of the Cys35Arg mutation [165]. Repeated attempts to amplify the region with this RYR1.17F/275R primer pair failed to generate discrete products. Successful amplification of the 390 bp product was achieved using a longer, 645 bp RYR1.17F/163R product as a substrate. It was noted that both products amplified from the control cDNA sample appeared as doublets after prolonged electrophoretic separation. In contrast, the equivalent products amplified from the MHS c221 cDNA appeared as a single band.

No candidate point mutations were observed in this sequence. However, sequence derived from the MHS sample revealed an apparent 27 bp deletion of nucleotides -89 to -63 in the 5' UTR when aligned with the published sequence [160] (Figure 5-5). Such a deletion was unlikely to be responsible for MH in the CH family, as all previously reported mutations involved single missense point mutations [25]. Furthermore, the sequence was devoid of any background peaks which would have been expected if the deletion was peculiar to one allele. In addition, sequence analysis of the equivalent PCR product from the control sample (c154) also revealed a deletion, though in this case a 24 bp section was omitted. After the point of the deletion, the sequence was superimposed over background sequence derived from a longer product, in keeping with the appearance of the twin bands on the agarose gel.

To determine whether the apparent deletions existed in the genomic DNA, the region was amplified from both MHS (M221) and control (M154) genomic DNA samples. Sequence from nucleotide position -148 to the end of exon1 was examined for evidence of deletions or mutations that might introduce a cryptic splice site. The sequence obtained from both the MHS and control DNA samples was entirely consistent with published data [160]. The different sized products amplified from cDNA were unlikely to represent alternatively spliced transcripts, as the deleted sections were not flanked by potential consensus (C/T)AG acceptor or G(T/C) donor splice site sequences [160]. The apparent deletions in the amplified cDNA were probably PCR-induced artifacts resulting from "slippage" during re-amplification of repeated GC-rich SpI and muscle-specific promotor elements (underlined in Figure 5-5). Although secondary PCR with nested primers can greatly improve the specificity of PCR reactions, this practice reduced the fidelity of PCR and was avoided in subsequent analyses.

Figure 5-5 PCR-associated deletions in RYR1 5' UTR amplified from cDNA.

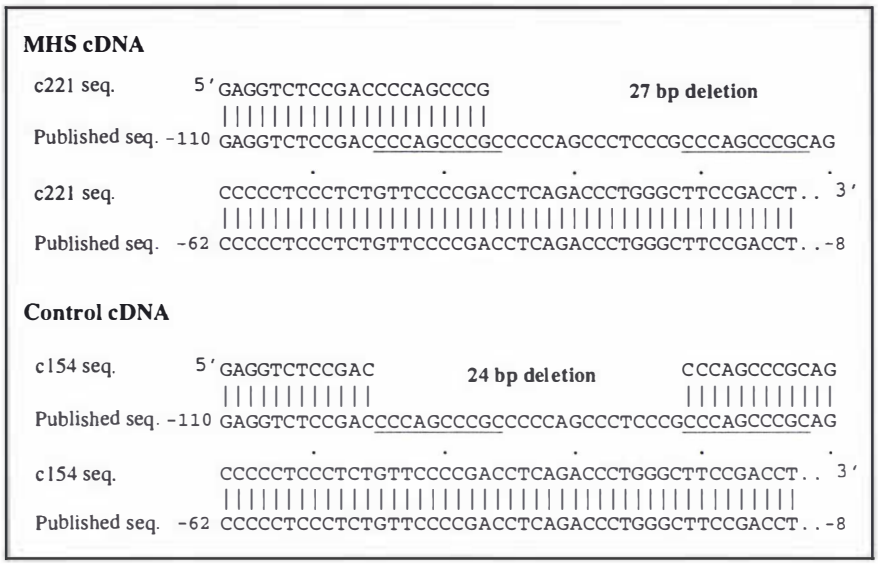

RYR1 cDNA was amplified with the -1.17F/275R primer set. Sequence was generated with the 275R reverse primer; reverse complemented and aligned with published exon one sequence [160] (Genbank accession U48449). Repeated sequence elements containing the Sp1 promoter elements [160] are underlined.

5.4.4 Detection of RYR1 sequence polymorphisms

A candidate MH mutation was not detected in the RYR1 N-terminal or central regions. This was confirmed by sequence analysis of cDNA synthesized from a second MHS individual (c369). However, fifteen differences between the MHS (c221) and control (c154) sequences were detected that corresponded to published polymorphisms [107,168] proving the chosen sequencing strategy enabled the successful detection of heterozygous mutations. The MHS trait coincided with the common allele at each of these polymorphisms, corresponding to the published sequence. The non disease-linked haplotype inherited by the control individual (c154) included the rarer allele for most of the RYR1 polymorphisms. Previously corrected sequence errors at Leu792 [107] and a correction of RGAP1368 to QEAPQ1369 [168] were confirmed.

One new sequence discrepancy was encountered (in both MHS and MHE sequences) resulting from the resolution of a probable GCCG compression in the original sequence to GCGC, changing valine 2550 to leucine. In addition, seven new silent polymorphisms were encountered within the sequence as described in Table 5-3. Sequence profiles for the Cys2363 and Pro2366 polymorphism are shown in Figure 5-6. The latter mutation changes RE recognition sites for *Bsl* I and *Bsp* MI and may be potentially useful for future haplotype analysis. The MHS trait appears to be in phase with the normal allele at each of the new silent polymorphisms.

A novel C to G transversion was detected in the sequence from the MHE individual that changed amino acid glutamine 3756 to glutamate (Figure 5-6 B). This conservative substitution was not considered to be a candidate MH mutation since the corresponding residue in the rabbit [155] and porcine [203] RYR1 sequences is also glutamate [203] (See Chapter6, Figure 6.8). Furthermore, the mutation was unique to the MHE(h) individual.

Figure 5-6 Detection of novel RYR1 polymorphisms by sequence analysis of cDNA

A. Cys2363, Pro2366 B. Gln3756Glu

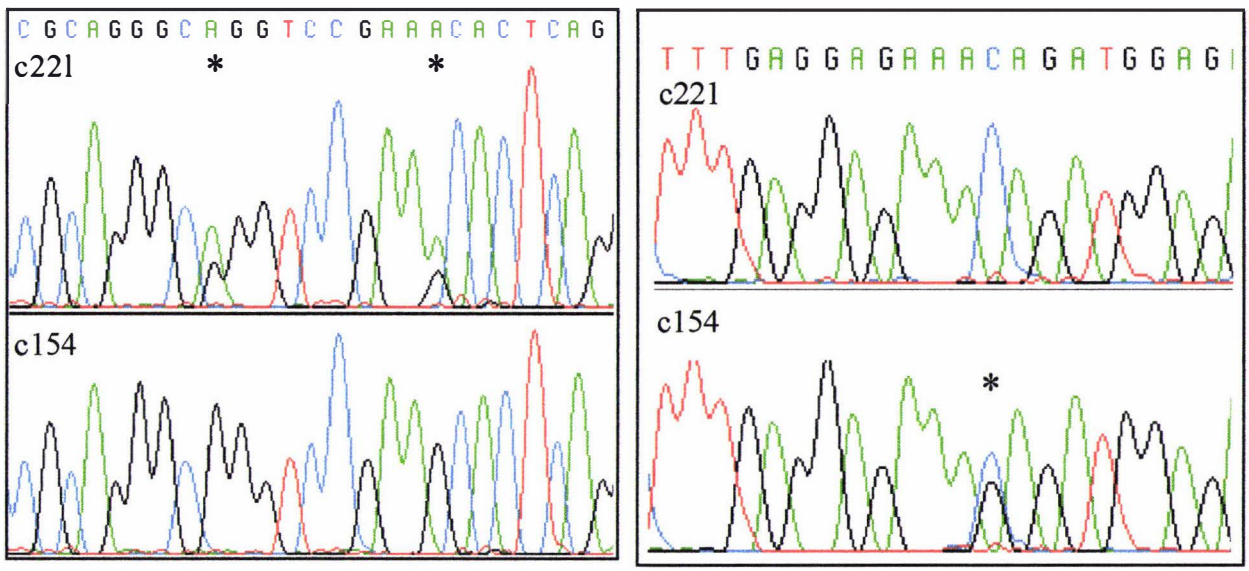

A. Sequence analysis of the 6376/47exR PCR product showing position of two new polymorphisms. The control sequence (c154) is homozygous for the base change in both cases. Sequence was generated using an ABI-377-18 automatic sequencer with dye terminator chemistry. Sequence was initiated with the 47exR PCR primer. Antisense sequence is shown.

B. Sequence analysis of the 10809/11359 PCR product showing the C to G transversion that substitutes glutamine 3756 for glutamate (unique to the c154 control sequence). Sequencing reactions were primed with the forward 10809 PCR primer (performed as described above).

Table 5-3 Novel silent RYR1 polymorphisms

Amino Acid[a]	Substitution	MHS c221	MHE c154	Amino acid change	R E site changed
Cys 2363	TGC>TGT	C/T	T/T	None	None
Pro 2366	CCC>CCT	C/T	T/T	None	N*la* IV, B*sl* I loss, B*sp* MI gain
Arg 2403[b]	CGC>CGT	C/C	C/C	None	H*ha* I, T*ha* I loss
Ala 2427[b]	GCC>GCT	C/C	C/C	None	B*bv* I, T*se* I gain
Gln 3756	CAG>GAG	C/C	C/G	Gln > Glu	S*cr* FI gain
Thr 3918	ACT>ACA	T/T	A/T	None	None
Ala 4293	GCG>GCC	G/G	G/C	None	N*la* IV, B*sl* I gain
Thr 4752	ACA>ACC	A/A	A/T	None	H*ph* I gain

[a] Amino acids are numbered according to the corrected RYR1 sequence [160].
b Detected in cDNA from MHS individual c479.

5.4.5 Detection of a novel Thr4826Ile mutation

No candidate mutations were detected after sequencing almost the entire 15.3 kb coding region of the MHS individual from the CH family. Three short gaps of 30 - 50 bp remained where sequence was initiated further than anticipated from the sequencing primer. Sequence analysis of the three remaining regions exposed a candidate C14477 to T transition in exon 100 that substituted isoleucine for threonine 4826 in the sequence derived from the MHS individual. This candidate mutation was detected in a 630 bp fragment amplified with the 13903- 14512 primer set and was located 52 bp away from the 14512 sequencing primer. The C14477T mutation was not observed in the initial attempt to sequence the 13903-14512 product because the sequence was initiated approximately 58 bp from the 14512 primer. The candidate C14477T mutation overlaps with the binding site of 14456 forward primer that was used to amplify the adjacent 3' cDNA segment. Consequently, the mutation was not detected in the sequence analysis of this final 3' fragment either. The presence of the C14477T polymorphism was confirmed by sequence analysis of the reverse strand and by the analysis of the same regions amplified from cDNA from a second MHS individual. Automatic sequence electropherograms obtained for the MHS and MHE individuals are shown in Figure 5-7.

The MHS and MHE siblings selected for the sequencing project shared the same maternal chromosome 19 but different paternal chromosomes from their MHS father. The mutation was detected only in the cDNA from the MHS sibling thus it coincided with the inheritance of the MH-associated paternal haplotype in this individual. The Thr4826Ile substitution was therefore a strong candidate for a causative mutation in view of the preliminary study that linked the inheritance of this haplotype with the inheritance of MHS in the CH pedigree. In addition, the Thr4826Ile mutation was the only disease-linked substitution encountered during the sequencing of the entire RYR1 coding region. Furthermore, the strict conservation of the predicted transmembrane loop encompassing threonine 4826 across all published RYR1, RYR2 and RYR3 [126,192,203,204,217] sequences implies functional significance of this residue (As discussed in Chapter 6, Figure 6.9).

Figure 5-7 Sequence analysis of the T4826I mutation

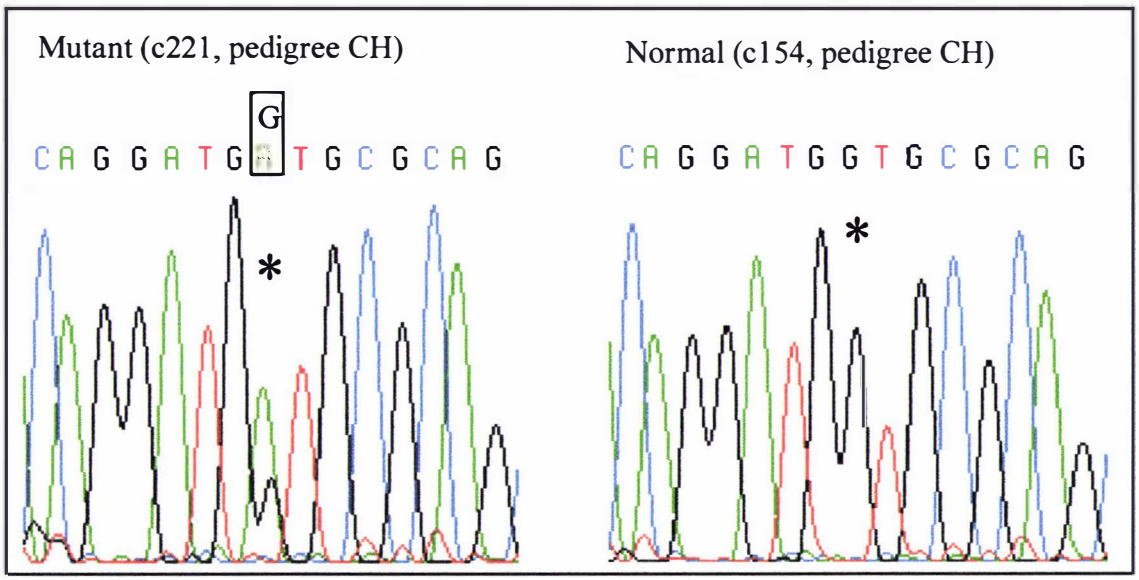

Nucleotide sequence of the RYR1 cDNA PCR fragment (13903-14512) bearing the C14477T mutation detected in the CH pedigree. Sequence was obtained an ABI-377-18 automatic sequencer with dye-terminator chemistry, using the 14512 primer. Antisense sequence is shown. The mutation changes the threonine 4826 (ACC) to an isoleucine (ATC). The mutation was unique to the sequence from the cDNA from the MHS individual (c221).

5.4.6 SSCP detection of the T4826I mutation in genomic DNA

As the Thr4826Ile had not previously been reported and was positioned well outside the known RYR1 mutation regions, it was important to rule out the possibility that the mutation might represent a common, coincidental sequence polymorphism. This necessitated the development of a cost-effective and efficient method to detect the mutation in genomic DNA samples from 100 members of the normal population.

Analysis of exon 100 sequence [160], (Genbank accession number; U484505) indicated the C14477T transition did not alter any restriction sites for an affordable restriction endonuclease that would facilitate RFLP detection. Although the mutation removed a recognition site for *Sfa* NI, financial considerations excluded the use of this enzyme in a large-scale RFLP mutation screen. A non-radioactive SSCP technique employing ethidium bromide detection was therefore developed to screen for the mutation in a 208 bp PCR fragment which was amplified from genomic DNA with the 14662/100iR primer set. The presence of the mutation was revealed by the appearance of an additional single-stranded DNA band (or bands) migrating below a band corresponding to the normal allele as shown in Figure 5-8 A. While there is a difference in the banding pattern produced from normal and mutant alleles, this was not consistently reproducible or immediately obvious to the untrained eye. An alternate forward primer (14486F) was therefore designed to amplify a shorter, 185 bp product in an attempt to improve the differentiation of the mutant and normal SSCP bands.

The mutation was readily detected in the 185 bp product by the appearance of two additional SSCP bands, as shown in Figure 5-8B, though SSCP analysis of the shorter products prepared using the 14486/100iR primer set was particularly susceptible to alterations in the buffer composition or gel running conditions.

Figure 5-8 SSCP detection of the Thr4826Ile mutation

A.

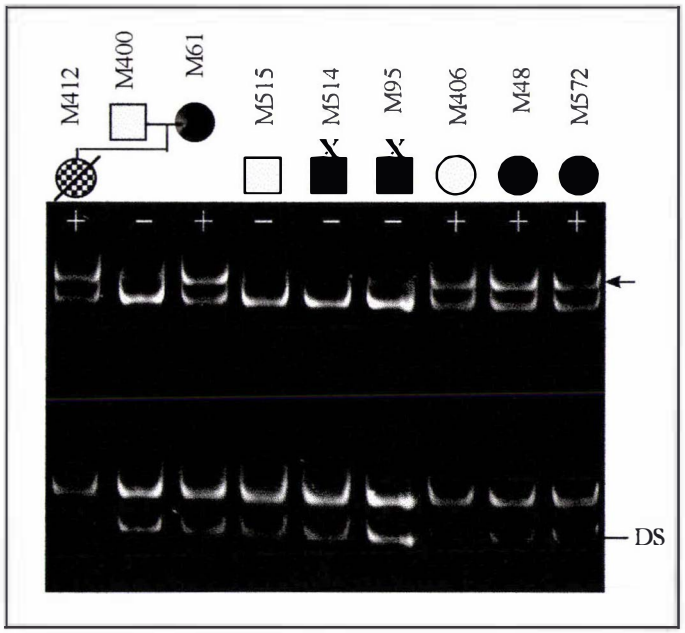

A. SSCP analysis of the T4826I mutation in members of the CH family. The 208 bp fragment was amplified with the 144462/100iR primer set and separated by non-denaturing 9 % PAGE in 0.5 X TBE for 3 hr, 35 min. at 3-4W (constant power) at 4 °C. The gel was stained in 0.5 μg/ml EtBr, and photographed under UV light. The mutation-specific band is indicated with an arrow. DS = double stranded DNA. Black symbols represent MHS individuals. Clear symbols represent individuals not examined by IVCT. The chequered symbol represents a child (M412) who suffered sudden infant death. MHS individuals M514 and M95 are recombinant (X) with respect to the T4826I mutation.

B.

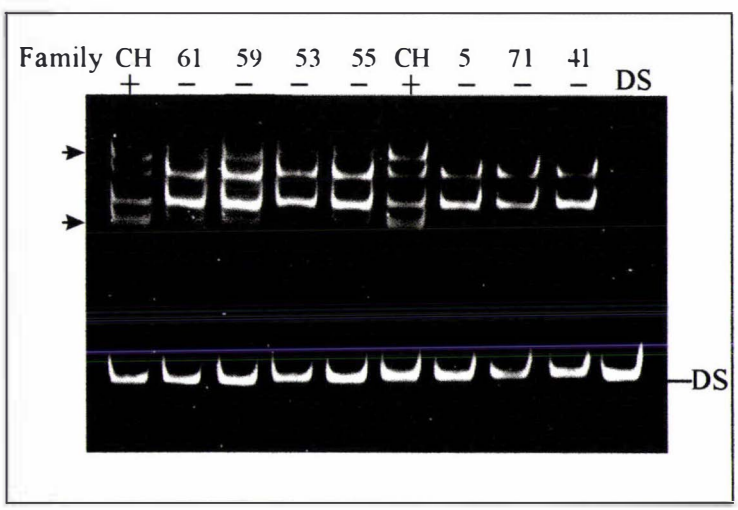

B. SSCP analysis of the T4826I mutation in unrelated NZ MHS probands. The 185 bp fragment was amplified with the 14486/100iR primer set, resolved by non-denaturing 9 % PAGE at 4°C for 3 hr 40 min. at 3W, constant power (~280 V). The gel was stained in 0.5 μg/ml EtBr and visualised under UV light. The mutation is revealed by the appearance of two extra bands (marked with arrows) in an MHS member of the CH family (M74: lanes 1 and 6). The T4826I mutation was not detected in representative MHS members of other MH pedigrees examined. (lanes 2-5 and 7-9)

5.4.6.1 Screening control DNA samples for the Thr4826Ile mutation

To investigate whether the Thr4826Ile mutation could be a neutral polymorphism, SSCP analysis was employed to screen for the mutation in 220 normal chromosomes from unrelated control subjects. Samples were selected from the unaffected parents of MHS individuals and unrelated MHN individuals from other NZ MH families, in addition to spouses married into the CH family. The control sample population included individuals of both Maori and Caucasian descent and was

therefore representative of the ethnic background of the family in which the mutation was identified. The Thr4826Ile mutation was not detected in the DNA from any of the 220 normal chromosomes investigated, indicating it was not a common polymorphism. The segregation of the Thr4826Ile mutation with MHS in members of the CH family and the relationship between phenotype and genotype for IVCT tested members of the family is explored in detail in Chapter 6.

5.5 IDENTFICATION OF RYR1 MUTATIONS IN OTHER MHS PROBANDS

After the acquisition of an automatic sequence facility and primers and methodology for the amplification of RYR1 cDNA, the sequence analysis of RYR1 cDNA became the method of choice to search for both published and novel RYR1 mutations in MHS probands. Since RT-PCR using skeletal muscle RNA proved successful in detecting a number of novel polymorphisms as well as a unique mutation in RYR1in the CH family, this approach was used to investigate additional NZ families. Probands from three new MH families referred for genetic analysis were selected in a screen for candidate mutations in the N-terminal and central mutation-rich regions of RYR1 cDNA. Fresh skeletal muscle tissue specimens (100 – 500 mg) obtained from individuals undergoing muscle biopsy operations for the IVCT were frozen immediately and stored in liquid nitrogen. RNA was extracted from approximately 100 mg of each tissue sample, and cDNA synthesized using random hexamers using the Superscript™ system (as described in the analysis of the CH family). The N-terminal and central mutation-rich regions were amplified in three fragments (as described in Table 5-4 and Figure 5-9) and subjected to automatic DNA sequence analysis. Case reports for the three probands investigated from families 36, 24 and 70 are presented in appendix 6.

Table 5-4 Amplification of RYR1 mutation-rich regions from cDNA

Region	F primer	primer	Size	Amino acid	[$MgCl_2$]	T	Sequencing primers
N1	409	403R	816 bp	144 - 401	1.5 mM	59°C	163F, 341F 1204
N2	649	1993	1345 bp	224 - 634	1.5 mM	59°C	952, 522F, 614R
Central	6376	47exR	1100 bp	2134 - 2486	1.5 mM	61°C	6763, 2434F, 47exR

Figure 5-9 PCR products encompassing RYR1 mutation-rich regions

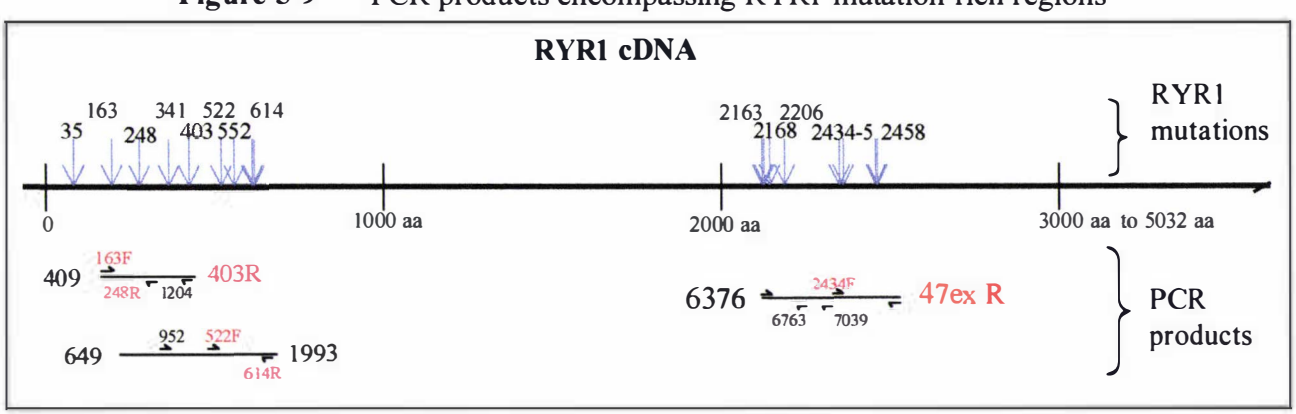

RYR1 mutation-rich regions were amplified from cDNA of MHS probands and sequenced for novel mutations. Sites of previously published mutations are indicated with blue arrows. Forward and reverse sequencing primers are indicated with arrows above and below the PCR fragments, respectively. Primer details as described for Figure 5-3. Primer sequences are given in appendix 1. Primer positions and additional sequencing primers are shown in appendix 2.

5.5.1 Identification of a novel Arg2452Trp mutation in family 36

Muscle tissue and DNA from a representative MHS member of family 36 became available when the proband (who had suffered MH in infancy) presented for IVCT examination at the age of 13. This case was of particular interest due to the rarity of MH reactions in infancy and the suspicion of sub-clinical CCD in this patient (N. Pollock, personal communication).

The mutation-rich regions were amplified and sequenced from cDNA as described above. None of the nine published mutations [25,110,161,167-169] were detected. However, a novel C7354T nucleotide transition was identified which resulted in a substitution of arginine 2452 for tryptophan. Sequence analysis of the reverse strand confirmed the presence of the Arg2452Trp mutation.

Figure 5-10 SSCP detection of the Arg2452Trp mutation in Family 36

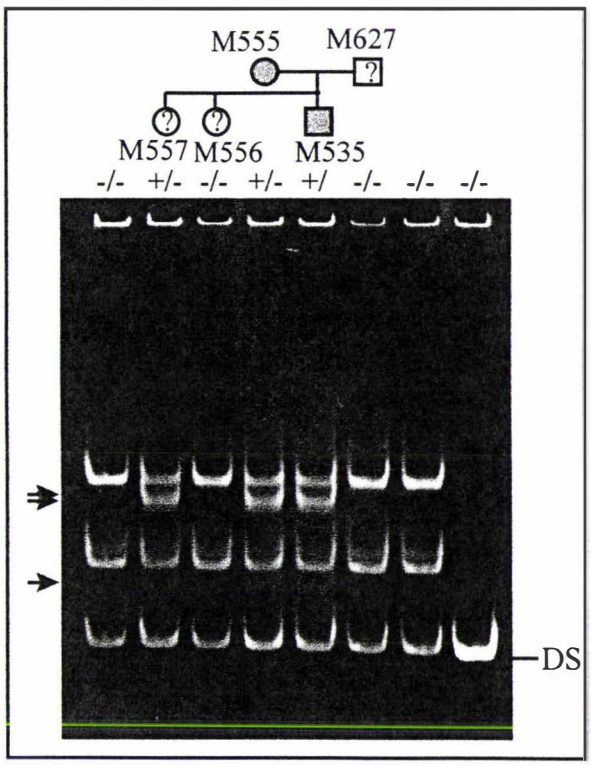

Genomic DNA samples were amplified with the 45iF/7361 primer set, denatured and resolved by 8% non-denaturing PAGE in 0.5X TBE, Electrophoresis was performed at 3W (constant power) at 4°C (until the bromophenol blue due front had migrated off the bottom of the gel). DNA was stained with 0.5 μg/ml EtBr and visualised under UV light. Mutation-specific bands are indicated with arrows. DS = Double stranded DNA. Filled symbols = MHS, ? = Untested.

The mutation did not alter any recognition sites for restriction endonucleases that would allow the implementation of a simple RFLP detection procedure. Therefore, genomic DNA samples of relatives were amplified with the 45iF/7361 primer set and screened for the Arg2452Trp mutation by SSCP analysis as shown in Figure 5-10. The presence of the mutation was revealed by the appearance of three additional SSCP bands. SSCP detection of the Arg2452Trp mutation was found to be robust and relatively insensitive to variations in gel buffer and running conditions.

The Arg2452Trp mutation was not found in 100 normal chromosomes examined by SSCP or in the DNA of 32 unrelated MH probands from other NZ families, indicating it is not a common polymorphism. The amplified region also includes the site of the Arg2458His and Arg2458Cys mutations [169]. These were not detected in any of the NZ probands examined. DNA samples were obtained from both parents of the proband and two siblings and screened for the mutation by

SSCP and/or DNA sequence analysis. However, further study of the Arg2452Trp mutation in family 36 was limited by the small size of the pedigree.

The father of the proband (family 36) was negative for the mutation. This individual has declined muscle biopsy but has normal creatine kinase levels. Both SSCP and DNA sequence analysis revealed the mother of the proband to be positive for the Arg2452Trp mutation. Upon examination, this individual was found to have elevated creatine kinase and was subsequently diagnosed MHS by IVCT (with a 4.3g response to 2% halothane and a 3.7g response to 2 mM caffeine). This confirmed maternal inheritance of MHS in the proband, consistent with the occurrence of the Arg2452Trp substitution. The mutation was present in the DNA of one of two siblings investigated, but these individuals have not yet been examined by IVCT. Further work awaits collection of specimens from the maternal grandparents to determine the origin of the mutation in this family and the IVCT examination of additional individuals. The fact that MH was unveiled during surgery for cleft palate is noteworthy, since an association between cleft palate and susceptibility to MH has been previously noted [412,413].

5.5.2 Identification of a novel Arg401Cys mutation in family 70

An MHS individual from a Maori family (M479, family 70) was selected for RYR1 cDNA sequence analysis based on the ethnic background, documentation of a fulminant MH crisis in this family and the availability of muscle tissue from a recent muscle biopsy. A clinical case report for the MHS proband is given in appendix 6.8. The N-terminal and central RYR1 mutation-rich regions were amplified from cDNA and sequenced in both directions. Two novel silent polymorphisms were detected at residues Arg2403 and Ala2437 (as described in Table 5-3), however no candidate MH mutations were detected in the central mutation region. Sequence analysis of the N-terminal PCR products encompassing residues 137 to 411 revealed a novel C1201 to T transition that substitutes Arg401 for Cys (Figure 5-11). This mutation is situated two residues upstream of an Ile403Met mutation that was associated with MH and CCD in a single overseas pedigree [13].

Having identified a mutation by direct sequencing of products made by RT-PCR, primers were designed to amplify a 195 bp fragment from genomic DNA to screen for the Arg401Cys mutation in family members by SSCP (Figure 5-11B).

Figure 5-11 Identification of the Arg401Cys mutation

A. Sequence analysis of cDNA B. SSCP analysis of genomic DNA

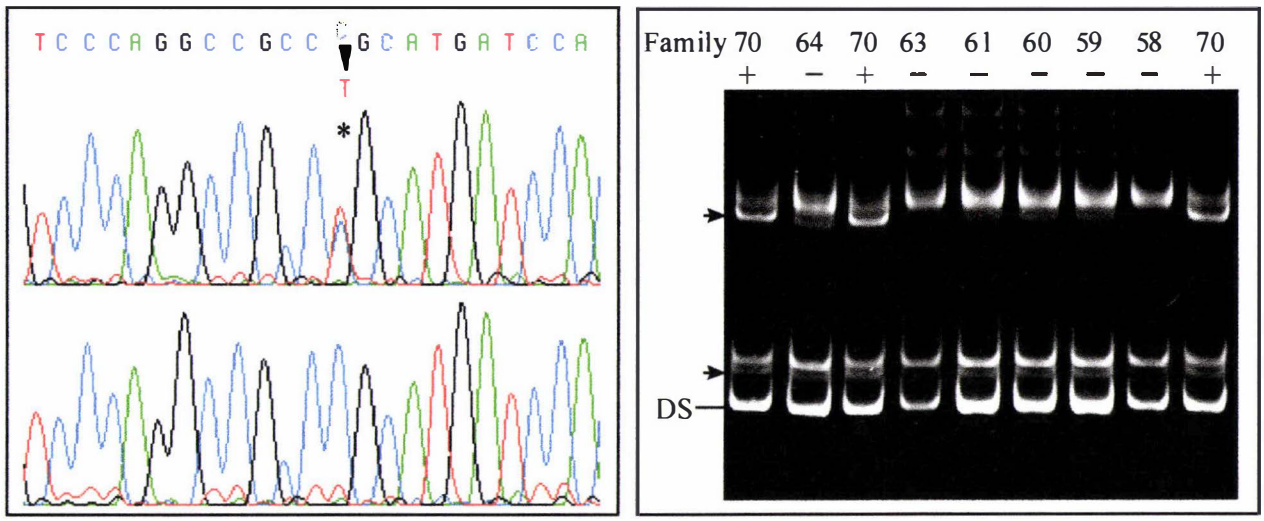

A. DNA sequence of RYR1 cDNA amplified with the 409F/403R-bio primer pair. The C1201T transition that substitutes Arg401 for Cys was detected in cDNA from individual 479 (family 70) (top). Normal cDNA sequence from MHE individual (154) is shown in the bottom panel. Sequence was obtained using an ABI-377-36 automatic sequencer with dye-terminator chemistry, initiated with the 341F primer.

B. SSCP analysis of a 195 bp fragment amplified with the 403F-seq/401iR primer set by 8 % non-denaturing PAGE in 0.5X TBE. Electrophoresis was carried out at 3W (constant power) for 3hr 20 min at 4°C. DNA was visualised by staining in 0.5 µg/ml EtBr and photographed under UV light. The R401C mutation was detected by a band shift in the SSCP profile for MHS members of family 70 (M479: lanes 1 and 3, M542: lane 9). Mutation-specific bands are indicated with arrows. The mutation was not detected in DNA from probands of other MHS families examined (lanes 2, 3-8).

Figure 5-12 Segregation of the Arg401Cys mutation in family 70.

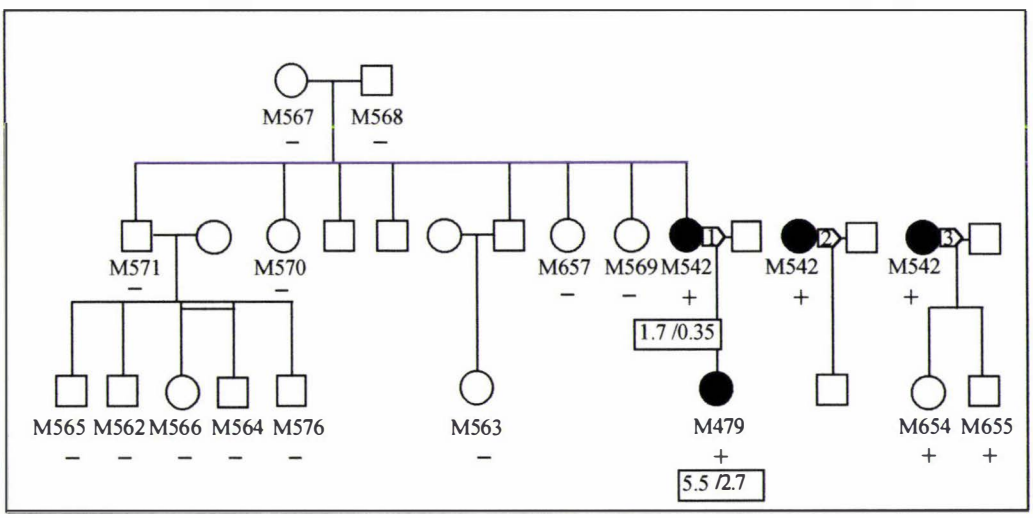

The presence (+) or absence (-) of the Arg401Cys mutation is indicated for members of family 70 screened by SSCP and automatic DNA sequence analysis. Contracture responses to 2% halothane and 2 mM caffeine (respectively) are presented in boxes for two individuals diagnosed MHS (black symbols) by IVCT. M479 is the proband.

5.5.3 Segregation of MHS with the Arg401Cys mutation in family 70

The segregation of the mutation in members of family 70 screened by SSCP and/or automatic DNA sequence analysis is presented in Figure 5-12. The mutation was detected in the mother of the proband (M542) who was also diagnosed MHS by IVCT. Two half-sisters of the proband were also positive for the Arg401Cys mutation, as determined by automatic sequence analysis of amplified genomic DNA. Neither has been investigated by IVCT. Interestingly, both parents of M542, and four of her siblings (investigated by DNA sequence analysis) were all negative for the Arg401Cys mutation. This would indicate that the Arg401Cys mutation has occurred *de novo* in individual M542, assuming the alleged paternity is valid.

The novel Arg401Cys mutation was not detected in 46 normal chromosomes from unrelated individuals or in the DNA of 32 other NZ MHS probands screened by SSCP, indicating it is not a common polymorphism. Residue Arg401 is strictly conserved across all known sequences from the RyR family (Chapter 6, Figure 6.7A). This, together with the proximity of this mutation to a previously reported Ile403Met mutation [13] implies functional significance of this residue and importance of the region in the MH disorder. However, it is not possible at this point to establish a causative role for the Arg401Cys mutation based on the limited IVCT data from this pedigree.

5.5.4 Detection of the Gly341Arg mutation in family 24

RNA was extracted from muscle tissue obtained from the MHS father (M445) of the proband from family 24. The N-terminal and central mutation-rich regions of RYR1 were amplified from cDNA and examined by automatic sequence analysis as described in Table 5.4. None of the published RYR1 mutations were identified in the second N-terminal (649/1993) or central (6376-47exR) fragments. Visual inspection of the sequence of the first N-terminal (409/403R-bio) fragment revealed a weak C/T signal overlap as shown in Figure 5-14A. The sequence polymorphism corresponded to the site of the published G1021A (Gly341Arg) mutation in the coding strand [109]. The G1021A mutation was clearly visible in the forward sequence derived from a second PCR product amplified with the 409/403R primer pair (Figure 5-14B). The presence of the G1021A transition was subsequently confirmed in genomic DNA samples from four MHS individuals from family 24 by SSCP analysis (Figure 5-13) and automatic DNA sequence analysis (Figure 5-14).

SSCP analysis of the Gly341Arg mutation (Figure 5-13) was particularly sensitive to PCR and electrophoretic variables, consequently further members of family 24 family were screened for the mutation by direct sequence analysis of amplified genomic DNA. The segregation of the mutation in members of family 24 is displayed in Figure 5-15. The mutation was also detected in two MHS siblings (M475 M537) of the proband but was not detected in the DNA from one MHN uncle (M548). MH susceptibility is thought to have been inherited via the paternal grandmother who registered an abnormally high creatine kinase levels (N. Pollock, personal communication, data not available).

Figure 5-13 SSCP analysis of the G1021A (Gly341Arg) mutation in family 24

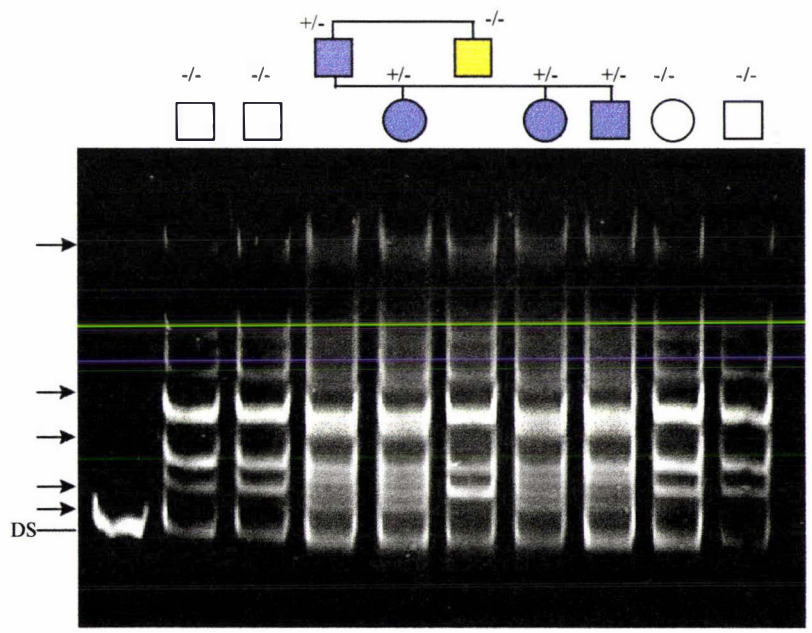

The 121 bp 341F/341R PCR products were amplified from genomic DNA and resolved electrophoresis on a 15 % non-denaturing 29:1 bis-acrylamide gel in 1 X TBE. Electrophoresis was carried out at 4°C for 5 1/2 hours at 3W (constant power) and ~ 325 V. Arrows indicate mutation-specific SSCP bands. Symbols: Blue = MHS, = MHN (family 24), Clear = unrelated MHS individuals.

Figure 5-14 Detection of the G1021A (Gly341Arg) mutation by automated sequence analysis of cDNA

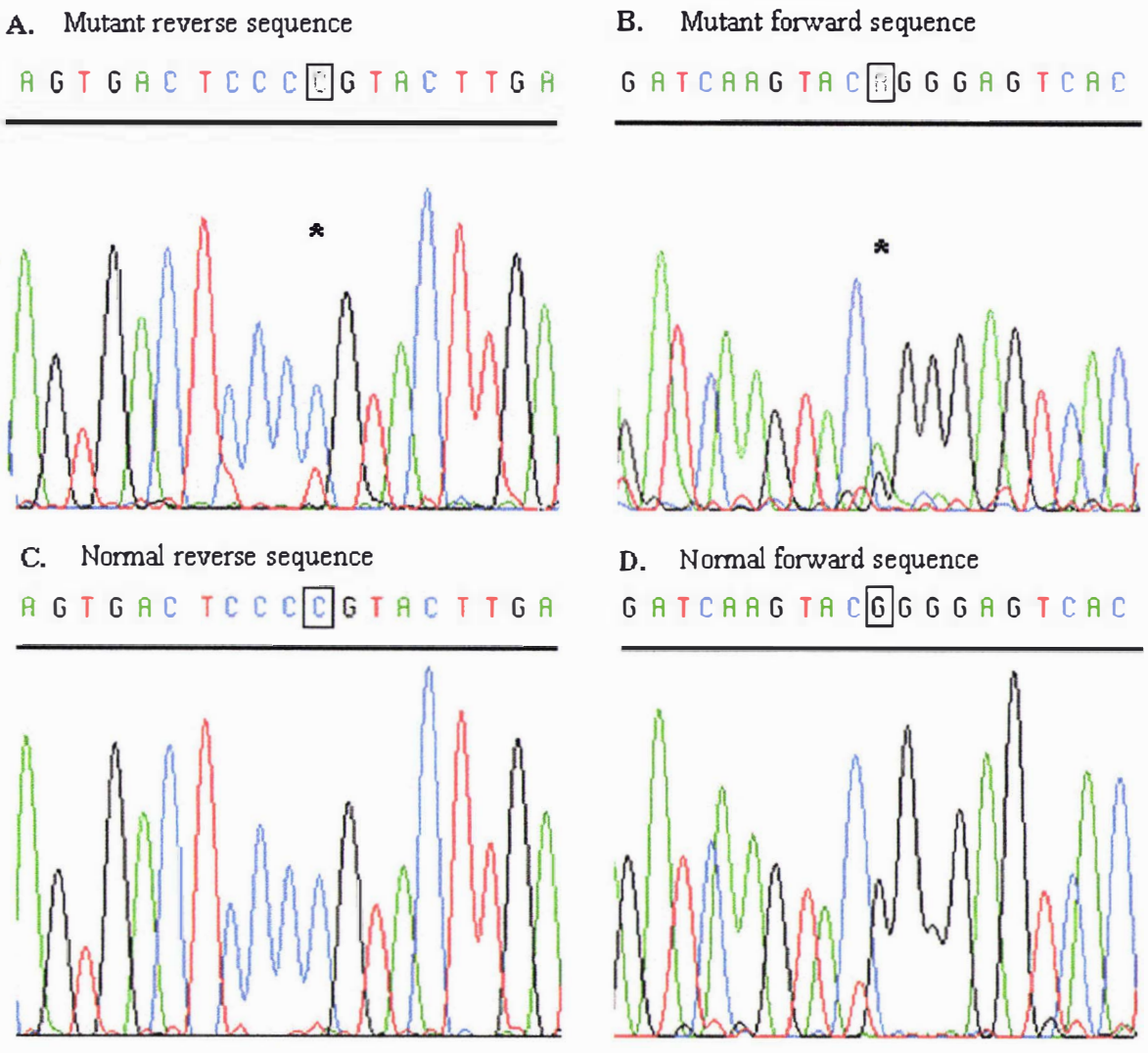

A. Sequence from 409/403R-bio PCR product amplified from cDNA from an MHS individual (445, family 24) indicating the C1021 to T mutation in the antisense sequence. Sequence was obtained using an ABI-377-18 automatic sequencer with dye-terminator chemistry and an internal reverse sequencing primer (1024).

B. Sequence from amplified control MHN cDNA (c154), representing the homozygous normal C1021 genotype. Sequence was generated, as above, using the reverse 1024 primer.

C. Sequence from the 409/403R-bio PCR product amplified from cDNA (c445) from MHS individual indicating the G1021A mutation in the coding sequence. Sequence initiated with forward 952 primer.

D. Sequence from the 409/403R-bio PCR product from MHN control cDNA, bearing the homozygous, normal G1021 genotype. Sequence initiated with the 341F primer.

Figure 5-15 Segregation of the Gly341Arg mutation with MH in Family 24

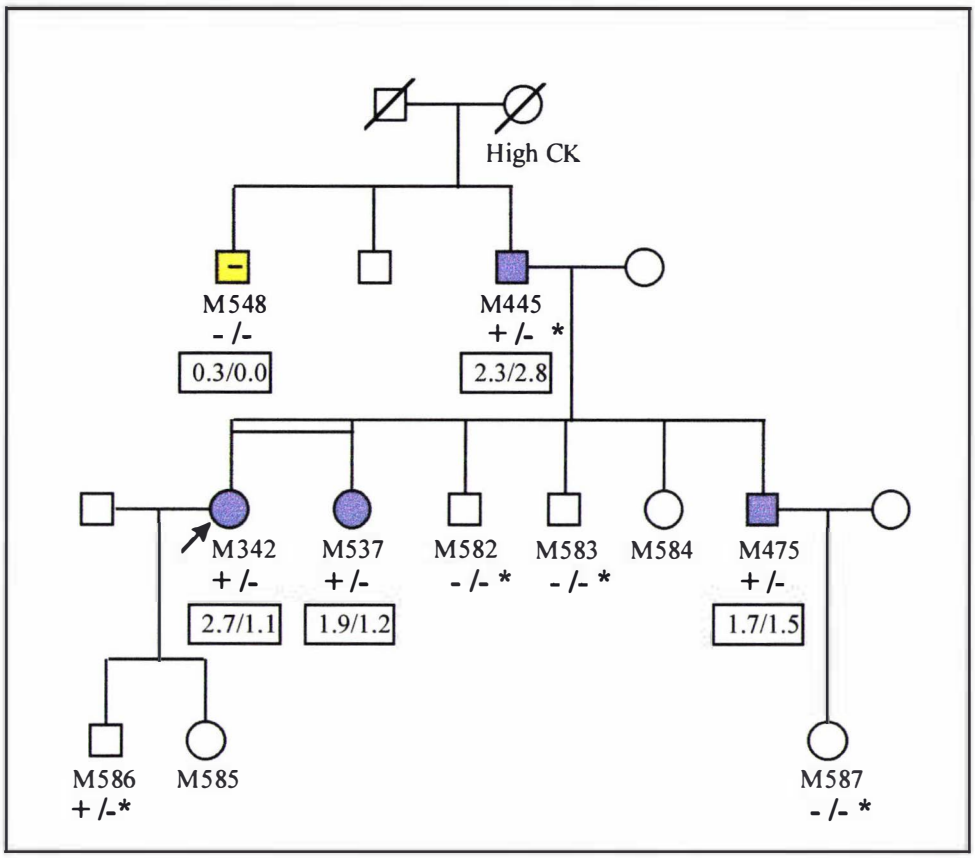

Pedigree structure for family 24. Siblings connected by double lines are identical twins. The G1021A (G341R) mutation (+/-) was detected in the genomic DNA of four individuals diagnosed MHS by IVCT (blue symbols). The MHS proband is indicated with an arrow (clinical case report presented in appendix 6.4. The mutation was absent (-/-) from the MHN individual (Yellow symbol). Boxed values refer to the IVCT contracture responses to 2 % halothane and 2 mM caffeine respectively. Genotype was determined by SSCP, and/or automatic DNA sequence analysis (*) of the 341F/341R-bio PCR product.

Evidence in favour of linkage between the Gly341Arg mutation and MH was investigated statistically using Linkage 5.1. Program parameters included a disease and allele frequency of 1/10000, a mutation rate of 1 X 10^{-6}, and penetrance of 0.99 and 0.01 for the mutant and normal alleles respectively. A maximum lod score of 0.88 (at $\theta = 0$) was calculated for the pedigree depicted in Figure 5-15. Linkage analysis was constrained by insufficient phenotype data for the family; thus, the analysis was inconclusive.

5.6 IDENTIFICATION OF NOVEL RYR1 MUTATIONS IN MHS PROBANDS BY SSCP ANALYSIS OF GENOMIC DNA

The automatic sequence analysis of RYR1 cDNA revealed three novel candidate MH mutations (Thr4826Ile, Arg2452Trp, and Arg401Cys) and one of the previously published mutations (Gly341Arg). In each case, the SSCP technique was employed to detect the mutation in short fragments amplified from genomic DNA in order to screen for the mutation in family members and normal control subjects. SSCP is more technically demanding and less reliable than other methods commonly employed to screen genomic DNA (such as allele specific PCR, ARMS or RFLP) but offers several advantages. SSCP with ethidium bromide detection is economical and therefore ideal for screening large number of samples simultaneously. Unlike RFLP, SSCP analysis can often reveal other mutations in the region of interest. This is particularly applicable to the study of MH in which mutations are tightly clustered in so-called 'hot-spot' regions. SSCP was employed to screen the remaining NZ MHS probands for three novel mutations (Arg401Cys, Thr4826Ile, and His4833Tyr) that were detected in the cDNA sequence analysis. Any novel SSCP variants identified in this screen were then characterised by automatic DNA sequence analysis.

5.6.1 Identification of a novel His4833Tyr mutation by SSCP analysis

A 208 bp fragment encompassing the site of the Thr4826Ile mutation was amplified from genomic DNA of MHS individuals from 32 NZ families and subjected to SSCP analysis. Thr4826Ile substitution was not detected in any of the individuals examined by SSCP including three of Maori descent. In the process of screening other families for the Thr4826Ile mutation, two additional SSCP variants were detected in unrelated MHS probands. One variant resulted from an T to A transition 28 bp downstream of the start of intron 100. This was detected in a single MHE individual of Polynesian descent (data not shown). The base-change was not detected in DNA from his MHS daughter and was therefore not likely to be a disease-causing mutation.

The second SSCP variant was characterised by the appearance of an additional single-stranded DNA species that migrated behind the band associated with the Thr4826Ile mutation, as shown in Figure 5-16. Sequence analysis of the 14462/100iR PCR product revealed a novel C14997T transition that substituted histidine 4833 for tyrosine (Figure 5-17). The Tyr4833His mutation is positioned only seven amino acid residues downstream of the Thr4826Ile mutation, as depicted in Figure 5-18.

Figure 5-16 SSCP detection of the His4833Tyr mutation.

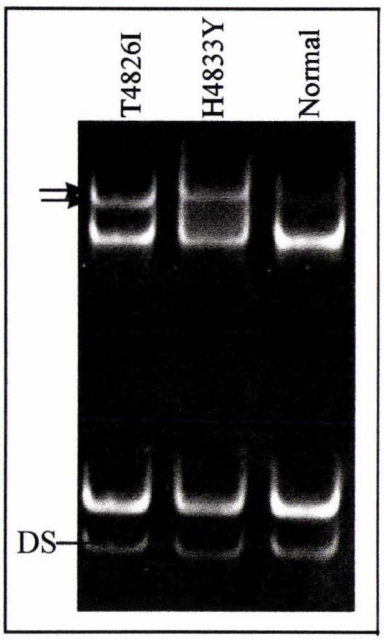

SSCP analysis of a 208 bp fragment amplified from genomic DNA of MHS probands with the 14462/100iR primer pair. Denatured PCR products were resolved by 8 % non-denaturing PAGE, in 0.5 X TBE, at 4°C for 3 hr 20 min. at 3W, constant power. DNA was visualised by staining in 0.5 μg/ml EtBr, and photographed under UV light.

Lane 1: SSCP pattern characteristic of the T4826I mutation (MHS individual M74, CH family). Lane 2: SSCP variant resulting from a C14497T transition that changes His 4833 to Tyr (MHS individual M470, family 1). Lane 3: Normal SSCP pattern from unrelated proband (MHS individual M169, family 94).

Figure 5-17 Characterisation of the Tyr4833His mutation

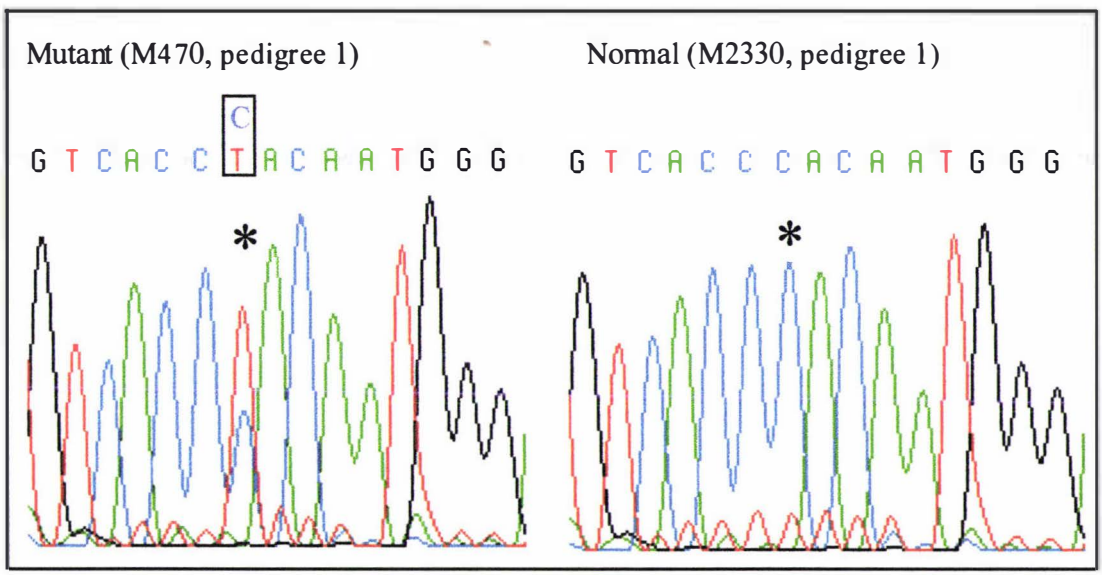

Nucleotide sequence of the 14462/100iR fragment amplified from genomic DNA, bearing the C14497T mutation detected in the family 1. Sequence was obtained an ABI-377-18 automatic sequencer with dye-terminator chemistry, using the 14462 primer. Antisense sequence is shown . The mutation changes the tyrosine 4833 to histidine.

Figure 5-18 Proximity of C-terminal RyR1 mutations detected in two MHS Maori families

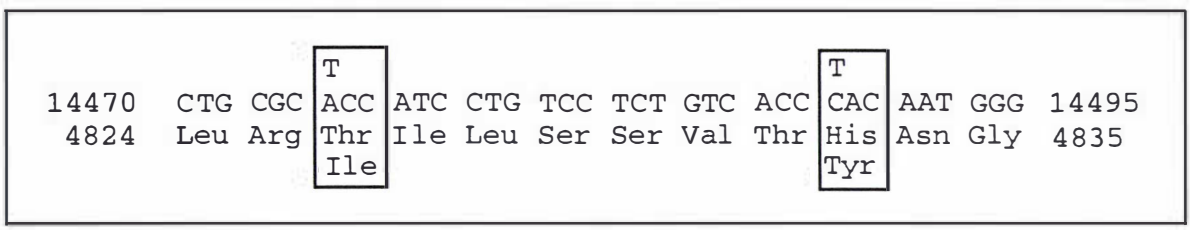

Figure 5-19 Segregation of the His4833Tyr mutation in Family 1

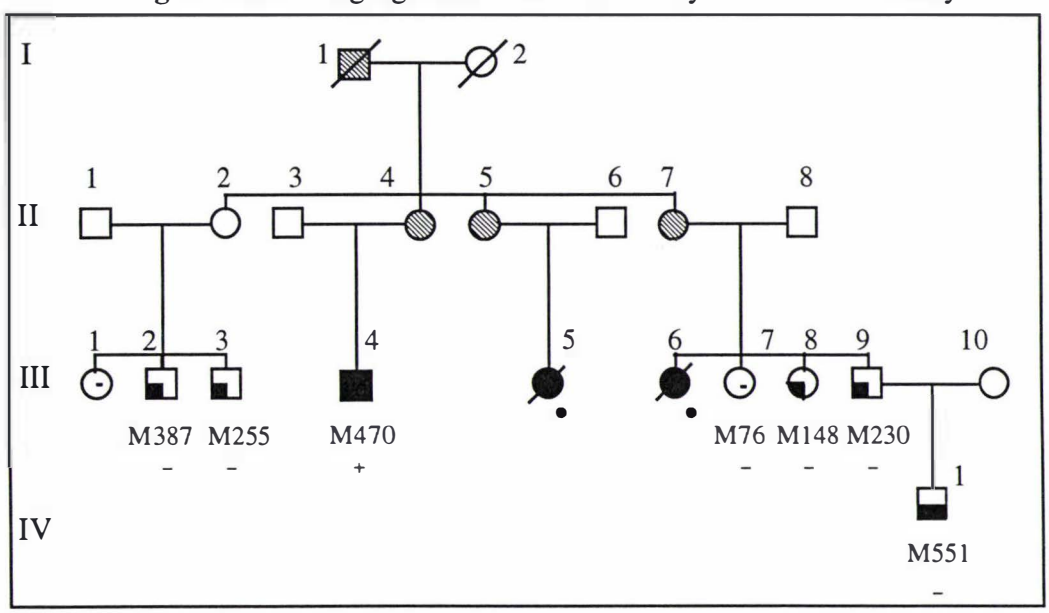

Individuals were diagnosed positive (+) or negative (-) for the His4833Tyr mutation by automatic DNA sequence analysis of a 208 bp fragment amplified from genomic DNA with the 144462/100iR primer set. The mutation was detected in a single MHS individual (M470, filled black symbol) who registered strong IVCT tensions. MHN individuals are represented by clear symbols with a negative sign. Individuals diagnosed MHE and MHS by EMHG criteria are represented with quarter and half-filled symbols, respectively. Diagonally shaded symbols depict obligate MHS carriers.

Seven individuals from the family were screened for the His4833Tyr mutation by SSCP and/or automatic DNA sequence analysis of amplified genomic DNA. Two fatal MH reactions have been documented in this pedigree (Figure 5-19, individuals II5 and II 6). Case reports are described for family 1 in appendix 6.2.

The His4833Tyr mutation was not present in one MHN (M76) or in four MHE(h) individuals (M387, M255, M148, and M230) investigated by SSCP. Individual M470 is the only family member identified with the His4833Tyr mutation, and is also the only family member examined by IVCT who registered a strong contracture response to caffeine (with tensions of 3.8 g at 2 mM

caf. and 3.2 g at 2 % hal.). However, the His4833Tyr mutation does not segregate completely with the MHS phenotype in family 1 (Figure 5-19). One MHS patient with relatively weak MHS contracture responses (M551; 0.2 g at 2 mM caf, 1.1 g at 2 % hal) also displayed the SSCP profile characteristic of the normal genotype (subsequently confirmed by DNA sequence analysis).

The His4833Tyr mutation was not observed in 220 normal chromosomes screened by SSCP, indicating it is not a common polymorphism. Jointly with residue threonine 4826, histidine 4833 is strictly conserved across all published RYR1, RYR2, and RYR3 implying functional significance of these residues (discussed in Chapter 6, Figure 6.9). However, due to the small size of the pedigree, it is possible that His4833Tyr represents a rare polymorphism that is not related to MHS. IVCT examination and genetic testing of additional family members is required before the causative role of this mutation in MH can be investigated further.

5.6.2 Identification of a novel Arg2454His mutation by SSCP analysis

The Arg2452Trp mutation was detected in a single MHS family. While screening NZ probands for this mutation, a SSCP variant was identified in an MHS proband (M119) from family 58 (Figure 5-20C). The SSCP pattern generated for this individual was distinct from the SSCP pattern characteristic of the Arg2452Trp genotype. Sequence analysis of the amplified genomic DNA revealed the presence of a G7361A transition that substitutes Arg2454 for His (Figure 5-20B). This second mutation was identified in a young male who developed a fulminant MH reaction during an emergency orthopedic procedure, and was diagnosed MHS with strong positive IVCT responses (the case report is documented for family 58 in appendix 6.7). The Arg2454His substitution was positioned only two amino acids downstream of the Arg2452Trp mutation identified in family 1 and only four residues upstream of published mutations at residue Arg2458 as depicted in Figure 5-20D.

Two family members were investigated for the Arg2454His mutation by automatic DNA sequence analysis. Both the mother and sister of the proband tested negative with respect to the mutation, but neither has been examined by IVCT. The expected paternal inheritance of MHS has not been confirmed, as the father of the proband has not been examined by IVCT. A DNA sample from this individual was not available to test for the Arg2454Trp mutation.

As there is no family history of MH in family 58, and only one family member was examined by IVCT, it was not possible to investigate the relationship between the Arg2454His mutation and MHS in this family. Therefore, it is possible that the mutation represents a polymorphism that is not causative of MH. However, the Arg2454His mutation was not detected in 100 chromosomes representative of the normal population, or in any of the 30 other MHS probands investigated by SSCP thus it is highly unlikely to be a common, coincidental polymorphism.

Figure 5-20 Identification of the Arg2454His and Arg2452Trp mutations by SSCP and sequence analysis of genomic DNA

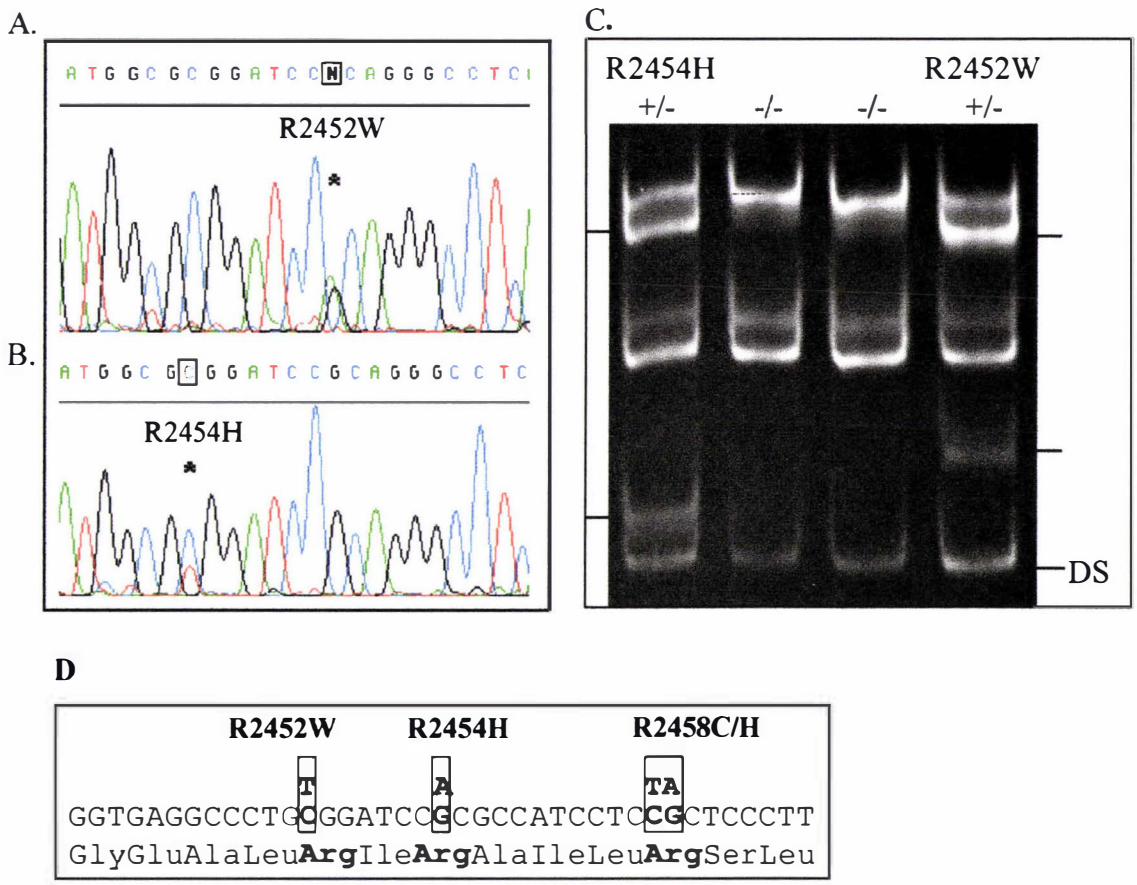

A. Identification of a novel RYR1 C7354T transition resulting in an Arg2452Trp mutation. The mutation was detected in cDNA from individual M535 (family 36) who suffered an MH crisis in infancy. The region was amplified with the 6376/47exR primer pair and sequenced with using an ABI-377-18 automatic sequencer, using the 47exR primer, with dye-terminator chemistry. Antisense sequence is shown.

B. Identification of a G7361A transition that changes Arg2454 to histidine. The region was amplified from genomic DNA from MHS individual M119 (family 58) with the 45iF/7393 primer pair and sequenced (as above) using the 47exR primer. Antisense sequence is shown .

C. SSCP detection of the Arg2454His (lane 1, individual M119, family 58) and Arg2452Trp (lane 4, individual M535, family 36) mutations. Lanes 2 and 3 represent the normal genotype in two unrelated MHS probands. PCR products were amplified from genomic DNA with the 45iF/7393 primer pair. Denatured PCR products were resolved by 8 % non-denaturing PAGE, in 0.5X TBE, Electrophoresis was conducted at 3W (constant power), ~325V, for 3 hr and 5 min. at 4°C. The gel was stained with 0.5 μg/ml EtBr, and photographed under UV light. Mutation-specific bands are indicated with arrows. DS = double stranded DNA.

D. The two novel arginine substitutions (Arg2452Trp and Arg2454His) occur in close proximity to two previously described MH mutations at the Arginine 2458 residue. (Arg2458His and Arg2458Cys [169]).

5.7 OVERVIEW OF RYR1 MUTATION ANALYSIS

In view of the genetic heterogeneity of MH and the relatively low incidence of each RYR1 mutation, a screen for individual reported mutations in new MHS probands by RFLP and sequence analysis of genomic DNA (chapter 3) is no longer cost-effective. Unless a commercially feasible system for multiplex PCR and simultaneous automated analysis of all RYR1 mutations is developed for the analysis of MH mutations, the screening of genomic DNA for individual mutations is not likely to be applied in future.

The sequence analysis of RYR1 cDNA proved an efficient alternate method to screen probands for reported RYR1 mutations and also enabled the detection of any novel mutations. Mutations were identified in each of the four probands examined in this way. Three were novel (Thr4826Ile, Arg401Cys, Arg2452Trp) while the fourth (Gly341Arg) has been associated with many MH families in overseas studies [109]. The sequence analysis of cDNA also pinpointed particular regions likely to contain mutations in other probands. For example, two novel mutations; Arg2454His and His4833Tyr were unveiled when regions containing the Arg2452Trp and Thr4826Ile mutations were amplified from genomic DNA of other MHS probands and subjected to SSCP analysis.

The N-terminal and C-terminal mutation–rich regions were sequenced in both directions from two MHS individuals as the most probable sites for a causative mutation in the CH family. The Thr4826Ile mutation eventually identified was found well outside these recognized mutation regions. However, a thorough initial analysis of mutation-rich regions as the most probable sites for a mutation should still be viewed as a valid approach to the analysis of this large gene. This was reinforced by the identification of three novel mutations (Arg401Cys, Arg2452Trp, and Arg2454His) in the mutation-rich RYR1 regions of other NZ families. Moreover, the detection of the Thr4826Ile, the His4833Tyr and the recently published Ile4898Thr mutation [164] has now established the RYR1 sequecne encoding the C-terminal channel domain of RyR1 as a third mutation "hot-spot" region for analysis in MH. Accordingly, sequence encoding the C-terminal domain should be included in addition to the N-terminal and central hot-spot regions in the analysis of MHS probands in future.

5.7.1 Quality of the cDNA

Total RNA was used as a template for the synthesis of cDNA rather than purified mRNA. This approach was chosen since relatively low yields of RNA were obtained from human skeletal muscle [307] and additional steps required to isolate mRNA are costly and can result in a further reduction in the overall yields. Both oligo-dT primed and RH-primed cDNA preparations were subsequently used to generate PCR products for sequencing. Oligo-dT primed cDNA is generally a more specific substrate for PCR compared to that synthesised with random hexamers [309,311]. However, the synthesis of full-length RYR1 cDNA transcripts with oligo-dT is reportedly obstructed by a 75% GC-rich sequence in the 12600- 13400 bp region [126], (T. McCarthy, personal communication). Furthermore, an adenine-rich region between residues 8501 and 8512 is thought to serve as a secondary priming site that may stop transcription from the 3' end [126]. It was therefore anticipated that amplification of products in the 8000-13000 nucleotide region would be difficult using oligo-dT primed cDNA as the substrate. However, the successful amplification of the 8068 - 8640 region from the oligo-dT primed cDNA indicated that RYR1 cDNA transcripts of at least 7.5 kb in length had been synthesised. Premature termination of oligo-dT cDNA synthesis at either the GC-rich region or the proposed secondary priming site [126] therefore did not appear to compromise RT-PCR using Superscript™ RT .

This contrasts with results obtained by groups using the Promega reverse transcriptase system, which employs an avian myeloblastosis virus RT (T. McCarthy, personal communication). In contrast, the Superscipt™ enzyme is a relatively heat stable, modified Moloney Murine leukemia virus RT suited to the synthesis of long templates [410].

In early cDNA cloning experiments, the human RYR1 transcription start point was positioned 105 bp upstream of the initiation methionine codon [126]. More recently, the transcription start-point has been assigned to -130 bp [160] by comparison with the rabbit transcription start-point (which was positioned by primer extension analysis [155]). In order to amplify and sequence the 5' RYR1 terminus, the forward 1.17F primer was designed to anneal 114 bp upstream of the initiator codon. The successful amplification of cDNA using the 1.17F primer supports the assignment of the human RYR1 start point to -130 bp [160].

The quality of the sequence obtained by automatic sequencing was a function of the specificity of the PCR and the purity of the template DNA [409]. Sequence derived from impure PCR products was ambiguous even when primed with internal oligonucleotides. Various methods were therefore employed to optimize PCR reactions in order to generate pure PCR products for sequencing, as outlined in Chapter 2

5.7.2 Strategies employed to improve PCR specificity

A hot-start procedure was used in all PCR reactions to reduce the amplification primer-dimers and contaminating products generated from non-specific priming during the reaction preparation at ambient temperatures. Optimal results were achieved using hot-start PCR with 0.05 µl of the random hexamer-primed cDNA template per 50 µl PCR reaction which was much less than the 2 µl volume recommended in the Superscript manufacturers' instructions. However, the addition of excess cDNA template was found to produce smeared bands, reduce PCR specificity and inhibit some reactions.

"Touchdown" PCR programs involving successive cycles with gradually decreasing annealing temperatures proved the most efficient procedure for optimizing PCR reactions. When standard attempts at PCR optimisation failed to generate discrete bands, the fragment of interest was isolated away from contaminating PCR products and primers by gel-purification from agarose gel slices. UV light can introduce nicks in the PCR template, introducing stops and noise in the sequencing reaction [409,411]. Gel purification was therefore employed only where other optimisation methods had failed since the sequence derived from gel-purified fragments was generally of reduced quality, and signal strength tended to fade rapidly.

The nested-primer secondary PCR approach to obtaining discrete products from non-specific PCR reactions was avoided. Secondary amplification of too-few copies of the target sequence can result in allele bias and a risk of false negative result [311]. Alternatively, false-positive signals could result from amplification of PCR-errors introduced in the first round of PCR. Furthermore, the second PCR reaction is particularly sensitive to contamination from other templates generated in the first round of amplification [414]. Re-amplification of gel-purified PCR products using nested primers [411] was also avoided due to the risk of amplification of a UV-induced mutation [304]. A single PCR product purified by this approach was found to contain a PCR-induced mutation that appeared to substitute Val2715 for Ala.

5.7.3 Identification of PCR contamination by polymorphism analysis

The possibility of contamination of PCR reactions with the products of previous reactions is a common problem in all PCR procedures, particularly those in forensic applications that involve low-copy number DNA templates [311,411]. Minute quantities of PCR product can act as extremely efficient templates and rapidly out-compete the amplification of the genomic DNA or cDNA substrate. Once established, such contamination can be difficult to eradicate, particularly if primers or template DNA solutions are affected. Contamination of this nature could result in identical sequence profiles for both the MHS and control sequences and failure to detect a mutation. However, evidence that PCR cross-contamination had occurred in the amplification of at least one product was revealed by inconsistencies in the sequence profiles for obtained for known polymorphisms.

A segment encompassing amino acid residues 2462 to 2868 including eight published known silent RYR1 polymorphisms [107,168] was amplified with the 7361/8752 primer pair to search for a novel mutation. Sequence analysis of this region revealed that the cDNA from the MHS and MHE individuals displayed identical genotypes for several polymorphisms. This conflicted with earlier results from RFLP and sequence analysis of the Asp2729 and Ile2406 polymorphisms. The reverse, 8752R PCR primer sequence encompassed the site of the Ser2862 polymorphism. The possibility that this may have lead to inefficient priming and allele bias in the amplification of the MHS c221 sample was excluded by further sequence analysis of the 7361/8572 product. This revealed heterozygosity at the Arg2623 and Arg2620 polymorphisms for both MHS and MHE individuals, indicating both alleles were equally represented in the PCR products.

These inconsistencies were therefore suggestive of contamination of the PCR reaction from the MHS individual with DNA derived from the control, MHE individual. However, the negative PCR controls, containing water in place of DNA, had not yielded visible products. This pointed to contamination of the MHS cDNA template with PCR product or cDNA from the MHE individual. Contamination of this nature would not be detected in the negative PCR control. The diluted cDNA solutions used in these reactions were subsequently discarded.

The identity of MHS cDNA samples was investigated by PCR-amplification of concentrated cDNA samples followed by RFLP or sequence analysis of established polymorphisms [107]. Genotype profiles for the Ile1151, Ser2862, Asp2729 and Leu197 polymorphisms were compared with those established earlier by RFLP genotyping or sequence analysis of corresponding genomic DNA samples. All genotypes were consistent with those previously defined for the MHS individual (c221) and were distinct from those established for the control individual (c154) (data not shown). This confirmed the cDNA used in the PCR was derived from the MHS individual (c221), as expected. The PCR cross-contamination may therefore been isolated to only one dilute solution of the cDNA and a single PCR product. However to be confident that a mutation in the hot-spot regions had not been obscured by sample cross-contamination, the N-terminal and central RYR1 regions from 410-4600 bp and 6380-8640 were re-amplified from the MHS cDNA (c221) and sequenced again in both directions. Alternate amplification strategies employing different primer combinations were used to amplify these regions, such that previously amplified products could not act as templates in the event of further PCR cross-contamination. Genotypes for the published polymorphisms were compared with results of the RFLP analysis of genomic DNA to confirm the identity of the amplified cDNA. The remainder of the RYR1 sequence was amplified from the new cDNA preparation, using barrier tips in all PCR procedures.

5.7.4 Amplification of a GC-rich region

DNA Polymerases do not work efficiently on target sequences that have over 65% GC content. The amplification of such regions can be assisted with the addition of denaturants to the reaction [411]. A region of the RYR1 sequence spanning residues 12890 - 13360 with 75%-81% GC content is difficult to amplify from cDNA. The formation of secondary structure in the mRNA template is thought to inhibit cDNA synthesis in this region [126]. This segment is consequently often omitted in the screening of RYR1 cDNA for MH mutations (Mark Davies, Dr. Patrick Lynch, personal communication). Other investigators had amplified this difficult region in short segments from genomic DNA, using co-solvents to aid denaturation [13].

The successful amplification of areas downstream of the GC-rich sequence from oligo-dT primed cDNA indicated that reverse transcription through the GC-rich RYR1 region was accomplished using the Superscript™ RT system. This prompted attempts to amplify the region from cDNA. A number of variables (including the addition of DMSO and glycerol co-solvents) were modified in attempts to improve the stringency of the reaction. DMSO destabilizes or decreases the Tm of the duplex and can increase the PCR specificity [415-417]. DMSO also destabilizes the *Taq* polymerase enzyme, thus concentrations of more than 10% were not used. Glycerol serves as a cosolvent in addition to helping to stabilise the enzyme and improve product yields [417]. After trial and error, a 802 bp PCR fragment with 76.2% GC content was successfully amplified from oligo-dT primed cDNA with the 12575/13356 primer set by including 7% glycerol and 8% DMSO in the PCR reaction.

5.7.5 Sequence quality and heterozygote detection

The value of automatic sequence analysis to detect mutations was demonstrated in this study by the identification of a number of novel candidate mutations and sequence polymorphisms. Mutations and sequence discrepancies were identified by aligning the sequence from the MHS individual with that from the MHE individual and the published RYR1 sequence [126]. In some cases, polymorphisms appeared as two overlapping peaks of equal height. These were readily detected as "N" signals. However, automatic sequence analysis with dye-terminator chemistry produces data with variable peak intensity and some mutations were not detected by sequence alignment alone. This necessitated visual comparison of the MHS sequence with the control sequence. Although the signal intensity varied for different nucleotides, the electropherogram patterns were found to be reproducible for a given template provided the same dye chemistry was used. Polymorphisms were thus revealed by the occurrence of overlapping signals in conjunction with a reduction in the relative peak intensity of the mutated nucleotide compared to the control sequence.

A sequencing artifact, termed "bleedthrough", which resulted in the appearance of T sub-peaks under principal C signals complicated the interpretation of sequence data. The majority of point mutations in human disease involve C to T transitions resulting either from the deamination of cytidine to uridine or of deamination of 5-methylcytidine to thymidine [418,419]. Therefore, the "bleedthrough" sequence artifact significantly hampered the differentiation of candidate mutations from sequence noise. Decreasing both the concentration of DNA in the sequencing reactions and the volume of reaction applied to the sequencing gel reduced the problem. True polymorphisms were distinguished from sequence artifacts by careful scrutiny of the corresponding sequence from the control sample, and by sequencing the region of interest in the opposite direction.

Sequence read lengths of up to 700 bp were obtained, however in most cases, sequence beyond the 400 bp region was deemed unreliable for heterozygote detection due to loss of signal resolution. The length of unambiguous sequence was generally shorter for gel-purified fragments. The distance between the position of the sequencing primer and the start of the readable sequence varied from 4 to 60 bp. This was a function of the recovery of smaller DNA species after purification of the sequencing reactions. The Thr4826Ile mutation was not detected in the initial sequence obtained which was initiated at an unusually long distance (52 bp) from the primer. It was unfortunate that the mutation happened to be positioned in one of only three such gaps in the sequence remaining after the sequence analysis of the entire 15.3 kb coding sequence, and well outside the mutation-rich regions that were sequenced repeatedly in both directions.

5.7.6 SSCP analysis of mutation regions

SSCP with non-radioactive detection proved an economical method to simultaneously screen genomic DNA samples of MHS probands for any new mutations. The use of this technique required a positive control and adherence to an empirically defined set of conditions to ensure sensitivity. SSCP is thus not a reliable method to screen of RYR1 mutations for which positive DNA samples are not available. Nevertheless, SSCP variants were identified, which when characterised by automatic DNA sequence analysis corresponded to novel candidate MH mutations.

The major drawback to SSCP is that the band patterns can differ significantly from one gel to another, and differences between the positive and normal samples may not always be observed. The analysis of the Arg2452Trp mutation was extremely robust a significant band shift was consistently associated with the presence of the mutation. In contrast, SSCP analysis of the Gly341Arg mutation depicted in (Figure 5-13) was not reproducible. Similarly, the SSCP analysis of the Thr4826Ile mutation in the 185 bp 14486/100iR product (Figure 5-8) was particularly susceptible to alterations in the buffer composition or gel running conditions. For example, an alteration in the SSCP patterns that obscured their interpretation was consistently associated with the substitution of Boehringer Manheim *Taq* polymerase for the Promega enzyme. A 0.7 difference in pH and the addition of 1 %Triton 100 detergent in the Promega PCR buffer were the only significant differences between the composition of the two buffers. Detergents are known to effect the mobility of single-stranded DNA under non-denaturing conditions [324] and could therefore have a marked influence on the SSCP patterns. PCR reactions for SSCP were thus prepared using cocktail reaction mixes to ensure uniformity of the buffer components and $MgCl_2$ concentration.

SSCP was used to screen "normal" individuals and relatives of probands identified with novel mutations. None of the novel candidate mutations were identified in the normal population, indicating they were not common polymorphisms. However, in most cases the families were too small to demonstrate a causative relationship between the mutation and MHS. In contrast, over 200 members of the CH family were screened for the Thr4826Ile mutation, providing data for a thorough study of phenotype/genotype relationships in the CH family. Various statistical methods are employed to investigate the association between the mutation and the IVCT responses, as described in Chapter 6.

6. GENOTYPE / PHENOTYPE RELATIONSHIPS FOR RYR1 MUTATIONS

In the following chapter, genotype/phenotype relationships are investigated for the RYR1 mutations identified in NZ families. The IVCT data sets for most families involved were too small to explore these relationships by genetic linkage analysis and other statistical methods. In contrast, the CH family is one of the largest characterized MH families in the world in terms of the number of patients examined by both the IVCT and genetic screening. The identification of the novel Thr4826Ile mutation in the CH family provided a unique opportunity to investigate a causative role for this mutation, to explore the performance of the IVCT and to test assumptions about the frequency of MHS in the population.

6.1 INVESTIGATING LINKAGE BETWEEN MHS AND T4826I

The Thr4826Ile polymorphism was a strong candidate for the causative MHS defect in the CH family, since it occurred in phase with the MHS-linked chromosome 19q haplotype and was not found in the normal population. The relationship between inheritance of Thr4826Ile and manifestation of the MHS phenotype was explored further by following the segregation of the mutation in key members of the large Maori pedigree. This screen focused initially on 130 IVCT-tested individuals and obligate MHS carriers.

A total of 212 members of the extended seven-generation Maori pedigree were sampled and typed for the C14477T (Thr4826Ile) mutation by SSCP analysis (as described in Chapter 5, section 5.4.6). A blind interpretation of the SSCP band patterns was performed without reference to the MHS status. The Thr4826Ile genotypes; mutated (+) or normal (-) were then aligned with the corresponding clinical diagnoses; MHS or MHE/MHN respectively via the DNA identification numbers. Any discrepancies were verified (or in one case, resolved) by repeating the PCR and SSCP analysis.

The first striking finding was that there was complete concordance between the inheritance of Thr4826Ile and the clinical MH episodes in the family. The mutation was detected in the DNA of five patients who have survived clinical MH crises, including one individual who suffered two MH crises. Immediate relatives of five patients who suffered fatal MH reactions tested positive for Thr4826Ile, as did all obligate carriers of the disease in four major branches of the pedigree. Details of documented MH episodes in the CH family and relevant DNA results are included with clinical case reports in appendix 6.1

Patients who had undergone the muscle biopsy test were categorised MHS, MHE(h), MHE(c) or MHN based on the standard EMHG thresholds of ≥ 0.2 g tension at 2 % halothane and 2 mM caffeine. The relationship between Thr4826Ile genotype and the IVCT phenotype amongst tested members of the CH family is summarised in Table 6-1. Of the 130 members diagnosed by IVCT in the extended pedigree, 94 were negative for the mutation and 36 were positive. All 36 mutation-positive subjects were diagnosed MHS by IVCT, consistent with a direct involvement of the mutation in the MHS phenotype. Of the 94 mutation-negative individuals, 27 were MHN, 43 were MHE(h), two were MHE(c) and 22 were MHS. The segregation of the mutation with MHS

was therefore incomplete. Of the 58 subjects diagnosed MHS by the standard EMHG parameters, only 36 (62 %) carried the mutant allele.

Discrepancies between phenotype and genotype were anticipated from the earlier analysis of RYR1-linked chromosome 19q markers (Chapter 4) in which several MHS individuals were found to lack the high-risk 6-1-4-1-3 haplotype. Results of the screen for Thr4826Ile were found to be entirely consistent with the segregation of the high-risk 6-1-4-1-3 haplotype. Therefore, the discordant MHS(-) individuals who lacked both the Thr4826Ile mutation and the associated 6-1-4-1-3 haplotype could not be readily accounted for by genotyping error or genetic recombination between the RYR1 mutation and flanking markers.

Table 6-1 Phenotypes for CH family members with (+) and without (-) the Thr4826Ile mutation

Genotype	MHS	MHE(h), (c)	MHN	Total
Positive (+)	36	0, 0	**0**	36
Negative (-)	**22**	43, 2	27	94
total	58	45	27	130

Patients registering abnormal (≥ 0.2 g) contracture responses to halothane only, or caffeine only are classified MHE(h) and MHE(c) respectively EMHG diagnostic thresholds applied. Numbers in bold highlight recombinant MHS(-) and MHN(+) categories.

6.1.1 Linkage analysis: methodology

To gauge statistical support for an association between the mutation and MHS, genetic linkage analysis was performed on the combined, complex pedigree, presented in appendix 9.
The pedigree file for linkage analysis included a total of 324 individuals who are linked over eight generations to a founding marriage. The complex CH pedigree includes five consanguinity and marriage loops (Appendix 9) individuals IDs: 13-4, 33-34, 56-57, 126-120 and 18-20). Each loop in a pedigree file exponentially increases the computer processing requirements for linkage analysis hence the linkage program permits a maximum of only three loops. To accommodate these constraints, one individual from each consanguinity loop was duplicated. The first was a simple marriage loop, which was broken by duplicating one unrelated individual (ID 4). As this person is not a disease carrier, this marriage loop has no bearing on the pattern of inheritance of the disease allele in the family. A second loop involving individuals 57 and 56 was broken by the duplication of individual 57. This is a consanguineous partnership between two distant MHN cousins who were both negative for the Thr4826Ile mutation. Three consanguineous loops each involving at least one possible carrier of the disease allele remained (33-34, 126-120 and 18-20).

The parameters for linkage analysis were set in accordance with agreed EMHG values as discussed in Chapter 4 (section 4.5.3). The MHS gene and Thr4816Ile gene frequencies were fixed at 0.0001. Two liability classes were used to define the penetrance of the MHS gene. In the first case a penetrance of 1.0 and a zero phenocopy rate was assumed for patients with a documented, fulminant MH crisis. In all other cases, the penetrance of the MHS gene was defined as 0.99 for MHS individuals, and phenocopy rate of 0.01 was assumed for homozygous normal individuals. An unknown status was assumed for MHE individuals. The mutation rate was taken

to be 0.00001. Pairwise lod scores for were calculated using MLINK and Z_{max} and θ_{max} values were estimated with ILINK [333].

6.1.2 Linkage results: MHS vs. Thr4826Ile.

Pairwise lod scores for linkage between MHS and the Thr4826Ile mutation are given in Table 6-2. Absolute linkage to the Thr4826Ile RYR1 mutation is not supported (Z= -1.714 at $\theta = 0$) under the standard diagnostic parameters that predicate 22 recombinant MHS individuals. However, a maximum lod score of Zmax = 11.103 at $\theta = 0.133$ was generated in favour of linkage between Thr4826Ile and MHS. This clearly shows that the mutation is linked to MHS in the extended pedigree, however the 22 MHS recombinants suggest that the RYR1 mutation is not causative of MHS. This result could also be explained by phenotyping errors, which can lead to an overestimation of the recombination fraction [378] and a loss of power of the linkage test [353]. The 3.5 - 11 % false positive rate of the IVCT [97] is therefore a significant impediment to linkage analysis.

Table 6-2 Two-point lod scores for linkage of the Thr4826Ile mutation to the MHS phenotype as defined under standard EMHG thresholds

IVCT MHS threshold		*MHS vs. Thr4826Ile*								
		Z at recombination fraction (θ) =								
Hal.	*Caf.*	θ_{MAX}	Z_{MAX}	0.00	0.01	0.05	0.10	0.20	0.30	0.40
≥ 0.2 g	≥ 0.2 g	0.133	11.10	-1.714	4.103	9.292	10.89	10.52	8.164	4.599

6.2 THE RELATIONSHIP BETWEEN IVCT THRESHOLDS AND EVIDENCE FOR LINKAGE

In chapter four, evidence for linkage to chromosome 19q markers in individual branches of the family was unveiled by the application of more stringent diagnostic thresholds. In these studies, the evidence for linkage increased with incremental increases in the thresholds together with the reclassification of recombinant borderline MHS individuals as MHE or MHN. This result suggested that false positive diagnosis was the probable explanation for the majority of MHS(-) individuals. Due to the computational demands associated with the analysis of complex, inbred pedigrees, it was not feasible to conduct the linkage analysis under a wide range of diagnostic parameters for the entire pedigree. An alternate approach was adopted in which IVCT data was scrutinized to determine the numbers of MHS and MHN recombinant individuals that would be assigned under increasingly stringent diagnostic schemes. Thresholds for the 2 % halothane test ranging systematically from 0.2 g to 1.8 g in 0.2 g increments were applied in combination with 2 mM caffeine thresholds ranging from 0.2 g to 1.2 g in 0.2 g increments. Individuals for whom the threshold values were attained in both the caffeine and halothane tests were recorded as MHS, while all others were classified MHN. Thus, there was no MHE category in this analysis.

Results are presented in Table 6-3. Note that the term "MHS recombinants" refers to individuals who have the normal genotype but are classified MHS while "MHN recombinants" correspond to mutation-positive individuals who are diagnosed MHN according to the arbitrary thresholds. These terms are broadly applied to refer to discrepancies between genotype and MHS phenotype

and do not necessarily signify meiotic recombination between the mutation and the disease locus *per se*.

The concordance between the Thr4826Ile mutation and the MHS phenotype increased with systematic increases in the applied diagnostic thresholds, as indicated by a concomitant reduction in the number of MHS(-) recombinants. Interestingly, no MHN(+) recombinants appeared until the threshold tension at 2 mM caffeine was raised above 1.2 g, at which point, three individuals who were positive for the mutation were re-classified MHN. Cut-off points of 1.2 g (at 2 mM caf.) and 1.8 g (at 2% hal.) completely distinguished the positive and negative genotype groups. Under this arbitrary diagnostic scheme, 35 individuals who were positive for the Thr4826Ile mutation were classified MHS whilst all 94 individuals with the normal genotype were classified MHN. Clearly, the MHS phenotype of mutation-positive individuals can be distinguished from the moderate phenotype of those individuals who are MHS under EMHG thresholds with normal genotype for the Thr4826Ile mutation. This result is therefore compatible with the assumption of false positive diagnosis in recombinant MHS(-) individuals.

Table 6-3 Effect of the diagnostic thresholds on the concordance between MHS and the Thr4826Ile mutation

Diagnostic criteria ≥ tension shown at 2mMcaf / 2%hal	No. of MHN[1]	No. of MHN recombinant [2]	No. of MHS[1]	No. of MHS recombinant [2]	Sensitivity [3]	Specificity [3]
MHS 0.0/0.2	30	0	100	64	100.0	31.9
MHS 0.2/0.0	70	0	60	24	100.0	74.5
MHS 0.2/0.2	72	0	58	22	100.0	76.6
MHS 0.4/0.4:	84	0	46	10	100.0	89.4
MHS 0.4/0.8:	85	0	45	9	100.0	90.4
MHS 0.6/0.6:	85	0	45	9	100.0	90.4
MHS 0.8/0.8:	89	0	41	5	100.0	94.7
MHS 1.0/1.0:	91	0	39	3	100.0	96.8
MHS 1.2/1.2:	93	0	36	1	100.0	98.9
MHS 1.4/1.4:	97	3	32	0	91.4	100.0
MHS 1.2/1.8:	94	0	35	0	100.0	100.0

MHS diagnosed if tensions ≥ the thresholds shown were generated at both 2 mM caffeine and 2% halothane. Subjects for whom the threshold tension is reached for only one or neither of the tests were classified as MHN.

MHN recombinants correspond to the number of MHN individuals who are positive for the Thr4826Ile mutation. MHS recombinants correspond to the number of MHS individuals who are negative for the mutation.

Specificity was calculated as the proportion of MHN diagnoses in patients without the Thr4826Ile mutation (n = 94). Sensitivity was calculated as the proportion of MHS diagnoses in patients with the Thr4826Ile mutation (n = 36).

To assess the relationship between the diagnostic thresholds and evidence for linkage, genetic linkage was calculated under the raised thresholds of 0.4 g at 2 mM caffeine and 0.8 g 2 % halothane (as applied by Healy et al., 1996). Results were compared to those obtained under the conventional thresholds in Table 6-4. A lod score of 21.74 at $\theta = 0$ was generated using the more stringent criteria that reduced the number of recombinant MH individuals from 22 to 9. A maximum lod score of $Z_{max} = 23.725$ was obtained at $\theta = 0.024$. This result provides overwhelming support for linkage between MHS and the Thr4826Ile mutation detected in the CH family

Table 6-4 Linkage of the Thr4826Ile mutation to MHS under conventional and stringent diagnostic criteria.

IVCT MHS threshold		*MHS vs. Thr4826Ile*								
		Z at recombination fraction (θ) =								
Hal.	*Caf.*	θ_{MAX}	Z_{MAX}	0.00	0.01	0.05	0.10	0.20	0.30	0.40
≥ 0.2 g	≥ 0.2 g	0.133	11.10	-1.714	4.103	9.292	10.89	10.52	8.164	4.599
≥ 0.8 g	≥ 0.4 g	0.024	23.73	21.74	23.52	23.43	22.06	18.03	12.96	6.97

6.2.1 The sensitivity and specificity of the IVCT

Sensitivity and specificity refer to the ability of a diagnostic test to discriminate between healthy individuals and patients at risk of life threatening reactions to anaesthesia. The sensitivity measures the proportion of truly susceptible individuals who are correctly identified as MHS in the test while the specificity measures the proportion of individuals without the disease who are correctly diagnosed MHN [101]. The evaluation of data from patients ranked "almost certainly MH" [44] and those from control individuals with no history of MH or any muscle disease has provided the basis for determination of the IVCT sensitivity and specificity respectively [97,102]. For example, an EMHG evaluation of 202 low-risk individuals and 105 high-risk individuals yielded a specificity of 93.6% and a sensitivity of 99% [97]. MHE individuals were included in the susceptible category in these estimates. The specificity increased to 98.2% and the sensitivity dropped to 85 % when the MHE individuals were included in the non-susceptible category [97].

The specificity and sensitivity of the NZ IVCT test has not been formally assessed in this way. Inter-lab variation in IVCT results has been well-documented [70,100,420]. Nevertheless, the assumption that the European based thresholds achieve the same degree of accuracy when applied to data from the Palmerston North IVCT data has never been tested.

The genetic data can be used in place of the clinical observations as a "gold standard" for determining true MH susceptibility, thus providing a fresh means of evaluating the specificity and sensitivity of the IVCT [34,162]. This approach is of course dependent on the assumption that the mutation is causative of MHS. In other words, we assume that individuals with the mutation are truly susceptible, and those without the mutation are unaffected. On this basis, the sensitivity and specificity of the IVCT were calculated from the genetic data as follows;

Sensitivity = 100 X [true positives / (true positives + false negatives)]
Specificity = 100 X [true negatives / (true negatives + false positives)]

'True positives' refer to MHS(+) patients who were diagnosed MHS and carry the Thr4826Ile mutation. 'False positives' correspond to MHS(-) individuals who were diagnosed MHS but lack the Thr4826Ile mutation. 'True negatives' refer to MHN(-) patients who have the normal genotype and are diagnosed MHN. 'False negatives' correspond to MHN(+) patients who carry the Thr4826Ile mutation but are diagnosed MHN by the chosen diagnostic criteria. An important point is that the specificity is calculated under the assumption that the putative false positive test results are not associated with an additional unknown mutation.

Estimates of sensitivity and specificity were calculated for the IVCT with these formulae under various diagnostic thresholds with increasing stringency, as shown in Table 6-3. Maximal estimates of sensitivity (100%) and specificity (100%) were achieved at caffeine and halothane thresholds of 1.2 g and 1.8 g respectively. In contrast, under the standard EMHG thresholds of 0.2 g , the NZ IVCT achieves a sensitivity of 100% and specificity of only 76.6% (95% C.I = 68 – 85.1%). The sensitivity compares favourably with sensitivity estimates of 99% [97] and 98.5% [162] from European studies. However, the specificity is considerably lower than the estimate of 93.6 % from the European IVCT analysis of control patients [97] and the 81.8 % estimate from another study [162].

The specificity of the NZ test drops even further when the MHE category is taken as susceptible. The European study achieved a high sensitivity only by including the MHE category as MHS [97], whereas in the NZ data analysis, MHE results were taken as MHN. When the NZ MHE results were included with the MHS category, the specificity declined to a very low value of 30 %. This was largely attributable to the apparent poor specificity of the halothane test. When assessing the tests independently, the 2 % halothane test achieved a specificity of just 32 % while the caffeine test alone conferred 74.5 % specificity.

The relationship between the IVCT and genetic data was further investigated by statistical tests and graphical representation of the data to assess the performance of the IVCT and the case for genetic heterogeneity within the CH family.

6.3 STATISTICAL ANALYSIS OF THE IVCT DATA

Linkage results provided evidence for a role of the Thr4826Ile mutation in MHS but were highly sensitive to the diagnostic criteria imposed. The classification of the data into discrete groups for linkage analysis also concealed differences between the phenotypes of the mutation-positive and negative individuals, such as the variation in dose response. Additional statistical tests were therefore employed to assess the phenotypes of patients with and without the Thr4826Ile mutation. The possibility that the two populations might be more clearly distinguished by different test concentrations to those applied in clinical diagnosis was explored. Data were scrutinized for evidence of additional MHS genes segregating in the family in patients lacking the Thr4826Ile mutation who registered strong abnormal contracture responses

6.3.1 Statistical analysis of the differences between sample means

Statistical tests of significant differences such as the students T-test examine whether the difference between two statistics (such as the mean tensions for mutation positive and negative

groups) is significant or merely a chance observation. Most classical statistical techniques assume that samples are drawn from populations with normal distributions and allow the estimation of population parameters (hence the term "parametric") [421,422]. The degree of confidence in the test result is compromised when the assumption of the test is violated [423].

The distribution of the data from the mutation-positive and negative groups was examined using a boxplot (Figure 6-1). Data from the mutation-positive samples was representative of a normally distributed population, with coincident mean, median and modes, and a symmetrical distribution of data about the mean. Most tensions registered by the mutation-negative group were close to zero and negative tensions were rarely recorded. Accordingly, the mutation-negative group data are more consistent with an L-type distribution [423]. The non-normal distribution of this data imposes restrictions on statistical methods employed.

Non-parametric tests operate without assumptions about the symmetry of the data distribution [424] and are appropriate non-normal distributions like the clinically non-susceptible group. A simple non-parametric test (the Mann-Whitney U-test) [422,423] was performed to test (at the 0.00001 level of significance) whether the average IVCT tensions registered for the mutation-positive group were higher than the tensions recorded for the negative group. Formulae are given in Appendix 8.2. The test yielded a Z score of 8.6 for both the caffeine and halothane data sets, which exceeded the critical value (4.27) for rejecting the null hypothesis. Muscle from the mutation-positive group is therefore statistically significantly more sensitive to the test agents than the mutation-negative group, and that the observed differences cannot possibly be attributed to chance.

Figure 6-1 Distribution of IVCT data for subjects with and without the Thr4826Ile mutation.

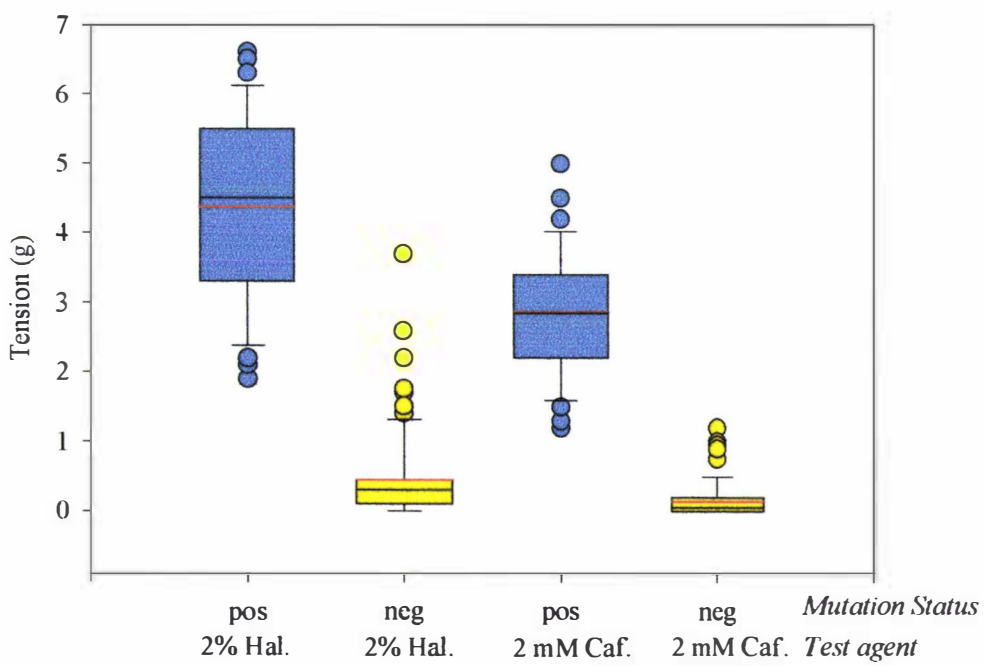

Data distributions for the mutation-positive (blue) and negative (yellow) group are shown at 2 % halothane and 2 mM caffeine. Black lines indicate the median, 25th and 75th percentiles. Red lines indicates data means. Black bars indicate the 10th and 90th percentiles. Circles represent outliers (data points falling outside the 10th and 90th percentiles). The data from the mutation-positive group is approximately normally distributed.

6.3.2 Comparison of the discriminatory power of the caffeine and halothane tests

Visual inspection of the raw IVCT data indicated that muscle contracture response is more sensitive to the 2% halothane challenge than the 2 mM caffeine challenge. The higher sensitivity of the halothane test is illustrated clearly in the distribution of contracture responses presented Figure 6-1. Compared to the halothane test, the caffeine test more effectively distinguished patients with theThr4826Ile mutation from those with the normal genotype. A suspicion that the NZ test results in unusually high sensitivity to halothane and an unusually high proportion of MHE(h) diagnoses under the conventional cut-points has led to the unofficial adoption of a 0.3 g halothane threshold in the more recent diagnoses (N. Pollock, personal communication).

6.3.3 Comparison of the discriminatory power of IVCT threshold drug concentration.

The 2% halothane test was shown to induce stronger muscle contractures and achieve relatively poor discrimination of the patients with and without the mutation, compared to the 2 mM caffeine test. A question that has not often been addressed in the MH literature is whether the specificity of the IVCT might be improved if the lower threshold concentrations of halothane and/or caffeine were used in diagnosis. A further question is whether the affected and unaffected patients might be more clearly distinguished by the slope of a dose response curve, rather than a single tension recorded at a particular drug concentration.

6.3.3.1 Dose response curves

The IVCT involves measurement of muscle tension with stepwise increases in the concentration of each test agent. Halothane is added at concentrations of 0.5%, 1.0%, 2 % and 3%, while caffeine is added at concentrations of 0.5 mM, 1.0 mM, 1,5 mM, 2.0 mM, 3.0 mM and 4 mM. Maximal muscle tensions recorded at each concentration of drug were transcribed from hospital records to construct dose response curves (see Figure 6-2). The mean drug-induced tension for the mutation and mutation negative groups are plotted against the drug concentration (logarithmic x-axis scale), with error bars representing one standard error of the mean. The dose response curves revealed conspicuous differences in both the maximal tensions and patterns of drug sensitivity between the mutation-positive and negative groups.

Muscle from patients harboring the Thr4826Ile mutation have increased sensitivity to lower concentrations of the test agents, as indicated by a shift of dose response curves to the left. Half-maximal tension-inducing drug concentrations for the mutation positive and negative groups are 0.57% and 1.2% respectively for halothane and 1.55 mM and 3.1 mM for caffeine.

The optimal drug concentration range for diagnostic purposes is that which yields the maximum difference between the slopes of the dose response curves of the positive and negative genotype groups [425]. This is observed in the 0.5 – 1.0 % halothane range and the 1.5 - 2 mM caffeine concentration range. The dose response curve for the positive group begins to plateau at 2% halothane while the slope for the mutation negative group is at a maximum in this range. This could account for the relatively poor separation of the positive and negative groups achieved at the standard 2% halothane concentration.

Figure 6-2. Dose response curves for patients with and without the Thr4826Ile mutation

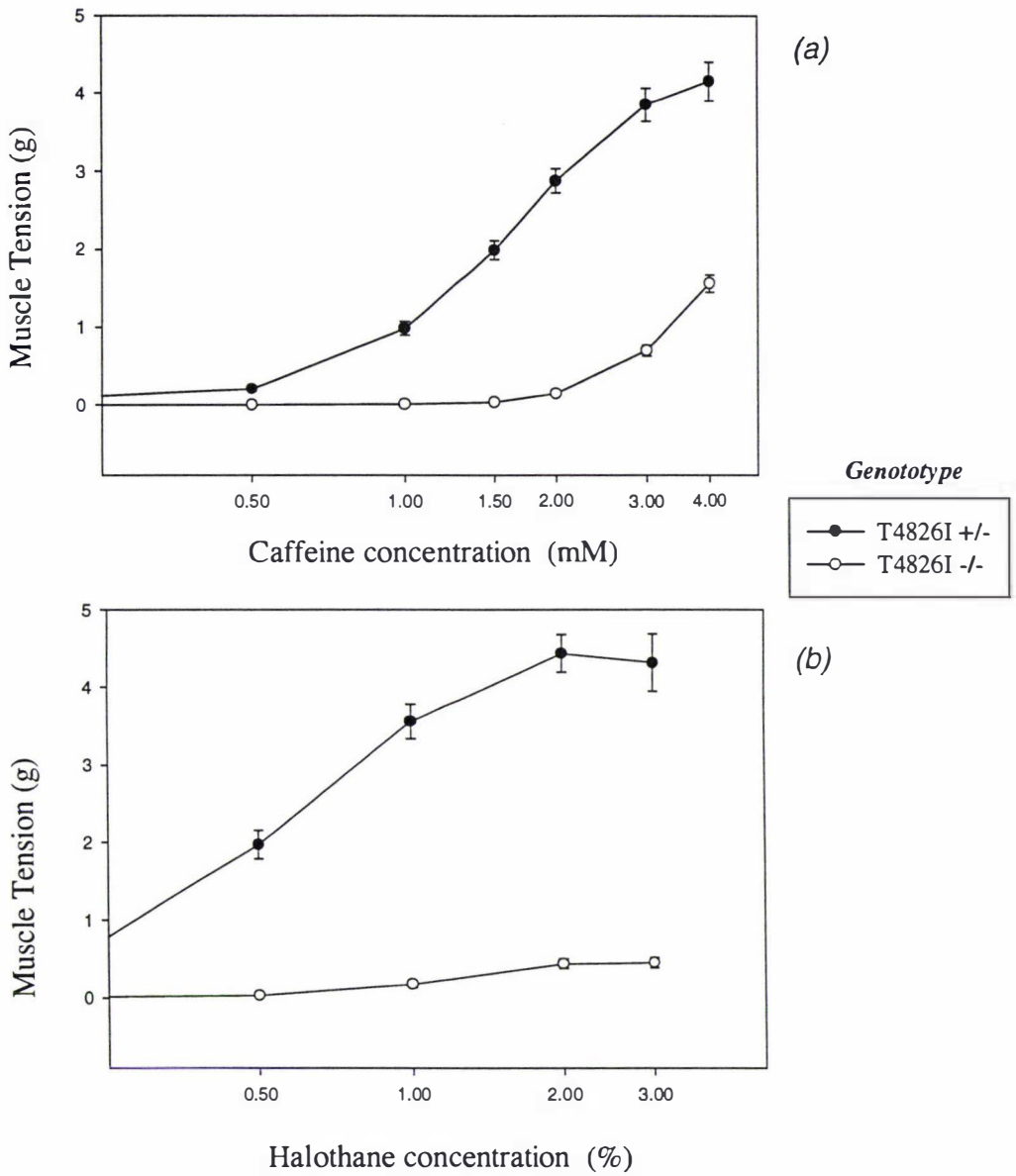

Mean (± SEM) caffeine (a) and halothane (b) contracture response in IVCT from members of CH family with (black circles) and without (clear circles) the T4826I mutation. Values are statistically significant between groups at all test levels of caffeine and halothane ($P < 0.0001$; paired two-sample t-test).

Sample size: Caffeine (a) n = 33, 35, 35, 34, 33, 28 (mutation +), n = 62, 90, 90, 91, 90, 85 (mutation -). Halothane (b) n = 36, 36, 35, 16 (mutation +), n = 91, 89, 90, 91, 86 (mutation -).

Figure 6-3 Distribution of IVCT data for patients with and without the Thr4826Ile mutation

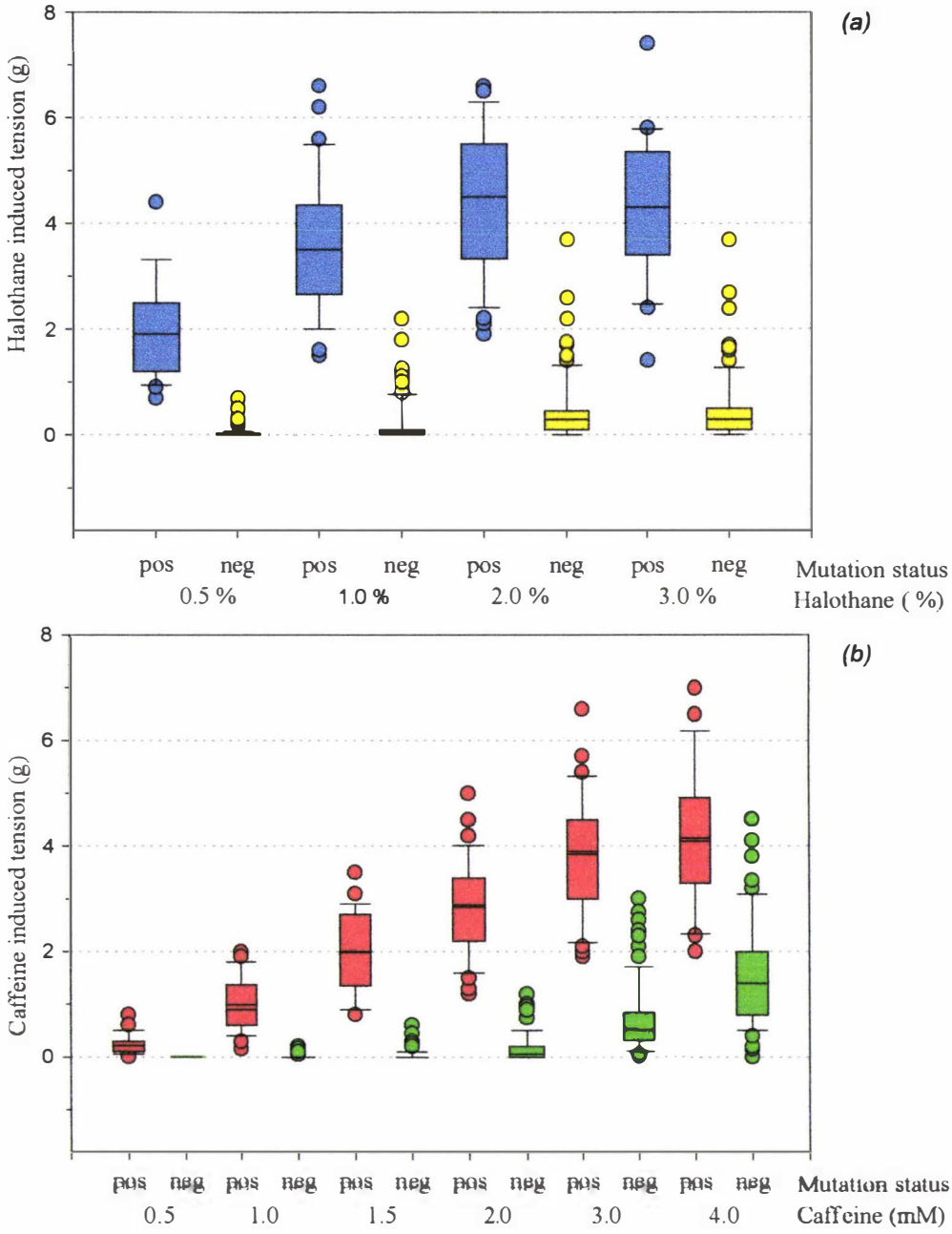

The distribution of IVCT contracture response to halothane (top) and caffeine (bottom) for individuals positive (blue, red) or negative (yellow, green) for the T4826I mutation. Bars represent the median, 10th, 25th, 75th, and 90th percentiles. Circles depict the outliers, falling outside the 10th and 90th percentile whisker-caps.

High concentrations of both caffeine (4 mM) and halothane (3 %) induce strong tensions in some unaffected individuals, and are not useful in diagnosis. For example, the caffeine response for the positive group approaches a maximum at 3 - 4 mM caffeine, while the contracture responses for the negative group are rising sharply from in this range. Consequently, the 3 and 4 mM test concentrations have poor discriminatory power.

6.3.3.2 The distribution of contracture data

The distribution of contracture responses induced at each drug concentration is illustrated with boxplots in Figure 6-3, which indicate the degree of overlap in contracture responses between the two groups at each concentration. A smaller spread of data and a clearer separation of the Thr4826Ile positive and negative groups was observed for the caffeine test compared to the halothane test. The 1.5 mM caffeine challenge completely differentiates the mutation positive from the mutation negative group, while a single point of overlap occurred at 2 mM caffeine. This corroborates well with the concentration used diagnostically and the observation that 1.0 - 2.0 mM caffeine solutions are the most discriminating in an EMHG study [70]. A halothane concentration of 1 % maximally differentiated the mutation-positive and mutation negative groups (seven points of overlap). In contrast, 20 points of overlap occur at the standard diagnostic 2% halothane level.

6.3.3.3 Concordance between genotype and MHS vs. threshold drug concentrations

The dose response curves and patterns of data distribution suggest that the performance of the NZ IVCT would be improved by the use of a 1.5 mM caffeine and 0.5 - 1.0% halothane threshold concentration in place of the current diagnostic concentrations of 2% halothane 2 mM caffeine. This proposal was examined using the genetic data from the CH family to assess the concordance between the genetic data and diagnosis of MHS under a range of threshold concentrations. Results are summarised in Table 6-5. Estimates of the IVCT sensitivity and specificity were calculated as in section 6.2.1. Alteration of MHS diagnostic criteria with respect to the threshold test concentrations required to generate ≥0.2g tension showed that as the diagnostic concentrations were made increasingly stringent (lowered), the number of MHS discordants decreased.

The performance of the IVCT was significantly improved with application of lower drug threshold concentrations. The combination of drug threshold concentrations of 1.5 mM caffeine and 1.0 % halothane achieved high specificity (92.6 %) whilst maintaining absolute sensitivity (100%). Only those subjects registering threshold contracture responses (≥ 0.2 g) to both drugs to be classified MHS in the calculation of these estimates. The equivalent EMHG estimates of specificity and sensitivity using the standard diagnostic thresholds were 84.8 % and 98.5 % respectively [97].

Table 6-5 Effect of the threshold drug concentration on the concordance between MHS and the Thr4826Ile mutation in the CH family.

MHS ≥ 0.2g tension at caf/hal conc.	No. of MHN[1]	No. of MHN recombinant[2]	No. of MHS[1]	No. of MHS recombinant[2]	Sensitivity (%)	Specificity (%)
MHS 0.5/0.5:	115	21	15	0	41.7%	100
MHS 1.0/0.5	94	2	38	2	94.4	97.9
MHS 1.0/1.0:	93	1	37	2	97.2	97.9
MHS 1.5/0.5:	88	1	42	7	97.2	92.6
MHS 1.5/1.0:	87	0	43	7	100	92.6
MHS 2.0/1.0	82	0	48	12	100	87.2
MHS 2.0/2.0	**72**	**0**	**58**	**22**	**100**	**76.5**

Specificity was calculated as the proportion of MHN diagnoses in patients without the Thr4826Ile mutation (n = 94). Sensitivity was calculated as the proportion of MHS diagnoses in patients with the Thr4826Ile mutation (n = 36). Subjects are classified MHS if ≥ 0.2 g tension is registered at both the drug concentrations shown. Results for standard EMHG diagnostic thresholds are in bold.

6.4 IDENTIFICATION AND DISCUSSION OF DATA INCONSISTENCIES

Amongst the 130 IVCT tested individuals, 22 subjects had not inherited Thr4826Ile, but were diagnosed MHS according to standard criteria. In view of the increasing concordance between genotype and phenotype observed with each stepwise increase in the stringency of the diagnostic cut-points, poor IVCT specificity was accepted as a likely source of many of the 22 discrepancies. However, under the maximum raised diagnostic criteria of 0.4 g and 0.8g applied by Healy *et. al.*, 1996 [105], nine CH individuals without the mutation remained MHS. False positive diagnosis is less feasible for these individuals, since their contracture responses exceeded those reported for subjects identified with the Gly341Arg mutation [105].

Four alternate explanations can be invoked to explain these discrepancies; 1) A second MHS gene (non RYR1-linked) was introduced from unrelated spouses or by *de novo* mutation; 2) Environmental factors in combination confer abnormally high sensitivity to the test agents (age, metabolic status, influence of drugs, body mass and composition, existing muscle damage, previous anesthetic exposure); 3) Alternate modes of disease transmission are acting in addition to the autosomal dominant inheritance, which might include modifier genes, sub-clinical myopathies or imprinting. 4). IVCT error (random error or procedural error).

Individuals with a true genetic predisposition to MH (the Thr4826Ile mutation) demonstrated consistently abnormal contracture responses, a strong correlation between the caffeine and halothane-induced contracture responses and a distinctive dose response, due to increased sensitivity to lower concentrations of the test reagents. Data from the discordant MHS(-) group was scrutinised for inconsistencies that pointed to the involvement of IVCT error or extraneous environmental influences rather than an inherent susceptibility to MH. These included: significant variation between duplicate tests; poor correlation between the caffeine and halothane

contracture responses, and; atypical dose response curves. Statistical methods were explored to identify apparent outliers within the MHS group of patients that did not fit a model for the MHS(+) data distribution. Such outliers may provide an insight into the involvement of extraneous environmental or genetic factors that might be leading to an MHS-like phenotype. A multivariate approach was adopted to consider both the caffeine and halothane responses together since a linear relationship between these two variables has been described [426].

The contracture responses to 2% halothane were plotted against the 2 mM caffeine-induced tensions for patients identified with (blue) and without (yellow) the Thr4826Ile mutation (Figure 6-4). A strong linear correlation between the caffeine and halothane data was found (r^2 =0.83). The IVCT data for the "with" and "without" mutation groups can be distinguished by the position of data points along the diagonal with subjects identified as carrying the mutation producing relatively strong tensions to both agents and falling on the upper right quadrant of the graph. The majority of the mutation-negative responses fall on the lower left quadrant, and are clearly distinguishable from the group harboring the mutation. Among the 43 individuals diagnosed MHS according to raised diagnostic cutpoints (indicated by the dotted lines), the nine subjects without the mutation produced the weakest responses. While there is some overlap in the halothane-induced tensions between the two groups, inspection of the caffeine test responses indicated cut-point of 1.2 g for 2 mM caffeine would distinguish the mutation positive group from the negative group. Accordingly, the discordant individuals classified MHS under the raised diagnostic criteria could be considered to be in a different phenotypic category from the MHS(+) patients.

6.4.1 Identification of outliers: Discriminant analysis

A useful way of detecting multivariate outliers is to measure the distance of each observation from the center of the data using the Mahanalobis distance statistic (D^2) [427] [428,429]. This statistic estimates the multivariate equivalent of how many standard deviations a data point is from the mean of a normally distributed group of data, and thus gives an indication as to the likelihood of the data point belonging to a group. The Mahanalobis distance discriminatory test was applied to the caffeine and halothane IVCT data to assess whether or not the phenotypes for the discordant MHS(-) subjects are statistically significantly distinct from the mutation-positive group. Formulae are described in Appendix 8.3. Assuming the IVCT data represents a multivariate normal distribution (acceptable for the MHS group), the distance (D^2) from the combined mean should follow a chi-squared distribution with two degrees of freedom (2 variables) [428]. If an individual does come from that distribution there is a 95 % chance of their distance from the mean (D^2) being less than 5.99 and a 99% chance of the distance from the mean being less than 9.21 [428].

Of the 94 individuals from the mutation negative group, nine discordant MHS(-) individuals scored D^2 values indicating a 1.5%-8 % chance of belonging to the distribution defined by the mutation-positive group (indicated on Figure 6.4). Therefore, at the 1 % levels of significance there is no statistical justification for dismissing the nine MHS(-) cases on the assumption that their responses are "significantly different" to the group harboring the mutation. IVCT data from the remaining mutation-negative individuals was representative of less than 1% of the positive group ($D^2 > 9.21$). Further overlap with the mutation negative-group data is anticipated as the number of biopsy tests increase. An assessment of the MHS(+) data distribution revealed that 99 % of the total mutation-positive population would be expected to record IVCT responses >0.3 g (caf.) and > 0.45 g (hal) at the standard concentrations (assuming a multivariate normal distribution) . Therefore, the adoption of clinical diagnostic thresholds below these values could result in an unacceptable risk of potentially fatal false negative diagnosis.

Figure 6-4 Correlation between IVCT response and the Thr4826Ile substitution

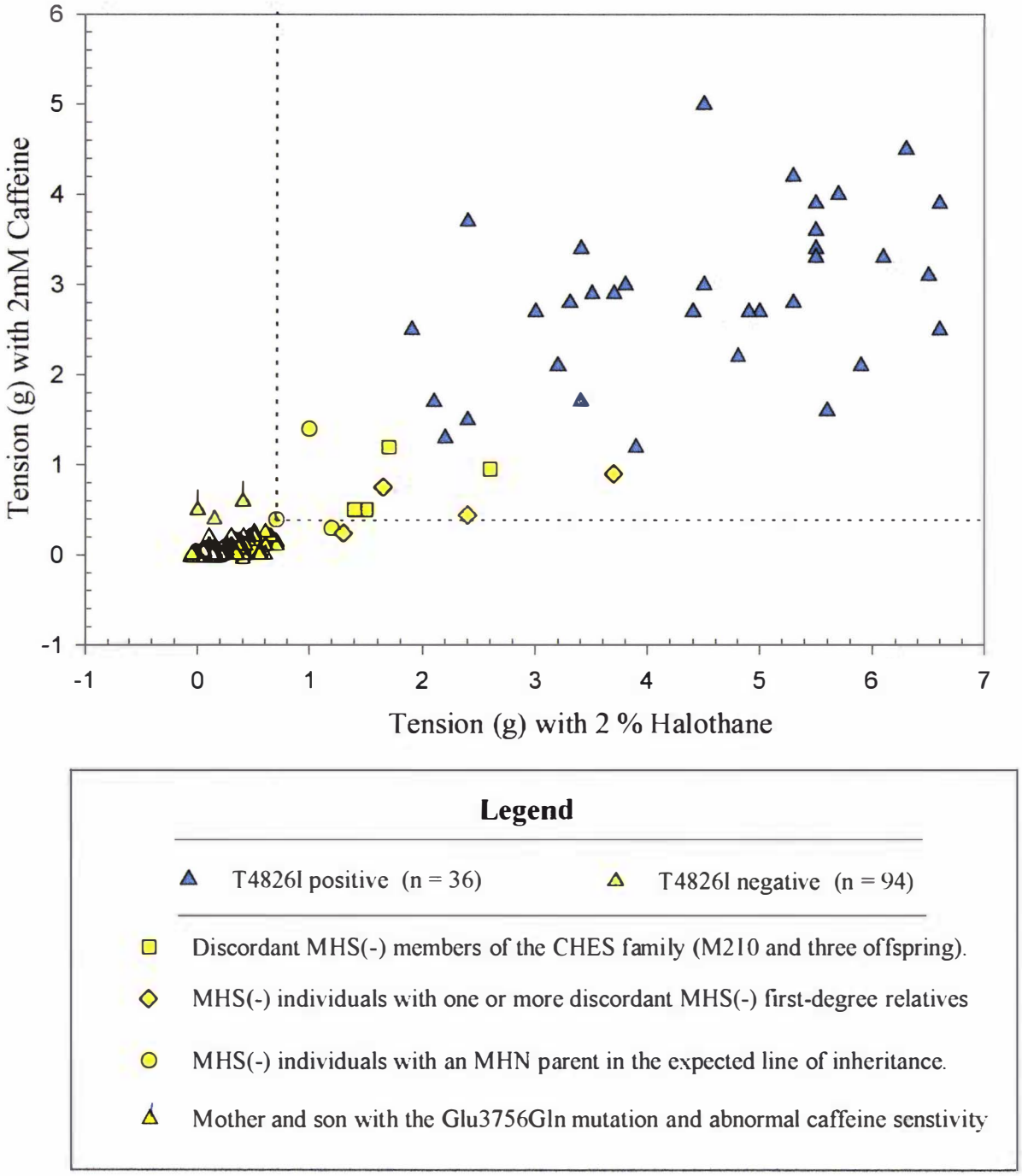

Maximal IVCT contracture response in subjects from CH family with (blue symbols, n = 36) and without (yellow symbols, n = 94) the T4826I substitution. Dotted lines mark the raised diagnostic cut-off tensions applied in the genetic linkage analysis(MHS*). Other symbols distinguish discordant MHS(-) individuals from families in which an additional MH gene may be segregating.

6.5 FACTORS CONTRIBUTING TO GENOTYPE/PHENOTYPE DISCREPANCIES IN THE CH FAMILY.

A group of patients who are MHS according to raised diagnostic criteria were identified as having an intermediate phenotype, based on the IVCT responses to caffeine and halothane. In some cases, the halothane responses fell into the range defined by the mutation positive group, and thus they cannot easily be dismissed as false positive diagnoses. According to their statistical measure of multivariate distance from the mean IVCT values, the contracture response from this intermediate group are not statistically significantly different to the MHS(+) group ($P > 0.01$). Alternate explanations, including the influence of additional environmental or genetic factors (as described at the beginning of section 6.4) were considered.

6.5.1 External factors

Extraneous environmental factors may be contributing to false positive diagnosis, however, age and fiber type distribution have been found to have no influence on MH diagnosis based on EMHG protocol [430]. There were no measurable differences between men and women in the average sensitivity of muscle to test agents (data not shown). The discordant MHS(-) group was not over-represented by any particular gender or age-group.

The influence of environmental factors or random error on the MHS IVCT results was explored by reviewing the consistency of contracture responses for the duplicate muscle strips. An interesting finding is that the Thr4826Ile mutation was completely penetrant *in vitro*. Of the 145 muscle bundles tested from individuals harbouring the Thr4826Ile mutation, every specimen registered a significantly abnormal response. The lowest tension produced by 2% halothane was 0.8 g, while the lowest contracture response to 2 mM caffeine was 0.6 g. Stronger tensions were registered from additional strips examined, in each case. All of the 145 muscle bundles examined from the mutation positive group registered tensions sufficiently strong to secure an MHS diagnosis under the raised diagnostic thresholds applied in the second linkage analysis.

Data from duplicate tests were reviewed for 94 patients who were negative for the Thr4826Ile mutation. 72 of these patients failed to yield contracture responses above the 0.2 g threshold in any of the strips examined. Amongst the 22 discordant MHS(-) individuals, all but two could be distinguished from the mutation positive group by having at least one marginal (< 0.3 g) or normally reacting muscle strip. Only two of the 94 mutation-negative individuals consistently registered tensions above the minimum 0.8 g (halothane) and 0.6 g (caffeine) contracture responses recorded for the mutation positive group. They were M394 and M397 from the discordant ES branch (Figure 6-5). This suggests that the inherent variability of the IVCT may underlie a significant proportion of the discordant MHS results. Discordant members of the CHES branch are the exception, displaying consistently abnormal results.

6.5.2 Genetic heterogeneity: Clustering of discordant results in families

A suspicion of genetic heterogeneity is particularly compelling where discordant MHS results are clustered in family members who do not a share common RYR1 haplotype. Four of the nine discordant individuals identified with a susceptible phenotype under the stringent diagnostic thresholds, and in the multivariate analysis are clustered in the CHES branch of the pedigree.

The CHES family pedigree is reproduced in Figure 6-5. Individual M210 and his three offspring (M394, 395, 397) are all clearly MHS yet lack the Thr4826Ile mutation or any common chromosome 19q haplotype. The IVCT contracture responses for these individuals are marked with squares in Figure 6-5. The highly abnormal contracture responses and the localization of the discordant individuals in one family challenged the presumption of false positive diagnosis. Furthermore, three siblings of the father (M210) and the grandfather (individual II 6, Figure 6-5) were diagnosed MHS but lack the mutation and associated chromosome 19q haplotype. These individuals were tested before the introduction of the standard EMGH test and data is not available for comparison. If the MHS results from these earlier tests are accepted as valid, the occurrence of eight discordant MHS(-) diagnoses in closely related individuals spanning three generations strongly indicates the segregation of a second MHS gene defect, not related to RYR1. As Thr4826Ile segregated with MHS in the left-hand side of the pedigree, the inheritance of a mutation from one of the first generation individuals (I1 or I2) is unlikely. A *de novo* mutation in MHS individual II6 would explain the data. Future work may reveal a mutation in one of the other identified candidate genes. Currently, the candidate MH locus of choice for linkage studies is the CACNL1A3 gene encoding the α_1-subunit of the skeletal muscle voltage-dependent calcium channel (DHPR) in which two MH mutations have been identified [33,40]. Two discordant members of the family (M210, M395) were negative for the published Arg1086His mutation in this gene.

Interestingly, a neurological examination of MHS(-) individual M210 revealed evidence of an underlying myopathy. Symptoms included definite progressive and generalised muscle weakness and impaired muscle reflexes. These observations may or may not be related to MH susceptibility (Dr. M. Pollock, Neurologist, personal communication). However, neuromuscular complaints of this nature have not been reported in any patients identified with the Thr4826Ile mutation. The abnormal contracture responses registered by individual M210 and his three children may be caused by a mild undiagnosed muscle disorder, unrelated to MH.

In three of the five remaining MHS(-) individuals identified as having strong abnormal contracture responses (M95, M98, M175) a discordant MHS(-) result in at least one other first degree relative raises the possibility of further genetic heterogeneity in the CH family. These cases are summarised in Table 6-7 and are represented with diamond symbols in Figure 6-4.

Figure 6-5 Discordance between the Thr4826Ile mutation and MHS in the CHES branch of the large Maori family

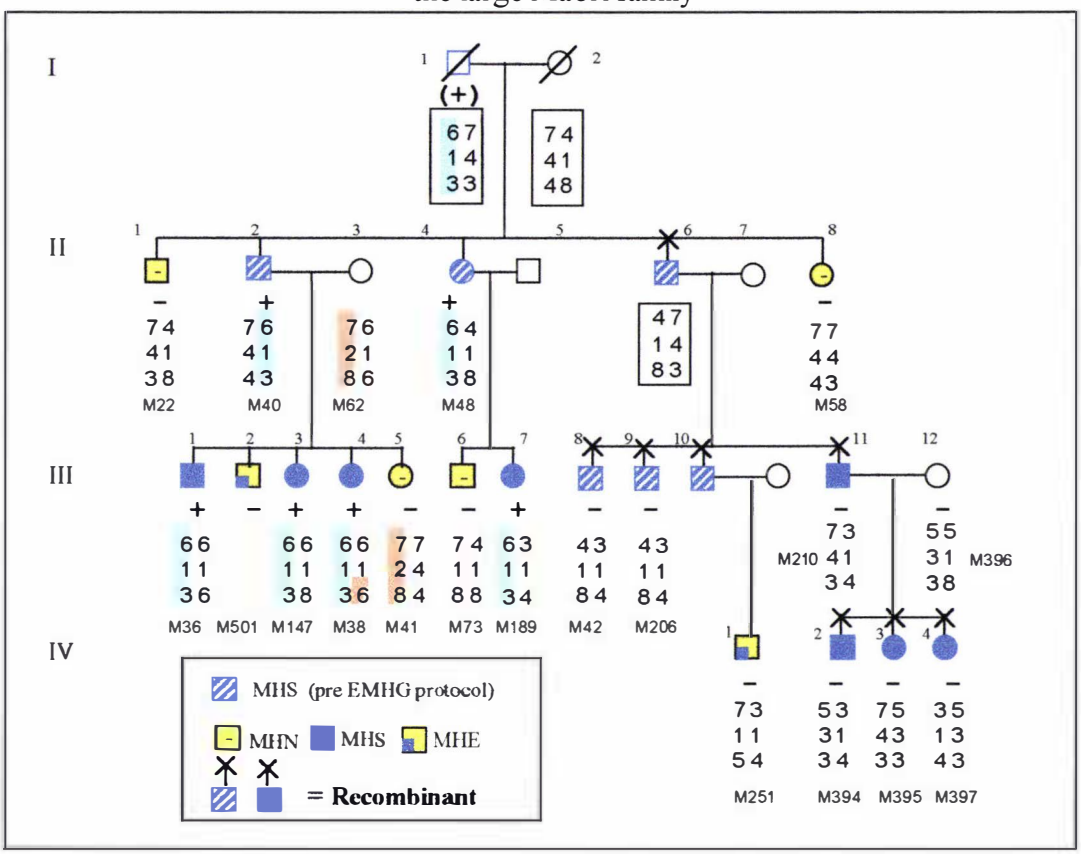

The presence (+) or absence (-) of the T4826I mutation is indicated below each symbol. T4826I failed to segregate with MHS in 8 individuals (marked recombinants) on the right hand side of the pedigree. Haplotypes for the D19S220, RYR-RFLP and D19S47 markers are indicated. Discordant individuals do not share a common chromosome 19q haplotype, suggesting the introduction of defect at a second MHS locus in generation II.

Table 6-7 Closely related discordant MHS(-) individuals in the CH family

MHS(-) individual	Pedigree branch	Relationship	MHS(-) Relatives	IVCT data 2 mM Caf.	2 % Hal.
M210	CHES	- - -	- - -	0.5 g	1.5 g
		daughter	M394	1.2 g	1.7 g
		son	M397	0.95 g	2.6 g
		Son	M395	0.5 g	1.4 g
M95	CHKC	- - -	- - -	0.7 g	1.75g
		son	M96	0.25 g	0.5 g
M98	CHKM	- - -	- - -	1.0 g	1.75 g
		daughter	M99	0.2 g	0.65 g
		sister	M199	0.2 g	0.45 g
		son	No DNA	0.5 g	0.25 g
M175	CHEA	- - -	- - -	0.9 g,	3.7 g
		brother	M33	0.25 g	1.3 g

6.5.4 Apparent "Generation skipping"

Prior to the discovery of a genetic determinant of MHS status, a diagnosis of MHS in individuals descended from an MHN or MHE parent led to concern about the accuracy of the IVCT MHN diagnosis. In the absence of genetic data, explanations invoked to explain the inconsistencies included non-paternity and false negative diagnosis in the parent. A further suggestion was that the MHS phenotype had "skipped" a generation, through compensatory mechanisms that masked true MH susceptibility in the MHN parent.

The genetic study of the CH family has resolved some cases, and has verified both the alleged paternity and the reliability of the MHN diagnosis. An MHS diagnosis in an individual descended from an MHN or MHE parent in a family that is clearly negative for the Thr4826Ile mutation indicates false positive diagnosis has occurred, or alternatively, that MHS was inherited via the parent who was married into the family.

A striking example is the strong abnormal contracture response recorded for MHS(-) individual M54, (CHEA, Figure 4-11; 1.0 g at 2 mM caf., 1.4 g at 2 % hal.). Variable caffeine results, ranging from 0.1g to 1g tension, distinguish the phenotype of this individual from that associated with the Thr4826Ile mutation. Nevertheless, the maximum contracture responses from this individual fall well into the distribution of subjects who were positive for the Thr4826Ile mutation. The mother of this individual was diagnosed MHE and lacks the mutation. Either M54 has inherited MHS paternally, has incurred a *de novo* mutation, or has inherited benign mutations from both parents, which only manifest as MHS in combination. Testing of the father of M54 may help resolve this discrepancy in the future.

The same conclusion can be reached for individual M130 (CHEH branch, Figure 4- 10) who was diagnosed MHS (0.25 g at 2 mM Caf, 1.2 g at 2 % Hal.). Her father (assumed obligate carrier) was diagnosed MHN. Neither individual had inherited the Thr4826Ile mutation, and chromosome 19q haplotypes support the alleged paternity. This strongly suggests that the MHN diagnosis in the father was valid, corroborating the observed rarity of MHN diagnoses [41,42]. This anomaly could be explained by a false-positive halothane response in M130 (duplicate hal. test = 0.6 g). Alternatively some factor in the combined genetic background of this individual may confer moderately atypical halothane sensitivity.

A third example of apparent generation skipping occurred in a branch of the family otherwise considered to be a non-susceptible (M86, CHEM branch, Figure 4-13; 0.4 g caf., 0.6 g hal.). The parents of the boy tested MHN and MHE. Haplotypes were consistent with alleged paternity. The occurrence of an MHS diagnosis in an individual with two MHN parents has been previously described in eight families [431] and a fatal MH reaction has been documented in a child whose parents were both diagnosed MHN [432]. Such cases are indicative of the presence of alternate recessive patterns of inheritance, or sub-clinical myopathies. In the case of individual M86, a mildly abnormal pattern recorded in an electromyogram supports the latter conclusion (N. Pollock personal communication).

There were no common chromosome 19q haplotypes within or between discordant branches, ruling out the likelihood of a putative second RYR1 mutation segregating throughout the family. Key discordant individuals were tested for 10 reported RYR1 mutations by RFLP (R163C, I403M, R552W, R614C, G2434R, R2435H [25] and the published Arg1086His CACNLIA3 mutation [33]. None of these mutations were detected.

6.5.4.1 Abnormal phenotype associated with the Gln3756Glu mutation

An additional RYR1 mutation segregating in the CHEH branch (Figure 4-10) may have conferred heightened sensitivity to caffeine. A mutation that substituted glutamate for glutamine 3756 occurred in phase with the 5-7-4-1-5 haplotype shared by four MHE individuals. A mother and son who both registered abnormal responses to caffeine (0.5g, 0.6g) but were negative for Thr4826Ile also share this haplotype (represented by tailed triangles in Figure 6-4). IVCT results for the two susceptible carriers of the Gln3756Glu mutation were atypical for an MHS diagnosis in that the maximal response to caffeine exceeded the halothane response in both cases. The glutamine 3756 to glutamate substitution was not considered to be a candidate MH mutation since was first detected in a MHE individual, the residue is not conserved, and the equivalent residue is glutamate in all other RyR isoforms (Figure 6-8).

Three individuals are compound heterozygotes, having inherited both Thr4826Ile and the Gln3756Glu substitution. All three compound heterozygotes registered strong caffeine tensions (>3.4 g) and one individual with both mutations exhibited the highest halothane response of all 36 members of the mutation-positive group. A one-tailed student T-test was performed to test whether the caffeine tensions recorded for the compound heterozygotes were higher than the tensions registered by individuals with just the Thr4826Ile mutation. The difference approached statistical significance at the 0.05 level ($P = 0.061$, $T = 1.59$, $df = 32$). At present, there is insufficient data to attribute the apparent relationship between the Gln3756Glu substitution and caffeine sensitivity to more than a chance observation. Since the 5-7-4-1-5 haplotype is present in other related MHN and borderline MHE(h) patients, any phenotypic manifestation of the associated mutation evidently has low penetrance or requires the existence of additional genetic factors.

6.6 COMPARISON OF PHENOTYPES ASSOCIATED WITH DIFFERENT RYR1 MUTATIONS

A study of the IVCT data from European MHS families identified with various RYR1 mutations indicated that particular RYR1 mutations were associated with a more pronounced MHS phenotype [25]. For example, a more severe halothane phenotype was tentatively associated with mutations in the central portion of the gene compared to those in the N-terminal region [25]. A relatively mild IVCT phenotype has been attributed to patients identified with the Cys35Arg mutation [165]. Calcium photometry assays of cells transfected with wild type and mutated forms of the ryanodine receptor had also revealed differences in the sensitivity to caffeine and halothane among the ryanodine receptor mutants [16]. In contrast to European studies that have reported MHE diagnoses in patients with RYR1 mutations [109,174], no MHE subjects were identified with the Thr4826Ile mutation suggesting a more severe phenotype is conferred by the Thr4826Ile mutation compared to other RYR1 defects.

To investigate this hypothesis the IVCT data from each NZ family identified with a RYR1 defect was investigated for evidence of differences in the severity of the phenotype conferred by the various mutations. The caffeine and halothane responses for each individual are plotted against the position of the RYR1 mutation in Figure 6-6. While direct examination of the data indicated that certain mutations conferred a more sensitive MHS phenotype compared to others, considerable variability in the muscle tensions was noted within each group and the sample sizes

in most cases were small. Statistical methods were employed to test whether or not the apparent differences in the MHS phenotypes were significant. Two mutations (Arg2452Trp, Arg2454His) were excluded because the sample sizes were too small (n < 2). Average contracture responses (and SEM) for the remaining mutations are shown in Table 6-8.

Table 6-8 Mean contracture responses for patients identified with RYR1 mutations

A. 2 mM caffeine

Mutation	N	Mean (g)	Std Error	Median
Arg163Cys	2	3.85	1.45	3.85
Thr4826Ile	34	2.906	0.152	2.85
Gly341Arg	4	1.65	0.393	1.35
Gly2434Arg	4	1.588	0.349	1.65
Arg401Cys	2	1.5	1.2	1.5

B. 2% halothane

Mutation	N	Mean (g)	Std Error	Median
Arg163Cys	2	4.95	2.65	4.95
Thr4826Ile	35	4.4	0.246	4.5
Gly341Arg	4	2.150	0.221	2.1
Gly2434Arg	4	3.625	0.585	4.05
Arg401Cys	2	3.6	1.9	3.6

Mean muscle tension (g) at 2 mM caffeine (A) and 2% halothane for NZ patients identified with RYR1 mutations. .

Figure 6-6 Comparison of IVCT data associated with RYR1 mutations identified in NZ MHS families

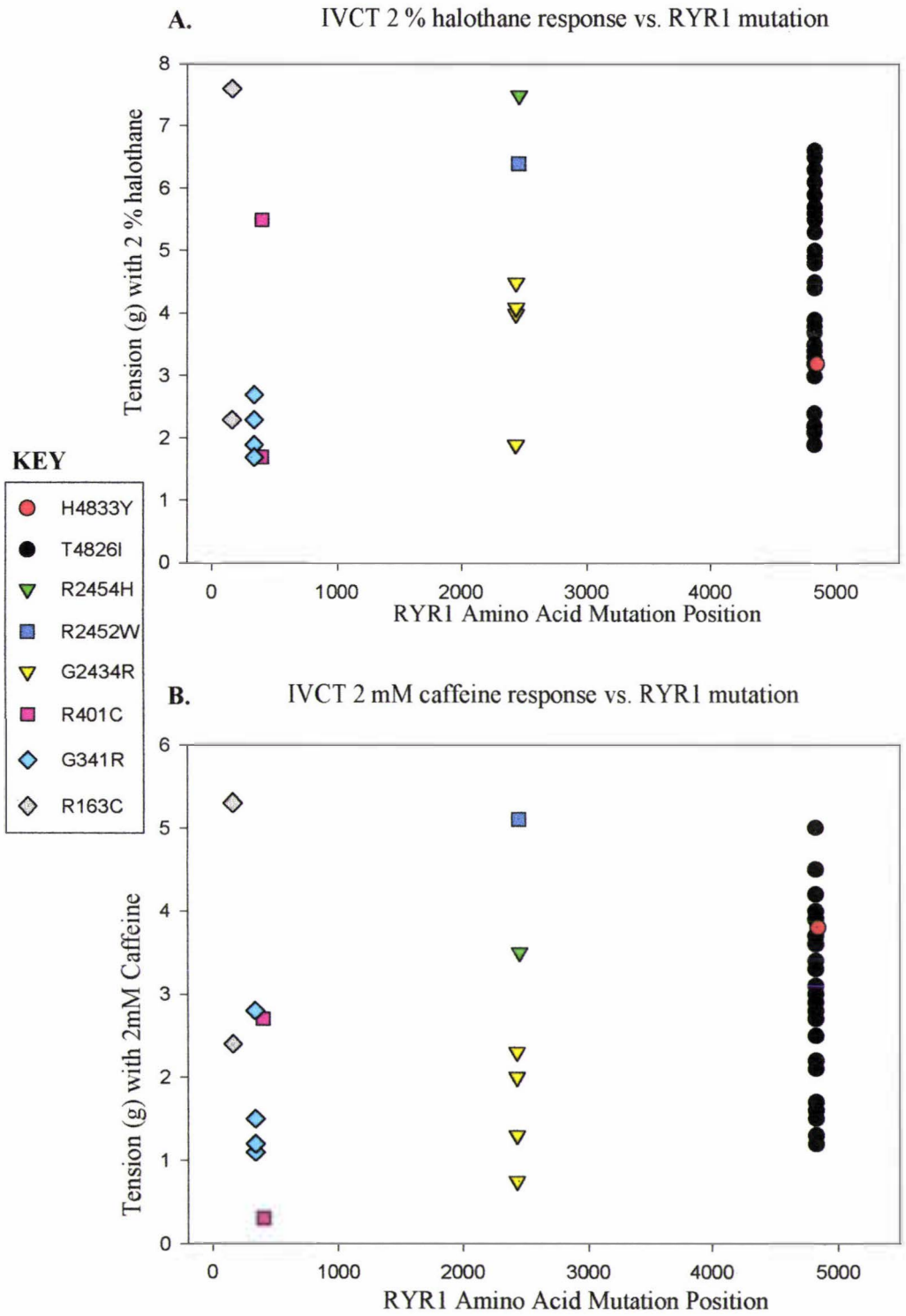

6.6.1 Statistical comparison of phenotypes for RYR1 mutations

Phenotypes associated with each of the mutations were compared using the one–way ANOVA test (analysis of variance)[433-436]. The ANOVA test is described in detail in appendix 8.4. Briefly, ANOVA is used to test the equality of three or more population means, assuming data are sampled from normal populations. The key idea is that variability among the contracture values can be divided into variability among mutation-group means and variability within the groups. If phenotypic differences between the mutation groups are discernible over the background of random variation occurring within each mutation group, the phenotype appears to be influenced by the nature of the RYR1 mutation. The result of the ANOVA test is expressed as the F ratio; calculated as the ratio of the between-group versus the within-group mean square differences. If the difference between the groups is not different, an F value close to 1.0 is expected.

The ANOVA test was applied in separate tests to the 2 mM caffeine data and 2% halothane data for the Arg4826Ile, Gly2434Arg, Gly341Arg, Arg163Cys and Arg401Cys mutations (i.e. five groups). Results are presented in Table 6-9. The ANOVA analysis was limited by the small sample size (n <5), nevertheless, the differences between the caffeine values for the different mutations are very significant (P = 0.0038). In contrast, the differences between the halothane values were not statistically significant (P = 0.0781), due to the inherent variability of the halothane-induced tensions.

After rejecting the hypothesis that the mean caffeine responses associated with the different mutations were equal, the Tukey-Kramer multiple comparisons test [433,435] was performed to discover which group means were significantly different. Results approaching statistical significance (0.05 > P <0.08) were obtained when the Thr4826Ile group was compared to the data from the Gly2434Arg and Gly341Arg groups, and when the Arg163Cys group was compared with the Gly2434Arg, Gly341Arg and Arg401Cys groups.

Table 6-9 ANOVA Table: Comparison of IVCT phenotypes for RYR1 mutations.

Source of variation	Degrees of freedom	Sum of Squares	Mean square	F ratio	P value
Halothane					
Between group	4	21.16	5.29		
Within group	42	98.043	2.334		
total	46	119.2		2.266	0.0781
Caffeine					
Between group	4	16.26	4.065		
Within group	41	35.46	0.89		
total	45	52.716		4.572	0.0038

The F ratio is calculated as the between-group mean square value divided by the within-group mean square value. P values < 0.05 are statistically significant (where the P value represents the probability of obtaining the data if there is no difference between the means). ANOVA tests were performed with GraphPad InStat version 3.00 for Windows 95 [433].

Small sample size prohibited comparison of the phenotypes associated with mutations in the N-terminal, central, and C-terminal regions of RyR1. Nevertheless, the ANOVA test and direct examination of the data plotted for individuals identified with each mutation (Figure 6-6) suggests that the Gly341Arg and Gly2434Arg mutations might confer a relatively mild phenotype, while the Thr4826Ile and Arg163Cys mutations were associated with the strongest contracture

responses. The emerging picture is that different mutations have graded influences on the open probability of the calcium channel, therefore it is plausible that carriers of the less severe mutations can occasionally test MHE or even test MHN in the IVCT [274]. The weaker phenotypes recorded for patients with the Gly2434Arg and Gly341Arg mutations corroborates with reports of MHE diagnoses in patients harbouring the Gly341Arg mutation [109,174], MHE and MHN results in patients harbouring the Gly2434Arg mutation [167], and the expression of the severe CCD phenotype in some carriers if the Arg163Cys mutation [13]. A similar pattern was recorded in calcium photometry assays of mutant channel proteins expressed in HEK-293 cells [16]. In these studies, the Arg163Cys mutant channel was more sensitive to lower concentrations of caffeine and halothane than the Gly341Arg, Gly2434Arg and Ile403Met mutants [16].

6.6.2 Comparison of the NZ and overseas IVCT tensions for known RYR1 mutations

The frequency of discordant MHS(-) from the CH family suggests that some feature unique to the NZ IVCT might confer heightened sensitivity to the test agents, leading to a high false positive rate when the European MH group diagnostic thresholds are applied. IVCT results from subjects identified with the previously published mutations; Arg163Cys, Gly341Arg and Gly2434Arg mutations were compared to the corresponding published data from the Irish MH group [25] to test this hypothesis (using the student pairwise T-test). Differences between the NZ and Irish IVCT data were not statistically significant. While direct examination of the data suggested that the minimum halothane thresholds required to elicit a 0.2 g response are lower for the NZ test, statistical analysis of a larger data set will be necessary to clarify this point.

6.7 MHS IN ASSOCIATION WITH SUDDEN INFANT DEATH IN THE LARGE MAORI FAMILY

Two distantly related young children from the CHKW and CHEA branches of the large Maori family aged 9 and 24 months died sudden unexplained deaths in the absence of any known triggering agents. Clinical details are limited, but both deaths were preceded by generalized muscle rigidity, masseter spasm and hyperthermia, resembling an awake episode of MH. Body core temperatures at the time of death were not recorded; however, a clinician described "steam" rising from one of the deceased children (N. Pollock, personal communication). The death of the 9-month-old child was recorded as sudden infant death. In the case of the 24-month-old child, analysis of post-mortem eye fluid did not reveal raised CK or lactic acid typically associated with MH events.

These cases of sudden death in young children were of particular interest because anecdotal reports have previously implied a link between MHS and sudden infant death. Cases of sudden infant death in connection with MH susceptibility has been documented in Australian [71], Scandinavian [70] and American [72] studies. A higher incidence of the sudden infant death syndrome (SIDS) has been reported in MH families, and a higher than expected frequency of MHS in parents of SIDS children [70-72]. Denborough reported that in five out of fifteen cases of sudden infant death, malignant hyperthermia susceptibility was present in one of the parents [71]. However, the genetic basis of MHS had not been described in these families.

The parents of the 9-month-old infant were closely related and were both MHS and positive for the Thr4826Ile mutation. Their child thus had a 75% chance of inheriting one copy of the mutation and a 25% chance of being homozygous for the defect. This lead to speculation that the sudden death phenotype represented a more severe expression of MHS, manifesting as a result of the inheritance of two copies of the disease gene. This hypothesis was prompted by the observation that porcine MH, which is inherited as an autosomal recessive disorder, can be triggered by stress factors [437] and in particular, overheating [62,438] in the young animal.

SSCP and sequence analysis of the DNA extracted from paraffin embedded autopsy spleen tissue taken from the deceased infants revealed that both had inherited the Thr4826Ile mutation and the associated chromosome 19q haplotype. However, both children were heterozygous for both the mutation and RYR1 RFLP markers, indicating the SIDS did not result from homozygosity for Thr4826Ile. Nevertheless, the possible inheritance of multiple MHS genetic factors as a result of inbreeding in the case of the 9-month-old infant could be ruled out.

6.7.1 MH episodes in the absence of anaesthesia

Cases of MH in the absence of triggering anaesthetic are not unprecedented. So-called "awake" MH events in susceptible individuals have been triggered not only by anaesthetics, but by a range of mechanisms, including exercise [439,440], overheating in infants [62,441], infection [440], stress [67], gasoline fumes [442], alcohol [443] and exposure to bromochloro-difluoromethane (emitted from fire extinguishers) [441].

Overheating has been proposed as a link between MH and SIDS, since overheating alone can induce MH in susceptible piglets [62]. Furthermore, overheating is recognized both as an important risk factor in sudden infant death [444], and is a potential trigger in reported awake episodes of MH [445] in association with viral infection [446-448] and MH and rhabdomyolysis in MHS adults exercising in hot conditions [443-446]. Dantrolene, (a potent inhibitor of SR calcium release) has been used successfully to combat heat stroke [64] and an awake episode of MH in an individual with influenza [447]. Severe rhabdomyolysis was reported in an MHS family in which three men had suffered fatal or near-fatal attacks of rhabdomyolysis while infected with influenza [443]. Interestingly, the 9-month-old infant was feverish and suffering from influenza at the time of death. It is possible that the MH-like reaction may have been triggered by fever in this infant, and that dantrolene therapy may have been effective, had it been available.

The involvement of the autonomic nervous system in MHS is unclear. Stress is a recognized trigger for MHS in swine, leading to muscle rigidity, hyperthermia and rapid death in susceptible animals. Some authors contend that MHS patients are at increased risk of sudden death [67,446,449] and the significance of stress as a predisposing factor and the role of adrenergic stimulation has been presented [67,70,450,451]. For example, in a single MHS family, 31 fatal and near-fatal MH episodes were recorded, and only 11 occurred in association with anaesthesia [67]. The remaining episodes occurred outside the hospital and in association with some form of stress. The susceptible patients had evidence of hyperactive sympathetic nervous systems (tachycardia, profuse sweating cyanosis) with enhanced myotonias and fever during periods of emotional stress [67]. Clinical events in MHS individuals are more likely to be associated with trauma [67] and 38% of reactions in Sweden occurred during emergency surgery, reflecting the impact of stress on the probability of a susceptible individual developing MH [70]. Exam stress and alcohol consumption may have been precipitating factors in the separate sudden unexplained deaths of two brothers, whose father was diagnosed MHS and complained of muscle cramps after

exercise [449]. The recent finding that RYR1 is widely expressed in the brain has provided a possible mechanism for the neurogenic aetiology of malignant hyperthermia [452,453].

In view of the strong association between the Thr4826Ile substitution and susceptibility to MH in this family, it is possible that the inheritance of this mutation may have played some role in the sudden unexplained deaths of two young children. The circumstances of their deaths involving hyperthermia and muscle rigidity in the absence of anaesthesia could pertain to an awake episode of MH, however due to the lack of clinical data it is not possible to clinically classify these episodes as MH. To our knowledge, this is the first report of an MHS mutation detected in association with sudden deaths in any MH pedigree.

6.8 SUMMARY AND IMPLICATIONS FOR DIAGNOSIS

An extensive overview of the segregation of the Thr4826Ile substitution and the muscle contracture sensitivity in 212 member of the large Maori family strongly indicated that the Thr4826Ile mutation is causative of MH susceptibility in this family.

6.8.1 Summary of evidence supporting a causal role for Thr4826Ile in MHS

Evidence in favour of a causative role for the Thr4826Ile mutation in the CH family satisfies the standard criteria for accepting candidate MHS mutations, as listed below.

- Thr4826Ile was the only candidate mutation discovered in the sequence analysis of the entire RYR1 cDNA.
- The Thr4826Ile mutation was absent in the normal population, indicating it is not a common coincidental polymorphism.
- The mutation was detected in five individuals who had survived clinical MHS episodes and in the immediate relatives of five individuals who had suffered fatal episodes.
- The inheritance of Thr4826Ile coincided with strong MHS contracture responses in 36 members of the family, dispersed over several distantly related branches of the seven-generation pedigree.
- The Thr4826Ile mutation was not detected in any of 72 MHN or MHE members of the family. A lod score of > 3.0 was calculated for linkage between Thr4826Ile and MHS under the standard EMHG cut-points (≥ 0.2 g contracture at 2 % hal. and 2 mM caf.).
- Residue Thr4826 was conserved over 12 RyR isoforms and in RyR1 proteins from different species, implying functional significance of the residue.
- A nearby His4833Tyr mutation was discovered n a second MHS Maori family, supporting a functionally important role for this region in the calcium channel activity.

Finally and conclusively, since its discovery in the NZ family, theThr4826Ile mutation has been identified in an Australian MHS family, where it segregated (though incompletely) with MHS over three generations (Mark Davis personal communication, Royal Perth Hospital). It is highly likely that the Australian family is related to the large Maori CH family, since a number of CH family members now reside in Australia, and several branches of the CH family have not been traced. A comparison of RYR1 haplotypes from MHS members of each family deduced from the sequence analysis supported this assumption. In addition, MHS individuals from both families carry the rare D19S47 "3" allele in phase with Thr4826Ile, consistent with the proposed common

ancestry. Independent identification of Thr4826Ile in a second MHS family strongly supports a causative role for this substitution in MHS.

Taken together, this evidence strongly indicates that the Thr4826Ile mutation confers abnormal sensitivity to the SR calcium channel agonists and susceptibility to malignant hyperthermia.

6.8.2 The frequency of MHS in the population

In terms of drug sensitivity, and magnitude of muscle contractures induced by caffeine and halothane, nine discordant MHS(-) individuals registered an intermediate MHS phenotype. Intermediate contracture responses in these discordant individuals is compatible with either false positive IVCT diagnosis, or the presence of a defect at a different locus that bestows a milder IVCT phenotype. It is difficult to distinguish between these two scenarios since the invasive nature of the IVCT precludes re-testing of discordant individuals, and their clinical susceptibility can not be put to the test by exposure to triggering anaesthetics. However, strong MHS IVCT results in established negative lines of inheritance, and the clustering of MHS diagnoses in CH family members lacking a common RYR1 haplotype signalled the involvement of one or more additional MHS genes in the CHES, CHEA and CHKM branches of the family. It is possible that a second gene defect may have been spuriously introduced into various branches of the pedigree by marriage loops, since these occurred frequently in the family. Even so, the occurrence of two or more true MH genes in a single pedigree would be unlikely considering the rare incidence of MHS (estimated 1/8000 when age, sex and penetrance are taken into account [170]).

This study is not the first in which lack of concordance between a RYR1 mutation and MHS conflicted with the reported incidence of MHS. In fact, the genotype/phenotype discrepancies encountered in the CH pedigree are comparable to observations from European genetic studies in which one discordant MHS individual was observed per six to eight patients subjected to the IVCT [99,105,170,175,176,454,455]. The occurrence of MHS/MHS or MHE/MHS marriages in one third of families investigated in a European study that examined both parents was also unexpected [432], based on the assumed prevalence of MH and the reported specificity of the IVCT. The IVCT specificity was measured on a low-risk group with normal histology that was over-represented by elderly women presenting for hip replacement [97]. Therefore, spectrum bias in the selection of the control group may have underestimated the incidence of MHS IVCT results in the population [15].

6.8.3 Recommendations for future linkage analysis

Genome scans have assigned five other MHS loci in addition to RYR1 (MHS-2 to MHS-6) [29,31-33,177]. However, in these studies only two families were conclusively linked to loci other than RYR1 [31-33]. Therefore, results from these studies do not support a second major locus explaining the MH families not linked to RYR1. Instead, the RYR1 locus may have been falsely excluded in a number of families [40]. In the current study, strong evidence in favour of linkage of MHS to Thr4826Ile ($Z = 21.7$ at $\theta = 0$) was unveiled under more stringent thresholds of 0.4 g at 2 mM caf and 0.8 g at 2 5 hal. These results have widespread implications for MH genetics and challenge the involvement of major alternate MHS loci that have been proposed [31,32], yet remain elusive [456]. Linkage toRYR1 was excluded in about 50% of MHS families investigated. Overseas families in which linkage to the RYR1 locus was excluded due to one or more discordant MHS individuals should therefore be re-evaluated under more stringent diagnostic schemes to gauge the actual involvement of RYR1 in MHS.

6.8.4 Implications and recommendations for future diagnosis of MHS.

Many anesthesiologists currently opt for non-triggering anesthetics for their patients for whom there was sufficient indication of MH to warrant IVCT examination, regardless of an MHN result (N. Pollock, personal communication), entering medico-legal, if not scientific, factors in the calculation of risk [34]. The absence of the Thr4826Ile mutation in any MHN or MHE individuals corroborates with clinical reports of near-absolute IVCT sensitivity [41,43,102], and validates the accuracy of the MHN diagnosis from the NZ testing center. The positive rate of 23% more than three times the 6.4% false positive rate reported for the EMHG IVCT [97].

6.8.4.1 Diagnostic criteria

The accuracy of the halothane test is compromised by the volatile nature of this drug and the use of four halothane test concentrations compared to six different concentrations of caffeine [96]. Contracture threshold concentration and tension values correlated well for the caffeine test but not for the halothane test, as was noted in an earlier study [25]. It has been suggested that halothane elicits a contracture response by an all-or–nothing mechanism, with a higher rate of non-specific effects [40]. The CH family data supports this notion, since all carriers of the mutation registered an abnormal response at a low 0.5% halothane concentration, average tensions actually decreased between 2 % and 3 % halothane in the dose response curves. The IVCT test might be improved by including extra halothane challenge at 0.75 % and 1.5%, since the 0.5% - 1.5% test concentration range appears the most discerning range, while the 3 % challenge is ineffectual in distinguishing MHS from MHN muscle. Scrutiny of dose response patterns revealed that threshold concentrations of 1.0 % halothane and 1.5 mM caffeine would more effectively discriminate positive and negative individuals than the conventional diagnostic thresholds of 2 % halothane and 2 mM caffeine

Non-specific reactions of normal muscle to the halothane test have resulted in an unsatisfactory level of MHE(h) classification. MHE diagnoses constitute 35 % of all diagnoses from the NZ testing center and 96 % of the diagnoses in the MHE category are MHE(h) (reacting to halothane only). Additional (and probably unnecessary) muscle biopsy tests are often conducted to ascertain the true MH status of branches of a family in which MHE results occur. Consequently, the effective cost of each muscle biopsy diagnosis is significantly increased when the equivocal results are factored into the equation.

A modest increase in clinical MHS halothane cut-off point from ≥ 0.2 g to ≥ 0.4 g could reduce the incidence of indeterminate MHE(h) category from 33% of diagnoses to 12 % and markedly improve the efficiency of the IVCT. The use of a 0.4 g halothane cut-point together with the conventional 0.2 g cut-off for the 2 mM caffeine test would continue to maintain the low risk (0.008) of a false negative diagnosis (based on the multivariate normal distribution of IVCT data for the population of affected individuals).

6.8.4.2 Selection for individuals for muscle biopsy examination

A further area where the IVCT could be improved is in the selection of individuals for muscle biopsy. Testing patients in a haphazard way is not only costly, but can lead to wrong assumptions about the pattern of segregation of the disease in the family. Parents in the large Maori family have tended to avoid testing by volunteering their children for examination, in the belief that a positive diagnosis sustained by one or more children automatically ascertains their own MHS status. When generations are skipped in this way, the pre-test probability of a patient being

positive is reduced from 0.5 to 0.25. Consequently the positive predictive value of the muscle biopsy test is reduced, and the likelihood of an MHS result being erroneous increases. In fact, if several generations are skipped, the probability of an individually being falsely diagnosed susceptible exceeds the likelihood that the patient has inherited MH [457].

6.8.5 The impact of the genetic analysis of NZ MHS families

The screen for RYR1 mutations in NZ MH probands indicated that the mutations frequent in European [13,108-111,165,166] and North American families [106,107,167,168] are not common causes of MH susceptibility in NZ families. The Arg163Cys, Gly341Arg and Gly2434Arg mutations were identified in three NZ families, and were found to segregate with the MHS phenotype in each case. Accordingly, the eight early RYR1 mutations are causative of MHS in only 9% of NZ MH families. This was lower than anticipated from the investigation of European families in which these mutations accounted collectively for up to 22 % of MHS cases [25,274]. Regional specificity in the frequency and distribution of MH mutations has documented in Danish [174,336], Swedish [459] and North American studies [460].

The search for 9 new mutations in NZ families focused primarily on families that were either well-characterised (families; 94, CH, 24) or of particular clinical interest (Families 36,70 and 1). None of the new RYR1 mutations were detected in any of the individuals investigated.
The project emphasis shifted to sequence analysis of the mutation-rich regions of RYR1 cDNA from key MH families, which was highly successful; mutations were detected in four families (Family CH, 1, 36, 24) investigated in this way. Two additional mutations; His4833Tyr and Arg2454His were identified in subsequent SSCP screening of the novel mutations regions in the remaining MHS families (summarised in Table 6-12).

For the remaining 24 MHS families, RYR1 cDNA analysis could be used to search for both novel and published RYR1 mutations in MHS individuals. However, with the exception of family 4, the majority of NZ MHS families are too small to demonstrate a causative relationships for any mutations found, and MHS skeletal muscle tissue is not available in some cases.

Assuming the published and novel RYR1 mutations detected in this study are causative of MHS, the genetic analysis of RYR1 mutations in NZ MH families has revealed the molecular basis of the MH disorder in approximately 25% of NZ MH families. However, the proportion of NZ individuals for which MHS has been characterised at the molecular level is much higher, bearing in mind that the Thr4826Ile, Gly2434Arg, His4833Tyr and Gly341Arg mutations were identified in the four largest NZ MHS families (families CH, 5, 1 and 24). Members of the eight families in which RYR1 mutations were identified accounted for 51 % of the 338 IVCT tests performed at the Palmerston North testing centre in the 11 year period from May, 1987 to August 1998. Members of the CH family alone comprise 41% of the tests performed, and 43% of the 134 MHS diagnoses. It is envisaged that as with the exponential growth in the family that will occur in the next generation, the number of individuals requiring MH diagnosis will far exceed the capacity of the Palmerston North testing centre. The investigation of genetic analysis of the MH in NZ families has made a substantial contribution to the understanding and future management MH in NZ.

Table 6.12 Mutations detected in members of NZ MH families diagnosed by IVCT

Family ID	Mutation	Initial method of identification	Ref.	MH diagnosis and proportion positive for mutation		
				MHS	MHE	MHN
35	Arg163Cys	RFLP (*Bst* UI)	[13]	2 (2/2)	0	0
24	Gly341Arg	cDNA sequencing	[109]	4 (4/4)	0	1 (0/1)
5	Gly2434Arg	RFLP (*Dde* I)	[110]	5 (5/5)	4 (0/4)	3 (0/5)
36	Arg2452Trp	cDNA sequencing	novel	2 (2/2)	0	0
58	Arg2454His	SSCP exon 46	novel	1 (1/1)	0	0
20	Arg401Cys	cDNA sequencing	novel	2 (2/2)	0	0
CH	Thr4826Ile	cDNA sequencing	novel	61 (36/58)	26 (0/24)	52 (0/48)
1	His4833Tyr	SSCP exon 100	novel	2 (1/2)	4 (0/4)	2 (0/1)

MHS status was determined by IVCT testing at the Palmerston North centre according to the EMHG thresholds of ≥ 0.2 g at 2mM caffeine and 2 % halothane. The numbers in brackets refer to the proportion of individuals in each category who tested positive for the respective mutation amongst individuals for whom DNA was available. 24 individuals from the CH family and 4 individuals from family 5 who were examined by IVCT at other testing centers are not included.

6.8.6 Prospects for future genetic testing of MHS in NZ

Previously published mutations

Genetic testing of individuals from select families is now underway at Massey University. Examples of forms for DNA test requests and results are given in appendices 7.3 and 7.4. Patients from families 36, 24, and 5 (Figures 3.6, 3.8 and 5.15) who test positive for the Arg163Cys, Gly341Arg and Gly2434Arg mutations respectively may now be designated MHS and exempt muscle biopsy. Support for the involvement of these mutations in MHS was provided in the first instance by the segregation of the Arg163Cys [13,161][336,454,461], Gly341Arg [105,109,173,300] and Gly2434Arg [110,161,167] mutations in MHS families, and their absence form the normal population. Further support was obtained using calcium release assays of cultured myotubes from patients with Arg163Cys [299], biochemical studies of RyR purified from MHS muscle of patients Gly2434Arg [300] and characterisation of mutated RyR proteins expressed in cell culture [16,303]. These three mutations segregated precisely with MHS in the respective NZ families.

The major impediment to the use of simple genetic testing in MH diagnosis is that a test for a mutation segregating with MHS within a family cannot assume the same high sensitivity of the IVCT raising serious medico-legal issues. Although individuals who are negative for the RYR1 mutations will be assumed to have a risk equivalent to that of any member of the population selected at random (~1/70, 000), in practical terms, patients who have negative genetic tests are not classified MHN, and must not be exposed to triggering agents until after their MHN status has been verified by IVCT.

Novel mutations

Genetic diagnosis in the small families identified with the novel Arg401Cys, Arg2454His Arg2452Trp, and His4833Tyr mutations awaits characterisation of family members with the IVCT. The recent independent identification of the Arg401Cys in two Australian families (M. Davies, Royal Perth Hospital, personal communication) and the Arg2454His [161] and the Arg2454Cys mutations [163] in European MHS families provides additional support for their association with MHS.

Proof that the Thr4826Ile mutation is directly causative of MH, and not merely a rare, tightly linked polymorphism requires further biochemical characterization. Regardless of causality, the presence of the Thr4826Ile mutation has been shown to be an absolute indicator of MH susceptibility. In future, related individuals found positive for the mutation (by DNA sequencing) will be assumed at risk of MH without need of confirmation with a highly invasive and costly muscle biopsy test for which there is a risk (albeit extremely low) of a false-negative diagnosis. Due to the suspected segregation of an additional (and perhaps less penetrant) MHS gene defect in the family, borderline MHS individuals who lack the mutation will continue to be managed as clinically susceptible until their MHN status is established by muscle biopsy and IVCT. Nevertheless, molecular genetic screening will enable more astute selection of key subjects for examination, thereby assisting the effective identification of negative branches of the family.

6.8.7 Future study of genetic heterogeneity in the CH family

Evidence supporting the presence of a second MHS mutation segregating within the CH family is particularly apparent in the CHES branch (Figure 6-5). Inspection of the chromosome 19q-haplotype data ruled out the possibility of a common RYR1 mutation segregating within the discordant family. The next step in defining the involvement of an alternate mutation in the CHES family would be to screen discordant members for known MHS mutations in other genes. Members of the family tested negative for the published Arg1086His CACNLIA3 mutation, however a second mutation has since been reported in this gene [40].

Muscle tissue from discordant members of the CHES family has been collected, enabling the cDNA sequence analysis of other candidate genes. An important point when selecting candidate loci for further analysis is that of the proposed MHS loci on chromosomes 7q21-22[29], 3q13.1[31] 17q11-24 [30,177] and 5p [32], convincing evidence for linkage (lod score > 3.0) was obtained only for the chromosome 1q31 (CACLIA3) [33] and chromosome 3q13.1 loci [31]. Before screening any of the proposed alternate loci for a candidate mutation it would be worthwhile to perform a preliminary linkage exclusion analysis [28] using SSLP markers. After RYR1, the CACNLIA3 gene (which encodes the α_1 subunit of the DHPR) is the principal candidate gene for MHS. Highly polymorphic markers for this gene have been described [32,33,462]. If linkage to this region was not excluded by genetic recombination, CACNLIA3 cDNA could then be sequenced for a candidate mutation. If linkage to CACNLIA3 was excluded the investigation could be extended to include markers for other candidate loci. The availability of automatic fluorescence technology for SSLP genotyping would greatly assist these investigations.

Since MHS mutations were found in the CACN1A3 gene [33], the three remaining genes for the regulatory subunits of the DHPR are further candidates for MHS defects. The CACNL2A gene, encoding the α/δ subunit gene maps to chromosome 7q [29] which is in the vicinity of the proposed MHS3 locus [29]. The CACNLG gene encoding the gamma subunit [181,463] and the CACNLB1 gene for the $\beta 1$ subunit of the DHPR [180,464] both map to the proposed MHS2 locus on chromosome 17q11.2-q24 [181]. The gene for the adult muscle sodium channel (SCNA4) has also been proposed as a candidate at the MHS2 locus in North American and South African pedigrees [30], however no candidate mutations have yet been described in this gene. Genes encoding other proteins at the triad junction that interact with RyR are candidates for further study, including 12 kDa FKBP12 [465], the 81.5 kDa triadin [466] and the 26 kDa junctin [259,467]. Owing to their small size, it might prove more economical in the future to amplify and sequence their respective cDNA's, thus avoiding the expense of fluorescent primers for linkage

analysis. No candidate genes have yet been identified at proposed MHS4 (3q)[31] and MHS5 (5p) loci [32].

A common theme in the genetics of skeletal muscle myopathies is that mutations within the same ion channel gene can give rise to remarkably different phenotypes. Conversely, mutations in different ion channels may present with a final common phenotype. For example, mutations in the CACNLIA3 gene affecting the S4 voltage-sensing segments give rise to hypokalemic periodic paralysis (hypoKPP), characterised by episodic weakness associated with decreased serum potassium concentrations [183]. In contrast, a CACNLIA3 Arg1086His mutation affecting the domain II-IV linker conferred an MHS phenotype, identical to that associated with RYR1 mutations [33]. RyR1 mutations give rise to both the CCD and MHS phenotypes. HypoKPP [183], paramyotonia congenita [468], potassium activated myotonia and succinylcholine-induced masseter muscle rigidity [154] all result from defects in the sodium channel SCNA4 gene [131], while mutations in the pore-forming subunit of the chloride channel (encoded by CLCN1) cause Becker's and Thomsen's myotonia [131]. MH is a secondary complication in many of these myopathies [34]. The fact that a discordant MHS member of the CHES family presented with symptoms of muscle weakness (myotonia) and impaired reflexes suggests the MHS IVCT phenotype results from an underlying muscle disease. Therefore, it may be productive to explore genes that are mutated in well-defined neuromuscular diseases for a mutation that is unveiled as the MHS phenotype in the IVCT. In addition to SCNA4, CACNLIA3, and CLN1, other candidates include the CHRNA1 gene that encodes the acetylcholine receptor (binding site of succinylcholine) mutated in congenital myesthenic syndrome [469], and the gene for carnitine palmitoyl transferase II. Deficiencies in this enzyme are clinically associated with rhabdomyolysis, and palmitoyl carnitine activates the SR calcium channel [470], therefore, a physiological link to MH is particularly plausible in this case [34].

In some instances the expression and/or activity of other proteins involved in calcium flux may be altered to compensate for the "leaky" SR calcium channels and modify the *in vitro* and *in vivo* response of MHS muscle [303]. For example, a 115-fold reduction in the transcripts for SkM2, a specific sodium channel alpha-subunit was found in biopsy sections of muscle from MHS patients [471]. In addition, the expression of endogenous sarco(endo)plasmic reticulum calcium-ATPase (SERCA2b), is up-regulated in HEK-293 cells expressing mutated RyR1, supporting the view that the SR calcium storage capacity is increased as a compensatory response to an enhanced calcium leak [303]. Genes encoding proteins that modify the MHS phenotype may also be candidates for primary MHS mutations. The application of cDNA microarray chips in expression screens [472-474] may, in the future enable a comprehensive study of the expression patterns in MHS muscle and assist the identification of modifying genes.

6.9 IMPLICATIONS FOR THE STRUCTURE AND FUNCTION OF THE CALCIUM RELEASE CHANNEL

An explosion in the interest surrounding the ryanodine receptor family of calcium release channels has occurred in the last decade. Numerous approaches to characterisation of the structure/function relationships include primary sequence analysis for known calcium binding and transmembrane domains [126,155,192,217], homology searches for conserved folding motifs and calcium, nucleotide and protein binding domains [126,155,475], calcium overlay experiments [301,476], functional studies of mutated [16,287,299,302,303] and truncated [127] proteins, antibody binding studies [300,477] and cross-linking experiments [289,478,479]. More recently attention has focussed on the molecular interaction between RYR1 and other proteins involved in excitation-contraction coupling including the DHPR [269,275,280,480,481], triadin [266,482,483] and calsequestrin [482,484]. Reviews on the structure and functional correlates for RyR and other proteins involved in excitation-contraction coupling, can be found in the following references; [15,20,236,251,274,275].

6.9.1 RyR sequence conservation

The average identity of human RYR1, RYR2 and RYR3 is 65%, excluding two large variable regions (VR1 and 2) of low identity equivalent to residues (1298- 1428) and (4249- 4626) of RYR1 [204,207]. The variable sequence regions may underlie the different regulatory properties observed among RyR isoforms. For example, the increased sensitivity to caffeine, calcium and caffeine observed for the RyR2 isoform has been attributed to a loss of calcium inactivation sites within the variable (VR2) region [241].

Other regions of the ryanodine receptor thought to be important in channel structure function and activation are highly conserved among the RyR isoforms, particularly in the transmembrane domain [274]. The predicted secondary structure for the RyR isoforms is similar, and they have similar overall topological maps [155,204,207]. The conservation of residues involved in MHS mutations within the RyR super-family suggests functional or structural significance and has been interpreted to support a causative role for a number of RYR1 mutations identified to date [25].

Five novel mutations were identified in single NZ MHS families; Arg401Cys, Arg2452Trp, Arg2454His, Thr4826Ile and His4833Tyr. To examine whether the residues involved were conserved within the RyR family, the amino acid sequences surrounding each mutation was aligned with the corresponding published RYR1, RYR2 and RYR3 sequences from various species [155,160,192,203,205,207,211,485-488] (Table 6-10).

6.9.1.1 Conservation of residues in the N-terminal and central MHS domains

The Agr401Cys mutation was detected in a single MHS NZ family. Both Arg401 and Ile403 [13] are completely conserved across all known RyR sequences, although the adjacent upstream region is relatively poorly conserved across the RyR2 and RyR3 isoforms (Figure 6-7 A).

Arg2452 and Arg2454 were also strictly conserved (Figure 6-7 B). The substitutions at arginine 2452 and 2454 detected in this study occur in close proximity to two previously described MH mutations at arginine 2458 [169]. The clustering of four MH mutations within a seven amino acid

region, and the conservation of the three affected arginine residues across all RYR1, RYR2 and RYR3 sequences implies a critical regulatory role for the positively charged amino acids in this domain of the ryanodine receptor. Interestingly, 11 of the 13 mutations reported in the central region of the ryanodine receptor involve the loss or gain of arginine residues [25,162]. This region is thought to constitute a regulatory domain of the RYR1 calcium channel and shares homology with the central regulatory region of the IP3 calcium channel [15].

A Gln3756Glu substitution was detected in the sequence analysis of cDNA from an MHE member from the CH family. This may have contributed to mildly atypical caffeine responses noted in two other individuals and possibly a more severe MHS phenotype in compound heterozygotes that had both the Thr48326Ile and Gln3756Glu mutations on different haplotypes. A multiple sequence alignment revealed that the Gln3756Glu substitution results in a reversion of glutamine 3756 back to the "ancestral" glutamate residue found at this position in all other RyR sequences (see Figure 6-8). This would suggest that the Gln3756Glu substitution is unlikely to seriously disrupt RyR1 function, consistent with the presence of this substitution in MHE and MHN individuals from the CHEH branch of the family (Figure 4-10).

Three glutamate-rich regions within the RyR1 are thought to act as low affinity calcium binding domains [126,204]. These encompass residues 1873 – 1924, 2025-2092 and residues 3675-3758 of the RYR1 sequence [126,204,301]. Interestingly, residue Gln3756 is positioned in the third glutamate-rich region, which is highly conserved between the RyR's suggesting it, might be a common important regulatory site. The Gln3756Glu substitution also falls within potential $^{45}Ca^{+2}$ and ruthenium red-binding sites assigned to residues 3657-3776 in overlay experiments with expressed fragments of the skeletal muscle Ca2+ release channel [301].

Figure 6-7 Conservation of amino acids surrounding published and novel MHS mutations

A. Conservation of Arg401 and Ile403 among RyR isoforms

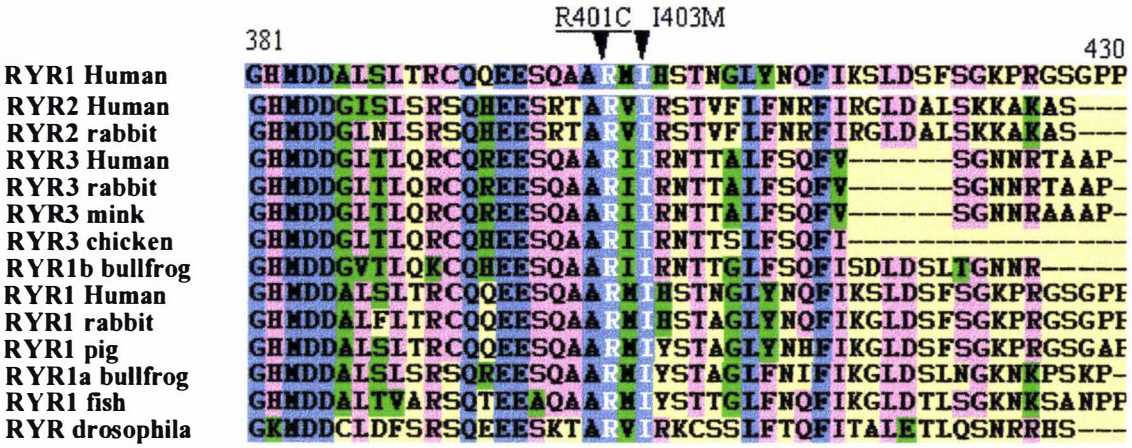

B. Conservation of sequence surrounding the published and novel (underlined) MHS mutations in the central RYR1 mutation region.

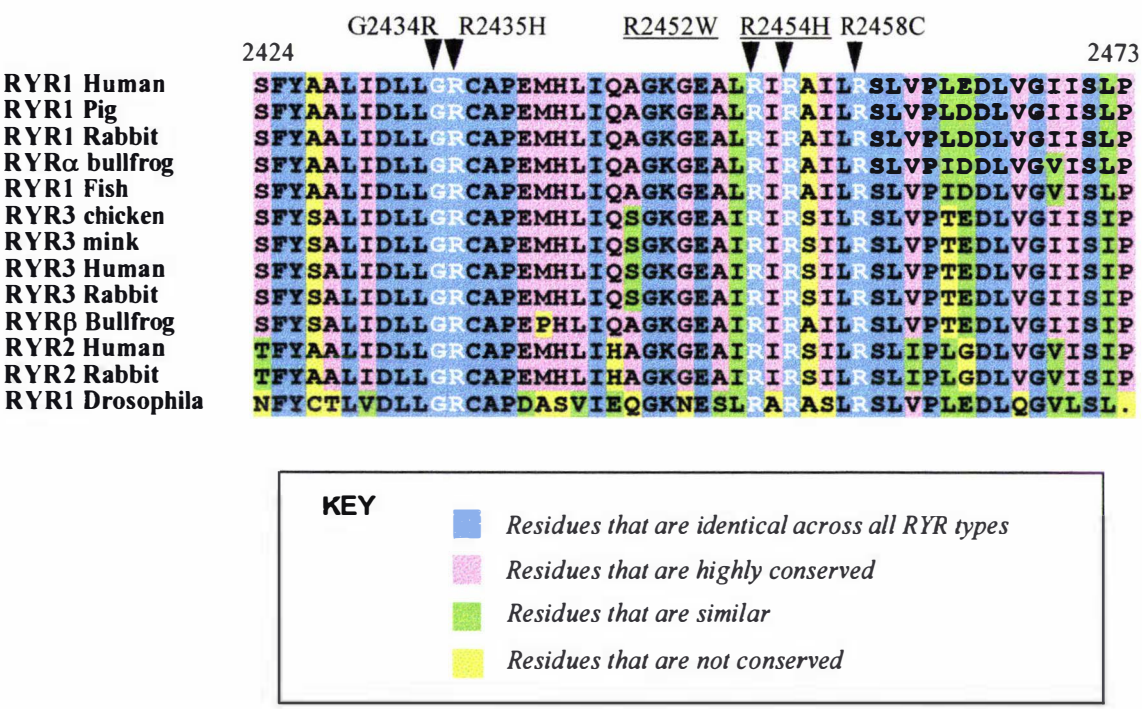

Novel substitutions identified in NZ families (Arg401Cys, Arg2452Trp and Arg2454His) are underlined. Alignments were generated with manually edited BLAST-P [489,490] output aligned with CLUTALW (www/ebi/ac/uk) [491]. CLUSTALW output was converted to multiple sequence file (msf) format using READSEQ (Don Gilbert, www.iubio.indiana.edu) and coloured with MacBoxshade software [492] according to residue group. Sequence details are provided in Table 6-10.

Figure 6-8 Glutamine 3756 in the Human RYR1 sequence is not conserved in other RyR sequences

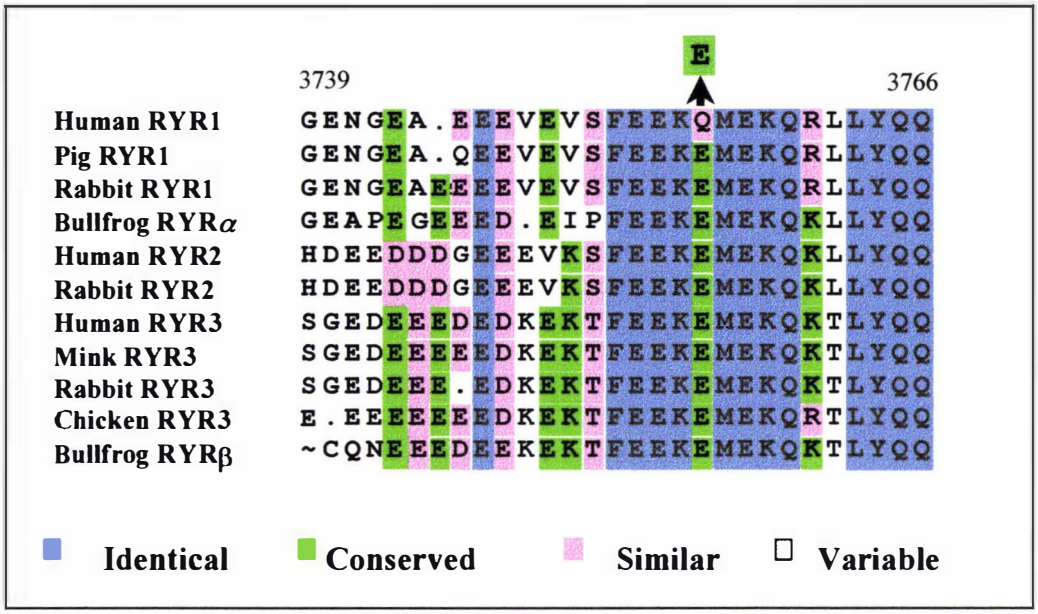

The Q3756E substitution was detected in an MHE individual from the CHEH family and does not segregate with MHS. The mutation reverts glutamine 3756 to a glutamate residue, which is maintained within a glutamate-rich region in all other RyR sequences investigated. Sequences were aligned as described in Figure 6-7. For sequence references, see Table 6-10.

Table 6-10 RyR sequence details

Sequence ID	Genbank accession number	Reference:
RYR1 human	U458508 P21817	[160]
RYR1 pig	P16960	[203]
RYR1 rabbit	226386 P11716	[155]
RYRα bullfrog	A54161 Q91383	[485]
RYR1 fish	AAB58117, Q13054	(unpublished)
RYR3 chicken	S66572, Q90985	[486]
RYR3 mink	CAA69029 Q95201	[211]
RYR3 human	NP_001027, AJ001515	[205]
RYR3 rabbit	S27272 X68650	[192]
RYRβ bullfrog	B54161 Q91319	[485]
RYR2 human	AAA93465 X98330	[487]
RYR2 rabbit	P30957 Q29621	[207]
RYR *Drosophila*	BAA41471 Q24498	[488]

6.9.1.2 Conservation of RyR transmembrane sequence

The C-terminal Thr4826Ile and His4833Tyr substitutions identified in two NZ families are positioned in the highly conserved calcium channel domain (see Figure 6-9). Flanking transmembrane domains (M2 and M3 [155]) share homology with transmembrane sequences from the IP_3 receptor, the rat sodium channel and the nicotinic acetylcholine receptor [493] M3

and M4 segments also share strong homology with the equivalent regions of the IP3 receptor and the rat sodium channel [493]. Threonine 4826 is conserved as a serine residue in the corresponding region of both the rat sodium channel and the nAchR [126,493].

Figure 6-9 Conservation of Thr4826 and His4833 and surrounding transmembrane sequence among RyR isoforms

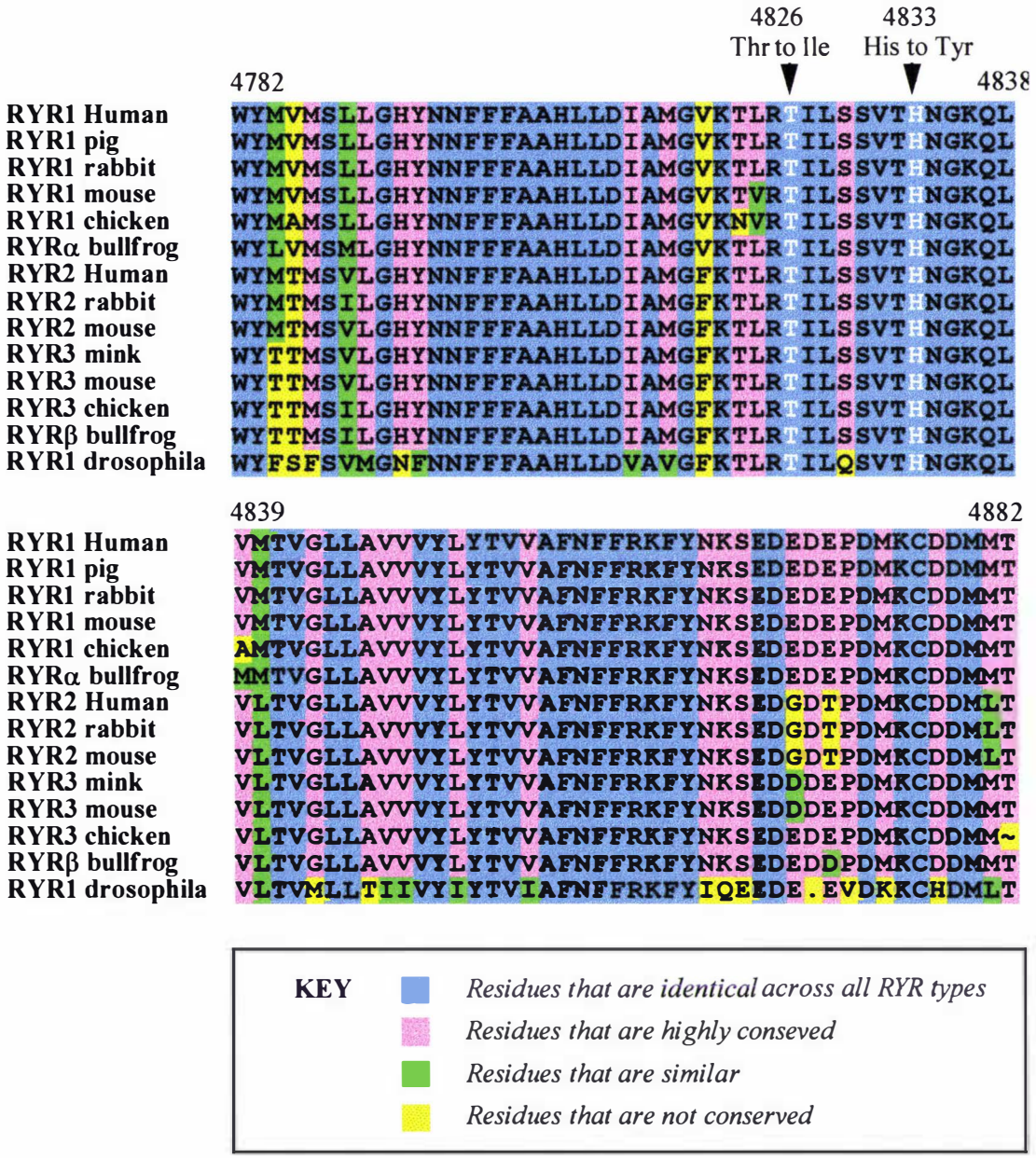

Multiple sequence alignment performed as described for Figure 6-7. Sequence details are provided in Table 6-10. Models for transmembrane topology are illustrated in Figure 6-10.

6.9.2 Molecular predictions for mutations in the C-terminal MHS domain

The majority of RyR1 MHS substitutions are clustered in two regions; in the N-terminal region of the protein between residues 35 and 614 or in the central region between residues 2163 and 2458. Shortly after the Thr4826Ile mutation was detected in the large Maori family, an isoleucine 4898 to threonine substitution was published in a Mexican family [164]. This was the only other

mutation known in the C-terminal channel region of the ryanodine receptor at this time [164]. The identification of two novel channel mutations in NZ families together with the recently described Ile4898Thr mutation [164] has now firmly establish a third MH domain, in the C-terminal region of the receptor.

6.9.2.1 The Ile4898Thr mutation

The Ile4898Thr mutation was associated with severe central core disease (CCD), a rare myopathy characterized by muscle weakness and mitochondrial depletion in the centre of the muscle cell. Studies of the expressed protein revealed increased Ca^{+2} sensitivity, and depleted Ca^{+2} stores consistent with a leaky channel and the proposed pathogenesis of the CCD disorder. Muscle of subjects harboring the Ile4898Thr substitution displayed only mildly abnormal sensitivity to these drugs in the IVCT, consistent with absence of MH events in the family despite repeated exposure to triggering anesthetics [164].

Both models of RYR1 membrane topology predicted a luminal position for the Ile4898Thr mutation [126,155], either at the end of transmembrane helix M9 in the 10-helix model [126] or in the luminal loop between transmembrane domains M3 and M4 in the 4-helix model [155], as described in Figure 6-10. Three mechanisms for the observed effects of the Ilr4898Thr mutation have been proposed [494]. Firstly, the mutation may perturb regulatory associations between RYR1 and acidic luminal proteins, such as triadin and calsequestrin [255,482,484]. However, such an effect would be unlikely to have been observed in the non-muscle expression system used by Lynch *et al.* [494]. A second possibility is that the Ile4898Thr mutation may perturb one of two proposed luminal calcium regulatory sites [494,495]. Thirdly, the M3-M4 loop may be inverted to form part of the transmembrane ion pore where the mutations may disrupt pore structure and channel ion selectivity [494]. A VGYG motif comprises the ion selectivity filter in the potassium channel [496]. An equivalent GGIG motif may act as an ion pore in RyR and IP_3 receptors [494]. Interestingly, this putative RyR1 channel pore motif encompasses Ile4898. A single substitution of alanine for glycine 4824 within the putative pore region of RyR2 reduced up ion conductance by 97%, suggesting the region constitutes an essential part of the ion conduction pathway and the ryanodine binding site [497].

The Thr4826Ile and His4833Tyr mutations described in the two Maori families study confer a profoundly different phenotype to the CCD phenotype associated with the Ile4898Thr mutation, and are the first mutations identified in the C-terminal regions of RyR1 associated with clinical MH susceptibility. There is no evidence of CCD in the Maori families and both mutations confer marked and fully penetrant sensitivity to the caffeine and halothane *in vitro* and susceptibility to MH *in vivo*. In contrast, individuals identified with the Ile4898Thr mutation recorded weak MHS IVCT responses and had not developed MH upon exposure to triggering anaesthetics [164].

6.9.2.2 The Thr4826Ile and His4833Tyr mutations

The location of the Thr4826Ile and His4833Tyr mutations with respect to ryanodine receptor channel structure can not be established without precise definition of the transmembrane topology. According to the 4-transmembrane spanning segment model, residues Thr4826 and His4833 reside in a 170-residue cytosolic loop between transmembrane sequences M2 and M3 [155](Figure 6-10 A) whereas the 10 transmembrane helix predicts an SR luminal position in a 16 residue loop between transmembrane segments M7 and M8 [126] (Figure 6-10 B). The hydropathy indices for predicted transmembrane sequences M7 and M9 are relatively weak [126], and these sections were not predicted to form transmembrane helices in the Takeshima *et al*

model. A third model predicts six transmembrane helices, in which the Zorzato *et al.* M9 domain is inverted to form a pore-forming segment between transmembrane domains M8 and M10 [497].

If residues Thr4826 and His4833 are situated within a loop on the luminal side of the membrane as predicted by the Zorzato *et. al.* model [126] (Figure 6-10 B), Thr4826Ile and His4833Tyr may disrupt possible regulatory interactions with luminal proteins as proposed for the Ile4898Thr mutation [164].

6.9.2.3 Current evidence favours a cytoplasmic location for the Thr4826Ile mutation

Images of the RyR tertiary structure from electron microscopy indicated the channel domain was large enough to accommodate 10 transmembrane helices per monomer [498]. However, combined evidence from proteolytic digests [288,499], single-channel recordings with tryptic fragments [500] antibody binding studies [218] and the formation of a functional channel by the carboxyl terminus of RyR cleaved at Arg-4475 [127,500] favours the 4-transmembrane domain model of Takeshima *et al* [155].

Proteolytic enzymes identify likely surface-exposed regions and have been employed to investigate RyR1 transmembrane topology. The tryptic cleavage sites at Arg4475 [288,499] and Arg4756 [501] and Lys-C and Glu-C cleavage sites at 4676 and 4782 [499] occurred within cytoplasmic loops according to both models, and therefore so not aid in discriminating the two models. A potential N-linked glycosylation site has been identified at asparagine 4864, which is luminal according to the Takeshima *et al.* model and cytoplasmic according to the Zorzato *et al.* model. Glycosylation would be only expected to occur if the residue is located on the luminal side of the SR membrane. Glycosylation of the RyR has not been detected in ligand overlay experiments with junctional face membrane proteins [257], however his region may be inaccessible to the ER glycosylation machinery [218].

The selective binding of antibodies raised to the 4860-4886 region to permeabilised SR vesicles indicated the region was exposed to the SR lumen. This was only compatible with the 4-transmembrane model [218]. The 10 transmembrane helix model placed the 4860-4886 region between a cytoplasmic loop and transmembrane sequence M9. In further support of the 4-transmembrane domain model, the homologous region from the IP3 receptor is luminal [218].

According to the 4-transmembrane domain model of Takeshima *et al* [155], residues Thr4826 and His4833 are positioned within a loop between transmembrane domains M2 and M3 on the cytoplasmic side of the membrane (Figure 6-10 A). The large loop encompassing threonine 4826 and histidine 4833 may therefore contain binding sites for cytosolic modulators of RyR1 activity. Alternatively, the mutations in this cytosolic loop may disrupt proposed long-range interactions [20,289] between the channel and regulatory regions within the foot domain of RyR1, and/or interactions between RyR monomers [251]. The intraluminal loops linking transmembrane segments M1-M2 and M3-M4 contain a high density of charged residues [155]. The negative surface charge at the luminal mouth of the channel might influence the ion channel and gating properties, or assist interactions with charged regions of luminal proteins, such as triadin [502]. In contrast, the M2-M3 loop including residues Thr4826 and His4833 does not include an area of concentrated charge density, in keeping a different role for this region on the cytoplasmic side of the membrane. The location of Thr4826Ile within the M2-M3 transmembrane loop on the opposite side of the SR membrane to the previously described Ile4898Thr mutation could account for the different MHS and CCD phenotypes respectively conferred by these mutations.

Figure 6-10 Relative positions of RYR1 channel mutations according to models for RyR1 transmembrane topology

A.

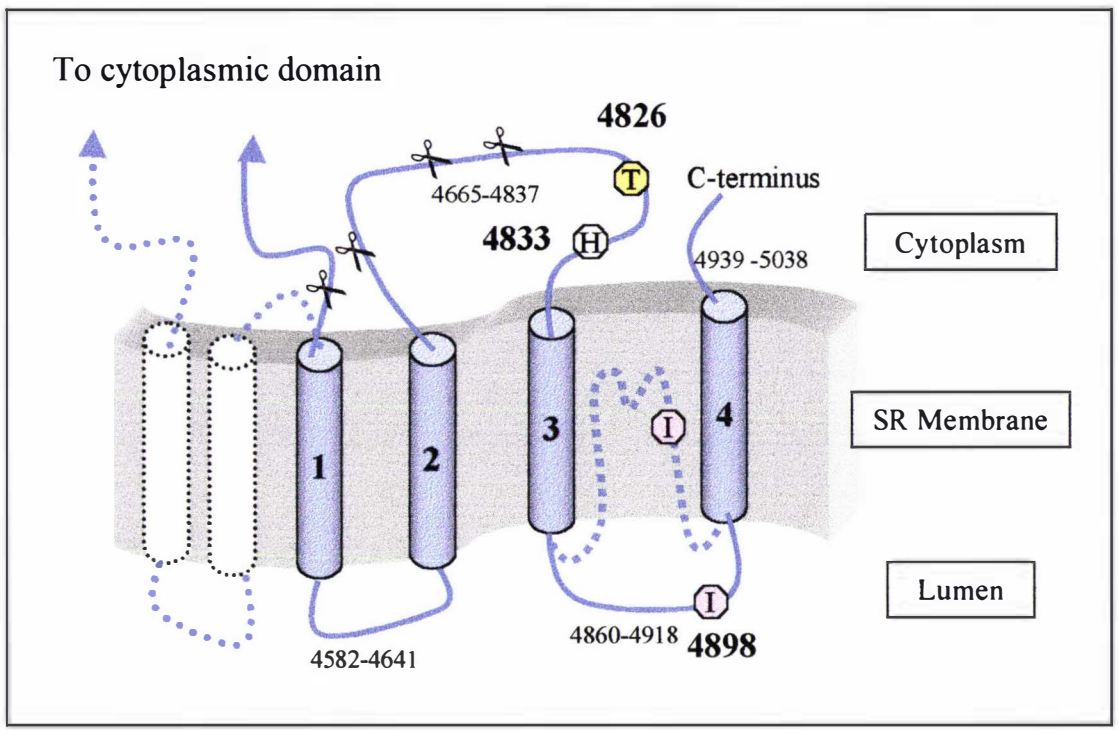

B.

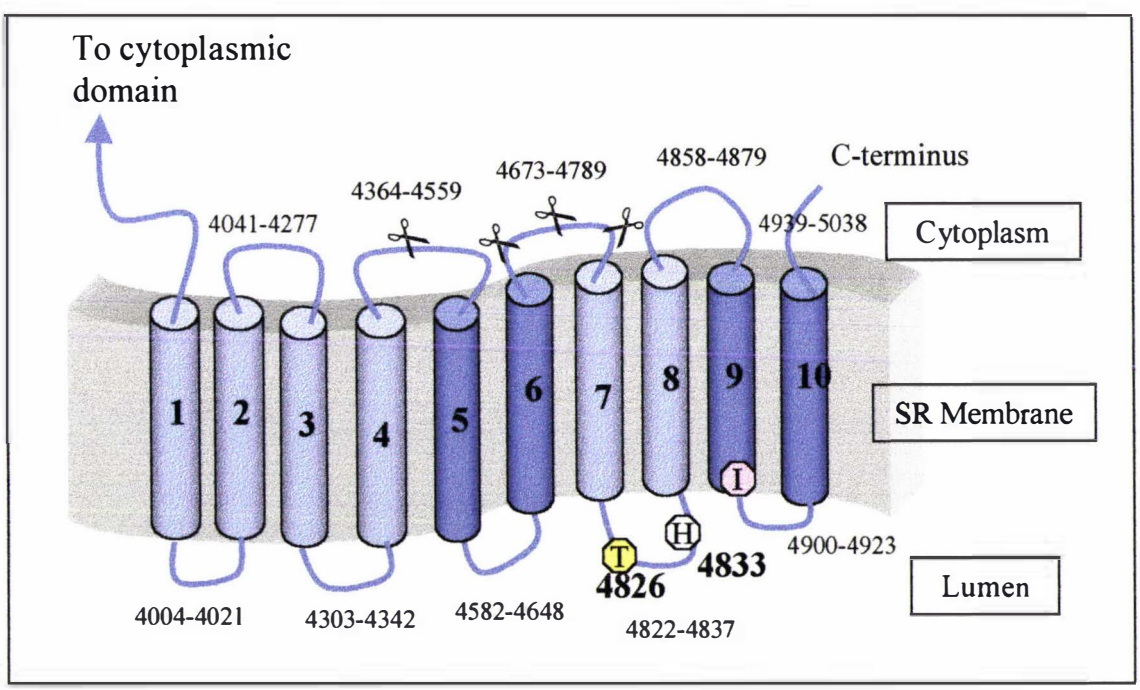

A. Blue cylinders represent the 4 TM models for the RyR1 channel membrane topology as predicted by Takeshima *et al.* [155]. Dotted lines and white cylinders depict an alternate 6 TM model, in which the M3-M4 region is a pore-forming segment [494,497]. The Thr4826Ile and His4833Tyr mutations identified in NZ Maori MHS families are positioned within a cytoplasmic loop, while the CCD Ile4898Thr mutation found in a Mexican family [164] is luminal. Scissors mark surface-exposed proteolytic cleavage sites [288,499,501].

B. 10 TM model as proposed by Zorzato *et al.* [126]. Thr4826Ile and His4833Tyr are positioned in the SR lumen. Helices 5,6,9 and 10 are common to both models.

6.9.2.4 Modulator binding sites mapped to the C-terminal RyR1 region

The C-terminal portion from residue Arg4475 contains structures sufficient to form a functional calcium release channel that activated by cytoplasmic calcium and regulated by ryanodine [127]. Both the high and low affinity binding ryanodine binding sites were positioned between Arg4475 and the C-terminus of the RyR1 [501]. In addition, three calcium binding and ruthenium red binding sites have been mapped to the carboxyl terminus of RyR1 [239,301,476], one of which was mapped to amino acids 4765 - 5038 [301], encompassing Thr4826 and His4833.

Rather than directly interfering with the modulator binding sites, RYR1 mutations may perturb protein-protein interactions, between the channel and cytoplasmic domains or between RyR monomers. Alternatively the mutations may perturb interactions with other proteins at the triad junction [251]. One of three calmodulin binding sites have been localized to residues 4534 – 4552 [249], a few residues upstream of the putative transmembrane segment M5/M1. A binding site for an EF-hand calcium binding protein (S100) [503], overlaps with the putative calmodulin binding site spanning residues 4534 to 4552 [249]. FKBP12 binding sites have been mapped to the periphery of the type 1 RyR, approximately 10 nm distant from the putative channel pore [224]. Both calmodulin and FKBP12 interact with a domain that connects directly to a cytoplasmic extension of the transmembrane assembly of the receptor, and thus might modulate channel gating indirectly. A mutation in one of the transmembrane loop regions on the cytoplasmic face of the SR membrane may perturb such interactions.

An existing destabilization of protein interactions caused by RyR channel mutations may be potentiated upon exposure to halothane, since halothane increases the fluidity of membranes and is known have a direct effect on hydrophobic protein-protein interactions between calcium regulatory proteins within skeletal muscle triads [260,504]. Halothane has been shown to induce oligomerization and activation of the skeletal muscle RyR [505]. This might trigger abnormal calcium homeostasis via oligomerization of the mutated protein causing the RyR channel to open for longer than normal channels, resulting in an increase in the cytosolic calcium concentrations sufficient to trigger the MH crisis [235,260].

In summary, current evidence favours a cytoplasmic position for the loop containing the Thr4826Ile and His4833Tyr substitutions. While various functions have been ascribed to the C-terminal region of the RyR1 protein, it is difficult to predict which of these functions, if any, might be perturbed by the C-terminal MHS mutations while the true transmembrane architecture of the channel region is unknown. There is still considerable debate in the literature as to the locations of calmodulin binding sites [249] and calcium activation and inactivation sites [241]. The mechanism by which triadic proteins; triadin, calsequestrin, junctin and the DHPR) interact with the receptor to modulate calcium release is a further area for future investigation [251]. A better understanding of the mechanism by which the novel MHS confer a hypersensitive phenotype also awaits biochemical characterisation of the mutant RyR protein.

6.10 FUTURE MOLECULAR CHARACTERISATION OF THE NOVEL THR4826ILE MUTATION

An investigation of the functional consequences of the Thr4826Ile mutation on the calcium release properties on the mutated protein at the molecular level is required to conclusively prove the mutation is directly causative of MH. A number of approaches to the molecular characterisation of MHS mutations have been described, most of which employ radiolabelled ryanodine binding assays as a means to assess the open state of the channel [235].

Biochemical studies of the porcine MHS mutation focussed on the measurement of the kinetics of calcium release, calcium inactivation and the [^{3}H]–ryanodine binding properties of heavy SR vesicles in response to clinically relevant agonists, including caffeine and halothane [17,18,506,507]. An analogous study of the human condition has been limited by the availability of muscle tissue specimens, the quality of muscle and the genetic heterogeneity within the sample population. In a single unprecedented experiment, RyR activity was examined in SR vesicles prepared from muscle tissue of patients heterozygous for the Gly2434Arg mutation. Using high affinity [^{3}H]-ryanodine binding Richter *et al.*, [300] demonstrated that this mutation enhanced the sensitivity of RYR1 to activating concentrations of calcium which was enhanced by caffeine [300]. Approximately 2.2 g of MHS tissue was used in this study [300]. The advantage of this method is that it circumvents cloning procedures, and proteins at the triadic junction that are associated with RyR are retained in the SR vesicles. Sufficient amounts of frozen tissue (stored at –20°C) was collected from MHS patients undergoing muscle biopsy. However, the SR vesicles prepared from this frozen tissue may not be comparable to vesicles prepared from tissue which had been frozen immediately in liquid nitrogen [300].

Earlier studies had investigated the ryanodine binding of solubilised RyR receptors, purified from human MHS muscle and inserted into planar lipid bilayers [295]. Single channel recordings revealed that pooled human MHS RyR displayed an unusually high sensitivity to calcium (doubled) which was augmented by caffeine and halothane [295]. However single channel recordings on human MHS muscle were highly variable due to the different populations of tetramers made up of between zero and four mutant subunits [3,19]. Furthermore, luminal or cytoplasmic components that might mediate the effects of the T4826I mutation are absent.

An alternate approach would be to measure cellular calcium homeostasis in cultured human muscle cells derived from MHS muscle tissue. This technique was used successfully to investigate muscle cells harbouring the RYR1 Arg163Cys mutation, which was shown to confer a 2-fold increase in halothane sensitivity [299]. The principal advantage of this method is that large muscle tissue specimens are not required, and the experimental system faithfully reproduces the muscle cell environment. An important component of the experiment of Censier *et al.* was the demonstration that cultured MHN muscle cells displayed the hypersensitive calcium release properties when transfected with RyR cDNA containing the Arg163Cys mutation, thus pinpointing RyR as the site of the defect [299]. With recent advances in tissue culture systems for primary muscle cells and rapid calcium imaging techniques, this approach promises to be of use in future biochemical characterisation of MHS and diagnosis.

The functional expression of mutated RyR receptors offers prospects for the molecular characterisation of MHS mutations without the requirement of human MHS muscle specimens. A

further advantage is that the effects of the mutation can be explored independently of the heterogeneous human genetic background, in which compensatory factors may modify the effects of mutations. Rabbit RYR1, cloned and expressed in Chinese hamster ovary cells (CHO) [508-510] COS cells [302,511], and HEK-293 cells [16,164,303,512-514] is modulated by endogenous and pharmacological effectors like the native channel.

A cellular calcium photometry assay, involving fluorescence imaging of fura-2-loaded cells has been exploited to measure the caffeine and halothane-induced calcium release in HEK-293 cells transfected with various mutated forms of the RYR1, corresponding to the reported RYR1 mutations [16,164,303]. These experiments revealed alterations in the sensitivity to caffeine and halothane that were associated with all but one of the mutations investigated. Furthermore, the patterns of sensitivity mirrored those observed in the IVCT even though the assay used cells of kidney origin. However a potential pitfall with the application of this method is envisaged for future characterisation of the T4826I mutation. T4826I may be located within the SR lumen where it may perturb protein interactions with muscle-specific luminal proteins (e.g. calsequestrin or triadin). Functional effects of this nature would not be reproduced in the kidney cell. A myogenic cell line (IB5) developed from homozygous RYR1-knockout primary fibroblast cell lines has been described [515]. IB5 cells can be induced to form multinucleated myotubes and express key triadic proteins, including skeletal triadin, calsequestrin, FKBP12, SERCA1, and DHPR. The IB5 cell line might prove a useful alternative to HEK-2993 cells for future functional expression of RYR1 mutations [515], particularly those located within the channel domain. A comparison of the properties of normal and mutated channels expressed in HEK-293 and IB5 cells might clarify the involvement other skeletal muscle proteins in the expression of the MHS phenotype.

A key objective in the future characterisation of RyR channel mutations is to establish the true transmembrane topography of the channel so that the cytoplasmic versus luminal position of the mutations can be unambiguously defined. Studies of the comparative binding affinities of intact and permeabilised SR vesicles to antibodies raised to the loop containing residues T4826 and H4833 mutations may shed light on the location of these mutations and discriminate, once and for all between the alternate models for the RyR receptor structure. While the large size and membraneous nature of the RyR1 tetramer is obstructive to structural determination at atomic detail using of standard X-ray crystallographic techniques, this approach may be feasible if efforts to produce ordered two dimensional crystals of individual domains prove successful. Advances in the development of cryoelectron microscopy and single-particle image processing techniques have allowed major progress to be made in the determination of the receptor's structure over the past decade [122,219,224-226,516]. This technology may soon yield more detailed information about the 3-D structure of the RyR channel domain [226].

REFERENCES

1 Denborough M, Lovell R. Anaesthetic deaths in a family. *Lancet* 1960; **2**: 45.

2 Lopez JR, Allen PD, Alamo L, Jones D, Sreter FA. Myoplasmic free [Ca2+] during a malignant hyperthermia episode in swine. *Muscle Nerve* 1988; **11**: 82-8.

3 Nelson TE. Halothane effects on human malignant hyperthermia skeletal muscle single calcium-release channels in planar lipid bilayers. *Anesthesiology* 1992; **76**: 588-95.

4 Louis CF, Zualkernan K, Roghair T, Mickelson JR. The effects of volatile anesthetics on calcium regulation by malignant hyperthermia-susceptible sarcoplasmic reticulum. *Anesthesiology* 1992; **77**: 114-25.

5 Gronert GA, Mott J, Lee J. Aetiology of malignant hyperthermia. *Br J Anaesth* 1988; **60**: 253-67.

6 Rosenberg H. Clinical presentation of malignant hyperthermia. *Br J Anaesth* 1988; **60**: 268-73.

7 Harrison GG. Pale, soft exudative pork, porcine stress syndrome and malignant hyperpyrexia--an identity? *J S Afr Vet Assoc* 1972; **43**: 57-63.

8 Kukoyi EA, Addis PB, McGrath CJ, Rempel WE, Martin FB. Porcine stress syndrome and postmortem muscle characteristics of two purebreds and three specific terminal crosses. *J Anim Sci* 1981; **52**: 278-84.

9 Ellis FR, Halsall PJ, Harriman DG. Malignant hyperpyrexia and sudden infant death syndrome. *Br J Anaesth* 1988; **60**: 28-30.

10 Allen GC. Malignant hyperthermia and associated disorders. *Curr Opin Rheumatol* 1993; **5**: 719-24.

11 Denborough M. Malignant hyperthermia. *Lancet* 1998; **352**: 1131-6.

12 Wedel DJ. Malignant hyperthermia and neuromuscular disease. *Neuromuscul Disord* 1992; **2**: 157-64.

13 Quane KA, Healy JM, Keating KE, Manning BM, Couch FJ, Palmucci LM, Doriguzzi C, Fagerlund TH, Berg K, Ording H, et al. Mutations in the ryanodine receptor gene in central core disease and malignant hyperthermia. *Nat Genet* 1993; **5**: 51-5.

14 Mulley JC, Kozman HM, Phillips HA, Gedeon AK, McCure JA, Iles DE, Gregg RG, Hogan K, Couch FJ, MacLennan DH, et al. Refined genetic localization for central core disease. *Am J Hum Genet* 1993; **52**: 398-405.

15 Loke J, MacLennan DH. Malignant hyperthermia and central core disease: disorders of Ca2+ release channels. *Am J Med* 1998; **104**: 470-86.

16 Tong J, Oyamada H, Demaurex N, Grinstein S, McCarthy TV, MacLennan DH. Caffeine and halothane sensitivity of intracellular Ca2+ release is altered by 15 calcium release channel (ryanodine receptor) mutations associated with malignant hyperthermia and/or central core disease. *J Biol Chem* 1997; **272**: 26332-9.

17 Mickelson JR, Gallant EM, Litterer LA, Johnson KM, Rempel WE, Louis CF. Abnormal sarcoplasmic reticulum ryanodine receptor in malignant hyperthermia. *J Biol Chem* 1988; **263**: 9310-5.

18 Fill M, Coronado R, Mickelson JR, Vilven J, Ma JJ, Jacobson BA, Louis CF. Abnormal ryanodine receptor channels in malignant hyperthermia. *Biophys J* 1990; **57**: 471-5.

19 Fill M, Stefani E, Nelson TE. Abnormal human sarcoplasmic reticulum Ca2+ release channels in malignant hyperthermic skeletal muscle. *Biophys J* 1991; **59**: 1085-90.

20 Franzini-Armstrong C, Protasi F. Ryanodine receptors of striated muscles: a complex channel capable of multiple interactions. *Physiol Rev* 1997; **77**: 699-729.

21 MacLennan DH, Duff C, Zorzato F, Fujii J, Phillips M, Korneluk RG, Frodis W, Britt BA, Worton RG. Ryanodine receptor gene is a candidate for predisposition to malignant hyperthermia. *Nature* 1990; **343**: 559-61.

22 McCarthy TV, Healy JM, Heffron JJ, Lehane M, Deufel T, Lehmann-Horn F, Farrall M, Johnson K. Localization of the malignant hyperthermia susceptibility locus to human chromosome 19q12-13.2. *Nature* 1990; **343**: 562-4.

23 Fujii J, Otsu K, Zorzato F, de Leon S, Khanna VK, Weiler JE, O'Brien PJ, MacLennan DH. Identification of a mutation in porcine ryanodine receptor associated with malignant hyperthermia. *Science* 1991; **253**: 448-51.

24 Otsu K, Khanna VK, Archibald AL, MacLennan DH. Cosegregation of porcine malignant hyperthermia and a probable causal mutation in the skeletal muscle ryanodine receptor gene in backcross families. *Genomics* 1991; **11**: 744-50.

25 Manning BM, Quane KA, Ording H, Urwyler A, Tegazzin V, Lehane M, O'Halloran J, Hartung E, Giblin LM, Lynch PJ, Vaughan P, Censier K, Bendixen D, Comi G, Heytens L, Monsieurs K, Fagerlund T, Wolz W, Heffron JJ, Muller CR, McCarthy TV. Identification of novel mutations in the ryanodine-receptor gene (RYR1) in malignant hyperthermia: genotype-phenotype correlation. *Am J Hum Genet* 1998; **62**: 599-609.

26 Levitt RC, Nouri N, Jedlicka AE, McKusick VA, Marks AR, Shutack JG, Fletcher JE, Rosenberg H, Meyers DA. Evidence for genetic heterogeneity in malignant hyperthermia susceptibility. *Genomics* 1991; **11**: 543-7.

27 Deufel T, Golla A, Iles D, Meindl A, Meitinger T, Schindelhauer D, DeVries A, Pongratz D, MacLennan DH, Johnson KJ, et al. Evidence for genetic heterogeneity of malignant hyperthermia susceptibility. *Am J Hum Genet* 1992; **50**: 1151-61.

28 Sudbrak R, Golla A, Hogan K, Powers P, Gregg R, Du Chesne I, Lehmann-Horn F, Deufel T. Exclusion of malignant hyperthermia susceptibility (MHS) from a putative MHS2 locus on chromosome 17q and of the alpha 1, beta 1, and gamma subunits of the dihydropyridine receptor calcium channel as candidates for the molecular defect. *Hum Mol Genet* 1993; **2**: 857-62.

29 Iles DE, Lehmann-Horn F, Scherer SW, Tsui LC, Olde Weghuis D, Suijkerbuijk RF, Heytens L, Mikala G, Schwartz A, Ellis FR, et al. Localization of the gene encoding the alpha 2/delta-subunits of the L- type voltage-dependent calcium channel to chromosome 7q and analysis of the segregation of flanking markers in malignant hyperthermia susceptible families. *Hum Mol Genet* 1994; **3**: 969-75.

30 Olckers A, Meyers DA, Meyers S, Taylor EW, Fletcher JE, Rosenberg H, Isaacs H, Levitt RC. Adult muscle sodium channel alpha-subunit is a gene candidate for malignant hyperthermia susceptibility. *Genomics* 1992; **14**: 829-31.

31 Sudbrak R, Procaccio V, Klausnitzer M, Curran JL, Monsieurs K, van Broeckhoven C, Ellis R, Heyetens L, Hartung EJ, Kozak-Ribbens G, et al. Mapping of a further malignant hyperthermia susceptibility locus to chromosome 3q13.1. *Am J Hum Genet* 1995; **56**: 684-91.

32 Robinson RL, Monnier N, Wolz W, Jurg M, Reis A, Nuernberg G, Curran JL, Monsieurs K, Stieglitz P, Heytens L, Fricker R, van Broeckhoven C, Deufel T, Hopkins PM, Lunardi J, Mueller CR. A genome wide search for susceptibility loci in three European malignant hyperthermia pedigrees. *Hum Mol Genet* 1997; **6**: 953-61.

33 Monnier N, Procaccio V, Stieglitz P, Lunardi J. Malignant-hyperthermia susceptibility is associated with a mutation of the alpha 1-subunit of the human dihydropyridine-sensitive L-type voltage-dependent calcium-channel receptor in skeletal muscle [see comments]. *Am J Hum Genet* 1997; **60**: 1316-25.

34 Hogan K. The anesthetic myopathies and malignant hyperthermias. *Curr Opin Neurol* 1998; **11**: 469-76.

35 Kalow W, Britt BA, Terreau ME, Haist C. Metabolic error of muscle metabolism after recovery from malignant hyperthermia. *Lancet* 1970; **2**: 895-8.

36 Britt BA, Locher WG, Kalow W. Hereditary aspects of malignant hyperthermia. *Can Anaesth Soc J* 1969; **16**: 89-98.

37 Britt BA, Kalow W. Malignant hyperthermia: a statistical review. *Can Anaesth Soc J* 1970; **17**: 293-315.

38 Ball SP, Johnson KJ. The genetics of malignant hyperthermia. *J Med Genet* 1993; **30**: 89-93.

39 Kalow W, Britt BA, Chan FY. Epidemiology and inheritance of malignant hyperthermia. *Int Anesthesiol Clin* 1979; **17**: 119-39.

40 Jurkat-Rott K, McCarthy T, Lehmann-Horn F. Genetics and pathogenesis of malignant hyperthermia. *Muscle and Nerve* 2000; **23**: 4-17.

41 Ording H, Hedengran AM, Skovgaard LT. Evaluation of 119 anaesthetics received after investigation for susceptibility to malignant hyperthermia. *Acta Anaesthesiol Scand* 1991; **35**: 711-6.

42 Bendixen D, Skovgaard LT, Ording H. Analysis of anaesthesia in patients suspected to be susceptible to malignant hyperthermia before diagnostic in vitro contracture test. *Acta Anaesthesiol Scand* 1997; **41**: 480-4.

43 Halsall PJ, Cain PA, Ellis FR. Retrospective analysis of anaesthetics received by patients before susceptibility to malignant hyperexia was recognised. *British Journal of Anaesthesia* 1979; **51**: 949-54.

44 Larach MG, Localio AR, Allen GC, Denborough MA, Ellis FR, Gronert GA, Kaplan RF, Muldoon SM, Nelson TE, Ording H, et al. A clinical grading scale to predict malignant hyperthermia susceptibility. *Anesthesiology* 1994; **80**: 771-9.

45 Rutberg H, Henriksson KG, Jorfeldt L, Larsson J, Martensson J, Schildt B. Metabolic changes in a case of malignant hyperthermia. *Br J Anaesth* 1983; **55**: 461-7.

46 Heffron JJ. Malignant hyperthermia: biochemical aspects of the acute episode. *Br J Anaesth* 1988; **60**: 274-8.

47 MacLennan DH, Phillips MS. Malignant hyperthermia. *Science* 1992; **256**: 789-94.

48 Kosko JR, Brandom BW, Chan KH. Masseter spasm and malignant hyperthermia: a retrospective review of a hospital-based pediatric otolaryngology practice. *Int J Pediatr Otorhinolaryngol* 1992; **23**: 45-50.

49 Kalow W, Britt BA. Drugs causing rigidity in malignant hyperthermia. *Lancet* 1973; **2**: 390-1.

50 Britt BA, Kalow W. Malignant hyperthermia: aetiology unknown. *Can Anaesth Soc J* 1970; **17**: 316-30.

51 Gronert GA. Malignant hyperthermia. *Anesthesiology* 1980; **53**: 395-423.

52 Galloway GJ, Denborough MA. Suxamethonium chloride and malignant hyperpyrexia. *Br J Anaesth* 1986; **58**: 447-50.

53 Hall GM, Lucke JN, Lister D. Proceedings: Neuromuscular blocking drugs in porcine malignant hyperthermia. *Br J Anaesth* 1976; **48**: 270-1.

54 Herrmann-Frank A, Richter M, Sarkozi S, Mohr U, Lehmann-Horn F. 4-Chloro-m-cresol, a potent and specific activator of the skeletal muscle ryanodine receptor. *Biochim Biophys Acta* 1996; **1289**: 31-40.

55 Herrmann-Frank A, Richter M, Lehmann-Horn F. 4-Chloro-m-cresol: a specific tool to distinguish between malignant hyperthermia-susceptible and normal muscle. *Biochem Pharmacol* 1996; **52**: 149-55.

56 Ording H, Glahn K, Gardi T, Fagerlund T, Bendixen D. 4-Chloro-m-cresol test--a possible supplementary test for diagnosis of malignant hyperthermia susceptibility.[see comments]. *Acta Anaesthesiol Scand* 1997; **41**: 967-72.

57 Wappler F, Roewer N, Kochling A, Braune H, Reissinger T, Schulte am Esch J. Fulminant malignant hyperthermia associated with ketoacidotic diabetic coma. *Intensive Care Med* 1996; **22**: 809-12.

58 Franks RD, Aoueille Bd, Mahowald MC, Masson N. ECT use for a patient with malignant hyperthermia. *Am J Psychiatry* 1982; **139**: 1065-6.

59 Levenson JL. Tricyclic antidepressants and malignant hyperthermia [letter; comment]. *Am J Psychiatry* 1989; **146**: 1359-60.

60 van den Hende C, Lister D, Muylle E, Ooms L, Oyaert W. Malignant hyperthermia in Belgian Landrace pigs rested or exercised before exposure to halothane. *Br J Anaesth* 1976; **48**: 821-9.

61 Denborough M, Hopkinson KC. Death caused by overheating in piglets susceptible to malignant hyperthermia [letter]. *Med J Aust* 1994; **160**: 731-2.

62 Denborough M, Hopkinson KC, O'Brien RO, Foster PS. Overheating alone can trigger malignant hyperthermia in piglets [see comments]. *Anaesth Intensive Care* 1996; **24**: 348-54.

63 Bourdon L, Canini F. On the nature of the link between malignant hyperthermia and exertional heatstroke. *Med Hypotheses* 1995; **45**: 268-70.

64 Denborough MA. Heat Stroke and Malignant Hyperthermia. *Medical Journal of Australia* 1982; **1**: 204 - 205.

65 Hopkins PM, Ellis FR, Halsall PJ. Evidence for related myopathies in exertional heat stroke and malignant hyperthermia [see comments]. *Lancet* 1991; **338**: 1491-2.

66 Jardon OM. Heat stroke, stress, and malignant hyperthermia. *Nebr Med J* 1985; **70**: 195-9.

67 Wingard DW. Malignant hyperthermia: A Human stress syndrome? *The Lancet* 1974; **2**: 1450-1.

68 Wingard DW. Letter: Malignant hyperthermia: a human stress syndrome? *Lancet* 1974; **2**: 1450-1.

69 Fletcher R, Ranklev E, Olsson AK, Leander S. Malignant hyperthermia syndrome in an anxious patient. *Br J Anaesth* 1981; **53**: 993-5.

70 Ording H, Ranklev E, Fletcher R. Investigation of malignant hyperthermia in Denmark and Sweden. *Br J Anaesth* 1984; **56**: 1183-90.
71 Denborough MA, Galloway GJ, Hopkinson KC. Malignant hyperpyrexia and sudden infant death. *Lancet* 1982; **2**: 1068-9.
72 Peterson DR, Davis N. Sudden infant death syndrome and malignant hyperthermia diathesis. *Aust. Pediatr. J.* 1986; **22 (suppl)**: 33-5.
73 Harrison GG. Control of the malignant hyperpyrexic syndrome in MHS swine by dantrolene sodium. *Br J Anaesth* 1975; **47**: 62-5.
74 Kolb ME, Horne ML, Martz R. Dantrolene in human malignant hyperthermia. *Anesthesiology* 1982; **56**: 254-62.
75 Anderson IL, Jones EW. Porcine malignant hyperthermia: effect of dantrolene sodium on in-vitro halothane-induced contraction of susceptible muscle. *Anesthesiology* 1976; **44**: 57-61.
76 Friesen CM, Brodsky JB, Dillingham MF. Successful use of dantrolene sodium in human malignant hyperthermia syndrome: a case report. *Can Anaesth Soc J* 1979; **26**: 319-21.
77 Ward A, Chaffman MO, Sorkin EM. Dantrolene. A review of its pharmacodynamic and pharmacokinetic properties and therapeutic use in malignant hyperthermia, the neuroleptic malignant syndrome and an update of its use in muscle spasticity. *Drugs* 1986; **32**: 130-68.
78 Douglas MJ, McMorland GH. The anaesthetic management of the malignant hyperthermia susceptible parturient. *Can Anaesth Soc J* 1986; **33**: 371-8.
79 Davies W, Harbitz I, Fries R, Stranzinger G, Hauge JG. Porcine malignant hyperthermia carrier detection and chromosomal assignment using a linked probe. *Anim Genet* 1988; **19**: 203-12.
80 Webb AJ. The halothane test: a practical method of eliminating porcine stress syndrome. *Vet Rec* 1980; **106**: 410-2.
81 Gallant EM, Mickelson JR, Roggow BD, Donaldson SK, Louis CF, Rempel WE. Halothane-sensitivity gene and muscle contractile properties in malignant hyperthermia. *Am J Physiol* 1989; **257**: C781-6.
82 Fletcher JE, Calvo PA, Rosenberg H. Phenotypes associated with malignant hyperthermia susceptibility in swine genotyped as homozygous or heterozygous for the ryanodine receptor mutation. *Br J Anaesth* 1993; **71**: 410-7.
83 Fletcher JE, Tripolitis L, Rosenberg H, Beech J. Malignant hyperthermia: halothane- and calcium-induced calcium release in skeletal muscle. *Biochem Mol Biol Int* 1993; **29**: 763-72.
84 Foster PS, Gesini E, Claudianos C, Hopkinson KC, Denborough MA. Inositol 1,4,5-trisphosphate phosphatase deficiency and malignant hyperpyrexia in swine. *Lancet* 1989; **2**: 124-7.
85 Duthie GG, Arthur JR. The antioxidant abnormality in the stress-susceptible pig. Effect of vitamin E supplementation. *Ann N Y Acad Sci* 1989; **570**: 322-34.
86 Rempel WE, Lu M, el Kandelgy S, Kennedy CF, Irvin LR, Mickelson JR, Louis CF. Relative accuracy of the halothane challenge test and a molecular genetic test in detecting the gene for porcine stress syndrome. *J Anim Sci* 1993; **71**: 1395-9.
87 O'Brien PJ, Shen H, Cory CR, Zhang X. Use of a DNA-based test for the mutation associated with porcine stress syndrome (malignant hyperthermia) in 10,000 breeding swine. *J Am Vet Med Assoc* 1993; **203**: 842-51.
88 O'Brien PJ, Pook HA, Klip A, Britt BA, Kalow BI, McLaughlin RN, Scott E, Elliott ME. Canine stress syndrome/malignant hyperthermia susceptibility: calcium- homeostasis defect in muscle and lymphocytes. *Res Vet Sci* 1990; **48**: 124-8.
89 Nelson TE. Malignant hyperthermia in dogs. *J Am Vet Med Assoc* 1991; **198**: 989-94.
90 Isaacs H, Barlow MB. Malignant hyperpyrexia. Further muscle studies in asymptomatic carriers identified by creatinine phosphokinase screening. *J Neurol Neurosurg Psychiatry* 1973; **36**: 228-43.
91 Britt BA, Endrenyi L, Peters PL, Kwong FH, Kadijevic L. Screening of malignant hyperthermia susceptible families by creatine phosphokinase measurement and other clinical investigations. *Can Anaesth Soc J* 1976; **23**: 263-84.
92 Paasuke RT, Brownell AK. Serum creatine kinase level as a screening test for susceptibility to malignant hyperthermia. *Jama* 1986; **255**: 769-71.
93 Ording H. Diagnosis of susceptibility to malignant hyperthermia in man. *Br J Anaesth* 1988; **60**: 287-302.

94 Ellis FR, Keaney NP, Harriman DG, Sumner DW, Kyei-Mensah K, Tyrrell JH, Hargreaves JB, Parikh RK, Mulrooney PL. Screening for malignant hyperpyrexia. *Br Med J* 1972; **3**: 559-61.

95 Britt BA. Recent advances in malignant hyperthermia. *Anesth Analg* 1972; **51**: 841-50.

96 GROUP E. A protocol for the investigation of malignant hyperpyrexia (MH) susceptibility. The European Malignant Hyperpyrexia Group. *Br J Anaesth* 1984; **56**: 1267-9.

97 Ording H, Brancadoro V, Cozzolino S, Ellis FR, Glauber V, Gonano EF, Halsall PJ, Hartung E, Heffron JJ, Heytens L, Kozak-Ribbens G, Kress H, Krivosic-Horber R, Lehmann-Horn F, Mortier W, Nivoche Y, Ranklev-Twetman E, Sigurdsson S, Snoeck M, Stieglitz P, Tegazzin V, Urwyler A, Wappler F. In vitro contracture test for diagnosis of malignant hyperthermia following the protocol of the European MH Group: results of testing patients surviving fulminant MH and unrelated low-risk subjects. The European Malignant Hyperthermia Group [see comments]. *Acta Anaesthesiol Scand* 1997; **41**: 955-66.

98 Larach MG. Standardization of the caffeine halothane muscle contracture test. North American Malignant Hyperthermia Group. *Anesth Analg* 1989; **69**: 511-5.

99 Serfas KD, Bose D, Patel L, Wrogemann K, Phillips MS, MacLennan DH, Greenberg CR. Comparison of the segregation of the RYR1 C1840T mutation with segregation of the caffeine/halothane contracture test results for malignant hyperthermia susceptibility in a large Manitoba Mennonite family [see comments]. *Anesthesiology* 1996; **84**: 322-9.

100 Ording H, Bendixen D. Sources of variability in halothane and caffeine contracture tests for susceptibility to malignant hyperthermia. *Eur J Anaesthesiol* 1992; **9**: 367-76.

101 Larach MG. Should we use muscle biopsy to diagnose malignant hyperthermia susceptibility? [editorial; comment] [see comments]. *Anesthesiology* 1993; **79**: 1-4.

102 Allen GC, Larach MG, Kunselman AR. The sensitivity and specificity of the caffeine-halothane contracture test: a report from the North American Malignant Hyperthermia Registry. The North American Malignant Hyperthermia Registry of MHAUS. *Anesthesiology* 1998; **88**: 579-88.

103 Allen GC, Rosenberg H, Fletcher JE. Safety of general anesthesia in patients previously tested negative for malignant hyperthermia susceptibility [see comments]. *Anesthesiology* 1990; **72**: 619-22.

104 Isaacs H, Badenhorst M. False-negative results with muscle caffeine halothane contracture testing for malignant hyperthermia [see comments]. *Anesthesiology* 1993; **79**: 5-9.

105 Healy JM, Quane KA, Keating KE, Lehane M, Heffron JJ, McCarthy TV. Diagnosis of malignant hyperthermia: a comparison of the in vitro contracture test with the molecular genetic diagnosis in a large pedigree. *J Med Genet* 1996; **33**: 18-24.

106 Gillard EF, Otsu K, Fujii J, Khanna VK, de Leon S, Derdemezi J, Britt BA, Duff CL, Worton RG, MacLennan DH. A substitution of cysteine for arginine 614 in the ryanodine receptor is potentially causative of human malignant hyperthermia. *Genomics* 1991; **11**: 751-5.

107 Gillard EF, Otsu K, Fujii J, Duff C, de Leon S, Khanna VK, Britt BA, Worton RG, MacLennan DH. Polymorphisms and deduced amino acid substitutions in the coding sequence of the ryanodine receptor (RYR1) gene in individuals with malignant hyperthermia. *Genomics* 1992; **13**: 1247-54.

108 Quane KA, Keating KE, Healy JM, Manning BM, Krivosic-Horber R, Krivosic I, Monnier N, Lunardi J, McCarthy TV. Mutation screening of the RYR1 gene in malignant hyperthermia: detection of a novel Tyr to Ser mutation in a pedigree with associated central cores. *Genomics* 1994; **23**: 236-9.

109 Quane KA, Keating KE, Manning BM, Healy JM, Monsieurs K, Heffron JJ, Lehane M, Heytens L, Krivosic-Horber R, Adnet P, et al. Detection of a novel common mutation in the ryanodine receptor gene in malignant hyperthermia: implications for diagnosis and heterogeneity studies. *Hum Mol Genet* 1994; **3**: 471-6.

110 Keating KE, Quane KA, Manning BM, Lehane M, Hartung E, Censier K, Urwyler A, Klausnitzer M, Muller CR, Heffron JJ, et al. Detection of a novel RYR1 mutation in four malignant hyperthermia pedigrees. *Hum Mol Genet* 1994; **3**: 1855-8.

111 Keating KE, Giblin L, Lynch PJ, Quane KA, Lehane M, Heffron JJ, McCarthy TV. Detection of a novel mutation in the ryanodine receptor gene in an Irish malignant hyperthermia pedigree: correlation of the IVCT response with the affected and unaffected haplotypes. *J Med Genet* 1997; **34**: 291-6.

112 MacKenzie AE, Allen G, Lahey D, Crossan ML, Nolan K, Mettler G, Worton RG, MacLennan DH, Korneluk R. A comparison of the caffeine halothane muscle contracture test with the molecular genetic diagnosis of malignant hyperthermia [see comments]. *Anesthesiology* 1991; **75**: 4-8.

113 Hopkins PM, Hartung E, Wappler F. Multicentre evaluation of ryanodine contracture testing in malignant hyperthermia. The European Malignant Hyperthermia Group. *Br J Anaesth* 1998; **80**: 389-94.

114 Gilly H, Musat I, Fricker R, Bittner RE, Steinbereithner K, Kress HG. Classification of malignant hyperthermia-equivocal patients by 4-chloro- M-cresol. *Anesth Analg* 1997; **85**: 149-54.

115 Hartung E, Koob M, Anetseder M, Schoemig P, Krauspe R, Hogrefe G, Engelhardt W. Malignant hyperthermia (MH) diagnostics: a comparison between the halothane-caffeine- and the ryanodine-contracture-test results in MH susceptible, normal and control muscle. *Acta Anaesthesiol Scand* 1996; **40**: 437-44.

116 Gronert GA, Milde JH, Theye RA. Role of sympathetic activity in porcine malignant hyperthermia. *Anesthesiology* 1977; **47**: 411-5.

117 Clapham DE. Calcium signaling. *Cell* 1995; **80**: 259-68.

118 Berridge MJ, Bootman MD, Lipp P. Calcium - a life and death signal. *Nature* 1998; **395**: 645-48.

119 Wingertzahn MA, Ochs RS. Control of calcium in skeletal muscle excitation-contraction coupling: implications for malignant hyperthermia. *Mol Genet Metab* 1998; **65**: 113-20.

120 Wrogemann K, Pena SD. Mitochondrial calcium overload: a general mechanism for cell necrosis in muscle diseases. *Lancet* 1976; **1**: 672-674.

121 Berridge MJ. Cell signalling. A tale of two messengers [news; comment]. *Nature* 1993; **365**: 388-9.

122 Wagenknecht T, Radermacher M. Ryanodine receptors: structure and macromolecular interactions. *Curr Opin Struct Biol* 1997; **7**: 258-65.

123 Block BA, Imagawa T, Campbell KP, Franzini-Armstrong C. Structural evidence for direct interaction between the molecular components of the transverse tubule/sarcoplasmic reticulum junction in skeletal muscle. *J Cell Biol* 1988; **107**: 2587-600.

124 Rios E, Ma JJ, Gonzalez A. The mechanical hypothesis of excitation-contraction (EC) coupling in skeletal muscle. *J Muscle Res Cell Motil* 1991; **12**: 127-35.

125 Franzini-Armstrong C. Studies of the triad. 3. Structure of the junction in fast twitch fibers. *Tissue Cell* 1972; **4**: 469-78.

126 Zorzato F, Fujii J, Otsu K, Phillips M, Green NM, Lai FA, Meissner G, MacLennan DH. Molecular cloning of cDNA encoding human and rabbit forms of the Ca2+ release channel (ryanodine receptor) of skeletal muscle sarcoplasmic reticulum. *J Biol Chem* 1990; **265**: 2244-56.

127 Bhat MB, Zhao J, Takeshima H, Ma J. Functional calcium release channel formed by the carboxyl-terminal portion of ryanodine receptor. *Biophys J* 1997; **73**: 1329-36.

128 Franzini-Armstrong C. The sarcoplasmic reticulum and the control of muscle contraction. *Faseb J* 1999; **13 Suppl 2**: S266-70.

129 Franzini-Armstrong C. Functional significance of membrane architecture in skeletal and cardiac muscle. *Soc Gen Physiol Ser* 1996; **51**: 3-18.

130 Lamb GD. DHP receptors and excitation-contraction coupling. *J Muscle Res Cell Motil* 1992; **13**: 394-405.

131 Cooper EC, Jan LY. Ion channel genes and human neurological disease: recent progress, prospects, and challenges [In Process Citation]. *Proc Natl Acad Sci U S A* 1999; **96**: 4759-66.

132 Gronert GA, White DA. Failure of norepinephrine to initiate porcine malignant hyperthermia. *Pflugers Arch* 1988; **411**: 226-8.

133 Ording H. Pathophysiology of malignant hyperthermia. *Ann Fr Anesth Reanim* 1989; **8**: 411-6.

134 Heffron JJ. Mitochondrial and plasma membrane changes in skeletal muscle in the malignant hyperthermia syndrome. *Biochem Soc Trans* 1984; **12**: 360-2.

135 Hall GM, Bendall JR, Lucke JN, Lister D. Porcine malignant hyperthermia. II: Heat production. *Br J Anaesth* 1976; **48**: 305-8.

136 Gronert GA, Ahern CP, Milde JH, White RD. Effect of CO2, calcium, digoxin, and potassium on cardiac and skeletal muscle metabolism in malignant hyperthermia susceptible swine. *Anesthesiology* 1986; **64**: 24-8.

137 Harrison GG. Control of the malignant hyperpyrexic syndrome in MHS swine by dantrolene sodium. 1975 [classical article]. *Br J Anaesth* 1998; **81**: 626-9; discussion 625.

138 Harrison GG. Malignant hyperthermia. Dantrolene--dynamics and kinetics. *Br J Anaesth* 1988; **60**: 279-86.
139 King JO, Denborough MA. Anesthetic-induced malignant hyperpyrexia in children. *J Pediatr* 1973; **83**: 37-40.
140 Isaacs H, Badenhorst ME. Dominantly inherited malignant hyperthermia (MH) in the King-Denborough syndrome. *Muscle Nerve* 1992; **15**: 740-2.
141 Chitayat D, Hodgkinson KA, Ginsburg O, Dimmick J, Watters GV. King syndrome: a genetically heterogenous phenotype due to congenital myopathies. *Am J Med Genet* 1992; **43**: 954-6.
142 Shuaib A, Paasuke RT, Brownell KW. Central core disease. Clinical features in 13 patients. *Medicine (Baltimore)* 1987; **66**: 389-96.
143 De Cauwer H, Heytens L, Lubke U, Ceuterick C, Martin JJ. Discordant light microscopic, electron microscopic, and in vitro contracture study findings in a family with central core disease. *Clin Neuropathol* 1997; **16**: 237-42.
144 Ma JS, Mak SC, Liu AM, Yang MT, Chi CS. Central core disease associated with scoliosis: report of one case. *Chung Hua Min Kuo Hsiao Erh Ko I Hsueh Hui Tsa Chih* 1997; **38**: 297-9.
145 Heiman-Patterson TD, Natter HM, Rosenberg HR, Fletcher JE, Tahmoush AJ. Malignant hyperthermia susceptibility in X-linked muscle dystrophies. *Pediatr Neurol* 1986; **2**: 356-8.
146 Marchildon MB. Malignant hyperthermia. Current concepts. *Arch Surg* 1982; **117**: 349-51.
147 Wappler F, Scholz J, von Richthofen V, Fiege M, Kochling A, Matschke J, Winkler G, Schulte am Esch J. [Incidence of disposition for malignant hyperthermia in patients with neuromuscular diseases]. *Anasthesiol Intensivmed Notfallmed Schmerzther* 1998; **33**: 373-80.
148 Smith CL, Bush GH. Anaesthesia and progressive muscular dystrophy. *Br J Anaesth* 1985; **57**: 1113-8.
149 Stelzner J, Kretz FJ, Rieger A, Reinhart K. [Anesthetic-induced heart arrest. A case report of 2 infants with previously unrecognized muscular dystrophy]. *Anaesthesist* 1993; **42**: 44-6.
150 Heiman-Patterson TD, Rosenberg H, Fletcher JE, Tahmoush AJ. Halothane-caffeine contracture testing in neuromuscular diseases. *Muscle Nerve* 1988; **11**: 453-7.
151 George AL, Jr. Molecular genetics of ion channel diseases. *Kidney Int* 1995; **48**: 1180-90.
152 Lehmann-Horn F, Jurkat-Rott K. Voltage-gated ion channels and hereditary disease. *Physiol Rev* 1999; **79**: 1317-72.
153 Greenberg DA. Calcium channels in neurological disease. *Ann Neurol* 1997; **42**: 275-82.
154 Vita GM, Olckers A, Jedlicka AE, George AL, Heiman-Patterson T, Rosenberg H, Fletcher JE, Levitt RC. Masseter muscle rigidity associated with glycine1306-to-alanine mutation in the adult muscle sodium channel alpha-subunit gene [see comments]. *Anesthesiology* 1995; **82**: 1097-103.
155 Takeshima H, Nishimura S, Matsumoto T, Ishida H, Kangawa K, Minamino N, Matsuo H, Ueda M, Hanaoka M, Hirose T, et al. Primary structure and expression from complementary DNA of skeletal muscle ryanodine receptor. *Nature* 1989; **339**: 439-45.
156 MacKenzie AE, Korneluk RG, Zorzato F, Fujii J, Phillips M, Iles D, Wieringa B, Leblond S, Bailly J, Willard HF, et al. The human ryanodine receptor gene: its mapping to 19q13.1, placement in a chromosome 19 linkage group, and exclusion as the gene causing myotonic dystrophy. *Am J Hum Genet* 1990; **46**: 1082-9.
157 Harbitz I, Chowdhary B, Thomsen PD, Davies W, Kaufmann U, Kran S, Gustavsson I, Christensen K, Hauge JG. Assignment of the porcine calcium release channel gene, a candidate for the malignant hyperthermia locus, to the 6p11----q21 segment of chromosome 6. *Genomics* 1990; **8**: 243-8.
158 Hogan K, Couch F, Powers PA, Gregg RG. A cysteine-for-arginine substitution (R614C) in the human skeletal muscle calcium release channel cosegregates with malignant hyperthermia. *Anesth Analg* 1992; **75**: 441-8.
159 Quane KA, Keating KE, Healy JM, Heffron JJ, Lehane M, Krivosic-Horber R, Heytens L, McCarthy TV. Haplotype analysis of the BYR1 gene in malignant hyperthermia and central core disease. *Biochem Soc Trans* 1995; **23**: 372S.
160 Phillips MS, Fujii J, Khanna VK, DeLeon S, Yokobata K, de Jong PJ, MacLennan DH. The structural organization of the human skeletal muscle ryanodine receptor (RYR1) gene. *Genomics* 1996; **34**: 24-41.

161 Barone V, Massa O, Intravaia E, Bracco A, Di Martino A, Tegazzin V, Cozzolino S, Sorrentino V. Mutation screening of the RYR1 gene and identification of two novel mutations in Italian malignant hyperthermia families. *J Med Genet* 1999; **36**: 115-8.

162 Brandt A, Schleithoff L, Jurkat-Rott K, Klingler W, Baur C, Lehmann-Horn F. Screening of the ryanodine receptor gene in 105 malignant hyperthermia families: novel mutations and concordance with the in vitro contracture test [In Process Citation]. *Hum Mol Genet* 1999; **8**: 2055-62.

163 Gencik M, Gencik A, Mortier W, Epplen JT. Novel mutation in the RYR1 gene (R2454C) in a patient with malignant hyperthermia. *Hum Mutat (Online)* 2000; **15**: 122.

164 Lynch PJ, Tong J, Lehane M, Mallet A, Giblin L, Heffron JJ, Vaughan P, Zafra G, MacLennan DH, McCarthy TV. A mutation in the transmembrane/luminal domain of the ryanodine receptor is associated with abnormal Ca2+ release channel function and severe central core disease [see comments]. *Proc Natl Acad Sci U S A* 1999; **96**: 4164-9.

165 Lynch PJ, Krivosic-Horber R, Reyford H, Monnier N, Quane K, Adnet P, Haudecoeur G, Krivosic I, McCarthy T, Lunardi J. Identification of heterozygous and homozygous individuals with the novel RYR1 mutation Cys35Arg in a large kindred [see comments]. *Anesthesiology* 1997; **86**: 620-6.

166 Quane KA, Ording H, Keating KE, Manning BM, Heine R, Bendixen D, Berg K, Krivosic-Horber R, Lehmann-Horn F, Fagerlund T, McCarthy TV. Detection of a novel mutation at amino acid position 614 in the ryanodine receptor in malignant hyperthermia. *Br J Anaesth* 1997; **79**: 332-7.

167 Phillips MS, Khanna VK, De Leon S, Frodis W, Britt BA, MacLennan DH. The substitution of Arg for Gly2433 in the human skeletal muscle ryanodine receptor is associated with malignant hyperthermia. *Hum Mol Genet* 1994; **3**: 2181-6.

168 Zhang Y, Chen HS, Khanna VK, De Leon S, Phillips MS, Schappert K, Britt BA, Browell AK, MacLennan DH. A mutation in the human ryanodine receptor gene associated with central core disease. *Nat Genet* 1993; **5**: 46-50.

169 Manning BM, Quane KA, Lynch PJ, Urwyler A, Tegazzin V, Krivosic-Horber R, Censier K, Comi G, Adnet P, Wolz W, Lunardi J, Muller CR, McCarthy TV. Novel mutations at a CpG dinucleotide in the ryanodine receptor in malignant hyperthermia. *Hum Mutat* 1998; **11**: 45-50.

170 Adeokun AM, West SP, Ellis FR, Halsall PJ, Hopkins PM, Foroughmand AM, Iles DE, Robinson RL, Stewart AD, Curran JL. The G1021A substitution in the RYR1 gene does not cosegregate with malignant hyperthermia susceptibility in a British pedigree. *Am J Hum Genet* 1997; **60**: 833-41.

171 Steinfath M, Singh S, Scholz J, Becker K, Lenzen C, Wappler F, Kochling A, Roewer N, Schulte am Esch J. C1840-T mutation in the human skeletal muscle ryanodine receptor gene: frequency in northern German families susceptible to malignant hyperthermia and the relationship to in vitro contracture response. *J Mol Med* 1995; **73**: 35-40.

172 MacLennan DH. Discordance between phenotype and genotype in malignant hyperthermia. *Curr Opin Neurol* 1995; **8**: 397-401.

173 Monsieurs KG, Van Broeckhoven C, Martin JJ, Van Hoof VO, Heytens L. Gly341Arg mutation indicating malignant hyperthermia susceptibility: specific cause of chronically elevated serum creatine kinase activity. *J Neurol Sci* 1998; **154**: 62-5.

174 Fagerlund T, Ording H, Bendixen D, Islander G, Ranklev-Twetman E, Berg K. RYR mutation G1021A (Gly341Arg) is not frequent in Danish and Swedish families with malignant hyperthermia susceptibility. *Clin Genet* 1996; **49**: 186-8.

175 Deufel T, Sudbrak R, Feist Y, Rubsam B, Du Chesne I, Schafer KL, Roewer N, Grimm T, Lehmann-Horn F, Hartung EJ, et al. Discordance, in a malignant hyperthermia pedigree, between in vitro contracture-test phenotypes and haplotypes for the MHS1 region on chromosome 19q12-13.2, comprising the C1840T transition in the RYR1 gene [published erratum appears in Am J Hum Genet 1995 Aug;57(2):520]. *Am J Hum Genet* 1995; **56**: 1334-42.

176 Fagerlund TH, Ording H, Bendixen D, Islander G, Ranklev Twetman E, Berg K. Discordance between malignant hyperthermia susceptibility and RYR1 mutation C1840T in two Scandinavian MH families exhibiting this mutation. *Clin Genet* 1997; **52**: 416-21.

177 Levitt RC, Olckers A, Meyers S, Fletcher JE, Rosenberg H, Isaacs H, Meyers DA. Evidence for the localization of a malignant hyperthermia susceptibility locus (MHS2) to human chromosome 17q. *Genomics* 1992; **14**: 562-6.

178 Iles DE, Segers B, Heytens L, Sengers RC, Wieringa B. High-resolution physical mapping of four microsatellite repeat markers near the RYR1 locus on chromosome 19q13.1 and apparent exclusion

of the MHS locus from this region in two malignant hyperthermia susceptible families. *Genomics* 1992; **14**: 749-54.

179 Pessah IN, Lynch C, 3rd, Gronert GA. Complex pharmacology of malignant hyperthermia [editorial]. *Anesthesiology* 1996; **84**: 1275-9.

180 Iles DE, Segers B, Sengers RC, Monsieurs K, Heytens L, Halsall PJ, Hopkins PM, Ellis FR, Hall-Curran JL, Stewart AD, et al. Genetic mapping of the beta 1- and gamma-subunits of the human skeletal muscle L-type voltage-dependent calcium channel on chromosome 17q and exclusion as candidate genes for malignant hyperthermia susceptibility. *Hum Mol Genet* 1993; **2**: 863-8.

181 Iles DE, Segers B, Weghuis DO, Suikerbuijk R, Wieringa B. Localization of the gamma-subunit of the skeletal muscle L-type voltage- dependent calcium channel gene (CACNLG) to human chromosome band 17q24 by in situ hybridization and identification of a polymorphic repetitive DNA sequence at the gene locus. *Cytogenet Cell Genet* 1993; **64**: 227-30.

182 Iles DE, Segers B, Olde Weghuis D, Suijkerbuijk R, Mikala G, Schwartz A, Wieringa B. Refined localization of the alpha 1-subunit of the skeletal muscle L- type voltage-dependent calcium channel (CACNL1A3) to human chromosome 1q32 by in situ hybridization. *Genomics* 1994; **19**: 561-3.

183 Ptacek LJ, Tawil R, Griggs RC, Engel AG, Layzer RB, Kwiecinski H, McManis PG, Santiago L, Moore M, Fouad G, et al. Dihydropyridine receptor mutations cause hypokalemic periodic paralysis. *Cell* 1994; **77**: 863-8.

184 Brownell AK. Malignant hyperthermia: relationship to other diseases. *Br J Anaesth* 1988; **60**: 303-8.

185 Curran JL, Hall WJ, Halsall PJ, Hopkins PM, Iles DE, Markham AF, McCall SH, Robinson RL, West SP, Bridges LR, Ellis FR. Segregation of malignant hyperthermia, central core disease and chromosome 19 markers. *Br J Anaesth* 1999; **83**: 217-22.

186 Fagerlund TH, Islander G, Ranklev-Twetman E, Berg K. Recombination between the postulated CCD/MHE/MHS locus and RYR1 gene markers. *Clin Genet* 1996; **50**: 455-8.

187 Otsu K, Fujii J, Periasamy M, Difilippantonio M, Uppender M, Ward DC, MacLennan DH. Chromosome mapping of five human cardiac and skeletal muscle sarcoplasmic reticulum protein genes. *Genomics* 1993; **17**: 507-9.

188 Sorrentino V, Giannini G, Malzac P, Mattei MG. Localization of a novel ryanodine receptor gene (RYR3) to human chromosome 15q14-q15 by in situ hybridization. *Genomics* 1993; **18**: 163-5.

189 Kuwajima G, Futatsugi A, Niinobe M, Nakanishi S, Mikoshiba K. Two types of ryanodine receptors in mouse brain: skeletal muscle type exclusively in Purkinje cells and cardiac muscle type in various neurons. *Neuron* 1992; 9: 1133-42.

190 Furuichi T, Furutama D, Hakamata Y, Nakai J, Takeshima H, Mikoshiba K. Multiple types of ryanodine receptor/Ca2+ release channels are differentially expressed in rabbit brain. *J Neurosci* 1994; **14**: 4794-805.

191 Sei Y, Gallagher KL, Basile AS. Skeletal muscle type ryanodine receptor is involved in calcium signaling in human B lymphocytes. *J Biol Chem* 1999; **274**: 5995-6002.

192 Hakamata Y, Nakai J, Takeshima H, Imoto K. Primary structure and distribution of a novel ryanodine receptor/calcium release channel from rabbit brain. *FEBS Lett* 1992; **312**: 229-35.

193 Giannini G, Clementi E, Ceci R, Marziali G, Sorrentino V. Expression of a ryanodine receptor-Ca2+ channel that is regulated by TGF-beta. *Science* 1992; **257**: 91-4.

194 Giannini G, Sorrentino V. Molecular structure and tissue distribution of ryanodine receptors calcium channels. *Med Res Rev* 1995; **15**: 313-23.

195 Murayama T, Ogawa Y. Characterization of type 3 ryanodine receptor (RyR3) of sarcoplasmic reticulum from rabbit skeletal muscles. *J Biol Chem* 1997; **272**: 24030-7.

196 Witcher DR, Strifler BA, Jones LR. Cardiac-specific phosphorylation site for multifunctional Ca2+/calmodulin-dependent protein kinase is conserved in the brain ryanodine receptor. *J Biol Chem* 1992; **267**: 4963-7.

197 McPherson PS, Campbell KP. Characterization of the major brain form of the ryanodine receptor/Ca2+ release channel. *J Biol Chem* 1993; **268**: 19785-90.

198 Hakamata Y, Nishimura S, Nakai J, Nakashima Y, Kita T, Imoto K. Involvement of the brain type of ryanodine receptor in T-cell proliferation. *FEBS Lett* 1994; **352**: 206-10.

199 Guse AH, da Silva CP, Berg I, Skapenko AL, Weber K, Heyer P, Hohenegger M, Ashamu GA, Schulze-Koops H, Potter BV, Mayr GW. Regulation of calcium signalling in T lymphocytes by the second messenger cyclic ADP-ribose. *Nature* 1999; **398**: 70-3.

200 Airey JA, Grinsell MM, Jones LR, Sutko JL, Witcher D. Three ryanodine receptor isoforms exist in avian striated muscles. *Biochemistry* 1993; **32**: 5739-45.
201 Flucher BE, Conti A, Takeshima H, Sorrentino V. Type 3 and type 1 ryanodine receptors are localized in triads of the same mammalian skeletal muscle fibers. *J Cell Biol* 1999; **146**: 621-30.
202 Bertocchini F, Ovitt CE, Conti A, Barone V, Scholer HR, Bottinelli R, Reggiani C, Sorrentino V. Requirement for the ryanodine receptor type 3 for efficient contraction in neonatal skeletal muscles. *Embo J* 1997; **16**: 6956-63.
203 Harbitz I, Kristensen T, Bosnes M, Kran S, Davies W. DNA sequence of the skeletal muscle calcium release channel cDNA and verification of the Arg615----Cys615 mutation, associated with porcine malignant hyperthermia, in Norwegian landrace pigs. *Anim Genet* 1992; **23**: 395-402.
204 Tunwell RE, Wickenden C, Bertrand BM, Shevchenko VI, Walsh MB, Allen PD, Lai FA. The human cardiac muscle ryanodine receptor-calcium release channel: identification, primary structure and topological analysis. *Biochem J* 1996; **318**: 477-87.
205 Nakashima Y, Nishimura S, Maeda A, Barsoumian EL, Hakamata Y, Nakai J, Allen PD, Imoto K, Kita T. Molecular cloning and characterization of a human brain ryanodine receptor. *FEBS Lett* 1997; **417**: 157-62.
206 Leeb T, Brenig B. cDNA cloning and sequencing of the human ryanodine receptor type 3 (RYR3) reveals a novel alternative splice site in the RYR3 gene. *FEBS Lett* 1998; **423**: 367-70.
207 Otsu K, Willard HF, Khanna VK, Zorzato F, Green NM, MacLennan DH. Molecular cloning of cDNA encoding the Ca2+ release channel (ryanodine receptor) of rabbit cardiac muscle sarcoplasmic reticulum. *J Biol Chem* 1990; **265**: 13472-83.
208 Zucchi R, Ronca-Testoni S. The sarcoplasmic reticulum Ca2+ channel/ryanodine receptor: modulation by endogenous effectors, drugs and disease states. *Pharmacol Rev* 1997; **49**: 1-51.
209 Futatsugi A, Kuwajima G, Mikoshiba K. Tissue-specific and developmentally regulated alternative splicing in mouse skeletal muscle ryanodine receptor mRNA. *Biochem J* 1995; **305**: 373-8.
210 Miyatake R, Furukawa A, Matsushita M, Iwahashi K, Nakamura K, Ichikawa Y, Suwaki H. Tissue-specific alternative splicing of mouse brain type ryanodine receptor/calcium release channel mRNA. *FEBS Lett* 1996; **395**: 123-6.
211 Marziali G, Rossi D, Giannini G, Charlesworth A, Sorrentino V. cDNA cloning reveals a tissue specific expression of alternatively spliced transcripts of the ryanodine receptor type 3 (RyR3) calcium release channel. *FEBS Lett* 1996; **394**: 76-82.
212 Takeshima H, Iino M, Takekura H, Nishi M, Kuno J, Minowa O, Takano H, Noda T. Excitation-contraction uncoupling and muscular degeneration in mice lacking functional skeletal muscle ryanodine-receptor gene. *Nature* 1994; **369**: 556-9.
213 Balschun D, Wolfer DP, Bertocchini F, Barone V, Conti A, Zuschratter W, Missiaen L, Lipp HP, Frey JU, Sorrentino V. Deletion of the ryanodine receptor type 3 (RyR3) impairs forms of synaptic plasticity and spatial learning. *Embo J* 1999; **18**: 5264-73.
214 Tarroni P, Rossi D, Conti A, Sorrentino V. Expression of the ryanodine receptor type 3 calcium release channel during development and differentiation of mammalian skeletal muscle cells. *J Biol Chem* 1997; **272**: 19808-13.
215 Barone V, Bertocchini F, Bottinelli R, Protasi F, Allen PD, Franzini Armstrong C, Reggiani C, Sorrentino V. Contractile impairment and structural alterations of skeletal muscles from knockout mice lacking type 1 and type 3 ryanodine receptors. *FEBS Lett* 1998; **422**: 160-4.
216 Takeshima H, Komazaki S, Hirose K, Nishi M, Noda T, Iino M. Embryonic lethality and abnormal cardiac myocytes in mice lacking ryanodine receptor type 2. *Embo J* 1998; **17**: 3309-16.
217 Nakai J, Imagawa T, Hakamat Y, Shigekawa M, Takeshima H, Numa S. Primary structure and functional expression from cDNA of the cardiac ryanodine receptor/calcium release channel. *FEBS Lett* 1990; **271**: 169-77.
218 Grunwald R, Meissner G. Lumenal sites and C terminus accessibility of the skeletal muscle calcium release channel (ryanodine receptor). *J Biol Chem* 1995; **270**: 11338-47.
219 Radermacher M, Rao V, Grassucci R, Frank J, Timerman AP, Fleischer S, Wagenknecht T. Cryo-electron microscopy and three-dimensional reconstruction of the calcium release channel/ryanodine receptor from skeletal muscle. *J Cell Biol* 1994; **127**: 411-23.

220 Serysheva, II, Orlova EV, Chiu W, Sherman MB, Hamilton SL, van Heel M. Electron cryomicroscopy and angular reconstitution used to visualize the skeletal muscle calcium release channel. *Nat Struct Biol* 1995; **2**: 18-24.

221 Serysheva, II, Schatz M, van Heel M, Chiu W, Hamilton SL. Structure of the skeletal muscle calcium release channel activated with Ca2+ and AMP-PCP. *Biophys J* 1999; **77**: 1936-44.

222 Samso M, Trujillo R, Gurrola GB, Valdivia HH, Wagenknecht T. Three-dimensional location of the imperatoxin A binding site on the ryanodine receptor. *J Cell Biol* 1999; **146**: 493-9.

223 Wagenknecht T, Berkowitz J, Grassucci R, Timerman AP, Fleischer S. Localization of calmodulin binding sites on the ryanodine receptor from skeletal muscle by electron microscopy. *Biophys J* 1994; **67**: 2286-95.

224 Wagenknecht T, Grassucci R, Berkowitz J, Wiederrecht GJ, Xin HB, Fleischer S. Cryoelectron microscopy resolves FK506-binding protein sites on the skeletal muscle ryanodine receptor. *Biophys J* 1996; **70**: 1709-15.

225 Wagenknecht T, Radermacher M, Grassucci R, Berkowitz J, Xin HB, Fleischer S. Locations of calmodulin and FK506-binding protein on the three- dimensional architecture of the skeletal muscle ryanodine receptor. *J Biol Chem* 1997; **272**: 32463-71.

226 Samso M, Wagenknecht T. Contributions of electron microscopy and single-particle techniques to the determination of the ryanodine receptor three-dimensional structure. *J Struct Biol* 1998; **121**: 172-80.

227 Takagi A, Sunohara N, Ishihara T, Nonaka I, Sugita H. Malignant hyperthermia and related neuromuscular diseases: caffeine contracture of the skinned muscle fibers. *Muscle Nerve* 1983; **6**: 510-4.

228 Donaldson SK, Gallant EM, Huetteman DA. Skeletal muscle excitation-contraction coupling. I. Transverse tubule control of peeled fiber Ca2+-induced Ca2+ release in normal and malignant hyperthermic muscles. *Pflugers Arch* 1989; **414**: 15-23.

229 Meissner G, el-Hashem A. Ryanodine as a functional probe of the skeletal muscle sarcoplasmic reticulum Ca2+ release channel. *Mol Cell Biochem* 1992; **114**: 119-23.

230 Coronado R, Morrissette J, Sukhareva M, Vaughan DM. Structure and function of ryanodine receptors. *Am J Physiol* 1994; **266**: C1485-504.

231 Meissner G. Ryanodine receptor/Ca2+ release channels and their regulation by endogenous effectors. *Annu Rev Physiol* 1994; **56**: 485-508.

232 Meissner G, Rios E, Tripathy A, Pasek DA. Regulation of skeletal muscle Ca2+ release channel (ryanodine receptor) by Ca2+ and monovalent cations and anions. *J Biol Chem* 1997; **272**: 1628-38.

233 Melzer W, Herrmann-Frank A, Luttgau HC. The role of Ca2+ ions in excitation-contraction coupling of skeletal muscle fibres. *Biochim Biophys Acta* 1995; **1241**: 59-116.

234 Ogawa Y. Role of ryanodine receptors. *Crit Rev Biochem Mol Biol* 1994; **29**: 229-74.

235 Mickelson JR, Louis CF. Malignant hyperthermia: excitation-contraction coupling, Ca2+ release channel, and cell Ca2+ regulation defects. *Physiol Rev* 1996; **76**: 537-92.

236 Ogawa Y, Kurebayashi N, Murayama T. Ryanodine receptor isoforms in excitation-contraction coupling. *Adv Biophys* 1999; **36**: 27-64.

237 Ma J, Fill M, Knudson CM, Campbell KP, Coronado R. Ryanodine receptor of skeletal muscle is a gap junction-type channel. *Science* 1988; **242**: 99-102.

238 Yano M, el-Hayek R, Ikemoto N. Role of calcium feedback in excitation-contraction coupling in isolated triads. *J Biol Chem* 1995; **270**: 19936-42.

239 Chen SR, Zhang L, MacLennan DH. Antibodies as probes for Ca2+ activation sites in the Ca2+ release channel (ryanodine receptor) of rabbit skeletal muscle sarcoplasmic reticulum. *J Biol Chem* 1993; **268**: 13414-21.

240 Chen SR, Ebisawa K, Li X, Zhang L. Molecular identification of the ryanodine receptor Ca2+ sensor. *J Biol Chem* 1998; **273**: 14675-8.

241 Du GG, MacLennan DH. Ca(2+) inactivation sites are located in the COOH-terminal quarter of recombinant rabbit skeletal muscle Ca(2+) release channels (ryanodine receptors). *J Biol Chem* 1999; **274**: 26120-6.

242 Smith JS, Coronado R, Meissner G. Techniques for observing calcium channels from skeletal muscle sarcoplasmic reticulum in planar lipid bilayers. *Methods Enzymol* 1988; **157**: 480-9.

243 Lamb GD, Junankar PR, Stephenson DG. Raised intracellular [Ca2+] abolishes excitation-contraction coupling in skeletal muscle fibres of rat and toad. *J Physiol (Lond)* 1995; **489**: 349-62.

244 Ikemoto N, el-Hayek R. Signal transmission and transduction in excitation-contraction coupling. *Adv Exp Med Biol* 1998; **453**: 199-207.

245 Herrmann-Frank A, Luttgau HC, Stephenson DG. Caffeine and excitation-contraction coupling in skeletal muscle: a stimulating story. *J Muscle Res Cell Motil* 1999; **20**: 223-37.

246 Tripathy A, Xu L, Mann G, Meissner G. Calmodulin activation and inhibition of skeletal muscle Ca2+ release channel (ryanodine receptor). *Biophys J* 1995; **69**: 106-19.

247 Fuentes O, Valdivia C, Vaughan D, Coronado R, Valdivia HH. Calcium-dependent block of ryanodine receptor channel of swine skeletal muscle by direct binding of calmodulin. *Cell Calcium* 1994; **15**: 305-16.

248 Buratti R, Prestipino G, Menegazzi P, Treves S, Zorzato F. Calcium dependent activation of skeletal muscle Ca2+ release channel (ryanodine receptor) by calmodulin. *Biochem Biophys Res Commun* 1995; **213**: 1082-90.

249 Menegazzi P, Larini F, Treves S, Guerrini R, Quadroni M, Zorzato F. Identification and characterization of three calmodulin binding sites of the skeletal muscle ryanodine receptor. *Biochemistry* 1994; **33**: 9078-84.

250 Jayaraman T, Brillantes AM, Timerman AP, Fleischer S, Erdjument-Bromage H, Tempst P, Marks AR. FK506 binding protein associated with the calcium release channel (ryanodine receptor). *J Biol Chem* 1992; **267**: 9474-7.

251 MacKrill JJ. Protein-protein interactions in intracellular Ca2+-release channel function. *Biochem J* 1999; **337**: 345-61.

252 Brillantes AM, Allen P, Takahashi T, Izumo S, Marks AR. Differences in cardiac calcium release channel (ryanodine receptor) expression in myocardium from patients with end-stage heart failure caused by ischemic versus dilated cardiomyopathy [published erratum appears in Circ Res 1992 Dec;71(6):1538]. *Circ Res* 1992; **71**: 18-26.

253 Ahern GP, Junankar PR, Dulhunty AF. Subconductance states in single-channel activity of skeletal muscle ryanodine receptors after removal of FKBP12. *Biophys J* 1997; **72**: 146-62.

254 Gilchrist JS, Katz S, Belcastro AN. Improved resolution of the initial fast phase of heavy sarcoplasmic reticulum Ca2+ uptake by Ca2+:antipyrylazo III dual-wavelength spectroscopy. *Biochem Biophys Res Commun* 1990; **168**: 364-71.

255 Guo W, Campbell KP. Association of triadin with the ryanodine receptor and calsequestrin in the lumen of the sarcoplasmic reticulum. *J Biol Chem* 1995; **270**: 9027-30.

256 Kim KC, Caswell AH, Talvenheimo JA, Brandt NR. Isolation of a terminal cisterna protein which may link the dihydropyridine receptor to the junctional foot protein in skeletal muscle. *Biochemistry* 1990; **29**: 9281-9.

257 Knudson CM, Stang KK, Jorgensen AO, Campbell KP. Biochemical characterization of ultrastructural localization of a major junctional sarcoplasmic reticulum glycoprotein (triadin). *J Biol Chem* 1993; **268**: 12637-45.

258 Carl SL, Felix K, Caswell AH, Brandt NR, Brunschwig JP, Meissner G, Ferguson DG. Immunolocalization of triadin, DHP receptors, and ryanodine receptors in adult and developing skeletal muscle of rats. *Muscle Nerve* 1995; **18**: 1232-43.

259 Jones LR, Zhang L, Sanborn K, Jorgensen AO, Kelley J. Purification, primary structure, and immunological characterization of the 26-kDa calsequestrin binding protein (junctin) from cardiac junctional sarcoplasmic reticulum. *J Biol Chem* 1995; **270**: 30787-96.

260 Froemming GR, Ohlendieck K. Oligomerisation of Ca2+-regulatory membrane components involved in the excitation-contraction-relaxation cycle during postnatal development of rabbit skeletal muscle. *Biochim Biophys Acta* 1998; **1387**: 226-38.

261 Froemming GR, Dillane DJ, Ohlendieck K. Complex formation of skeletal muscle Ca2+-regulatory membrane proteins by halothane. *Eur J Pharmacol* 1999; **365**: 91-102.

262 Karon BS, Geddis LM, Kutchai H, Thomas DD. Anesthetics alter the physical and functional properties of the Ca- ATPase in cardiac sarcoplasmic reticulum. *Biophys J* 1995; **68**: 936-45.

263 Franks NP, Lieb WR. Molecular and cellular mechanisms of general anaesthesia. *Nature* 1994; **367**: 617-14.

264 Eckenhoff RG, Johansson JS. Molecular interactions between inhaled anesthetics and proteins. *Pharmacol Rev* 1997; **49**: 343-67.
265 Kosk-Kosicka D, Fomitcheva I, Lopez MM, Eckenhoff RG. Heterogeneous halothane binding in the SR Ca2+-ATPase. *FEBS Lett* 1997; **402**: 189-92.
266 Murray BE, Ohlendieck K. Complex formation between calsequestrin and the ryanodine receptor in fast- and slow-twitch rabbit skeletal muscle. *FEBS Lett* 1998; **429**: 317-22.
267 Fruen BR, Mickelson JR, Louis CF. Dantrolene inhibition of sarcoplasmic reticulum Ca2+ release by direct and specific action at skeletal muscle ryanodine receptors. *J Biol Chem* 1997; **272**: 26965-71.
268 Nelson TE, Lin M, Zapata-Sudo G, Sudo RT. Dantrolene sodium can increase or attenuate activity of skeletal muscle ryanodine receptor calcium release channel. Clinical implications. *Anesthesiology* 1996; **84**: 1368-79.
269 Meissner G, Lu X. Dihydropyridine receptor-ryanodine receptor interactions in skeletal muscle excitation-contraction coupling. *Biosci Rep* 1995; **15**: 399-408.
270 Cheng H, Lederer MR, Xiao RP, Gomez AM, Zhou YY, Ziman B, Spurgeon H, Lakatta EG, Lederer WJ. Excitation-contraction coupling in heart: new insights from Ca2+ sparks. *Cell Calcium* 1996; **20**: 129-40.
271 Flucher BE, Franzini-Armstrong C. Formation of junctions involved in excitation-contraction coupling in skeletal and cardiac muscle. *Proc Natl Acad Sci U S A* 1996; **93**: 8101-6.
272 Shoshan-Barmatz V, Ashley RH. The structure, function, and cellular regulation of ryanodine-sensitive Ca2+ release channels. *Int Rev Cytol* 1998; **183**: 185-270.
273 Wasserstrom JA. New evidence for similarities in excitation-contraction coupling in skeletal and cardiac muscle. *Acta Physiol Scand* 1998; **162**: 247-52.
274 Leeb T, Brenig B. Ryanodine receptors and their role in genetic diseases (Review). *Int J Mol Med* 1998; **2**: 293-300.
275 Leong P, MacLennan DH. Complex interactions between skeletal muscle ryanodine receptor and dihydropyridine receptor proteins. *Biochem Cell Biol* 1998; **76**: 681-94.
276 Adams BA, Tanabe T, Mikami A, Numa S, Beam KG. Intramembrane charge movement restored in dysgenic skeletal muscle by injection of dihydropyridine receptor cDNAs. *Nature* 1990; **346**: 569-72.
277 Tanabe T, Beam KG, Adams BA, Niidome T, Numa S. Regions of the skeletal muscle dihydropyridine receptor critical for excitation-contraction coupling. *Nature* 1990; **346**: 567-9.
278 Nakai J, Tanabe T, Konno T, Adams B, Beam KG. Localization in the II-III loop of the dihydropyridine receptor of a sequence critical for excitation-contraction coupling. *J Biol Chem* 1998; **273**: 24983-6.
279 Lu X, Xu L, Meissner G. Activation of the skeletal muscle calcium release channel by a cytoplasmic loop of the dihydropyridine receptor. *J Biol Chem* 1994; **269**: 6511-6.
280 Leong P, MacLennan DH. A 37-amino acid sequence in the skeletal muscle ryanodine receptor interacts with the cytoplasmic loop between domains II and III in the skeletal muscle dihydropyridine receptor. *J Biol Chem* 1998; **273**: 7791-4.
281 Slavik KJ, Wang JP, Aghdasi B, Zhang JZ, Mandel F, Malouf N, Hamilton SL. A carboxy-terminal peptide of the alpha 1-subunit of the dihydropyridine receptor inhibits Ca(2+)-release channels. *Am J Physiol* 1997; **272**: C1475-81.
282 Leong P, MacLennan DH. The cytoplasmic loops between domains II and III and domains III and IV in the skeletal muscle dihydropyridine receptor bind to a contiguous site in the skeletal muscle ryanodine receptor. *J Biol Chem* 1998; **273**: 29958-64.
283 Yamazawa T, Takeshima H, Shimuta M, Iino M. A region of the ryanodine receptor critical for excitation-contraction coupling in skeletal muscle. *J Biol Chem* 1997; **272**: 8161-4.
284 Nakai J, Dirksen RT, Nguyen HT, Pessah IN, Beam KG, Allen PD. Enhanced dihydropyridine receptor channel activity in the presence of ryanodine receptor. *Nature* 1996; **380**: 72-5.
285 Nakai J, Ogura T, Protasi F, Franzini-Armstrong C, Allen PD, Beam KG. Functional nonequality of the cardiac and skeletal ryanodine receptors. *Proc Natl Acad Sci U S A* 1997; **94**: 1019-22.
286 Ponting CP. Novel repeats in ryanodine and IP3 receptors and protein O-mannosyltranseferase. *TIBS* 2000; **25**: 48-50.

287 Zorzato F, Menegazzi P, Treves S, Ronjat M. Role of malignant hyperthermia domain in the regulation of Ca2+ release channel (ryanodine receptor) of skeletal muscle sarcoplasmic reticulum. *J Biol Chem* 1996; **271**: 22759-63.

288 Chen SR, Airey JA, MacLennan DH. Positioning of major tryptic fragments in the Ca2+ release channel (ryanodine receptor) resulting from partial digestion of rabbit skeletal muscle sarcoplasmic reticulum. *J Biol Chem* 1993; **268**: 22642-9.

289 Wu Y, Aghdasi B, Dou SJ, Zhang JZ, Liu SQ, Hamilton SL. Functional interactions between cytoplasmic domains of the skeletal muscle Ca2+ release channel. *J Biol Chem* 1997; **272**: 25051-61.

290 Ohnishi ST. Effects of halothane, caffeine, dantrolene and tetracaine on the calcium permeability of skeletal sarcoplasmic reticulum of malignant hyperthermic pigs. *Biochim Biophys Acta* 1987; **897**: 261-8.

291 Kim DH, Sreter FA, Ohnishi ST, Ryan JF, Roberts J, Allen PD, Meszaros LG, Antoniu B, Ikemoto N. Kinetic studies of Ca2+ release from sarcoplasmic reticulum of normal and malignant hyperthermia susceptible pig muscles. *Biochim Biophys Acta* 1984; **775**: 320-7.

292 Mickelson JR, Ross JA, Reed BK, Louis CF. Enhanced Ca2+-induced calcium release by isolated sarcoplasmic reticulum vesicles from malignant hyperthermia susceptible pig muscle. *Biochim Biophys Acta* 1986; **862**: 318-28.

293 Carrier L, Villaz M, Dupont Y. Abnormal rapid Ca2+ release from sarcoplasmic reticulum of malignant hyperthermia susceptible pigs. *Biochim Biophys Acta* 1991; **1064**: 175-83.

294 Endo M, Yagi, S. Ishizuka, T., Horiuti, K., Koga, Y. and Amaha, K. Changes in the calcium induced calcium release mechanism in the sarcoplasmic reticulum of of the muscle from a patient with malignant hyperthermia. *Biomedical Research* 1983; **4**: 83-92.

295 Valdivia HH, Hogan K, Coronado R. Altered binding site for Ca2+ in the ryanodine receptor of human malignant hyperthermia. *Am J Physiol* 1991; **261**: C237-45.

296 O'Driscoll S, McCarthy TV, Eichinger HM, Erhardt W, Lehmann-Horn F, Herrmann-Frank A. Calmodulin sensitivity of the sarcoplasmic reticulum ryanodine receptor from normal and malignant-hyperthermia-susceptible muscle. *Biochem J* 1996; **319**: 421-6.

297 Shomer NH, Louis CF, Fill M, Litterer LA, Mickelson JR. Reconstitution of abnormalities in the malignant hyperthermia- susceptible pig ryanodine receptor. *Am J Physiol* 1993; **264**: C125-35.

298 Shomer NH, Mickelson JR, Louis CF. Caffeine stimulation of malignant hyperthermia-susceptible sarcoplasmic reticulum Ca2+ release channel. *Am J Physiol* 1994; **267**: C1253-61.

299 Censier K, Urwyler A, Zorzato F, Treves S. Intracellular calcium homeostasis in human primary muscle cells from malignant hyperthermia-susceptible and normal individuals. Effect Of overexpression of recombinant wild-type and Arg163Cys mutated ryanodine receptors. *J Clin Invest* 1998; **101**: 1233-42.

300 Richter M, Schleithoff L, Deufel T, Lehmann-Horn F, Herrmann-Frank A. Functional characterization of a distinct ryanodine receptor mutation in human malignant hyperthermia-susceptible muscle. *J Biol Chem* 1997; **272**: 5256-60.

301 Chen SR, MacLennan DH. Identification of calmodulin-, Ca(2+)-, and ruthenium red-binding domains in the Ca2+ release channel (ryanodine receptor) of rabbit skeletal muscle sarcoplasmic reticulum. *J Biol Chem* 1994; **269**: 22698-704.

302 Treves S, Larini F, Menegazzi P, Steinberg TH, Koval M, Vilsen B, Andersen JP, Zorzato F. Alteration of intracellular Ca2+ transients in COS-7 cells transfected with the cDNA encoding skeletal-muscle ryanodine receptor carrying a mutation associated with malignant hyperthermia. *Biochem J* 1994; **301**: 661-5.

303 Tong J, McCarthy TV, MacLennan DH. Measurement of resting cytosolic Ca2+ concentrations and Ca2+ store size in HEK-293 cells transfected with malignant hyperthermia or central core disease mutant Ca2+ release channels. *J Biol Chem* 1999; **274**: 693-702.

304 Sambrook J, Fritsch EF, Maniatus T. *Molecular cloning: A laboratory manual.*: Cold Spring Harbour Laboratory Press, Cold Spring Harbour., 1989.

305 Kunkel LM, Smith KD, Boyer SH, Borgaonkar DS, Watchel SS, Miller OJ, Breg WR, ones HW, Rary JM. *Proc. Natl. Acad. Sci.* 1977; **74**: 1245-49.

306 Goelz SE, Hamilton SR, Vogelstein B. Purification of DNA from fomaldehyde fixed and parafin embedded human tissue. *Biochem. Biophys. Res. Commun.* 1985; **130**: 118-26.

307 Hood DA, Simoneau JA. Rapid isolation of total RNA from small mammal and human skeletal muscle. *Am J Physiol* 1989; **256**: C1092-6.
308 Chomczynski P, Sacchi N. Single-step method of RNA isolation by acid guanidinium thiocyanate-phenol-chloroform extraction. *Anal Biochem* 1987; **162**: 156-9.
309 Farrell RE. *RNA methodologies: A laboratory guide for isolation and characterisation.*: San Diego Academic Press, 1993.
310 Chomczynski P. A reagent for the single-step simultaneous isolation of RNA, DNA and proteins from cell and tissue samples. *Biotechniques* 1993; **15**: 532-4, 536-7.
311 White BA. *PCR Protocols, current methods and applications*, Vol. 15. Totawa, New Jersey: Humana Press, 1993.
312 Eckert KA, Kunkel TA. High fidelity DNA synthesis by the Thermus aquaticus DNA polymerase. *Nucleic Acids Res* 1990; **18**: 3739-44.
313 Williams JF. Optimization strategies for the polymerase chain reaction. *Biotechniques* 1989; **7**: 762-9.
314 Ellsworth DL, Rittenhouse KD, Honeycutt RL. Artifactual variation in randomly amplified polymorphic DNA banding patterns. *Biotechniques* 1993; **14**: 214-7.
315 Carbonari M, Sbarigia D, Cibati M, Fiorilli M. Optimization of PCR performance. *Trends Genet* 1993; **9**: 42-3.
316 Hecker KH, Roux KH. High and low annealing temperatures increase both specificity and yield in touchdown and stepdown PCR. *Biotechniques* 1996; **20**: 478-85.
317 Don RH, Cox PT, Wainwright BJ, Baker K, Mattick JS. 'Touchdown' PCR to circumvent spurious priming during gene amplification. *Nucleic Acids Res* 1991; **19**: 4008.
318 Sharkey DJ, Scalice ER, Christy KG, Jr., Atwood SM, Daiss JL. Antibodies as thermolabile switches: high temperature triggering for the polymerase chain reaction. *Biotechnology (N Y)* 1994; **12**: 506-9.
319 Huang MM, Arnheim N, Goodman MF. Extension of base mispairs by Taq DNA polymerase: implications for single nucleotide discrimination in PCR. *Nucleic Acids Res* 1992; **20**: 4567-73.
320 Rozen S, Skaletsky HJ. Primer3. In.: Whitehead Institute, 1996, 1997.
321 Orita M, Iwahana H, Kanazawa H, Hayashi K, Sekiya T. Detection of polymorphisms of human DNA by gel electrophoresis as single-strand conformation polymorphisms. *Proc Natl Acad Sci U S A* 1989; **86**: 2766-70.
322 Hayashi K, Yandell DW. How sensitive is PCR-SSCP? *Hum Mutat* 1993; **2**: 338-46.
323 Hongyo T, Buzard GS, Calvert RJ, Weghorst CM. 'Cold SSCP': a simple, rapid and non-radioactive method for optimized single-strand conformation polymorphism analyses. *Nucleic Acids Res* 1993; **21**: 3637-42.
324 Glavac D, Dean M. Optimization of the single-strand conformation polymorphism (SSCP) technique for detection of point mutations. *Hum Mutat* 1993; **2**: 404-14.
325 Weissenbach J, Gyapay G, Dib C, Vignal A, Morissette J, Millasseau P, Vaysseix G, Lathrop M. A second-generation linkage map of the human genome [see comments]. *Nature* 1992; **359**: 794-801.
326 Gyapay G, Morissette J, Vignal A, Dib C, Fizames C, Millasseau P, Marc S, Bernardi G, Lathrop M, Weissenbach J. The 1993-94 Genethon human genetic linkage map [see comments]. *Nat Genet* 1994; **7**: 246-339.
327 Couch FJ, Hogan K, McCarthy TV, Gregg RG. Dinucleotide repeat polymorphism at the RYR1 locus (19q13.1). *Nucleic Acids Res* 1991; **19**: 5094.
328 Weber JL, May PE. Abundant class of human DNA polymorphisms which can be typed using the polymerase chain reaction. *Am J Hum Genet* 1989; **44**: 388-96.
329 Iles DE, Segers B, de Jong P, Alleman J, Wieringa B. Trinucleotide repeat polymorphism at the D19S190 locus. *Nucleic Acids Res* 1992; **20**: 1170.
330 Dracopoli NC, Haines, J.I., Korf, B.R., Moir, D.T., Morton, C.C., Seidman, C.E., Seidman J.G. and Smith, D.R. *Current protocols in human genetics*. New York: John Whiley and Sons, Inc., 1995.
331 Lathrop GM, Lalouel JM. Easy calculations of lod scores and genetic risks on small computers. *Am J Hum Genet* 1984; **36**: 460-5.
332 Lathrop GM, Lalouel JM, Julier C, Ott J. Strategies for multilocus linkage analysis in humans. *Proc Natl Acad Sci U S A* 1984; **81**: 3443-6.

333 Terwilliger JD, Ott J. *Handbook of human genetic linkage analysis.* Baltimore: The Johns Hopkins University Press, 1994.
334 CHLC. In., 1999.
335 Alestrom A, Fagerlund TH, Berg K. A simple method to detect the RYR1 mutation G1021A, a cause of malignant hyperthermia susceptibility. *Clin Genet* 1995; **47**: 274-5.
336 Fagerlund T, Ording H, Bendixen D, Berg K. Search for three known mutations in the RYR1 gene in 48 Danish families with malignant hyperthermia. *Clin Genet* 1994; **46**: 401-4.
337 Tabor S, Richardson CC. Effect of manganese ions on the incorporation of dideoxynucleotides by bacteriophage T7 DNA polymerase and Escherichia coli DNA polymerase I. *Proc Natl Acad Sci U S A* 1989; **86**: 4076-80.
338 Ott J. *Analysis of human genetic linkage*: Johns Hopkins University Press, Baltimore, 1991.
339 Conneally PM, Rivas ML. Linkage analysis in man. *Adv Hum Genet* 1980; **10**: 209-66.
340 Collins FS. Of needles and haystacks: finding human disease genes by positional cloning. *Clin Res* 1991; **39**: 615-23.
341 Royer-Pokora B, Kunkel LM, Monaco AP, Goff SC, Newburger PE, Baehner RL, Cole FS, Curnutte JT, Orkin SH. Cloning the gene for an inherited human disorder--chronic granulomatous disease--on the basis of its chromosomal location. *Nature* 1986; **322**: 32-8.
342 Knowlton RG, Cohen-Haguenauer O, Van Cong N, Frezal J, Brown VA, Barker D, Braman JC, Schumm JW, Tsui LC, Buchwald M, et al. A polymorphic DNA marker linked to cystic fibrosis is located on chromosome 7. *Nature* 1985; **318**: 380-2.
343 Wallace MR, Marchuk DA, Andersen LB, Letcher R, Odeh HM, Saulino AM, Fountain JW, Brereton A, Nicholson J, Mitchell AL, et al. Type 1 neurofibromatosis gene: identification of a large transcript disrupted in three NF1 patients [published erratum appears in Science 1990 Dec 21;250(4988):1749]. *Science* 1990; **249**: 181-6.
344 Goate A, Chartier-Harlin MC, Mullan M, Brown J, Crawford F, Fidani L, Giuffra L, Haynes A, Irving N, James L, et al. Segregation of a missense mutation in the amyloid precursor protein gene with familial Alzheimer's disease [see comments]. *Nature* 1991; **349**: 704-6.
345 Strittmatter WJ, Saunders AM, Schmechel D, Pericak-Vance M, Enghild J, Salvesen GS, Roses AD. Apolipoprotein E: high-avidity binding to beta-amyloid and increased frequency of type 4 allele in late-onset familial Alzheimer disease. *Proc Natl Acad Sci U S A* 1993; **90**: 1977-81.
346 Gusella JF, Wexler NS, Conneally PM, Naylor SL, Anderson MA, Tanzi RE, Watkins PC, Ottina K, Wallace MR, Sakaguchi AY, et al. A polymorphic DNA marker genetically linked to Huntington's disease. *Nature* 1983; **306**: 234-8.
347 Wunderle VM, Ramkissoon YD, Kwok C, Kom RM, King VE, Goodfellow PN. Breakpoint break for consortium studying adult polycystic kidney disease. *Cell* 1994; **77**: 785-6.
348 Futreal PA, Liu Q, Shattuck-Eidens D, Cochran C, Harshman K, Tavtigian S, Bennett LM, Haugen-Strano A, Swensen J, Miki Y, et al. BRCA1 mutations in primary breast and ovarian carcinomas. *Science* 1994; **266**: 120-2.
349 GDB. Human Genome Database [database online]. Toronto (Ontario, Canada): The Hospital for Sick Children, Baltimore (Maryland, USA): Johns Hopkins University. In., 1990-.Updated daily.
350 Blackwelder WC, Elston RC. A comparison of sib-pair linkage tests for disease susceptibility loci. [published erratum appears in Genet Epidemiol 1986;3(5):379]. *Genet Epidemiol* 1985; **2**: 85-97.
351 Weeks DE, Lange K. The affected-pedigree-member method of linkage analysis. *Am J Hum Genet* 1988; **42**: 315-26.
352 Lio P, Morton NE. Comparison of parametric and nonparametric methods to map oligogenes by linkage. *Proc Natl Acad Sci U S A* 1997; **94**: 5344-8.
353 Martinez M, Khlat M, Leboyer M, Clerget-Darpoux F. Performance of linkage analysis under misclassification error when the genetic model is unknown. *Genet Epidemiol* 1989; **6**: 253-8.
354 Freimer NB, Sandkuijl LA, Blower SM. Incorrect specification of marker allele frequencies: effects on linkage analysis. *Am J Hum Genet* 1993; **52**: 1102-10.
355 Britt BA. Etiology and pathophysiology of malignant hyperthermia. *Fed Proc* 1979; **38**: 44-8.
356 Morton NE. Sequential tests for the detection of linkage. *Am. J. Hum. Genet.* 1955; **7**: 277-318.
357 White RaL, J. Chromosome Mapping with DNA Markers. *Scientific American* 1988; **258**: 20 - 28.
358 Botstein D, White RL, Skolnick M, Davis RW. Construction of a genetic linkage map in man using restriction fragment length polymorphisms. *Am J Hum Genet* 1980; **32**: 314-31.

359 Donis-Keller H, Barker DF, Knowlton RG, Schumm JW, Braman JC, Green P. Highly polymorphic RFLP probes as diagnostic tools. *Cold Spring Harb Symp Quant Biol* 1986; **51 Pt 1**: 317-24.
360 Messler W, Li S, Stewart C. The birth of microsatellites. *Nature* 1996; **381**: 483.
361 Weber JL. Human DNA polymorphisms and methods of analysis. *Curr Opin Biotechnol* 1990; **1**: 166-71.
362 Edwards MC, Clemens PR, Tristan M, Pizzuti A, Gibbs RA. Pentanucleotide repeat length polymorphism at the human CD4 locus. *Nucleic Acids Res* 1991; **19**: 4791.
363 Buard J, Bourdet A, Yardley J, Dubrova Y, Jeffreys AJ. Influences of array size and homogeneity on minisatellite mutation. *Embo J* 1998; **17**: 3495-502.
364 Garcia E, Elliott J, Gorvad A, Brandriff B, Gordon L, Soliman KM, Ashworth LK, Lennon G, Burgin M, Lamerdin J, et al. A continuous high-resolution physical map spanning 17 megabases of the q12, q13.1, and q13.2 cytogenetic bands of human chromosome 19. *Genomics* 1995; **27**: 52-66.
365 Ott J. Strategies for characterising highly polymorphic markers in human gene mapping. *Am. J. Hum. Genet.* 1992; **51**: 283-90.
366 Boehnke M. Allele frequency estimation from data on relatives. *Am. J. Hum. Genet.* 1991; **48**: 22-5.
367 Elston RC, Yelverton KC. General models for segregation analysis. *Am J Hum Genet* 1975; **27**: 31-45.
368 Lalouel JM, Rao DC, Morton NE, Elston RC. A unified model for complex segregation analysis. *Am J Hum Genet* 1983; **35**: 816-26.
369 Thompson EA. A scoring method for multi-point linkage analysis: application to the Utah 11-p data. *Genet Epidemiol Suppl* 1986; **1**: 171-6.
370 Greenberg DA. Inferring mode of inheritance by comparison of lod scores. *Am J Med Genet* 1989; **34**: 480-6.
371 Elston RC. Man bites dog? The validity of maximizing lod scores to determine mode of inheritance [editorial]. *Am J Med Genet* 1989; **34**: 487-8.
372 Weeks DE, Lehner T, Squires-Wheeler E, Kaufmann C, Ott J. Measuring the inflation of the lod score due to its maximization over model parameter values in human linkage analysis. *Genet Epidemiol* 1990; **7**: 237-43.
373 Schlamp CL, Poulsen GL, Nork TM, Nickells RW. Nuclear exclusion of wild-type p53 in immortalized human retinoblastoma cells [see comments]. *J Natl Cancer Inst* 1997; **89**: 1530-6.
374 Amos CI, Elston RC, Srinivasan SR, Wilson AF, Cresanta JL, Ward LJ, Berenson GS. Linkage and segregation analyses of apolipoproteins A1 and B, and lipoprotein cholesterol levels in a large pedigree with excess coronary heart disease: the Bogalusa Heart Study. *Genet Epidemiol* 1987; **4**: 115-28.
375 Lomas DA. New insights into the structural basis of alpha 1-antitrypsin deficiency. *Qjm* 1996; **89**: 807-12.
376 McGue M, Gottesman, II. The genetic epidemiology of schizophrenia and the design of linkage studies. *Eur Arch Psychiatry Clin Neurosci* 1991; **240**: 174-81.
377 Todorov AA, Rao DC. Trade-off between false positives and false negatives in the linkage analysis of complex traits. *Genet Epidemiol* 1997; **14**: 453-64.
378 Ott J. Linkage analysis with misclassification at one locus. *Clin Genet* 1977; **12**: 119-24.
379 Gutmann DH, Wood DL, Collins FS. Identification of the neurofibromatosis type 1 gene product. *Proc Natl Acad Sci U S A* 1991; **88**: 9658-62.
380 Morton NE. The detection and estimation of linkage between the genes for elliptocytosis and the Rh blood group type. *Am. J. Hum. Genet.* 1956; **8**: 80-96.
381 Risch N. A new statistical test for linkage heterogeneity. *Am J Hum Genet* 1988; **42**: 353-64.
382 Haldane JBS, Smith CAB. A new estimate of the linkage between the genes for colour-blindness and hemophilia in man. *Ann. Eugenics* 1947; **14**: 10-31.
383 Ott J. Estimation of the recombination fraction in human pedigrees: Efficient computation of the likelihood for human linkage studies. *Am. J. Hum. Genet.* 1974; **26**: 588-97.
384 Bryant SP. Human genetic linkage analysis: A review. In: *Guide to human genome computing*: Academic Press limited., 1994: 59-110.
385 Lange K, Weeks D, Boehnke M. Programs for Pedigree Analysis: MENDEL, FISHER, and dGENE [letter]. *Genet Epidemiol* 1988; **5**: 471-2.

386 Elston RC, Stewart J. A general model for the genetic analysis of pedigree data. *Hum Hered* 1971; **21**: 523-42.
387 Cannings C, homson EA, Skolnick MH. Probability functions on complex pedigrees. *Adv. Adv. Prob.* 1978; **10**: 26-61.
388 Elston RC. The prior probability of autosomal linkage. *Ann Hum Genet* 1975; **38**: 341-50.
389 Ranklev E, Fletcher R. Investigation of malignant hyperthermia in Sweden. *Acta Anaesthesiol Scand* 1986; **30**: 693-6.
390 Donnelly AJ. Malignant hyperthermia. Epidemiology, pathophysiology, treatment. *Aorn J* 1994; **59**: 393-5, 398-400, 403-5.
391 Moslehi R, Langlois S, Yam I, Friedman JM. Linkage of malignant hyperthermia and hyperkalemic periodic paralysis to the adult skeletal muscle sodium channel (SCN4A) gene in a large pedigree. *Am J Med Genet* 1998; **76**: 21-7.
392 Wallace AJ, Wooldridge W, Kingston HM, Harrison MJ, Ellis FR, Ford PM. Malignant hyperthermia--a large kindred linked to the RYR1 gene. *Anaesthesia* 1996; **51**: 16-23.
393 Ball SP, Dorkins HR, Ellis FR, Hall JL, Halsall PJ, Hopkins PM, Mueller RF, Stewart AD. Genetic linkage analysis of chromosome 19 markers in malignant hyperthermia. *Br J Anaesth* 1993; **70**: 70-5.
394 Lathrop GM, Hooper AB, Huntsman JW, Ward RH. Evaluating pedigree data. I. The estimation of pedigree error in the presence of marker mistyping. *Am J Hum Genet* 1983; **35**: 241-62.
395 Kerem BS, Buchanan JA, Durie P, Corey ML, Levison H, Rommens JM, Buchwald M, Tsui LC. DNA marker haplotype association with pancreatic sufficiency in cystic fibrosis. *Am J Hum Genet* 1989; **44**: 827-34.
396 Chakravarti A, Li CC, Buetow KH. Estimation of the marker gene frequency and linkage disequilibrium from conditional marker data. *Am J Hum Genet* 1984; **36**: 177-86.
397 Ellis FR, Halsall PJ. Malignant hyperpyrexia. *Br J Hosp Med* 1980; **24**: 318-21, 323, 325-7.
398 Morton NE, MacLean CJ, Lew R, Yee S. Multipoint linkage analysis. *Am J Hum Genet* 1986; **38**: 868-83.
399 Sakagami M, Mashima S, K. H, Mukoyama H. The choice of DNA polymerase can affect the detection of short tandem repeat (STR) polymorphisms. In.: Elsevier trends journal technical tips online., 1997.
400 Smith JR, Carpten JD, Brownstein MJ, Ghosh S, Magnuson VL, Gilbert DA, Trent JM, Collins FS. Approach to genotyping errors caused by nontemplated nucleotide addition by Taq DNA polymerase. *Genome Res* 1995; **5**: 312-7.
401 Wolz W, Wendelmuth U, Rouquier S, Giorgi D, Muller CR. A complex satellite DNA polymorphism flanking the human ryanodine receptor gene (RYR1). *Cytogenet Cell Genet* 1996; **72**: 215-6.
402 Healy SJ, Heffron JJ, Lehane M, Bradley DG, Johnson K, McCarthy TV. Diagnosis of susceptibility to malignant hyperthermia with flanking DNA markers. *Bmj* 1991; **303**: 1225-8.
403 Ording H. Incidence of malignant hyperthermia in Denmark. *Anesth Analg* 1985; **64**: 700-4.
404 Durner M, Greenberg DA, Hodge SE. Inter- and intrafamilial heterogeneity: effective sampling strategies and comparison of analysis methods. *Am J Hum Genet* 1992; **51**: 859-70.
405 Brow MA, Oldenburg MC, Lyamichev V, Heisler LM, Lyamicheva N, Hall JG, Eagan NJ, Olive DM, Smith LM, Fors L, Dahlberg JE. Differentiation of bacterial 16S rRNA genes and intergenic regions and Mycobacterium tuberculosis katG genes by structure-specific endonuclease cleavage. *J Clin Microbiol* 1996; **34**: 3129-37.
406 Rossetti S, Englisch S, Bresin E, Pignatti PF, Turco AE. Detection of mutations in human genes by a new rapid method: cleavage fragment length polymorphism analysis (CFLPA). *Mol Cell Probes* 1997; **11**: 155-60.
407 Maddox LO, Li P, Bennett A, Descartes M, Thompson JN. Comparison of SSCP analysis and CFLP analysis for mutation detection in the human iduronate 2-sulfatase gene. *Biochem Mol Biol Int* 1997; **43**: 1163-71.
408 Lynch C, 3rd, Frazer MJ. Anesthetic alteration of ryanodine binding by cardiac calcium release channels. *Biochim Biophys Acta* 1994; **1194**: 109-17.
409 Corporation PE. Comparative PCR Sequencing: A guide to sequencing-based heterozygote detection. In. Foseter City: Applied Biosystems Division, 1995: 109.

410 Gerard G, Schidt B, Kotewicz M, Campbell J. cDNA Synthesis by Moloney murine leukemia virus RNase H-minus reverse transcriptase possessing full DNA polymerase activity. *Focus* 1992; **14**: 91.
411 McPherson MJ, Hames BD, Taylor GR. *PCR2, A practical approach*. New York: Oxford University press, 1995.
412 Froster-Iskenius UG, Waterson JR, Hall JG. A recessive form of congenital contractures and torticollis associated with malignant hyperthermia. *J Med Genet* 1988; **25**: 104-12.
413 Stewart CR, Kahler SG, Gilchrist JM. Congenital myopathy with cleft palate and increased susceptibility to malignant hyperthermia: King syndrome? *Pediatr Neurol* 1988; **4**: 371-4.
414 Erlich HA. *PCR technology: Principles and applications for DNA amplification*. New York: W. H. Freeman and Company, 1992.
415 Filichkin SA, Gelvin SB. Effect of dimethyl sulfoxide concentration on specificity of primer matching in PCR. *Biotechniques* 1992; **12**: 828-30.
416 Seto D. An improved method for sequencing double stranded plasmid DNA from minipreps using DMSO and modified template preparation. *Nucleic Acids Res* 1990; **18**: 5905-6.
417 Pomp D, Medrano JF. Organic solvents as facilitators of polymerase chain reaction. *Biotechniques* 1991; **10**: 58-9.
418 Schorderet DF, Gartler SM. Analysis of CpG suppression in methylated and nonmethylated species. *Proc Natl Acad Sci U S A* 1992; **89**: 957-61.
419 Lindahl T. Instability and decay of the primary structure of DNA [see comments]. *Nature* 1993; **362**: 709-15.
420 Larach MG, Landis JR, Bunn JS, Diaz M. Prediction of malignant hyperthermia susceptibility in low-risk subjects. An epidemiologic investigation of caffeine halothane contracture responses. The North American Malignant Hyperthermia Registry. *Anesthesiology* 1992; **76**: 16-27.
421 Sheskin D. *Handbook of parametric and nonparametric statistical procedures*. Boca Raton, Fla.: CRC Press, 1997.
422 Sprent P. *Quick statistics : an introduction to non-parametric methods*. Harmondsworth: Penguin, 1981, 1981.
423 Freund JE. *Modern elementary statistics*, 7th ed edn.: Englewood Cliffs, N.J. : Prentice-Hall, 1988.
424 Rowntree D, 1936-. *Statistics without tears : a primer for non-mathematicians*: Harmondsworth : Penguin, 1991.
425 Hopkins PM, Ellis FR, Halsall PJ, Stewart AD. An analysis of the predictive probability of the in vitro contracture test for determining susceptibility to malignant hyperthermia. *Anesth Analg* 1997; **84**: 648-56.
426 Hopkins PM, Ellis FR, Halsall PJ. Comparison of in vitro contracture testing with ryanodine, halothane and caffeine in malignant hyperthermia and other neuromuscular disorders. *Br J Anaesth* 1993; **70**: 397-401.
427 McLachlan GJ. *Discriminant analysis and statistical pattern recognition*. New York: Wiley, 1992.
428 Manly BFJ. *Multivariate statistical methods : a primer*. London: Chapman and Hall, 1994.
429 Flury B. *Multivariate statistics : a practical approach*. London ; New York: Chapman and Hall, 1988.
430 Ording H, Hansen U, Skovgaard LT. Age, fiber type composition and in vitro contracture responses in human malignant hyperthermia. *Acta Anaesthesiol Scand* 1988; **32**: 121-4.
431 Fagerlund TH, Islander G, Ranklev Twetman E, Berg K. Malignant hyperthermia susceptibility, an autosomal dominant disorder? *Clin Genet* 1997; **51**: 365-9.
432 Islander G, Bendixen D, Ranklev-Twetman E, Ording H. Results of in vitro contracture testing of both parents of malignant hyperthermia susceptible probands. *Acta Anaesthesiol Scand* 1996; **40**: 579-84.
433 Inc. GS. GraphPad InStat. In:, Version 3.01 edn.: San Diego California USA, 1998.
434 Lowry R. Concepts and inferential statistics. In:, Vol. 1999: Vassar College, Pougkeepsie, New York , U.S.A, 1999.
435 Christensen R. *Analysis of variance, design and regression : applied statistical methods*. London: Chapman & Hall,, 1996.
436 Milliken GA, Johnson DE. *Analysis of messy data*: Belmont, Calif. : Lifetime Learning Publications, 1984.

437 Lucke JN, Hall GM, Lister D. Malignant hyperthermia in the pig and the role of stress. *Ann N Y Acad Sci* 1979; **317**: 326-37.
438 Lucke J, Hall G. Thermogenesis in stress-susceptible pigs: a review. *J R Soc Med* 1983; **76**: 514-7.
439 Ryan JF, Tedeschi LG. Sudden unexplained death in a patient with a family history of malignant hyperthermia. *J Clin Anesth* 1997; **9**: 66-8.
440 Denborough MA. Clinical classification and clinical incidence of malignant hyperthermia in Australia. In: *Proceedings of the 3rd symposium on malignant hyperthermia, 1994.* (Mrio MK, H., Yuge, O., ed): Springer-Verlag, Tokyo, 1996: 43 -7.
441 Denborough MA, Hopkinson KC, Banney DG. Firefighting and malignant hyperthermia. *Br Med J (Clin Res Ed)* 1988; **296**: 1442-3.
442 Antognini JF, Gronert GA. Continued puzzles in malignant hyperthermia [editorial]. *J Clin Anesth* 1997; **9**: 1-3.
443 Denborough MA, Collins SP, Hopkinson KC. Rhabdomyolysis and malignant hyperpyrexia. *Br Med J (Clin Res Ed)* 1984; **288**: 1878.
444 Ponsonby AL, Dwyer T, Gibbons LE, Cochrance DA, Jones ME, McCall MJ. Thermal environment and sudden infant death syndrome: case control study. *BMJ* 1992; **304**: 277-282.
445 Lucke JN, Hall GM, Lister D. Letter: Body temperature and malignant hyperthermia. *Lancet* 1976; **1**: 1405.
446 Denborough M. Malignant hyperthermia [see comments]. *Lancet* 1998; **352**: 1131-6.
447 Kasamatsu Y, Osada M, Ashida K, Azukari K, Yoshioka K, Ohsawa A. Rhabdomyolysis after infection and taking a cold medicine in a patient who was susceptible to malignant hyperthermia. *Intern Med* 1998; **37**: 169-73.
448 Schiller HH. Letter: Chronic viral myopathy and malignant hyperthermia. *N Engl J Med* 1975; **292**: 1409.
449 Ranklev E, Fletcher R, Krantz P. Malignant hyperpyrexia and sudden death. *Am J Forensic Med Pathol* 1985; **6**: 149-50.
450 Williams CH, Shanklin MD, Hedrick HB, Muhrer ME, Stubbs DH, Krause GF, Payne CG, Benedict JD, Hutcheson DP, Lasley JF. The fulminant hyperthermia-stress syndrome: genetic aspects, hemodynamic and metabolic measurements in susceptible and normal pigs. pp. 113-40. *In: Aldrete JA, Britt BA, ed. Malignant hyperthermia. New York, Grune & Stratton*, 1978: 113-40.
451 Lucke JN, Denny HR. The role of the sympathetic nervous system in the pathogenesis of halothane-induced malignant hyperthermia in the pietrain pig [proceedings]. *Br J Anaesth* 1978; **50**: 75-6.
452 Ledbetter MW, Preiner JK, Louis CF, Mickelson JR. Tissue distribution of ryanodine receptor isoforms and alleles determined by reverse transcription polymerase chain reaction. *J Biol Chem* 1994; **269**: 31544-51.
453 Giannini G, Conti A, Mammarella S, Scrobogna M, Sorrentino V. The ryanodine receptor/calcium channel genes are widely and differentially expressed in murine brain and peripheral tissues. *J Cell Biol* 1995; **128**: 893-904.
454 O'Brien RO, Taske NL, Hansbro PM, Matthaei KI, Hogan SP, Denborough MA, Foster PS. Exclusion of defects in the skeletal muscle specific regions of the DHPR alpha 1 subunit as frequent causes of malignant hyperthermia. *J Med Genet* 1995; **32**: 913-4.
455 Robinson R, Curran JL, Hall WJ, Halsall PJ, Hopkins PM, Markham AF, Stewart AD, West SP, Ellis FR. Genetic heterogeneity and HOMOG analysis in British malignant hyperthermia families. *J Med Genet* 1998; **35**: 196-201.
456 Steinfath M, Scholz J, Singh S, Wappler F. [What significance to genotype changes have in diagnosis of malignant hyperthermia? (see comments)]. *Anasthesiol Intensivmed Notfallmed Schmerzther* 1996; **31**: 334-43.
457 Loke JC, MacLennan DH. Bayesian modeling of muscle biopsy contracture testing for malignant hyperthermia susceptibility [published erratum appears in Anesthesiology 1998 Aug;89(2):555 and 1998 Dec;89(6):1615]. *Anesthesiology* 1998; **88**: 589-600.
458 Kalow W, Sharer S, Britt B. Pharmacogenetics of caffeine and caffeine-halothane contractures in biopsies of human skeletal muscle. *Pharmacogenetics* 1991; **1**: 126-35.
459 Fagerlund TH, Islander G, Twetman ER, Berg K. A search for three known RYR1 gene mutations in 41 Swedish families with predisposition to malignant hyperthermia. *Clin Genet* 1995; **48**: 12-6.

460 Stewart SL, Rosenberg H, Fletcher JE. Failure to identify the ryanodine receptor G1021A mutation in a large North American population with malignant hyperthermia. *Clin Genet* 1998; **54**: 358-61.

461 Fletcher JE, Tripolitis L, Hubert M, Vita GM, Levitt RC, Rosenberg H. Genotype and phenotype relationships for mutations in the ryanodine receptor in patients referred for diagnosis of malignant hyperthermia. *Br J Anaesth* 1995; **75**: 307-10.

462 Gregg RG, Couch F, Hogan K, Powers PA. Assignment of the human gene for the alpha 1 subunit of the skeletal muscle DHP-sensitive Ca2+ channel (CACNL1A3) to chromosome 1q31-q32. *Genomics* 1993; **15**: 107-12.

463 Powers PA, Liu S, Hogan K, Gregg RG. Molecular characterization of the gene encoding the gamma subunit of the human skeletal muscle 1,4-dihydropyridine-sensitive Ca2+ channel (CACNLG), cDNA sequence, gene structure, and chromosomal location. *J Biol Chem* 1993; **268**: 9275-9.

464 Gregg RG, Powers PA, Hogan K. Assignment of the human gene for the beta subunit of the voltage-dependent calcium channel (CACNLB1) to chromosome 17 using somatic cell hybrids and linkage mapping. *Genomics* 1993; **15**: 185-7.

465 Standaert RF, Galat A, Verdine GL, Schreiber SL. Molecular cloning and overexpression of the human FK506-binding protein FKBP. *Nature* 1990; **346**: 671-4.

466 Taske NL, Eyre HJ, O'Brien RO, Sutherland GR, Denborough MA, Foster PS. Molecular cloning of the cDNA encoding human skeletal muscle triadin and its localisation to chromosome 6q22-6q23. *Eur J Biochem* 1995; **233**: 258-65.

467 Kagari T, Yamaguchi N, Kasai M. Biochemical characterization of calsequestrin-binding 30-kDa protein in sarcoplasmic reticulum of skeletal muscle. *Biochem Biophys Res Commun* 1996; **227**: 700-6.

468 Yang N, Ji S, Zhou M, Ptacek LJ, Barchi RL, Horn R, George AL, Jr. Sodium channel mutations in paramyotonia congenita exhibit similar biophysical phenotypes in vitro. *Proc Natl Acad Sci U S A* 1994; **91**: 12785-9.

469 Sine SM, Ohno K, Bouzat C, Auerbach A, Milone M, Pruitt JN, Engel AG. Mutation of the acetylcholine receptor alpha subunit causes a slow-channel myasthenic syndrome by enhancing agonist binding affinity. *Neuron* 1995; **15**: 229-39.

470 el-Hayek R, Valdivia C, Valdivia HH, Hogan K, Coronado R. Activation of the Ca2+ release channel of skeletal muscle sarcoplasmic reticulum by palmitoyl carnitine. *Biophys J* 1993; **65**: 779-89.

471 Fletcher JE, Wieland SJ, Karan SM, Beech J, Rosenberg H. Sodium channel in human malignant hyperthermia. *Anesthesiology* 1997; **86**: 1023-32.

472 Afshari C, Nuwaysir E, Barrett J. Application of complementary DNA microarray technology to carcinogen identification, toxicology, and drug safety evaluation. *Cancer Res* 1999; **59(19)**: 4759-60.

473 Kurian K, Watson C, Wyllie A. DNA chip technology [editorial]. *J Pathol* 1999; **187(3)**: 267-71.

474 Bucher P. Regulatory elements and expression profiles. *Curr Opin Struct Biol* 1999; **9(3)**: 400-7.

475 Ponting C, Schultz J, Bork P. SPRY domains in ryanodine receptors (Ca(2+)-release channels). *Trends Biochem Sci* 1997; **22**: 193-4.

476 Chen SR, Zhang L, MacLennan DH. Characterization of a Ca2+ binding and regulatory site in the Ca2+ release channel (ryanodine receptor) of rabbit skeletal muscle sarcoplasmic reticulum. *J Biol Chem* 1992; **267**: 23318-26.

477 Fill M, Mejia-Alvarez R, Zorzato F, Volpe P, Stefani E. Antibodies as probes for ligand gating of single sarcoplasmic reticulum Ca2(+)-release channels. *Biochem J* 1991; **273**: 449-57.

478 Carroll S, Skarmeta JG, Yu X, Collins KD, Inesi G. Interdependence of ryanodine binding, oligomeric receptor interactions, and Ca2+ release regulation in junctional sarcoplasmic reticulum. *Arch Biochem Biophys* 1991; **290**: 239-47.

479 Murray BE, Ohlendieck K. Cross-linking analysis of the ryanodine receptor and alpha1-dihydropyridine receptor in rabbit skeletal muscle triads. *Biochem J* 1997; **324**: 689-96.

480 Nakai J, Sekiguchi N, Rando TA, Allen PD, Beam KG. Two regions of the ryanodine receptor involved in coupling with L-type Ca2+ channels. *J Biol Chem* 1998; **273**: 13403-6.

481 Grabner M, Dirksen RT, Suda N, Beam KG. The II-III loop of the skeletal muscle dihydropyridine receptor is responsible for the Bi-directional coupling with the ryanodine receptor. *J Biol Chem* 1999; **274**: 21913-9.

482 Ohkura M, Furukawa K, Fujimori H, Kuruma A, Kawano S, Hiraoka M, Kuniyasu A, Nakayama H, Ohizumi Y. Dual regulation of the skeletal muscle ryanodine receptor by triadin and calsequestrin. *Biochemistry* 1998; **37**: 12987-93.

483 Groh S, Marty I, Ottolia M, Prestipino G, Chapel A, Villaz M, Ronjat M. Functional interaction of the cytoplasmic domain of triadin with the skeletal ryanodine receptor [In Process Citation]. *J Biol Chem* 1999; **274**: 12278-83.

484 Szegedi C, Sarkozi S, Herzog A, Jona I, Varsanyi M. Calsequestrin: more than 'only' a luminal Ca2+ buffer inside the sarcoplasmic reticulum. *Biochem J* 1999; **337**: 19-22.

485 Oyamada H, Murayama T, Takagi T, Iino M, Iwabe N, Miyata T, Ogawa Y, Endo M. Primary structure and distribution of ryanodine-binding protein isoforms of the bullfrog skeletal muscle. *J Biol Chem* 1994; **269**: 17206-14.

486 Ottini L, Marziali G, Conti A, Charlesworth A, Sorrentino V. Alpha and beta isoforms of ryanodine receptor from chicken skeletal muscle are the homologues of mammalian RyR1 and RyR3. *Biochem J* 1996; **315**: 207-16.

487 Imagawa T, Nakai J, Takeshima H, Nakasaki Y, Shigekawa M. Expression of Ca(2+)-induced Ca2+ release channel activity from cardiac ryanodine receptor cDNA in Chinese hamster ovary cells. *J Biochem (Tokyo)* 1992; **112**: 508-13.

488 Takeshima H, Nishi M, Iwabe N, Miyata T, Hosoya T, Masai I, Hotta Y. Isolation and characterization of a gene for a ryanodine receptor/calcium release channel in Drosophila melanogaster. *FEBS Lett* 1994; **337**: 81-7.

489 Altschul SF, Gish W, Miller W, Myers EW, Lipman DJ. Basic local alignment search tool. *J Mol Biol* 1990; **215**: 403-10.

490 Altschul SF, Madden TL, Schaffer AA, Zhang J, Zhang Z, Miller W, Lipman DJ. Gapped BLAST and PSI-BLAST: a new generation of protein database search programs. *Nucleic Acids Res* 1997; **25**: 3389-402.

491 Higgins DG, Thompson JD, Gibson TJ. Using CLUSTAL for multiple sequence alignments. *Methods Enzymol* 1996; **266**: 383-402.

492 Baron MD. MacBoxshade, A program for creating printouts from multiple aligned protein or DNA sequences. In.

493 Noda M, Furutani Y, Takahashi H, Toyosato M, Tanabe T, Shimizu S, Kikyotani S, Kayano T, Hirose T, Inayama S, et al. Cloning and sequence analysis of calf cDNA and human genomic DNA encoding alpha-subunit precursor of muscle acetylcholine receptor. *Nature* 1983; **305**: 818-23.

494 Balshaw D, Gao L, Meissner G. Luminal loop of the ryanodine receptor: a pore-forming segment? [comment]. *Proc Natl Acad Sci U S A* 1999; **96**: 3345-7.

495 Gyorke I, Gyorke S. Regulation of the cardiac ryanodine receptor channel by luminal Ca2+ involves luminal Ca2+ sensing sites. *Biopysical J.* 1998; **75**: 2801-10.

496 Doyle DA, Cabral J, Pfeutzner RA, Kuo A, Gulbis JM, Cohen SL, Chait BT, MacKinnon R. The structure of the potassium channel: molecular basis of K+ conduction and selectivity. *Science* 1998; **280**: 69-76.

497 Zhao M, Li P, Li X, Zhang L, Winkfein RJ, Chen SR. Molecular identification of the ryanodine receptor pore-forming segment. *J Biol Chem* 1999; **274**: 25971-4.

498 Wagenknecht T, Radermacher M. Three-dimensional architecture of the skeletal muscle ryanodine receptor. *FEBS Lett* 1995; **369**: 43-6.

499 Marks AR, Fleischer S, Tempst P. Surface topography analysis of the ryanodine receptor/junctional channel complex based on proteolysis sensitivity mapping. *J Biol Chem* 1990; **265**: 13143-9.

500 Wang JP, Needleman DH, Seryshev AB, Aghdasi B, Slavik KJ, Liu SQ, Pedersen SE, Hamilton SL. Interaction between ryanodine and neomycin binding sites on Ca2+ release channel from skeletal muscle sarcoplasmic reticulum. *J Biol Chem* 1996; **271**: 8387-93.

501 Callaway C, Seryshev A, Wang JP, Slavik KJ, Needleman DH, Cantu C, 3rd, Wu Y, Jayaraman T, Marks AR, Hamilton SL. Localization of the high and low affinity [3H]ryanodine binding sites on the skeletal muscle Ca2+ release channel. *J Biol Chem* 1994; **269**: 15876-84.

502 Guo W, Jorgensen AO, Jones LR, Campbell KP. Biochemical characterization and molecular cloning of cardiac triadin. *J Biol Chem* 1996; **271**: 458-65.

503 Treves S, Scutari E, Robert M, Groh S, Ottolia M, Prestipino G, Ronjat M, Zorzato F. Interaction of S100A1 with the Ca2+ release channel (ryanodine receptor) of skeletal muscle. *Biochemistry* 1997; **36**: 11496-503.

504 Ohnishi ST, Waring AJ, Fang SR, Horiuchi K, Flick JL, Sadanaga KK, Ohnishi T. Abnormal membrane properties of the sarcoplasmic reticulum of pigs susceptible to malignant hyperthermia: modes of action of halothane, caffeine, dantrolene, and two other drugs. *Arch Biochem Biophys* 1986; **247**: 294-301.

505 Fromming GR, Ohlendieck K. Isoform-specific interactions between halothane and the ryanodine receptor Ca(2+)-release channel: implications for malignant hyperthermia and the protein theory of anaesthetic action. *Naturwissenschaften* 1999; **86**: 584-7.

506 Mickelson JR, Gallant EM, Rempel WE, Johnson KM, Litterer LA, Jacobson BA, Louis CF. Effects of the halothane-sensitivity gene on sarcoplasmic reticulum function. *Am J Physiol* 1989; **257**: C787-94.

507 Mickelson JR, Litterer LA, Jacobson BA, Louis CF. Stimulation and inhibition of [3H]ryanodine binding to sarcoplasmic reticulum from malignant hyperthermia susceptible pigs. *Arch Biochem Biophys* 1990; **278**: 251-7.

508 Bhat MB, Zhao J, Zang W, Balke CW, Takeshima H, Wier WG, Ma J. Caffeine-induced release of intracellular Ca2+ from Chinese hamster ovary cells expressing skeletal muscle ryanodine receptor. Effects on full-length and carboxyl-terminal portion of Ca2+ release channels. *J Gen Physiol* 1997; **110**: 749-62.

509 Suda N, Franzius D, Fleig A, Nishimura S, Bodding M, Hoth M, Takeshima H, Penner R. Ca2+-induced Ca2+ release in Chinese hamster ovary (CHO) cells co- expressing dihydropyridine and ryanodine receptors. *J Gen Physiol* 1997; **109**: 619-31.

510 Takekura H, Takeshima H, Nishimura S, Takahashi M, Tanabe T, Flockerzi V, Hofmann F, Franzini-Armstrong C. Co-expression in CHO cells of two muscle proteins involved in excitation-contraction coupling. *J Muscle Res Cell Motil* 1995; **16**: 465-80.

511 Chen SR, Vaughan DM, Airey JA, Coronado R, MacLennan DH. Functional expression of cDNA encoding the Ca2+ release channel (ryanodine receptor) of rabbit skeletal muscle sarcoplasmic reticulum in COS-1 cells. *Biochemistry* 1993; **32**: 3743-53.

512 Du GG, Imredy JP, MacLennan DH. Characterization of recombinant rabbit cardiac and skeletal muscle Ca2+ release channels (ryanodine receptors) with a novel [3H]ryanodine binding assay. *J Biol Chem* 1998; **273**: 33259-66.

513 Du GG, MacLennan DH. Functional consequences of mutations of conserved, polar amino acids in transmembrane sequences of the Ca2+ release channel (ryanodine receptor) of rabbit skeletal muscle sarcoplasmic reticulum. *J Biol Chem* 1998; **273**: 31867-72.

514 Chen SR, Leong P, Imredy JP, Bartlett C, Zhang L, MacLennan DH. Single-channel properties of the recombinant skeletal muscle Ca2+ release channel (ryanodine receptor). *Biophys J* 1997; **73**: 1904-12.

515 Moore RA, Nguyen H, Galceran J, Pessah IN, Allen PD. A transgenic myogenic cell line lacking ryanodine receptor protein for homologous expression studies: reconstitution of Ry1R protein and function. *J Cell Biol* 1998; **140**: 843-51.

516 Radermacher M, Wagenknecht T, Grassucci R, Frank J, Inui M, Chadwick C, Fleischer S. Cryo-EM of the native structure of the calcium release channel/ryanodine receptor from sarcoplasmic reticulum. *Biophys J* 1992; **61**: 936-40.

517 Tunwell REA, Lai FA. Ryanodine receptor expression in the kidney and a non-excitable kidney epithelial cell. *J Biol Chem* 1996; **271**: 29583-8.

518 Guerrini R, Menegazzi P, Anacardio R, Marastoni M, Tomatis R, Zorzato F, Treves S. Calmodulin binding sites of the skeletal, cardiac, and brain ryanodine receptor Ca2+ channels: modulation by the catalytic subunit of cAMP- dependent protein kinase? *Biochemistry* 1995; **34**: 5120-9.

519 Makita N, Sloan-Brown K, Weghuis DO, Ropers HH, George AL, Jr. Genomic organization and chromosomal assignment of the human voltage-gated Na(+) channel beta-1 subunit gene (SCN1B). *Genomics* 1994; **23**: 628-34.

520 Wallace RH, Wang DW, Singh R, Scheffer IE, George AL, Jr., Phillips HA, Saar K, Reis A, Johnson EW, Sutherland GR, Berkovic SF, Mulley JC. Febrile seizures and generalized epilepsy

associated with a mutation in the Na(+)-channel beta-1 subunit gene SCN1B. *Nature Genet.* 1998; **19**: 366-70.

521 Watanabe TK, Shimizu F, Nagata M, Kawai A, Fujiwara T, Nakamura Y, Takahashi E, Hirai Y. Cloning, expression, and mapping of CKAPI, which encodes a putative cytoskeleton-associated protein containing a CAP-GLY domain. *Cytogenet Cell Genet* 1996; **72**: 208-11.

522 OMIM. Online Mendelian Inheritance in Man, OMIM (TM). In:, Vol. 1999: Center for Medical Genetics, Johns Hopkins University (Baltimore, MD) and National Center for Biotechnology Information, National Library of Medicine (Bethesda, MD), 1999.

523 Chen LS, Lo CF, Numann R, Cuddy M. Characterization of the human and rat phospholemman (PLM) cDNAs and localization of the human PLM gene to chromosome 19q13.1. *Genomics* 1997; **41**: 435-43.

524 Levitt RC, Liu Z, Nouri N, Meyers DA, Brandriff B, Mohrenweiser HM. Mapping of the gene for hormone sensitive lipase (LIPE) to chromosome 19q13.1-->q13.2. *Cytogenet Cell Genet* 1995; **69**: 211-4.

525 Trask B, Fertitta A, Christensen M, Youngblom J, Bergmann A, Copeland A, de Jong P, Mohrenweiser H, Olsen A, Carrano A, et al. Fluorescence in situ hybridization mapping of human chromosome 19: cytogenetic band location of 540 cosmids and 70 genes or DNA markers. *Genomics* 1993; **15**: 133-45.

526 Levitt RC, McKusick VA, Fletcher JE, Rosenberg H. Gene candidate [letter]. *Nature* 1990; **345**: 297-8.

527 Fletcher JE, Tripolitis L, Erwin K, Hanson S, Rosenberg H, Conti PA, Beech J. Fatty acids modulate calcium-induced calcium release from skeletal muscle heavy sarcoplasmic reticulum fractions: implications for malignant hyperthermia. *Biochem Cell Biol* 1990; **68**: 1195-201.

528 Fletcher JE, Mayerberger S, Tripolitis L, Yudkowsky M, Rosenberg H. Fatty acids markedly lower the threshold for halothane-induced calcium release from the terminal cisternae in human and porcine normal and malignant hyperthermia susceptible skeletal muscle. *Life Sci* 1991; **49**: 1651-7.

529 Baggio G, Manzato E, Gabelli C, Fellin R, Martini S, Enzi GB, Verlato F, Baiocchi MR, Sprecher DL, Kashyap ML, Brewer HBJ, Crepaldi G. Apolipoprotein C-II deficiency syndrome: clinical features, lipoprotein characterization, lipase activity, and correction of hypertriglyceridemia after apolipoprotein C-II administration in two affected patients. *J. Clin. Invest.* 1986; **77**: 520-27.

530 Pollock N, Hodges M, Sendall J. Prolonged malignant hyperthermia in the absence of triggering agents [see comments]. *Anaesth Intensive Care* 1992; **20**: 520-3.

531 Hodges M, Pollock NA, Couchman K, Hall KH, Spiers AD. Improving management following a malignant hyperthermia crisis. *Anaesth Intensive Care* 1990; **18**: 116-9.

532 Wedel DJ. The effect of age on the development of MH in susceptible piglets. *Anesthesiology* 1994; **81 No. 3A**: A426.

533 Bennett EJ, Bowyer DE. Principles of Paediatric Anaesthesia. In: (Thomas CC, ed). Illinois: Springfield, 1982: 66-71.

534 Wiswell TE, Bent RC, Solenberger R. Malignant hyperthermia in infancy. *South Med J* 1989; **82**: 1451-2.

535 Bailey AG, Bloch EC. Malignant hyperthermia in a three-month-old American Indian infant. *Anesth Analg* 1987; **66**: 1043-5.

536 Wilhoit RD, Brown RE, Jr., Bauman LA. Possible malignant hyperthermia in a 7-week-old infant [see comments]. *Anesth Analg* 1989; **68**: 688-91.

537 Pennington GP, Joeris L. Malignant hyperthermia in a 3-month-old infant: a case report. *J Med Assoc Ga* 1996; **85**: 162-3.

538 Meluch AM, Sibert KS, Bloch EC. Malignant hyperthermia following isoflurane anesthesia in an American Lumbee Indian. *N C Med J* 1989; **50**: 485-7.

539 Fahmy T. ***XlSTAT***. In:, Shareware edn., Vol. 2000: Thierry Fahmy, 1999.

APPENDICES

A 1 PRIMERS FOR PCR AND DNA SEQUENCING

RYR1 primers listed according to position on RYR1 sequence (from 5 ' terminus)

Primer	Forward/ Reverse	*Exon/ Intron*	Sequence 5' – 3'	*Template, /Function*	*Source*
RYR1-176F	F	E	CTTCCTCCCATCTCTGTCCA	Genomic seq	M
RYRintron1	R	I	CTAACCCAGAGAGACGCACC	Genomic seq	M
RYRex1.17F	F	E	CTCTGGTGTCTCCAGAGGTCTC	cDNA seq	M
-10	F	E	TTCCGACCTCGACATCATGGGTGACG	cDNA seq	TVM
RYRC35Fbio	F	I	B-TGGAGACGCTGCCCCTCGGTTC	Genomic seq	M
RYRC35-R	R	I	GGCCCCTCTTCCTCCTGCACAG	Genomic seq	M
RYRC35Rseq	F	I	CTTCCTCCTGCACAGACC	Genomic seq	M
RYR275R	R	E	GGATGACTCCACGCCAGCCTC	cDNA seq	M
409	F	E	CAGGAGGACGCAACAGGAGAG	cDNA seq	TVM
163F-bio	F	E	B-TCCAAGCAGAGGTCTGAAGGAGAA	RFLP	M
163R	R	E	AGCGCTCGGAGGAGACACTGACAA	RFLP	M
163i-R	R	I	CCCATGGTGAGAAGATGGGGAC	RFLP	M
163Rseq	R	I	GGAGACACTGACAAGGAT	RFLP	M
163Rseq	R	E	GGAGACACTGACAAGGAT	RFLP, seq	M
649	F	I	CACGTCCTCCGCCTCTTTCAT	cDNA seq	M
248F-bio	F	E	B-TGCTGACAGTGATGACCAGCGCAG	Genomic seq	M
248R	R	E	CTGATTCTCAGTGGCTCCAGCCTC	Genomic seq	M
248Rseq	R	E	GTGGCTCCAGCCTCCAGA	Genomic seq	M
952	F	E	TCCAAGGAGAAGCTGGATGT	cDNA seq	M
341F-bio	F	E	B-GAAGCTGGATGTGGCCCCCAAGCG	Genomic seq	M
341R	R	E	TCTGGAGCGGCATAGGTGAG	Genomic seq	M
341R-seq	R	E	CATAGGTGAGCCACAGTC	Genomic seq	M
403Fseq	F	E	GACGACGCACTGTCGCTGAC	RFLP	M
403Rbio	R	E	B-GTTGTATAGGCCATTGGTGCT	RFLP	M
RYR401iR	R	I	GTGTGGGGCAACAGAGGTAGAG	SSCP, Seq	M
RYR522F	F	E	GGAAAGAGATTGTGAATCTTGTCT	ARMS/seq	M
RYR522R-bio	R	E	B-ACCAGCCAGTCCAAGTTTGTGGAG	ARMS/seq	M
522F-Pst	F	E	CTCTCCATGGTCCTGAACTGCAGAGACCG	ARMS	M
522-F-wt	F	E	CTCTCCATGGTCCTGAATTGCATAGAC	ARMS	M
522 Rbio-Pst	R	E	GGACTGGACCCCTACCTAGGACTGCA	ARMS	M
RYR522F-NdeI	F	E	GGAAAGAGATTGTGAATCTTCCAT	ARMS	M
RYR552F-bio	F	I	TGGATCTGACACCTCTTCCCCC	RFLP	M
RYR552R	R	I	GGTGCCCAGAATGAGAGGTG	RFLP	M
RYR552R-seq	R	I	GAGAGGTGAAGCGGCCATC	RFLP	M
1755	R	E	TGCTTGTCCAGGAGGGAGATG	cDNA seq	TVM
614F-bio	F	E	GTCCTGGACGTGCTATGCTCCCTG	RFLP	M
614R	R	E	CTGGTGACATAGTTGATGAGGTTT	RFLP	M
614Rseq	R	E	AGTTGATGAGGTTTGTC	RFLP, seq	M
1927	F	E	CATCCGCCCCAACATCTTTGTG	cDNA seq	TVM

RYR 8132R	R	E	ATGAGGCATCCACATAGTCG	cDNA seq	M
8273	F	E	CGGAGTACACACACGAGAAGT	cDNA seq	TVM
8332	R	E	TCAGCTCCTCGTCTATGTTCTC	cDNA seq	TVM
8525	F	E	CACAAAGTGCCCAGACCTATG	cDNA seq	TVM
RYR2862F	F	E	GATCCTCGAGAAGGCTACAACCCT	RFLP linkage	M
RYR2862R	R	E	TTCTGCCAGTTGTTCTGCCATGGC	RFLP linkage	M
8582	R	E	GGGACAGGGTAACAGCACTAA	cDNA seq	TVM
8789	R	E	TAACCGCGTAGCCATTCATCT	cDNA seq	TVM
9022	R	E	GAGGCAGTGGTTGGTGAAGTA	cDNA seq	TVM
9178	F	E	GCCCCAGCTGTGGTCAACTG	cDNA seq	TVM
9234	R	E	TCAGGGCCTGACTTCATCACT	cDNA seq	TVM
RYR 9442	F	E	CAGCACCAGTTCGGAGATGA	cDNA seq	MTVM
9485	R	E	CAGCGTTCGGTAGCAAGAGA	cDNA seq	TVM
9696	F	E	CAACAGTGTGGAGGAGATGTGTC	cDNA seq	TVM
9769	R	E	TGTGTAGCGGGCACCTGACTC	cDNA seq	TVM
9916	F	E	GTCACCTCTGACCACCTCAACT	cDNA seq	TVM
10052	F	E	AGCTCCTGCAGTCCCACTTCA	cDNA seq	TVM
10109	R	E	CTCCTCCTCGGACACCACCT	cDNA seq	TVM
10298	R	E	TCTCGCCCACCATCCTGAACA	cDNA seq	TVM
10518	R	E	GGCAGCATCTTCTTCAGTGTG	cDNA seq	TVM
10648	R	E	CTTTCCCTGAAGGTGAAGGTT	cDNA seq	TVM
10809	F	E	CGAGCACCCTTACAAGTCTAA	cDNA seq	TVM
10884	R	E	AGGGGCGTCATACGGAAACAG	cDNA seq	TVM
11213	R	E	AGACCTCAACCTCCTCTTCAG	cDNA seq	TVM
11307	F	E	CGAGATGGTGCTGCAGATGAT	cDNA seq	TVM
11359	R	E	CAGCTTCAGGGTGGAGGACAC	cDNA seq	TVM
11514	F	E	TGCCTTTGAGAGACAGAACAA	cDNA seq	TVM
11725	F	E	TCATTTGCACTGTGGACTACCTC	cDNA seq	TVM
11787	R	E	ATGACATCCTTGCCCGAGTAG	cDNA seq	TVM
11924	R	E	TGCGTCCCATAGGCGACTGT	cDNA seq	TVM
12198	F	E	CTCTGAAGCCTTCCAGGACTAC	cDNA seq	TVM
12277	R	E	TGGACCGCTGAACTGCTTCTG	cDNA seq	TVM
12337	F	E	CGAAATGATCAACTGCGAAGAGTTC	cDNA seq	TVM
12418	R	E	ATGCTCCGACAGGTTGGTCAG	cDNA seq	TVM
12575	F	E	GAGACCAACCGCGCCCAGTG	cDNA seq	TVM
12643	R	E	AGCCTCGCCGCCCTCGTTCA	cDNA seq	TVM
12668	F	E	AGATGGAGCTCTTCGTGAGTTTCTG	cDNA seq	TVM
12753	R	E	CCCTCGTCCTCGTCGGTCTCC	cDNA seq	TVM
12892	F	E	GCCCTGCGAGGCCTCAGCTACC	cDNA seq	TVM
12974	R	E	CCAGAGCAGCGCCGCCACTG	cDNA seq	TVM
12985	F	E	CTGCTCTGGGCAGCAGTGAC	cDNA seq	TVM
13066	R	E	ACCAGGCCGCCGCCGAACAG	cDNA seq	TVM
13285	F	E	GACGGGGCGGTGGCCGTGAC	cDNA seq	TVM
13377	F	E	GCCCACACCCGAGGGCTCTC	cDNA seq	TVM
13356	R	E	GGTTCCGCAGGCGTCGTGTCC	cDNA seq	TVM
13731	R	E	TCCCCTGGTGGAGAGTCTGAG	cDNA seq	TVM
13903	F	E	GAACCCGCCCTGCGGTGTCTG	cDNA seq	TVM
13973	R	E	TTACCAGGGGCACCTTGAGAC	cDNA seq	TVM
14456	F	E	GCACCATCCTGTCCTCTGTCA	cDNA seq	TVM
RYR 14462	F	I	ACCTGGGCTGGTATATGGTG	SSCP seq	M

1993	R	R	AGTCACCTCGTCCACCATCAC	cDNA seq	TVM
RYR2536R	R	E	GGGCACGAAGTCGGTGTGTGA	cDNA seq	M
2477	F	E	CTCGAGAGCGACTCCATCTTG	cDNA seq	TVM
2770	F	E	TCTGGGGAGACGCTCAAGACT	cDNA seq	TVM
2824	R	E	GTTGTCCTCCGCCTTCTCATC	cDNA seq	TVM
RYR2859	F	E	ATGAGCAATGGGTACAAGCC	cDNA seq	TVM
3016	F	E	TACAGCGCAGTGCAGGACATC	cDNA seq	TVM
3065	R	E	CTTCATCCAGCAGGCGGTAGG	cDNA seq	TVM
3227	F	E	GCAGTCACCACAGGCGAGATG	cDNA seq	TVM
RYR1151F-	F	E	CAGCGCTGGCACTTGGGCAGT	RFLP linkage	M
RYR1151R	R	E	GAGGACCTCGCCATTGAGGGTGAA	RFLP linkage	M
3360	R	E	CGGTGCCCATTGAAGACATAG	cDNA seq	TVM
3586	F	E	GGCCAGGTGGGTCATCTGAAC	cDNA seq	TVM
3988	R	E	GCGGCGCAGGTTTTCGTAGTC	cDNA seq	TVM
3880	F	E	GTCCAGTTCCACCAGCACTTC	cDNA seq	TVM
4262	F	E	ACCCCGAGATCATCCTCAACA	cDNA seq	TVM
4296	R	E	GCAAAGACCCTCACGGAGTAA	cDNA seq	TVM
4520	F	E	TCAGCCACACGGACCTTGTCA	cDNA seq	TVM
4572	R	E	CCATTGGCTGTAAAGGTCATT	cDNA seq	TVM
4766	F	E	GCCCACCGCGGCTGGAGATG	cDNA seq	TVM
4800	R	E	GGCATGCGGCTCCAGGACACT	cDNA seq	TVM
5137	R	E	CACTTTCGAGGTGGATGCTGATGAG	cDNA seq	TVM
5285	F	E	CGGGAGTTGGAGTCACCACTT	cDNA seq	TVM
5430	R	E	GCCTCCCCCAGCATCCTCAGT	cDNA seq	TVM
5555	R	E	TCACATCCTCATCGCCAAAGA	cDNA seq	TVM
5880	F	E	TGCGGAGCGCTATGTGGACAA	cDNA seq	TVM
6082	R	E	GATGAAAGTCAAGCAAATCCTG	cDNA seq	TVM
6100	F	E	CATCAAGACCTGCTGGCACACT	cDNA seq	TVM
6163	R	E	CGGCTGCCCAGGGTGGTCTC	cDNA seq	TVM
6376	F	E	CAGTACGACGGGCTGGGTGAG	cDNA seq	TVM
6426	R	E	TCCACGGAGGACGGTGAGATG	cDNA seq	TVM
RYR 38intF	F	I	CAAAGCCTTGCATTGTCTCCT	gen. RFLP seq	M
RYR 39intR	R	I	ATGCAAAAGTAAGGGGAAGGG	gen. RFLP seq	M
RYR int 39 F	F	I	GATCTGTAAAGGCGGTCGGT	seq	M
RYR int 40 R	R	I	CCAGCACCTGCCTGGGCC	seq	M
6763	F	E	GCCACTGTTCTCCAGCAGGTA	cDNA seq	TVM
6426	R	E	TCCACGGAGGACGGTGAGATG	cDNA seq	TVM
7039	R	E	CACCACCACATTGGCGTTCTC	cDNA seq	TVM
2434F	F	E	CTTTGGTGAGGAACCGCCTGAAG	RFLP	M
2434R-bio	R	I	B-GAGTGCCTGCATGAGGCGTTCAAAG	RFLP	M
RYR R2453W F	F	I	CCGGCAAGGGTGAGGCCCTGT	SSCP	M
RYR 47exR	R	E	GGATGCTGACATCTTTGGCT	SSCP, cDNA seq	M
7361	F	E	CCATCCTCCGCTCCCTTGTG	cDNA seq	TVM
7393	R	E	GAGGCTGATGATGCCCACAAG	cDNA seq	TVM
RYR47exR	R	E	GGATGCTGACATCTTTGGCT	Gen, cDNA seq	M
7642	F	E	GCCGTGAACCGCTACCTGTG	cDNA seq	TVM
7699	R	E	GTGTTCTGTGCCCGCAAAGAG	cDNA seq	TVM
8025	R	E	AAAGATGCCCCAGAAGAGTTTC	cDNA seq	TVM
RYR 2729F	F	E	AAATACGACCCGGAGCTGTAC	RFLP linkage	M
RYR 2729R	R	I	B-CAGGGTCAGCAGATGTTGGAG	RFLP linkage	M

RYR 14486	F	I	CCCTCTTGGGACACTACAACA	SSCP seq	M
RYR 100iR	R	I	TTATCCCTTCACCACCCACT	SSCP seq	M
14512	R	E	GTAGACGACCACCGCCAGAAG	cDNA seq	TVM
15137	R	E	GGGCTTGCTGTGAGAATAAGG	cDNA seq	TVM

I = intron based primer, E = Exon based primer
B =5′ biotinylated
M = Primers purchased by Dept. of Biochemistry, or IMBS, Massey University.
TVM = Primers donated by Prof. Tommie McCarthy, University of Cork, Ireland

A 1.2 PCR primers for microsatellite markers

Marker	Marker Type	Primer	Sequence (5′-3′)
D19S220	CA repeat	D19S220 F	ATGTTCAGAAAGGCCATGTCATTTG
		D19S220 2	TCCTCAACGGATACACAGCAACAC
RYRCA	CA repeat	RYRCA F	GCATCACGGTCTGCAATTCAT
		RYRCA R	GCAATGGCATAATCTCAGCT
D19S190	CAG repeat	D19S190F	CCCATTGGTTGATTTTGC
		D19S190R	TTCTACTTGGAGGAAGAGGAGG
D19S47	CA repeat	D19S47 F	GATGTCTCCTTGGTAAGTTA
		D19S47 R	AATACCTAGGAAGGGGAGGG

A 1.3 PCR primer pairs for the detection of novel RYR1 mutations in genomic DNA

Mutation	Method of detection	Primer F, R	PCR sequence (5′-3′)	I/E
Arg401Cys	SSCP/seq	403 Fseq	GACGACGCACTGTCGCTGAC	E
		RYR401iR	GTGTGGGGCAACAGAGGTAGAG	I
Arg2452Trp	SSCP	RYRR2453WF	CCGGCAAGGGTGAGGCCCTGT	I
Arg2454His	SSCP	RYR 47ex(1309)R	GGATGCTGACATCTTTGGCT	E
Thr4826Ile	SSCP	RYR 14462 F	ACCTGGGCTGGTATATGGTG	I
His4833Arg	SSCP/seq	RYR 14486 F (seq)	CCCTCTTGGGACACTACAACA	I
		RYR 100i R	TTATCCCTTCACCACCCACT	I

No introns?

A 2 RYR1 cDNA SEQUENCE AND POLYMORPHISMS

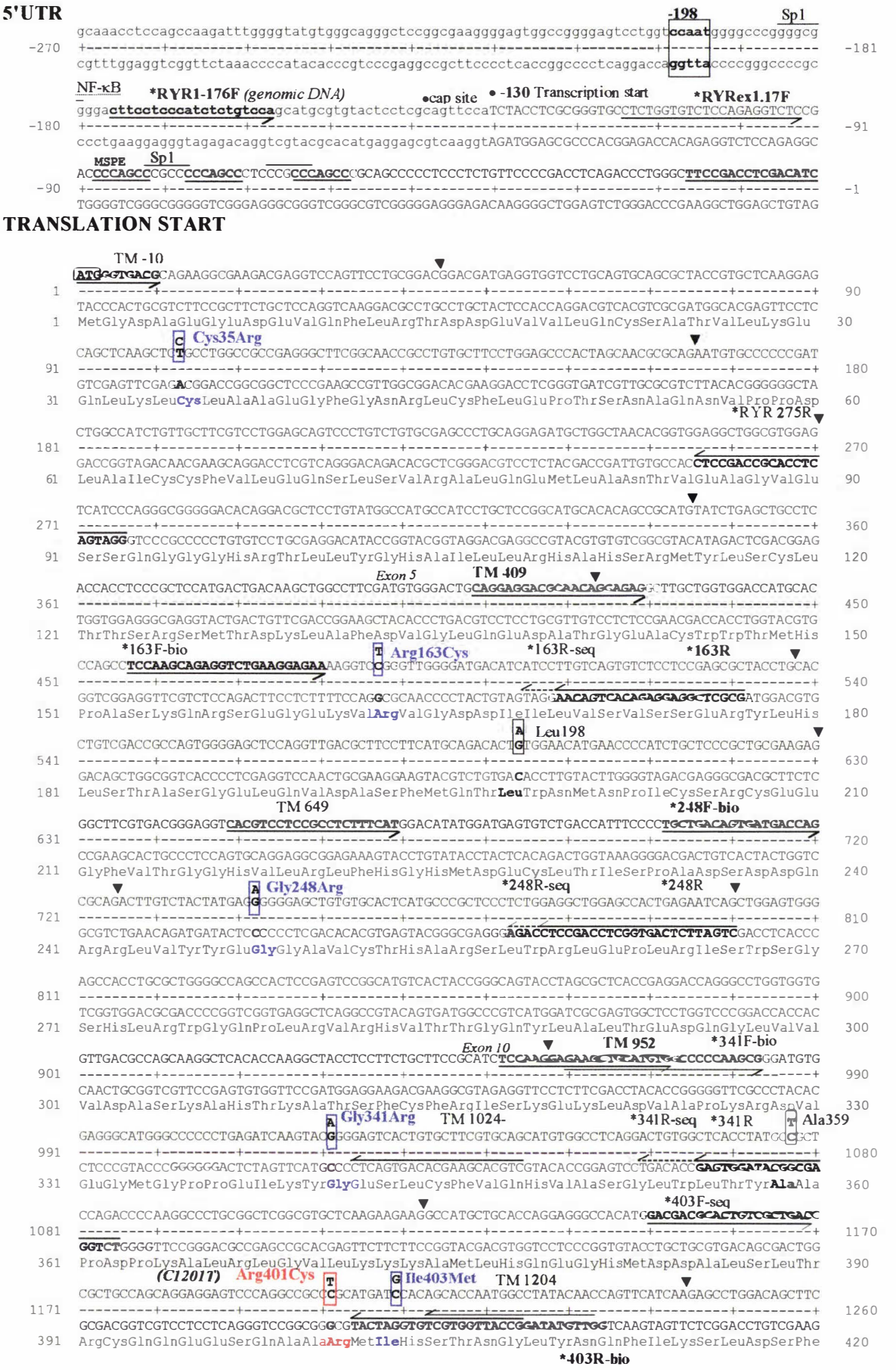

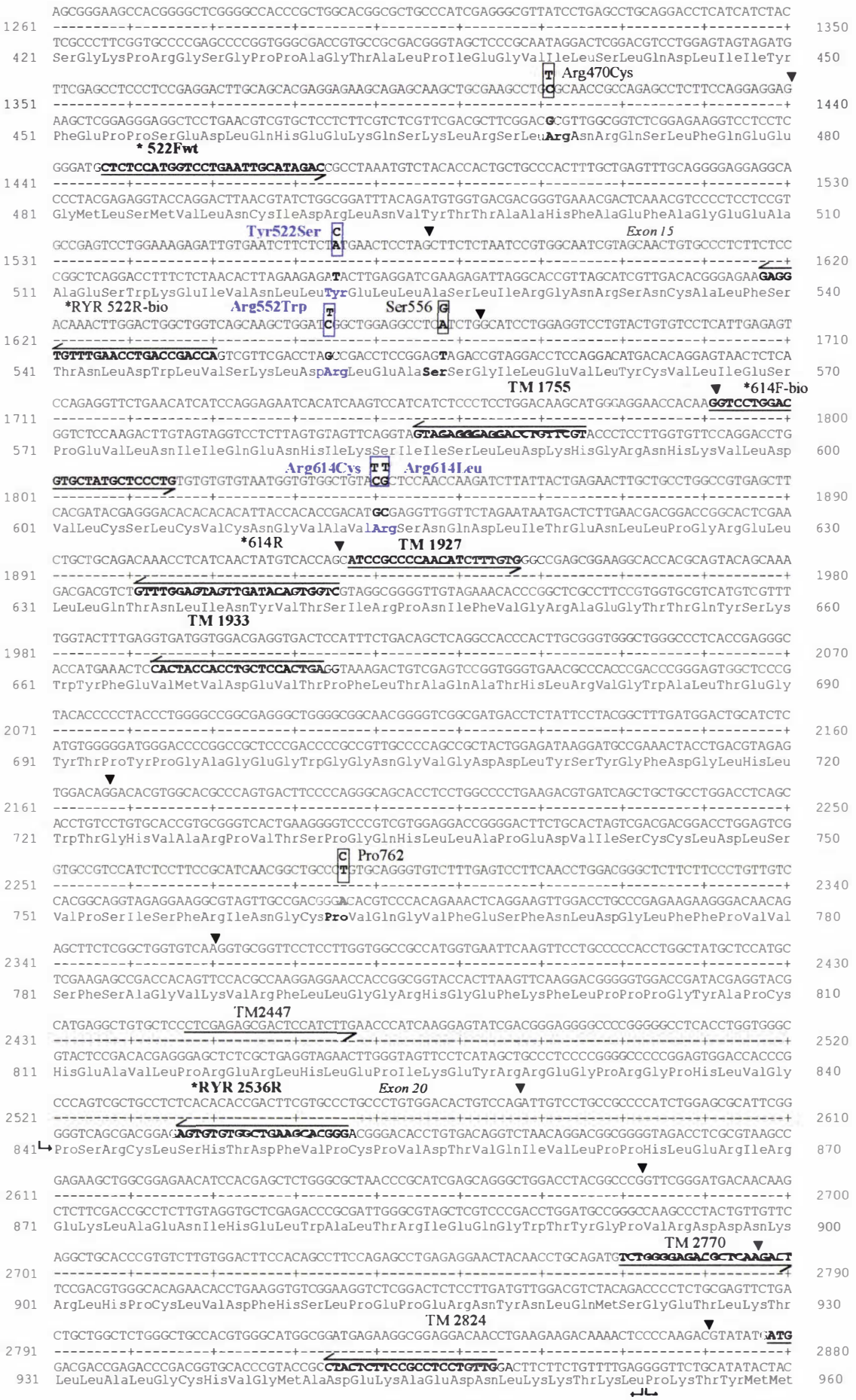
Arg470Cys
* 522Fwt
Tyr522Ser
Exon 15
*RYR 522R-bio
Arg552Trp
Ser556
TM 1755
*614F-bio
Arg614Cys
Arg614Leu
*614R
TM 1927
TM 1933
Pro762
TM2447
*RYR 2536R
Exon 20
TM 2770
TM 2824

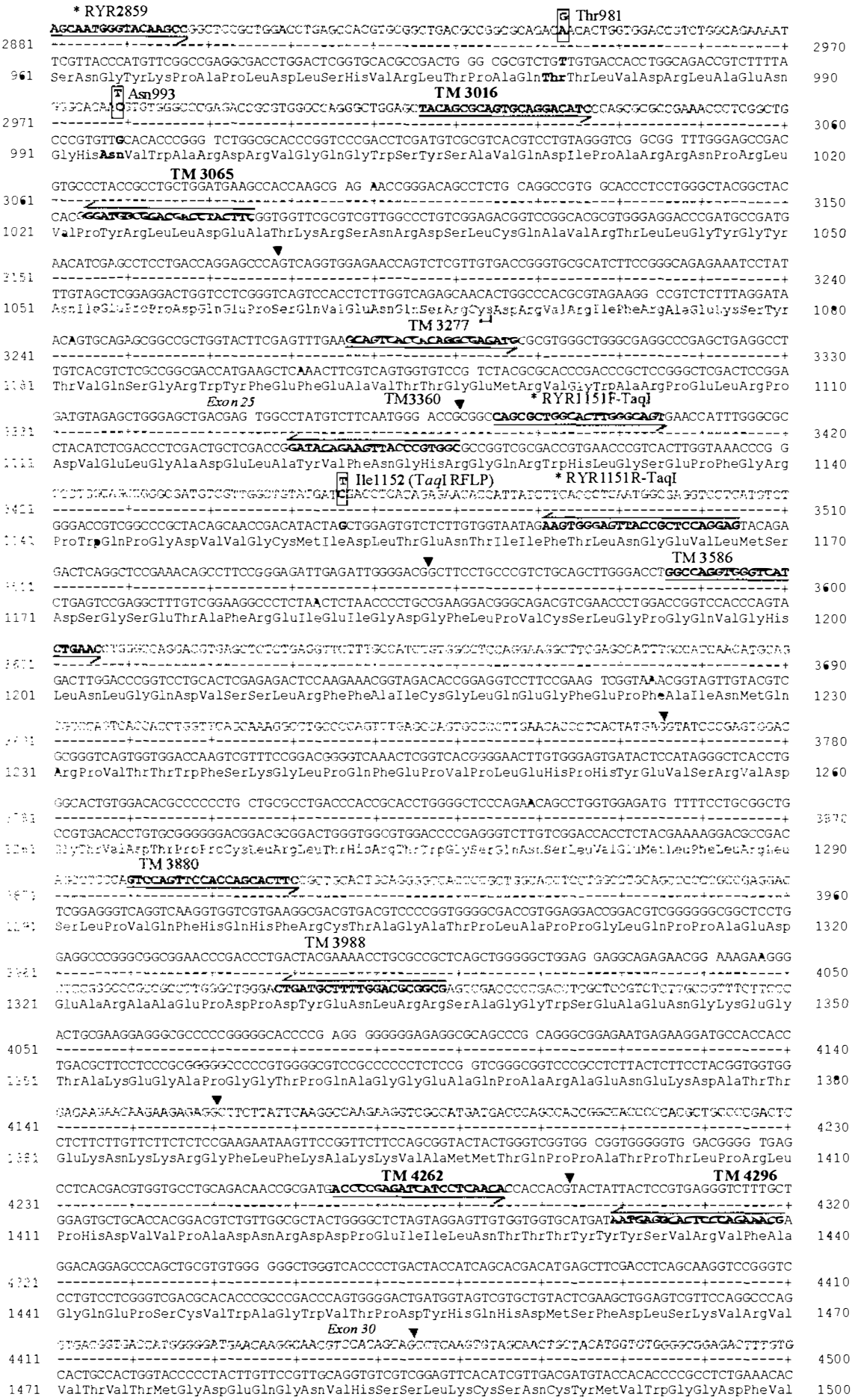
* RYR2859
Thr981
Asn993
TM 3016
TM 3065
TM 3277
TM3360
Exon 25
* RYR1151F-TaqI
Ile1152 (TaqI RFLP)
* RYR1151R-TaqI
TM 3586
TM 3880
TM 3988
TM 4262
TM 4296
Exon 30

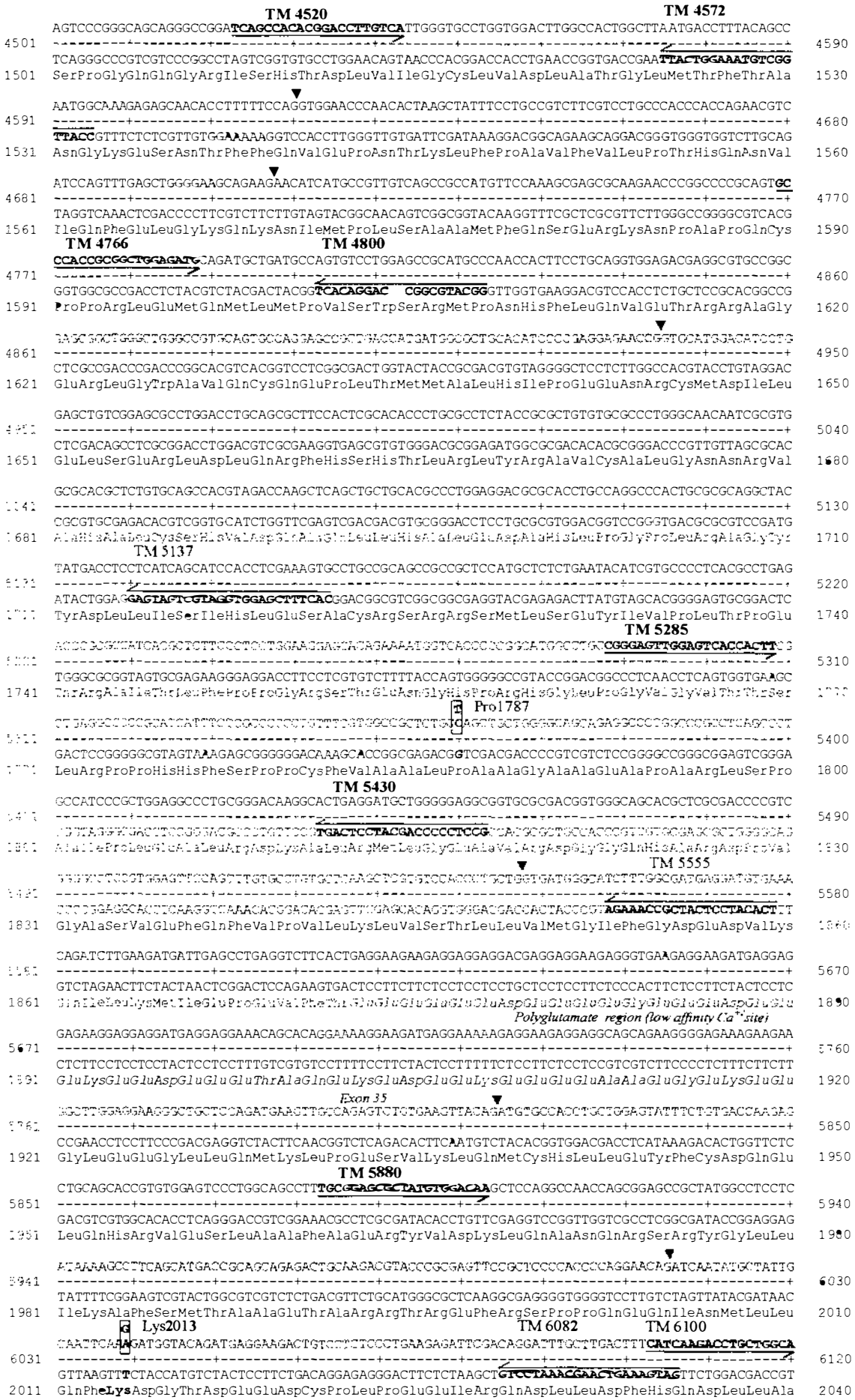
TM 4520
TM 4572
TM 4766
TM 4800
TM 5137
TM 5285
Pro1787
TM 5430
TM 5555
Polyglutamate region flow affinity Ca++ site
Exon 35
TM 5880
Lys2013
TM 6082
TM 6100


Gly2060Cys
TM 6376
TM 6426
Arg2163Cys
Arg2163His
Val2168Met
Thr2206Met
Exon 40
TM 6763
TM 7039
Cys2363 (NEW)
Pro2366 (NEW)
Arg2403 (NEW)
*2434F
Exon 45
A a2427 (NEW)
Gly2434Arg
Arg2435His/Leu
Arg2452Trp
(C7354T)
Arg2454His
(G7361A)
Arg2458Cys/His
TM 7361
TM 7393
*RYR 47ex (1309)R
Ala2500
Val2509
Val 2550 to Leu (corrected seq. error)

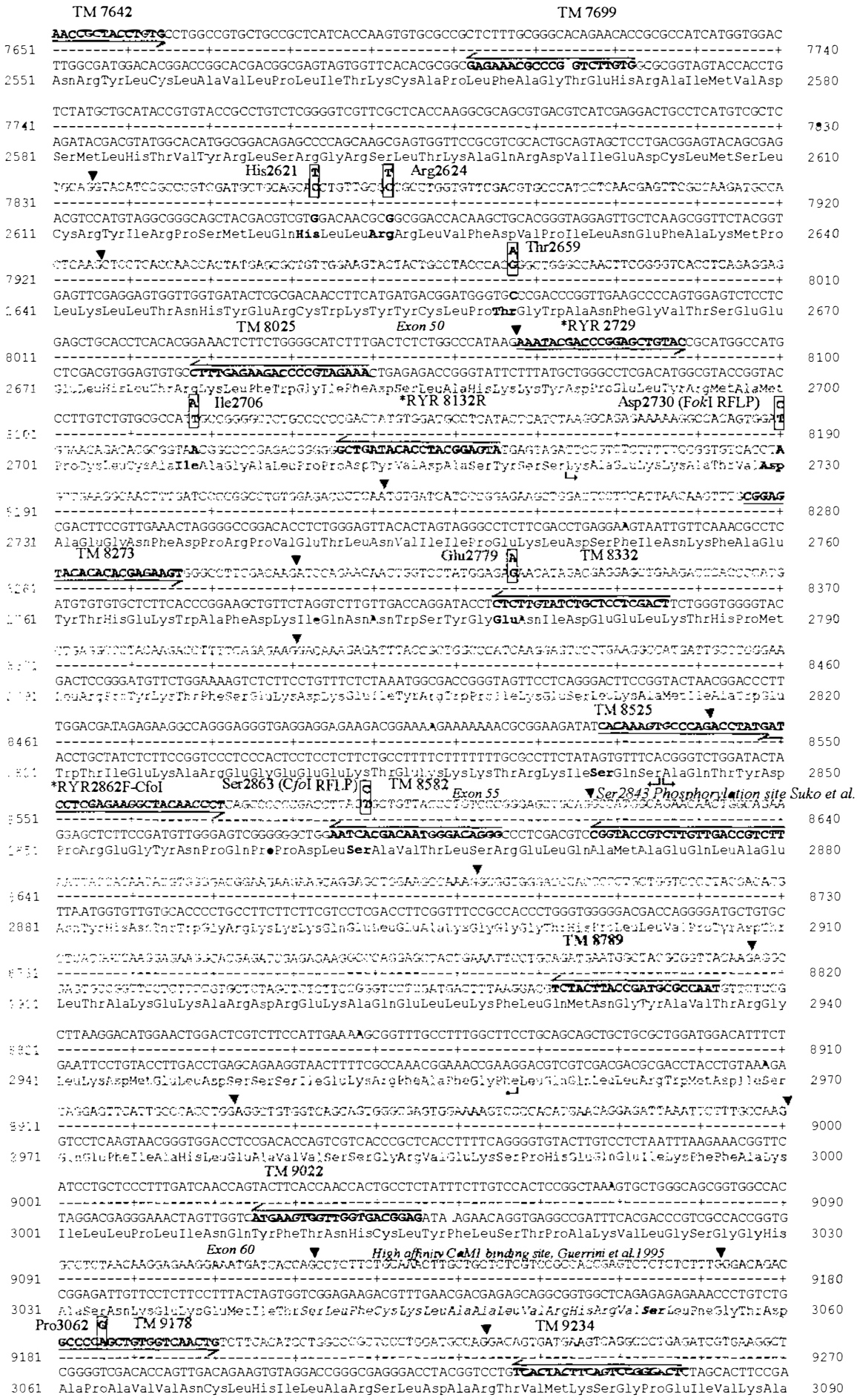
TM 7642
TM 7699
His2621
Arg2624
Thr2659
TM 8025
Exon 50
*RYR 2729
Ile2706
*RYR 8132R
Asp2730 (FokI RFLP)
TM 8273
Glu2779
TM 8332
TM 8525
*RYR2862F-CfoI
Ser2863 (CfoI RFLP)
TM 8582
Exon 55
Ser2843 Phosphorylation site Suko et al. 1993.
TM 8789
Exon 60
High affinity CaM1 binding site, Guerrini et al.1995
Pro3062
TM 9178
TM 9022
TM 9234

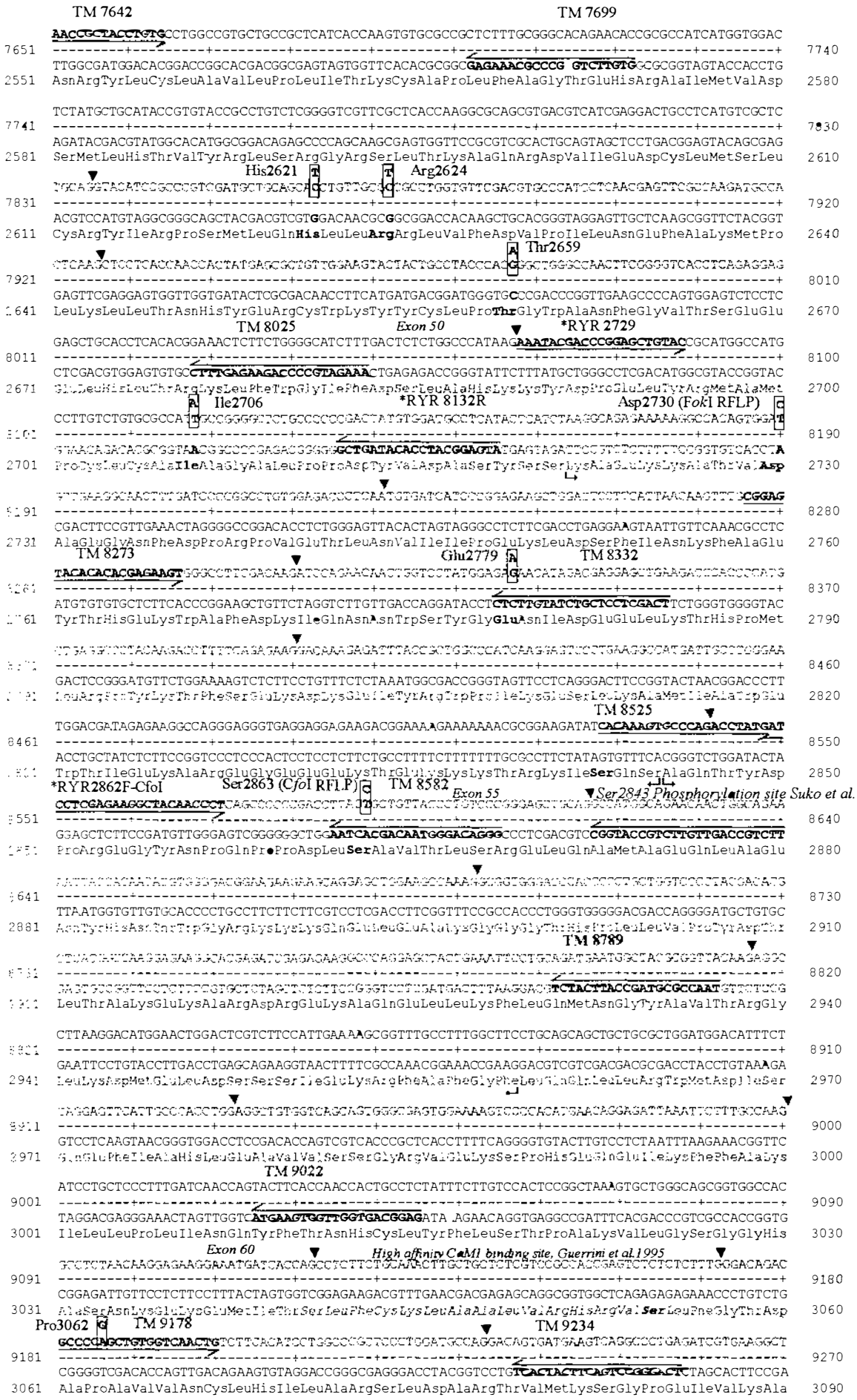
TM 7642
TM 7699
His2621
Arg2624
Thr2659
TM 8025
Exon 50
*RYR 2729
Ile2706
*RYR 8132R
Asp2730 (FokI RFLP)
TM 8273
Glu2779
TM 8332
TM 8525
*RYR2862F-CfoI
Ser2863 (CfoI RFLP)
TM 8582
Exon 55
Ser2843 Phosphorylation site Suko et al. 1993.
TM 8789
Exon 60
High affinity CaM1 binding site, Guerrini et al.1995
Pro3062
TM 9178
TM 9022
TM 9234

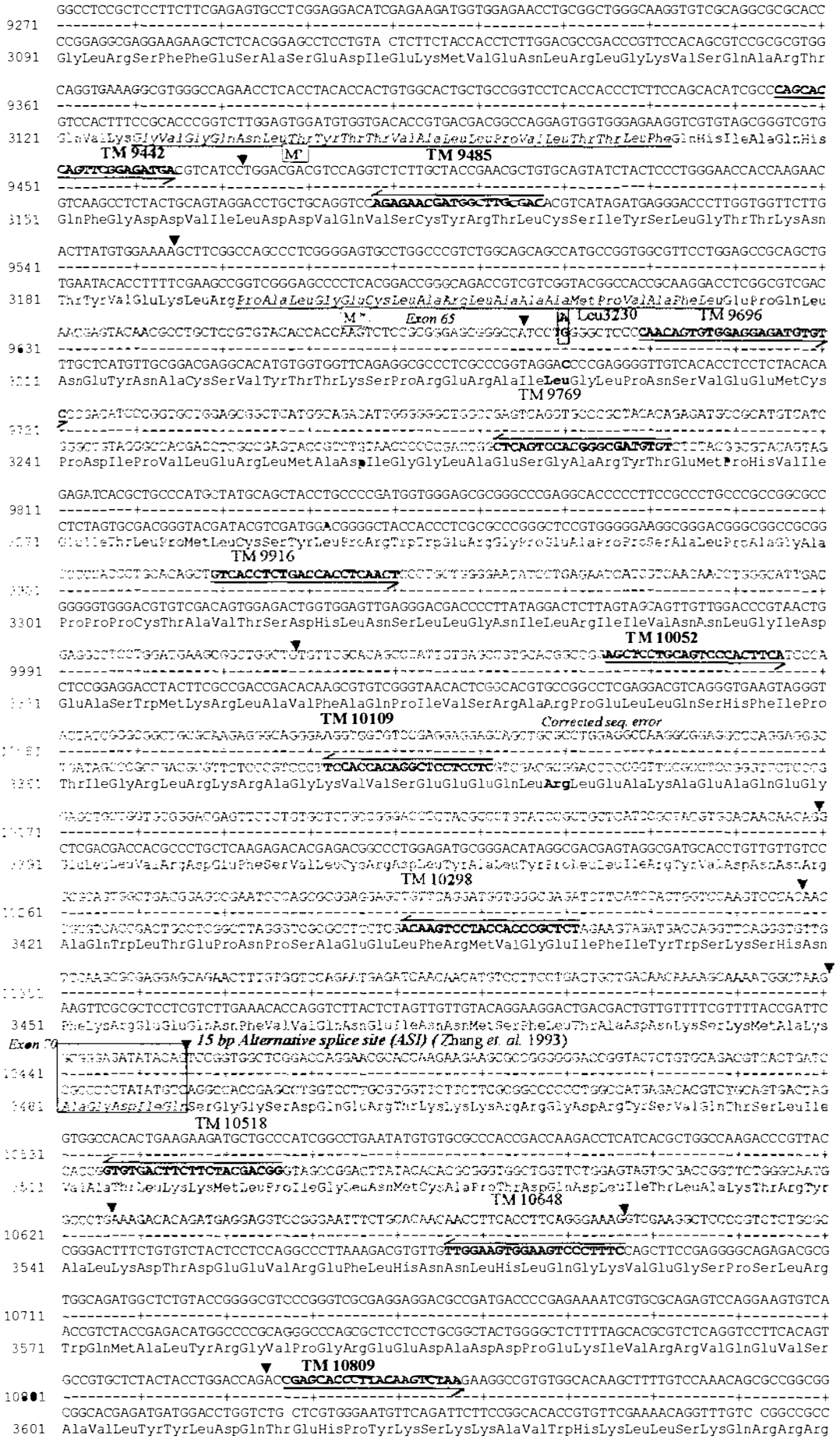
TM 9442
M'
TM 9485
Exon 65
Leu3230
TM 9696
TM 9769
TM 9916
TM 10052
TM 10109
Corrected seq. error
TM 10298
Exon 70
15 bp Alternative splice site (ASI) (Zhang et. al. 1993)
TM 10518
TM 10648
TM 10809

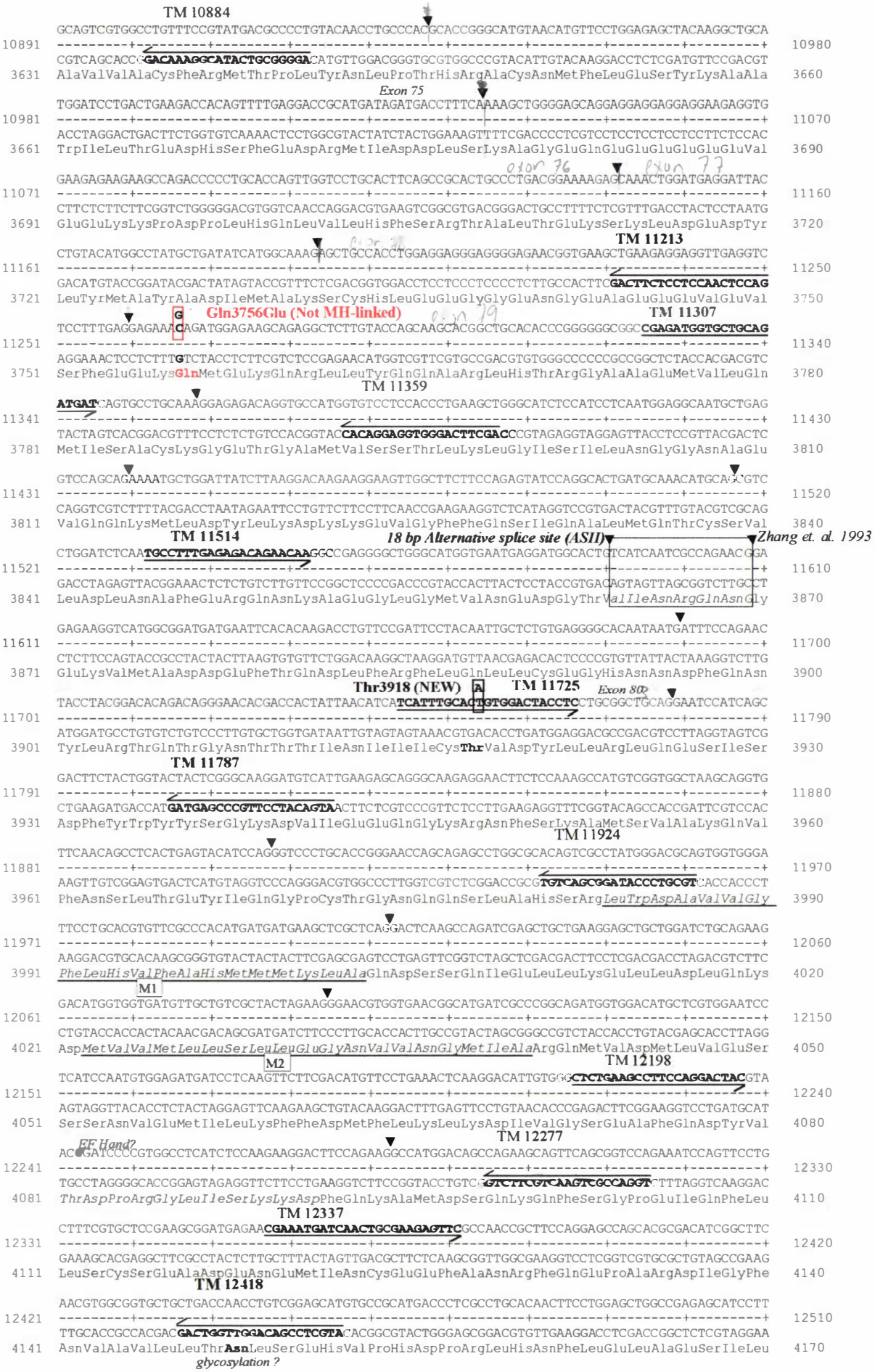
TM 10884
Exon 75
Exon 76
Exon 77
TM 11213
Gln3756Glu (Not MH-linked)
TM 11307
TM 11359
TM 11514
18 bp Alternative splice site (ASII)
Zhang et. al. 1993
Thr3918 (NEW)
TM 11725
Exon 80
TM 11787
TM 11924
M1
M2
TM 12198
EF Hand?
TM 12277
TM 12337
TM 12418
glycosylation ?

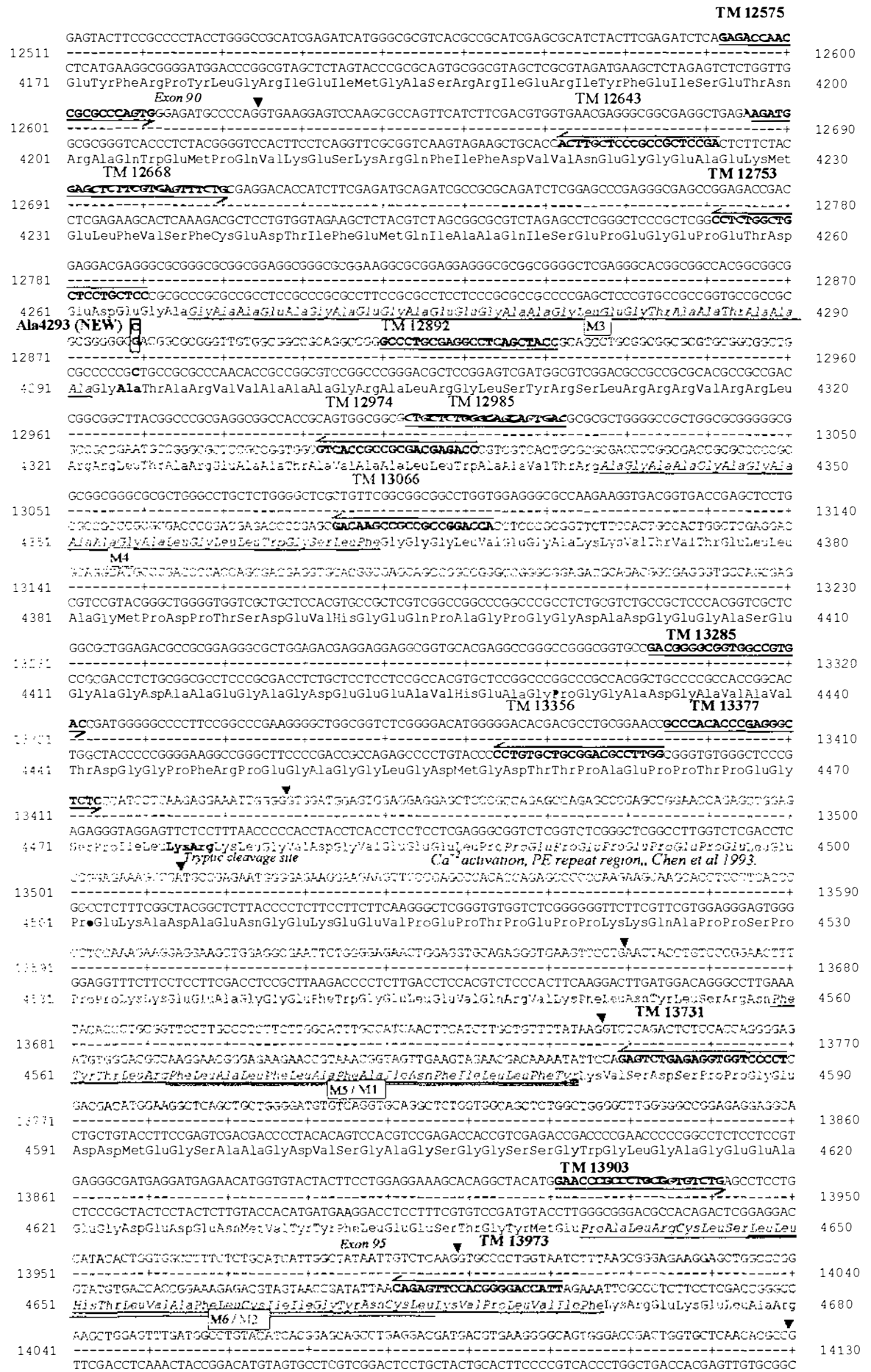
TM 12575
Exon 90
TM 12643
TM 12668
TM 12753
Ala4293 (NEW)
TM 12892
M3
TM 12974
TM 12985
TM 13066
M4
TM 13285
TM 13356
TM 13377
Tryptic cleavage site
Ca++ activation, PE repeat region,, Chen et al 1993.
TM 13731
M5 / M1
TM 13903
Exon 95
TM 13973
M6 / M2

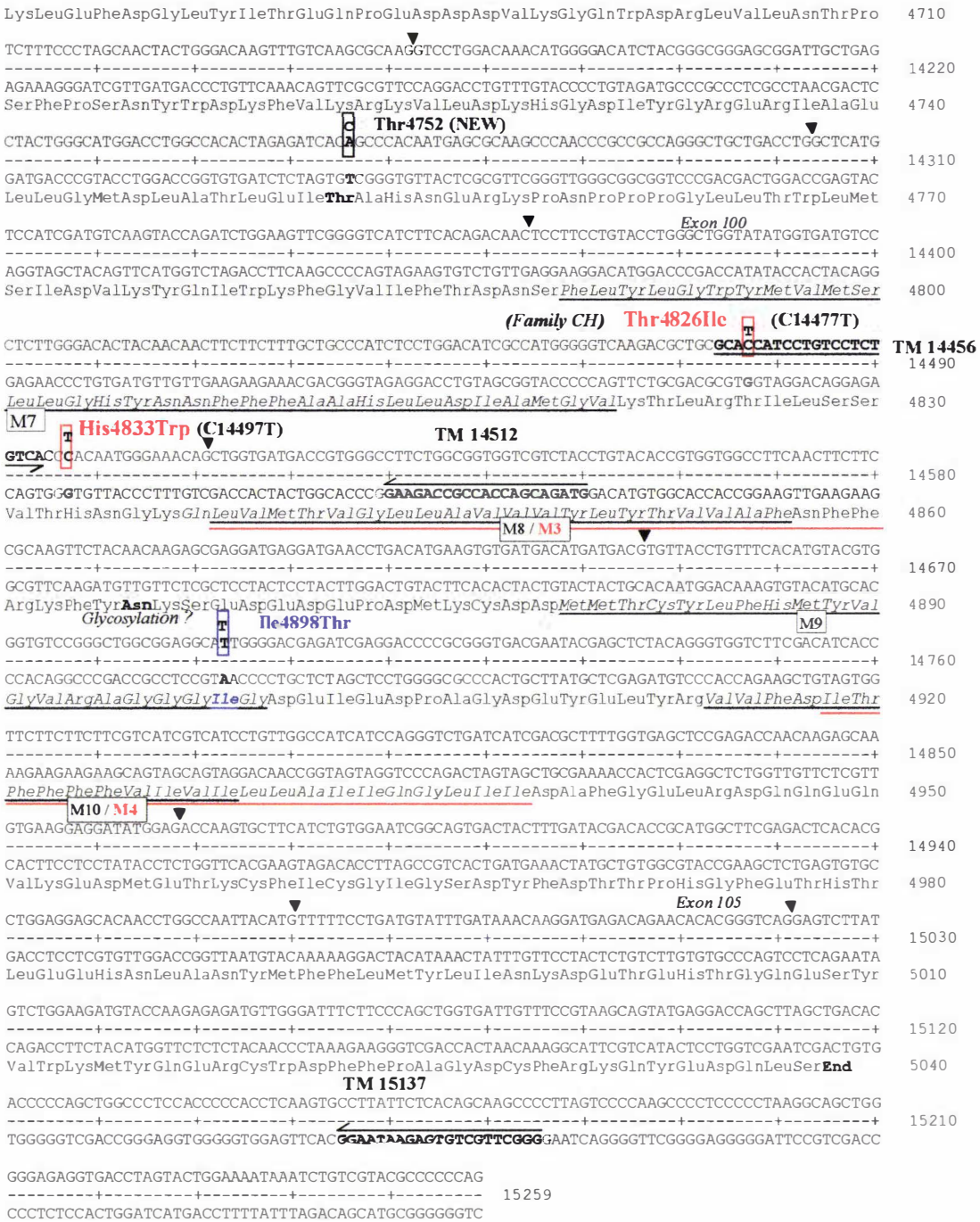

Updated RYR1 UTR and coding sequence. Locations of proposed CCAAT box, GC-rich muscle specific promotor elements (MSPE), cap site, SpI and NF-kB binding sites and putative transcription start sites in the 5' upstream region of the RYR1 gene are taken from Phillips *et al.* 1996 [160] (further sequence corrections are indicated). Primer sequences are highlighted and underlined. "TM" primers were provided by TVM McCarthy. Remaining oligonucleotide sequences (*) derived from exon sequences were designed for the amplification of MH mutation regions, RFLP genotyping of genomic DNA and cDNA amplification and sequencing. Primer labels in bold face were used successfully in RT-PCR amplification of cDNA. Nucleotide and amino acid substitutions for reported and novel sequence polymorphisms, reported MH/CCD mutations (blue) and novel MH mutations identified in NZ families (red) are indicated. Alternatively spliced regions ASI and ASII are boxed. Putative transmembrane spanning segments are underlined and labeled according to Zorzato *et al.* [126] (black) or Takeshima *et al.* [155] (red) models of membrane topology. Repeated sequence elements, conserved between RyR classes are marked with arrows [126,192,217,517]. Polyglutamate [126] proline-glutamate repeat [239], and putative EF hand Ca^{+2}- binding sequences [192] and a high affinity calmodulin binding site [518] in italics.

A 3 ONLINE RESOURCES :, GENETIC MAPS AND MARKERS

1. The genome database (GDB) maintained by Johns Hopkins University, Baltimore (http://gdbWWW.gdb.org/) is the primary resource for Human gene loci, mutations, probes, genetic maps and polymorphisms, including allele sizes and frequencies. Direct links to corresponding Genbank resources for detailed sequence and reference information are provided.

2. The Online Mendelian Inheritance in Man (OMIM) database provides information about human genetic diseases and their symptoms, and contains direct links to relevant genetic maps (GDB). OMIM is available via the NCBI site at http://www.ncbi.nlm.nih.gov/Omim/.

3. The data of the CEPH Genethon map is available from Genethon, with a browseable interface from the Baylor College of Medicine Genome Centre (http://gc.bcm.tmc.edu:8088/bio/access_gdata.html).

4. Integrated linkage maps, markers, and genotype data can also be retrieved at the Cooperative Human Linkage Center (CHLC) (http://www2.igh.cnrs.fr/HUM-Genome-DB.html).

5. Human expressed sequence tags (Est's) are catalogued at the ESTdb Database (gopher://gopher.gdb.org/77/.index/est/).

6. Information about the progress of the sequencing of the human genome is provided by the Human Genome Project Directory (http://www2.igh.cnrs.fr/HUM-Genome-DB.html).

A 4 CHROMOSOME 19q MAP

The involvement of alternate MH genes positioned nearby RYR1 was suggested to account for apparent recombinant between RYR1 markers and the MHS phenotype [1, 2]. The GDB comprehensive chromosome 19 map [349] was examined for the existence of potential candidate MH genes within a region extending 3 Mb proximal and distal to the RYR1 locus. 27 genes of known function have been mapped to this region, including 5 expressed in muscle tissue. The location of relevant genes and markers relative to the RYR1 locus is illustrated below.

Partial chromosome map: 19q13.1-13.2

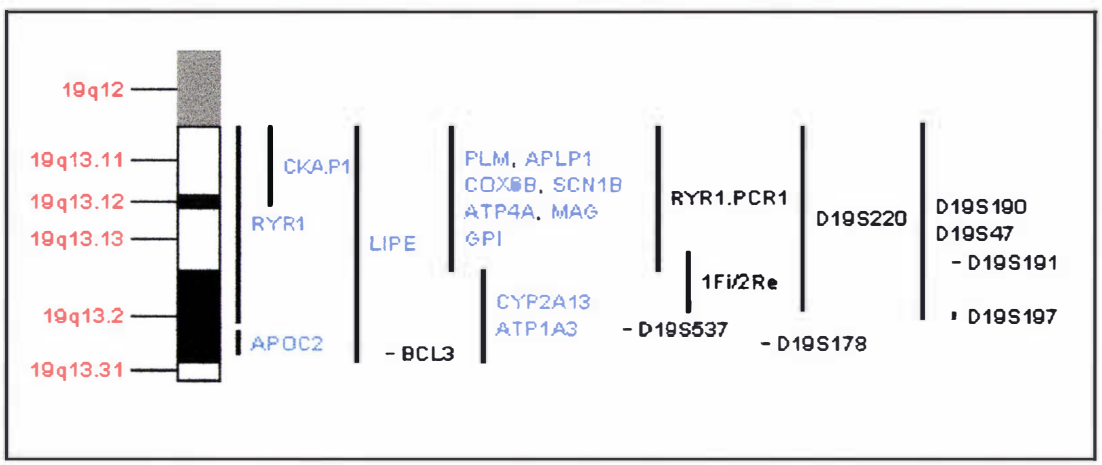

Combined CHLC and GDB integrated sex-averaged chromosome 19 map query (MAPVIEW) included 3Mb either side of the RYR1 locus [349]. Selected genes of interest are printed in blue test, markers in black. Markers and genes not relevant linkage of MH to the region are not included. 1F1/2Re refers to a RYR1 RFLP amplimer. RYR1.PCR1 is the RYR1 CA repeat marker.

1.1.1 Alternate gene candidates in the chromosome 19q13.1-13.2 region

SCNB1 The gene encoding the beta subunit (SCNB1) of the type 1 voltage-gated sodium channel modulates the sodium channel inactivation kinetics, and is therefore a candidate for hereditary disorders affecting membrane excitability. SCNB1 was mapped to chromosome 19q13.1[519]. Note that the SCN4A gene encodes the alpha subunit of the voltage gated Na^+ channel and has been proposed as the MHS2 locus in families demonstrating linkage to the chromosome 17q region [30,391]. SCN4A defects are causative of generalised nondystrophic myotonias, hyperkalemic periodic paralysis, succinylcholine-induced masseter muscle rigidity (MMR) and abnormal IVCT responses [154]. Mutations in the sodium channel beta-1 subunit gene (SCN1B) on chromosome 19q13.1 are associated with a disorder characterised by febrile seizures in early childhood and generalised epilepsy [520] but have not been linked to MH-type myopathies.

CKAP1 Encodes the cytoskeleton-associated protein 1, expressed in a variety of tissues. Assigned to 19q13.11-q13.12 by fluorescence in situ hybridisation (FISH) [521]. Disease phenotypes associated with CKAP1 gene defects have not been described [522].

PLM Encodes Phospholemman, a plasma membrane expressed highly in skeletal muscle and heart. PLM is phosphorylated in response to insulin and adrenergic stimulation and induces a hyperpolarization-

LIPE Mapped to 19q13.1-q13.2 by FISH [524] near to the APOC2 gene [525]. LIPE encodes hormone-sensitive lipase (HSL), involved in the mobilization of FFA from adipose. Proposed as a potential MH gene candidate [526] on account of the raised free fatty acid levels observed in porcine MHS muscle [527] togther with observations that freefatty acids markedly lower the threshold for halothane-induced calcium release from the SR of skeletal muscle [527,528]. Apolipoprotein C-II (apoC-II) is a necessary cofactor for the activation of lipoprotein lipase, the enzyme that hydrolyzes triglycerides in plasma and transfers the fatty acids to tissues [529]. The LIPE and APOC2 genes, are located approximately 7 cM telomeric to RYR1 (GDB integrated chromsome 19q map). LIPE, APOC2 and other MH gene candidates distal to D19SS47 were excluded as candidate MHS genes in the CH family by a recombination between the disease trait and the D19S47 locus, which lies between the RYR1 and APOC2 gene (Figure 4-12).
Other genes of interest mapped to the 19q13.1 region include the myelin asociated glycoprotein (MAG), cytochrome C-oxidase, (COX7A1) glucose phosphate isomerase (GPI) and the ATPase H^+/K^+ transporting alpha polypeptide (ATP4A) [349].

A 5 NZ MHS FAMILIES : SUMMARY OF IVCT AND GENETIC INVESTIGATION

Family	MHS	MHE	MHN	Selected DNA	IVCT result *	Mutation Identified **	.....RYR1 Mutation screen.....				CAC
							RFLP	Seq	RFLP/ cDNA seq	SSCP	RFLP
1	2	4		M470	S (3.8/3.2)	H4833Y (19)	1-7	8, 9	13-17	15,16, 18-22	23
"				M230	E (0.8/0.0)	Neg	1-7	8, 9			
3		2	1	M92	E (0.8/0)	-	1-7	8, 9		15,16, 18-22	23
"				M77	E (0.7/0)	-	1-7	8, 9			
4	3		1	M293	S (6.3/3.0)	-	1-7	8			23
5	7	4	4	M330	S (4.5/2.0)	G2434R (4)	1-7	6, 8-12	13, 14	15,16, 18-22	23
7	2	2		M15	S (1.2/0.9)	-	1-7	8, 9	13, 14	15,16, 18-22	23
17		1		M49	E (0.9/0)	-	1-7	8, 9		15,16, 18-22	23
19	3			M9	S (3.5/3.4)	-	1-7	6, 8-12	13-16	15,16, 18-22	23
24	4		1	M342	S (2.7/1.1)	G341R (8)	1-7	8-12			
"				M445	S (2.3/2.8)	G341R (8)		8-12	13 -17	15,16,18-22	23
25	3			M285	S (1.8/0.6)	-	1-7	8, 9		15,16,18-22	23
32	1			M270	S (3.8/2.0)	-	1-7	8, 9		15,16,18-22	23
35	2			M218	S (2.3/2.4)	R163C (1)	1-7	8, 9		15, 16,18-22	23
36	2			M535	S (4.3/2.7)	R2452W (20)	1-7	8-12	13-17	15, 16,18-22	23
41	1			M203	S (1.3/0.3)	-	1-7	8, 9		15, 16,18-22	23
48	2	1		M200	S (0.7/0.6)	-	1-7	8, 9		15, 16,18-22	23
49	2			M299	S (3.9/3.5)	-				15, 16,18-22	23
51	1			M88	S (1.1/0.8)	-	1-7	8, 9		15, 16,18-22	23
52	2	3	6	M128	S (2.7/0.2)	-	1-7	6, 8-10		15, 16,18-22	23
53-	1		1	M63	S (2.6/1.9)	-	1-7	8, 9		15, 16,18-22	23
55	1	1		M72	S (0.7/0.3)	-	1-7	8, 9		15, 16,18-22	23
58	1		1	M119	S (7.5/5.4)	R2454H (21)	1-7	8, 9	13-17	15, 16,18-22	23
59	1	1	2	M124	S (2.2/0.2)	-	1-7	8, 9		15, 16,18-22	23
60	1			M55	E (0.6/0.05)	-	1-7	8, 9		15, 16,18-22	23
61	1		4	M123	S (0.7/0.6)	-	1-7	8-10		15, 16,18-22	23
63	1			M70	S (0.4/0.2)	-	1-7	8, 9		15, 16,18-22	23
64	2			M122	S (3.8/1.7)	-	1-7	8, 9		15, 16,18-22	23
65		1		M134	E (0.4/0.1)	-	1-7	8, 9		15, 16,18-22	23
70	2			M479	S (5.5/2.7)	R401C (22)	1-7	8-12	13-17	15, 16,18-22	23
71		2	3	M126	E (1.4/0.1)	-	1-7	8, 9		15, 16,18-22	23
73	3	2	2	M176	S (2.8/0.9)	-	1-7	8, 9		15, 16,18-22	23

A 5 NZ MHS FAMILIES: IVCT AND GENETIC INVESTIGATION

74	2			**M181**	S (CCD, 1.5/0.5)	-	1-7	8, 9	13-16	15, 16,18-22	23
76	2			**M90**	S (1.0/ 0.7)	-	1-7	8, 9		15, 16,18-22	23
77	1	1	2	**M117**	S (1.1/0.3)	-	1-7	8, 9		15, 16,18-22	23
78				**M180**	S (1.4/0.5)	-	1-7	8, 9		15, 16,18-22	23
80		1		**M167**	E (1.4/0.1)	-	1-7	8, 9		15, 16,18-22	23
94	1			**M169**	S (5.5/5.0)	-	1-7	6,8, 9	13 -16	15, 16,18-22	23
95	2			**M410**	S (4.6/1.3)	-	1-7			15, 16,18-22	23
96	1	2		**M481**	S (died, MH)	-	1-7			15, 16,18-22	23
97	2		1	**M489**	S (2.6/0.9)	-	1-7			15, 16,18-22	23
98		1		**M506**	S (1.3/0.2)	-	1-7			15, 16,18-22	
99	1			**M511**	S (3.8/2.4)	-	1-7			15, 16,18-22	
CHEA	58	45	27	**M2 / M60**	S (1.6/0.9)	T4826I (18)	1-7	6, 8-12	13-16	18, 19	23
CHKM				**M121**	S (5.7/4.0)	T4826I (18)	1-7	8-12	13-16	18, 19	23
CHEH				**M221**	S (4.9/2.7)	T4826I (18)	1-7	8-12	13-17	18-22	23
CHRA				**M74**	S (3.6/2.1), MH	T4826I (18)	1-7	8-12	13-17	18-22	23
CHKM				**M98**	S (1.7/1.0)	Neg	1-7	9-11	13-16		23
CHKW				**M102**	S (0.2-1.0/0.2)	Neg	1-7	8-12	13-16	18-22	23
CHEA				**M54**	S (1.4/1.0)	Neg	1-7	9-11	13-16	18-22	23
CHEA				**M175**	S (3.7/0.9)	Neg	1-7	9-11	13-16	18-22	23
CHES				**M210**	S (1.5/0.5)	Neg	1-7	9-11	13-16	18-22	23
CHEH				**M130**	S (1.2/0.3)	Neg	1-7	9-11	13-16	18-22	23

* Maximum IVCT tensions recorded at 2 % halothane/ 2 mM caffeine
** Mutation, code (see below)

Code (novel mutations in italics)

Number	RYR1 Mutation	Number	RYR1 Mutation
1	R163C	12	Y522S
2	I403M	13	R2163C
3	Y522S	14	R2163H
4	R552W	15	R2458C
5	R614C	16	R2458H
6	G2434R	17	V2206M
7	R2435C	18	*T4826I*
8	G248R	19	*H4833Y*
9	G341R	20	*R2452W*
10	C35R	21	*R2454H*
11	R614L	22	*R401C*
		23	R1086C (CACNLIA3 Mutation)

A 6 CLINICAL CASE REPORTS:

Example case reports for probands identified with RYR1 mutations are summarised below Information for the CH family was provided by Dr. Neil Pollock (specialist anaesthetist, Palmerston North hospital). Details of other MH crises were obtained from the Palmerston North hospital Department of anaesthesia and intensive care MH database.

A6.1 CH Family.

Ethnic group: Maori pedigree,
Pedigree size: 1400 members traced over seven generations
Pedigree diagram: Complex pedigree illustrated in Appendix 9. Select branches in Figures 4-10 to 4-13
Mutation: Thr4826Ile

Clinical MH events in the CH family

Case No.	Pedigree Branch	Ped. ID no.	Reaction details	IVCT	MHS confirmed relatives	DNA ID	DNA result
1	CHEA	294	Fatal	NT	4 MHS Nieces	NA	NT
2	CHEA	337	Fatal	NT	Sister MHS	NA	NT
3	CHNG	55	Fatal	NT	Nephew MHS	NA	NT
4	CHNG	63	Fatal	NT	Sister MHS	NA	NT
5	CHRA	90	Fatal	NT	Son MHS	NA	NT
6	CHRA	92	X 2,	MHS	(Mother died MH)	M74	POS
7	CHRA		X 1,	NT	Mother MHS	M633	POS
8	CHEH	244	X 2,	MHS	Sister MHS	M10	POS
9	CHKM	154	X 2,	NT	Sister, Brother (x2) MHS	M29	POS
10	CHKC	169	X 1,	NT	Brother MHS	M404	POS
11	CHKM	136	X 1,	NT	Father, sister MHS	M573	POS
12	CHKW	125	X 1,	NT	Aunt MHS	NT	NT

NT = not tested, Pos = positive for the Thr4826Ile mutation
NA = DNA samples not available for testing.
X2 = Two separate MH events

Documented case reports

Case 1: CHEA branch, ID294, Figure 4-11, A9
A 20 year old male was admitted for wiring of mandible following a rugby injury. He had a normal past history. Anaesthesia was induced with thiopentone, nasotracheal intubation facilitated with suxamethonium, and anaesthesia maintained with halothane breathing spontaneously. One hour after induction of anaesthesia he was noted to be pyrexic, sweating, rigid and exhaustion of the soda lime was noted. He developed ventricular tachycardia followed by fibrillation and resuscitation attempts were unsuccessful. One son was diagnosed MHS by IVCT.

Case 6: CHRA branch , ID 92, M74, Figure 4-13, A9
This case has been reported previously [530]. The patient was an 18 year-old male who presented for insertion of a Russell-Taylor rod into an unstable tibial fracture. He had previously developed an MH reaction at another hospital which responded to cooling and supportive measures. Subsequent IVCT was positive. On this occasion a trigger free anaesthetic was administered but 4 hours post-induction he developed a respiratory acidosis (pCO2 52mm), pyrexia 40°C, metabolic acidosis and subsequently an

increase in CK (17,000iu). He required prolonged treatment with dantrolene, cooling, management with vasoactive drugs and eventually made a good recovery.

Case 8: CHEH branch, ID 244, M10, Figure 4-10, A9
This 31 year old woman had had 3 previous anaesthetics for short procedures, and on each occasion developed masseter spasm. In different anaesthetics she was noted to be hyperventilating, tachycardic and pyrexic. With the fourth anaesthetic she again developed masseter spasm and the family history of MH was then noted. MHS diagnosis was confirmed by a positive IVCT result.

Case 9 CHKM branch, ID 154, M29, Figure 4-12, A9
This reaction has been reported previously [531]. The 23 year male presented for wiring and bone grafting of a cervical fracture. A previous anaesthetic for an eye injury at age 5 was uneventful. Anaesthesia was induced with thiopentone, suxamethonium and pancuronium and maintained with 0_2, N_2O and isoflurane. First abnormality developed over 2 hours after induction with an increase in heart rate to 100 beats/min. and a decrease in saturation to 88%. The soda lime was noted to be very hot and temperature was recorded at 41.9 °C. Vigorous resuscitation ensued for the next 2 hours including administration of dantrolene, cooling. correction of metabolic acidosis and treatment of cardiac arrhythmias including a brief period of asystole. He eventually made an almost normal recovery with a minor neurological defect the only abnormality. IVCT of siblings gave an MHS diagnosis.

Case 11: CHKM branch, ID136. M573, Figure 4-12, A9
An 18 year old woman presented for removal of a stone in the duct of the right sublingual gland. She was premedicated with omnopon, and hyoscine and anaesthesia was induced with thiopentone 300mg, the trachea intubated following 100 mg suxamethonium and anaesthesia maintained with N_2O and 2% halothane, breathing spontaneously. The surgeon found difficulty in opening the patient's mouth, in retrospect secondary to masseter spasm and the procedure was abandoned after 25 min. Tachycardia (170 beats/min) and tachypnoea (32/min) were immediately noted in recovery. The patient noted severe muscle aches. CK was measured at 5176 units (normal = 0 - 110). Recovery was uneventful. The patient declined IVCT but a sister and brother both had positive IVCT diagnoses.

A6.2 Family 1
Ethnic group: Caucasian/Maori
Pedigree diagram: Figure 5-19
Mutation: His4833Tyr

Two clinical MH events have been recorded. Few details are available. In the first case, a woman suffered a fatal MH reaction while undergoing an emergency appendectomy. The reaction was triggered by suxamethonium and ranked 4 on the clinical grading scale. Symptoms included inappropriate sinus tachycardia and inappropriate tachyhypnoea (pulse and respiratory rates were measured at 160 and 40 respectively). Generalised muscle rigidity was noted and severe muscle pain post-operatively. The patient died in recovery.

The second case occurred in 1980 whilst the proband was undergoing an elective procedure (suction clearance of the ear). Drugs administred include thiopentone, suxamethonium and halothane. The episode ranked 2 on the clinical grading scale. First symptoms were noted 20 minutes after induction and included cardiac arrythmia and inappropriate sinus tachycardia. Dantrolene was not administered.

A 6.3 Family 5
Ethnic group: Caucasian/Maori
Pedigree diagram: Figure 3--7
Mutation: Gly2434Arg

The proband (M317) was a 15 year old male suffered a suspected MH event, 55 minutes into emergency repair of a fractured humerous in 1983. The first symptom was hyperthermia (Temperature = 39 °C). Tachycardia was not observed, ET CO2 was not recorded. The reaction was ranked 3 on the clinical grading scale..

A6.4 Family 24

Ethnic group: Caucasian
Pedigree diagram: Figure 3-9
Mutation: Gly341Arg

The proband (M342) exhibited symptoms consistent with the onset of an MH crisis while undergoing a tonsillectomy in Australia. Symptoms included generalised muscle rigidity upon exposure to suxamethonium and halothane, in addition to tachycardia, high CK (87,500 iU), flushing and hyperthermia (a temperature of 39°C was recorded). The reaction scored a ranking of 5 on the MH clinical grading scale, indicating a high likelihood of MH [44]. Susceptibility to MH was subsequently confirmed in this family by IVCT. Strong positive MHS diagnoses were registered for the proband (M342), her twin sister (M537) her father (M445).and a brother (M475)

A 6.5 Family 35

Ethnic group: Caucasian
Pedigree diagram: Figure 3-6
Mutation: Arg163Cys

The proband (M142) was a 23 year-old female who presented for repair of the ulnar collateral ligament of the left thumb. There was no family history of MH despite extensive numbers of relatives on both parents' sides. Anaesthesia induced with propofol, alfentanil and droperidol and maintained with isoflurane, nitrous oxide and oxygen. The first symptoms were noted 45 minutes after the onset of anaesthesia with an increase of End tidal (ET) CO_2 from a baseline of 54 mm Hg to a level of 60 mm Hg and an increase of respiratory rate. $ETCO_2$ increased to a peak of 107 mm Hg, heart rate increased from 80 to 168 beats per minute, respiratory rate rose to 37 breaths per minute and hypertension was noted (BP 175/80). Temperature rose from 38.1C to 38.8C over a 5-10 minute period before therapy was instituted. Isoflurane was discontinued, 100% oxygen administered, and dantrolene commenced at a dose of 3.5 mg per kg. Cooling commenced with intravenous fluids (4°C), ice packs and bladder irrigation. There was a rapid response with a fall in $ETCO_2$ to normal levels and a fall of HR to <100 beats/min within 5-10 minutes. Initial arterial blood gases showed pH 7.32, pCO_2 44, pO_2 544 and a base deficit of 3.5 mM. Peak creatine kinase (normal 20-140 IU) measured 275 units 12 hours post reaction and had returned to normal by 24 hours. Myoglobinuria was not detected. A further dose of 60 mg Dantrolene was administered for a subsequent increase in temperature to 38.3° C noted in recovery. No further problems occurred. The reaction achieved rank 5 on the MH clinical grading scale indicating malignant hyperthermia was almost certain. The proband was diagnosed MHS by IVCT.

A 6.6 Family 36

Ethnic group: Caucasian
Pedigree diagram: Figure 5-10
Mutation: Arg2452Trp

The proband (M535) suffered a fulminant MH reaction characterised by hyperthermia (T = 39°C), tachycardia, masseter muscle rigidity and Tachypnoea at the age of 6 months when presenting for repair of cleft palate. The crisis ranked a maximum score of 6 (almost certainly MH) on the MH clinical grading scale[44]. This reaction was unusual in that MH in infancy is considered extremely rare [532,533]. In fact, an initial diagnosis of MH was rejected when hyperthermia was noted in the infant, as MH was not known

to occur in this age group. Isolated cases indicating MH reactions in infants have been reported [534-538] however MHS diagnoses were not confirmed by positive IVCT diagnosis in the proband or in immediate relatives in these cases. The proband responded to dantrolene therapy and made a full recovery. The diagnosis of MHS in the young proband was confirmed by positive IVCT at the age of 13 years. Strong positive contracture responses of 6.4 g to 2% halothane and 5.1g to 2 mM caffeine were registered.

A6.7 Family 58

Ethnic group: Caucasian
Pedigree diagram: Figure 5-20
Mutation: Arg2454His

The proband (M119) had suffered a fulminant MH crisis upon exposure to suxamethonium and isoflurane, exhibiting masseter spasm, tachycardia and hypercarbia. He was subsequently diagnosed MHS by IVCT, registering highly abnormal contracture responses of 7.5 g and 3.5 g to 2% halothane and 2 mM caffeine respectively. This second mutation was identified in an unrelated young male who developed a fulminant MH reaction with masseter spasm, significant hypercapnia, tachycardia and rhabdomyolysis during an emergency orthopaedic procedure

A6.8 Family 70

Ethnic group: Caucasian/Maori
Pedigree diagram: Figure 5-12
Mutation: Arg401Cys

The proband (M) suffered an MHS crisis when undergoing a dental procedure. Tachycardia (pulse 145) was noted 20 minutes after induction of anaesthesia with suxamethonium, propofol and halothane. A respiratory rate of 26 and end tidal CO_2 of 70 was recorded. Acidosis was not observed.
Generalised muscle rigidity and hyperthermia (temperature = 38.2°C) were noted and anaesthesia was discontinued. Dantrolene was not administered. Myoglobinuria and high CK (165, 300) were noted post-operatively.

A 7 PATIENT CONSENT FORMS, GENETIC TESTING

A 7.1 Patient consent form for the provision of venous blood samples for DNA analysis

CONSENT FORM

Institute of
Molecular BioSciences,
MASSEY UNIVERSITY.

.....
(Name)

DNA Sampling and Analysis

DNA (our genetic material) is analysed by molecular techniques to determine carrier status, or for presymptomatic diagnosis. It can also be stored, in our DNA Bank, against future research developments in Malignant Hyperthermia. Thus, it may be used by future generations.

I/We understand that **my/our** DNA will be extracted and stored in the MH DNA Bank (Director, Dr. K.M. Stowell)

I/We give consent for this DNA to be:

(Please sign for your choice of the options listed.
Cross out options which do not apply.)

a) Stored indefinitely for the use of our family in the future.

b) Used in a Diagnostic DNA test

c) Used for research purposes.

I have understood the information given to me and have had the opportunity to ask questions. I understand that I may withdraw or modify this consent at any stage, and that such withdrawal will not affect my further health care.

Signature: ..... **Date** .....

Clinician: ..... **Date** .....

Telephone No: (06)356-9099 Extn: 7517 **Fax No:** (06) 350-5688

A 7.2 Patient consent form for the provision of skeletal muscle tissue samples.

Genetic Testing for Malignant Hyperthermia

INFORMATION SHEET

My name is Kathryn Stowell and I, together with my PhD student, Rosemary Brown, want to develop a new simple test for Malignant Hyperthermia. We can be contacted during working hours by telephoning 3504801.

As you know common anaesthetics can affect people with Malignant Hyperthermia in many ways. There may be very little effect to quite long-term side effects and in very rare cases people can die. We want to find out what causes Malignant Hyperthermia so that we can develop a new test to replace the muscle biopsy test that is used now.

You will already have had explained to you the biopsy that you are about to have. We invite you to allow us to use a small piece of the muscle tissue, that will be removed, for our new test. No extra muscle will be taken. This small piece of muscle will be used to find out the cause of Malignant Hyperthermia so that we will then be able to develop our new test.

Your rights are in no way affected by signing the consent form. It is simply a record that on the basis of your present understanding, you agree to allow us to use a small piece of your muscle tissue after it has been collected. You have the right to withdraw your permission for us to use your muscle at any time by telephoning me at the above number. It will not be used without your consent for any other research. If you decide later that you do not want us to use your muscle, it can be returned to you if you wish, by telephoning me.

As we are trying to find a way to do this new test there will be no results from this research until it has been completed and a new test has been developed. The identity of your muscle sample and the results of the test will be strictly confidential to us, the researchers.

A 7.3 Genetic test request form

REQUEST FOR MOLECULAR GENETIC ANALYSIS FOR MALIGNANT HYPERTHERMIA

Institute of
Molecular BioSciences,
MASSEY UNIVERSITY.

NAME: **DOB:**

GENDER: M / F

REFERRING CLINICIAN:

COLLECTED AT: **DATE:**

SPECIMEN TYPE:

MUTATION TESTED FOR: (TICK REQUIRED MUTATION)

R163C	
G341R	
G2433R	
R2455H	
T4826I	

Cost per test: $350.

REASON FOR REFERRAL:

CONSENTING SIGNATURE:_____. **DATE:**_____
Patient

WITNESSED: _____.
Medical Professional.

PLEASE COURIER BLOOD SPECIMENS ON DAY OF COLLECTION TO ENSURE INTEGRITY OF DNA.

Delivery Address:

ATTN: Dr. K. Stowell,
Institute of Molecular Biosciences,
Science Tower D,
Massey University,
Palmerston North.

Genetic Testing for Malignant Hyperthermia

CONSENT FORM

I have read the Information Sheet and have had the details of the study explained to me. My questions have been answered to my satisfaction, and I understand that I have the right to ask any further questions at any time.

I understand that I have the right to withdraw my consent to the use of my muscle at any time.

I agree to allow the researchers to use a small piece of my muscle for the research on Malignant Hyperthermia on the understanding that my name will not be used without my permission and that the tissue will not be used for any other purpose. (The information generated from this study will be used only for this research and publications arising from this research project.)

I agree to participate in this study under the conditions set out in the Information Sheet.

At the end of the study (tick one box)

- ❑ I would like my muscle returned to me
- ❑ I would like my muscle destroyed

Signed: .....

Name: .....

Date: .....

A 7.3 Example of genetic test result form – (positive result)

REQUEST FOR MOLECULAR GENETIC ANALYSIS FOR MALIGNANT HYPERTHERMIA

Institute of
Molecular BioSciences,
MASSEY UNIVERSITY.

NAME: **DOB**

GENDER:

LOCATION: **CLINICIAN:** Dr. Neil Pollock

COLLECTED: **ARRIVED:**

TEST NUMBER: **TEST DATE:**

SPECIMEN TYPE: Whole venous blood.

REASON FOR REFERRAL:
Family history of Malignant Hyperpyrexia.
Pre Symptomatic Testing

METHOD:
PCR amplification of genomic DNA representing the region of the skeletal muscle ryanodine receptor containing T4826I mutation, followed by direct sequencing. Positive and negative control samples were analysed in parallel.

RESULTS:

The T4826I mutation was detected in this patient.

INTERPRETATIONS:

The T4826I mutation in the skeletal muscle ryanodine receptor has been shown to segregate with susceptibility to Malignant Hyperthermia in this kindred (manuscript in preparation). The presence of the T4826I mutation in this individual is indicative of an MH positive diagnosis. This individual can be considered to be at high risk of presenting with an MH episode.

REPORTED BY:_____.
Robyn Marston
Research Assistant

_____.
Dr. Kathryn Stowell
Consultant Scientist

Comment: These results are provided with the understanding that Genetic Counselling is available through Central Regional Genetic Services, if the patient desires it. If there are any questions regarding this report please contact Dr. K. Stowell, by phoning (06) 350 5515 ext 7517

A 7.3 Example of genetic test result form – Negative result

REQUEST FOR MOLECULAR GENETIC ANALYSIS FOR MALIGNANT HYPERTHERMIA

Institute of
Molecular BioSciences,
MASSEY UNIVERSITY.

NAME: **DOB:**

GENDER:

LOCATION: **CLINICIAN:** Dr. Neil Pollock

COLLECTED: **ARRIVED:**

TEST NUMBER: **TEST DATE:**

SPECIMEN TYPE: Whole venous blood.

REASON FOR REFERRAL:
Family history of Malignant Hyperpyrexia.
Pre Symptomatic Testing

METHOD:
PCR amplification of genomic DNA representing the region of the skeletal muscle ryanodine receptor containing T4826I mutation, followed by direct sequencing. Positive and negative control samples were analysed in parallel.

RESULTS:

The T4826I mutation was not detected in this patient.

INTERPRETATIONS:

The T4826I mutation in the skeletal muscle ryanodine receptor has been shown to segregate with susceptibility to Malignant Hyperthermia in this kindred (manuscript in preparation). Subject to the presence of a *de novo* mutation or inheritance of a second mutation causative of Malignant Hyperthermia, this individual can be considered to be at the same risk to Malignant Hyperthermia as the general population. This is considered as 1 chance in 50,000 (Britt and Kalow, 1970. *Canadian Anaesthetic Society Journal*:**17**, 293-315)

REPORTED BY:_____.
Robyn Marston
Research Assistant

_____.
Dr. Kathryn Stowell
Consultant Scientist

Comment: These results are provided with the understanding that Genetic Counselling is available through Central Regional Genetic Services, if the patient desires it. If there are any questions regarding this report please contact Dr. K. Stowell, by phoning (06) 356-9099 ext 7517

A 8 STATISTICAL METHODS AND FORMULAE

Software

Graphical presentations were prepared with SigmaPlot™ (Jandel Scientific for PC) and Kaleidograph (Mac) statistical drawing programs. Basic statistical functions were performed using Microsoft Exel™ version 4.0. ANOVA was performed with GraphPad InStat. Software [433]. Multivariate analysis was performed using Microsoft Exel™ version 4.0 with XLSTAT extension software [539], and customised formulae.

1.1.5 A 8.1 Student T-test

The two sample student T-test appraises the difference between two sample means to determine whether samples are likely to have come from the same underlying population, by testing the null hypothesis that the two means are equal. The test is appropriate for small samples ($n < 30$) or where the population variances σ_1^2 and σ_2^2 are unknown and assumes that the unknown population variances are equal. The population variance is estimated from the pooled sample variances as described by the denominator in the following formula.

$$t = \frac{\bar{x}_1 - \bar{x}_2 - \delta}{\sqrt{\frac{(n_1-1)s_1^2 + (n_2-1)s_2^2}{n_1+n_2-2} \cdot \left(\frac{1}{n_1} + \frac{1}{n_2}\right)}}$$

Equation 1

Where $\bar{x}_1$ and $\bar{x}_2$ represent the means of the two samples, δ is the difference between the means assumed by the null hypothesis (usually zero). s_1 and s_2 represent the sample variances. The null hypothesis is rejected when t exceeds the critical value (obtained from statistical tables according to degrees of freedom, df = n – 1). The corresponding P value is the probability of a type one error (rejecting the null hypothesis though it is true), interpreted as the probability that an observed difference between two sample means can be attributed to chance.

References:

[421,423,424]

1.1.6 A 8.2 Non-parametric testing

A simple non-parametric test for the comparison of means from two continuous non-normal populations is the Mann-Whitney U-test (or the rank sum test). The data from the two samples is combined, ordered and ranked. Where ties occur between samples, each of the tied observations is assigned the mean of the jointly occupies rank. The ranks are summed, to give W1 (the sum of the ranks of the first sample) and W2 (the sum of the ranks of the second sample). The U statistic is calculated with the following formula.

$$U_1 = W_1 - \frac{n_1(n_1+1)}{2}$$

Equation 2

The mean and the standard deviation of sampling distribution of U_1 are given by

$$\mu_{U1} = \frac{n_1 n_2}{2}$$

$$\sigma_{U1} = \sqrt{\frac{n_1 n_2 (n_1 + n_2 + 1)}{12}}$$

Equation 3

If n_1 and n_2 are both greater than eight, the sampling distribution of U_1 is approximately normal. In this case, the z statistic can be used to test the null hypothesis that $\mu_1 = \mu_2$.

$$z = \frac{U_1 - \mu}{\sigma_{U1}}$$

Equation 4

References:
[421-424]

1.1.7 *A 8.3 Multivariate analysis*

Multivariate tests allow simultaneous comparison of more than one variable between two groups. Multivariate tests take into consideration several problems: unequal dispersion of variables within and between groups, and also the problem that variables can be mutually correlated within groups (covariance).

Mahanalobis distance statistic (D^2)

For defining multivariate outliers. The Mahanalobis distance statistic (D^2) estimates the multivariate equivalent of how many standard deviations a data point is from the mean of the sample. Two factors are taken into account in defining the statistical measure of Mahanalobis distance: (1) the differing variability (s^2) of the variables (which can occur if the variables have been scaled differently) and (2) the correlation between the variables. The Mahanalobis distance is smaller for strong positive correlations, because some of the distance along one dimension (or variable) is predictable from the correlation with the other.

D^2 is calculated with the following formula, which is the equation of a two-dimensional elipsoid, whose contour traces the path of points $(x_i y_i)$ with equal Mahanalobis distance from the centre (x, y).

In the IVCT data analysis of MHS patients, x any y were substituted with the means of the caffeine and halothane test variables for the mutation positive group, while r (0.433) is the correlation coefficient for the two variables.

$$D^2 = \frac{1}{(1-r^2)} \left(\frac{(x_i - x)^2}{s^2_x} + \frac{(y_i - y)^2}{s^2_y} - \frac{2r\,(x_i - x)(y_i - y)}{s_x s_y} \right)$$

Equation 5

Assuming the samples come from a multivariate normal distribution, their distance from its mean (D^2) should follow a chi-squared distribution with two degrees of freedom (2 variables). If an individual does come from that distribution there is a 95 % chance of their distance from the mean (D^2) being less than 5.99 and a 99% chance of the distance from the mean being less than 9.21. The D^2 statistic was estimated for all the individuals in the mutation positive group (n= 34).

In support of the assumption of multivariate normality, a plot of the ordered $D^2_{(i)}$ values versus $\chi^2_{(1-\alpha_i)}$ for two degrees of freedom did yield an approximate straight line, where $(1-\alpha_i) = (i - 0.5)/n$, for the ordered distances of D_i^2, i = 1,2,3 .....n [428].

The multivariate analysis was performed and interpreted with support from Duncan Hedderley from the Massey Statistics research and consulting center. The correlation coefficient and D^2 values were calculated using Microsoft Excel Version 4 (programed with equation 5).

References: [427-429]

A 8.4 One way Analysis Of Variance (ANOVA)

ANOVA (analysis of variance) is used to compare data from three or more groups, assuming the data follow a normal distribution. The method is based on the logic of the pairwise T-test test. For any single pairwise t-test, if an observed result is found to be significant at the basic 0.05 level, what this means is that there is a 5% chance of its having occurred through mere chance. If three pair-wise comparisons were performed to compare three sets of data, the probability that one or another of them might end up "significant" at the .05 level by mere chance, would be on the order of .3 x 0.05 = 0.15. Therefore, performing multiple pairwise t-tests to compare data from a number of groups leads to type 1 errors (rejecting the null hypothesis although it is true) [433].

Like any test of statistical significance, the ANOVA test compares an observed fact to a measure of the random variability in which it is embedded. The aim of the comparison in this case is to determine whether the aggregate difference among the a group of sample means is greater than that expected from mere random variability. The variability between the groups is measured and compared to the variability between groups to test whether the factor under scrutiny is having a significant influence on the data.

For any set of N values of x_i, a deviate is the difference between an individual value of Xi and the mean of the set (Mx), i.e. Xi - Mx. A squared deviate is the square of that quantity, and the sum of squared deviates (S.S) is the sum of the squared deviates in the set. Between-group and within-group S.S are calculated as shown below [434]:

Total summed squared deviates: $S.S_T = \Sigma x_i^2 - \frac{(\Sigma x_i)^2}{N_T}$

Summed squared deviates within each group: $S.S_g = \Sigma x_{gi}^2 - \frac{(\Sigma x_{gi})^2}{N_g}$

Total within-group summed squared deviates: $S.S\ wg = S.S\ a + S.S\ b + S.S\ c.....$

Between-group summed squared deviates: $S.S\ bg = S.S_T - S.S\ wg$

Degrees of freedom (k = no, of groups)

$df_T = NT - 1$

$df_{wg} = k - 1$

$df_{bg} = N_T - k$

Mean square values $MS_{bg} = \frac{S.S_{bg}}{df_{bg}}$ $MS_{wg} = \frac{S.S_{wg}}{df_{wg}}$

F statistic: $F = \frac{MS\ bg}{MS\ wg}$ A measure of the aggregate difference among the means of k groups / A measure of the amount of random variation that exists inside k groups

Even if the null hypothesis is true, values are expected to be closer to their group means than the overall mean [433]. The calculation of the degrees of freedom and the mean square account for this. The F ratio is the end result. If the null hypothesis is true (the means of the groups are the same) then F values close to 1.0 are expected. The differences between the groups are said to be significant when F exceeds a particular critical value. The critical values of F for which the decision is based at either the 0.01 and 0.05 level of significance depend on both the between-group and within-group degrees of freedom [433]. Critical F values were calculated from the sampling distribution of F using the Microsoft™ Excel (version 4.0). The P value associated with F can be interpreted as the chance that randomly selected groups with the same mean would produce an F ratio as big (or bigger) as the one obtained in the experiment.

References: [435,436]

APPENDIX 9 : CH family pedigree

APPENDIX 9: CH FAMILY PARTIAL PEDIGREE

INCLUDES 325 INDIVIDUALS / 1400 TOTAL